Deutscher Wetterdienst

Annalen der Meteorologie

44

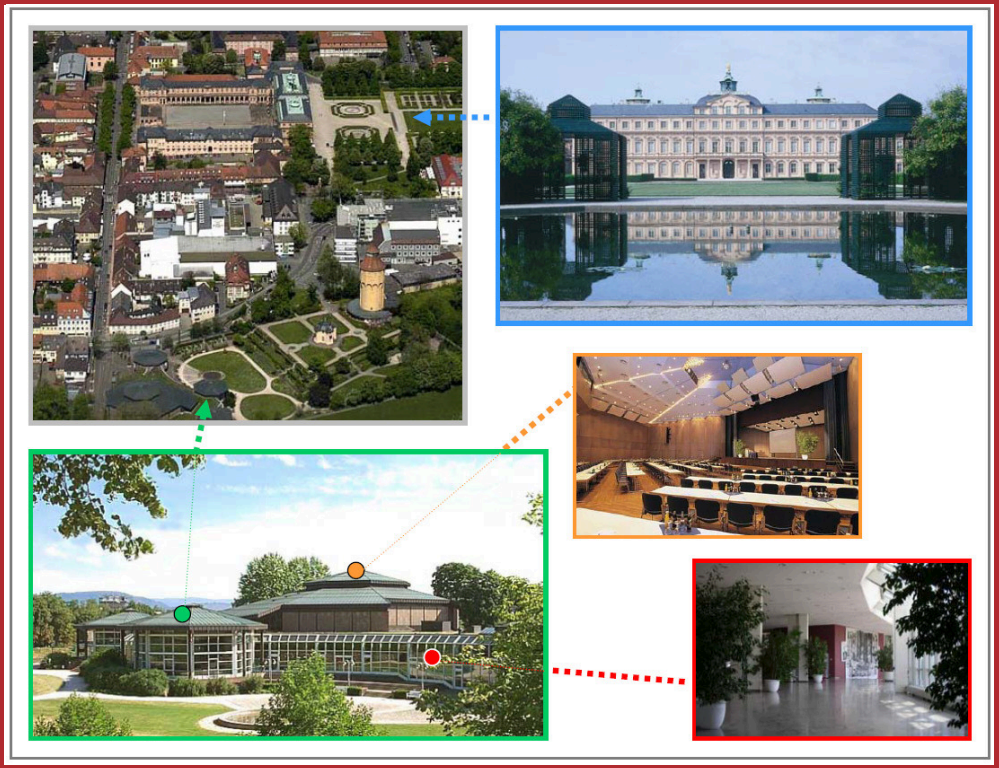

Programme & Extended Abstracts

30th International Conference on Alpine Meteorology

11 – 15 May 2009

Badnerhalle, Rastatt, Germany

Offenbach am Main 2009

Selbstverlag des Deutschen Wetterdienstes

Annalen der Meteorologie

		Erscheinungsjahr
Nr. 1	H.G. Cannegieter: The history of the International Meteoro-logical Organization 1872-1951	1963
Nr. 2	A. Hofmann: Der internationale Stand des Problems der Langfrist-Vorhersage	1963
Nr. 3	Die Meteorologen-Tagung in München vom 27.-30.April 1966	1967
Nr. 4	Meteorologen-Geophysiker-Tagung in Hamburg vom 1.-6.April 1968, Meteorologische Vorträge	1969
Nr. 5	XI. Internationale Tagung für Alpine Meteorologie in Oberstdorf 22.- 26.September 1970	1971
Nr. 6	Meteorologische Vorträge, gehalten auf der 36. Physikertagung 1971 in Essen	1973
Nr. 7	F. Wippermann: The Planetary Boundary-Layer of the Atmosphere	1973
Nr. 8	F. Klemm: Die Entwicklung der meteorologischen Beobachtungen in Franken und Bayern bis 1700	1973
Nr. 9	Die Meteorologen-Tagung in Bad Homburg v.d.H. vom 27.-29.März 1974	1974
Nr. 10	F. Klemm: Die Entwicklung der meteorologischen Beobachtungen in Nord- und Mitteldeutschland bis 1700	1976
Nr. 11	Simulation of large-scale atmospheric processes. International Conference Hamburg, Aug. 30-Sept.4, 1976	1976
Nr. 12	Die Meteorologen-Tagung in Garmisch Partenkirchen vom 13. bis 16. April 1977	1977
Nr. 13	F.Klemm: Die Entwicklung der meteorologischen Beobachtungen in Südwest-deutschland bis 1700	1979
Nr. 14	100 Jahre Wetterdienst in Bayern, 1878-1978	1979
Nr. 15	Deutsche Meteorologentagung 1980 in Berlin	1980
Nr. 16	Societas Meteorologica Palatina 1780-1795, Symposium Mannheim	1980
Nr. 17	Festsymposium "200 Jahre meteorologische Beobachtungen auf dem Hohenpeißenberg"	1981
Nr. 18	Symposium über Strahlungstransportprobleme und Satellitenmessungen in der Meteorologie und der Ozeanographie	1982
Nr. 19	17.Internationale Tagung für Alpine Meteorologie, Berchtesgarden, 21. bis 25.September 1982	1982
Nr. 20	Deutsche Meteorologentagung 1983 in Bad Kissingen	1983
Nr. 21	F.Klemm: Die Entwicklung der meteorologischen Beobachtungen in Österreich einschließlich Böhmen und Mähren bis zum Jahr 1700	1983
Nr. 22	Internationale Tagung für Human-Biometeorologie vom 2. bis 4. Oktober 1985 in Freiburg	1985
Nr. 23	Deutsche Meteorologentagung 1986 in Münster	1986
Nr. 24	Gedächtniskolloquium für K. H. Hinkelmann am 14. Mai 1987 in Mainz	1988
Nr. 25	Xth International Cloud Physics Conference, Bad Homburg 1988, 2 Vol.	1988
Nr. 26	Deutsche Meteorologentagung 1989 in Kiel	1989
Nr. 27	Deutsche Meteorologentagung 1992 in Berlin	1992
Nr. 28	Internationale Tagung für Human-Biometeorologie, Freiburg 1992	1992
Nr. 29	100 Jahre Meteorologisches Observatorium Potsdam	1994
Nr. 30	23. Internationale Tagung für Alpine Meteorologie 1994 in Lindau	1994
Nr. 31	Deutsche Meteorologen-Tagung 1995 in München	1995
Nr. 32	Herbstschule Radarmeteorologie 1995	1995
Nr. 33	3. Fachtagung BIOMET am 4. und 5. Dezember 1996 in München	1997
Nr. 34	4. Deutsche Klimatagung, Frankfurt am Main 1997	1997
Nr. 35	3rd European Conference on Applications of Meteorology 23 - 26 September 1997 in Lindau	1997
Nr. 36	Symposium: Vorhersage-Wetter, Klima, Umwelt, Berlin 1997	1998
Nr. 37	Deutsche Meteorologen-Tagung 1998 in Leipzig	1998
Nr. 38	Herbstschule Radarmeteorologie 1998	1998
Nr. 39	4. Fachtagung BIOMET (19.-20. April 1999 in München) des Fachausschusses BIOMET der DMG gemeinsam mit der Ges. zur Förderung Medizin-Meteorologischer Forschung e.V.	1999
Nr. 40	CD ,SIRWEC 2004, 12th Internat. Road Weather Conference, Bingen	2004
Nr. 41	17th International Congress of Biometeorology, ICB 2005	2005
Nr. 42	50 Jahre Überwachung der Radioaktivität in der Atmosphäre durch den DWD	2006
Nr. 43	125 Jahre Deutsche Meteorologische Gesellschaft, Festveranstaltung am 7.November 2008 in Hamburg	2008

Deutscher Wetterdienst

Annalen der Meteorologie

44

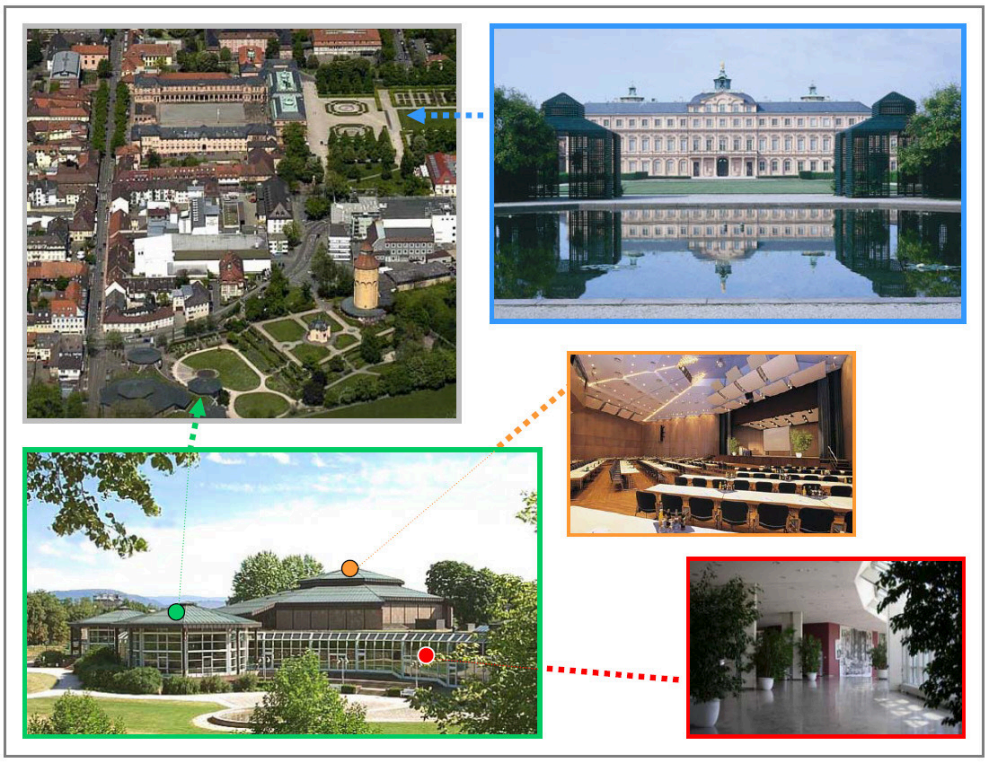

Programme & Extended Abstracts

30th International Conference on Alpine Meteorology

11 – 15 May 2009

Badnerhalle, Rastatt, Germany

Offenbach am Main 2009

Selbstverlag des Deutschen Wetterdienstes

Collage of images on the cover – in cyclonic order:

top left: aerial view of Rastatt town centre with *Schloss* (castle; upper middle) and *Badnerhalle* (lower left)
bottom left: *Badnerhalle* complex at the edge of the former extended castle park with view towards Black Forest
bottom right: interior of *Türkenlouis Saal* (lecture hall; orange) and park-side foyers (poster sessions; red)
top right: garden-side baroque façade of Rastatt castle mirrored in a fountain basin

ICAM sponsors: Five institutions supported the conference through contributions in money or in kind

WMO	World Meteorological Organization, Geneva, CH
NEC	NEC Deutschland GmbH, Düsseldorf, D
DLR-IPA	Deutsches Zentrum für Luft- und Raumfahrt, Institut für Physik der Atmosphäre, D
DWD	Deutscher Wetterdienst, Offenbach, D
KIT-IMK	Karlsruhe Institute of Technology, Institut für Meteorologie und Klimaforschung, D

This volume was assembled for Deutscher Wetterdienst at the Institut für Physik der Atmosphäre (IPA) of Deutsches Zentrum für Luft- und Raumfahrt e.V. (DLR), D-82234 Oberpfaffenhofen, Germany:
Editing: Hans VOLKERT *Compilation*: Jana FREUND *Author Index:* Romy MAY

ISSN 0072-4122
ISBN 978-3-88148-440-4

Publisher: Deutscher Wetterdienst, Frankfurter Straße 135, D-63067 Offenbach am Main, Germany

FOREWORD

The *International Conference on Alpine Meteorology* (ICAM) series was started in 1950 in Italy by Mario BOSSOLASCO, a far sighted geophysicist and meteorologist. The meteorological services and some research institutes in the then six Alpine countries Italy, Austria, Switzerland, France, Germany and Yugoslavia (today: Slovenia and Croatia) acted as regular hosts at biennial intervals. A nine-month-shift to odd years in 2003 resulted in a better synchronization with the *Mountain Meteorology Conference* series of the *American Meteorological Society* taking place in even years. The 30th realization of ICAM in Rastatt, Germany, concludes the fifth cycle through the Alpine countries before a new routine will be started in 2011 in the United Kingdom, which recently joined the ICAM-countries.

Scientific conferences constitute an important method to establish new cooperative links and to further existing cooperation. They provide occasions for the exchange of new ideas and techniques between staff and students from universities, research laboratories, and meteorological services. The communication of ideas is regularly enhanced, when the venue is situated in a town of modest size and with some cultural backcloth. In summer 2007 the *Badnerhalle* in Rastatt was found to meet these criteria well. Good public transportation links and the proximity to Black Forest and Vosges, where the COPS operations took place from June to August 2007, are additional advantages.

The settlement of Rastatt was first mentioned in written documents as early as 1084. Around 1700 the grown village gained town-rights, just before margrave *Ludwig-Wilhelm* moved his residence from Baden-Baden to here in 1705. The castle was completed during the following years. Today it preserves the state-rooms, richly ornamented in rococo-style, and several museums. After numerous changes of the political situation in the border region of Germany and France, today's population of nearly 50,000 inhabitants could enjoy several decades of stability in a central region of the European Union. We take this spirit of cooperation as a good *omen* for the success of ICAM-2009.

The response to the call for papers was impressive indeed. The programme committee structured the submitted contributions in two different, but equally important classes: short oral presentations to the plenary and poster presentations for in-depth discussions with interested colleagues during extended poster sessions. All contributors were given the possibility to submit a two-page extended abstract five weeks before the conference in order to aid individual selections during the event. Around 125 *Extended Abstracts* were received and are collected here following the ICAM-2009 *Programme* (pp. *ii-xvii*) in two large blocks:

A) Oral Presentations (pp. 1–125) and
B) Poster Presentations (pp. 127–253)

The *Author Index* (pp. 257–259) helps to find contributions by their originators. It is hoped that this volume serves the intended purpose during the conference and that it will later conserve some of the spirit in the tradition of previous ICAM volumes. For cost reasons the figures are printed in black-and-white; numerous colour versions are contained in the electronic issue which can be downloaded from the conserved ICAM-2009 website under www.pa.op.dlr.de/icam2009/extabs .

In conclusion we express our gratitude to all contributors to this volume for adhering well to dates and guidelines (cf. pp. 254–255), to our colleagues on the organisation and programme committees for their combined efforts to set up a balanced programme and to stage the event, and to our sponsors from industry, international agencies and meteorologically oriented German institutions for their confidence and support.

Around Easter in April 2009

Hans VOLKERT & Günther ZÄNGL

30th International Conference on Alpine Meteorology (ICAM)

Structure of sessions and overview timetable

Time	*Monday 11 May 2009*	*Tuesday 12 May 2009*	*Wednesday 13 May 2009*	*Thursday 14 May 2009*	*Friday 15 May 2009*
09:00 – 10:30	**Opening** short addresses 2 'historic' talks 1 review talk	**Session 04** *BoundLayer* Turbulence 6 talks	**Session 08** *PRECIP* D-PHASE 1review, 4talks	**Session 12** *BoundLayer* Cold Pools 6 talks	**Session 16** *PRECIP* other regions 6 talks
	Coffee	*Coffee*	*Coffee*	*Coffee*	*Coffee*
11:00 - 12:30	**Session 01** *PRECIP* COPS-Observation 6 talks	**Session 05** *BoundLayer* Therm. driven flows 6 talks	**Session 09** *NWP* COPS-DPHASE 6 talks	**Session 13** *SNOW* 6 talks	**Session 17** *NWP* Towards the future 6 talks
	Lunch	*Lunch*	*Lunch* & guided tour through baroque residence 15:30	*Lunch*	**Awards+Discuss.** 13:00 *Lunch*
14:00 - 15:00	**Session 02** *PRECIP* Idealized 4 talks	**Session 06** *DYNAMICS* Synoptic scale 4 talks		**Session 14** *DYNAMICS* Meso.mount.flows 1 4 talks	
15:00 – 16:30	**Poster Session A** *PRE & CLI-1* (with refreshments)	**Poster Session B** *BL & CLI-2* (with refreshments)	**Session 10** *PRECIP* Aerosols 4 talks	**Poster Session C** *DYN & SNOW* (with refreshments)	
16:30 – 18:00	**Session 03** *PRECIP* Convect. Initiation 6 talks	**Session 07** *CLIMATE* 6 talks	*Coffee* **Session 11** *PRECIP* Analyses 4 talks	**Session 15** *DYNAMICS* Meso.mount.flows 2 6 talks	
19:30 - 21:30	***ICEBREAKER***		***DINNER***		
22:30					

Note: All submissions were grouped in topical categories, most of them with sub-categories:

CLIMATE	climate aspects	*BoundLayer*	boundary layer processes
DYNAMICS	dynamical aspects	*PRECIP*	precipitation processes
NWP	numerical weather prediction	*SNOW*	snow pack

Typically, packets of 4 or 6 presentations are assembled to fill the 17 oral sessions as given above.

Poster groups *PRE*, *BL* and *DYN* are accompanied by the remaining posters in such a way as to achieve fairly equal numbers of poster presentations for each day (~36).

The programme also serves as table of contents for the 2-page Extended Abstracts
(these are available for all contributions for which a page number is given)

as of 15 April 2009

Part A) Sequence of events and oral presentations

Sunday, 10 May 2009		
17:00-19:00		***R e g i s t r a t i o n***

Monday, 11 May 2009		
08:00-09:00	***page***	***R e g i s t r a t i o n*** (continued)
Opening session		***Welcome*** *and* ***short address*** Chair: *Hans Volkert*
09:10-09:20	***002***	*Gerhard* ***Adrian*** (DWD, Offenbach, D): ICAM as a regular visitor: Back to Germany for the fifth time
		Two 'historic' talks with some modern ingredients:
09:20-09:40	***004***	*Haraldur* ***Ólafsson*** (Univ. of Reykjavík, Iceland & Univ. of Bergen, N) and *Ágústsson*: Mountain Meteorology in the Middle Ages
09:40-10:00	***008***	*Arnold* ***Tafferner*** (DLR, Oberpaffenhofen, D), *Hoinka, Zängl* & *Weber* : The 'miraculous' föhn in Bavaria of January 1704
		Overview after a recent field campaign in the neighbourhood:
10:00-10:30		*Volker* ***Wulfmeyer*** (University of Hohenheim, Stuttgart, D): The Convective and Orographically-induced Precipitation Study (COPS): A unique data set for studying the initiation and organization of convection in low-mountain regions
10:30-11:00		***C o f f e e***
Session 01		***Precipitation Processes:*** Chair: *Mathias Rotach* ***Observations during COPS***
11:00-11:15		*Stephen* ***Mobbs*** (Univ. of Leeds, UK): Observations of shallow convection over the Black Forest during COPS
11:15-11:30	***010***	*Andrew* ***Russell*** (Univ. of Manchester, UK) and *Vaughan*: An examination of atmospheric lids during COPS
11:30-11:45	***012***	*Jan* ***Handwerker*** (KIT, Karlsruhe, D), *Träumner, Grenzhäuser, Wieser*: Wind measurements with lidar and cloud radar during COPS
11:45-12:00	***014***	*Paolo* ***di Girolamo*** (Univ. Basilicata, Potenza, I), *Summa, Bhawar, di Iorio, Vaughan, Norton and Peters*: Lidar and Radar Measurements of the melting layer in the frame of the Convective and Orographically-induced Precipitation Study
12:00-12:15	***016***	Rohini ***Bhawar*** (Univ. Basilicata, Potenza, I), *di Girolamo, Summa, di Iorio and Demoz*: Study of an MCS using Raman Lidar in the frame of the Convective and Orographically induced Precipitation Study
12:15-12:30	***018***	*Alan* ***Blyth*** (Univ. of Leeds, UK), *Huang, Brown, Cotton, Jones, Coe, Choularton, McFiggans* and *Irwing*: Influence of orography and aerosols on the microphysics of convective clouds observed during COPS
12:30-14:00		***L u n c h***
Session 02		***Precipitation Processes: Idealized studies*** Chair: *Dale Durran*
14:00-14:15	***020***	*Ulrich* ***Blahak*** (KIT, Karlsruhe, D): Idealized numerical sensitivity studies on shallow-convection-triggered storms in a low mountain range
14:15-14:30		*Daniel J.* ***Kirshbaum*** (Univ. of Reading, UK): Lee-wave triggering of deep convection
14:30-14:45	***022***	*Axel* ***Seifert*** (DWD, Offenbach, D) and *Zängl*: Scaling relations in warm orographic precipitation
14:45-15:00	***024***	*Günther* ***Zängl*** (DWD, Offenbach, D): The influence of the freezing level on orographic precipitation patterns at small scales

Monday, 11 May 2009 (continued)		
15:00-16:30		**POSTER SESSION A** ***with refreshments*** ***Precipitation Processes*** *and* ***Climate***
Session 03	***page***	***Precipitation Processes:*** Chair: *Ron McTaggart-Cowen* ***Convective initiation***
16:30-16:45		*Christoph* ***Kottmeier*** (KIT, Karlsruhe, D), *Kalthoff, Corsmeier, Barthlott, Träumner, Arnold, Wieser* and *Mahlke*: Initiation and coherent structures of PBL convection over low mountains during the campaigns ESCOMPTE, VERTIKATOR, CSIP, and COPS
16:45-17:00	***026***	*Ulrich* ***Corsmeier*** (KIT, Karlsruhe, D), *Barthlott, Kalthoff, Konow* et al.: Driving processes for convection initiation over complex terrain: COPS observations and respective COSMO simulations
17:00-17:15	***028***	*Evelyne* ***Richard*** (Lab. d'Aérologie, Toulouse, F), *Chaboureau, Flamant*: Forecasting summer convection over the Black Forest: A case study from the COPS experiment
17:15-17:30	***030***	*Christian* ***Barthlott*** (KIT, Karlsruhe, D), *Schipper, Kalthoff, Adler* and *Kottmeier*: COSMO model simulation of convergence zones in complex terrain: A case study from COPS
17:30-17:45	***032***	*Martin* ***Hagen*** (DLR, Oberpfaffenhofen, D), *van Baelen* and *Richard*: Influence of the wind profile on the location of hotspots of convection in mountainous terrain
17:45-18:00		*Andreas* ***Behrendt*** (Univ. of Hohenheim, Stuttgart, D), *Pal, Radlach, Aoshima* and *Wulfmeyer*: Analysis of convection initiation processes in complex terrain with the synergy of COPS remote sensing data
19:30-21:30		***ICEBREAKER***

Tuesday, 12 May 2009		
Session 04		***Boundary Layer Processes: Turbulence*** Chair: *Christian Barthlott*
09:00-09:15	***034***	*Branko* ***Grisogono*** (Univ. of Zagreb, CRO): Generalizing the local mixing length-scale for stable atmospheric boundary layers
09:15-09:30	***036***	*Željko* ***Vecenaj*** (Univ. of Zagreb, Zagreb, CRO), *Belušić* and *Grisogono*: Characteristics of the near-surface turbulence during a bora event
09:30-09:45	***038***	*Marwan* ***Katurji*** (Univ. of Canterbury, New Zealand), *Sturman, Zawar*: An investigation into ridge-top turbulence characteristics: A New Zealand case study of in situ measurements and large eddy simulation
09:45-10:00	***040***	*Rebecca* ***Mott*** (SLF, Davos, CH) and Lehning: The application of microscale airflow simulations for quantifying snow drift processes over complex terrain
10:00-10:15		*Stefano* ***Serafin*** (Univ. of Trento, I), *Caresia, Panelatti* and *Zardi*: A numerical investigation of the potential temperature and turbulent kinetic energy budgets in thermally driven winds in alpine valleys
10:15-10:30		*Stephan* ***de Wekker*** (Univ. of Virginia, Charlottesville, USA), *Lee, Craven, George* and *Tertell*: A preliminary investigation of atmospheric boundary layer evolution over the Blue Ridge Mountains in Virginia
10:30-11:00		***Coffee***
Session 05		***Boundary Layer Processes:*** Chair: *Branko Grisogono* ***Thermally driven flows***
11:00-11:15	***042***	*Jürg* ***Schmidli*** (IAC ETH, Zurich, CH) and *Rotunno*: Mechanisms of along-valley winds
11:15-11:30	***044***	*Dino* ***Zardi*** (Univ. of Trento, I): A conceptual model for the daytime evolution of the thermal structure in a mountain valley under fair weather conditions

11:30-11:45	***046***	*Bart* ***Geerts*** (Univ. of Wyoming, Laramie, USA) and *Demko*: Observations and numerical simulations of the interaction between the thermally-forced orographic circulation in the convective boundary layer and deep convection
11:45-12:00	***048***	*Jian-Wen* ***Bao*** (NOAA, Boulder, USA), *E. Grell, Michelson* and *G. Grell*: Investigation of orographic venting of atmospheric boundary layer air using observations and the WRF-Chem model
12:00-12:15	***050***	*Stefan* ***Emeis*** (KIT, Garmisch, D), *Schäfer, Forkel, Obleitner* & *Suppan*: Assessment of air quality and mixing-layer height in an Alpine valley from measurements and numerical modelling
12:15-12:30	***052***	*Cyrille* ***Flamant*** (IPSL, Paris, France), *Champollion, Richard, Masson, Cuesta* et al. : Complex valley flows and their impact on water vapor transport in pre-convective and convective environments: a case study
12:30-14:00		***L u n c h***
Tuesday, 12 May 2009 (continued)		
Session 06	***page***	***Dynamics: Synoptic scale aspects*** Chair: *Manfred Dorninger*
14:00-14:15	***054***	*Ron* ***McTaggart-Cowan*** (Env. Canada, Dorval, CAN), *Galernau* and *Bosart*: Development of an Alpine lee cyclone during MAP D-PHASE: Forcings for cyclogenesis
14:15-14:30		*Kristian* ***Horvath*** (DHMZ, Zagreb, CRO), *Ivatek-Šahdan*, *Ivančan-Picek* and *Grubišić*: Evolution and structure of two severe cyclonic Bora events: Contrast between the northern and southern Adriatic
14:30-14:45	***056***	*Sylvain* ***Mailler*** (LMD/CNRS, Paris, F) and *Lott*: A dynamical influence of the Himalayas on the winter south-eastern Asian monsoon
14:45-15:00	***058***	*Sixiong* ***Zhao*** (CAS, Beijing, China) and *Fu*: Dynamics of a vortex with heavy rainfall east of the Tibetan Plateau
15:00-16:30		**Poster session B *with r e f r e s h m e n t s*** ***Boundary Layer Processes*** *and* ***Climate***
Session 07		***Climate aspects*** Chair: *David Whiteman*
16:30-16:45		*Reinhold* ***Steinacker*** (Univ. of Vienna, A), *Sperka* and *Mayer*: A new high resolution Alpine re-analysis
16:45-17:00	***060***	*Simona* ***Fratianni*** (Univ. of Turin, I) and *Aquaotta*: Climate variability in North-Western Italy through the use of reconstructed and homogenized thermo-pluviometric series
17:00-17:15	***062***	*Sophie* ***Fukutome*** (MeteoSwiss, Zurich, CH), *Liniger* and *Frei*: An Alpine climatology of extreme events
17:15-17:30	***064***	*Monika* ***Rauthe*** (KIT, Karlsruhe, D), *Kunz* and *Mohr*: Winter storms with high loss potential in a changing climate: A regional perspective
17:30-17:45	***066***	*Rebekka* ***Posselt*** (MeteoSwiss, Zurich, CH), *Dürr, Stöckli* and *Müller*: Satellite-based retrieval of global radiation over complex terrain: A climatology for the Alps
17:45-18:00	***068***	*Jochen* ***Wagner*** (Univ. Bodenkultur, Vienna, A), *Arola, Blumthaler, Fitzka, Kift, Kreuter, Rieder, Simic* et al.: Comparison of ground-based UV irradiance measurements with satellite-derived values: 1-D and 3-D-radiative transfer model calculations in mountainous terrain

Wednesday, 13 May 2009		
Session 08	***page***	***Precipitation Processes: D-PHASE*** Chair: *Andreas Behrendt*
09:00-09:30	***070***	*Mathias* ***Rotach*** (MeteoSwiss, Zurich, CH), *Arpagaus, Dorninger, Hegg, Montani* and *Ranzi*: MAP D-PHASE: Lessons learned and future developments *(overview presentation)*
09:30-09:45	***072***	*Tanja* ***Weusthoff*** (MeteoSwiss, Zurich, CH), *Ament, Arpagaus* and *Rotach*: Verification of precipitation forecasts of the D-PHASE data set
09:45-10:00		*Luca* ***Panziera*** (MeteoSwiss, Zurich, CH) and *Germann*: Probabilistic nowcasting of orographic rainfall
10:00-10:15		*Simon* ***Jaun*** (WSL, Birmensdorf, CH), *Walser, Schär* and *Zappa*: Evaluation of a coupled meteorologic-hydrologic (ensemble) prediction system within the MAP D-PHASE
10:15-10:30	***074***	*Uwe* ***Ehret*** (TUniv. München, D) Evaluation of operational weather forecasts: Applicability for flood forecasting in Alpine Bavaria
10:30-11:00		***C o f f e e***
Session 09		***Numerical Weather Prediction:*** Chair: *Andrea Buzzi* ***COPS*** *and* ***D-PHASE***
11:00-11:15	***076***	*Stefano* ***Mariani*** (ISPRA, Roma, I), *Casaioli, Lanciani, Accadia* and *Tartaglione*: A multi-model intercomparison study for quantitative precipitation forecast using the 6-month MAP D-PHASE dataset
11:15-11:30		*Hans Stefan* ***Bauer*** (Univ. of Hohenheim, Stuttgart, D), *Wulfmeyer, Zus, Schwitalla, Dick, Bender, Wickert* and *Gendt*: The SPP1167 Project COPS-GRID and results of first studies using GPS and radar data
11:30-11:45		*Matthias* ***Zimmer*** (Univ. of Mainz, D) and *Wernli*: Verification of precipitation forecasts from different regional NWP model categories
11:45-12:00	***078***	*Kathrin* ***Wapler*** (DWD, Offenbach, D), *Seifert* and *Ritter*: Using COPS data for the validation of the high-resolution NWP model COSMO-DE
12:00-12:15	***080***	*Olivier* ***Caumont*** (Météo-France, Toulouse, F), *Wattrelot, Jaubert* and *Ducrocq*: Assimilation of weather radar reflectivity in the AROME model for the COPS-IOP9
12:15-12:30	***082***	*Geneviève* ***Jaubert*** (Météo-France, Toulouse, F), *Yan, Ducrocq, Brousseau, Champollion* and *Flamant* : Impact of GPS data assimilation on the convective scale prediction of COPS-IOP9
12:30-15:30		***L u n c h &*** ***guided tour through baroque residence***
Session 10		***Precipitation Processes: Aerosols*** Chair: *Mark Žagar*
15:30-15:45	***084***	*Jean-Pierre* ***Chaboureau*** (Univ. of Toulouse, F), *Richard, Pinty, di Girolamo, Kiemle* and *Flamant*: Long-range transport of Saharan dust from CALIPSO, airborne and ground-based lidars, and a regional model during COPS
15:45-16:00		*Gregor* ***Gläser*** (Univ. of Mainz, D) and *Knippertz*: Influence of the Atlas Mountains on large-scale dust storms in the Sahara desert
16:00-16:15	***086***	*Céline* ***Planche*** (LaMP, Clermont-Ferrand, F), *Flossmann* and *Wobrock*: The influence of aerosol particle number and hygroscopicity on the evolution of convective cloud systems and their precipitation: A numerical study based on the COPS observations on 12 and 13 August 2007
16:15-16:30	***088***	*Heike* ***Noppel*** (KIT, Karlsruhe, D), *Blahak, Seifert* and *Beheng*: Investigations of the impact of aersols on a hailstorm in the Black Forest
16:30-17:00		***C o f f e e***

Wednesday, 13 May 2009 (continued)		
Session 11	***page***	***Precipitation Processes: Analyses*** Chair: *Ronald B. Smith*
17:00-17:15	***090***	*Idar* ***Barstad*** (Univ. of Bergen, N), *Heikkila* and *Mesquita*: Precipitation downscaling at western Norway: Time-step precipitation intensity
17:15-17:30	***092***	*Mark* ***Liniger*** (MeteoSwiss, Zurich, CH), *Schiemann* and *Frei*: Gridding daily precipitation from sparse surface networks in complex topography: A reduced space optimal interpolation approach
17:30-17:45	***094***	*Theresa* ***Gorgas*** (Univ. of Vienna, A), *Dorninger* and *Steinacker*: High resolution analyses based on the D-PHASE & COPS GTS and non-GTS data sets
17:45-18:00		*Stefan* ***Schneider*** (Univ. of Vienna, A), *Steinacker, Dorninger* and *Gorgas*: High resolution precipitation measurements during COPS
19:30-22:30		***D I N N E R***

Thursday, 14 May 2009		
Session 12		***Boundary Layer Processes: Cold Pools*** Chair: *Kristian Horvath*
09:00-09:15	***096***	*David* ***Whiteman*** (Univ. of Utah, Salt Lake City, USA), *Hoch, Lehner* & *Hahnenberger*: Nocturnal cold air intrusions at Arizona's Meteor Crater
09:15-09:30		*Sharon* ***Zhong*** (Mich. State Univ., East Lansing, USA) and *Yao*: Atmospheric conditions leading to the formation of a strong temperature inversion in an enclosed basin
09:30-09:45	***098***	*Manfred* ***Dorninger*** (Univ. of Vienna, A): Aspects of cold pool life cycle in Austrian sinkholes
09:45-10:00		*Daniel* ***Martínez*** (Univ. Illes Bal., Palma, E), *Cuxart* and *Jiménez*: Analysis of a cold pool formed in a large basin
10:00-10:15		*Sebastian* ***Hoch*** (Univ. of Utah, Salt Lake City, USA), *Whiteman* and *Mayer*: Topographic effects on radiative cooling in valleys and basins
10:15-10:30	***100***	*Thomas* ***Haiden*** (ZAMG, Vienna, A): The role of subsidence in valley and basin warming
10:30-11:00		***C o f f e e***
Session 13		***Snow pack*** Chair: *Massimiliano Fazzini*
11:00-11:15		*Justin* ***Minder*** (Univ. of Washington, Seattle, USA), *Wayand, Durran*, and *Roe*: The sensitivity of mountain snowpack accumulation to climate warming: Insights from a hierarchy of models
11:15-11:30	***102***	*Christian* ***Wüthrich*** (MeteoSwiss, Zurich, CH), *Beggert, Scherrer, Croci-Maspoli, Appenzeller* and *Weingartner*: Analyses of newly digitised snow series over the last 100 years in Switzerland
11:30-11:45		*Michi* ***Lehning*** (SLF, Davos, CH), *Stössel, Manes, Guala* and *Fierz*: Measurements and simulations of surface mass- and energy balance over snow at a mountain site
11:45-12:00		*Markus* ***Engelhardt*** (KIT, Karlsruhe, D), *Lehner, Salzmann* and *Hauck*: Ground-atmosphere modelling of Alpine permafrost and the significance of the snow cover
12:00-12:15	***104***	*Heidi* ***Escher-Vetter*** (BAdW, Munich, D) and *Weber*: Determination of snow accumulation in high mountains based on data from climate stations
12:15-12:30	***106***	*Roberto* ***Barbiero*** (DPCTT, Trento, I), *Fazzini* and *Gaddo*: The exceptional meteorological conditions of the December 2008 in the Trentino area (north east Italy): Synoptic and nivological analysis at mesoscale

Thursday, 14 May 2009 (continued)		
12:30-14:00		***L u n c h***
Session 14	***page***	***Dynamics: Mesoscale mountain flows I*** Chair: *Vanda Grubišić*
14:00-14:15	***108***	*Hans* ***Richner*** (IAC ETH, Zurich, CH): Estimating foehn dynamics from train and cable car accidents
14:15-14:30		*Marius Opsanger* ***Jonassen*** (Univ. of Bergen, N), *Ólafsson* and *Reuder*: Flow structures over Hofsjökull glacier, Iceland, during the FLOHOF 2007 experiment
14:30-14:45		*Michael* ***Würsch*** (IAC ETH, Zurich, CH), *Sprenger* and *Jenker*: Lagrangian-based analysis of airflow during foehn in the Alps
14:45-15:00		*Simon* ***Vosper*** (MetOffice, Exeter, UK), *Wells, Yan* and *Arnold*: Using satellite data to constrain gravity-wave drag parametrizations
15:00-16:30		**Poster Session C with *r e f r e s h m e n t s*** ***Dynamics*** *and* ***Snow***
Session 15		***Dynamics: Mesoscale mountain flows II*** Chair: *Günther Zängl*
16:30-16:45		*Vanda* ***Grubišić*** (Univ. of Vienna, Austria), *Haimov, French, Oolman* and *Xiao*: Wave-induced turbulence in the lee of the Medicine Bow mountains
16:45-17:00	***110***	*Ivana* ***Stiperski*** (DHMZ, Zagreb, CRO) and *Grubišić*: Trapped lee wave interference in presence of surface friction
17:00-17:15		*Dale* ***Durran*** (Univ. of Washington, Seattle, USA) and *Reinecke*: The over-amplification of gravity waves in numerical solutions to flow over topography
17:15-17:30		*Patrick* ***Reinecke*** (NRL, Monterey, USA) and *Durran*: Initial condition sensitivities and the predictability of downslope winds
17:30-17:45		*Daniel* ***Reinert*** (Univ. of Mainz, D) and *Wirth*: The role of gravity waves for banner cloud dynamics
17:45-18:00		*Helen* ***Wells*** (MetOffice, Exeter, UK) and *Vosper*: Predictability of orographic drag for realistic atmospheric profiles

Friday, 15 May 2009		
Session 16		***Precipitation Processes: A look outside of the Alps*** Chair: *Christian Keil*
09:00-09:15		*Ronald B.* ***Smith*** (Yale Univ., New Haven, USA) and *Kirshbaum*: Orographic precipitation in the tropics: Linear theory of triggered convection
09:15-09:30		*Claus-Jürgen* ***Lenz*** (KIT, Karlsruhe, D), *Kottmeier* and *Corsmeier*: Dynamics and predictability of Mediterranean cyclones: The influence of sea surface and steep orography
09:30-09:45		*Michael* ***Sprenger*** (IAC ETH, Zurich, CH), *Schlemmer* and *Martius*: Disentangling the forcing mechanisms of heavy precipitation events along the Alpine south side using potential vorticity inversion
09:45-10:00	***112***	*Véronique* ***Ducrocq*** (Météo-France, Toulouse, F), *de Saint Aubin, Bresson, Nuissier* and *Ricard*: A numerical study of the combined processes leading to Mediterranean quasi-stationary MCS
10:00-10:15	***114***	*Ulrike* ***Romatschke*** (Univ. of Washington, Seattle, USA), *Medina, Houze* and *Rasmussen*: Topographic and diurnal effects on tropical and sub-tropical convection in South America
10:15-10:30	***116***	*Socorro* ***Medina*** (Univ. of Washington, Seattle, USA), *Houze, Williams* and *Kingsmill*: Structure of mid-latitude cyclones crossing the California Sierra Nevada as seen by vertically pointing radar
10:30-11:00		**Coffee**

Friday, 15 May 2009 (continued)		
Session 17	***page***	***Numerical Weather Prediction: Towards the future*** Chair: *Evelyne Richard*
11:00-11:15	***118***	*Christian* ***Keil*** (DLR, Oberpfaffenhofen, D) and *Craig*: Sources of uncertainty determined by high-resolution ensemble modelling
11:15-11:30	***120***	*Kirstin* ***Kober*** (DLR, Oberpfaffenhofen, D), *Craig, Keil* and *Tafferner*: Probabilistic forecasting of thunderstorms through combining nowcasting methods and numerical weather prediction
11:30-11:45		*Chiara* ***Marsigli*** (ARPA-SIM, Bologna, I), *Montani* and *Paccagnella*: Intercomparison of limited-area ensemble systems during the MAP D-PHASE operation period
11:45-12:00	***122***	*Javier* ***Garcia Hernandez*** (LCH EPF, Lausanne, CH), *Sirvent, Jordan, Boillat* and *Schleiss*: Ensemble meteorological forecast for the upper Rhone river basin
12:00-12:15	***124***	*Jason* ***Milbrandt*** (Env. Canada, Dorval, CAN), *Mailhot* and *McTaggart-Cowen*: The Canadian high-resolution NWP system for the 2010 winter Olympics
12:15-12:30		*Trevor* ***Smith*** (Env. Canada, Vancouver, CAN), *Synder* and *McLennan*: Some forecasting challenges for the 2010 Olympic and Paralympic winter games
Closing session		Chair: *Stephen Mobbs*
12:30		**A w a r d s**
-		*David* ***Parsons*** (WMO, THORPEX-IPO, Geneva, CH): Towards ICAM-2011: Resumé of current research efforts and envisioned trends
13:00		**D i s c u s s i o n** and **a d j o u r n**
13:00- ...		***L u n c h***

Part B) Poster blocks

All posters are on display for the full week. Authors are asked to be ready for discussions at the poster times on Monday, Tuesday and Thursday afternoon, respectively.

Monday

Poster blocks Pnn** and **Cnn:** **Session A "Precipitation Processes** and **Climate-1"

page

P01 *Lindsay **Bennett*** (University of Leeds, UK), *Blyth, Weckwerth, Burton* and *Gadian*:
Observations of convection initiation and development from the Doppler on Wheels radars and comparison with high resolution WRF simulations ***128***

P02 *Andreas **Schäfler*** (DLR, Oberpfaffenhofen, D), *Craig, Dörnbrack, Kiemle, Rahm* and *Wirth*:
Characterising the convective environment with direct measurements of moisture flux from airborne wind and water vapour lidars

P03 *Samuel **Buisán*** (AEMET, Zaragoza, E), *Espero, Sanz, Cortés* and *Lafragüeta*:
Characterization of convective activity in the Eastern Iberian Range, Spain ***130***

P04 *Bianca **Adler*** (KIT, Karlsruhe, D), *Kalthoff, Barthlott, Corsmeier, Mobbs, Crewell, Träumner, Kottmeier, Wieser* and *V. Smith*:
The initiation of deep convection by boundary layer convergence zones during COPS ***132***

P05 *Mamina **Kamara*** (Senegal Met Office, Senegal), *Ba* and *Ndiaye*:
Case study: impact of the exceptional rains on the floods in Senegal

P06 *Vanja **Kovač*** (ARSO, Ljubljana, SI*), Cedilnik, N. Žagar* and *M. Žagar*:
Influence of local orography on forecast of precipitation in case of flash floods in Slovenia on September 18, 2007 ***134***

P07 *Wolfgang **Langhans*** (IAC ETH, Zurich, CH), *Gohm* and *Zängl*:
The orographic impact on patterns of embedded convection during the August 2005 Alpine flood ***136***

P08 *Jože **Rakovec*** (Univ. of Ljubljana, SI), *Žabkar* and *M. Žagar*:
Analysis of different ALADIN forecast runs for the flash flood case in Slovenia, 18 September 2007 ***138***

P09 *Jianhua **Sun*** (CAS, Beijing, China) and *Zhao*:
The impact of multi-scale systems on freezing rain and snow storms over southern China ***140***

P10 *Günther **Zängl*** (DWD, Offenbach, D) and *Seifert*:
Misrepresentation of the seeder-feeder mechanism by Kessler-type auto-conversion schemes ***142***

P11 *Idar **Barstad*** (Univ. of Bergen, N):
[contents of intented poster amalgamated with oral presentation in session 11]

P12 *Raffaele **Salerno*** (Epson Meteo Centre, Milano, I):
Predictability analyses in global and regional scale applications

P13 - moved to Session 09 -

P14 *Thomas* ***Schwitalla*** (Univ. of Hohenheim, Stuttgart, D), *Bauer, Zus* and *Wulfmeyer*: ***page***
The WRF modeling system and first results of its application within the COPS period

P15 *Andrea* ***Buzzi*** (ISAC-CNR, Bologna, I), *Diavolio, Drofa* and *Malguzzi*:
The PROSA project: monitoring, nowcasting and short range forecasting over the Alps and other areas of Italy

P16 *Kirsty E.* ***Hanley*** (Univ. of Reading, UK), *Belcher, Clark* and *Kirshbaum*:
Predictability of convection in COPS: high-resolution ensemble forecasts from the Unified Model

P17 *Suraj D.* ***Polade*** (Univ. of Hamburg, D) and *Ament*:
Towards a verification of the hydrological cycle in the D-PHASE models: An evaluation of integrated water vapor

P18 *Mathieu* ***Reverdy*** (LaMP, Clermont-Ferrand, F), van *Baelen, Walpersdorf, Dick, Hagen* and *Richard*: Water vapor fields retrieved with tomography software. ***144***

P19 *Frédéric* ***Tridon*** (LaMP, Clermont-Ferrand, F), *van Baelen* and *Pointin*:
Simultaneous X-band and K-band study of precipitation to derive localized Z-R relationships ***146***

P20 *Helge* ***Tuschy*** (DLR, Oberpfaffenhofen, D), *Hagen* and *Mayr*:
Environmental conditions and radar observations of organized thunderstorms ***148***

P21 *Holger* ***Mahlke*** (KIT, Karlsruhe, D), *Corsmeier* and *Kottmeier*:
Modification of atmospheric parameters by deep convection over complex terrain during COPS ***150***

P22 *Uwe* ***Ehret*** (TUniv. München, D):
Convergence index: A new performance measure for the jumpiness of operational rainfall forecasts ***152***

P23 *Véronique* ***Ducrocq*** (Météo-France, Toulouse, F*), Drobinski, Lionello* et al. :
HyMeX: An experimental programme dedicated to the hydrological cycle in the Mediterranean ***154***

P24 *Frédéric* ***Jordan*** (E-DRIC, Epalinges, CH), *Garcia Hernadez* and *Gal*:
Operational performance of discharge prediction in Alpine regions ***156***

P25 *Giacomo* ***Poletti*** (Univ. of Trento, I), *de Franceschi, Bellin* and *Zardi*:
Analysis of precipitation patterns on Mount Baldo (Italy) ***158***

P26 *Matthias* ***Grzeschik*** (Lab. d'Aérologie, Toulouse, F), *Jaubert, Flamant* and *Richard*:
Assimilation of LEANDRE2 water vapor observations with the AROME 3D-Var cycle for COPS ***160***

C01 *Fiorella* ***Acquaotta*** (Univ. of Turin, I) and *Fratianni*:
A contribution to the study of the methods to create the references series ***162***

C02 *Stefan* ***Sperka*** (Univ. of Vienna, A), *Mayer* and *Steinacker*: ***page***
A quality control and bias correction method developed for irregularly spaced time-series of observational pressure- and temperature-data ***164***

C03 *Dino* ***Zardi*** (Univ. of Trento, I) and *Rampanelli*:
History and analysis of the temperature series of Trento, Italy (1816-2008)

C04 *Joan* ***Cuxart*** (Univ. IB, Palma, E), *Molinos, Martínez, Jiménez* and *Cunillera*:
Conditioned climatology of the stably stratified nights in the Ebro basin

C05 *Mark* ***Žagar*** (Univ. of Ljubljana, SI) and *Strajnar*:
Radar-based hail climatology of eastern Slovenia ***166***

C06 *Michael* ***Kunz*** (KIT, Karlsruhe, D) and *Puskeiler*:
Spatial variability and trends of hailstorm frequency and the relation to atmospheric characteristics in southwest Germany ***168***

C07 *Pavol* ***Faško*** (SHI, Bratislava, SK), *Lapin, Pecho* and *Mikulová*:
Analysis of snow cover change in Slovakia in 1981-2008 ***170***

C08 *Nadejda* ***Petkova*** (BAS, Sofia, BG), *Andronov* and *Koleva*:
Snow cover variability in Bulgaria

C09 *Michael* ***Fitzka*** (Univ. Bodenkultur, Vienna, A), *Simic, Weihs* and *Kromb-Kolb*:
15 years of spectral UV-measurements at Sonnblick observatory: Investigation of short- and long-term changes at a high altitude alpine station ***172***

C10 *Maria* ***Zoran*** (National Institute for Optoelectronics, Bukuresti, ROM):
Satellite remote sensing assessment of climate risks and their impact on Romanian mountain forests ***174***

C11 *Michael* ***Sprenger*** (IAC ETH, Zurich, CH), *Schlemmer* and *Martius*:
Detection and climatology of fronts in a high–resolution model reanalysis over the Alps

C12 *Christophe* ***Lavaysse*** (LMD/IPSL, Palaiseau, F), *Drobinski* and *Vrac*:
Downscaling precipitation and wind in the complex French Mediterranean region

Tuesday
Poster blocks Bnn *and* ***Cmm: Session B "Boundary Layer Processes*** *and* ***Climate-2"***

B01 *Peter* ***Sheridan*** (MetOffice, Exeter, UK), *Wells, Vosper, Price, Ross, Brown, Mobbs* and *Horlacher*: COLPEX - Cold Pool Experiment

B02 *Meinolf* ***Kossmann*** (DWD, Offenbach, D), *Hoch, Whiteman* and *Sievers*:
Modelling of nocturnal drainage winds at Meteor Crater, Arizona, using KLAM_21 ***182***

B03 *Josep R.* ***Miró*** (MSC, Barcelona, E) and *Pagès*:
Minimum temperatures classification at the Pyrenees area using Empirical Orthogonal Functions (EOF) ***184***

B04 *Marina* ***Mileta*** (DHMZ, Zagreb, CRO):
Fog water collection with SFC during the period 2000-2008 in Croatia ***186***

B05 *Lin-lin* ***Qi*** (CAS, Beijing, China) and *Sun*: ***page***
The application of the coupling model in the numerical simulation of the local radiation fog ***188***

B06 *Renzo* ***Richiardone*** (Univ. of Turin, I), *Manfrin, Ferrarese, Frantone* and *Fernicola*:
Temperature measurement with sonic anemometers: an instrument characterization

B07 *Mathias* ***Bavay*** (SLF, Davos, CH), *Dawes, Lehning, Aberer* and *Parlange*:
Swiss Experiment: Application of a collaborative research platform to spatial interpolation validation

B08 *Christof* ***Gromke*** (SLF, Davos, CH), *Walter, Manes* and *Lehning*:
Aerodynamic roughness lengths of snow surfaces ***190***

B09 *Stephan* ***de Wekker*** (Univ. of Virginia, Charlottesville, USA), *Godwin* and *Emmitt*:
Wind- and aerosol structure in the Salinas Valley and adjacent mountains in California from airborne Doppler lidar data

B10 *Haraldur* ***Ólafsson*** (Univ.s of Bergen, N & Reykjavík, Iceland), *Rögnvaldsson, Reuder, Ágústsson, Kristjánsson* and *Petersen*:
Monitoring the atmospheric boundary-layer in the Arctic at Gufuskálar, Iceland ***192***

B11 *Sandip* ***Pal*** (Univ. of Hohenheim, Stuttgart, D), *Behrendt, Riede, Schiller* and *Wulfmeyer*:
High resolution measurements of water vapor and aerosol fields with UHOH scanning DIAL system at Hornisgrinde

B12 *Marcus* ***Radlach*** (Univ. of Hohenheim, Stuttgart, D) *Behrendt, Pal* and *Wulfmeyer*:
Measurement of temperature and aerosol fields with rotational Raman lidar during the field campaign COPS at Hornisgrinde on 20th July 2007

B13 *Tammy M.* ***Weckwerth*** (NCAR, Boulder, USA), *Wulfmeyer, Behrendt, Pal* and *Aoshima*:
Water Vapor DIAL and DOW Observations and Comparisons with Mesoscale Models in COPS

B14 *Luciana* ***Rossato*** (INPE, Sao Jose dos Campos, Brazil), *de Jeu* and *Alvalá*:
Validation of soil moisture in Brazil as derived from AMSR-E sensor observations for cerrado regions

B15 *Yann* ***Largeron*** (LEGI, Grenoble, F), *Staquet* and *Chemel*:
Mixing and transport in the stable atmosphere of an idealized Alpine valley ***194***

B16 *Delia* ***Arnold*** (INTE, Barcelona, E), *Schicker, Seibert* and *Vargas*:
High resolution modelling of mountain and valley stations and its applications to complex dispersion conditions ***196***

B17 *Ahmad* ***Moghaddam*** (Univ. of Hormozgan, Iran), *Taghavi* and *Khorsandi*:
Study convective cells impact on air pollution dispersion in boundary layer on Bandar Abbas costal city in the south of Iran

B18 *Željko* ***Vecenaj*** (Univ. of Zagreb, CRO), *de Wekker* and *Grubišić*:
Mountain wave related turbulence derived from sonic anemometers and an elastic backscatter Lidar ***198***

B19 *Željko* ***Vecenaj*** (Univ. of Zagreb, CRO), *Grubišić* and *Grisogono*: ***page***
Along-coast features of the bora related turbulence ***200***

B20 *Dino* ***Zardi*** (Univ. of Trento, I), *de Franceschi, Tagliazucca* and *Tampieri*:
Analysis of second order moments in the surface layer turbulence in an Alpine valley ***202***

B21 *Pak Wai* ***Chan*** (Hong Kong Observatory, China):
Validating turbulence parameterization schemes of a numerical model using eddy dissipation rate measurements in terrain-disrupted airflow ***204***

B22 *Norbert* ***Kalthoff*** (KIT, Karlsruhe, D), Bischoff-*Gauss, Khodayar, Fiebig-Wittmaack* and *Montecinos*: The diurnal cycle of the convective boundary layer over an arid Andes valley: Observations and model simulations

B23 - withdrawn -

B24 *Tammy M.* ***Weckwerth*** (NCAR, Boulder, USA) and *Wilson*:
Radar climatology of convection initiation in the COPS Region

B25 *Victoria* ***Smith*** (Univ. of Leeds, UK), *Hobby, Mobbs* and *Burton*:
Detailed analysis of valley flows in complex terrain: A case study from the COPS field experiment

B26 *Sharon* ***Zhong*** (Mich.State Univ., East Lansing, USA), *Vandeuse, Shortridge* and *Bian*:
Estimating and testing the topographic amplification factor using GIS method and weather data from the western United States ***206***

B27 *Thierry* ***Robert-Luciani*** (ARPAV, Arabba, I), and *Marigo*:
Winter high pressare: Mixing air mechanism in the Belluno pre-Alpine basin ***208***

B28 *Rahela* ***Žabkar*** (Univ. of Ljubljana, SI) and *Rakovec*:
WRF-Chem study of the high ozone episode dynamics over the complex terrain of Slovenia ***210***

B29 *Ralph* ***Burton*** (Univ. of Leeds, UK), *Mobbs, Gadian* and *V. Smith*:
Sensitivity of the WRF model to boundary-layer forcing: Orographic test cases and idealised studies

B30 *Dana* ***Micu*** (Romanian Academy, Bukuresti, ROM), *Cheval* and *Baciu*:
Heat waves in the Romanian Carpathians during the cold season ***212***

B31 *Kirsten* ***Warrach-Sagi*** (Univ. of Hohenheim, Stuttgart, D):
Streamflow data assimilation for root zone soil moisture analysis

B32 *Andrew* ***Ross*** (Univ. of Leeds, UK):
Topographic effects on boundary-layer/forest-canopy exchange of gases

C13 *Zeljko* ***Majstorovic*** (Hydromet. Institute, Sarajevo, BiH), Zulum, Voljevica and Hodzic:
Impacts of climate changes to the wider Sarajevo region

C14 *Jan* ***Kysely*** (IAP, Prague, CZ): ***page***
Trends in heavy precipitation in mountainous and lowland areas in central Europe: Are the differences related to changes in circulation? ***176***

C15 *Milan* ***Lapin*** (Univ. Bratislava, SK) and *Kremler*:
Scenarios of air humidity and saturation deficit change for Slovakia ***178***

C16 *Marian* ***Melo*** (Univ. Bratislava, SK), *Lapin* and *Damborska*:
Shift of climatic regions in mountainous parts of Slovakia

C17 *Luis Mendes* ***Cherno*** (Météo. Nationale, Bissau, Guinée-Bissau):
Étude de l´impact de la variabilité du climat et des changements climatiques sur la Guinée-Bissau ***180***

Thursday
Poster blocks Dnn *and* ***Snn:*** ***Session C "Dynamics*** *and* ***Snow"***

D01 *Martina* ***Tudor*** (DHMZ, Zagreb, CRO):
Case study of bura of 1st and 3rd February 2007 ***214***

D02 *Ivana* ***Stiperski*** (DHMZ, Zagreb, CRO*), Ivančan-Picek* and *Grubišić*:
The complex bora flow in the lee of southern Velebit ***216***

D03 *G. Nína* ***Petersen*** (Met Office, Reykjavík, Iceland), *Renfrew* and *Moore*:
An overview of barrier winds off southeastern Greenland during the Greenland flow distortion experiment

D04 *Richard* ***Werner*** (Dornbirn, A):
Synchronous strong wind conditions in the middle alpine Region

D05 *Michael* ***Sprenger*** (IAC ETH, Zurich, CH), *Jenker, Schwierz* and *Dierer*:
Objective foehn prediction based upon the Adaboost algorithm

D06 *Florian* ***Pfurtscheller*** (IMGI, Innsbruck, A) and *Gohm*:
Orographic enhancement of severe windstorms in the Austrian Alps: Two case studies ***218***

D07 *Klaus* ***Burri*** (AGF, Zurich, CH), *Dürr, Gutermann, Häberli, Neururer, Richner* and *Werner*:
Foehn diagnosis and model verification ***220***

D08 *Christoph* ***Knigge*** (Univ. of Hannover, D*), Etling, Paci* and *Eiff*:
Laboratory experiments on mountain-induced rotors ***222***

D09 - withdrawn -

D10 *Susanne* ***Drechsel*** (IMGI, Innsbruck, A), *Mayr* and *Chow*:
Comparison of scanning strategies for 3D wind retrieval from dual Doppler lidar measurements

D11 *Vanda* ***Grubišić*** (Univ. of Vienna, A*), Xiao, Haimov, French* and *Oolman*:
Lower-tropospheric waves and wave-induced turbulence zones: Insights from T-REX

D12 *Ivana* ***Stiperski*** (DHMZ, Zagreb, CRO) and *Grubišić*: ***page***
Boundary layer effects on lee wave resonance in the semi-T-REX environment

D13 *Thomas* ***Raab*** (Univ. of Innsbruck, A), *Mayr* and *Zängl*:
WRF performance in complex terrain: A parameter study on downslope windstorms

D14 *Haraldur* ***Ólafsson*** (Univ.s of Bergen, N and Reykjavík, Iceland), *Shapiro, Ágústsson* and *Kristjánsson*: The Cape Tobin jet ***224***

D15 *Tiina* ***Kilpeläinen***, (Univ. of Bergen, N) and *Ólafsson*:
Simulations of mesoscale flow over an Arctic fjord ***226***

D16 *Kristian* ***Horvath***, (DHMZ, Zagreb, CRO), *Bajić* and *Ivatek-Šahdan*:
Dynamical downscaling of wind resources in complex terrain of Croatia

D17 *Eirik M.* ***Samuelsen*** (Meteorological Institute, Tromsø, N), *Grønås* and *Ólafsson*:
Local winds during a cold air outbreak in northern Norway

D18 *Hálfdán* ***Ágústsson*** (Univ. of Iceland, Reykjavík, Iceland) and *Ólafsson*:
Extreme turbulence in the wake of SE-Iceland ***228***

D19 *Beathe* ***Tveita*** (Storm Weather Centre, Bergen, N), *Ólafsson, Sandvik* and *Hagen*:
The sensitivity of the atmospheric flow to Greenland in a case of extreme winds ***230***

D20 *Berit* ***Hagen*** (Meteorological Institute, Bergen, N), *Ólafsson, Sandvik* and *Tveita*:
Greenland, the sea ice and extreme winds ***232***

D21 *Pak Wai* ***Chan*** (Hong Kong Observatory, China) and *Cheung*:
"Up-hill effect" on the winds at the Hong Kong International Airport in strong northerly winds associated with tropical cyclones ***234***

D22 *Haraldur* ***Ólafsson*** (Univ.s of Bergen, N and Reykjavík, Iceland) and *Petersen*:
Cyclogenesis in the lee of Iceland

D23 *Uroš* ***Strajnar*** (EARS, Ljubljana, SI):
Are tornadoes possible also in Slovenia? Case study of the extreme event of 13 and 14 July 2008 ***236***

D24 *Shuhua* ***Yu*** (CMA, Chengdu, China), *Gao* and *Xiao*:
Diagnosis of the effect of south-westerlies on the Tibetan vortex moving east

D25 *Walburga* ***Wilms-Grabe*** (KIT, Karlsruhre, D), *Corsmeier, Junkermann, Kottmeier, Holland, Geiss* and *Neiniger*:
Transport and chemical conversion in convective systems above complex terrain ***238***

D26 *Andrea* ***Buzzi*** (ISAC-CNR, Bologna, I) and *Catania*:
Dynamical and physical processes characterizing upper-level cut-off lows in winter ***240***

D27 *Alan* ***Gadian*** (Univ. of Leeds, UK), *Lock, Coals* and *Mobbs*:
Exploring a cut-cell approach for model simulations of flow over hills ***242***

D28 *Hans* ***Volkert*** (DLR, Oberpfaffenhofe, D):
The summer of COPS-2007: Multi-scale dynamics visualized by variable-speed time-lapse satellite imagery ***244***

S01 *Massimiliano* ***Fazzini*** (Univ. of Ferrara, I), *Romeo* and *Giallatini*: ***page***
Snow in the central Apennines (peninsular Italy): The first analysis on 30 years of snow and temperature data

S02 *Massimiliano* ***Fazzini*** (Univ. of Ferrara, I) and *Gaddo*:
Relationship between climatic parameters and morphology and duration of snow cover at microscale: Preliminary study in three major ski areas of the territory of Trentino (Italian Eastern Alps) ***246***

S03 *Silvia* ***Terzago*** (Univ. of Turin, I), *Cremonini* and *Fratianni*:
Snow precipitation variability in the Western Alps of Italy: Evaluation of an algorithm for the survey of the snow cover through satellites images ***248***

S04 *Ralf* ***Becker*** (DWD, Offenbach, D) and *Bisolli*:
Using polar-orbiting weather satellite data to estimate the snowlines of central-European mountains ***250***

S05 *Clemens* ***Teutsch*** (Univ. of Innsbruck, A) and *Mayr*:
The correlation of new snow density and water equivalent

S06 *Manfred* ***Dorninger*** (Univ. of Vienna, A):
A new device for accurate measurements of meteorological parameters in a snow rich environment ***252***

S07 *Christian* ***Hauck*** (Univ. de Fribourg, CH), *Engelhardt* and *Hilbich*:
Numerical modelling and geophysical monitoring of the sensitivity of alpine permafrost to climate change

Part A

Extended Abstracts of

Oral presentations

The order is chronologically as in the programme (pages *iii-ix*)

ICAM AS A REGULAR VISITOR: BACK TO GERMANY FOR THE FIFTH TIME

Gerhard Adrian[1] and Hans Volkert [2]

[1] Deutscher Wetterdienst, Forschung und Entwicklung, Offenbach, Germany
E-mail: *Gerhard.Adrian@dwd.de*

[2] Deutsches Zentrum für Luft-und Raumfahrt, Institut für Physik der Atmosphäre, Oberpfaffenhofen, Germany
Email: *Hans.Volkert@dlr.de*.

Abstract: As an introduction to the Extended-Abstract-Volume of all contributions to the 30th ICAM, the development of this long conference series is reflected in conjunction with a brief summary of current research initiatives in Germany that address aspects of weather forecasting in high spatial resolution above complex terrain.

Keywords: *Introduction, Overview*

1 ICAM BACK TO GERMANY

The *International Conference on Alpine Meteorology* comes to Germany for the fifth time in 2009 after having stayed here before in Garmisch (1958), Oberstdorf (1970), Berchtesgaden (1982) and Lindau (1994). As format, size and language(s) of communication gradually changed over more than five decades (details in Volkert, 2009), also the orographic focus became more general. The *Alps* in the centre of Europe remain to be of high interest, but studies of atmospheric phenomena around other high mountain ranges as the *Himalayas* or the *Rocky Mountains* are also presented. In addition, topographic features of lower elevation also became of significant interest, like the *Vosges* or the *Black Forest* and their intricate rôle in sparking off (occasionally also suppressing) summer convection or a small meteoritic cater in Arizona, which served as a very special natural laboratory for a measuring campaign.

The numerous contributions collected in this volume certainly provide a snapshot of the large variety of research projects which are currently undertaken to reduce uncertainties in the basic understanding of atmospheric processes, not only near mountains, as well as to enhance the spatio-temporal realism of high-resolution model simulations that are the basis of daily weather forecasts. This contribution is intended to put into perspective relevant German research initiatives, in particular those where the authors' affiliations are involved.

A larger sample of 24 more consolidated studies, which were first presented at the previous ICAM-2007 in Chambéry (France), can be found in Richard et al. (2009).

2 CURRENT RESEARCH INITIATIVES IN GERMANY

2.1 Basic research and new applications

Currently *Deutsche Forschungsgemeinschaft* (DFG) supports a six-year priority research programme *Quantitative Precipitation Forecast* (cf. Hense and Wulfmeyer, 2008), which had the *Convective and Orographically-induced Precipitation Study* (COPS; Wulfmeyer et al., 2008) as a field phase during June-August 2007. The latter received support from many countries and became endorsed as a Research and Development Programme of WMO-WWRP. A large number of oral and poster presentations during ICAM-2007 deals with episodes intensively probed obtained during COPS and general issues inspired by COPS data.

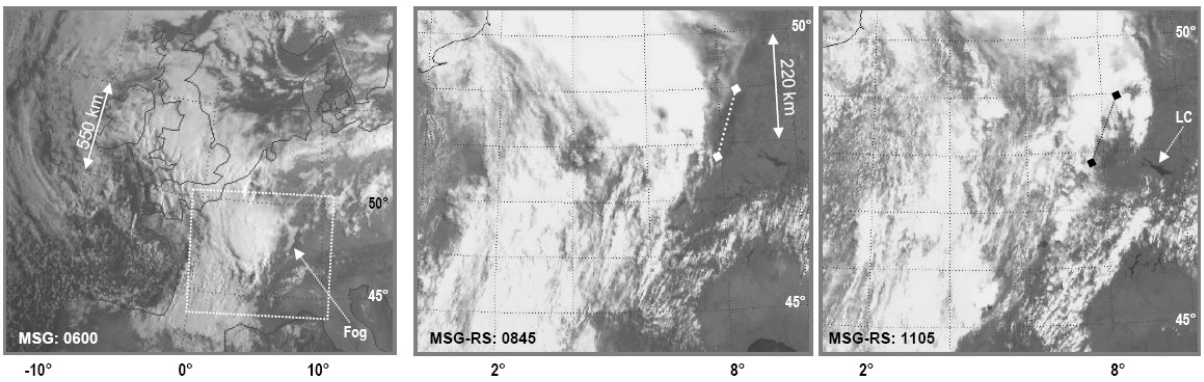

Figure 1: Cloud systems moving fast across central Europe and experiencing orographic modification on 20 July 2007 during COPS as viewed by Meteosat second generation (MSG) satellites – left: normal scan at 0600 with the cloud mass of a frontal system from Scotland to the Pyrenées approaching the upper Rhine valley covered by morning fog; middle: zoom (dotted frame in left image) into rapid scan at 0845 where cloud edge is starting to reach the Black Forest crest line (dots between diamonds); right: rapid scan at 1105 with freshly developed squall-line cloud about 100 km to the east of the Black Forest crest. LC: Lake of Constance; dotted lat./lon. grids on stereographic projections aid the orientation.

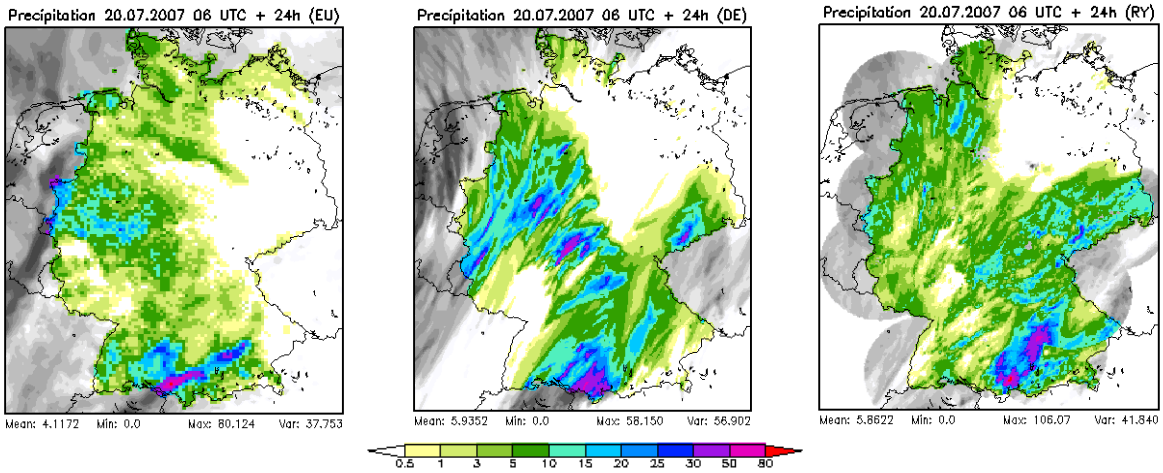

Figure 2. 24-hour accumulated precipitation (mm) on 20 July 2007, (a) predicted by COSMO-EU, (b) predicted by COSMO-DE and (c) determined from measurements obtained by the DWD radar network.

Rapid scans with 5'-intervals (normally 15') obtained from Meteosat were among the novel observing techniques during COPS. The moving frontal cloud systems of IOP-9c on 20 July are exemplified in Figure 1. The images reveal a suppression of clouds (and precipitation) at the southern end of the Black Forest, posing a severe challenge for high-resolution modelling. Display of satellite loops at variable speed can provide intuitive insights regarding the acting processes.

2.2 Orientated towards daily operations

Since 1999 DWD operates a non-hydrostatic numerical prediction model for short range weather forecasts, in close cooperation with European partners. Its version *COSMO-DE* covers Germany with a grid of 2.8 km horizontal resolution on 50 levels in a rapid update cycle of 3 h (8 runs per day over 21 h each). It is one-way nested into *COSMO-EU*, which uses a horizontal mesh size of 7 km and covers large parts of Europe.

An important difference between both model versions is that *COSMO-DE* does not use a convection parameterization and thus simulates convection cells explicitly. As a consequence, convection cells behave as a dynamical entity and move with the ambient flow field. This becomes evident from Figure 2, where accumulated precipitation fields are displayed for 20 July from *COSMO-EU* and *COSMO-DE* runs together with the corresponding estimate from radar observations. While the predominantly parameterized precipitation of *COSMO-EU* exhibits a very patchy structure, *COSMO-DE* shows clear band-like structures indicative of individual convection cells advected with the south-westerly flow. These bands are also evident in the radar-derived field, though not as pronounced as in the *COSMO-DE* forecast.

3 OUTLOOK

All contributions to this volume highlight the international collaborative spirit in meteorology. It is reassuring to note that 23 (of some 90) oral presentations and 20 (of some 100) poster presentations have lead authors working at institutions in Germany, be it at university institutes, at research laboratories of the *Helmholtz Gemeinschaft* or at *Deutscher Wetterdienst*. ICAM continues to be a vivid international forum of exchange and interaction. It is looking forward to its 31st meeting in 2011 in the United Kingdom, which recently joined the 'club' of the ICAM-countries.

Acknowledgements:
Axel Seifert and Günther Zängl provided Figure 2 and useful information. We thank them and all contributors to this volume for their cooperation on a voluntary basis as well as the ICAM-2009 sponsors for their support.

REFERENCES

Hense, A. and V. Wulfmeyer (eds.), 2008: *The Germany Priority Program SPP1167 "Quantitative Precipitation Forecast"*, special issue with 16 articles, *Meteorol. Z.* **17**, 703–948.

Richard, E., A. Buzzi, S. Mobbs, H. Volkert and M. Žagar (eds.), 2009: *Weather and Climate around Mountains: A collection of 24 papers first presented at ICAM-2007*. Special volume, *Meteorol. Atmos. Phys.* **103** , ii + 287 pp.

Volkert, H., 2009: The International Conferences on Alpine Meteorology: Characteristics and trends from a 57-year-series of scientific communication. *Meteorol. Atmos. Phys.* **103** , 5–12, DOI 10.1007/s00703-008-0312-9.

Wulfmeyer, V., A. Behrendt, H.-S. Bauer, C. Kottmeier, U. Corsmeier et *xxiii* alii, 2008: The Convective and Orographically-induced Precipitation Study: A research and development project of the world weather research program for improving quantitative precipitation forecasting in low-mountain regions. – *Bull. Amer. Meteor. Soc.* **89**, 1477–1486, DOI 10.1175/2008BAMS2367.1.

METEOROLOGY IN THE MIDDLE AGES
PART I – THERMALLY DRIVEN COASTAL WINDS

Haraldur Ólafsson[1] and Hálfdán Ágústsson[2]

[1] Háskóli Íslands, Iceland and Bergen School of Meteorology, Geophysical Institute, University of Bergen
E-mail: *haraldur68@gmail.com*
[2] Reiknistofa í veðurfræði and Háskóli Íslands, Iceland

Abstract: An investigation of Egil's Saga, written in Iceland in the early 13th century reveals a profound knowledge of local coastal wind circulations. The story-teller describes the sea breeze and the night-time returning flow, characterizing it as katabatic wind, and not land-breeze as in many modern textbooks. Numerical simulations confirm the katabatic nature of the return flow. The knowledge of these winds proved to be important for the downfall of Eric Haraldsson Bloodaxe, king of Norway.

Keywords: *Egils´ Saga, Middle Ages, Land-breeze, Sea-breeze,*

1 INTRODUCTION

In most modern textbooks, a night-time land breeze is explained as the opposite of a day-time sea breeze. This is typically illustrated by schematic figures featuring symmetric two-dimensional thermal fields and circulations, but with opposite signs, such as Fig.10.21 in Ahrens (1994) or in the internet-based Wikipedia. In this study, this concept is tested by numerical simulations. The impact of mountains on the night-time flow from land to the sea is also tested. Texts on coastal winds in Egils´s Saga Skallagrímssonar, written in the first part of the 13th century, are studied and compared to the results of the numerical simulations and modern textbooks.

2 THERMALLY DRIVEN FLOWS IN EGIL´S SAGA AND IN MODERN TIME TEXTBOOKS

Egil´s Saga Skallagrímssonar tells about the history of Egill Skallagrímsson and his family. During the reign of Haraldur Fairhair, son of Hálfdán the Blac, in the late 9th century, Egil´s father and grandfather fled from Norway to Iceland. The author of Egil´s Saga is not known, but generally considered to be Snorri Sturluson. Snorri was a well educated, wealthy and powerful personality in Iceland in the early 13th century. He wrote the history of Norway from before the settlement of Iceland, stories of the pagan gods and poetic treasures of pre-Christian times. Snorri himself was a descendant of Egill. He was fostered by the grandson of Magnus Ólafsson, king of Norway at Oddi in South-Iceland. Snorri was assassinated at his residence in Reykholt, Iceland by order from king Hákon of Norway on 23 September 1241. Egill travels to Norway to collect inheritance on behalf of his wife. In Norway, Egill does not get any money and the king, Eric Bloodaxe Haraldsson, declares Egill an outlaw. Egill is not satisfied and kills a number of the king´s men, including his son, Rögnvaldur. Perhaps more importantly, Egill raises a curse-pole with the head of a horse on top of it on the island of Herdla at the west coast of Norway. In short, the curse was that king Eric and Gunnhildur would lose their kingdom. Soon after, the curse came true. As Egill prepares the plundering and killings of the king´s men (Bergonund and others), he sails at the west coast of Norway, close to Alrekstead (now the city of Bergen):

The weather was calm, a fell-wind blew by night, a sea breeze by day. *One evening Egil sailed out to sea, but the fishermen were then rowing in to land, those, to wit, who had been set as spies on Egil's movements. They had this to tell, that Egil had put out and sailed to sea, and was gone. This news they carried to Bergonund. And when he knew these tidings, then he sent away all those men that he had had before for protection. Thereafter he rowed in to Alrekstead, and bade Frodi to his house, for he had a great ale-drinking there. (Egil´s Saga, Ch.59)…….Egil sailed out to sea for the night, as was written above. And when morning came the wind fell and there was a calm. They then lay drifting, letting the ship ride free for some nights. (Egil´s Saga, Ch.60)*

This text contains a description of the diurnal circulation of the winds during "calm" weather. Interestingly, the nocturnal wind is called "fell-wind", a translation of "fjallvindr" – mountain wind. The author attributes, in other words, the nocturnal wind to the mountains.

Most modern time meteorological textbooks present sea-breeze and land-breeze in the same context (e.g. Ahrens, 1994; Wikipedia at *http://en.wikipedia.org/wiki/Sea_breeze#Land_breezes*), and not necessarily together with slope-driven circulations, such as katabatic winds. The dynamics of the coastal nocturnal winds are thus explained in exactly the same way as the dynamics of the sea-breeze.

3 NUMERICAL SIMULATIONS

The diurnal circulation in June has been simulated with the numerical model MM5 (see Ágústsson & Ólafsson; Ólafsson & Ágústsson, 2008). Figure 1 shows the simulated sea-breeze in the afternoon and the late – night flow, with and without mountains. The simulated set-up is North-Iceland, a region well known by Snorri Sturluson and resembling West-Norway in terms of topography and fjords.

The simulations reveal firstly that there is no symmetry between the nocturnal flow and the sea-breeze. The sea-breeze is much stronger than the flow in the late night. Secondly, and most importantly in this context, there is no nocturnal flow if the land is flat, but winds of several m/s where the mountains are present.

4 DISCUSSION

The simulations show that the nocturnal wind in N-Iceland is of a katabatic nature, not a land-breeze. Consequently, many textbook descriptions of thermally driven nocturnal circulations may be characterized as misleading, at least for this part of the world. The dynamics are on the other hand in agreement with Egils´s Saga, assuming that the thermally driven flows in W-Norway are similar as in N-Iceland.

The author of Egil´s saga, and most likely Egill himself were well informed about the diurnal circulation. This is true, not only for the dynamics of the nocturnal winds, but the offshore extent of the winds. Bergonund appears to be ignorant about this and believes that Egill is leaving Norway when he sails to the west in the katabatic flow. Egill does of course not reach any further than a very short distance, and sails in with the sea breeze a few days later. Bergonund pays for his ignorance with his life and king Eric loses his kingdom for having such an idiot on his team.

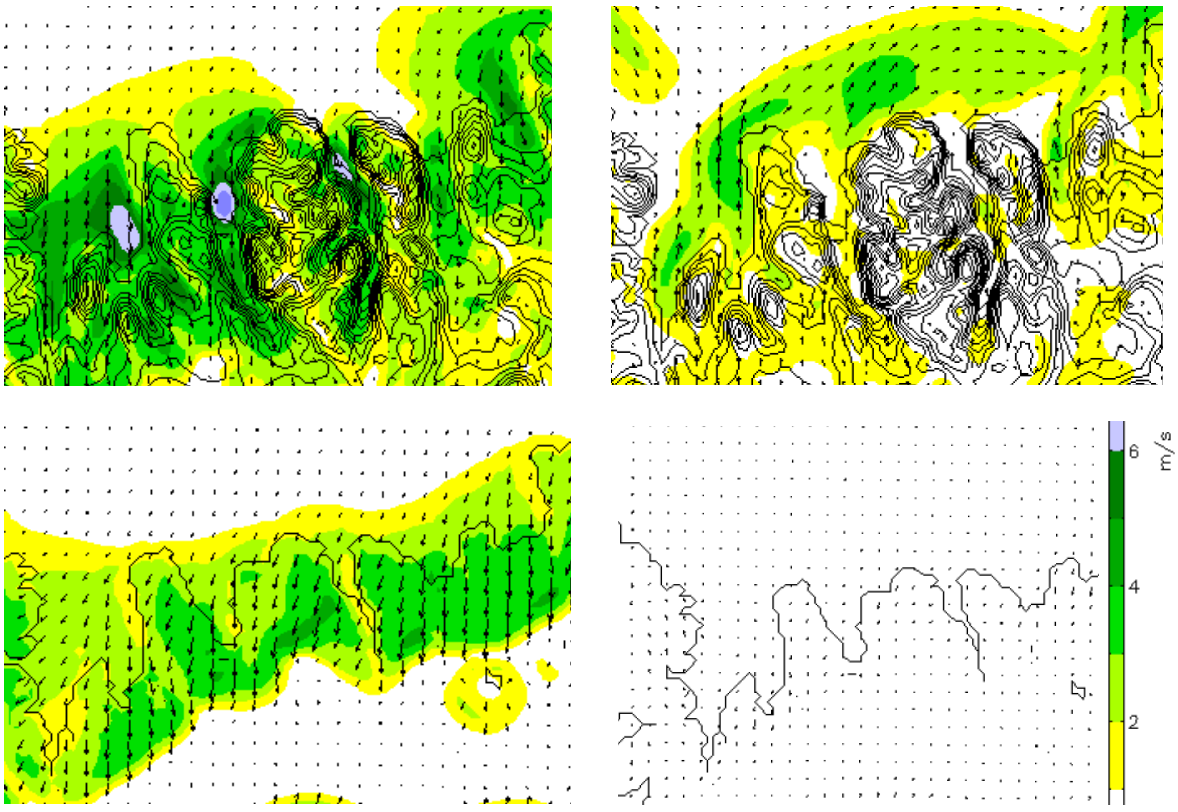

Figure 1. Simulated summer-time thermally driven surface winds at the north coast of Iceland and topographic height contours (intervals of 100 m). Top left: Afternoon. Top right: late night. Bottom left: Afternoon over flat Iceland. Bottom right: Late night over flat Iceland.

REFERENCES

Ahrens, C. D., 1994: Meteorology Today, 5th Ed., West Publishing Company, Minneapolis/St.Paul, USA. 589 p.

Ágústsson, H. and H. Ólafsson, 2008: Idealized simulations of katabatic flows in Iceland: Katabatic winds or land breeze? *Proc. Amer. Meteorol. Soc. Conf. Mountain Meteorology*, Whistler Canada. 5 p.

Egils´s Saga Skallagrímssonar, by an unknown author. Mál og menning, Reykjavík, Iceland, 1992. English translation by W.C. Green (1893) provided by the Icelandic Saga Database.

Ólafsson, H. and H. Ágústsson, 2008: Summer-time thermal winds over Iceland: Impact of topography. *Proc. Amer. Meteorol. Soc. Conf. Mountain Meteorology*, Whistler Canada. 7 p.

METEOROLOGY IN THE MIDDLE AGES
PART II – A DOWNSLOPE WINDSTORM IN LAXDÆLA SAGA

Haraldur Ólafsson[1] and Hálfdán Ágústsson[2]

[1] Háskóli Íslands, Iceland and Bergen School of Meteorology, Geophysical Institute, University of Bergen
E-mail: *haraldur68@gmail.com*
[2] Reiknistofa í veðurfræði and Háskóli Íslands, Iceland

Abstract: The texts of Laxdæla Saga, taking place in Iceland the 10th century and written in the 13th century are explored. It is argued that the saga contains a brief description of a downslope windstorm. A similar windstorm in modern times is presented to illustrate the nature of the windstorm.

Keywords: *Laxdæla Saga, Downslope windstorm, Iceland, Navigation, Middle Ages*

1 INTRODUCTION

Laxdæla Saga (Laxdale Saga) is one of the most romantic of the Icelandic Sagas, written in the middle of the 13th century. Laxdæla Saga is not signed, but its authorship has been attributed to Ólafur Þórðarson, a close relative of Snorri Sturluson, the alleged writer of Egil´s Saga Skallagrímssonar. Snorri was a celebrated scholar and a meteorologist (see Meteorology of the Middle Ages, Part I, in this publication). The story takes place in Norway, Iceland and in several other islands in the North-Atlantic, spanning from the period of the reign of Haraldur the Fairhaired in Norway and the settlement of Iceland in the late 9th century into the 11th century. This paper discusses a description of an important weather event in Laxdæla. A simulation from a similar event in modern times is presented and it is argued that we may have an example of a downslope windstorm.

2 A DOWNSLOPE WINDSTORM IN LAXDÆLA SAGA

Upon the end of the annual local parliament in Breiðafjörður at the west coast of Iceland, Þorsteinn (Thorstein) surtur sets sails for his farm Hrappsstaðir in Laxárdalur valley. This happened most likely in the month of June. Þorsteinn is hit by strong winds at the north coast of the Snæfellsnes peninsula, he wrecks the ship and everybody dies, except one person. The event is described as follows in a translation to English by M.A.C. Press, published in 1880:

Thorstein fell in with a high south-westerly gale, and they sailed up towards the roosts, and into that roost which is called Coal-chest-Roost,which is the biggest of the currents in Broadfirth. They made little way sailing, chiefly because the tide was ebbing, and the wind was not favourable, the weather being squally, with high wind when the squalls broke over, but with little wind between whiles.
(Laxdæla Saga, Ch. 18, English translation by Muriel A. C. Press, 1880)

There is intermittent rain and the strong winds that contribute to the accident are not present all the time, but they are associated with the precipitation events. This is quite usual in convective situations in south-westerly winds in the winter, but not as usual in the summer. A new translation, published in 1903 presents a different view of things:

Thorstein fell in with a fresh southwester; they sail inwards through the streams into that stream that hight Coal-kiststream; that is by far the greatest of those streams that are in Broadfirth; ill sped they with their sailing, and that was the more so, that by then was come the ebbing of the sea, but the breeze was not friendly to them; for the weather was showery and the wind was strong when it grew clear, but blew little between-whiles.
(Laxdæla Saga, Ch. 18, English translation by Robert Proctor, 1903)

Here, the strong winds are still intermittent, but they occur during clearings in between precipitation events, not during the precipitation. This must be characterized as unusual, but agrees with the original text:

Þorsteinn tók útsynning hvassan. Sigla þeir inn að straumum í þann straum er hét Kolkistustraumur. Sá er í mesta lagi þeirra strauma er á Breiðafirði eru. Þeim tekst siglingin ógreitt. Heldur það mest til

þess að þá var komið útfall sjávar en byrinn ekki vinveittur því að skúraveður var á og var hvasst veðrið þá er rauf en vindlítið þess í milli.
(Laxdæla Saga, the original in Icelandic)

Here the meaning of the text is closely linked to the interpretation of the word "rauf". The verb "rjúfa" means to open or to take apart and is commonly employed in the context of the sky clearing up. The strong winds are in other words associated with clearings in between precipitation events and we must conclude that Proctor´s translation from 1903 is more correct on this issue than the previous translation from 1880.

3 A NUMERICAL SIMULATION

The region is known for downslope windstorms, but to illustrate a windstorm similar to the one that killed Þorsteinn surtur and most of his crew, a summer windstorm is simulated and presented in Fig.1. The flow is simulated with a horizontal resolution of 3 km with the numerical model MM5 (for a detailed study of downslope windstorms in this region, see Ágústsson and Ólafsson, 2009). There is strong acceleration along the lee slopes of the mountains, and the strong winds do reach a short distance into the sea in some areas. The flow is quite non-stationary and sensitive to the representation of the topography. The exact position of the strong winds should therefore not be taken too literally.

4 DISCUSSION AND CONCLUSION

The windstorm described in Ch.18 in Laxdæla saga is associated with a clearing in the sky. This clearing is presumably being generated by downdrafts in the strong downslope flow. During period(s) of weaker winds, the downdrafts are weaker or absent and a precipitation system (a weak front) may overcome the barrier of the Snæfellsnes peninsula more easily and give precipitation on its northern side, as observed by Þorsteinn surtur. In order to generate strong downslope acceleration, a stably stratified atmosphere at low levels is required. Such a stratification is very common in winds from the southeast or south, while south-westerly winds are typically associated with an unstable atmosphere with convective precipitation. However, south-westerly flows are certainly not always unstable and they have produced many events of downslope windstorms in this region.

We conclude therefore that there is evidence that a downslope windstorm that led to a major accident at sea is being described in Laxdæla Saga, written in Iceland in the middle of the 13th century. The authors of this paper do not know of an older documentation of a downslope windstorm.

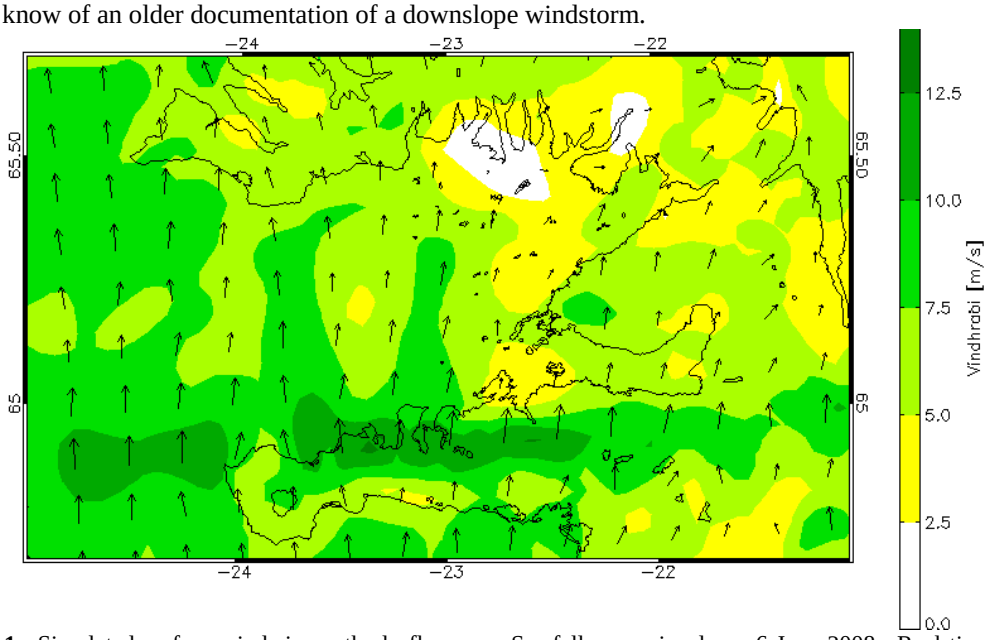

Figure 1. Simulated surface winds in southerly flow over Snæfellnes peninsula on 6 June 2008. Real-time simulations of this kind are available at http://www.belgingur.is

REFERENCES

Ágústsson, H. and H. Ólafsson, 2009: Forecasting wind gusts in complex terrain. Meteorology and Atmospheric Physics, in press

Laxdæla Saga by an unknown author. Mál og menning, Reykjavík, Iceland, 1993. English translations by Muriel A. C. Press (1880) and Robert Proctor (1903) provided by the Icelandic Saga Database.

Ólafsson, H. and H. Ágústsson, 2009: Meteorology in the Middle Ages – Part I: Thermally driven coastal winds. *Meteorologische Annalen, Proc. Int. Conf. Alpine Meteorology, Raststatt, Germany.*

THE 'MIRACULOUS' FÖHN IN BAVARIA OF JANUARY 1704

A. Tafferner[1], K.P. Hoinka[1], G. Zängl[2], L. Weber [3]

[1] Deutsches Zentrum für Luft- und Raumfahrt, Oberpfaffenhofen, Germany. (*arnold.tafferner@dlr.de)*
[2] Deutscher Wetterdienst, Offenbach, Germany;
[3] Philosophisch-Theologische Hochschule der Salesianer Don Boscos, Benediktbeuern, Germany

Abstract: According to the historic records from the monk Carolus Meichelbeck (1669–1734) the föhn of 28 January 1704 dramatically melted the frozen swamps very close to the Alpine baseline which in effect prevented the monastery of Benediktbeuern of being plundered by Tyrolian troops. In this paper we investigate whether realistic meteorological conditions during this föhn event would allow the reported strong and rapid melting of the water in the marshes. This is performed both by analytical calculation and a numerical simulation.

Keywords: *Föhn, ice melting, numerical simulation, Anastasia miracle*

1 INTRODUCTION

Before the establishment of systematic weather observations in the nineteenth century, there was a significant interest in observing the weather by individuals such as priests, writers and artists. These observations were sometimes performed unsystematically and yet there are known historical weather events which are reasonably well documented by location, date, intensity and even daily evolution. An example is the southerly föhn, one of the dominant weather phenomena in Bavaria, southern Germany. One particular event occurred on 28 January 1704, documented by the monk Meichelbeck at the Monastery Benediktbeuern. He reported that this föhn rapidly melted the frozen marshes surrounding the monastery and saved the monastery from being plundered by Tyrolean troops during the Spanish Succession War. This melting was so impressive that the chronicler praised this saving of the monastery as a divine marvel, the so-called 'Anastasia' or 'Lake Kochel' miracle.

2 TOPOGRAPHICAL BACKGROUND

The Monastery of Benediktbeuern (MB in Fig. 1) is located close to the Alpine baseline. Between Lake Kochel and Lake Walchen (LK and LW) south of the monastery there is a mountain gap (at the yellow line in Fig. 1), with nearby mountain summits reaching more than 1400 m. It is well known that mountain gaps enhance and intensify strong downslope windstorms, for example, the Chinook of Colorado. For centuries the monastery was surrounded by swamps with imbedded small swamp ponds and hamlets. These wet areas hampered approaching invaders providing a natural defence.

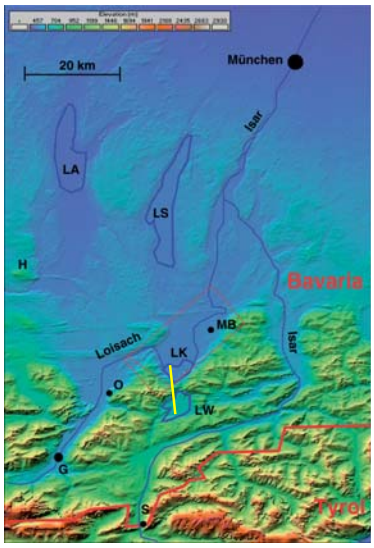

Figure 1. Map of southern Bavaria and parts of Tyrol showing the Isar and Loisach rivers. Garmisch-Partenkirchen (G), Ohlstadt (O), Hohenpeissenberg (H), Scharnitz (S), Monastery of Benediktbeuern (MB), Lake Ammer (LA), Lake Starnberg (LS), Lake Kochel (LK), Lake Walchen (LW). The scale is 1:100.000. (Elevation data, © U.S. Geological Survey.). The yellow line marks the location of the cross section of figure 2.

3 28 JANUARY 1704

In the morning of 28 January 1704, 2000 Tyrolean horsemen and soldiers started from Scharnitz (**S**, Fig. 1). They moved to Garmisch (**G**) and then along the Loisach River Valley, passing Ohlstadt (**O**) towards Großweil close to Lake Kochel. From there they planned to move along a dead-straight line over the frozen swamps and the River Loisach towards the monastery. It was hoped to arrive at the monastery in the evening. Meichelbeck pointed out that Lake Kochel was so strongly frozen that heavy load cars and 1000 men could have moved comfortably towards Benediktbeuern. When first notices of the troop's advance arrived, it was too late to organize an effective defence of the monastery. Therefore its salvation was entrusted to God. Because next day, the 29 January, was the festival day in honour of St Anastasia, the monks started to pray to Anastasia for her help in this dangerous situation. Meichelbeck reports that at 1400 h when the Tyrolean troops were about one hour away from the frozen swamps, a very warm wind appeared. Three to four hours later, the frozen swamps turned from white to black indicating that they were impassable for horses. As soon as the troops had reached the swamp areas they recognized that it was impossible for them to cross these melting surfaces because horses and men broke into the unsound ice surface. Meichelbeck mentioned also that the wind was persistently warm.

4 FÖHN AND ICE MELTING

The effect of the sudden föhn-related warming and the resulting melting of the frozen swamp must have been so impressive that for Meichelbeck the only explanation was that it was a miracle. Here a rough estimate is made to evaluate the melting effect, taking into account temporal limits and intensity reported by Meichelbeck (for details ref. to Hoinka et al., 2009). The minimum ice-layer thickness which is necessary for bearing the mean weight of a horse with horseman of about 700 kg can be estimated to between 10 and 20 cm above lakes. For the meltwater production an energy balance is considered where the available melt energy results from the radiation balance as well as sensible and latent heat fluxes. For reasons of simplicity, only the sensible heat flux is evaluated. The sensible heat flux S is calculated by a simple bulk approach $S = -\alpha (T_s - T_a)$, where $(T_s - T_\alpha)$ is the surface/air temperature difference. The heat transfer coefficient α is approximated by $\alpha = 5.7 \bullet v^{0.5}$ where v is the horizontal wind in m s^{-1}. The water-equivalent melt rate M_w is then calculated by $M_w = S\,(\rho_w \bullet r)^{-1}$. With density of water ρ_w , heat of fusion r ($3.35 \bullet 10^5$ J kg^{-1}) and S in Wm^{-2}, M_w is given in m s^{-1}. Assuming a wind of 35 m s^{-1} and a temperature difference ($T_a - T_s$) of 20 K we arrive at an ice melt rate of about 7.3 mm h^{-1}. Thus a solid lake ice-layer would be reduced by roughly 2.5 cm within 3 hours. One has to keep in mind that the solidity of lake ice and of a frozen swamp surface are quite different because the latter consists of a frozen mixture of grass, small plants, soil and water. Assuming a melting of swamp layer to be twice as effective compared to lake ice, we arrive at an estimate of about 5 cm within 3 hours. The evaluated thickness reduction is not very dramatic but sufficient to change a frozen surface from bearing to non-bearing capacity.

5 NUMERICAL SIMULATION

A numerical simulation has been set up using the MM5 model with 5 nests and highest resolution of 333m. A strong south-westerly geostrophic flow over the mountains has been initialised with linear vertical shear, with 15 m/s at 1000mb up to 33 m/s at tropopause level (for details see Zängl, 2003). As seen from the cross sections in Fig. 2 after 6 (left) and 12 (right) hours forecast time, the initial cold air pool over lake Kochel has been erased by the strong föhn flow through the mountain gap with a corresponding temperature rise of about 15 K in that area. Also strong winds spread out over the swamp area around Lake Kochel reaching 15 m/s (not shown).

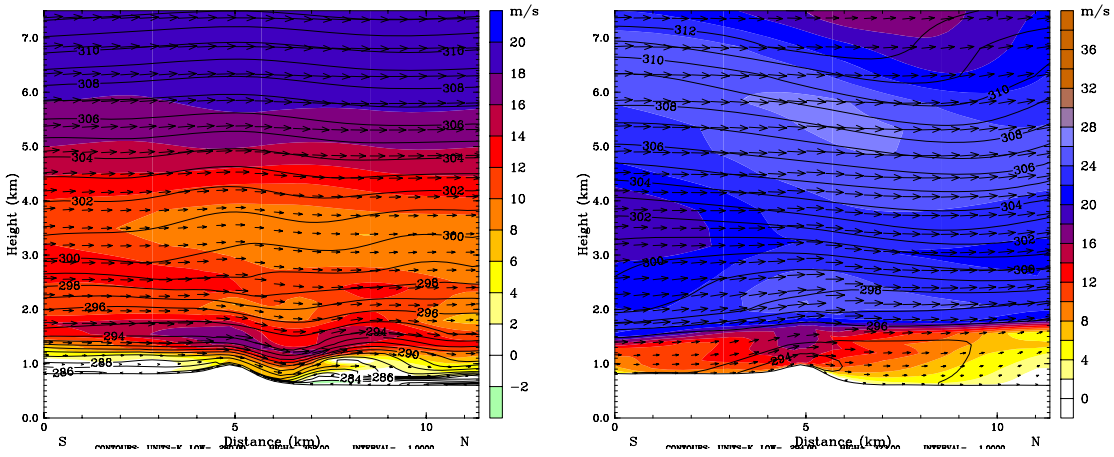

Figure 2. Cross sections of potential temperature and wind over the line indicated in fig.1 after 6 (left) and 12 (right) hours.

6 CONCLUSIONS

Inserting the wind and temperature values (15 m/s, 15 K) of the numerical föhn simulation in the equation for the melt rate M_w results in a much smaller melting rate of only about 1cm in 3 hours, or to 2 cm when taking into account the swamp surface. Meichelbeck might have dramatized the event's intensity by shortening the impact period in order to increase the 'miracle's' significance. Increasing the period up to 6 hours between the outbreak of the föhn and the recognition of the non-bearing capacity, the abovementioned values increase to 10 cm (extreme values) and 4 cm (numerical simulation). Even the smaller value would be sufficient to change a frozen surface from bearing to non-bearing capacity. Summarising one can say that no compelling evidence is indicated that a 'miracle' occurred. It suggests that the föhn of 28 January 1704 was an extraordinary event.

REFERENCES

Hoinka, K.-P., A. Tafferner, L. Weber, 2009: The 'miraculous' föhn in Bavaria of January 1704. Weather. **64** , 9-14.

Zängl, G., 2003: Deep and shallow south Foehn in the region of Innsbruck: Typical features and semi-idealized numerical simulations. Meteorol. Atmos. Phys., **83,** 237-261

AN EXAMINATION OF ATMOSPHERIC LIDS DURING COPS

Andrew Russell and Geraint Vaughan

Centre for Atmospheric Science, University of Manchester, Manchester, UK
E-mail: *andrew.russell-2@manchester.ac.uk*

Abstract: The understanding of the nature, origin and prevalence of atmospheric lids is low. There is, therefore, an opportunity to contribute significantly to this area of meteorology - this is the goal of this work. The context for this paper is the Convective and Orographically-induced Precipitation Study (COPS). The COPS observational campaign, which was undertaken in 2007, was based around the Black Forest region with the aim of improving precipitation forecasts in low mountainous regions. However, the project also represents a great data archive with which to analyse isolated features, such as atmospheric lids. In short, lids play a vital role in the development of convective storms. For example, evidence from the Convective Storm Initiation Project (CSIP), which was run in the UK in 2005, has shown that lids are important not only in determining whether a storm occurs but also when and where they develop and how intense they are – sometimes, counter-intuitively, they appear to increase the intensity. This extended abstract is intended as a brief overview of the previous literature on lids in order to place the work presented at ICAM-2009 in the wider scientific context.

Keywords: *inversions, capping, convection, convective inhibition, stability*

1 INTRODUCTION AND TERMINOLOGY

The term *lid* is often used in the context of atmospheric science. It is a useful concept, in addition to measures of lifting, when analysing or forecasting the development of convection. Therefore, it comes as little surprise that one of the first uses of the term in the scientific literature was in the description of the conditions leading to the severe storms in the Midwestern United States (Carlson and Ludlam 1968).

Why are atmospheric lids important? In the absence of the lid, the convection that develops is often widespread but shallow, unless the profile is unusually unstable. The presence of a lid can allow the lowest levels of the atmosphere to accumulate heat and moisture, creating the potential for deep convection. Release of this potential can occur at selected points along the capped region when there is sufficient boundary-layer forcing (i.e. convergence or orographic uplift). Alternatively, the lid may be weakened by large-scale uplift, or there may be a combination of the two effects. This rather complex interplay between the lid and deep convection is one reason why *convective available potential energy* (CAPE) by itself is not a good predictor of thunderstorm magnitude (McCaul and Weisman 2001).

The key feature of a lid is its *stability* (i.e. increasing potential temperature with height). Once a thermal is initiated in the atmosphere it will only remain buoyant whilst it is warmer than the air around it. Lids, or stable layers, are, therefore, very often associated with temperature *inversions* i.e. where the vertical temperature gradient changes from cooling with height to warming. Indeed, the top of the atmospheric boundary layer, which traps the turbulence that is induced at the surface, is frequently referred to as the *capping inversion* and, similarly, lids are often referred to as *caps*. However, a temperature inversion is not strictly necessary for a lid – a slowing of the lapse rate is all that is required for a previously buoyant air parcel to encounter some *convective inhibition* (CIN).

The origin of lids on the climatological has not been studied in any great depth but, given their characteristics and results from individual case studies, it is likely that the majority are derived from *residual layers* (i.e. remnants of the previous day's boundary layer) or *dry layers* that have descended from the upper-troposphere/lower-stratosphere.

2 A DEFINITION OF ATMOSPHERIC LIDS

Carlson et al. (1980) developed a Lid Strength Index (LSI) in the context of severe storm initiation in the Midwestern United States. The LSI compares buoyancy of an atmospheric profile with the lid effect thus:

$$LSI = \left(\overline{\theta}_w - \tilde{\theta}_{sw}\right) - \left(\theta_{swl} - \overline{\theta}_w\right) \tag{1}$$

Where, in the presence of a lid, $\overline{\theta}_w$ equals the mean wet-bulb potential temperature in the lowest 50 hPa, θ_{swl} equals the maximum saturation wet-bulb potential temperature and $\tilde{\theta}_{sw}$ equals the mean saturation wet-bulb potential temperature between θ_{swl} and 500 hPa. Therefore, a positive LSI means there is potential for convection without further forcing (e.g. lifting, heating) and a negative LSI implies that convection would be inhibited. However, the LSI give little indication of the thickness of the lid, whether there are multiple lids or what the relative rates of change of the lid strength and the surface layer temperature are.

3 PREVIOUS STUDIES OF ATMOSPHERIC LIDS

A number of cases from a recent UK field campaign – the Convective Storm Initiation Project (CSIP) – highlighted the importance of lids in the development of convective storms. In a summary of that project, Browning et al. (2007) discussed the role of lids in general whilst Morcrette et al. (2007), Russell et al. (2008, 2009) and Bennett et al. (2008) examined their role in individual cases in much greater detail. In particular, Russell et al. (2008) were concerned with the origin of the lid that they examined. In their case the lid had descended from the upper-troposphere but it is unclear whether the main source of lids is from descent, residual layers or differential advection, as speculated by Graziano and Carlson (1987).

Bennet et al. (2008) examined a case from the UK where multiple stable layers influenced the development of convection that led to some small showers. In particular, they consider how best to interpret radiosonde data with respect to understanding how convection develops. It would be interesting to extend their study and try to determine where these multiple stable layers came from.

Graziano and Carlson (1987) conducted an analysis of lid strength versus severe storm activity over a six month period in 1982 for the central two-thirds of the USA. Their study, representing one of the only systematic analyses of the role of lids in the initiation of convection, revealed that in order to understand the onset of severe convection both lid strength and buoyancy must be considered. For example, they found an LSI "cut-off value" above which severe convection was rarely observed. However, whilst the probability of deep convection decreases with increasing LSI, they found that when considering a given value of buoyancy the deep convection probability increased with increasing LSI.

4 SUMMARY

This extended abstract represents a short overview of the scientific literature on the subject of atmospheric lids. A suitable way to summarise this paper, therefore, is the following brief list of research questions that this review has thrown up. Here is this list:

- How important are lids in determining the strength of convective storms?
- How important are lids in determining the location of convective storms?
- How well do numerical weather prediction (NWP) models represent lids?
- Has the climatological occurrence of lids changed in recent time?
- Where do lids come from?
- Are the answers to the above questions significantly different in different geographical areas?

The data collected and the NWP models run during the COPS campaign, as summarised by Wulfmeyer et al. (2008), provide an ideal dataset to answer some of these questions.

Acknowledgements:
We would like to thank all the COPS team for the smooth running of the campaign and the high quality data that was collected. Thanks are also due to the Natural Environment Research Council (NERC) who funded UK-COPS.

REFERENCES

Bennett, L. J., A. M. Blyth, K. A. Browning, E. G. Norton, 2008: Observations of the development of convection through a series of stable layers during the Convective Storm Initiation Project. Q. J. R. Meteorol. Soc. **134**, 2079-2091.

Browning, K. A. and co-authors, 2007: The convective storm initiation project. Bull. Amer. Meteorol. Soc. **88**, 1939-1955.

Carlson, T. N. and F. H. Ludlam, 1968: Conditions for the occurrence of severe local storms. Tellus **20**, 203-226.

Carlson, T. N., R. A. Anthes, M. Schwartz, S. G. Benjamin and D. G. Baldwin, 1980: Analysis and prediction of severe storm environments. Bull. Amer. Meteorol. Soc. **61**, 1018-1032.

Graziano, T. M. and T. N. Carlson, 1987: A statistical evaluation of lid strength on deep convection. Weather Forecast. **2**, 127-139.

McCaul, E. W. and M. L. Weisman, 2001: The sensitivity of simulated supercell structure and intensity to variations in the shapes of environmental buoyancy and shear profiles. Mon. Wea. Rev. **129**, 664-687.

Morcrette, C. J., H. Lean, K. A. Browning, J. Nicol, N. Roberts, P. A. Clark, A. Russell and A. M. Blyth, 2007: Combination of mesoscale and synoptic mechanisms for triggering of an isolated thunderstorm: a case study of CSIP IOP 1. Mon. Wea. Rev. **135**, 3728-3749.

Russell, A., G. Vaughan, E. G. Norton, H. M. A. Ricketts, C. J. Morcrette, T. J. Hewison, K. A. Browning and A. M. Blyth, 2009: Convection forced by a descending dry layer and low-level moist convergence. Tellus A **61**, 250-263.

Russell, A., G. Vaughan, E. G. Norton, C. J. Morcrette, K. A. Browning, A. M. Blyth. 2008: Convective inhibition beneath an upper-level PV anomaly. Q. J. R. Meteorol. Soc. **134**, 371-383.

Wulfmeyer V. and co-authors, 2008: The Convective and Orographically Induced Precipitation Study. Bull. Amer. Meteorol. Soc. **89**, 1477–1486.

Wind measurements with lidar and cloud radar during COPS

Jan Handwerker, Katja Träumner, Jens Grenzhäuser, Andreas Wieser

Karlsruhe Institute of Technology (KIT) — Institut für Meteorology und Klimaforschung (IMK)
E-mail: *jan.handwerker@imk.fzk.de*

Abstract: The 35.5 GHz scanning cloud radar MIRA36-S and the 2 µm Doppler lidar Windtracer were collocated on the highest mountain of the Northern Black Forest (Hornisgrinde) during the COPS campaign. This study investigates wind speed data measured with these two instruments. We assume, that horizontal components should be independent of the used wavelength, delivering a unique quality check opportunity and allowing an extention of the individual measurements. Vertical components should differ in case of sedimenting particles, giving access to further physical properties of the scatterers, e.g. on the drop size distribution.

Keywords: *COPS, Radar, Lidar, Wind*

1 INTRODUCTION AND MEASUREMENT SETUP

During COPS ("Convective and Orographically-induced Precipitation Study") MIRA36-S and Windtracer were collocated on top of Hornisgrinde (1160 m asl, cf. Fig. 1). Sometimes the instruments were both vertical oriented, leading (besides further information) to direct measurements of the vertical scatterer velocity, sometimes they performed more or less complicated scan patterns, consisting of several successive PPI and RHI scans. Here, we show results from equal or comparable scan patterns for both instruments.

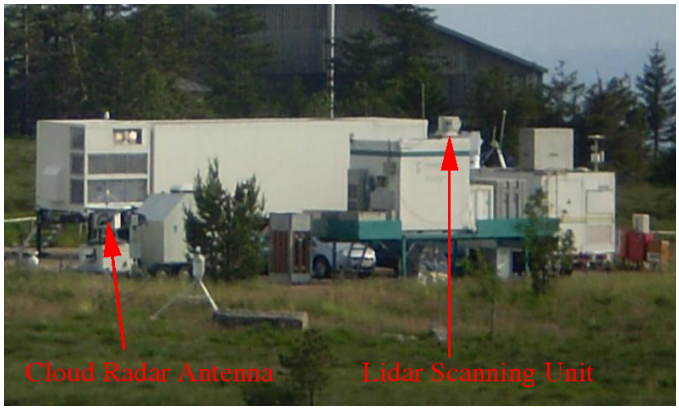

Figure 1: MIRA36-S and Windtracer at Supersite Hornisgrinde

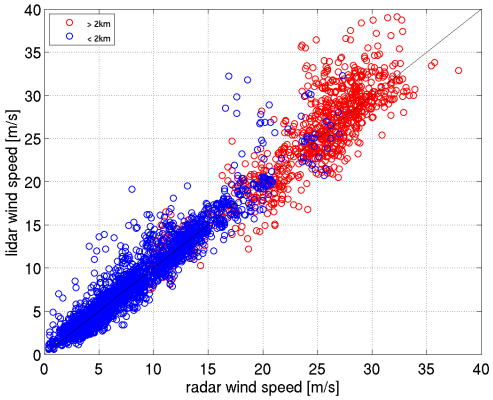

Figure 2: Intercomparison of horizontal wind speeds (radar measurements at 45°).

2 HORIZONTAL WIND SPEED

From cloud radar measurements horizontal wind speeds are derived by an improved VAD algorithm (Browning and Wexler , 1986; Tabary et al. , 2001) from PPI scans which lasted approx. 60 s. The radar performed PPI scans at 15° and 45° zenith angle, only the latter are presented here. Lidar based horizontal winds from a 10-minute scan pattern, containing two PPI scans (at 45° and 86° zenith angles) and some RHI scans. The horizontal winds are derived by a least square method, similar to the VAD algorithm. Our radar measurements are finer resolved in time and space than the lidar measurements. For comparisons we always used the nearest radar bin to a lidar measurement, i.e. there is no interpolation applied.

The scatterplot in Fig. 2 shows the correspondence of the two measurements. Blue marks measurements in the lower 2 km agl.; this height is an approximation for the maximum PBL thickness in summer on Hornisgrinde. 57 % of all measurements have a deviation of less than 1 m/s and only 3 % of more than 5 m/s.

In case of missing scatterers no horizontal wind can be derived. Radar and lidar show to be complementary. Below 2 km only 8.2 % of the possible measurements lead to simultaneously measurements of both instruments. In 16.2 % the radar could derive a horizontal wind, in 22.9 % the lidar was successful. Both instruments together provide a horizontal wind speed in 47.3 %. Above 2 km the numbers are 2.3 % (coinciding), 12.9 % (radar), 8.7 % (lidar) and 19.3 % (combined).

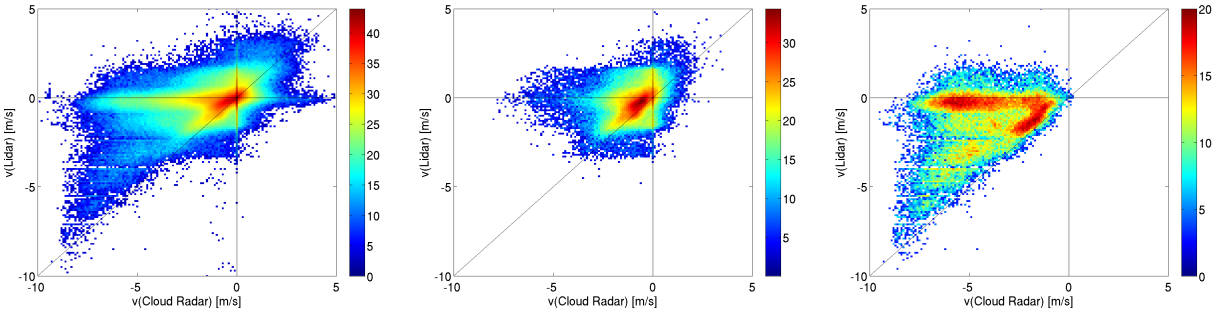

Figure 3: 2D frequency distributions of observed vertical velocities measured by radar (abscissa) and lidar (ordinate) for all measurements (left) measurements with clouds (middle) and in rain (right). Colors are coded on logarithmic scales.

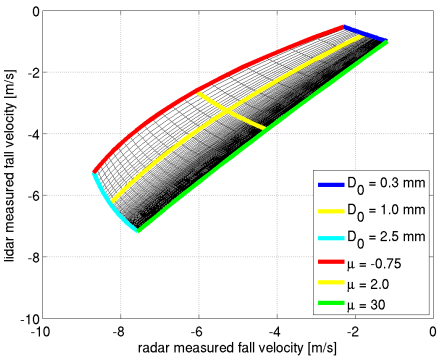

Figure 4: Expected distribution of radar and lidar measured vertical velocities for Gamma shaped drop size spectra. D_0 is varied between 0.3 mm and 2.5 mm, μ between -0.75 and 30.

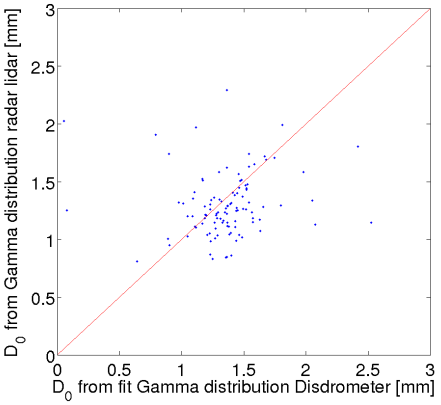

Figure 5: Reference Dropsizes measured by a Joss-Waldvogel Disdrometer compared to radar and lidar derived values.

3 VERTICAL VELOCITY COMPONENT

Due to their different wavelengths the two devices are sensitive to different scatterer sizes. Vertical wind components differ because of the size dependent sedimentation velocity of the scatterers. Scatter plots of the 2-dimensional distribution of vertical velocity measurements are shown in Fig. 3. These data are measured with vertical pointing instruments. Note, that the color codes are given in a logarithmic (dB) scale.

For all measurements (left panel of Fig. 3) upward velocities up to roughly 3 m/s are measured. In clouds (discriminated by a lidar backscatter value $\geq$ -6.8 dB, middle panel) movements are significant slower, but centered around a slow downward motion (not around 0). The fast downward motions only occur in rain events (discriminated by a radar reflectivity $\geq 0\,\mathrm{dB}_Z$ in 500 m agl).

In the latter case (rain) the different vertical velocities may be used to determine information on the drop size distribution. We (i) substract vertical wind motion (determined from lidar aerosol peak), (ii) assume a Gamma-shaped drop size distribution $N(D) = N_0 D^\mu \exp(-\lambda D)$ which has a reference drop size $D_0 = (\mu + 4)/\lambda$ and (iii) the terminal fall velocity from Atlas et al. (1973) ($v = 9.65 - 10.3\exp(-0.6D)$). With these assumptions Fig. 4 indicates the area where we expect the measured vertical velocities. The lidar software always uses the most intense peak to determine the vertical velocity. In most cases this is the aerosol peak, as can seen from Fig: 3 and by analysing the raw lidar spectra. Identifying the rain drop peak and applying the described method, leads to reference sizes (D_0) as shown in Fig. 5 in comparison to measurments of a colocated Joss-Waldvogel Disdrometer. These results are satisfactory.

4 CONCLUSIONS

Cloud radar and wind lidar are complementary in measuring horizontal winds. They allow mutual quality control. Using vertical fall velocities from both instruments yields information on microphysical parameters at least in rain.

REFERENCES

K. A. Browning and R. Wexler: A determination of kinematic properties of a wine field using doppler radar. *J. Appl. Meteor.*, **7**, 105 – 113, 1968.

P. Tabary, G. Scialom, and U. Germann: Real-time retrieval of the wind from aliased velocities measured by doppler radars. *J. Atmos. Oceanic Technol.*, **18**, 875–882, June 2001.

D. Atlas, R.C. Srivastava, and R.S. Sekhon: Doppler Radar Characteristics of Precipitation at Vertical Incidence, *Rev. Geophys. Space Phys.*, **11**, 1–35, 1973.

LIDAR AND RADAR MEASUEMENTS OF THE MELTING LAYER IN THE FRAME OF THE CONVECTIVE AND OROGRAPHICALLY-INDUCED PRECIPITATION STUDY

Paolo Di Girolamo[1], Donato Summa[1], Rohini Bhawar[1],
Tatiana Di Iorio[2], Geraint Vaughan[3], Emily Norton[3], Gerhard Peters[4]

[1] DIFA, Università degli Studi della Basilicata, Potenza, Italy
Email: digirolamo@unibas.it
[2] Dipartimento di Fisica, Università degli Studi di Roma "La Sapienza", Roma, Italy
[3] School of Earth, Atmospheric & Environmental Sciences, University of Manchester, Manchester, UK
[4] Meteorologisches Institut, Universität Hamburg, Hamburg, Germany

Abstract: During the Convective and Orographically-induced Precipitation Study (COPS), lidar dark/ bright and bands were observed by the Univ. of BASILicata Raman lidar system (*BASIL)* on several IOPs and SOPs (among others, 23 July, 15 August, 17 August). Dark/bright band signatures appear in the lidar measurements of the particle backscattering. Lidar data are supported by measurements from the University of Hamburg cloud radar *MIRA 36* (36 GHz), the University of Hamburg dual-polarization micro rain radars (24.1 GHz) and the University of Manchester Radio UHF clear air wind profiler (1.29 GHz). Results from *BASIL* and the radars will be illustrated and discussed at the Conference to support in the comprehension of the microphysical and scattering processes responsible for the appearance of the lidar dark band and radar bright band.

Keywords: *Dark and bright band, synergy of remote sensors, Raman Lidar and radars, COPS.*

1 INTRODUCTION

Changes in scattering properties of precipitating particles are found to take place during the snowflake-to-raindrop transition in the proximity of the freezing level. A maximum in radar reflectivity, known as the radar bright band, is observed in the microwave domain, while a minimum in lidar echoes appears at optical wavelengths, this phenomenon being referred as lidar dark band [1].

The radar bright band has been known and studied for more than three decades and it is presently a well understood phenomenon [2,3]. On the contrary, the lidar dark band has been poorly investigated and, to date, no systematic and coordinated observation are available. Lidar observations of the lidar dark band have been reported by Sassen and Chen [1], Demoz et al. [5] and Roy and Bissonnette [6]. Model simulations of this phenomenon have been provided by several authors [7,8]. The lidar dark band is believed to be the result of two conflicting microphysical processes: a) the structural collapse of severely melted snowflakes, leading to a decrease of lidar backscattering due to the reduced particles size and concentration and b) the completion of the melting process, leading to a sudden increase of lidar backscattering associated with spherical particle backscattering mechanisms coming into prominence [1]. The radar bright band peak occurs low in the melting region, just above (approx. 200 m) the lidar dark-band minimum. This position is close to where radar Doppler velocity reaches its plateau.

A comprehensive study of the dark and bright band phenomena has been recently published by Sassen et al. [9]. In this paper, authors report measurements performed by a single-wavelength (532 nm) backscatter lidar system and a three-wavelength Doppler radar (0.32-, 0.86-, and 10.6 cm). Unfortunately, lidar and radar depolarization data, which would have provided further information on the state of the melting particles, were not available from the instruments involved. Instead, lidar and radar depolarization measurements were performed during COPS by *BASIL* and *MIRA 36*, respectively.

2 LIDAR AND RADAR SYSTEMS

The measurements illustrated in this paper were performed in the framework of *COPS – Convective and Orographically-induced Precipitation Study* - held in the period 01 June-31 August 2007. The Univ. of BASILicata Raman lidar system (*BASIL)* was deployed throughout the duration of COPS in Supersite R (Achern, Rhine Valley, Lat: 48.64 ° N, Long: 8.06 E, Elev.: 140 m). *BASIL*, capable to provide measurements of atmospheric temperature and water vapour, particle backscatter at 355, 532 and 1064 nm, particle extinction coefficient at 355 and 532 nm and particle depolarization at 355 and 532 nm, operated between 25 May and 30 August 2007 and collected more than 500 hours of measurements, distributed over 58 measurement days.

During COPS, lidar data were supported by measurements from the University of Hamburg cloud radar MIRA 36 (36 GHz, 0.83 cm, Ka-band), the University of Hamburg dual-polarization micro rain radars (24.1 GHz, 1.24 cm, K-band) and the University of Manchester Radio clear air wind profiler (1.29 GHz, 23.24 cm,

UHF band). Additional ancillary information on the state of the atmosphere was provided by radiosondes, launched every three hours during each measurement session, as well as by a sodar and a microwave radiometer.

3 RESULTS

The time evolution of *BASIL* measurements of the particle backscatter ratio at 1064 nm (not shown) over a period of approx. 1.5 hours from 13:00 UTC to 14:35 UTC on 23 July 2007 reveal the presence of stratiform clouds, with cloud base at 3.4-3.8 km. Around 14:15 UTC melting hydrometeors start precipitating from clouds.

The left panel in figure 1 shows the vertical profile of temperature as measured by the radiosonde launched at 14:06 UTC, revealing the height of the freezing level at ~ 3.35 km. The second panel shows the vertical profile of radar reflectivity at 36 GHz, 24.1 GHz and 1.29 GHz, revealing the presence of the radar bright band at 2.95-3.0 km, i.e. 350-400 m below the freezing level at a temperature of 3.4 - 3.9 0C. The third panel shows the vertical profile of backscattering coefficient at 1064 nm, revealing the presence of the lidar dark band at 2.85-2.9 m, i.e. 450-500 m below the freezing level at a temperature of 4.4 - 4.9 0C, while the lidar bright band is approx. 200 further down at 2.7-2.75 km. The fourth panel shows the vertical profile of vertical velocity measured at 36 GHz and 1.29 GHz, with values of 2-2.5 m/s high in the melting layer and values of 3.5-4 m/s in the lower portion of the melting layer. Lidar (at 355 nm) and radar depolarization are shown in the right panel of figure 1. Enhanced radar reflectivity, increased radar depolarization and abrupt change in Doppler-derived particle velocities are found in the melting layer. Radar depolarization is most commonly increased due to the presence of wetted, asymmetric ice shapes. Lidar depolarization at 355 nm shows values of 25-30 % high in the melting layer and values of 5-10 % at the heights of the lidar dark and bright bands. These unexpectedly low values of lidar depolarization may imply that precipitating particles are almost spherical or have a more regular shapes.

Lidar measurements were stopped at 14:35 UTC because of the rain reaching surface and entering the telescope, but the lidar dark band phenomenon presumably continued for approx. 2 hours.

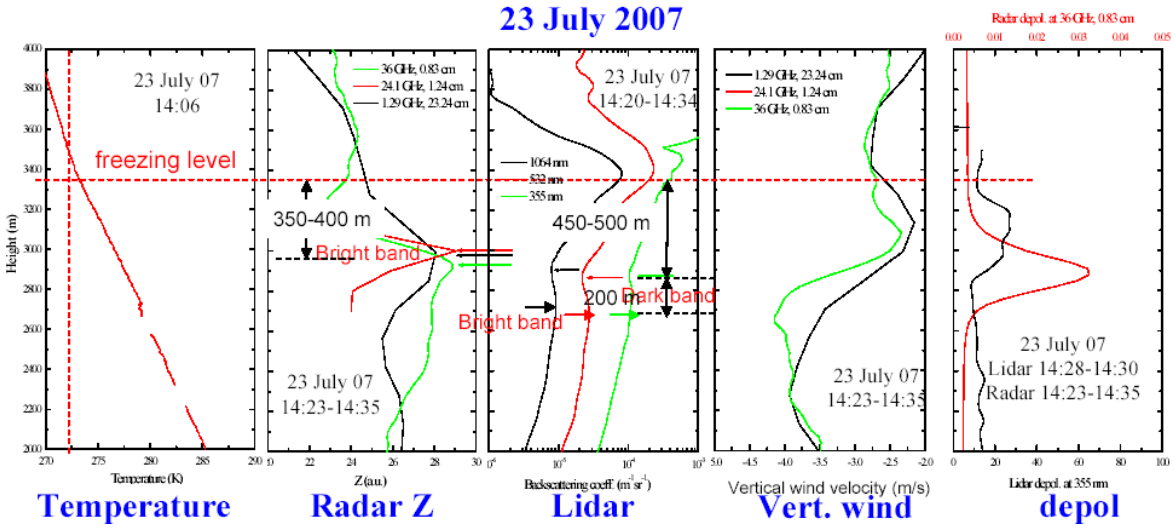

Figure 1. Vertical profile of temperature as measured by the radiosonde launched at 14:06 UTC (left panel); vertical profile of radar reflectivity at 36 GHz, 24.1 GHz and 1.29 GHz (second panel from left); vertical profile of backscattering coefficient at 1064 nm (third panel from left); vertical profile of vertical velocity measured at 36 GHz and 1.29 GHz (fourth panel from left); lidar depolarization at 355 nm (right panel).

REFERENCES

Sassen, K., and T. Chen, 1995: The lidar dark band: An oddity of the radar bright band. *Geophys. Res. Lett.*, **22**, 3505–3508.

Battan, L. J. Radar Observations of the Atmosphere, Univ. of Chicago Press, 1973, pp. 279.

Meneghini; R., and L. Liao, 2000: Effective Dielectric Constants of Mixed-Phase Hydrometeors. *J. Atm. Oceanic Tech.*, **17**, 628– 640.

Demoz, B. B., D. Starr, D. Whiteman, K. Evans, D. Hlavka, and R. Peravali, 2000: Raman LIDAR Detection of Cloud Base. *Geophys. Res. Lett.*, , **27**(13), 1899– 1902.

Roy, G., and L. R. Bissonnette,2001: Strong dependence of rain-induced lidar depolarization on the illumination angle: Experimental evidence and geometrical- optics interpretation, *Appl. Opt.*, **40**, 4770– 4780.

Di Girolamo, P., B. B. Demoz, and D. N. Whiteman, 2003: Model simulations of melting hydrometeors: A new lidar bright band from melting frozen drops, *Geophys. Res. Lett.*, 2003, **30** (12), 1626, doi:10.1029/2002GL016825.

Griaznov, V., I. Veselovskii, P. Di Girolamo, B. Demoz, D. N. Whiteman, 2004: Numerical Simulation of Light Backscattering by Spheres With Off-Center Inclusion. Application for Lidar Case. *Applied Optics*, **43**, 5512-5522.

Sassen, K., J. R. Campbell, J. Zhu, P. Kollias, M. Shupe, C. Williams, 2005: Lidar and triple-wavelength Doppler radar measurements of the melting layer: A revised model for dark and bright band phenomena, *J. Appl. Met.*, **44**, 301–312.

STUDY OF AN MCS USING RAMAN LIDAR IN THE FRAME OF THE CONVECTIVE AND OROGRAPHICALLY-INDUCED PRECIPITATION STUDY

Rohini Bhawar[a] , Paolo Di Girolamo[a], Donato Summa[a], Tatiana Di Iorio[b], Belay B. Demoz[c]

[a] *DIFA, Università degli Studi della Basilicata,Viale dell'Ateneo Lucano n. 10, 85100 Potenza, Italy*
Email: *rohinibhawar@yahoo.com*
[b] *Dipartimento di Fisica, Università degli Studi di Roma "La Sapienza", Piazzale Aldo Moro, 2, 00100 Roma, Italy*
[c] *Department of Physics and Astronomy, Howard University, 2400 Sixth Street, NW, Washington, DC , USA*

Abstract: During the *Intensive Observation Period* (IOP) 9c of the *Convective and Orographically-induced Precipitation Study* (*COPS)* on 20 July 2007 a frontal zone passed over the COPS region, with a Mesoscale Convective System (MCS) imbedded in it. The Raman lidar system *BASIL* which was deployed in Achern (Supersite R, Lat: 48.64 ° N, Long: 8.06 ^{0} E, Elev.: 140 m) in the frame of the *COPS* was operated continuously during this day. The lidar data determined the lowering of the anvil clouds, which is a signature for the approaching thunderstorm. During the time frame 10:46-11:37 UTC cloud deck is present around 2 km, which represents a mid-level outflow from the thunderstorm. Wind profiler data reveal that the wind flow at higher levels is opposite with respect to low level winds. The effect of this is to moisten that level and precipitate (mostly virga) to recycle back. Waves like structures were also seen in the data just prior to the arrival of the thunderstorm, which are due to shear between inflow or outflow regions. Thus, two primary processes stand out: the elevated outflow region above the BL (2-3.5 km) and the presence of associated shear, which helped in modifying the environment. Measurements in terms of particle backscatter and water vapour mixing ratio are discussed to illustrate the above phenomena.

1. INTRODUCTION

On 20 July 2007, an *Intensive Observation Period* (IOP) 9c of the *Convective and Orographically-induced Precipitation Study* (*COPS)* a vorticity maximum at the east side of a jet initiated over middle eastern France triggered cyclogenesis and a Mesoscale System (MCS) propagated north-eastwards. Thus, IOP 9 was particularly an experimental platform to study the development of frontal zones and their influence on the intensity of convection. The MCS reached the measurement site Archen, Rhine valley at around 09:30 UTC. Ahead of the weak cold front related to the cyclone, in which the MCS was imbedded, outflow boundaries produced a squall line with severe thunderstorm activity. The University of Basilicata Raman Lidar (*BASIL)* visualized the interaction of the MCS with the prevailing pre-storm environment and its modification. Additionally during the passage of the squall line, deep convection was triggered in the COPS region modifying the structure of the squall line and of related precipitation pattern. The cold front can also transport aerosols and trace gases from the boundary layer to the free troposphere [Cooper et al 2001, Esler et al, 2003, Stohl et al. 2001]. Water vapor is useful in studying many of the atmospheric dynamic features as it is conserved in all meteorological processes except condensation and evaporation.

The Raman Lidar system *BASIL,* deployed in Achern (Supersite R, Lat: 48.64 ° N, Long: 8.06 ^{0} E, Elev.: 140 m), operated between 25 May and 30 August 2007 and collecting more than 500 hours of measurements, distributed over 58 measurement days. The major feature of *BASIL* is represented by its capability to perform high resolution and accurate measurements of atmospheric temperature and water vapour, both in daytime and night-time, based on the application of the rotational and vibrational Raman lidar techniques in the UV. Besides temperature and water vapour, *BASIL* is capable to provide measurements of particle backscatter at 355, 532 and 1064 nm, particle extinction coefficient at 355 and 532 nm and particle depolarization at 355 and 532 nm. The Raman Lidar system *BASIL* was operated continuously during 20 July 2007 from 04:33 to 19:22 UTC. Below we present analysis of a MCS observed on 20 July 2007.

2. IMPORTANT FEATURES

Figure 1 shows the range corrected signals at 1064 nm during the total observation period from 04:33 to 19:22 UTC. There was presence of low clouds or fog in the valley till 09:30 UTC and development of convective clouds during the afternoon with different precipitation intervals throughout the day. The lidar visualized the interaction of the MCS with the prevailing pre-storm environment and also how it was modified. A signature of thunderstorm approaching is present in the 1064 nm range corrected lidar signals in figure 1, visible in the lowering of the anvil clouds up high. Low level wind below about 1km was towards the centre of the thunderstorm i.e. positive motions towards the centre within the cold air mass at an altitude range of 0.5 to 2.5 Km during the time period 10 to 12 UTC as seen in the wind profiler data from University of Manchester.

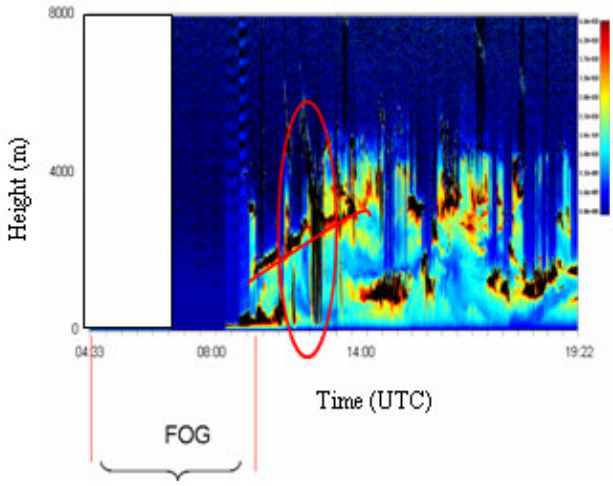

FIGURE 1. Range-corrected signals at 1064 nm during the MCS event.

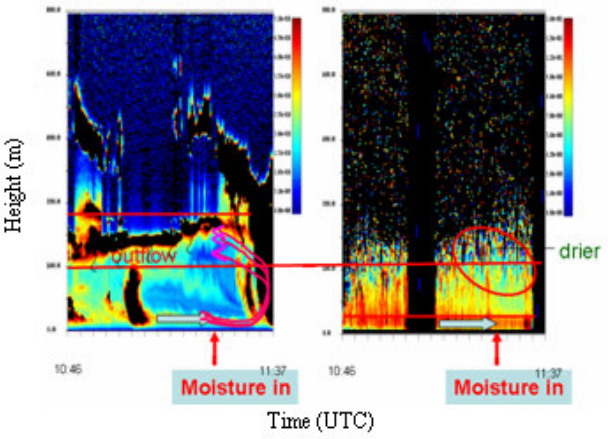

FIGURE 2. Range corrected signals at 1064 nm together with the water vapour mixing ratio data during the MCS (time frame 10:46-11:37 UTC).

The highest wind speed observed was around 15 m/s. Figure 2 shows the range corrected signals at 1064 nm together with the water vapour mixing ratio data during the MCS (time frame 10:46-11:37 UTC). An interesting fact is the cloud deck at 2km, which represents a mid-level outflow from the Thunderstorm/MCS. The wind flow at higher levels is opposite with respect to low level winds. The effect of this is to moisten that level and precipitate (mostly virga). So, we can see a conveyor belt of things here where the thunderstorm mid-level outflow spits out hydrometeor-debris and it is recycled back into it. In the water vapor mixing ratio we observe the moist layer below about 1 km and a drier layer about 2 km. This means that the MCS was modifying the environment at 1.6-2.5 km directly (outflow) and the lower levels through the virga/precipitation. In addition, the MCS can only survive by pulling in moisture from a large area (~100km radius or more) around it (below about 1km), which is somewhat modified by the virga. There is a wave like structure seen in the data just prior to the arrival of the thunderstorm present due to shear between inflow or outflow regions. Two primary and important processes which can be clearly observed are: the elevated outflow region above the BL (2-3.5km) and the presence of associated shear. Shear and mid-tropospheric moistening are important parameters to consider in convection: shear can inhibit convection, but also aid if the waves break and create self sustaining turbulence at the right level. In support of this the 09:08 UTC radiosonde showed a moist layer below about 1 km and a drier layer in the region above 1km: this was the time when the MCS entered the COPS area.

Results shown here demonstrate the excellent capability of Raman lidars in visualizing the detailed vertical and temporal structure of the atmosphere. Fine-scale structures of the boundary layer and between air masses at different altitudes detected, explaining the dynamic processes involved will be presented in the conference.

REFERENCES

1. Cooper, O.R., J.L.Moody, D.D.Parrish, M.Trainer, T.B.Ryeson, J.S. Holloway, G.Hubler, F.C.Fehsenfeld, S.J.Oltmans, and M.J.Evans, " Trace gas signatures of the airstreams within North Atlantic Cyclones:Case studies from the North Atlantic Regional Experiment (NARE'97) aircraft intensive" *J. Geophys. Res.,* **106**, 2001,5437-5456.

2. Esler, J.G., P.H.Haynes, K.S.Law, H.Barjat, K.Dewey, J.Kent, S.Schmitgen, and N.Brough, "Transport and mixing between airmasses in cold frontal regions during Dynamics and Chemistry of Frontal Zones (DCFZ), *J. Geophys. Res.,* **108**, 2003, doi:10.1029/2001JD001494.

3. Stohl, A., "A 1-year Lagrangian "climatology" of airstreams in the Northern Hemisphere troposphere and lowermost strastosphere" *J. Geophys. Res.,* **106**, 2001, 7263-7279.

INFLUENCE OF OROGRAPHY AND AEROSOLS ON THE MICROPHYSICS OF CONVECTIVE CLOUDS OBSERVED DURING COPS

Alan Blyth[1], Yahui Huang[2], Phil Brown[3], Richard Cotton[3], Hazel Jones[4], Tom Choularton[4], Gordon McFiggans[4], Martin Irwin[4], Hugh Coe[4]

[1] National Centre for Atmospheric Science, University of Leeds, Leeds LS2 9JT, UK
E-mail: blyth@*env.leeds.ac.uk*
[2] Institute for Climate and Atmospheric Science, University of Leeds, Leeds LS2 9JT, UK
[3] UK Met Office, Exeter EX1 3PB, UK
[4] School of Earth, Atmospheric and Environmental Sciences, University of Manchester, Manchester M13 9PL, UK

Abstract: Analysis is presented of microphysical data gathered on 2 days during COPS with instruments on the BAe 146 research aircraft. High concentrations of ice particles larger than 150 μm were observed in the 11 July 2007 cloud at temperatures of between -3 and -8 ˚C. In contrast, on 15 July 2007, large ice particles were barely detectable. However, the concentration of small ice particles was significantly higher than observed in the 11 July cloud. This is possibly due to the higher peak concentrations of aerosols that were observed on 15 July consistent with the model prediction of the presence of Saharan dust and the venting of aerosols from the Murg Valley.

Keywords: *COPS, aerosols, venting, convection, ice particles*

1 INTRODUCTION

The Convective Orographically-induced Precipitation Study (COPS) took place over the Black Forest mountains in the summer of 2007. The primary focus was on the formation and development of convective precipitation systems over the mountains. One goal of the project is to determine the properties of aerosol in the convective cloud inflow and to understand the formation and growth of ice and precipitation in the clouds as influenced by the aerosols.

The BAe-146 aircraft, which was equipped with state-of-art microphysics instruments such as the Cloud Particle Imager (CPI) and Small Ice Detector, penetrated developing cumulus clouds on 11 and 15 July 2007 near cloud top. Legs were also made below cloud base to investigate the properties of aerosol particles.

2 ANALYSIS OF IN SITU MEASUREMENTS

Several clouds were penetrated on 11 July as they advected across the COPS domain. It is believed that in one cloud, penetrated near the ascending top, first ice was observed with concentration of 0.04 L^{-1} at temperature of -6 ˚C. In a different cloud, which was in a mature to decaying stage, the concentration of ice particles larger than 150 μm reached to 124 L^{-1} . The high concentration of ice particles exceeds the value estimated from the Meyers formula (Meyers et al., 1992) derived from typical ice nuclei measurements for cloud tops estimated from radar. The observation of the co-existence of numerous ice particles, pristine columns, graupel particles and supercooled drops within the temperature range of -3 to -9 ˚C, suggests that the Hallett-Mossop process of splintering during riming (Hallett and Mossop, 1974) may be responsible for the ice development. Figure 1 shows the details from the penetration of Run 6.1made at a temperature of -5˚C.

Large ice particles were not measured in the clouds penetrated on 15 July. However, the concentration of ice particles smaller than about 55 μm was significantly higher than observed on 11 July. Interestingly, model results suggest that a plume of Saharan dust arrived in the COPS region early on 15 July 2007. There is a difference in the properties of the aerosol measured at the ground-based facility on Hornisgrinde on 11 and 15 July that is consistent with these model results. Higher peak concentrations of aerosols were also observed on the aircraft on 15 July. The analysis of the distributions of aerosol particles from the PCASP averaged over the legs made at similar altitudes in the two cases shows that the total concentration of aerosol and the concentration in each size range are greater on 15 July than on 11 July.

A leg was made over the Murg Valley on 15 July at an altitude of 1.7 km above MSL and below the altitude of cloud base. The track was approximately along the wind direction from SW to NE. Figure 2 shows the vertical wind and the concentrations from the PCASP and CPC. The updraft over the valley is strong with a maximum speed of 5.2 m/s. The width of the updraft is about 2.4 km (Fig. 2). In the core of the updraft the concentrations detected by the PCASP and CPC reached about 1300 cm^{-3} and 5600 cm^{-3}, respectively, while their peak values (1600 cm^{-3} and 7000 cm^{-3}, respectively) were encountered a little later. The concentration remained higher downwind of the valley than on the upwind side.

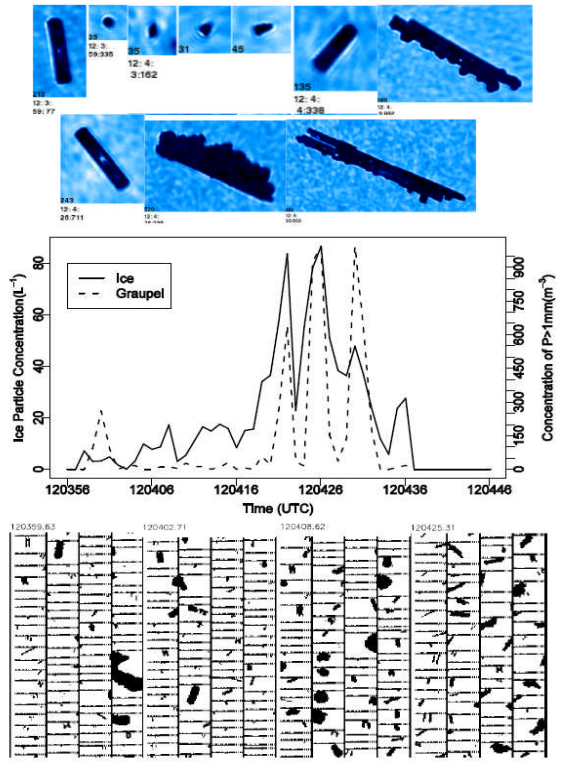

Figure 1. Ice particle concentration (solid line). Examples of particle images from CPI and 2DC are included.

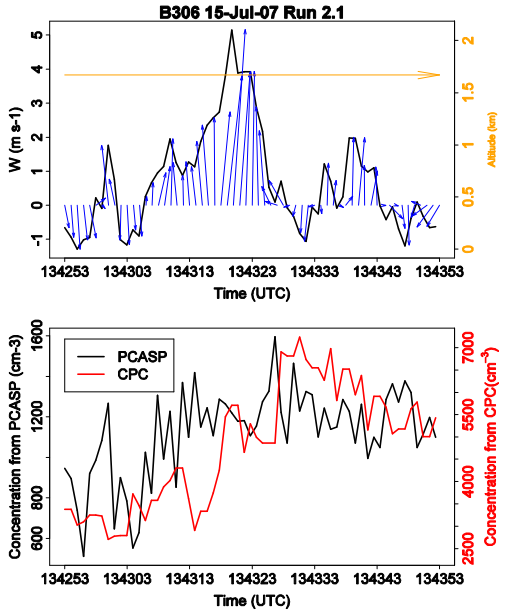

Figure 2. Wind field and aerosol concentration.

3 CONCLUSIONS

The concentration of large ice particles was greater than expected from primary ice nucleation in 11 July cloud. The observations suggest that the Hallett-Mossop process of secondary ice particle production was active and it is likely that the high concentrations could be explained with this mechanism. There are some issues to resolve however. Observations were also made near the ascending tops of some of the clouds that formed near the famous, much-photgraphed 15 July cloud. The analysis offers interesting twists to consider for modelling this cloud: mainly high concentration of aerosols probably associated with Saharan dust; and also venting of aerosols out of the Murg Valley, which likely contributes to the high concentrations. There is some support from the observations, but more modelling and data synthesis needs to be carried out. Venting from the valley was observed on a few other days during COPS suggesting that not only are the valley flows responsible for the convergence lines that help with the initiation of convection, but they may cause transport of aerosols into the clouds. Thus it is possible that the orography played a significant role in altering the microphysical behaviour of the clouds that formed or advected over the Black Forest.

Acknowledgements:
We thank the pilots of the FAAM BAe aircraft for making the flights and all the people involved in the field campaign. The COPS project is supported by the Natural Environment Research Council.

REFERENCES

Hallett, J. and S. C. Mossop, 1974: Production of secondary ice particles during the riming process. Nature, 249, 26-28.

Kalthoff, N., B. Adler, Ch. Barthlott, U. Corsmeier, S. Mobbs, S. Crewell, K. Träumner, Ch. Kottmeier, A. Wieser, and V. Smith, 2009: The impact of convergence zones on the initiation of deep convection: A case study from COPS. Atmospheric Research, doi:10.1016/j.atmosres.2009.02.010

Meyers, M. P., P. J. DeMott, and W. R. Cotton, 1992: New primary ice-nucleation parameterizatios in an explicit cloud model. J. Appl. Meteor., 31, 708-721.

Idealized Numerical Sensitivity Studies on Shallow-Convection-Triggered Storms in a Low Mountain Range

Ulrich Blahak[1]

[1] Institut für Meteorologie und Klimaforschung, Karlsruhe Institute of Technology (KIT), Karlsruhe, Germany
E-mail: *ulrich.blahak@imk.fzk.de*

Abstract: In this paper, the explicit numerical simulation of shallow convective motions and subsequent triggering of an ensemble of interacting convective cells using the COSMO-model and the newly modified Seifert-Beheng two moment bulk microphysical scheme is investigated, applying horizontal grid spacings of 100 - 500 m. Using idealized orography and initial conditions, shallow convection is forced by specifying suitable sensible and latent heat fluxes at the surface. It is shown that the used model setup and turbulence parameterization are adequate to simulate the spin-up of an ensemble of cells with, after a certain time of self-organization, take on realistic mutual distances and maximum vertical updraft speeds. In comparison with the more traditional idealized single storm simulations (triggered by, e.g., "warm bubble" or mountain wave flow) the presence of interactions with neighbouring cells leads to a (possibly) more realistic framework for sensitivity studies (microphysics, triggering mechanisms) on convective clouds.

***K*eywords:** *Shallow convection, deep convection, transition, cloud microphysics, precipitation, idealized simulations*

1 INTRODUCTION

In order to elaborate parameters crucially influencing the characteristics of convective cells, idealized high resolution cloud resolving simulations with the COSMO-model are performed using the two-moment bulk microphysical scheme of Seifert and Beheng (2006). A newly modified version is used, based on the recent extention of the scheme by considering a class of high density particles ("hail") in addition to cloud droplets, rain, cloud ice, snow and graupel.

In past idealized simulations, single convective systems have been artificially triggered either by the classical "warm bubble" approach or by wave flow over idealized orography. The numerical results often exhibited rather strong maximum updraft speeds (w > 50 m s^{-1}) and a rather quick lateral spreading of multicell/supercell type systems over the entire model domain, often accompanied by a comparatively low precipitation efficiency and low simulated radar reflectivity in the upper part of the cells.

Only a slight improvement has been obtained by changing microphysical parameters and process descriptions in the 2-moment microphysics scheme (Blahak, 2008). Therefore, we guess that another parts of the problem may be 1) the highly artificial trigger mechanism and 2) the fact that the simulated systems developed isolated and in a rather "pristine" environment, lacking interactions with neighbouring circulation patterns.

Accordingly, idealized simulations are altered by specifying an idealized daily cycle of the surface fluxes over hilly terrain (idealized hills, ridges), repesentative for a sunny summer day, such that a broad spectrum of convective structures simultaneously appears. In this way, the relevant circulation scales (shallow convection) spin up by themselves and, after removal of CIN, deep convective cells develop. To resolve the necessary spatial scales, we use model resolutions down to 100 m horizontally and approx. 50 m vertically within the PBL.

This kind of "quasi" LES simulations has been performed in the past by various authors to investigate warm shallow cumulus clouds. However, most of them did not apply such a detailed cloud microphysical parameterization and did not focus on sensitivity studies on deep convective mixed phase clouds. Balaji (1988) is one of the few who simulated the development of a deep convective cloud in a very similar fashion (but with coarser grid spacing).

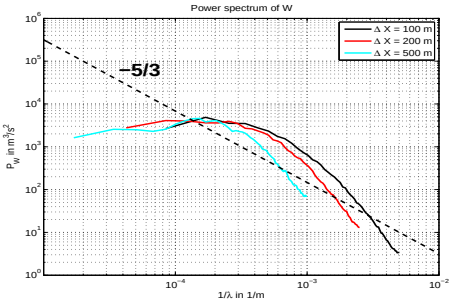

Figure 1: Mean horizontal power spectra of W in Y-direction in m^{3}s^{-2} as function of inverse wavelength in m^{-1} for simulations with ΔX = 100 m, 200 m and 500 m.

2 FROM SHALLOW TO DEEP CONVECTION

For our idealized simulations, the original soil- and radiation modules as well as any convection parameterization are turned off. The idealized daily cycle of sensible and latent heat fluxes H and E (max. H = 300 W m^{-2}) takes into account the effects of sloping terrain, slant cloud shadows and precipitation. Fully periodic lateral boundary conditions are used. Typical horizontal grid spacings for our simulations range from 100 m to 1 km. A suitable 3D turbulence closure is used which combines a Smagorinsky-type LES formulation of the turbulent lenght scale with a 1.5th order TKE closure for the turbulent diffusion coefficients (Herzog et al., 2002). The ratio of the horizontal to vertical turbulent diffusion coefficients is chosen to be 3.

Fig. 1 shows space-time-average power spectra of W in Y-direction within the planetary boundary layer (PBL) for simulations of dry shallow convection as function of the model grid spacing for a weak wind situation. Initially, the PBL is slightly stable, and shallow convection patterns develop gradually from small initial noise into a developing convective boundary layer. It is evident that, even at ΔX = 100 m, the scales of shallow convection ($\approx$ 200 – 500 m) lie within the slightly over-damped short-wave tail and not all details of this phenomenon are realistically simulated.

However, the spatial distribution of updrafts and downdrafts, updraft strengths of thermals as well as organization patterns look qualitatively ok up to $\Delta X = 300$ m, also for simulations with higher windspeed (no figures shown). Therefore, it seems that for our purpose (which is triggering of deep convective cells with realistic mutual distances), the coarsest possible grid spacing may be in the range of 300 m.

Using $\Delta X = 300$ m and activating the cloud microphysics parameterization results in an ensemble of interacting cells, like it is shown in Fig. 2 as a MAX-Cappi picture of simulated radar reflectivity. A gaussian mountain (height 500 m, half-width 20 km) in the center of the domain generated a first cell by anabatic winds (overheated south-eastern flank), and the figure captures about the time at which other cells in the surrounding area begin to develop (1:40 h after simulation start).

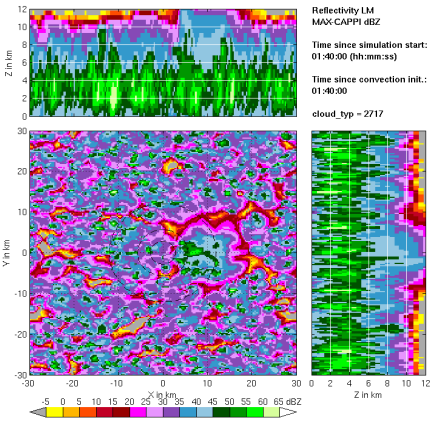

Figure 2: MAX-CAPPI of simulated radar reflectivity in dBZ after 1:40 h for the simulation with "low CCN" and "warm" environment.

3 SENSITIVITY ON TEMPERATURE REGIME AND AEROSOL CONDITIONS

In continuation of the work presented in Blahak et al. (2006), in which a single multicellular system has been initiated by pure mountain wave flow, the effect of different temperature levels in combination with low-CCN- and high-CCN-aerosol regimes on shallow-convection-triggered cells is investigated.

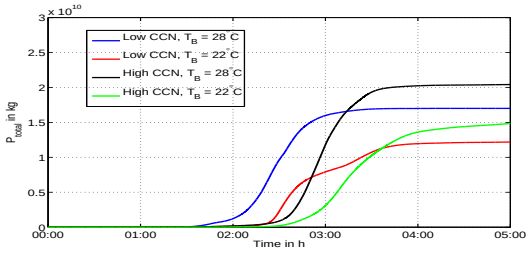

Figure 3: Time series of accum. precip. for the 4 cases. "warm" = "28°C"; "cold" = "22°C"

To this end, four simulations of the type described at the end of the last section are presented, which constitute all possible combinations of a "warm" and "cold" environment with "high-CCN" and "low-CCN" conditions, each with the same initial $CAPE \approx 1900\ \mathrm{J\,kg^{-1}}$ and at low windspeed. To summarize the results, the time series of the total accumulated precipitation (Fig. 3) show that for the simulated type of widespread "popcorn like" convection and for the specific prescribed atmospheric conditions, the effect of increased aerosol load is mainly a time delay of the precipitation, but no reduction of its amount. The "cold" environment leads to less precipitation compared to the "warm".

The simulated convection exhibits a typical life cycle of about 4 – 5 h, caused by the widespread convective vertical exchange processes and removal of $CAPE$, and maximum updraft speeds are $\approx 40\ \mathrm{m\,s^{-1}}$. Vigorous lateral spreading of cells (which has been observed the earlier study mentioned above) is hindered by interactions with neighbouring cells. Such interaction-effects will be explored in more detail in the future.

However, the sensitivities presented above strongly depend on details of the parameterizations of autoconversion, cloud nucleation and ice phase processes, which means that our results may not be generalized, and further investigations are necessary.

4 CONCLUSIONS

To study cloud microphysical sensitivities in an idealized framework using the COSMO-model and an advanced cloud microphysics parameterization, an ensemble of interacting neighbouring convective cells is triggered by (differential) surface heating and the resulting shallow convective motions. Using a simple LES 3D turbulence closure and grid spacings smaller than 300 m leads to results which seem to be "realistic enough" for this purpose. Such studies are a valuable alternative to the more traditional idealized "warm bubble" triggered single-convective-system studies and enlarge the scope to interaction effects of neighbouring cells.

REFERENCES

Balaji, V. and T. L. Clark, 1988: Scale selection in locally forced convective fields and the initiation of deep cumulus, *J. Atmos. Sci.*, **45**, 3188–3211.

Blahak, U., H. Noppel and K. D. Beheng, 2006: Influence of ambient environmental conditions and orography on the characteristics of deep convective cells as simulated with a sophisticated two-moment (bulk) microphysical scheme, 12. AMS Conference on Cloud Physics, 10. – 14.7.2006, Madison, Wisconsin, available online: http://ams.confex.com/ams/pdfpapers/113531.pdf.

Blahak, U., 2008: Towards a better representation of high density ice particles in a state-of-the-art two-moment bulk microphysical scheme, International Conference on Clouds and Precipitation, 7.7. – 11.7.2008, Cancun, Mexico.

Herzog, H.-J., G. Vogel and U. Schubert, 2002: LLM – A nonhydrostatic model applied to high-resolution simulations of turbulent fluxes over heterogeneous terrain, *Theor. Appl. Climatol.*, **73**, 67–86.

Seifert, A. and K. D. Beheng, 2006: A two-moment cloud microphysics parameterization for mixed-phase clouds. Part I: Model description, *Meteorol. Atmos. Phys.*, **92**, 45–66.

Scaling relations in warm-rain orographic precipitation

Axel Seifert, Günther Zängl

Deutscher Wetterdienst, Offenbach, Germany
E-mail: *axel.seifert@dwd.de*

Abstract: Warm rain orographic precipitation at an isolated mountain is studied by numerical experiments using the non-hydrostatic COSMO model. The simulations are analyzed in terms of precipitation amounts, precipitation efficiency and spillover factor as a function of the relevant microphysical and advective timescales and Froude numbers. For the microphysical conversion timescale a new formulation is applied based on an analysis of the stochastic collection equation. This new estimate of the warm rain microphysical timescale couples the rain formation to the forcing by condensation, i.e. updraft velocity and liquid water lapse rate, and microphysical properties like the cloud droplet number concentration. Using this microphysical timescale the scaling relations for warm-rain orographic precipitation for an isolated mountain are revisited.

***K*eywords:** *ICAM, orographic precipitation, precipitation formation, mountain flow, aerosol-cloud-precipitation effects*

1 INTRODUCTION

Understanding the warm rain formation at an isolated mountain is a classical, yet to some extent unsolved problem. The inherent difficulties arise due to the coupling of two non-linear systems, the hydrodynamic mountain flow and the rain formation by collision-coalescence. Various attempts have been made to formulate the orographic rain formation by simple scaling relations, see e.g. Jiang and Smith (2003) and the review of Smith (2006). A weak point of the previous studies is the oversimplified approach to cloud microphysics, often just described by a constant rain formation timescale. In the following a new rain formation timescale is presented which can be traced back to the stochastic collection equation itself. This timescale is then used to analyze and rationalize the results of a three-dimensional non-hydrostatic model.

2 WARM-RAIN TIMESCALE

The rain formation timescale follows the ideas of Stevens and Seifert (2008) and Seifert and Stevens (2009). They define the time τ_*, a measure for the onset of the first in-cloud rain, by a balance of production of cloud water by condensation and its depletion by the collision-coalescence process. For brevity the derivation of τ_*, which is based on the Seifert and Beheng (2001, SB2001 hereafter) warm rain scheme, is not repeated here, but the result is simply stated from Eq. (29) of Stevens and Seifert (2008):

$$\tau_* = \left[\beta_* + \sqrt{\beta_* + \frac{\tau_0^4}{(1-\epsilon_*)^4 \phi_{cc}(\epsilon_*)}} \right]^{1/2} \qquad \text{with} \qquad \beta_* = \frac{k_{cr}\, N_c^2}{2\, k_{\text{au}}} \, \frac{\epsilon_* \, \phi_{cr}(\epsilon_*)}{(1-\epsilon_*)^3 \phi_{cc}(\epsilon_*)} \tag{1}$$

and $\tau_0 = N_c^{1/2}\, \tau_{\text{cond}}^{3/4}\, k_{\text{au}}^{-1/4}$. Here N_c is the cloud droplet number concentration, τ_{cond} the condensation timescale, and ϵ_* the rain fraction at the time τ_*. The ϕ_{cc} and $\phi_{cr}(\epsilon)$ are the similarity functions of SB2001 for autoconversion and accretion. The autoconversion parameter k_{au} depends on the shape parameter ν of the cloud droplet size distribution, k_{cr} is the kernel coefficient for accretion. For further details, e.g. how to estimate ϵ_*, it is referred to Seifert and Stevens (2009). This warm-rain timescale has two advantages over previous formulations: First, it has been derived from the stochastic collection equation and includes all relevant microphysical sensitivities. Second, by including the condensation timescale τ_{cond} it is coupled to the dynamics of the cloud, since $\tau_{\text{cond}}^{-1} = w\, \Gamma_l$ with the updraft velocity w and the liquid water lapse rate Γ_l.

3 MODEL SETUP

Using the non-hydrostatic COSMO model we investigate the 3-d mountain flow across an isolated bell-shaped hill with height $h(x) = H/(1 + x/a)^{3/2}$ and a mountain half-width a. As initial condition we use a moist stable stratification, with the moisture in the lowest kilometer being close the saturation value. The simulations are performed with 1 km grid spacing on a 250×101 domain with 50 vertical levels. As microphysics scheme we use the SB2001 warm rain scheme with a fixed cloud droplet number concentration. Using a fixed initial condition for moisture and temperature we investigate the dependency of the flow and the resulting clouds and precipitation on the wind speed U_0, the mountain height H, mountain width a, and the cloud droplet number concentration N_c.

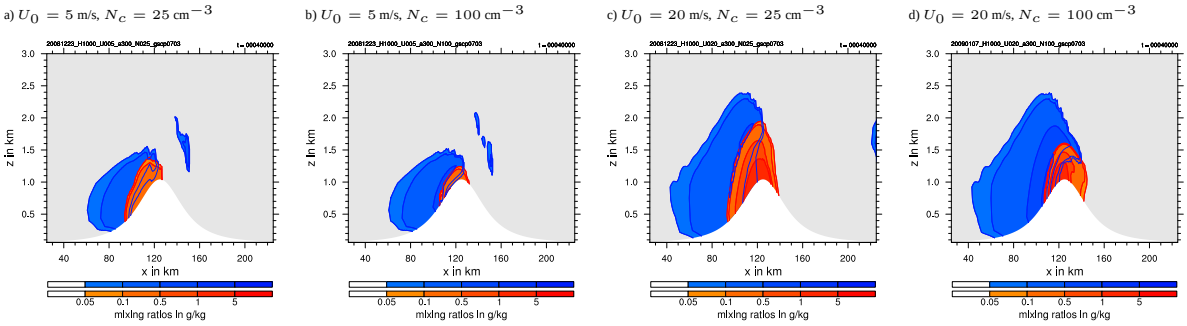

Figure 1: Vertical cross sections of cloud (blue) and rain (red) mixing ratios for different wind speeds and cloud droplet number concentrations ($H = 1000$ m, $a = 30$ km).

4 A FEW PRELIMINARY RESULTS

Figure 1 shows cross sections of the simulated orographic cloud for 4 different configurations. As expected, increasing the cloud droplet number concentration from 25 cm^{-3} to 100 cm^{-3} slows down the rain formation in the cloud resulting in less rain that is shifted to the mountain top. Increasing the wind speed leads to a bigger and thicker cloud which produces more rain, but is also susceptible to variations in the cloud droplet number concentration. Overall more than 1000 simulations of this type have been performed.

Figure 2 shows a result for the precipitation efficiency E_c, defined as surface precipitation amount over total condensate in the volume, for various simulations varying U_0 and N_c only. E_c is plotted as a function of the ratio of the advective timescale $\tau_{\text{adv}} = a/U_0$ and the microphysical timescale $\tau_*(N_c)$. For each U_0 there is a certain ratio τ_{adv}/τ_*, i.e. a certain N_c, at which surface precipitation starts. For large τ_* (higher N_c) no surface rain occurs, for smaller τ_* (lower N_c) we find first a linear increase of the precipitation efficiency with τ_{adv}/τ_*, and then the system goes into saturation when an efficiency of about 40-50 % is reached. Unfortunately, the curves for different U_0 do not fall onto each other. We argue that this is due to the oversimplified formulation of the advective timescale $\tau_{\text{adv}} = a/U_0$. There are probably two modifications necessary: (1) For larger U_0, or U_0/N with Brunt-Vaisala frequency N, the mountain wave becomes larger and therefore the advective timescale decreases more slowly than U_0^{-1}. (2) For small Froude numbers $U_0/(N\ H)$ the flow will prefer flow-around instead of flow-across the mountain resulting in a larger advective timescale.

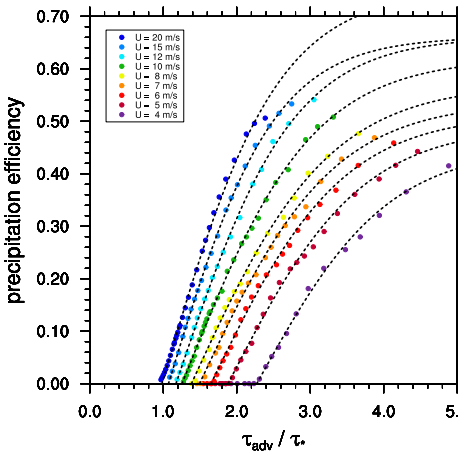

Figure 2: Precipitation efficiency for various simulations with $U_0 \in [4-20]$ m/s and $N_c \in [20-700]$ cm^{-3} as a function of the ratio of the advective timescale $\tau_{\text{adv}} = a/U_0$ and the microphysical timescale τ_* ($H = 1000$ m, $a = 30$ km).

5 CONCLUSIONS AND OUTLOOK

We presented a refined approach to rationalize the warm-rain orographic precipitation problem. The basic idea follow previous work of Jiang and Smith (2003) an others, but is now extended to a more sophisticated microphysical timescale. We argue that a more detailed formulation of the advective time scale is also necessary that includes the linear mountain wave effect as well as non-linear Froude number effects.

REFERENCES

[1] Jiang, Q., and Smith, R.B., 2003: Cloud timescale and orographic precipitation. *J. Atmos. Sci.*, **60**, 1543–1559.

[2] Stevens, B. and Seifert, A., 2008: On the sensitivity of simulations of shallow cumulus convection to their microphysical representation. *J. Meteorol. Soc. Jap.*, **86**, 143–162.

[3] Smith R.B., 2006: Progress on the theory of orographic precipitation. *in Willett, S.D. et al. Tectonics, Climate and Landscape evolution*, Geological Society of America Special Paper 298.

[4] Seifert, A. and Beheng, K.D., 2001: A double-moment parameterization for simulating autoconversion, accretion and selfcollection. *Atmos. Res.*, **59-60**, 265–281.

[5] Seifert, A. and Stevens, B., 2009: Microphysical scaling relations in a kinematic model of isolated shallow cumulus clouds, *J. Atmos. Sci.*, submitted.

THE INFLUENCE OF THE FREEZING LEVEL ON OROGRAPHIC PRECIPITATION PATTERNS AT SMALL SCALES

Günther Zängl

Deutscher Wetterdienst, Offenbach, Germany
E-mail: *Guenther.Zaengl@dwd.de*

Abstract: Idealized numerical simulations have been conducted to investigate the influence of the freezing level on precipitation patterns over narrow mountain ridges. The focus is on precipitation enhancement via the seeder-feeder mechanism, implying that widespread precipitation is locally enhanced by orographic lifting. The results indicate a marked sensitivity to the location of the freezing level with respect to the mountain peak height. For freezing levels significantly below or above the peak height, a single precipitation maximum near the mountain peak dominates, whereas for a freezing level near the peak height, the precipitation maximum tends to be shifted towards the lee slope. Analysis of the model results indicates that this is partly related to the fall-speed-difference between snow and rain and partly to the higher accretion efficiency of snow than of rain.

***K*eywords:** *Orographic precipitation, seeder-feeder mechanism*

1 INTRODUCTION

It has been known for quite a long time that mountainous orography can induce marked small-scale variability of precipitation, not only for single events but also on climatological time scales. This variability is related to various mechanisms of orographic precipitation enhancement, the most important of which being orographic triggering of convection and local intensification of stratiform precipitation via the seeder-feeder mechanism. A systematic spatial variability in climatological rainfall amounts appears in the first case if there are preferred triggering locations of convection, whereas in the second case the largest effect arises when precipitation predominantly falls in a narrow range of wind directions. At small scales, precipitation enhancement through the seeder-feeder mechanism usually leads to local precipitation maxima somewhere over the lee slopes of individual mountain ridges because of hydrometeor advection (e.g. Carruthers and Choularton, 1983). A more subtle aspect of seeder-feeder-induced precipitation enhancement, which was recently discovered by Zängl (2008) and Zängl et al. (2008), is an apparent temperature dependence of the enhancement intensity. Specifically, data analysis suggested that climatological precipitation enhancement over the lower lee slope of individual mountain ridges exhibits a correlation between ridge height and the height of the freezing level, in the sense that higher (lower) mountains induce larger precipitation enhancement for higher (lower) freezing levels. To gather more insight into this phenomenon, particularly into the underlying physical processes, idealized numerical simulations with the Penn State/NCAR mesoscale model MM5 have been conducted.

2 MODEL SETUP

The simulations discussed in the following have been conducted with four interactively nested model domains, having a finest horizontal mesh size of 750 m. The model topography is composed of a wide plateau-like elongated ridge with a height of 1000 m, and four small-scale mountains located on the upper windward slope of the basic ridge with an excess height of 400 m, 800 m, 1200 m and 1600 m, respectively (see Fig. 1a). The purpose of the basic ridge is to generate large-scale atmospheric lifting and thereby widespread moderate precipitation, providing the basis for seeder-feeder-induced enhancement over the small-scale mountains. The atmospheric conditions assumed in the simulations involve a ridge-normal flow with positive shear from 12.5 m s^{-1} at sea level to 25 m s^{-1} at tropopause level, and constant wind speed higher above, and a nearly saturated moisture field up to a pressure of 400 hPa. Seven different temperature profiles are considered with freezing levels ranging from 2800 m (T1) to 400 m (T7) at nearly equal steps, each having a lower-tropospheric moist Brunt-Väisälä-frequency of about 5×10^{-3} s^{-1}. The simulations use a PBL parameterization to account for surface friction and a sophisticated mixed-phase microphysics scheme including graupel (Tao and Simpson, 1993). For further details see Zängl (2008).

3 RESULTS

Simulated precipitation amounts are displayed in Fig. 1b,c along cross-sections through the 800-m and 1600-m mountains (lines AA' and BB' in Fig. 1a). They refer to an accumulation period of 6 hours, starting at a simulation time of 9 h. Inspecting the results for the different temperature profiles, one notices that the warmest (T1) and the two coldest (T6, T7) profiles produce a single precipitation maximum near the mountain top (dashed line). However, substantially different precipitation patterns are found for the intermediate temperature profiles: For the

800-m mountain (Fig. 1b), T2 still has a single maximum near the peak but a slower precipitation decay in the lee than T1. Continuing this trend, T3 exhibits a secondary maximum over the lower lee slope ($x \approx 5$ km), turning into the primary maximum for T4. With further decreasing temperatures (T5), the leeside precipitation maximum starts to shift back to the mountain peak. A qualitatively similar behaviour is found for the 1600-m mountain (Fig. 1c), but the pattern sequence is shifted towards higher temperatures. Now, the T2 run already features a marked secondary precipitation maximum over the lee slope, turning into the primary one for T3. The T4 run now shows a single maximum over the lee slope as the T5 run did for the lower mountain, whereas for the T5 run, the precipitation maximum has almost retreated to the mountain top. Obviously, these model results are consistent with the above-mentioned temperature-dependence of observed precipitation enhancement in the immediate lee of small-scale mountains.

Further inspection of the results suggested that a complex interaction between cloud microphysics and hydrometeor transport is responsible for the apparent temperature-dependence of the precipitation patterns. The first factor arises from the fact that the accretion efficiency of snow and graupel is higher than that of rain because of their slower fall speed and larger surface area. Thus, hydrometeor growth attains a maximum right above the freezing level when the freezing level intersects the mountain or lies close to the mountain top (otherwise, the vertical decrease of lifting compensates for this effect). This favours a leeside precipitation maximum when the freezing level is close to the mountain peak height. The second factor is related to the fall-speed difference between snow/graupel and rain. In case of strong winds following the topography and the freezing level crossing the topography, this fall-speed difference induces a local minimum (maximum) of the surface precipitation rate on the windward (lee) side above (below) the freezing level due to a local divergence (convergence) of hydrometeor trajectories. For a freezing level close to the mountain peak height, this again favours a precipitation maximum over the lee slope.

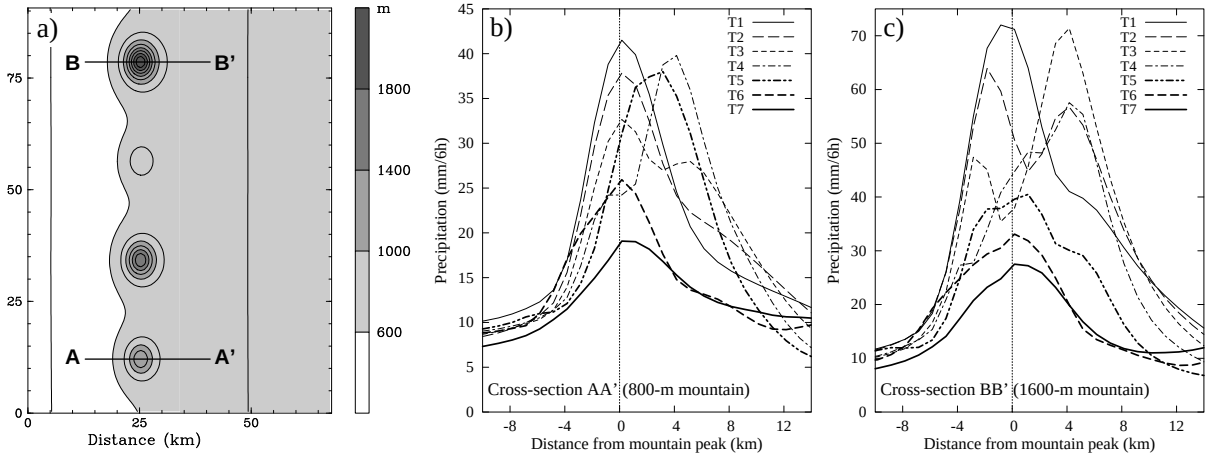

Figure 1: (a) Topography of the finest model domain, contour interval 200 m with additional shading increments every 400 m. Bold lines denote the cross-sections shown in (b,c). (b,c) Accumulated precipitation (mm/6h; accumulation period 9h–15h) for the 800-m and 1600-m mountains, respectively. See text for further explanation.

4 CONCLUSIONS

Based on these results, it can be concluded that the idealized simulations presented here qualitatively reproduce the observed phenomenon and provide plausible hypotheses about the underlying physical mechanisms

REFERENCES

Carruthers, D. J., and T. W. Choularton, 1983: A model of the feeder-seeder mechanism of orographic rain including stratification and wind-drift effects. *Quart. J. Roy. Met. Soc.*, **109,** 575–588.

Tao, W-K, and J. Simpson, 1993: Goddard cumulus ensemble model. Part I: Model description. *Terr., Atm. Ocean. Sci.*, **4,** 35–72.

Zängl, G., 2008: The temperature dependence of small-scale orographic precipitation enhancement. *Quart. J. Roy. Met. Soc.*, **134**, 1167–1181.

Zängl, G., D. Aulehner, C. Wastl, and A. Pfeiffer, 2008: Small-scale precipitation variability in the Alps: Climatology in comparison with semi-idealized numerical simulations. *Quart. J. Roy. Met. Soc.*, **134**, 1865–1880.

DRIVING PROCESSES FOR DEEP CONVECTION OVER CONPLEX TERRAIN: COPS OBSERVATIONS AND RESPECTIVE COSMO SIMULATIONS

Ulrich Corsmeier[1], Christian Barthlott[1], Norbert Kalthoff[1], Heike Konow[1], Christoph Kottmeier[1], Volker Wulfmeyer[2], Andreas Behrendt[2], and the COPS Team

[1] Institute for Meteorology and Climate Research, Karlsruhe Institute of Technology, Karlsruhe, Germany
E-mail: *ulrich.corsmeier@imk.fzk.de*
[2] Institute of Physics and Meteorology, University of Hohenheim, Stuttgart, Germany

Abstract: Data of COPS IOP 9c measured at July 20, 2007 were used to analyse the interaction of convection initiating processes of different scales. A weak cold front passing the COPS area in the morning from west to east was further weakened over the Rhine valley and partly strengthened by a gust front resulting from a MCS behind the front. Further convection initiation appears from a thermally driven convergence zone east of the Black Forest and valley and slope winds over the low mountain range. This leads to a series of severe convective systems in front of the former cold front. Model simulations with COSMO-DE show a not sufficient representation of the sub synoptic scale convection driving processes. Although moisture convergence and CAPE are simulated roughly at the right location, they are not strong enough to initiate deep convection und subsequent precipitation.

Keywords: *COPS, convection initiation, observation, modelling, scale interaction, moisture convergence, ICAM*

1 INTRODUCTION

The "Convective and Orographically induced Precipitation Study" (COPS), aims on the forecast improvement of convectively driven precipitation by mesoscale models. COPS was mainly funded by the DFG and took place from June to August 2007 in southwestern Germany and eastern France over the low mountain ranges of the Black Forest and the Vosges mountains.

2 MEASUREMENTS

During IOP 9c a mesoscale convective system (MCS), visible by a distinct surface low over eastern France, propagated north-eastward and a gust front of the MCS reached the COPS region in the morning. During the passage of the gust front from west to east through the Rhine valley, the convective weather activity was significantly reduced. When the air reached the western slope of the Black Forest, the air has been lifted to propagate over the mountain range. More to the east the sky was still free of clouds and radiation led to a high air temperature of up to 30 °C, to the formation of local slope and valley circulations, and on larger scale to the development of a north – south orientated convergence line over the northern Black Forest. The interaction of local scale orographic winds, the regional scale gust front, the mesoscale convergence line and the cold front led to organized deep convection over the eastern Black Forest and the Swabian Jura.

The transformation of stable air masses passing the Rhine Valley into air masses of high instability when passing the Black Forest is studied by analysis of airborne measurements and data of ground based in situ and remote sensing instruments. Upper tropospheric forcing and ground based lifting processes are discussed with special emphasis of the high spatial and temporal variability of the atmospheric stability and the humidity within the boundary layer.

3 COSMO-DE MODELLING

Model simulations of COSMO-DE without convection parameterisation are compared with the measurements. It is shown that larger scale features with horizontal scales far above the model resolution of 2.8 km like the cold front of the MCS and partly the convergence line with the resulting moisture convergence and CAPE over the Black Forest are reasonably represented in the model. The amplification of the convergent flow especially over the northern Black Forest by small scale forces (gust front and orographic winds) are suboptimal resolved in COSMO-DE. This results in missing deep convection and subsequent precipitation along the convergence line in the model and leads to insufficient precipitation forecast.

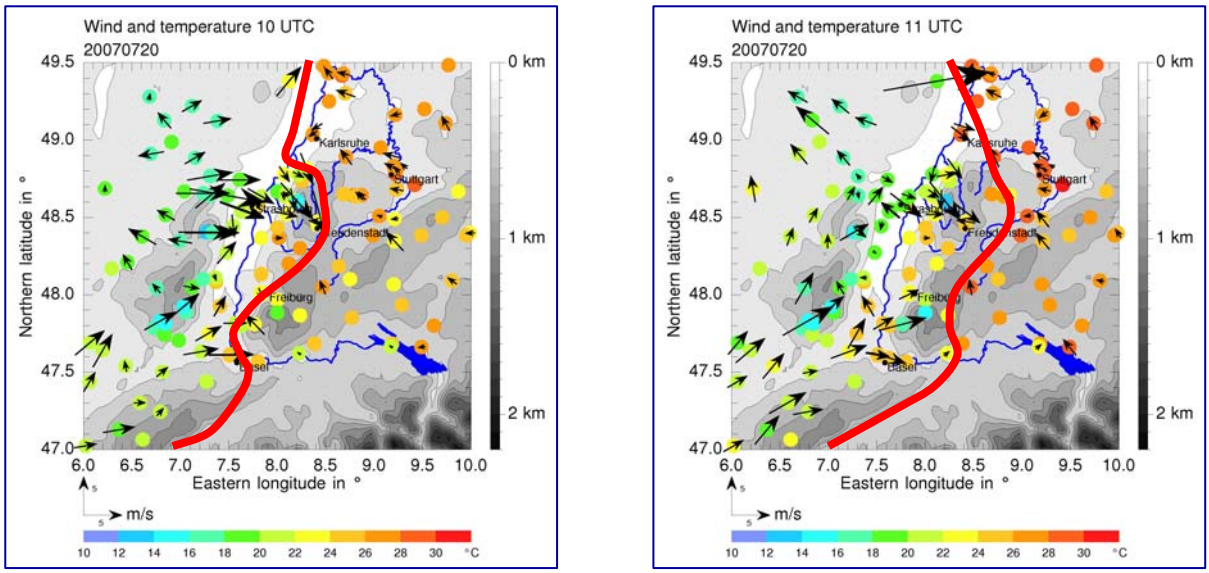

Fig. 1: A gust front is reaching the northern Black Forest. There are still easterly winds in the East. The temperature gradient is increasing (14 K). There is high cloud coverage in the West (10 UTC, left). A convergence line is developing east of Black Forest. Wind increases up to 6 ms^{-1} from opposite directions. The gust front is locally enhanced by orography. The temperature gradient is increasing. Convection is initiated (11UTC, right).

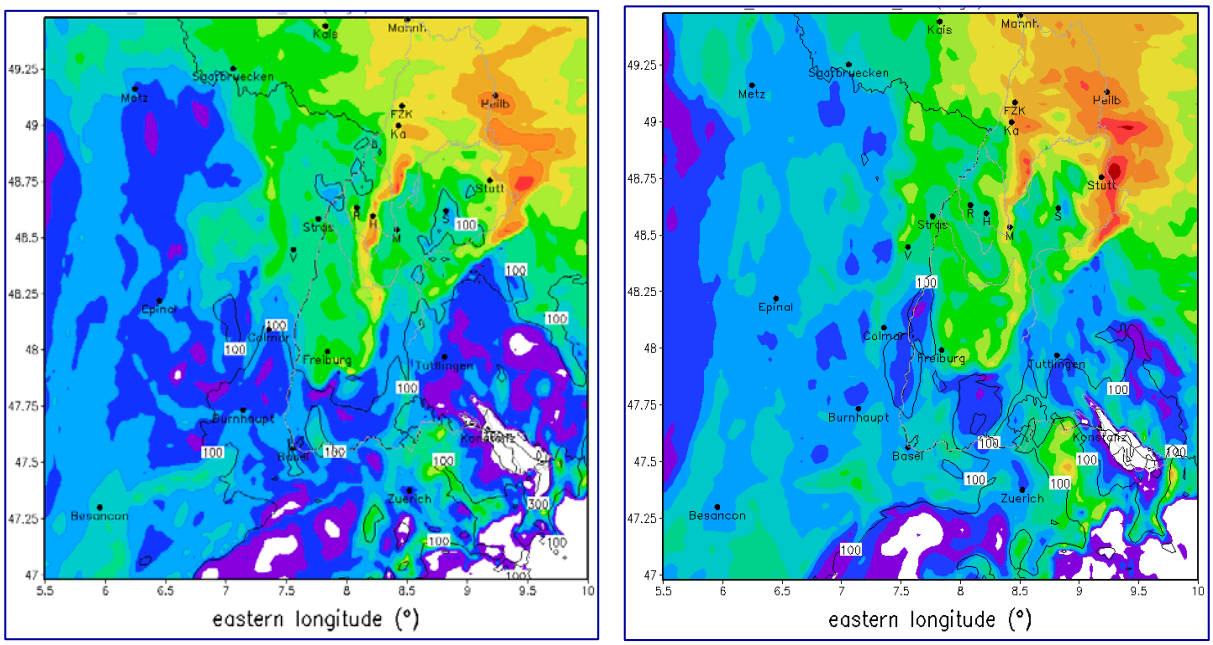

Fig. 2: Simulated CAPE increasing along simulated moisture convergence and observed gust front (~2500 J kg-1). CI is detected by radar along the high CAPE line (10 UTC, left). Weak convergence causes CAPE line moving east and CAPE maximum near Stuttgart moving west and increasing. CI observed in reality but not in the model (11 UTC, right).

REFERENCES

Kalthoff, N., B. Adler, Ch. Barthlott, U. Corsmeier, S. Mobbs, S. Crewell, K. Träumner, Ch. Kottmeier, A. Wieser, V. Smith, P. Di Girolamo, 2009: The impact of convergence zones on the initiation of deep convection: A case study from COPS, Atmos. Research, in press.

Kottmeier, Ch., N. Kalthoff, U. Corsmeier, Ch. Barthlott, J. Van Baelen, A., Behrendt, R. Behrendt, A. Blyth, R. Coulter, S. Crewell, M. Dorninger, C., Flamant, Th. Foken, M. Hagen, C. Hauck, H. Höller, H. Konow, M. Kunz, H., Mahlke, S. Mobbs, E. Richard, R. Steinacker, T. Weckwerth, A. Wieser, and V. Wulfmeyer, 2008: Mechanismus initiating deep convection over complex terrain during COPS, Meteorol. Z., **17** (6), 931-948, DOI 10.1127/0941-2948/2008/0348.

Wulfmeyer, V., Behrendt, A., Kottmeier, Ch., Corsmeier, U., et. al., 2008: The Convective and Orographically-induced Precipitation Study: A Research and Development Project of the World Weather Research Program for Improving Quantitative Precipitation Forecasting in Low-mountain Regions Bull. Amer. Meteor. Soc., **89** (10), 1477-1486.

FORECASTING SUMMER CONVECTION OVER THE BLACK FOREST: A CASE STUDY FROM THE COPS EXPERIMENT

Evelyne Richard[1], Jean-Pierre Chaboureau[1], Cyrille Flamant[2], Cédric Champollion[3]

[1] Laboratoire d'Aérologie, CNRS and Université Paul Sabatier, Toulouse, France
E-mail: *Evelyne.Richard@aero.obs-mip.fr*

[2] LATMOS, CNRS and Université Pierre et Marie Curie, Paris, France
[3] Géosciences Montpellier, France

Abstract: On 15 July 2007, in a very warm but also very dry environment, an isolated short-lived deep convective storm developed over the Black Forest in the late afternoon. Very few of the high-resolution models involved in COPS were able to capture this event. Based on various Meso-NH simulations, the conditions leading to the development of the storm have been investigated and carefully checked against a variety of observations. Although the modelled storm tends to appear a few kilometres south of the observed one, it is clear that the triggering and propagation of the storm are strongly controlled by the presence of a low-level convergence line, roughly north-south oriented, located along the crest line of the Black Forest massif and propagating eastwards.

Keywords: *ICAM, convection, mountainous area, COPS*

1 INTRODUCTION

On 15 July 2007, the COPS area is located in the transition zone between an eastern European ridge, stretching from the Mediterranean Sea to Poland and a high amplitude eastern Atlantic trough. The associated large scale forcing is very weak (Kottmeier et al. 2008). The different soundings performed in the COPS area exhibit only moderate values of Convective Available Potential Energy (CAPE) and relatively high values of Convective Inhibition (CIN, Adler et al. 2009). Under such conditions, convection triggering is unlikely. However a line of deep convective clouds reaching 12 km develop over the southern Black-Forest during the early afternoon.

2 MODEL RESULTS

The numerical simulations are performed with the French non-hydrostatic mesoscale model Meso-NH. During the COPS field experiment the model is run on three interactive 2-way nested domains with horizontal mesh sizes of 32, 8, and 2 km. The convection scheme is activated for the coarser grids while convection is assumed to be explicitly resolved for the 2-km grid. The bulk explicit microphysical scheme accounts for seven water species (vapor, cloud water, liquid water, pristine ice, snow, graupel, and hail). The initial conditions are obtained from the ECMWF analysis of 15 July 00:00 UTC and the boundary conditions for the outermost domain are interpolated in time from the 6-hourly ECMWF forecasts.

Model results are first assessed in terms of satellite and radar pseudo-observations. The brightness temperature as measured in the METEOSAT 10.8 μm channel is compared with the brightness temperature as reconstructed from the model fields. The time evolution of the 280 K contour, representative of mid- to high-level clouds, is used to monitor the convective activity. Model results are in good agreement with observations: convection starts to develop around 13:00 UTC and only lasts for a couple of hours. The triggering occurs on the eastern slope of the North tip of the southern Black Forest (48N, 8.35E) and the storm propagates towards the north-east. The main departure from the observations is a slower propagation and thus a shorter trajectory of the storm. However this effect might also be artificially amplified due to the parallax error of the satellite observations.

A similar comparison is performed using the time evolution of the 1dBZ reflectivity contour measured by the Montancy radar every 15 minutes during its 1° elevation scan. At the location of the storm, this elevation roughly corresponds to 1000m ASL. The agreement between the observations and the simulation is remarkable. Initiation time, duration, and trajectory of storm are quite well captured by the model. Taking into account the weak likelihood for convective development on this particular day as well as the great difficulty of accurately predicting isolated storms, the Meso-NH forecast can be considered as very successful but the question is whether it was obtained for the good reasons?

3 TRIGGERING PARAMETERS

In the absence of large scale forcing, the triggering of convection essentially depends on three parameters: the moisture supply in the low levels of the atmosphere, the potential instability of the air-mass and a vertical ascending motion resulting from either orographic lifting or diurnal thermal heating of the ground.

At 14 UTC, the CIN is very weak in the mountainous areas but only the Black Forest region exhibits significant amounts of CAPE. Two spots with CAPE exceeding 3000 J/kg are present in the model domain: one over the western slope of the southern Black Forest (corresponding to the steepest orography of the domain) and a second one, less intense but spatially wider, over the area where the convection is triggered. According to the model, high CAPE appears to be necessary but not sufficient. The comparison with the observed soundings does not show any inconsistency but unfortunately no soundings are located sufficiently close to the area of interest.

A real achievement of the COPS experiment is the fairly exhaustive documentation of the water vapor field which was sampled by several in situ and remote, ground based and airborne instruments. Model results were carefully checked against this very dense and unique data set. The main conclusions are i) the model results tend to have a moist bias in the layer 1km-3km – this bias is quite moderate in the morning but reaches 2g/kg in the afternoon, and ii) the model results depict very well the spatial variability of the moisture field including the observed accumulation of moisture above and in the lee of the two massifs.

This accumulation directly results from the presence of convergence lines generated in response to the diurnal heating and located along the crest lines of the two massifs. Patchy in the morning, these lines becomes more organized in the afternoon especially over the Black Forest (see Fig.1). Furthermore, at the northern tip of the southern Black Forest, the vertical motion is significantly reinforced by the lee-side convergence. The Doppler velocity observations from the Feldberg radar support the model results regarding the occurrence and location of such convergence. This mechanism plays a crucial role in the triggering of the convection.

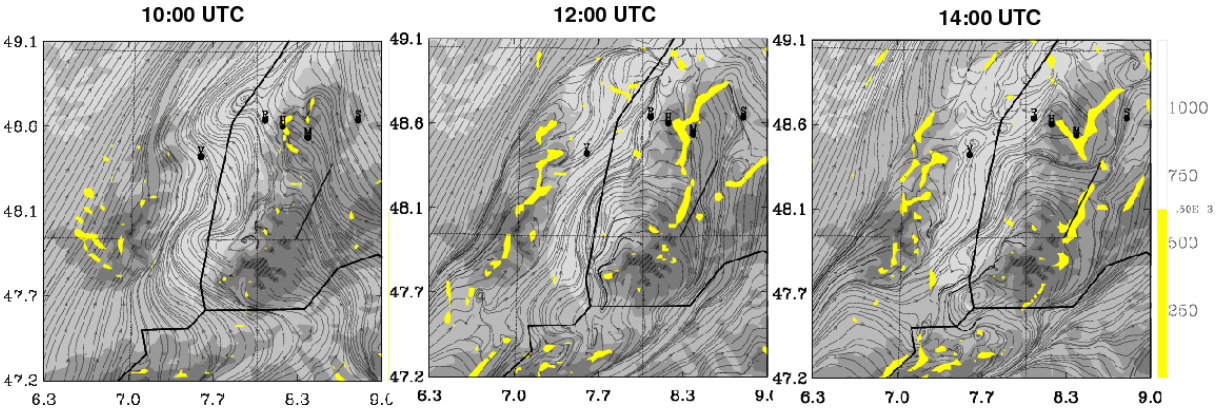

Figure 1: Streamlines and convergence in excess of 0.5 10^{-3} s^{-1} at 1000 m ASL. The thick black line indicates the trajectory of the storm.

4 CONCLUSIONS

The Meso-NH forecast of July 15 storm appears fairly realistic. The initiation time, duration, and trajectory of the storm are quite well captured. According to the model, convection is mainly triggered by the convergence which developed in the lee of the southern Black Forest. Despite these good results, the positive bias found in the humidity fields has to be further investigated. The envisaged model intercomparison exercise on this case will help to clarify this issue and to understand why others models (see for instance Barthlott et al., 2009) were not as successful.

REFERENCES

Adler, B., et al.., 2009: The impact of convergence zones on the initiation of deep convection: A case study from the COPS campaign. Atmos. Res., submitted.

Barthlott, Ch., Schipper, J.W., Kalthoff, N., Adler, B. and Kottmeier, Ch., 2009 : Model representation of boundary-layer convergence triggering deep convection over complex terrain: A case study from COPS, Atmos. Res., submitted.

Kottmeier, C. et al., 2008: Mechanisms initiating convection during the COPS experiment. Meteor. Z., 17, 931-948.

COSMO MODEL SIMULATION OF CONVERGENCE ZONES IN COMPLEX TERRAIN: A CASE STUDY FROM COPS

Christian Barthlott, Janus Willem Schipper, Norbert Kalthoff, Bianca Adler, Christoph Kottmeier

Institute for Meteorology and Climate Research, Karlsruhe Institute of Technology (KIT), Karlsruhe, Germany
E-mail: *christian.barthlott@imk.fzk.de*

Abstract: An isolated thunderstorm from the Convective and Orographically-induced Precipitation Study in southwest Germany and east France in 2007 is analysed. On July 15, deep convection developed east of the Black Forest crest, although convective available potential energy (CAPE) was only moderate and convective inhibition (CIN) was high. Data analysis revealed that convection was triggered by updrafts penetrating the capping inversion of the planetary boundary layer as a result of low-level convergence. Although the numerical weather prediction model COSMO-DE of the German Weather Service (2.8 km grid resolution) simulated a convergence line and the evolution of a line of low clouds in good agreement with radar and satellite observations, no precipitating deep convection developed from this line of clouds. For an improved representation of orographic effects, simulations with a finer grid resolution of 1 km were performed. Despite almost optimal conditions, i. e. moderate amount of CAPE and almost vanishing CIN, the updrafts required to overcome CIN were not reached in both model configurations. Although both simulations did not initiate deep convection, the results suggest that in an air mass convection situation without mid-tropospheric forcing, the simulated location and timing of convergence lines with coexistent large values of CAPE and low values of CIN can be used as diagnostic parameters for deep convection nowcasting.
Keywords: *Moist convection, Convergence zones, COSMO model, Black Forest*

1 INTRODUCTION

Quantitative Precipitation Forecasting (QPF) still is a challenge for state-of-the-art numerical weather prediction (NWP) models. The existing QPF deficiencies are determined mainly by the model's capacity to forecast the initiation of convection at the right location and time. The international field campaign COPS (Convective and Orographically-induced Precipitation Study) took place in southwest Germany and east France in summer 2007 with the overall goal to advance the quality of forecasts of orographically-induced convective precipitation by four-dimensional observations and modeling of its life cycle (Wulfmeyer et al., 2008).

During the intensive observation period (IOP) 8b on July 15, a single convective cell developed east of the Black Forest crest (Fig. 1), although convective available potential energy (CAPE) was only moderate and convective inhibition (CIN) was high. The break-out of deep convection and subsequent precipitation had not been predicted by the convection-resolving model COSMO-DE used by the German Weather Service (DWD) for operational forecasting. Data analysis by Kottmeier et al. (2008) and Kalthoff et al. (2009) revealed that convection was triggered by low-level convergence zones. As a result of the convergent flow, strong updrafts were observed above the mountains which penetrated the PBL-capping inversion and reached the level of free convection (LFC).

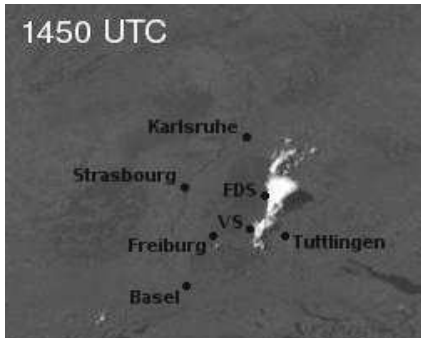

Figure 1: MSG visible image on 15 July 2007.

2 NUMERICAL SIMULATIONS

The non-hydrostatic limited-area atmospheric prediction model COSMO-DE (version 4.0) of the German Weather Service was used for simulations with 2.8 and 1 km horizontal grid resolution (hereinafter referred to as COSMO_2.8 and COSMO_1, respectively). Initial and hourly boundary data come from the COSMO-EU forecast, initial time was 0000 UTC.

COSMO_2.8 succeeds well in reproducing the observed mesoscale convergence line, i. e. its location and timing and the subsequent formation of shallow clouds (Fig. 2). The absence of deep convection in the model despite almost optimal conditions (CAPE $> 2000\ \mathrm{J\,kg^{-1}}$, CIN $< 5\ \mathrm{J\,kg^{-1}}$) may possibly be explained by the vertical extent of the updrafts caused by low-level convergence. In the COSMO_2.8 simulations (Fig. 3, left), the convergence zone extends up to 1400 m amsl with maximum vertical wind speeds of $0.07\ \mathrm{m\,s^{-1}}$. It is obvious that the rising air does not reach the LFC which has a height of around 3100 m amsl. The results with COSMO_1, (Fig. 3, right) show a thinner convergence zone, whereas its vertical extent at the position of maximum convergence is comparable to that of the COSMO_2.8 simulation. Horizontal convergence itself is higher by a factor of 5, thus inducing maximum vertical wind speeds of $0.6\ \mathrm{m\,s^{-1}}$. Despite the higher vertical wind speeds, the rising air reaches a level of 2200 m amsl only, which equals the level in the COSMO_2.8 simulation. As a consequence, CAPE cannot be released, since the LFC is not reached by ascending parcels.

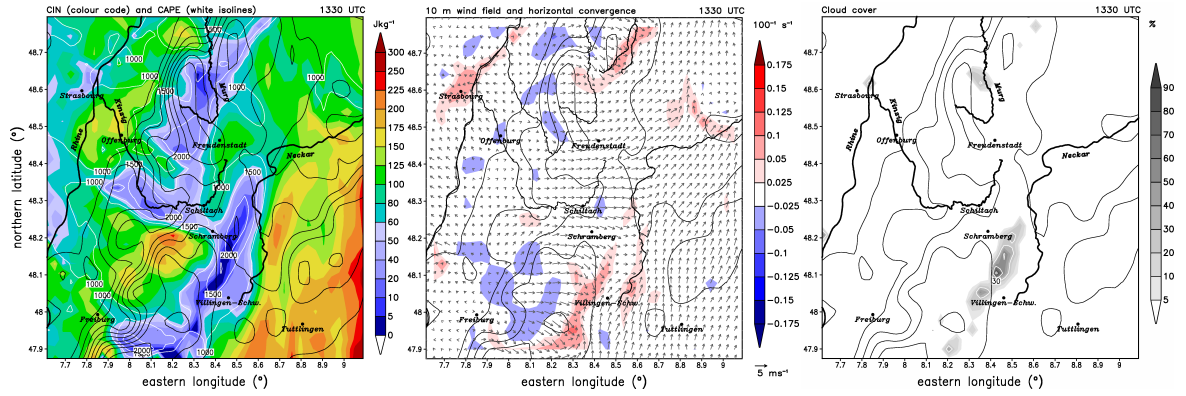

Figure 2: CIN and CAPE (left), 10 m horizontal wind field and convergence (middle), and cloud cover (right) at 1330 UTC as simulated by COSMO_2.8. Black isolines indicate model topography.

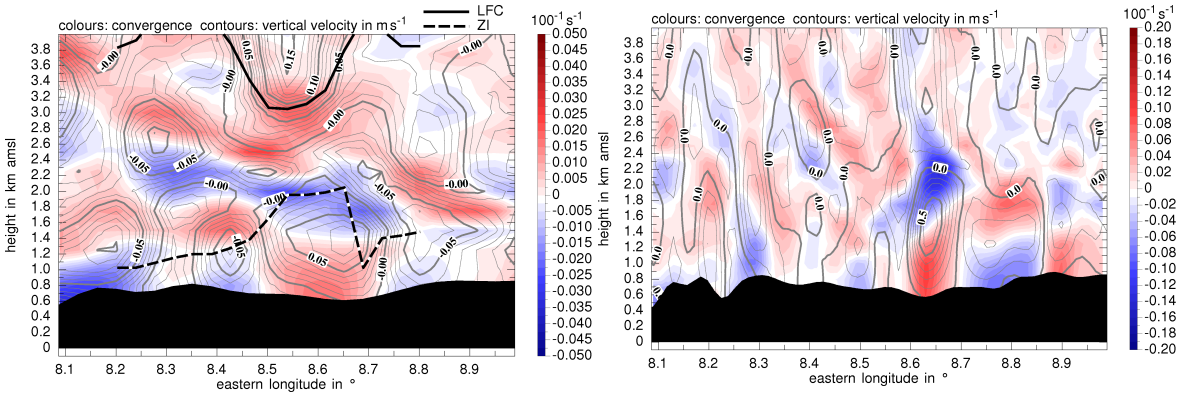

Figure 3: Vertical cross-section of horizontal convergence and vertical wind speed at 1400 UTC along the northern latitude of 48.19° N simulated with COSMO_2.8 (left) and COSMO_1 (right).

3 CONCLUSIONS

COSMO_2.8 succeeds well in reproducing the location and timing of the observed mesoscale convergence line and the subsequent formation of shallow clouds but generates no deep convection. Although the increase of horizontal grid resolution from 2.8 to 1 km increases the strength of the convergence zone and the vertical wind speeds, the vertical extent of the updrafts remains the same and the capping inversion inhibits the breakout of deep convection in the simulation. In comparison to the measured vertical wind speeds, the simulated ones are considerably smaller and, hence, considered to be decisive for the missing initiation of deep convection.

Besides an accurate specification of the thermodynamic and kinematic fields, the results highlight the role of boundary layer convergence features for QPF. It is hypothesized that the lifting depth of a convergence line must be simulated well enough to correctly account for its triggering effect on deep moist convection. Although both simulations did not initiate deep convection, the results suggest that in an air mass convection situation without mid-tropospheric forcing, the simulated location and timing of convergence lines with coexistent large values of CAPE and low values of CIN can be used as diagnostic parameters for deep convection nowcasting.

REFERENCES

Kalthoff, N., B. Adler, C. Barthlott, U. Corsmeier, S. Mobbs, S. Crewell, K. Träumner, C. Kottmeier, A. Wieser, and V. Smith, 2009: The impact of convergence zones on the initiation of deep convection: A case study from COPS. *Atmos. Res.*, doi:10.1016/j.atmosres.2009.02.010.

Kottmeier, C., N. Kalthoff, C. Barthlott, U. Corsmeier, J. Van Baelen, A. Behrendt, R. Behrendt, A. Blyth, R. Coulter, S. Crewell, P. D. Girolamo, M. Dorninger, C. Flamant, T. Foken, M. Hagen, C. Hauck, H. Höller, H. Konow, M. Kunz, H. Mahlke, S. Mobbs, E. Richard, R. Steinacker, T. Weckwerth, A. Wieser, and V. Wulfmeyer, 2008: Mechanisms initiating deep convection over complex terrain during COPS. *Meteorol. Z.*, **17**, 931–948.

Wulfmeyer et al., 2008: The Convective and Orographically-induced Precipitation Study: A Research and Development Project of the World Weather Research Program for improving quantitative precipitation forecasting in low-mountain regions. *Bull. Amer. Meteor. Soc.*, **89**, 1477–1486, doi:10.1175/2008BAMS2367.1.

INFLUENCE OF THE WIND PROFILE ON THE LOCATION OF HOTSPOTS OF CONVECTION IN MOUNTAINOUS TERRAIN

Martin Hagen[1], Joël Van Baelen [2], Evelyne Richard [3]

[1] Deutsches Zentrum für Luft- und Raumfahrt (DLR), Oberpfaffenhofen, Germany
E-mail: *martin.hagen@dlr.de*
[2] Université de Clermont-Ferrand, France
[3] Observatoire Midi-Pyrénées, Toulouse, France

Abstract: Radar observation of the initiation and life cycle of small convective cells during the COPS field campaign in south-western Germany and eastern France show a dependence on the prevailing wind profile. Several hotspots for convective initiation were identified. Orographic features favour convergent flow. On the days when weak winds were prevailing cells developed over the crest line, whereas on days when strong westerly wind were observed the initiation of convection took place in the lee of the mountains within convergent flow.

Keywords: *convection, mountainous area, radar observations*

1 INTRODUCTION

COPS (Convective and Orographically-induced Precipitation Study, Wulfmeyer et al., 2008) was an international field campaign that took place in the Upper Rhine Valley, the Black Forest and the Vosges Mountains during summer 2007. The aim of COPS was to study the orographic influence on the initiation and life cycle of convection, mainly by investigating the humidity structure. Observations with advanced instruments should help to improve the forecast skill of mesoscale numerical models, especially precipitation forecasts. Among the large number of observed convective systems we will concentrate on the observations of isolated small convective rain showers which developed in the Vosges Mountains on two consecutive days. While on one day the cells were initiated at the crest line of the mountain range, on the second day the cells developed on the lee side of the Vosges Mountains in the Rhine Valley.

2 THE COPS FIELD CAMPAIGN

For the COPS field campaign the polarimetric C-band Doppler radar POLDIRAD was deployed for 3 month in the foothills of the Vosges Mountains about 20 north-west of Strasbourg (Fig. 1) and about 100 m above the floor of the Rhine Valley. Volume scans were performed up to 120 km range every 10 minutes. A large set of instruments were set up at the super sites Aachern, Hornisgrinde, Deckenpfronn, and Bischenberg/ Meistratzheim. Additionally the ARM mobile facility was installed in the Murg Valley. At the French super site Bischenberg a high resolution (temporal 30 sec., radial 60 m) scanning X-band radar was installed. The maximum range was 20 km.

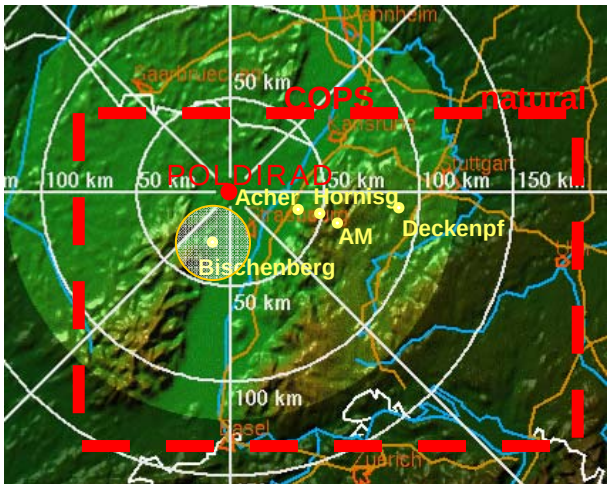

Fig. 1 The COPS region in South-Western Germany and North-Eastern France. Range rings are from POLDIRAD, yellow dots show locations of super sites. The highlighted circle around Bischenberg indicates the 20 km range of the X-band radar.

In addition to the observations several meso-scale numerical models were used to provide forecasts for the field campaign and to perform studies with different microphysics schemes. For the present study we used the simulations with the French MesoNH model.

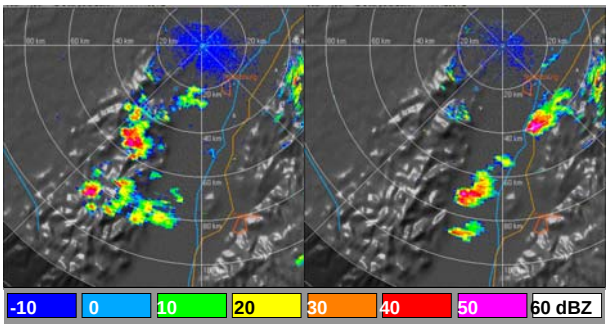

Fig. 2 PPI of reflectivity on 12 Aug. 2007 1440 UTC (left) and 13 Aug. 2007 1120 UTC (right).

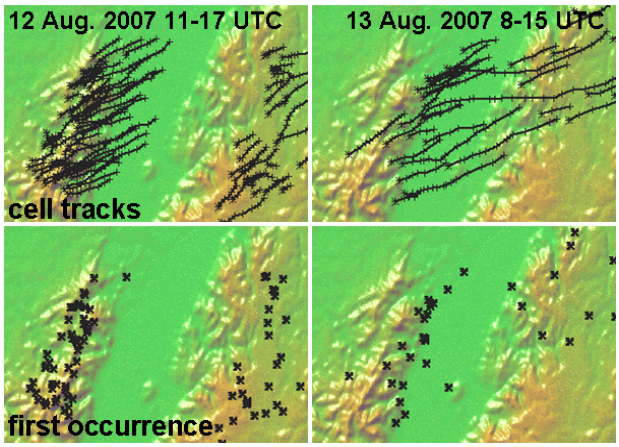

Fig. 3 Tracks of cells (top row) and location of first occurrence (bottom row) for 12 August and 13 August 2007.

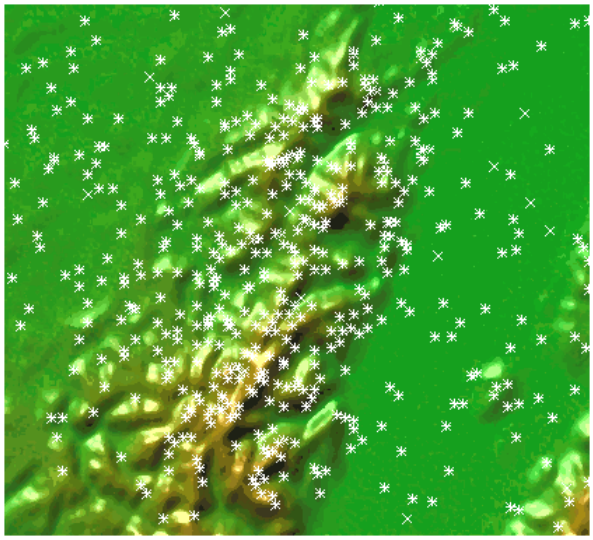

Fig. 4 Location of first occurrence of convective cells observed by POLDIRAD over the Vosges Mountains on 15 days during COPS.

3 OBSERVATIONS OF ISOLATED CELLS

In addition to stratification and the moisture field, topographic features have a strong influence on the initiation and development of convection. Mountains provide elevated heat surfaces which can destabilize the stratification in the boundary layer. Also, mountains can initiate flow convergence along the crest line providing a source for convection initiation. On a larger scale mountains can distort the flow generating convergence in relation the orography. During COPS on several days only small isolated shower or thunderstorm cells developed in the COPS region. A distinct situation was observed on August 12 and 13, 2007. On both days isolated cells developed in relation to the Vosges Mountains. Fig. 2 shows two sample PPI images of reflectivity for the two days. On 12 August cells developed over the Vosges and travelled afterwards with the mean south-westerly flow into the Rhine Valley while decaying there. On 13 August the cells developed in the lee of the Vosges, travelling across the Rhine Valley and some of them where enhanced again at the windward slopes of the Black Forest. Fig. 3 shows the cell tracks and location of first radar echo for the two days. In total 80 and 38 cells were tracked on 12 and 13 August, respectively. 51 (22) of them have been initiated in relation to the Vosges Mountains. On both days the life time was in the order of 0.5 to 2 hours, with some cells being active for even a longer time. This was mainly for 13 August.

Simulations with the mesoscale model MesoNH have been able to reproduce the diverse life cycle of the cells. The quite realistic simulations are also of great value to access atmospheric parameters which have not been observed in 3 dimensions, like the moisture structure and the wind field. While on 12 Aug. weak south-westerly winds are prevailing, strong westerly winds are simulated and observed on 13 Aug. The simulated cells correspond to the observed ones, not exactly in time and location, but with similar life time and cell initiation.

Fig. 4 shows the convective initiation over the Vosges Mountains on 15 days in 2007 (June 4+5, 8-12, July 17, Aug. 3, 6, 12, 13, 17, 23, 24). Wind direction and profile were varying and radar observations were available only every 10 minutes. Despite the large variability of the initiation points common features can be identified: (i) initiation tends to be located along mountain ridges; (ii) initiation is concentrated along mountain peaks; (iii) initiation occurs along the edge of ridges towards the Rhine Valley (right side); (iv) there is a gap region between the crest line and the edge towards the Rhine Valley.

4 CONCLUSIONS

Observations with radar during the COPS field campaign in Central Europe of isolated shower cells show a strong dependence on the orography and the prevailing wind field. The simulations with MesoNH were able to reproduce the observations in a quite realistic manner, even reproducing “hot spots” of cell initiation in relation to orography. The X-band radar at Bischenberg allowed for observations with high temporal resolution at one of the north-eastern hot spots. Convergences along ridges favours the initiation of convection.

REFERENCES

Wulfmeyer, V., et al., 2008: The Convective and Orographically-induced Precipitation Study. *Bull. Amer. Meteor. Soc.*, **89**, 1477-1486.

GENERALIZING THE LOCAL MIXING LENGTH-SCALE FOR STABLE ATMOSPHERIC BOUNDARY LAYERS

Branko Grisogono

Dept. of Geophysics, University of Zagreb, Zagreb, Croatia
Email: *bgrisog@gfz.hr*

Abstract: Excessively diffusive and much-too-deep modeled stable ABL flow is remedied by using a new generalized „z-less" mixing length-scale, Λ, including the vertical wind shear, S explicitly. This generalization of Λ is based on a simplified turbulent kinetic energy (*TKE*) eqn. yielding $\Lambda \sim (TKE)^{1/2}/|S|$, almost regardless of other parameterization details. The proportionality depends on known model constants and a function of Ri and turbulent Prandtl number, Pr; Λ approaches Ozmidov scale (determined by the turbulent dissipation and buoyancy frequency) in the limit $Ri >> 1$. Tests with mesoscale MIUU model and a calibrated 1D semi-analytic Prandtl model prove this generalization of Λ correct and useful.

***Keywords**: ICAM, katabatic flow, modeling, parameterization, Prandtl, Richardson number, strongly stratified turbulence*

1 INTRODUCTION

Recent research suggests that the evolution of the stable atmospheric boundary layers (SABL) is poorly understood, especially so over inclined (mountainous) areas. The emphasis is on parameterizing turbulent effects in the SABL. The "classical" SABL is always stratified weakly (i.e. the gradient Richardson number, $Ri << \infty$, usually, $0 < Ri \leq 1$) and modeled reasonably well during past decades; however, the strongly- or very stably-stratified SABL (VSABL, typically $Ri >> 1$) is not understood well. Various problems with current turbulence parameterization schemes become more apparent as the refining model resolution is used over complex terrain (e.g. Gohm et al. 2008, Grisogono and Belušić 2009); these problems include over-diffusion, frictional decoupling, etc. Excessively diffusive, much-too-deep SABL flows, as often modeled numerically, are assessed in the light of a recently proposed alleviation of this problem, using a calibrated Prandtl model (Grisogono and Belušić 2008, later GB08) and extended to other SABL flows. The latter demanded an explicit inclusion of the vertical shear of quasi-horizontal wind, S, in the local, so called „z-less" mixing length. A potential weakness of the mixing length in GB08 was the lack of its smoothness (it used min-max option).

A generalization of this proposal is given via simplified turbulent kinetic energy (*TKE*) eqn. and a set of related parameterizations for the eddy diffusivity and conductivity with respect to "z-less" mixing length, Λ. It will be shown that $\Lambda \sim \Lambda_0 = (TKE)^{1/2}/|S|$, almost regardless of other closure details. The dimensionless factor of proportionality in Λ is a simple function of Ri and turbulent Prandtl number, Pr, derived from a particular parameterization chosen and the model's known details. This new Λ mitigates over-diffusive SABL in models. For example, Λ proposed here may improve forecasting the minimum near-surface temperature and the low-level wind in mountainous areas (e.g. katabatic wind) since the VSABL is now simulated more reliably.

2 GENERALIZED „Z-LESS" MIXING LENGTH-SCALE

Begin with the *TKE* eqn. under the usual simplifications: horizontal homogeneity, the x-axis mean flow alignment, Boussinesq and the absence of mean vertical motions; thus:

$$\frac{\partial (TKE)}{\partial t} = -\overline{u'w'}\frac{\partial \bar{u}}{\partial z} + \frac{g}{\theta}\overline{w'\theta'} - \frac{\partial}{\partial z}\left[\overline{w'\left(\frac{p'}{\rho_0} + TKE\right)}\right] - \varepsilon \qquad (1)$$

where the terms have their very typical meaning. The change of *TKE* is balanced by the shear production, buoyant destruction (in the SABL), transport due to pressure- and turbulence-correlations and dissipation, respectively. Assuming steadiness, and neglecting transport terms, we parameterize the momentum and heat fluxes in (1) as $K_m\$$, $K_h\$$, where K_m, K_h are eddy diffusivity and conductivity and $\$ \equiv |S|$. Also in (1) we use $\varepsilon = b(TKE)^{3/2}/\Lambda$, where b is a model constant and Λ is a new mixing length. Hence, (1) yields:

$$0 = K_m \$^2 - K_h N^2 - \frac{b}{\Lambda}(TKE)^{3/2}. \qquad (2)$$

This gives a simple eqn. for Λ. A 1st order closure assumes $K_m = a_1\Lambda^2\$$, $K_h = a_1\Lambda^2\$/Pr$, a_1 is a model constant; moreover, typically $Pr \geq 1$ and $Pr > Ri$ in the SABL (e.g. Zilitinkevich et al. 2008). An advanced parameterization, i.e. a higher-order closure, may take a form $K_m = a_2\Lambda(TKE)^{1/2}$, $K_h = a_2\Lambda(TKE)^{1/2}/Pr$. When either closure type is plugged in (2), expanding it in $Ri/Pr << 1$, the corresponding Λ ensues, Table 1.

K_m	$\Lambda(\Lambda_0)$	$\Lambda(\Lambda_N)$
$a_1\Lambda^2\|S\|$	$\Lambda_0(b/a_1)^{1/3}[1+Ri/(3Pr)]$	$\Lambda_N\,(b/a_1)^{1/3}\,Ri^{1/2}[1+Ri/(3Pr)]$
$a_2\Lambda(TKE)^{1/2}$	$\Lambda_0(b/a_2)^{1/2}[1+Ri/(2Pr)]$	$\Lambda_N(b/a_2)^{1/2}Ri^{1/2}[1+Ri/(2Pr)]$
$a_3(TKE)/N$	$\Lambda_0(b/a_3)Ri^{1/2}[1+Ri/Pr]$	$\Lambda_N(b/a_3)Ri[1+Ri/Pr]$

Table 1. Generalized mixing length, Λ. For three typical types of eddy diffusivity, K_m, $K_h = K_m/Pr$, Λ is derived in terms of either Λ_0 or Λ_N, (Ozmidov length) including explicity shear or buoyancy frequency, i.e. $\Lambda_0=(TKE)^{1/2}/|S|$ or $\Lambda_N=(TKE)^{1/2}/N$. Richardson gradient and turbulent Prandtl numbers are Ri and Pr; $0 < a_i < 1$, $0 < b < 0.1$ are constants ($Pr >> Ri$).

Next, the MIUU model is used, as in GB08, where the same run as here was compared to Prandtl model. The default run with only Λ_N produces an over-diffusive and too deep SABL, Fig. 1, upper panels; the middle panels show the correct SABL, i.e. VSABL, corresponding to Prandtl model; the lower panels show the new result with generalized Λ, which is almost the same as in the middle panel (from GB08). This gives credit to our new Λ.

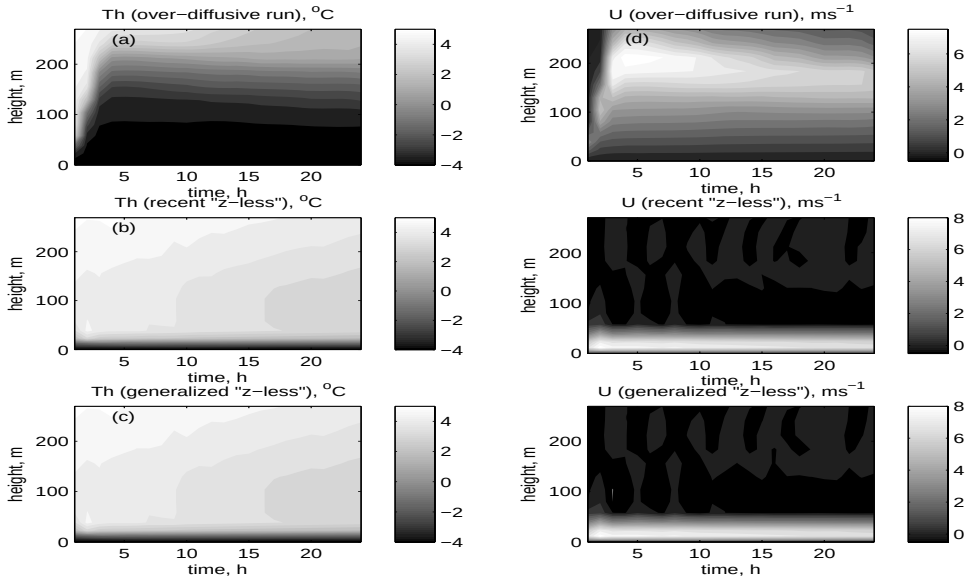

Figure 1. Left (a,b,c): potential temperature Th and right (d,e,f): downslope wind component U vs. time and height simulated using MIUU model. Upper two panels (a,d) show an over-diffusive SABL; middle: recent (b,e), correct results concuring to Prandtl model (GB08); lowest (c,f) use Λ_2 from Table 1; note that (c,f) are almost the same as (b,d), giving approval to the derivation of the generalized "z-less" mixing length Λ. The simulated flow assumes a constant slope -2.2°, windless background atmosphere, $\Delta\theta/\Delta z$ = 5K/km, and the surface potential temperature deficit 6.5 K, the low-level jet is at ~ 20 m.

3 CONCLUSION

A thin and „sharp" VSABL flow is obtained using the generalized mixing length, Λ, Table 1 and Fig. 1, giving the same result as recently recommended by GB08, where the low-level jet is imbedded in a sharp near-surface inversion. The strength of this approach is that Λ is not given but derived from the simplified *TKE* eqn.

Acknowledgements:
Danijel Belušić is thanked for his comments. The study is supported by the Croatian Ministry of Science, Education & Sports, project BORA, No. 119-1193086-1311 and by EMEP4HR, No. 175183/S30 provided by the Research Council of Norway.

REFERENCES

Gohm, A., G.J. Mayr, A. Fix and A. Giez, 2008: On the onset of bora and the formation of rotors and jumps near a mountain gap. Quart. J. Roy. Meteorol. Soc. **134**, 21-46.

Grisogono, B., and D. Belušić, 2008: Improving mixing length-scale for stable boundary layers. Quart. J. Roy. Meteorol. Soc. **134**, 2185-2192 (GB08).

Grisogono, B. and D. Belušić, 2009: A review of recent advances in understanding the meso- and micro-scale properties of the severe Bora wind. Tellus **61A**, 1-16.

Zilitinkevich, S.S., T. Elperin, N. Kleeorin, I. Rogachevskii, I. Essau, T. Mauritsen and M. W. Miles, 2008: Turbulence energetics in stably stratified geophysical flows: strong and weak mixing regimes. Quart. J. Roy. Meteorol. Soc. **134**, 793-799.

CHARASTERISTICS OF THE NEAR-SURFACE TURBULENCE DURING A BORA EVENT

Željko Večenaj, Danijel Belušić and Branko Grisogono

Department of Geophysics, Faculty of Science, Zagreb, Croatia
E-mail: *zvecenaj@gfz.hr*

Abstract: Wind velocity at the town of Senj was measured at 13 m above the ground with a 3D ultrasonic anemometer operating at 4 Hz sampling frequency. The severe bora case that occurred on 07 January and lasted to 11 January 2006 is analyzed here. This data set is used for evaluation of the turbulent kinetic energy, *TKE*, and its dissipation rate, ε. Some considerations about defining turbulent perturbations of the bora wind speed are pointed out. The inertial dissipation method for estimation of ε is used. The empirical length scale parameter for this event is estimated with respect to ε and *TKE*.

Keywords: bora wind, inertial dissipation technique, turbulent kinetic energy, dissipation rate, mixing length-scale

1 INTRODUCTION

Bora (locally *bura*) is a downslope windstorm that blows from the northeastern quadrant in the lee of the coastal mountains when the relatively cold northeasterly flow impinges on the Dinaric Alps (e.g. Yoshino, 1976; Grisogono and Belušić, 2009). Belušić and Klaić (2006) analyzed bora case with gusts speed maxima > 60 m s^{-1}. They found that the values of turbulent kinetic energy (*TKE*) can surpass 30 J kg^{-1}.

TKE dissipation rate (ε) describes dissipation of *TKE* by molecular viscosity into the heat. Improvements needed for a more faithful turbulence parameterization in e.g. air-pollution and dispersion calculations during bora events require a more detailed understanding of bora turbulence (e.g. Baklanov and Grisogono, 2007). This is impossible without a more complete knowledge of *TKE* and ε. Piper and Lundquist (2004) evaluated ε related to the cold front. Their results are compared with those derived here with the respect to the mean streamwise velocity component, giving also credibility to this study.

2 DATA AND METHODS

The 3D wind speed measurements were performed in the town of Senj (44.99°N, 14.90°E, 2 m above MSL) at a height of 13 m above the ground with the WindMaster ultrasonic anemometer (Gill Instruments). The anemometer records the data with a sampling frequency f = 4 Hz. The observed bora episode extends from 07 to 11 January 2006 (4 day time series). The coordinate system is rotated in the mean wind direction (55°). Figure 1 depicts the measured 4 day time series of the streamwise velocity component with 1 hr mean superimposed.

We used the inertial dissipation method (IDM) for evaluation of ε (e.g. Večenaj et al., 2007). Using Taylor's hypotheses of frozen turbulence (e.g. Stull, 1988), ε can be evaluated from:

$$\varepsilon = \frac{2\pi}{\overline{U}}\left[\frac{f^{5/3}S_u(f)}{\alpha}\right]^{3/2} \qquad (1)$$

where $\overline{U}$ is a mean streamwise velocity component, $S_u(f)$ is the spectrum and α is the Kolmogorov constant.

Starting from the local one-and-a-half-order closure, ε can be parameterized in numerical models using the mean value of *TKE* (e.g. Mellor and Yamada, 1974):

$$\varepsilon = \frac{TKE^{3/2}}{\Lambda} \qquad (2)$$

where $TKE = \frac{1}{2}\left(\overline{u'^2} + \overline{v'^2} + \overline{w'^2}\right)$ and u', v' and w' are turbulent perturbations of the streamwise, transverse and vertical velocity components, respectively, while bars represent a suitable averaging. The parameter Λ is the empirical length scale that is closely related to the size of dissipating turbulent eddies.

3 RESULTS

The relationship between the standard deviation of the streamwise velocity component (σ_u), and $\overline{U}$ in the surface layer is usually linear (e.g. Stull, 1988), which was shown by Belušić et al. (2006) to be valid for the local bora turbulence. Moving averages with lengths from 1 min to 1 h are subtracted from the entire 4 day bora episode to determine the perturbations. Then a power law of the form (3a) is fitted to the scatter diagrams of σ_u

vs. $\overline{U}$ for different moving averages. Expecting b to be 1, Fig. 2 shows that the closest value for $b \approx 1$ is achieved for the 1 min moving average. Therefore, we use the 1 min moving average for determination of the local turbulence perturbations in this bora episode. From (2) it follows that $\varepsilon \propto TKE^{1.5}$. This relation is tested by fitting the (3b) power law to the ε vs. *TKE* scatter diagram of 1 h mean values for the entire bora episode. This fit gives coefficient d and parameter $\Lambda = (c)^{-1}$ to be 1.3 and 60 m, respectively.

$$\sigma_u = a\left(\overline{U}\right)^b \quad \text{(3a)}; \qquad \varepsilon = c(TKE)^d \quad \text{(3b)}$$

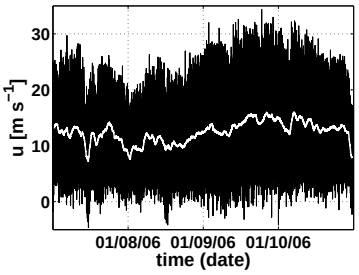

Figure 1. A 4 day raw 4 Hz data time series (07 to 11 January 2006) of the streamwise-wind component measured in Senj, with the 1 h mean superimposed.

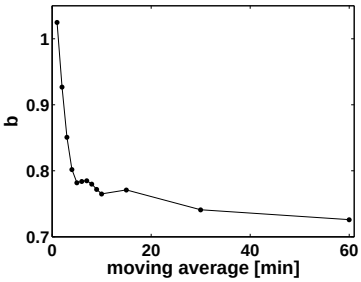

Figure2. The power coefficients b from (3a) for different moving averages subtracted from the entire bora episode.

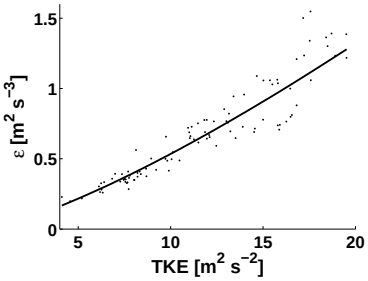

Figure3. Scatter plot ε vs. *TKE* for the entire bora episode. Solid line is the fit with the *a priori* unknown coefficients c and d from (3b).

4 CONCLUSIONS

Our data suggest that the 1 min moving average may be recommended for determination of the local turbulence perturbations for bora. Estimations of ε using IDM agree well with those of Piper and Lundquist (2004) with respect to the mean streamwise velocity component. In this bora episode ε is proportional to $TKE^{1.303}$. This model explains 91 % of ε vs. *TKE* variance. From (3b) it follows that $\Lambda \approx 60$ m.

Many current state-of-the-art models use Blackadar length-scale parameterization which would for this situation give $\Lambda \approx 25$ m. This is derived on the basis of the vertical *TKE* profiles from Belušić and Klaić (2004), using MEMO 6 mesoscale model to simulate several bora events. The same result is obtained using the WRF-ARW model with Mellor-Yamada-Janjic turbulence parameterization scheme. The model-based Λ obviously underestimates Λ derived here from *TKE* and ε values. This may imply the inadequacy of the Blackadar type of parameterizations for the bora related turbulence.

Future work related to the near-surface bora turbulence will include the 4 Hz data analysis of a variety of the bora episodes, categorized by their nature (type), severity (strength) and seasonal period. In this way, a comprehensive picture of the bora related near surface turbulence will be revealed.

Acknowledgements:
This study is supported by the Croatian Ministry of Science, Education & Sports, projects BORA No. 119-1193086-1311 and by EMEP4HR project number 175183/S30 provided by the Research Council of Norway.

REFERENCES

Baklanov, A. and B. Grisogono (Eds), 2007: Atmospheric Boundary Layers: Nature, Theory and Applications to Environmental Modelling and Security, Springer, New York, 241 pp.

Belušić, D. and Z.B. Klaić, 2006: Mesoscale dynamics, structure and predictability of a severe Adriatic bora case. Meteorol. Z. **15**, 157-168.

Belušić, D., M. Pasarić, Z. Pasarić, M. Orlić, and B. Grisogono, 2006: A note on local and non-local properties of turbulence in the bora flow. Meteorol. Z. **15**, 301-306.

Grisogono, B. and D. Belušić, 2009: A review of recent advances in understanding the meso- and micro-scale properties of the severe Bora wind. Tellus A **61**, 1-16.

Mellor, G.L. and T. Yamada, 1974: A hierarchy of turbulence closure models for planetary boundary layers. J. Atmos. Sci. **31**, 1791-1806.

Piper, M. and J.K. Lundquist, 2004: Surface layer turbulence measurements during a frontal passage. J. Atmos. Sci. **61**, 1768-1780.

Stull, R.B., 1988: An Introduction to Boundary Layer Meteorology, Kluwer Academic, 666 pp.

Večenaj, Ž., D. Belušić, and B. Grisogono, 2007: Estimation of turbulence kinetic energy dissipation rate in a bora event. *Proc. 29th Intern. Conf.on Alpine Meteorology*, Chambery, France, 745-748.

Yoshino, M.M., 1976: Local wind bora: a research summary. *Yoshino, M.M. (Ed.), Local wind bora*, University of Tokio Press, 277-282.

AN INVESTIGATION INTO RIDGE-TOP TURBULENCE CHARACTERISTICS: A CASE STUDY OF IN SITU MEASUREMENTS AND LARGE EDDY SIMULATION

Marwan Katurji, Peyman Zawar-Reza, Andrew Sturman

Centre for Atmospheric Research, University of Canterbury, Christchurch, New Zealand
E-mail: *mka94@student.canterbury.ac.nz*

Abstract: High Reynolds number turbulent flow over a ridge top in New Zealand is investigated through in situ measurements and large eddy simulations. Spectral analysis was performed for observed stream-wise and lateral velocity components for two different locations along the ridge. Multi-scale turbulent interactions are examined and the 3-dimensional isotropy assumption in the inertial sub-range of the spectrum assessed. Turbulent eddy length scales were derived showing increased dissipative length scales during day time. The Advanced Regional Prediction System (ARPS) large eddy simulation (LES) model was used in 2-D simulations over the experimental site to examine the sensitivity of surface layer turbulence to soil moisture initialization. Results for the dry soil runs showed a relative increase in daily averaged turbulent kinetic energy by 25 % and 23 % for two different locations in the domain. The nature of turbulent eddy evolution, structure and interaction over a complex ridge is examined.

Keywords: *Turbulence, velocity spectra, mountain ridge top, large eddy simulation.*

1 BACKGROUND AND INTRODUCTION

Atmospheric surface layer turbulence over flat terrain is well understood under different stability conditions. Turbulence over hill tops has also attracted interest in the research community, but there is still much knowledge to be gained. Large scale eddies having length scales larger than the hill length scale are transported over hills within a time period less than their own turnover time following the rapid distortion theory discussed by Townsend (1972). Panofsky et al. (1982) showed through observations of spectra over different fetch distances in complex terrain that the response rate differs for small and large eddies. They suggested that while the small high frequency turbulent eddies adjust to new terrain quickly the large low frequency ones still hold memory of the terrain upstream of the flow. More recent theories of turbulence structure and processes in the atmospheric surface layer have negated Monin-Obukhov similarity theory (Hunt and Morrison 2000), while McNaughton and Brunet (2002) have shown the existence of two interacting scales of turbulence initiated from the surface upward by rising unstable thermal eddies that interact with the mean flow. The current work provides an insight into turbulence in high Reynolds number ($\sim 10^9$) flow over a ridge top through in situ measurements and large eddy simulations in an attempt to critically assess previous theories. The main objective of this paper is to understand the turbulent structure and mechanisms of flow over a mountain ridge top in the South Island that is a potential site for wind turbines.

2 METHODOLOGY AND RESULTS

Two ultra-sonic anemometers were mounted on 20 metre towers 3 km apart along a ridge top. Sampling rate was 60 Hz, block averaged to 20 Hz. The p-welch fourier transform routine was used to produce spectral plots after de-trending and windowing the discrete data. Daytime and night time datasets were analyzed from the two towers, and spectral data were carefully examined to ensure that the time period represented the complete spectrum of energy production and dissipation. Dissipative eddy sizes were derived from spectral plots of eddy dissipation rate using the spectral model equation in the inertial sub-range after Kolmogorov (1941a & b) and Obukhov (1941). The power spectra were scaled by the variance of the wind speed and the frequency was scaled by z/L (Figure 1 a & d). Power ratios of cross-wise and vertical spectra to stream-wise spectra were derived to investigate the isotropic assumption of turbulence (Figures 1 b, c, e & f). Site 2 was more turbulent and had higher wind speeds than site 1 for both day and night time conditions, which relates to their relative exposure. The entire range of the energy spectrum was captured, from the large and low frequency eddies to the small and high frequency eddies. Day and night spectra differ slightly for the two sites and show a drop of energy for the night time period, which is evidence that the increase in energy during daytime was from thermally induced turbulence production. An interesting feature in the normalized spectral plots is the double peak depicted in the spectra of site 2.

The Advanced Regional Prediction System model (ARPS) was used to undertake 2-D sensitivity experiments, as it is capable of resolving atmospheric phenomena to a high degree of accuracy using large eddy simulation techniques. A north-west/south-east section was chosen since this direction represents the prevailing wind direction. Terrain data were selected from 25 m resolution digital elevation model output and was smoothed using a robust locally weighted scatter plot model. A silty-clay soil type and grassland with shrub

cover were selected to represent surface conditions. The main focus of this modelling exercise is to study the effect of homogenous soil moisture initialization on the turbulent kinetic energy and wind speeds, so two runs were performed – a wet soil run (65 % saturation) and a dry soil run (40 % saturation). The 2-D large eddy simulation soil moisture sensitivity experiments clearly show increase in turbulent activity during daytime for both moist and dry soil conditions with the dry soil simulation contributing more to the turbulent kinetic energy. Average daily values of turbulent kinetic energy show an increase of 23 % and 25 % relative to the wet soil run for the two locations.

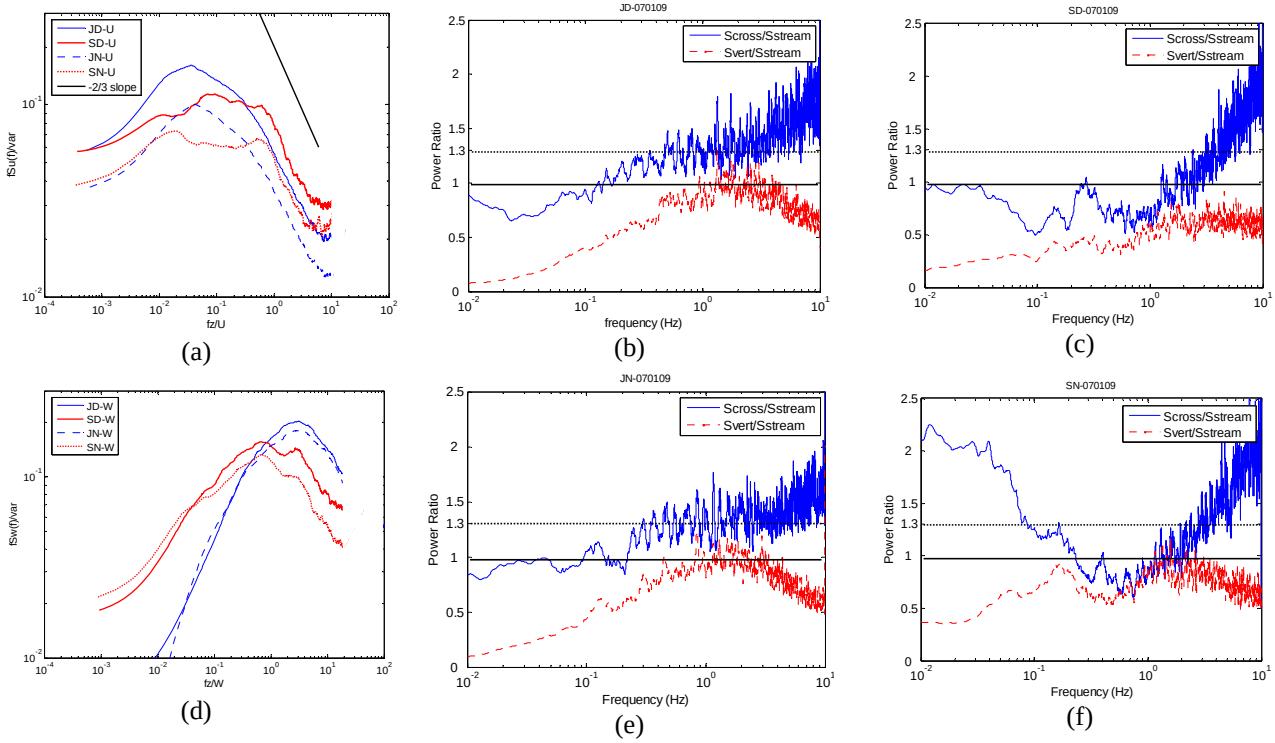

Figure 1. (a, b): Normalized power spectra for the day and night periods at the two sites for the stream-wise (U) and vertical (W) velocity component. (b, c, e, f): Spectral ratios of the lateral (or cross-wise) and vertical power to the longitudinal (or stream-wise) power for cases JD (site 1 day), SD (site 2 day), JN (site 1 night), and SN (site 2 night).

CONCLUSION

The value of high resolution meteorological data along ridge tops in complex terrain under high wind speed conditions is evident. Spectral data analysis for daytime and night time provided evidence about turbulent eddy sizes and structures in the atmospheric surface layer. The double peak in the spectrum occurred both during unstable and near neutral conditions and during night time, implying that the terrain upwind of the sensor and in the vicinity of the flux footprint can have an important influence on the turbulence spectra. The isotropic hypothesis held true during a night time case when turbulence was dominated by shear rather than thermal buoyancy. Model simulations showed that soil moisture can be an important factor in surface layer turbulence.

REFERENCES

Hunt, J.C.R, Morrison, J.F. (2000). Eddy structure in turbulent boundary layers. Euro J. Mech. B. Fluids, 19, 673-694.

Kolmogorov, A. N. (1941a). Energy dissipation in locally isotropic turbulence. Quarterly Journal of the Royal Meteorological Society, 32(1), 19-21.

Kolmogorov, A. N. (1941b). The Local Structure of Turbulence in Incompressible Viscous Fluid for Very Large Reynolds Numbers. Proceedings: Mathematical and Physical Sciences, 434(1890), 9-13.

McNaughton, K. G., & Brunet, Y. (2002). Townsend's hypothesis, coherent structures and Monin-Obukhov similarity. Boundary-Layer Meteorology, 102(2), 161-175.

Obukhov, A.M. (1941). Energy distribution in the spectrum of a turbulent flow. Ser. Geogr. Geofiz., 4-5, 453-466.

Panofsky, H. A., Larko, D., Lipschutz, R., & Stone, G. (1982). Spectra of velocity components over complex terrain. Quarterly Journal of the Royal Meteorological Society, 108, 215-230.

Townsend, A. A. (1972). Flow in a deep turbulent boundary layer over a surface distorted by water waves. Journal of Fluid Mechanics Digital Archive, 55(04), 719-735.

The application of microscale airflow simulations for quantifying snow drift processes over complex terrain

Rebecca Mott and Michael Lehning
Email: mott@slf.ch

WSL-Institute for Snow and Avalanche Research (SLF), Davos, Switzerland

Abstract:
The inhomogeneous snow distribution found in alpine terrain is the result of wind and precipitation interacting with the snow cover. In this study we compute high resolution wind fields for a specific snow fall event in October 2003 in order to explain zones of snow deposition/erosion and to investigate length scales of relevant snow transport and deposition processes. We use the wind fields as input for Alpine3D in order to quantify the redistribution of snow via saltation, suspension and the preferential deposition of precipitation. The results obtained with Alpine3D confirm the hypothesis that preferential deposition is active at the ridge scale and true redistribution, mainly via saltation, forms smaller scale deposition patterns such as dunes and cornices. A sensitivity analysis is presented using diverse numerical resolutions to separate numerical from physical effects concerning local erosion and deposition.

Keywords: *preferential deposition, snow drift processes, small scale windfields*

INTRODUCTION

In complex terrain, characteristic local wind flow patterns are induced by the topography. During snow fall events the modification of the near surface wind field results in a spatially varying preferential deposition of precipitation and in transport of already deposited snow. In high alpine terrain it is especially apparent that drift processes are active on many different scales.

The aim of our work is to explain zones of snow deposition/erosion which can be attributed to wind driven processes and to investigate length scales of relevant snow transport and deposition processes. Previous studies show that a horizontal resolution of 25m is sufficient to represent general deposition features (Mott et al., 2008, Dadic et al., submitted), especially on glaciers. However, recent investigations (Raderschall et al., 2008, Lehning et al., 2008) also suggest that preferential deposition is only active at the ridge scale and redistribution of snow by saltation and suspension is active on smaller scales.

In this study we discuss windfields and respective flow patterns on different scales. The effect of the representation of specific flow patterns on preferential deposition and pure snow drift processes is discussed. The relative contribution of the individual transport processes are presented. Finally we compare model simulation of snow distribution to observed snow variability at different numerical resolutions.

DATA AND METHODS

A steep mountain ridge, the Gaudergrat (Davos, Switzerland), was used as a test site for wind and snow drift experiments. Three automatic meteorological stations, located in the luff, top and lee of the mountain ridge, provide a long series of wind data. In summer 2003 the GAUDEX experiment was conducted at Gaudergrat with a total number of 33 measurement stations, consisting of 27 automatic weather stations and 6 turbulence stations (Lewis et al., 2008). This unique set of wind and turbulence data provides detailed insight into the mean flow patterns of this specific area. In this study we use this knowledge to compute high resolution wind fields for a specific snow fall event in October 2003.

Wind fields were computed with the non-hydrostatic and compressible weather model, Advanced Regional Prediction System (ARPS) and compared to the detailed data set available. The snow distribution after the snow fall event was measured by manual snow probing. We used the wind fields as an input for Alpine3D (Lehning et al., 2008) in order to quantify the redistribution of snow via saltation and suspension and the preferential deposition of precipitation.

A sensitivity analysis is presented using a number of numerical resolutions to separate numerical from physical effects with respect to local erosion and deposition. The sensitivity analysis is carried out by resampling the grid with the smallest scale (10m) to coarser grid resolutions. All sensitivity analysis runs were carried out with the same initial and boundary conditions. In order to discuss the individual transport processes a time series of precipitation and the total deposition is analyzed. The relative contribution of saltation/suspension versus preferential deposition has been evaluated by switching off saltation/suspension in the corresponding sensitivity cases as described by (Lehning et al., 2008).

RESULTS AND CONCLUSION

The results of drift simulations show two characteristic patterns of snow deposition. At ridge scale, strong snow loading is simulated in the lee-slope of the ridge, which is attributed to the cross-ridge flow and the associated strong wind gradient behind the ridge often leading to flow resolution. If the horizontal resolution is 10m, the maximum snow loading is found directly behind the ridge, whereas at 25m resolution the snow loading is distributed further down the lee slope. Secondary deposition features are found in the lee of smaller scale cross

slope ridges, and are caused by flow parallel to the main ridge. These deposition features, small scale snow dunes, were formed mainly due to pure drift-processes without the contribution of preferential deposition. Therefore these patterns are best represented in simulations with a horizontal resolution of 10m or less.

The results obtained with Alpine3D confirm the hypothesis that preferential deposition is active at the ridge scale and true redistribution mainly via saltation forms smaller scale deposition patterns such as dunes and cornices. The sensitivity analysis shows that a resolution of 10m or less is necessary to capture smaller scale deposition features observed, as suggested earlier by Lehning et al. (2008). With an increase of grid resolution the speed-up effect at the mountain ridge increases dramatically. This leads to stronger wind velocity gradients in the direction of the mean flow (see Figure 2 and Figure 3). The effect of the gradient (see Figure 3) is clearly represented by a maximum snow deposition where the velocity gradient becomes strongest, directly behind the ridge.

Overall the snow drift modelling shows that the mean flow characteristics observed and modelled at Gaudergrat explain the major drift zones observed after the snow fall event in October 2003. The choice of the numerical grid is shown to be crucial when explaining different drift zones on different scales.

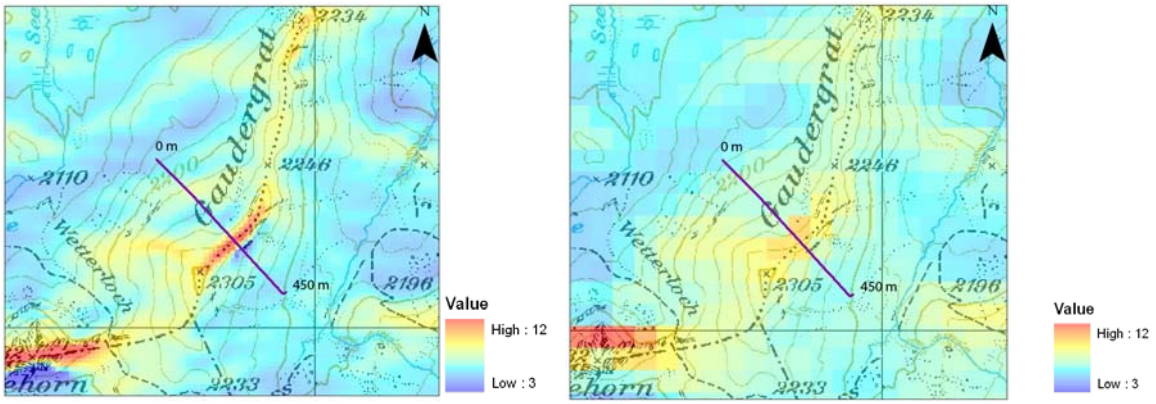

a) b)

Figure 1: Wind velocity [m/s] with resolutions of a) 10m and b) 50m under northwesterly wind condition. The line indicates the transect (see Fig. 2 and Fig. 3)

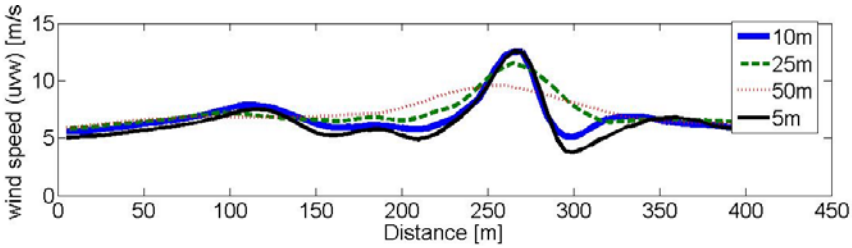

Figure 2: Transect of wind speed of different numerical resolutions (5, 10, 25, 50)

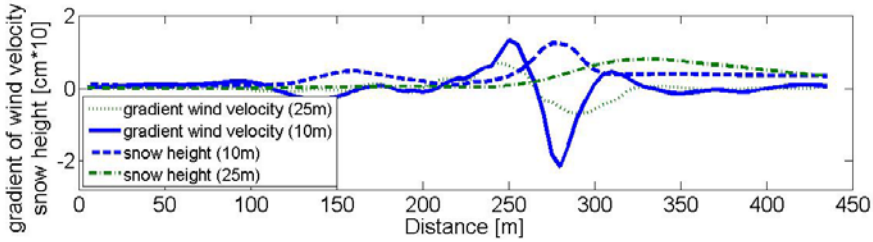

Figure 3: Transect of the gradient of wind speed and respective snow height simulation for dx, dy 10m and 25m

REFERENCES

Mott R., Faure F., Lehning M., Löwe H., Hynek B., Michlmayr G., Prokop A., Schöner W. 2008: Simulation of seasonal snow-cover distribution for glacierized sites on Sonnblick, Austria, with the Alpine3D model. Annals of Glaciology **49**. 155 -160.

Lehning, M., H. Löwe, M. Ryser, and N. Raderschall (2008), Inhomogeneous precipitation distribution and snow transport in steep terrain, Water Resour. Res., **44**, W07404, doi:10.1029/2007WR006545.

Raderschall N., M. Lehning, C. Schär (2008), Fine-scale modeling of the boundary layer wind field over steep topography, Water Resour. Res., **44**, W09425, doi:10.1029/2007WR006544.

Dadic R., Mott R., Lehning M., Burlando P., submitted: Wind Influence on Snow Distribution and Accumulation over Glaciers. Submitted to Journal of Geophysical Research. Doi:10.1029.

Lewis, H.W., Mobbs, S.D., Lehning M., 2008. Observations of cross-ridge flows across steep terrain, Q.J.R.Meteorol.Soc., 134, 801–816, doi: 10.1002/qj.259.

MECHANISMS OF ALONG-VALLEY WINDS

Juerg Schmidli[1], Richard Rotunno[2]

[1] Institute for Atmospheric and Climate Science, ETH, Zurich, Switzerland
[2] National Center for Atmospheric Research, Boulder, USA
E-mail: *jschmidli@env.ethz.ch*

Abstract: The physical mechanisms leading to the formation of along-valley winds are investigated. A diagnostic equation for the along-valley pressure gradient is developed and used in combination with numerical model simulations to clarify the relative role of various mechanisms such as the valley volume effect (TAF) and subsidence heating in the formation of along-valley winds. The setup for the numerical simulations consists of an idealized three-dimensional topography and two sets of thermal forcings: A simplified sinusoidal forcing in the first case, and a realistic forcing in the second case. The present analysis confirms the importance of the valley volume effect for the formation of along-valley winds, but also clarifies the role of subsidence heating and the limitations of the TAF argument.

***K*eywords:** *ICAM, valley winds, volume effect, topographic amplification factor, TAF, subsidence heating*

1 INTRODUCTION

Thermally driven slope and valley winds are an essential component of the fair-weather boundary layer over mountainous terrain. Together with turbulent processes they control the exchange of energy, momentum, moisture and pollutants between the land surface and the free atmosphere. Despite their importance there is still debate about the mechanisms driving the along-valley wind and their relative importance. Is the valley volume effect or topographic amplification factor (TAF; Steinacker , 1984) sufficient to explain the formation of the up-valley wind? How important is subsidence heating (Rampanelli et al., 2004; Weigel et al., 2006)? In order to clarify the relative role of the different mechanisms in the formation of the along-valley wind, a diagnostic equation for the along-valley pressure gradient is developed and used in combination with numerical model simulations.

2 METHOD OUTLINE

Starting from the along-valley momentum equation, and using the thermodynamic equation and the hydrostatic approximation, it is shown that the along-valley pressure gradient ΔP can be expressed by

$$\Delta P|_{x,z=0} = -\frac{gQ_p^n}{\theta_0}(\tau - 1) + \Delta P_h \tag{1}$$

where Q_p^n represents the net heat input into the control volume over the plain, ΔP_h represents the upper-level large-scale forcing, and the total amplification factor τ is given by

$$\tau = \tau_a \cdot \tau_v \cdot \tau_q \cdot \tau_e = \tau_a \cdot \tau_h. \tag{2}$$

Here τ_a is related to the geometry of the valley cross-section, τ_v is the topographic amplification factor, τ_q is the ratio of the valley to the plain surface sensible heat flux, and τ_e is related to the heat exchange of the valley with the free atmosphere. In summary, the diagnostic relation relates the along-valley pressure gradient to the topographic amplification factor (τ_v), the time evolution of the valley heat budget (τ_e, τ_q), and the large-scale forcing (ΔP_h).

3 MODEL SETUP

The setup for the numerical simulation of the thermally driven flows using the Advanced Regional Prediction System (ARPS) consists of an idealized three-dimensional topography and two sets of thermal forcing: A *simple forcing* assuming a spatially uniform sensible heat flux with sinusoidal variation in time (diurnal cycle) in the first case, and a *realistic forcing* determined by the full physics including radiation transfer, land surface processes and turbulence in the second case.

4 RESULTS

Fig. 1 shows a snap-shot of the simulated cross-valley and along-valley flow at 1200 local time (LT) at a location 20 km up-valley from the valley entrance for the two sets of thermal forcing. The stronger along-valley

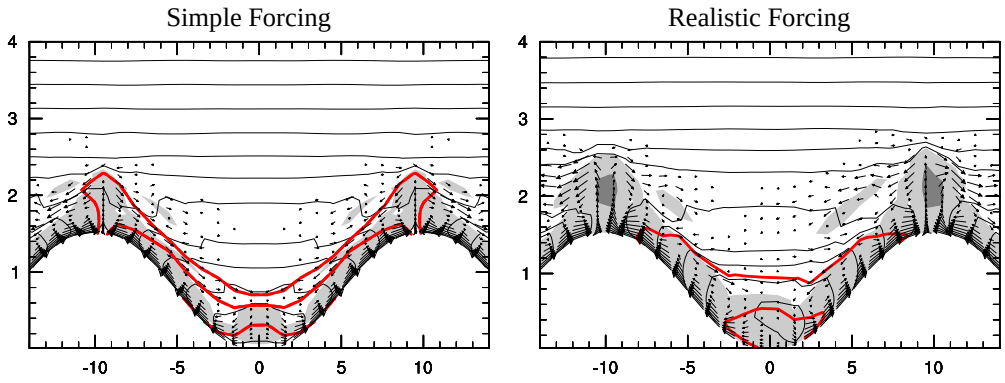

Figure 1: Simulated cross-valley wind vectors and along-valley flow (bold contours) 20 km up-valley from the valley mouth at 1200 LT for the two sets of thermal forcing. The thin lines indicate potential temperature and the shading indicates the vertical eddy diffusivity.

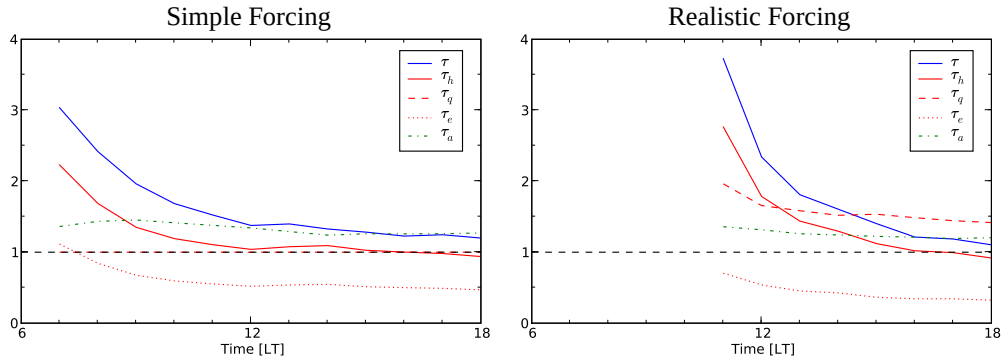

Figure 2: Time evolution of the valley wind forcing factors 20 km up-valley from the valley entrance. For the realistic forcing case, the factors can not be calculated prior to 1100 LT due to cooling instead of heating over the plain during the first few hours.

wind in the simple forcing case can be explained by the larger sensible heat flux during the first few hours in the simple forcing run. The deeper boundary layer in the realistic forcing run is the result of a larger sensible heat flux in the hour prior to the snap-shot (314 W m^{-2} versus 197 W m^{-2}). Note that the integrated forcing in the period 0600 – 1200 LT is very similar for the two cases. Fig. 2 portrays the temporal evolution of the different forcing factors introduced in Eq. (2). Note that $\tau_v = 2$ for the chosen valley geometry. It can be seen that the total amplification factor τ decreases rapidly with time due to significant and increasing heat exchange of the valley with the atmosphere above (τ_e). For the realistic forcing run there is an additional contribution to the forcing due to a larger sensible heat flux in the valley in comparison to the plain (τ_q).

5 CONCLUSIONS

The study finds that the underlying assumption of the valley volume argument, that there is no heat exchange with the free atmosphere, is not fulfilled for the case examined. The heat exchange is small during the first few hours, but rapidly increases thereafter. In the afternoon it is comparable in magnitude to the sensible heat input into the valley atmosphere. The present study confirms the importance of the valley volume effect for the formation of the along-valley wind, but also clarifies the role of subsidence heating and the limitations of the TAF argument. In summary, the analysis brings together different ideas of the valley wind into a unified picture.

REFERENCES

Steinacker, R., 1984: Area-height distribution of a valley and its relation to the valley wind. *Beitr. Phys. Atmosph.*, **57**, 64–71.

Weigel, A.P., F.K. Chow, M.W. Rotach, R.L. Street, and M. Xue, 2006: High-resolution large-eddy simulations of flow in a steep alpine valley. Part II: Flow structures and heat budgets. *J. Appl. Meteor. Climatol.*, **45**, 87–107.

Rampanelli, G., D. Zardi, and R. Rotunno, 2004: Mechanisms of up-valley winds. *J. Atmos. Sci.*, **61**, 3097–3111.

A CONCEPTUAL MODEL FOR THE DAYTIME EVOLUTION OF THE THERMAL STRUCTURE IN A MOUNTAIN VALLEY UNDER FAIR WEATHER CONDITIONS

Dino Zardi
Gruppo di Fisica dell'Atmosfera,
Dipartimento di Ingegneria Civile e Ambientale, Università di Trento, Trento, Italy
E-mail: *Dino.Zardi@ing.unitn.it*

Abstract: A simplified model is proposed to reproduce the essential features of the diurnal evolution of a convective boundary layer (CBL) in a mountain valley. A zero-order order mixed layer (ML) scheme is adopted for the thermal structure above the valley floor, while up-slope mass and heat flows are estimated by means of a Prandtl-like solution. The effects of compensating subsidence are evaluated by estimating the downward motion from mass conservation and assuming a linearly stratified free atmosphere. The resulting evolution equation for the ML height incorporates all the parameters controlling the diurnal evolution of the layer. Thus the model allows to compare CBL growth in the valley and over a plain and to estimate how various factors concur to determine the observed amplification of the diurnal temperature cycle in mountain valleys.

Keywords: *valley, slope, heat flux, convective boundary layer, subsidence, topographic amplification factor (TAF).*

1 INTRODUCTION

Under fair weather conditions in mountain valleys typical winds develop, driven by the along-valley pressure gradients determined by the enhanced heating of the valley atmosphere with respect to the adjacent plains. The factors producing such an amplified temperature range have been extensively explored (Steinacker, 1984, Whiteman, 2000, Rampanelli, et al. 2004). Recent contributions suggest that this effect cannot be explained in terms of geometric factors only (Serafin, 2006). Indeed the processes heating the valley atmosphere are: (a) the subsidence of potentially warmer air in the valley core compensating the development of up-slope flows along the sunny sidewalls; (b) the turbulent heat flux over the valley floor originated from solar radiation and driving the development of a Convective Boundary Layer (CBL). The latter typically displays a vertical structure significantly different than over flat terrain: in particular the mixed layer is usually shallower, whereas the stably stratified capping inversion layer is usually deeper, as a consequence of the core subsidence (Figures 1 and 2).

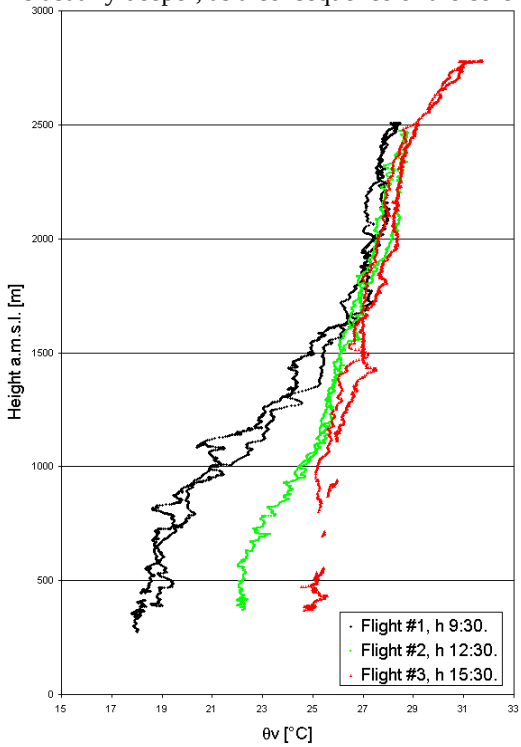

Figure 1: Profiles of virtual potential temperature θ_v during flights subsequently performed in the Adige Valley over Besenello on 1 October 1999 at times reported in the figure legend (adapted from de Franceschi et al., 2003).

2 OUTLINE THE MODEL

The proposed conceptual model assumes a simplified trapezoidal valley cross-section and adopts a zero-order mixed layer (ML) scheme to reproduce the thermal structure of the atmosphere up to the ML height above the valley floor, whereas the initial state of the atmosphere is given by $\theta(z)=\theta_0+\gamma z$.

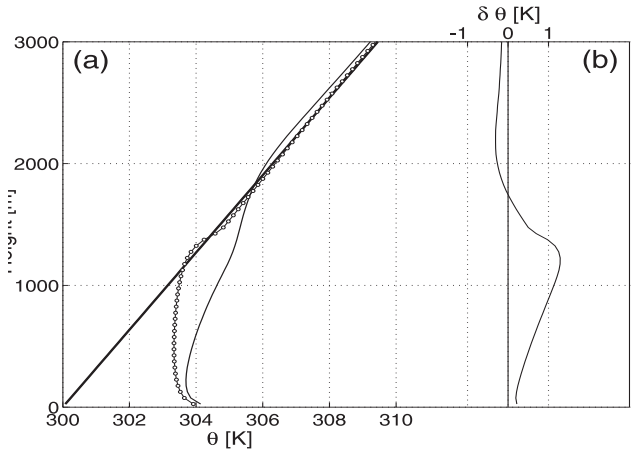

Figure 2: (a) Vertical profiles of potential temperature along the valley axis (thin solid line) and over the plain (bullets) at *t = 6h* after sunrise (the dark solid line shows the initial profile). (b) Difference between the two profiles at various heights (adapted from Rampanelli et al. 2004).

The up-slope mass and heat flow is estimated by means of a Prandtl-like scheme. Accordingly the effect of the subsidence warming is evaluated by estimating the compensating downward motion from mass conservation and evaluating the potential temperature of air parcels entering the top of the ML at any time after sunrise. By combining all these equations and related constraints deriving from continuity and consistency conditions, an evolution equation for the mixed layer height is obtained, which incorporates all the parameters concurring to control the diurnal evolution of the layer. As a result the model allows to evaluate how the air in the valley mixed layer gets warmed more than over the adjacent plain (Figure 3) . This also allows a first estimate of various factors determining the observed amplification of the diurnal temperature cycle in mountain valleys.

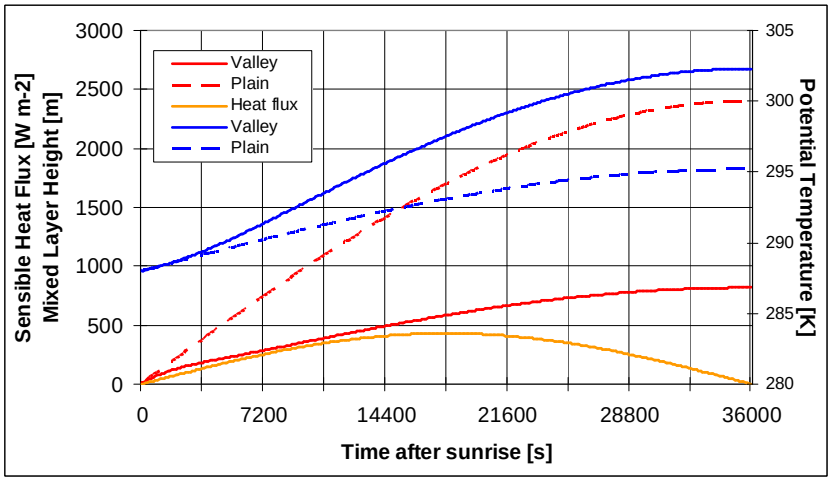

Figure 3: Simulated diurnal evolution of potential temperature (blue lines) and mixed layer height (red lines) respectively in the valley (solid lines) and over the plain (dashed lines) under the same sensible heat flux at ground (orange line) for a valley displaying a floor width of 3 km, a crest height of 3.5 km, a sidewall slope angle α=45° (θ_0 = 288 K, γ = 0.003 K km^{-1}).

Acknowledgements:
I am greatly indebted with Max de Franceschi, Gabriele Rampanelli, Stefano Serafin, Mathias Rotach, Richard Rotunno and Dave Whiteman for many fruitful discussions in these years. I am also very grateful to the late lamented prof. Ignaz Vergeiner for his warm encouragement to pursue my work on conceptual modeling at an early stage of my research activity.

REFERENCES

de Franceschi, M., G. Rampanelli, D. Sguerso, D. Zardi, and P. Zatelli: 2003, Development of a measurement platform on a light airplane and analysis of airborne measurements in the atmospheric boundary layer, Ann. of Geophys. **46**, 269-283.

Rampanelli, G. and D. Zardi: 2004, `A method to determine the capping inversion of the convective boundary layer'. J. Appl. Meteor. **43**, 925-933.

Rampanelli, G., Zardi, D., Rotunno, R., 2004, Mechanisms of Up-Valley Winds , J. Atmos. Sci., **61**, 3097-3111.

Serafin, S., 2006, Boundary-layer processes and thermally driven flows over complex terrain. Ph.D. thesis in Environmental Engineering, Univesity of Trento, Italy, 200 pp.

Steinacker, R., 1984: Area-height distribution of a valley and its relation to the valley wind. Contrib. Atmos. Phys., **57**, 64-71

Whiteman, C. D., 2000: Mountain Meteorology: Fundamentals and Applications. Oxford Univ. Press, New York, 355pp.

OBSERVATIONS AND NUMERICAL SIMULATIONS OF THE INTERACTION BETWEEN THE THERMALLY-FORCED OROGRAPHIC CIRCULATION IN THE CONVECTIVE BOUNDARY LAYER AND DEEP CONVECTION

Bart Geerts and Joshua C. Demko

University of Wyoming, Laramie, Wyoming
E-mail: *geerts@uwyo.edu*

Abstract: Surface and upper-air data, collected as part of the Cumulus Photogrammetric, In situ and Doppler Observations (CuPIDO) experiment during the 2006 monsoon season around the Santa Catalina Mountains in southeast Arizona, are used to study the development of the mountain-scale surface convergence and its interaction with deep convection, which develops very regularly in the afternoon over this mountain. High-resolution multi-nest WRF simulations are being conducted for several days to examine WRF's ability to reproduce the observed convective evolution. The model is validated with observed mountain-scale surface convergence and cloud top height.

Keywords: *ICAM, convection, mountainous area (9 pt in italics)*

1 INTRODUCTION

During the summer, cumulus convection erupts almost daily close to solar noon over the ranges of the interior Mountain West of the United States. The lower troposphere is marked by a deep convective boundary layer (CBL) and weak winds. The moist convection is essential to warm-season precipitation and to surface-troposphere exchange of water and heat in the region. Even relatively simple numerical simulations have shown that under sufficient solar radiation, weak stratification, and weak wind, a thermally-direct circulation develops over a mountain, with anabatic flow converging over a mountain [e.g., Fig. 1 in Demko et al. (2009)]. It is generally believed that the low-level convergence associated with this toroidal circulation, combined with heating over elevated terrain, is responsible for the initiation and maintenance of cumulus convection over or near the mountain [e.g., Fig. 8.15 in Whiteman (2000)].

Few observational studies have documented the thermally forced toroidal circulation over mountains, and they generally only describe the surface component (e.g., Garrett 1980; Banta 1984; Vergeiner and Dreiseitl 1987). Demko et al. (2009) used both aircraft and surface measurements to characterize this circulation around the relatively isolated Santa Catalina Mountains (SCM) in Arizona, a mountain peaking ~2000 m above the plains with a diameter of ~30 km. The surface measurements around the mountain clearly reveal the diurnal evolution of mountain-scale convergence (MSC), which tends to peak around solar noon. The divergent component of the toroidal circulation near the CBL top proved more difficult to capture, even with ~50 flight loops around the SCM. Surface measurements around and on top of the SCM show that the MSC was forced by a diurnally-varying pressure difference between the high terrain and the surrounding plains (Geerts et al. 2008). The diurnal signal of this perturbation pressure difference suggests that is due to heating of the CBL over elevated terrain.

Because the mountains that drive the CBL convergence and deep convection are generally small compared to model resolution, the resulting cloudiness and precipitation are poorly predicted by current numerical weather prediction (NWP) models. Even NWP models of sufficient resolution to resolve the thermally-direct orographic circulations are challenged in their ability to simulate the surface fluxes and CBL growth over complex terrain, and thus accurately predict the timing and intensity of ensuing thunderstorms. Several modeling studies have depicted the development of the CBL and of thermally-forced circulations, but most studies assumed an idealized vertical profile and an idealized mountain. Our study employs real cases to simulate CBL development of a real mountain range, i.e. the SCM. The selected cases occurred during the CuPIDO field campaign (Damiani et al. 2008), therefore detailed observations are available for some basic model validation. This study first verifies whether the model captures the observed MSC and its forcing. The objective then is to use the spatially and temporally continuous, dynamically consistent model output to shed light upon the nature and dynamics of CBL growth and orographic circulations. The first part focuses on cases with little cumulus convection over the SCM, of insufficient depth to produce precipitation and a cold pool. The second part examines the interaction between CBL flow and orographic deep convection.

2 RESULTS

Key observations are summarized in Demko et al. (2009) and Geerts et al. (2008). The WRF v.3.0.1 non-hydrostatic mesoscale model was run with an inner next resolution of 1 km for five days in CuPIDO, two with only Cu congestus, and three others with cumulonimbus development over the SCM. In general the model

captures the MSC (**Fig. 1**, for one of the 5 cases) and convective evolution (as measured by cloud top chronology, not shown) remarkably well. The model is then used to study the diurnal evolution of MSC, CBL depth, and deep convection (Fig. 2). On 9 July deep convection broke out around sunset (02:15 UTC).

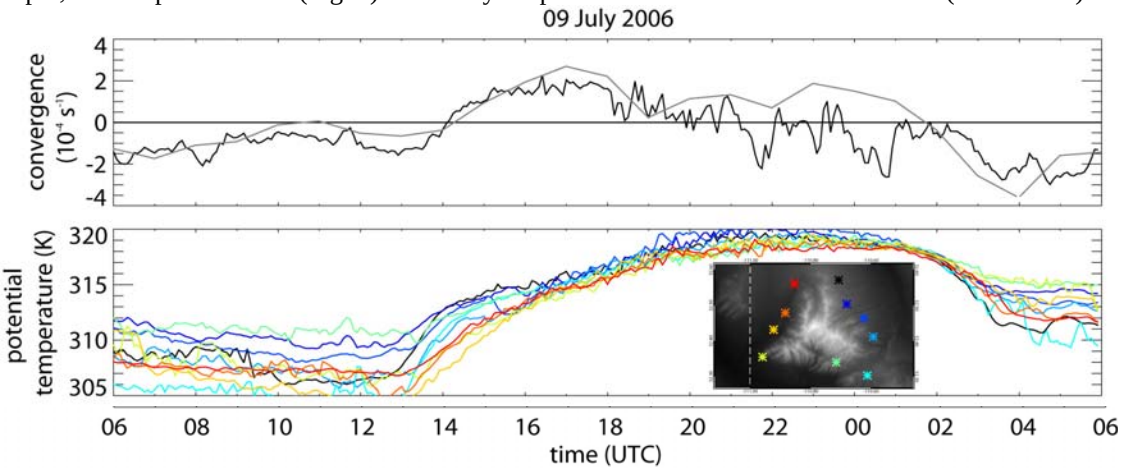

Figure 1: (top) Observed (black) and WRF-modeled (grey) MSC calculated from the 10 ISFF stations and WRF's closest grid point; (bottom) observed potential temperature at the ISFF stations color-coded as shown in the insert terrain map. Solar noon is at 19:30 UTC.

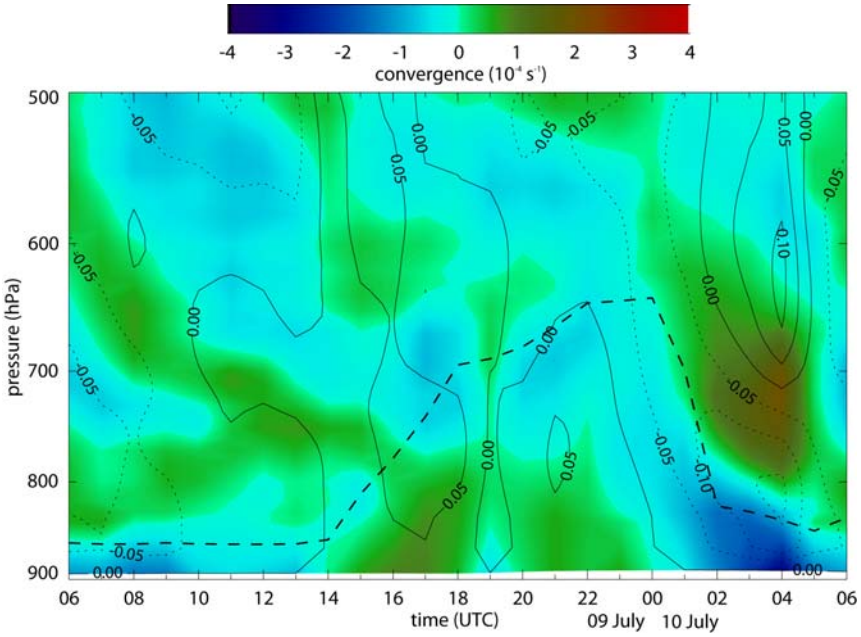

Figure 2: Time-height plot of MSC for the 900 km^2 box (color shaded), mean vertical velocity within this box inferred from mass continuity (solid lines for updrafts, dotted lines for downdrafts, contour interval 0.05 ms^{-1}), and mean CBL height (bold dashed line), for the 9 July case.

Acknowledgements: *This work is funded by National Science Foundation grant ATM-0444254.*

REFERENCES

Banta, R. M., 1984: Daytime boundary-layer evolution over mountainous terrain. Part I: Observations of the dry circulations. *Mon. Wea. Rev.*, **112**, 340-356.

Damiani, R., J. Zehnder, B. Geerts, J. Demko, S. Haimov, J. Petti, G.S. Poulos, A. Razdan, J. Hu, M. Leuthold, and J. French, 2008: Cumulus Photogrammetric, In-situ and Doppler Observations: the CuPIDO 2006 experiment. *Bull. Amer. Meteor. Soc.*, **89**, 57–73.

Demko, J. C., B. Geerts, Q. Miao, and J. Zehnder, 2009: Boundary-layer energy transport and cumulus development over a heated mountain: an observational study. *Mon. Wea. Rev.* , **137**, 447–468.

Garrett, A.J., 1980: Orographic cloud over the eastern slopes of Mauna Loa Volcano, Hawaii, related to insolation and wind. *Mon. Wea. Rev.*, **108**, 931–941.

Geerts, B., Q. Miao, and J.C. Demko, 2008: Pressure perturbations and upslope flow over a heated, isolated mountain. *Mon. Wea. Rev.*, **136**, 4272–4288.

Vergeiner, I., and E. Dreiseitl, 1987: Valley winds and slope winds: observations and elementary thoughts, *Meteorol. Atmos. Phys.*, **36**, 264–268.

Whiteman, C. D., 2000: *Mountain Meteorology: Fundamentals and Applications.* Oxford University Press, 376 pp.

INVESTIGATION OF OROGRAPHIC VENTING OF ATMOSPHERIC BOUNDARY LAYER AIR USING OBSERVATIONS AND THE WRF-CHEM MODEL

Jian-Wen Bao[1], Sara A. Michelson[2], Evelyn D. Grell[2], Georg A. Grell[2]

[1] NOAA/Earth System Research Laboratory/Physical Sciences Division, Boulder, Colorado, USA
E-mail: *Jian-Wen.Wao@noaa.gov*
[2] NOAA/Earth System Research Laboratory and CIRES/University of Colorado, Boulder, Colorado, USA

Abstract: Three-dimensional air-mass transport under fair weather conditions in California's Central Valley between the atmospheric boundary layer (ABL) to the free troposphere (FT) is investigated with a case study using the observations from the Central California Ozone Study (CCOS) 2000 field experiment and the WRF-Chem model.

Keywords: *CCOS, WRF-Chem, atmospheric boundary layer, pollution transport, orographic ventilation and recirculation*

1 INTRODUCTION

Orographic ventilation and recirculation of pollution in the Atmospheric Boundary Layer (ABL) have been recognized as important mesoscale transport processes in the formation of poor air quality in areas surrounded by complex topography (see, e.g., Henne et al. 2004). One such area is the Central Valley (CV) of California. Although state-of-the-art mesoscale models are capable of simulating the transport processes, it is not clear how accurate the simulated processes are, given the inevitable uncertainties in the physics and input parameters of the models. In addition, the conditions necessary for initiating and maintaining the processes are not well understood in terms of mesoscale and micrometeorological dynamics. These two issues need to be addressed in order to improve model-based air quality forecasts and control planning in the CV. In a pilot research effort, a combined field and modeling investigation is conducted to address these issues by taking observations within the ABL and the transition layer between the ABL and the free troposphere in the CV, and applying a numerical model to simulate and analyze the observed properties of the transport processes. In this investigation, orographic ventilation and recirculation processes taking place along both the Coast Range and the Sierra Nevada slopes are simulated and compared with observations.

2 MODEL SETUP AND OBSERVATIONS

The WRF-Chem model (Grell 2004) is used in this study. The results shown are from simulations on a 4-km domain that encompasses the Central California Ozone Study (CCOS) 2000 field study area, extending from the Pacific Ocean in the west to the Sierra Nevada in the east, and from north of Redding, CA, south to the Mojave Desert. The case highlighted here is the 29 July to 3 August 2000 high-ozone episode, which is one of the poor air quality events that occurred during the CCOS field experiment. The RACM-KPP chemical mechanism is used in the WRF-Chem simulations along with the physics configuration including the Mellor-Yamada-Janjic ABL and the Monin-Obukhov (Janjic) surface layer schemes, the NOAH land surface model, the Goddard short-wave, RRTM long-wave radiation schemes and the WSM 5-class microphysics parameterization. Brief descriptions of the physics parameterization schemes in the WRF model can be found in (Skamarock et al. 2005). There are 50 vertically stretched levels with 30 levels within the lowest 2 km and the lowest model layer is about 24 m thick. The initial and boundary conditions are generated using the 6-hourly 40-km National Center for Environmental Prediction (NCEP) Eta analysis.

The CCOS observations are used to evaluate the skills of the WRF-Chem meteorological model in reproducing the overall pattern of the observed low-level flows. The observational datasets used for the meteorological comparison include a network of 24 915-MHz wind profilers and one 449-MHz wind profiler along with the surface data at these sites. The wind profilers provide hourly averages of wind speed and direction, typically to heights of 3000 m AGL. In addition to winds, the profilers measure the vertical profile of virtual temperature up to 1000 m AGL using the Radio Acoustic Sounding System (RASS) technique.

3 MESOCALE CIRCULATION ASSOCIATED WITH THE VENTOLATION

Mesoscale circulation components are important in the orographic ventilation and recirculation of the ABL pollution in the CV. These components are dynamically complex because they interact with each other. Previous observational and modeling studies reveal the distinct features of these components (Bao et al. 2008; Michelson and Bao 2008). First, the low-level winds in the Sacramento Valley (SV) are characterized by the

diurnal variation of the up-valley flow and the down-valley flow. Second, the central CV is characterized by the splitting of the incoming flow from the San Francisco Bay area. Third, the flow in the San Francisco Bay area is characterized by the diurnal variation of the strength of the incoming flow from the Pacific Ocean that moves through the Carquinez Strait. Fourth, the flow in the San Joaquin Valley (SJV) is characterized by the incoming flow that moves towards the south, where a low-level jet typically develops at night and interacts with the downslope flows along the foothills of the eastern side of the SJV to form the Fresno Eddy. In addition to the Fresno Eddy, interaction between the northward inflow and the nocturnal down-valley flow in the SV often leads to the formation of a counterclockwise local eddy to the north or northwest of Sacramento, known as the Shultz Eddy during the night. It remains a question as to whether or not these two eddies play a significant role in local pollution recirculation.

As documented in (Bao et al. 2008), comparisons of the observations and the simulation indicate that the WRF-Chem meteorological model captures the major characteristics of the observed low-level winds in the CV, but quantitative differences are noticeable. These differences can, in theory, be attributed to the errors in the simulated topographically induced local forcing (largely due the errors in the atmospheric boundary layer physics) and the simulated interaction between the upper-level winds and the aforementioned low-level flows.

4 SUMMARY AND CONCLUSIONS

Three-dimensional air-mass transport under fair weather conditions in California's CV between the atmospheric boundary layer to the free troposphere is investigated with a case study using the observations from the CCOS 2000 field experiment and the WRF-Chem model. First, the comparisons of the observations and the model simulation are carried out to show that the WRF-Chem model simulates the meteorological processes of this case well. Then, the movement of the tracers simulated by the WRF-Chem model is analyzed to reveal the characteristics of the three-dimensional transport. Our results indicate that the three-dimensional air-mass transport is very complex under fair weather conditions in the CV. During the day, the development of the convective ABL acts as an efficient "air pump" that transports pollutants upward as the ABL grows. However, the slope wind system around the CV plays an important role in redistributing pollutants vertically as well as horizontally. The tracer movement indicts that once lifted to the FT, the pollutants that originate in the ABL are vertically recirculated downward toward the ABL and horizontally transported by the synoptic flow. During the night, as the two major horizontal mesoscale low-level eddies (i.e., the Schultz and Fresno Eddies) are formed, the remnants of the pollution in the ABL converge horizontally and are recirculated along the foothills, where they remain at low-levels until sunrise and are then vertically redistributed as the daytime ABL develops. Under typical fair weather conditions in summer, there are two major lower tropospheric pathways for the ABL air masses to move out the CV: eastward over the Sierra Nevada and southward through the Tehachapi Pass.

REFERENCES

Bao, J.-W., S. A. Michelson, P. O. G. Persson, I. V. Djalalova, and J. M. Wilczak, 2008: Observed and WRF-Simulated Low-Level Winds in a High-Ozone Episode during the Central California Ozone Study. *J. App. Meteor. and Climat.*, **47,** 2372–2394.

Gell, G. A., S. E. Peckham, R. Schmitz, S. A. McKeen, G. Frost, W. C. Skamarock, and B. Eder, 2005: Fully Coupled Online Chemistry Within the WRF Model. *Atmos Environ.*, **39**, 6957-6975.

Henne, S., M. Furger, S. Nyeki, M. Steinbacher, B. Neininger, S. F. J. deWekker, J. Dommen, N. Spichtinger, A. Stohl, and A. S. H. Prévôt, 2004: Quantification of topographic venting of boundary layer air to the free troposphere. *Atmos. Chem. Phys.*, **4**, 497-509.

Michelson, S A and J.-W. Bao, 2008: Sensitivity of Low-Level Winds Simulated by the WRF Model in California's Central Valley to Uncertainties in the Large-Scale Forcing and Soil Initialization. *J. App. Meteor. and Climat.*, **47**, 3131–3149.

Skamarock, W. C. , J. B. Klemp, J. Dudhia, D. O. Gill, D. M. Barker, W. Wang, and J. G. Powers, 2005: A description of the Advanced Research WRF Version 2. NCAR Tech Notes-468+STR. [Available from UCAR Communications, P.O. Box 3000, Boulder, CO 80307.]

ASSESSMENT OF AIR QUALITY AND MIXING-LAYER HEIGHT IN AN ALPINE VALLEY FROM MEASUREMENTS AND NUMERICAL MODELLING

Stefan Emeis[1], Klaus Schäfer[1], Renate Forkel[1] , Friedl Obleitner[2] , Peter Suppan[1]

[1] Institute for Meteorology and Climate Research – Atmospheric Environmental Research (IMK-IFU), Forschungszentrum Karlsruhe GmbH, Garmisch-Partenkirchen, Germany
E-mail: *Stefan.emeis@imk.fzk.de*
[2] Institute of Meteorology and Geophysics, University of Innsbruck, Innsbruck, Austria

Abstract: Due to their geometrical shape Alpine valleys are strongly vulnerable to high anthropogenic emissions. Within the project ALPNAP measurements and modelling efforts have been undertaken to analyse the air quality and noise situation in several valleys of the Alps through which major trans-European traffic routes (motorway and railway) are running. Here we will present results with respect to air quality from a section of the Inn Valley east of Innsbruck. In-situ observations at the valley floor and on the slope and from a tethered balloon together with horizontally path-averaging (DOAS) and vertical profiling (SODAR, ceilometer) remote sensing instruments during winter 2005/06 yielded meteorological and air pollution data for the valley atmosphere close to and further away from the motorway/railway lines running through this valley. The highest pollutant concentrations built up during a ten-day high pressure episode with permanent snow cover which was coined by a persistent multiple layer structure with inversions in the valley atmosphere which was not broken up neither by valley nor by slope winds. A mesoscale numerical model (MCCM), with a spatial resolution of 1 km in the inner nest, has been used to simulate the air quality in this part of the valley for January 2006. Measured data and model simulations together give a good basis for reliable mitigation strategies to reduce the air pollution effects on the health of the local population. The effects of changing climate could be estimated from future frequencies of snow cover occurring in such valleys.

Keywords: *air quality, mixing-layer height, Alpine valleys, in-situ measurements, remote sensing, numerical modelling*

1 INTRODUCTION

Due to their geometrical shape Alpine valleys are strongly vulnerable to high anthropogenic emissions. This is especially true for winter and early spring when nocturnal radiative cooling over snow surfaces leads to an extremely stable thermal stratification of the valley boundary layer and the formation of persistent inversions which allow for a high accumulation of air pollutants at the valley floor.

Within the European Union INTERREG IIIb project ALPNAP (Monitoring and Minimisation of Traffic-Induced Noise and Air Pollution Along Major Alpine Transport Routes) measurements and modelling efforts have been undertaken to analyse the air quality and noise situation in several valleys of the Alps through which major trans-European traffic routes (motorway and railway) are running. Main emphasis has been laid on wintry episodes during which the strongest adverse environmental impact on the local population is expected. The results presented here will focus on air quality. Apart from in-situ measurements two further tools (ground-based remote sensing and numerical modelling with a chemistry-transport model) have been employed and are evaluated here.

2 DATA AND MODEL SETUP

The in-situ observations at the valley floor and on the slopes comprised apart from classical meteorological and air quality measurements the operation of a tethered balloon in the valley centre and the retrieval of path-averaged pollution data with a DOAS across and away to the motorway A12.

Ground-based remote sensing yielding vertical wind and aerosol profiles with an acoustic (SODAR) and an optical device (ceilometer) were performed during winter 2005/06. Acoustic and optical backscatter intensities were processed to derive the mixing-layer height and the vertical structure of the valley atmosphere (Emeis et al. 2008).

The coupled mesoscale meteorology-chemistry model MCCM (Grell et al., 2000) has been used to simulate the air quality in this part of the valley for January 2006. The model contains several online-coupled tropospheric gas-phase modules, a photolysis module and a BVOC emission module. Aerosol processes are described with the modal MADE/SORGAM aerosol module. Three nested model domains were simulated with the innermost nest having a spatial resolution of 1 km.

3 RESULTS

The measurements yielded meteorological and air pollution data for the valley atmosphere close to and further away from the motorway/railway lines running through this valley (Emeis et al. 2007, Schäfer et al.

2008). The air quality data show a clear dependence on the thermal stratification of the valley atmosphere and on the occurrences of inversions within the wintry valley boundary layer. The highest pollutant concentrations built up during a ten-day high pressure episode in January 2006, which led to a persistent multiple layer structure with inversions in the valley atmosphere which was not broken up neither by valley nor by slope winds. Figure 1 shows an extreme example for the thermal structure of the valley atmosphere which can form over a longer-lasting snow cover.

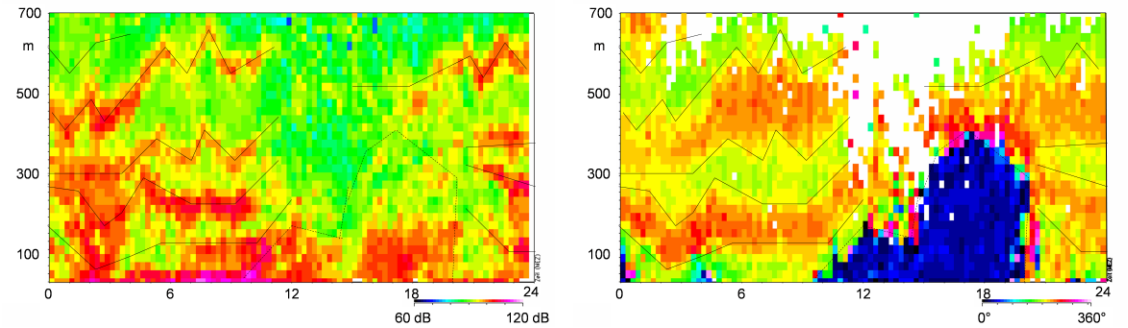

Figure 1. Acoustic backscatter intensity (left; purple and red: high, green: low) and wind direction (right; green: down-slope winds, red: down-valley winds, and blue: up-valley winds) from the SODAR measurements on January 29, 2006. The lines in the two Figures have been analysed from the wind direction changes in the right-hand frame (from: Emeis et al. 2007).

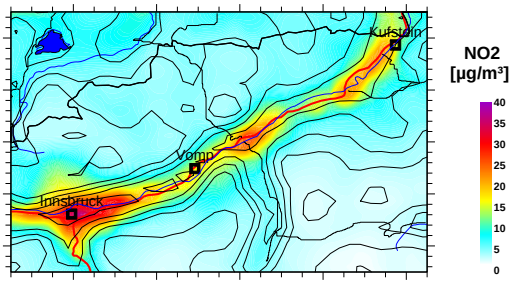

First results (Figure 2) of the mesoscale model MCCM show high concentrations of NO_2 at the valley ground and low concentrations on the mountain ridges. The high NO_2 concentrations are caused by the traffic of the highway at the valley floor, increasing by the medium and small cities as well as due to the mixing layer in which the air pollutants are trapped.

Figure 2. Simulated annual mean of NO_2 concentrations near the surface. Highest concentrations can be found at the valley floor along the highway route with peaks in and around cities. At higher altitude background concentrations of NO_2 are dominating.

4 CONCLUSIONS

Measured data and model simulations together give a good basis for the development of reliable mitigation strategies to reduce the air pollution effects on the health of the local population. As the snow cover was an important meteorological prerequisite for the formation of the extremely stable thermal stratification in the valley atmosphere, the effects of a changing climate on air quality in Alpine valleys could be estimated from future occurrence frequencies of a longer-lasting snow cover in such valleys. The possible corresponding long-term changes in atmospheric layering can influence the number of the exceedences of the EU threshold values of air pollutants as for NO_2 additionally to variances in the emission pattern and chemical processes.

Acknowledgements:
We thank the Austrian military for granting access to their Frundsberg barracks to place some of our remote sensing equipment there. The project ALPNAP (Monitoring and Minimisation of Traffic-Induced Noise and Air Pollution Along Major Alpine Transport Routes) has received European Regional Development Funding through the INTEREG IIIB Community Initiative.

REFERENCES

Emeis, S., C. Jahn, C. Münkel, C. Münsterer, K. Schäfer, 2007: Multiple atmospheric layering and mixing-layer height in the Inn valley observed by remote sensing. Meteorol. Z., **16**, 415-424.

Emeis, S., K. Schäfer, C. Münkel, 2008: Surface-based remote sensing of the mixing-layer height – a review. Meteorol. Z. **17**, 621-630.

Schäfer, K., J. Vergeiner, S. Emeis, J. Wittig, M. Hoffmann, F. Obleitner, P. Suppan, 2008: Atmospheric influences and local variability of air pollution close to a motorway in an Alpine valley during winter. Meteorol. Z., **17**, 297-309.

Grell, G. S. Emeis, W.R. Stockwell, T. Schoenemeyer, R. Forkel, J. Michalakes, R. Knoche, W. Seidl ,2000: Application of a Multiscale, Coupled MM5/Chemistry Model to the Complex Terrain of the VOTALP Valley Campaign. Atmospheric Environment, **34**, 1435-1453

COMPLEX VALLEY FLOWS AND THEIR IMPACT ON WATER VAPOUR TRANSPORT IN PRE-CONVECTIVE AND CONVECTIVE ENVIRONMENTS: A CASE STUDY

Cyrille Flamant[1], Cedric Champollion[2], Evelyne Richard[3], Laurent Labbouz[1], Frédéric Masson[4], J. Cuesta[5], P. Bosser[6], G. Pigeon[7]

[1] IPSL/LATMOS, CNRS and Université Pierre et Marie Curie, Paris, France
[2] Géosciences Montpellier, Université Montpellier II, CNRS, Montpellier, France
[3] Laboratoire d'Aérologie, CNRS et Université de Toulouse, Toulouse, France
[4] EOST, Institut de Physique du Globe de Strasbourg, Strasbourg, France
[5] IPSL/Laboratoire de Météorologie Dynamique, CNRS et Ecole Polytechnique, Palaiseau, France
[6] LOEMI/Institut Géographique National, Saint Mandé, France
[7] Centre National de Recherches Météorologiques, Météo-France and CNRS, Toulouse, France
E-mail: *cyrille.flamant@latmos.ipsl.fr*

Abstract: Complex valley flows in the Rhine Valley, as well as their impact on water vapour transport, are investigated in pre-convective and convective environments using airborne lidar data and GPS tomography, as well as high resolution numerical simulations. The analysis focuses on the 15 July case study during which an isolated convective storm was observed over the Black Forest. The reasons for null convective initiation over the Vosges are also investigated.

***K*eywords:** *Convection, airborne lidar, GPS tomography, mesoscale modelling*

1 INTRODUCTION

On 15 July 2007, an isolated convective storm was observed over the Black Forest in the framework of COPS (Convective and Orographically-induced Precipitation Study). Even though cumulus clouds were first observed to develop over the Vosges mountains (between 1130 and 1245 UTC), convective initiation (CI) was solely observed over the Black Forest on that day. Over the Black Forest, satellite imagery acquired every 15 min. show that shallow cumulii were first observed at 1145 UTC, and deep convection initiated shortly thereafter southeast of Freudenstadt (Kottmeier et al. 2008). The outputs from the European Centre for Medium-Range Weather Forecasts (ECMWF) model are broadly consistent with the satellite imagery and evidenced conditions favourable to CI over the Vosges in the 1200 UTC analysis, yet detrimental to CI in the 1500 UTC forecast issued from the 1200 UTC analysis. On the other hand, not so favourable conditions for CI were seen in the 1200 UTC analysis over the Black Forest, while the 1500 UTC forecast revealed favorable conditions for CI. The objective of this study is to understand the reason why CI did not occur over the Vosges on 15 June 2007.

2 DATA

In this study, we use a combination of high resolution observations from airborne lidar and Global Positioning System (GPS) tomography to analyse the water vapour variability in the region of the Rhine Valley associated with mountain flows. The airborne lidar LEANDRE 2 (Bruneau et al. 2001) was embarked on the SAFIRE Falcon 20 (F20). On 15 July 2007, the SAFIRE F20 performed two missions along a grid-type pattern (see Fig. 1) at an altitude of 5000 m above mean sea level (msl). The dynamics and thermodynamics at the meso-scale over the COPS domain are investigated using the mesocale model Meso-NH. Finally the synoptic situation is analysed using ECMWF analyses and forecasts.

3 THE ROLE OF DRY AIR MASSES WEST OF THE VOSGES

On this day, the synoptic situation was dominated by the presence of a deep eastern Atlantic trough and a ridge extending from the Mediterranean to Poland. In the low levels, the COPS region was under the influence of a strong southwesterly flow. In the morning, Meso-NH evidenced that a filament of dry air originating from the Mediterranean travelled northeastward reaching the Western part of the COPS domain, mostly to the West of and

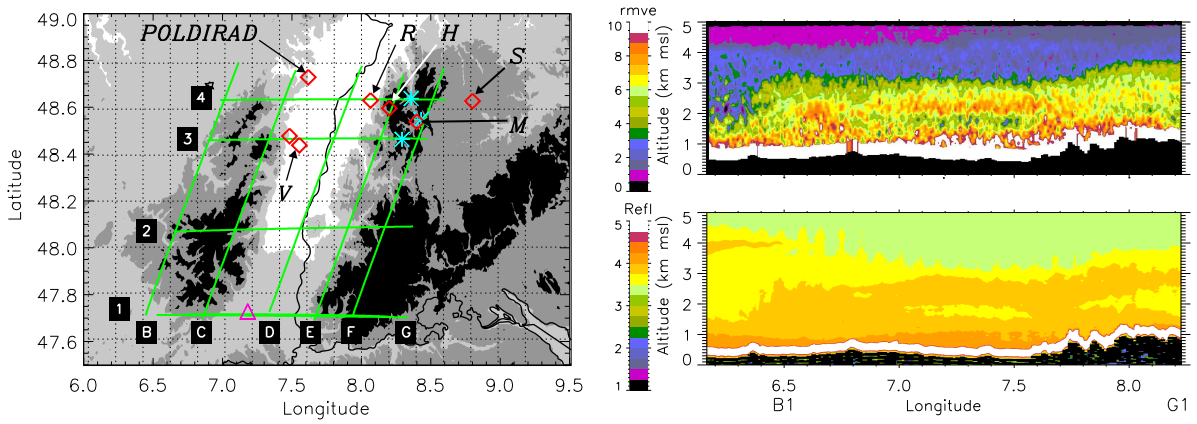

Figure 1: Left: Topography in the COPS domain. Overlain are the SAFIRE F20 flight track (green) and the location of the Supersites (red diamonds). Right: Atmopsheric reflectivity at 730 μm (bottom) and water vapour mixing ratio (top) issued from the airborne lidar LEANDRE 2 along leg B1-G1 between 0803 and 0830 UTC.

alongside the Vosges massif. This dry feature was observed in the morning by LEANDRE 2 (along leg G1-B1, West of B1, i.e. West of 6.4°E) between 2 and 3 km msl (Fig. 1). The Balloon soundings in Nancy revealed that this feature had the characteristics of a low-level jet and was present between 0000 and 1200 UTC (not shown). Airborne lidar measurements made in the afternoon (at times when CI was observed over the Black Forest) also show the presence of dry air masses West of the Vosges, and the accumulation of water vapour along the Eastern flank fo the Vosges (not shown). This was also corroborated by GPS tomography.

4 CONCLUSIONS

The variability of the water vapour field at the mesoscale investigated in pre-convective and convective environments using airborne lidar data and GPS tomography, as well as high resolution numerical simulations, suggest that the presence of a low-level jet transporting dry air masses from the Mediterranean region into the Western COPS region is mostly responsible for the absence of CI over the Vosges on 15 July 2007. The dry low-level jet feature appears to be responsible for preventing the moist air masses transported with the anabatic flow associated with the Rhine Valley-Vosges system from reaching the top of the Vosges. As a result, condistions detrimental to CI are observed over the Vosges.

Acknowledgements: *The authors wish to thank the SAFIRE (Service des Avions Français Instrumentés pour la Recherche en Environnement, www.safire.fr), the Institut Géographique National (IGN, www.ign.fr) and the Division Technique of the Institut National des Sciences de l'Univers (DT/INSU, www.dt.insu.cnrs.fr). The authors are grateful to D. Bruneau and P. Genau (LATMOS), F. Blouzon, A. Abchiche and N. Amarouche (DT/INSU) for re-fitting and operating the LEANDRE 2 system in the F/F20. Special thanks to A. Gribkoff, R. Cailloux and M. Laurens (SAFIRE) for operating the dropsonde system.*

REFERENCES

Bruneau, D., P. Quaglia, C. Flamant, M. Meissonnier, J. Pelon, 2001: The airborne lidar LEANDRE II for water-vapor profiling in the troposphere. I. System description. *Appl. Opt.*, **40**, 3450–3475.

Kottmeier, Ch., N. Kalthoff, U. Corsmeier, Ch. Barthlott, J. Van Baelen, A., Behrendt, R. Behrendt, A. Blyth, R. Coulter, S. Crewell, M. Dorninger, C., Flamant, Th. Foken, M. Hagen, C. Hauck, H. Höller, H. Konow, M. Kunz, H., Mahlke, S. Mobbs, E. Richard, R. Steinacker, T. Weckwerth, A. Wieser, and V. Wulfmeyer, 2008: Mechanisms initiating deep convection over complex terrain during COPS. *Meteorol. Z.*, **17**, 931–948.

DEVELOPMENT OF AN ALPINE LEE CYCLONE DURING MAP D-PHASE: FORCINGS FOR CYCLOGENESIS

Ron McTaggart-Cowan[1], T. J. Galarneau Jr.[2], L. F. Bosart[2] and J. A. Milbrandt[1]

[1]Environment Canada, Montreal, Canada
Email: ron.mctaggart-cowan@ec.gc.ca
[2]State University of New York at Albany, Albany, United States of America

Abstract: The development of a subsynoptic-scale cyclone in the Gulf of Genoa during the Mesoscale Alpine Project (MAP) Demonstration of Probabilistic Hydrological and Atmospheric Simulation of flood Events in the Alpine region (D-PHASE) project is investigated using analyses and model simulations. The cyclogenesis even, which led to the production of tropical storm force winds near the islands of Corsica and Sardinia, is shown to be related to the interaction between an upper-tropospheric short-wave disturbance and lower-level potential vorticity (PV) anomalies that occur as the flow in the Alpine region transitions from flow "over" to flow "around" the barrier. The role of the Alps in the initiation of these features is diagnosed using a set of model attribution tests involving modifications to the local orography. Moutain-scale PV banners and a lee-side warm anomaly are shown to combine to create a local environment conducive to sub-synoptic cyclogenesis, although the development pathway of the cyclone – as diagnosed by an eddy energy budget – depends strongly on the extent of the Alpine influence on the regional flow.

Keywords: ICAM, Alpine lee cyclogenesis, Genoa cyclones

1. INTRODUCTION

The rapid development of subsynoptic-scale cyclones in the Gulf of Genoa constitutes an important forecasting challenge for the western Mediterranean. One such event took place on 15 November 2007, during the Mesoscale Alpine Project (MAP) Demonstration of Probabilistic Hydrological and Atmospheric Simulation of flood Events in the Alpine region (D-PHASE) project Rotach and Coauthors (2009), and within 12~h led to the generation of tropical storm force winds near the islands of Corsica and Sardinia. This region is well known to favor the development of subsynoptic-scale cyclones (Buzzi and Tosi 1989), which generally occur as an upper-level trough over western Europe crosses the Alpine barrier [Pichler and Steinacker (1987) and others]. With dense coastal populations and numerous shipping lanes, such strong wind events in the western Mediterranean can have a large impact on the region despite their relatively small horizontal scale.

The present study presents a diagnosis of the key features that influence the development of the Genoa cyclone on 15 November 2007 and evaluates the ability of a set of control forecasts to simulate the evolution of the system. Section 2 briefly describes the datasets and model used for this investigation. A description of the cyclogenesis event and model simulations follows in Section 3.

2. DATA AND NUMERICAL MODEL

Two sources of analysis data form the basis for the analysis component of this study: the Canadian Meteorological Centre (CMC) global analysis (0.35° grid spacing) and the National Centers for Environmental Prediction final analysis (0.5° grid spacing). The latter data are used in calculations of air parcel trajectories and frontogenesis since the vertical motion field is not archived in the CMC analysis. A variety of observational platforms are used to both augment and evaluate the global analyses, including: an Italian radar composite for the D-PHASE project[1], Meteosat Second Generation visible and infrared satellite imagery, and QuikSCAT scatterometer data. Data from the World-Wide Lightning Location Network is used to evaluate the extent and intensity of deep convection associated with the GoG cyclone.

The GEM model is used for all simulations presented in this study. The nonhydrostatic model uses semi-implicit time-stepping and semi-Lagrangian advection (Cote et al. 1998). All simulations performed for this study are triply-nested, beginning with a global 0.35° forecast integrated from CMC analyses. A limited-area version of the GEM model (identified as CMCGEML during MAP D-PHASE) is launched simultaneously with a grid spacing of 0.135°, using the global model outputs as boundary conditions. A second nest (CMCGEMH/S) is started 6~h later with a grid spacing of 0.0225°. No convective parameterization is activated in integrations on the inner domain.

1Made available by the Agenzia Regionale Prevenzione e ambiente dell'Emilia-Romagna Servizio IdroMeteoClima (ARPA-SIM)

3. DIAGNOSIS OF FORCINGS FOR DEVELOPMENT

The development of an intense, subsynoptic cyclone in the Gulf of Genoa on 15-16 November 2007 has been analyzed, and a pair of forecast sequences have been evaluated. Three key components of the cyclogenesis event have been identified: 1) a long- ived upper-level CTD embedded in a synoptic-scale trough; 2) a lee-side surface thermal perturbation; and, 3) a primary orographic PV banner.

The passage of a short wave trough across the Alps leads to upwards-increasing PV advection and stability reduction over the Gulf of Genoa. The lower-level vortex develops along a lower-level horizontal shear line that forms in the confluence zone between easterly winds over the Gulf and the northerly Mistrals blowing off the coast of France. The influence of the Alps on the development of the GoG cyclone is highlighted by the transition of the flow from ”over” to “around” the Alpine barrier.The cold-frontal inversion near ridge-top and veering mid-level winds induce a transition to flow ``around'' the Alps on 15 November.

Before the transition, extensive precipitation occurred on the Alpine north side, and descent in the lee contributes – in conjunction with cold-frontal retardation – to the development of the lee-side warm anomaly. Following the flow transition, parcels curve cyclonically around the southwestern tip of the barrier, acquiring PV by differential friction and resulting in the formation of a primary PV banner. As shown in Fig. 1, the initiation of the cyclone in the model attribution tests occurred in a region of enhanced vorticity northwest of Sardinia that results from the superposition of these two PV features. This region is favoured for development since the ambient vorticity is readily streched by the extensive convection associated with the cold flow over the relatively warm Mediterranean waters. A noteworthy exception to this occurs in the COLD model simulation shown in Fig. 1. In this test the warm anomaly was removed, making the mountain-scale PV banner the primary feature in the Alpine lee. The upper-level disturbance couples with the banner in this case, leading to a development that occurs well to the west of the observed location (identified as Best Track in Fig. 1).

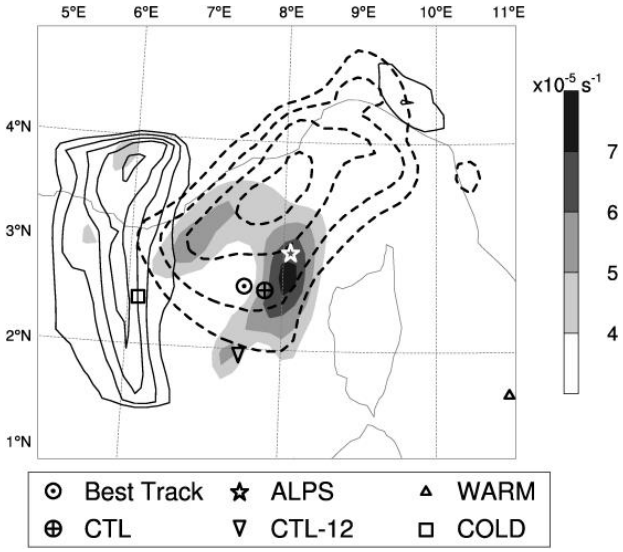

Figure 1: Relative vorticity (550-450 hPa) in shading as indicated on the greyscale bar, resulting from the combined inversion of the PV banner (solid lines show 950-600 hPa PV at 0.2 PVU intervals) and the lee-side warm anomaly (dashed ilnes show the surface potential temperature anomaly at 2 K intervals). The location of cyclogeneis in the attribution tests is shown with the symbols indicated in the legend.

The identification of the key components involved in this case of Gulf of Genoa cyclogenesis, and the interactions that occur between them during the flow transition, serve to illucidate the role of the Alps in rapid sub-synoptic scale development. A companion study investigates the sources of eddy energies associated with this event further illustrates the importance of the Alpine barrier in modulating the the development pathway (classical baroclinic versus convectively-driven) of the cyclone. These studies use modern models and high resolution datasets corroborate the findings of earlier studies and provide additional insight into the features and processes germante to Alpine lee cyclogenesis.

ACKNOWLEDGEMENTS

The authors would like to thank Kristen Corbosiero and Sergio Abarca who processed the WWLLN lighting used in this study, Mike Brennan who provided gridded QuikSCAT data, and Silvio Davolio who archived and granted us access to the ARPA-SIM radar composite.

REFERENCES

Buzzi, A. and E. Tosi, 1989: Statistical behaviour of transient eddies near mountains and implications for theories of lee cyclogenesis. *J. Atmos. Sci.,***43**, 2826-2837.

Pichler, H. and R. Steinacker, 1987: On the synoptics and dynamics of orographically induced cyclones in the Mediterranean. *Meteor. Atmos. Phys.*, **36**, 108-117.

Rotach, M. and Coauthors, 2009: MAP D-PHASE: Real time demonstration of weather forecast quality in the Alpine region. *Bull. Amer. Meteor. Soc.*, (in review).

Cote, J., S. Gravel, A. Method, A. Patoine, M. Roch and A. Staniforth, 1998: The operational CMC-MRB Global Environmental Multiscale (GEM) model. *Mon. Wea. Rev.*, **126**, 1373-1395.

A DYNAMICAL INFLUENCE OF THE HIMALAYAS ON THE WINTER MONSOON OVER SOUTHEASTERN ASIA

Sylvain Mailler[1,2], François Lott[1]

[1] Laboratoire de Météorologie dynamique, Paris, France
[2] Ecole Nationale des Ponts et Chaussées, Marne-La-Vallée, France
E-mail: *flott@lmd.ens.fr*

Abstract: Previous studies have shown (i) that the Tibetan plateau produces a significant fraction of the two components of the Equatorial Mountain Torque (EMT) in winter, (ii) that these torques are in part related to the East Asian cold surges, and (iii) that the cold surges affect the convection over the maritime continent. We show here that these relations are strong enough for the convection over the Equatorial South China Sea (ESCS) to be associated with significant signals on the two components of the EMT that can precede by a few days and more the convection. These signals are associated to surface pressure and temperature patterns that are strongly reminiscent of the East Asian cold surges. Our results therefore show that the Tibetan plateau couple dynamically the midlatitudes and the tropical region, and that the vectors of this dynamical coupling are the cold surges.

***K*eywords:** *Mountain torques, cold surges, tropical convection, winter monsoon*

1 INTRODUCTION

During the northern winter, the weather in eastern Asia, the South China Sea (SCS) and the maritime continent is dominated by the winter monsoon, where the active monsoon phase is characterized by northerly low-level winds along the East Asian coasts extending from Japan to the SCS and intense convective events over the SCS and Borneo (e.g. *Houze et al.*, 1981). As has been shown in earlier studies (e.g. *Chang et al.*, 2005), the Borneo vortex intensity and the East Asian cold surges are important in modulating this monsoon.

By showing that the convective events over the ESCS are often preceded by significant signals on the Equatorial Mountain Torque generated by the Tibetan plateau, we establish that the dynamical forcing of the Tibetan plateau on the East Asian winter monsoon is strong enough to have a direct impact on convection over this major monsoon variability center. We also verify that the vectors of this relationship between the Tibetan plateau and the monsoon convection are the cold surges.

2 DATA AND METHODS

The surface pressure and low-level temperature values are from the NCEP/NCAR reanalysis. After removing the annual and interannual variations, the resulting series will be noted $\widetilde{T}_{50m}$ and $\widetilde{P}_S$. The index $\widetilde{I}_C$ of the convective activity over the ESCS is the opposite of the average of the NOAA interpolated OLR over the sector $[105°\text{E};120°\text{E}]\times[0°\text{N};15°\text{N}]$. With this definition, positive values of $\widetilde{I}_C$ correspond to low OLR and active convection over the ESCS.

The two components $\widetilde{T}_{M,1}$ (along the Greenwich axis) and $\widetilde{T}_{M,2}$ (along the $90°$E equatorial axis) of the EMT due to the Tibetan plateau are computed following *Feldstein* (2006). A positive $\widetilde{T}_{M,1}$ results from a positive South-North pressure gradient over the topography while a negative $\widetilde{T}_{M,2}$ is associated to a West-East positive pressure gradient, as described in *Egger and Hoinka* (2008). Positive West-East pressure gradients also produce a positive polar torque $\widetilde{T}_{M,3}$ (*Lott et al.* (2004)).

The composite maps and series of Fig.1 are built using the 20 strongest positive peaks and the 20 strongest negative peaks of $\widetilde{I}_C$ from November through March (NDJFM) during the 1979-2007 period. A Student t-test is used to evaluate the confidence levels.

3 RESULTS

The composites of $\widetilde{T}_{M,1}$ and $\widetilde{T}_{M,2}$ keyed on $\widetilde{I}_C$ are shown in Fig.1a. In it we can see that there is a significant positive anomaly in $\widetilde{T}_{M,1}$ from D-6 to D-2 which peaks at D-5. After this peak in $\widetilde{T}_{M,1}$, Fig.1a shows that $\widetilde{T}_{M,2}$ becomes negative, and this lasts from D-4 to D0. To extract the intraseasonal variations that are visible on Fig.1a (periods around 20 days), we filter the series with the *Blackmon* (1976) low-pass filter that isolates signals with periods of 10 days and more.

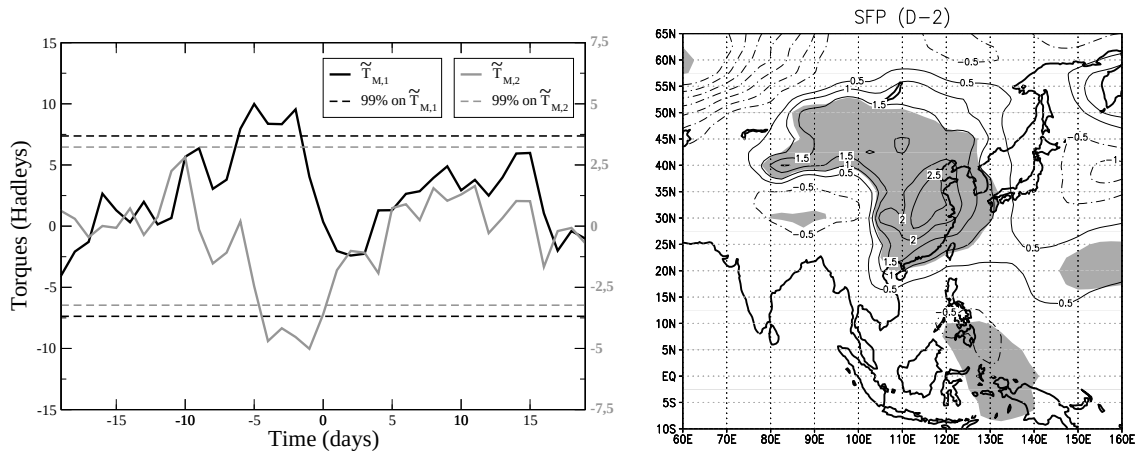

Figure 1: (a) Composite series of $\widetilde{T}_{M,1}$ (black solid) and $\widetilde{T}_{M,2}$ (gray solid) keyed on $\widetilde{I}_C$. Units for the torques are in Hadley: $1\,\mathrm{H} = 10^{18}\ \mathrm{kg\ m^2\ s^{-2}}$. The dotted lines correspond to the 99% significance level for $\widetilde{T}_{M,1}$ (black) and $\widetilde{T}_{M,2}$ (gray). (b) Composite of the IS $\widetilde{P}_S$ (hPa) two days before a peak of $\widetilde{I}_C$. Contour interval: $0.5\ \mathrm{hPa}$; positive values, light solid; negative values, light dotted; zero-contour omitted; 99% confidence, shaded.

Figure 1b shows that, two days before the convection peaks, there is a significant intraseasonal high pressure anomaly over East Asia. This signal is associated to a negative temperature anomaly, in a way that is typical of the East Asian cold surges (see *Mailler and Lott*, 2009). It is this surface pressure signal that produces the negative $\widetilde{T}_{M,2}$ at that time (Fig.1a).

4 CONCLUSIONS

The analyzes presented here reveal that the winter monsoon convective events over the ESCS are often preceded by large signals in both components of the EMT due to the Tibetan plateau. A detailed study of the surface pressure and surface temperature patterns associated to these EMT signals has been carried out by *Mailler and Lott* (2009). These authors show that the signals we described here on the two components of the EMT are associated with high surface pressure anomalies travelling from southern Siberia to the SCS within a week together with low temperature anomalies, and that this anomalies are closely linked to the East Asian cold surges.

Our results suggest that the EMT affects the onset and the break of the winter monsoon active phases. They have some predictive interest in the sense that the signals on the torques precede by a few days and more these on the convection. From a more theoretical point of view, our results are related to the fact that the orography triggers anticyclones. As there is a large body of theoretical literature in mountain meteorology related to the development of lee cyclones (see for instance *Smith* (1979)), we will need to check if these theories can be adapted to our cases in order to understand our statistical results from a theoretical point of view.

References

Blackmon, M. L. (1976), A climatological study of the 500 mb geopotential height of the Northern Hemisphere, *J. Atmos. Sci.*, *33*, 1607–1623.

Chang, C.-P., P. A. Harr, and H.-J. Chen (2005), Synoptic disturbances over the equatorial South China Sea and western Maritime Continent during boreal winter, *Mon. Weather Rev*, *133*, 489–503, doi:10.1175/MWR-2868.1.

Egger, J., and K.-P. Hoinka (2008), Mountain torque events at the Tibetan Plateau, *Mon. Weather Rev*, *136*, 389–404, doi: 10.1175/2007MWR2126.1.

Feldstein, S. B. (2006), Dynamical processes of equatorial atmospheric angular momentum, *J. Atmos. Sci.*, *63*, 565–581, doi: 10.1175/JAS3586.1.

Houze, R. A., S. G. Geotis, F. D. Marks, and A. K. West (1981), Winter monsoon convection in the vicinity of North Borneo. part I: Structure and time variation of the clouds and precipitation, *Mon. Weather Rev*, *109*, 1595–1614.

Lott, F., A. W. Robertson, and M. Ghil (2004), Mountain torques and northern hemisphere low-frequency variability. Part I: Hemispheric aspects, *J. Atmos. Sci.*, *61*, 1259–1271.

Mailler, S., and F. Lott (2009), Dynamical influence of the Tibetan Plateau on winter monsoon convection over southeast Asia, *Geophys. Res. Lett.*, *36*, L06708, doi:10.1029/2008GL036952.

Smith, R. B. (1979), Some aspects of the quasi-geostrophic flow over mountains, *J. Atmos. Sci.*, *36*, 2385–2392.

Dynamics on Vortex with Heavy Rainfall in East to Tibetan Plateau

Sixiong ZHAO[1] Shenming FU[1,2]

[1] Institute of Atmospheric Physics，Chinese Academy of Sciences, Beijing，100029, China

Email: *zhaosx @ mail.iap.ac.cn*

[2] Graduate University of Chinese Academy of Sciences，Beijing，100049, China

Abstract

Some vortexes form usually in east to Tibetan Plateau, which are called as the Southwest Vortex (SWV) because they appear in Southwest China.The majority of them form, develop and disappear in original places, only a few of them can move eastward, sometimes cause the strong heavy rainfall and severe flooding in East China. The formation and development of this kind of vortexes are the key scientific problems because of its importance in improving the prediction of disastrous weather in China. Therefore, the relevant investigation regarding this kind of the vortexes has been conducted. In this study, the vortex case of June 2008 , with the severe heavy rainfall in South China, is studied by using the reanalysis data from NCEP/NCAR, one-hour interval surface observation, intensive rawinsonde data, Satellite TBB data from FY-2C and conventional observation data. The results are as follows:

(1). The Southwest vortexes was the direct influencing system for the heavy rainfall, it developed ahead the trough in westerlies at 500 hPa and the vortex was steered by the trough, to move eastwards. The rainy area moved from west to east accompanying with SWV. The cold air played very important role and there existed significant cold advection at 500 hPa.

(2). There was the structure of weak warm core in the vortexes in upper troposphere rather than that of the cold core in the extra-tropical cyclones. However, the warm core of the SWV is weaker than that of tropical cyclone.

(3). The diagnostic analysis shows that the maintenance and intensification of vorticity were mainly associated with divergence term in vorticity equation which indicates the friction impact existed in low troposphere, especially that in planetary boundary layer in east to the Plateau.

(4). Convective activities and precipitation were always at the central area of SWV and the right-front side of the track of SWV. Convective cloud clusters were active during the heavy rainfall. Some of them belonged the meso-α or meso-β-scale systems, respectively, with the one-hour maximum of precipitation amount of 90 mm, longest period about 17 hours, and moved at almost as same as the speed of SWV. There were about 11 meso-scale rainy clusters, they are quasi-stationary or moved slowly. The interaction between the cloud clusters and the vortexes can be found and its formation mechanism seemed to be also related with The Second Kind of Conditional Instability (CISK). The release of latent heating contributed very significantly to development of the vortexes.

(5). The intensive air sounding of Guilin station, South China indicates that, the relative humidity was rich at the low levels whereas poor at the upper levels, the stratification at middle -- lower troposphere was neutral, with thermal inversion. After the SWV moved out, wind at low levels changed significantly, the CAPE decreased.

(6). Tropical system, that is, the monsoon trough extending from India, Bangladesh, Indo-China peninsula to South China and monsoon surges, associated with the monsoon trough, influenced the SWV and make the latter to re-intensify, also re-initiating the heavy rainfalls. There existed the obvious interaction between middle and lower latitude systems.

(7). Sufficient water vapor played very important role in occurrence of heavy rainfall, the Bay of Bengal and South China Sea, probably, are main water vapor source places.

(8). During the heavy rainfalls in June 2008, the SWV moved eastwards, and re-intensify in South China; the long persistence of the short wave trough at 500 hPa was closely responsible to the heavy rainfalls.

(9). The vortexes have the obvious characteristics of subtropical weather systems. This kind of vortexes is quite different from the cyclones in east to Rocky Mountains, North America and in east to Alps, Europe and more comparison studies between them should be conducted in future.

(10). The trough moved eastward accompanying with the eastward retreatment of subtropical high pressure and also the rainy area moved eastward. The subtropical high pressure system in West Pacific also plays the very important role in occurrence and maintenance of heavy rainfalls, at first, the subtropical high extend westward and quasi-stationary, so the short wave trough at 500 hPa moved very slowly, then the subtropical high pressure retreated eastward, the rainy area shifted from South China to East China with the eastward movement of the trough. A new vortex developed in the original SWV and then, replaced the latter.

(11). Based on the mentioned-above, one kind of vortex typed heavy rainfalls in South China during pre-rainy season has been proposed.

CLIMATE VARIABILITY IN NORTH-WESTERN ITALY THROUGH THE USE OF RECONSTRUCTED AND HOMOGENIZED THERMO-PLUVIOMETRIC SERIES

Simona Fratianni[1], Fiorella Acquaotta[1]

[1] Department of Earth Science, University of Turin, Turin, Italy
E-mail: *simona.fratianni@unito.it*

Abstract: In order to properly study climate variations, homogeneous series are needed. We have therefore analysed thirteen meteorological stations of Piedmont owned by SIMN (Hydrographic and Mareographic National Service) in the 1951-2006 period. We have set up a monthly series for every station and then we have applied the Standard Normal Homogeneity Test for their homogenization. These methods allowed us to estimate the real trend for each series. On the other hand, the non-parametric Mann-Kendall test has been used to understand the statistical meaning of the trend for the thermal-pluviometric series. We have calculated climate indices (frost days, days with no thaw, tropical nights, summer days, thermal sum, rainy days, density of precipitations) over WMO 30-years periods (1951-80, 1961-90, 1971-2000) and over the whole period.

Keywords: *Piedmont, temperature, precipitation, homogenization, climate change, climate indices.*

1 INTRODUCTION

In this study were analyzed climatic changes occurred in Piedmont, over the last fifty-six years. We studded the maximum and minimum temperatures and precipitation series extracted from the meteorological database of the ex-SIMN (Hydrographic National Service) now ARPA (Regional Agency for Environmental Protection) – Piedmont.

2 DATA AND METHODS

In order to create a complete database, without missing data, we have reconstructed the gap in the series We have identified the monthly, seasonal and annual gaps and considered as a gap not only the period with the total absence of records but also the range that did not have at least 80% of the data (Klein Tank and Konnen, 2003). For the reconstruction we have used three methods of spatial interpolation (Eischeid et al. 1995). For each candidate series, we have selected a maximum of four neighbouring stations.

Unfortunately, most data show non–climatic factors that may hide the real changes. The SNHT allows to detect and estimate the single shift variations of the mean value of a candidate series compared with a homogeneous reference series (Alexandersson et al. 1997). We have used the ratio for the precipitation series and the difference for the temperatures. Once identified the discontinuous value, the period antecedent must be corrected by the correction factors estimated by the test (Stépànek, 2005).

The trends have been calculated on the seasonal and annual precipitation series, on the maximum and minimum temperatures series and on the series of seasonal and annual anomalies standardized of the variable considered. In order to estimate the consistency of the series, a level of significance of 5% has been imposed, and the trends have been calculated using the non-parametric Mann-Kendall test (Bohm et al. 2001).

We have analyzed the average monthly values of the maximum and minimum temperatures and precipitation to obtain an overview of some climate indices defined by CCL/CLIVAR (Zhang et Yang, 2004).

3 RESULTS

Trends have been calculated on the reconstructed and homogenized series (Tab.1). The series with standardized anomalies of annual and seasonal precipitation of the stations located at less than 500 m of height, show decreasing trends mainly in winter and summer, save for the Varallo Sesia station, where a growing trend is recorded in winter, spring and autumn. For the stations located at a higher altitude than 500 m a.s.l., these patterns show instead a growing trend in almost all the seasons, except for winter and autumn at Salbertrand, the summer season at Piedicavallo and Bardonecchia and the winter and summer season at Valprato Soana. Despite that, for most of the series, both at an annual and seasonal level, the results of the Mann-Kendall test did not allow for the assimilation of the estimated trend. Only the trends associated with the spring and summer seasons at Vercelli and Oropa are significant in statistical terms.

The standardized anomalies of maximum and minimum temperatures show growing trends and the significance test allow for the assimilation of results. For both variables, the largest increase was determined in winter, save for the Vercelli station where, for minimum temperatures, the largest increase was found in spring, and Varallo Sesia maximum temperatures show a larger increase in summer. Growing and statistically

acceptable trends have also been calculated for the annual temperatures series (Tab.2). At the Vercelli, Turin and Luserna S. G. stations, the largest increase is recorded within the minimum temperature series, at Varallo Sesia and Asti within maximum temperatures.

Stations	Latitude	Longitude	Elev.[m]	Winter	Spring	Summer	Autumn	Year
Vercelli	45°19'32"	08°23'26"	135	(-)	(-)	(-) p=0.01	(+)	(-)
Asti	44°53'09"	08°12'48"	152	/	/	/	/	(-)
Torino	45°04'49"	07°40'25"	270	(-)	(-)	(-)	(-)	(-)
Cumiana	44°57'53"	07°23'31"	327	(-)	(-)	(-)	(-)	(-)
Varallo Sesia	45°49'14"	08°16'30"	453	(+)	(+)	(-)	(+)	(-)
Luserna S. G.	44°48'50"	07°14'32"	476	(-)	(-)	(-)	(-)	(-)
Susa*	45°08'10"	07°05'33"	520	/	/	/	/	(-)
Salbertrand*	45°04'20"	06°53'42"	1010	(-)	(+)	(+)	(-)	(-)
Piedicavallo*	45°41'35"	07°57'26"	1040	(+)	(+)	(-)	(+)	(+)
Oropa	45°37'40"	07°58'56"	1180	(+)	(+) p=0.01	(+)	(+)	(+)
Bardonecchia*	45°04'33"	06°43'03"	1353	(+)	(+)	(-)	(+)	(-)
Piamprato*	45°33'28"	07°34'27"	1555	(-)	(+)	(-)	(+)	(+)
Ceresole Reale*	45°28'08"	07°08'25"	2260	(+)	(+)	(+)	(+)	(+)

Table 1. Geographical location of the meteorological stations during the period 1951-2006. * Stations that have measured only the precipitation variable. Pattern of seasonal and annual trends found for every station: (-) decreasing trend; (+) growing trend; / not calculated trend. For Vercelli and Oropa stations, the probability value associated with the Mann Kendall test ($p<0.05$) is also shown, indicating that the trend calculated is statistically acceptable.

Stations	Maximum temperatures (°C/yr)		Minimum temperatures (°C/yr)	
Vercelli	+0.03±0.01	p=0.01	+0.05±0.01	p=0.001
Asti	+0.03±0.01	p=0.01	+0.006±0.008	p=0.001
Torino	+0.03±0.01	p=0.003	+0.04±0.01	p=0.001
Luserna S. G.	+0.05±0.01	p=0.001	+0.060±0.004	p=0.001
Varallo Sesia	+0.04±0.01	p=0.001	+0.03±0.01	p=0.001
Oropa	+0.04±0.01	p=0.001	+0.04±0.01	p=0.001

Table 2. Maximum and minimum annual temperatures trends; p shows the significance of the Mann-Kendall test.

We have also selected three periods of 30-years defined by WMO (1951-1980, 1961-1990 and 1971-2000) and we have individualized that the minimum values of the precipitation, the number of rainy days and the density of rain are always found in the second period, 1961-1990. Besides the changes individualized over time in all stations have also been revealed in the pluviometric regimes. The main change was the shift from a subalpine regime, with its main maximum in autumn to a prealpine regime with its main maximum in spring.

We have also analyzed the average monthly values of the maximum and minimum temperatures and some climate indices calculated on the three period of 30-years. By comparing the first and last 30-years period of the minimum temperature series, a 0.7 °C increase is shown, while for maximum temperatures the difference corresponds to 0.5°C; as a result, the number of tropical days has also grown. A decrease in the number of days of frost (from 80 to 67) and days without thaw (from 11 to 6 days) can be instead observed.

In accordance with the national and international bibliography, the minimum temperatures series have showed an increase greater than the maximum temperatures series and this have caused a decrease, over the years, in the number of months classified cold.

Acknowledgements: *The authors wish to thank ARPA Piedmont and in particular Roberto Cremonini, Manuela Bassi and Barbara Cagnazzi for supplying data and the suggestions given in this study.*

REFERENCES

Alexandersson, H. and A. Moberg, 1997: Homogenization of Swedish temperature data. Part 1: Homogeneity test for linear trends. Int. J. Climatol. Volume **17**, 25-34.

Bohm, R., I. Auer, M. Brunetti, M. Maugeri, T. Nanni and W. Schoner, 2001: Regional temperature variability in the European Alps: 1760-1998 from homogenized instrumental time series, Int. J. Climatol., Volume **21**, 1779-1801.

Eischeid, J., C. Baker, T. Karl and H. Diaz, 1995: The quality control of long-term climatological data using objective data analysis, Journal of Applied Meteorology, Volume **34**, 2787-2795.

Klein Tank, A. and G. Konnen, 2003: Trends in indices of daily temperature and precipitation extremes in Europe, 1946-99, Amer. Meteorol. Soc. **16**, 3665-3680.

Stèpànek, P., 2005: AnClim, software for time series analysis, Dept. of Geography, Fac. of Natural Sciences, MU Brno.

Zhang, X. and F. Yang, 2004: RclimDex (1.0), User manual, 23 pp.

AN ALPINE CLIMATOLOGY OF EXTREME EVENTS

Sophie Fukutome, Mark Liniger, Chritoph Frei

Federal Office of Meteorology and Climatology MeteoSwiss, Zurich, Switzerland
E-mail: *sophie.fukutome@meteoswiss.ch*

Abstract:
A climatology of extreme weather events is presented for the part of the Alpine region located in Switzerland. The General Extreme Value (GEV) Theory is used to estimate the distribution of maxima and/or minima of various climatological parameters at the stations of the Swiss Meteorological Observation Network. These parameters include precipitation, temperature, wind gusts and wind speed, snow, and consecutive dry days.

Keywords: *Extremes, Alps, climatology*

1 INTRODUCTION

Understanding today's climate requires knowledge of extreme aspects of the climate and their frequency. Especially in the Alpine Region, events such as heat waves, droughts, or heavy precipitation can have dire consequences. Our purpose is to provide a climatology of return periods and/or return values of climatological parameters relevant to extreme weather in Switzerland, which covers a large part of the alpine region.

2 DATA AND METHOD

The data used in the present study stems were measured at the stations of the Swiss Meteorological Observation Network. The parameters chosen encompass precipitation, temperature, wind, fresh snow, and the number of consecutive dry days. For precipitation and snow, various levels of aggregation, such as sums over 1, 2, 3, 4, 5, or 10 days are also examined. For precipitation, seasonal analyses are performed as well. For temperature, minima are also analyzed.

The Block Maxima method of the classical Extreme Value theory (Coles, 2001) is applied, in which the General Extreme Value (GEV) distribution is fitted to the maxima or minima of blocks of data. The parameters of the distribution are estimated with the maximum likelihood method. Confidence bounds with respect to the best estimate are estimated with the profile log-likelihood method.

Because of the large number of stations, the process is entirely automatized. The Kolmogorov-Smirnov test is implemented with a randomization procedure to automatically discard stations at which the data is incompatible with the best estimate.

3 RESULTS AND CONCLUSIONS

Maps of the 1-day and 5-day precipitation return values for a 30-year return period reveal some of the characteristics of the climate in the alpine region. In the summer, thunder-storms bring heavy precipitation to the pre-Alps, or the Tessin (Fig. 1 and 2, left-hand panel). In winter, low-pressure systems bring about precipitation events that extend over several days, hence the low values over the Swiss Plateau (Fig. 1 and 2, right-hand panel). These lasting winter events are also responsible for the smaller difference between summer and winter values in the Swiss Plateau for 5-day precipitation return values (fig. 2). The pattern of the 5-day precipitation return values reveal the lack of extended periods of rain in the summer in the Rhone Valley.

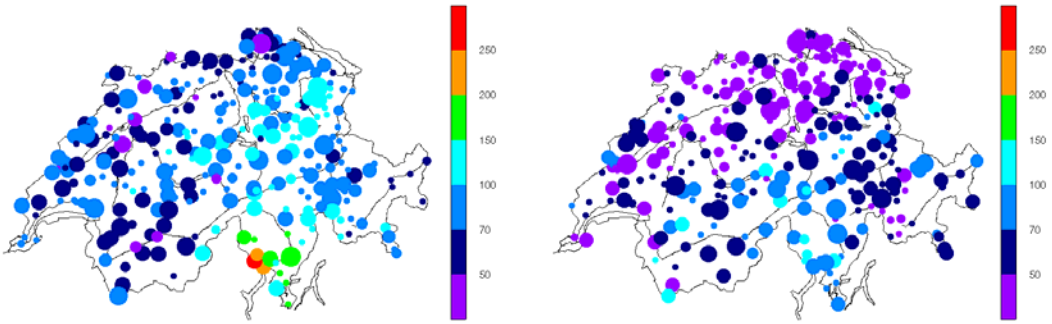

Figure 1. Return values of 1-day precipitation for a 30-year return period [mm]. Left: summer. Right: winter. The size of the dots is proportional to the length of the time series (longest: 1864-2008; shortest: 1964-2008).

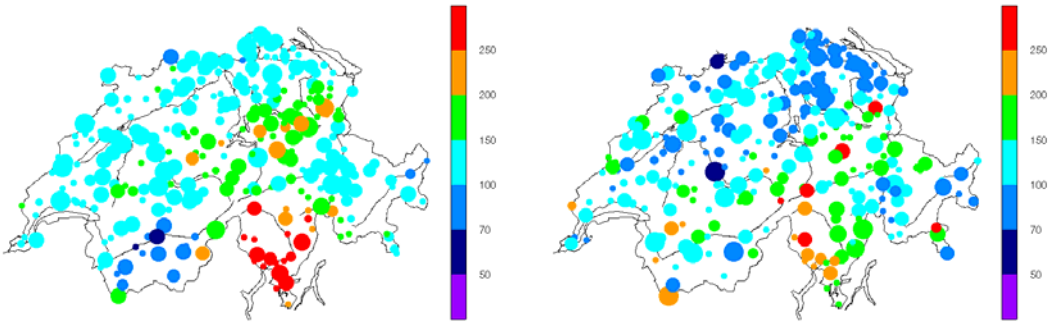

Figure 2. Return values of 5-day precipitation for a 30-year return period [mm]. Left: summer. Right: winter. The size of the dots is proportional to the length of the time series (longest: 1864-2008; shortest: 1964-2008).

Similar maps for fresh snow (not shown) show, as expected, an increase of the return values with altitude, but also highlight stations with particular extreme value behavior due to the topographical configuration. Valleys prone to Föhn can be recognized by the large return values of the mean wind speed.

In general, it can be said that the maps of return values for given return periods reflect the characteristics of the climate in the alpine region, and bring to light the areas liable to frequently suffer intense climatic events.

REFERENCES

Coles, S., 2001: An Introduction to Statistical Modeling of Extreme Values, 208 pp., Springer, New York.

Stephens, M. A., 1970: Use of the Kolmogorov-Smirnov, Cramer-von Mises and related statistics without extensive tables, J. Roy. Stat. Soc., **32B**, 115-122.

Winter storms with high loss potential in a changing climate: a regional perspective

Monika Rauthe[1], Michael Kunz[1], Susanna Mohr[1]

[1] Institute for Meteorology and Climate Research University Karlsruhe / Forschungszentrum Karlsruhe, Karlsruhe, Germany
E-mail: *monika.rauthe@imk.uka.de*

Abstract: In the RESTER (Strategien zur Reduzierung des Sturmschadenrisikos für Wälder) project the impacts of extreme storm events on the forests in Germany are analysed. The regional storm climate is quantified by means of wind gusts from regional climate models (REMO and CLM). Extreme value statistics are applied to estimate the gust wind speeds of a specific return period at every grid point. There is a systematic underestimation of the gust wind speeds in comparison to the observations (1971 – 2000), but the spatial patterns due to the orographic influences are well reproduced by the regional models. They are able to resolve partially the orographic amplifications on wind speeds, what is the big advantage over the coarse resolution of the global models. In the future (2021 – 2050) changes of the storm climate in Southern and Central Germany are not well-defined, while in Northern Germany an increase of the storm activity seems to be likely. Apart from the analysis of single model runs an ensemble composite of different models and scenarios is created to quantify the probability of the changes.

***K*eywords:** *winter storm, orography, climate change, RESTER*

1 INTRODUCTION

According to the recent publications of the IPCC, climate changes are unequivocal and changes in the global climate system will increase in the following decades (IPCC 2007). Concerning winter storms as reproduced by global climate models, an enhancement especially of severe cyclones over Europe is found (see review by Ulbrich et al. (2009) and references therein). Changes of the strength and/or occurrence of extreme natural hazards on the regional scale, however, are only partially known. Due to the low resolution of current global climate models, regional effects can be hardly estimated - especially for parameters like wind speed or precipitation, which are strongly amplified by local scale conditions (e.g. orographic effects). Because of the high loss potential of winter storms the knowledge about changes of the storm climate on a regional scale is very important. Our investigations are conducted in the framework of the research project "Herausforderung Klimawandel" funded by the federal state of Baden-Württemberg. Within the RESTER project, we characterises the changes in winter storm climate in Germany with a special focus on the region of Baden-Württemberg in the southwest of Germany.

2 DATA AND METHODS

This study is based on different data sets from regional climate models (REMO and CLM), which are are both forced by the global climate model ECHAM5. In contrast to ECHAM5 with a horizontal resolution of 2.5°, REMO and CLM have a resolution of about 10 and 18 km, respectively. For the projection period, the calculations include the IPCC emission scenarios A1B, A2 or B1 (IPCC 2007). Extreme value statistics are applied to quantify the storm climate. The analyses are based on the time series of wind gusts at each grid point. Using the method of independent storms with a minimum distance of 48 h for the hourly values and the peaks over threshold method, the maximum gusts of the 100 strongest events are fitted with the generalized Pareto distribution (Palutikof et al. 1999). The strength of storms of a specific return period is estimated from this distribution. This analysis is applied to every single grid point for both the control period (1971 – 2000) and the projection period (2021 – 2050).

3 RESULTS

To estimate the reliability of the regional climate models, they are evaluated for the control period against the so-called storm hazard map from CEDIM (Center for Disaster Management and Risk Reduction Technology) published by Heneka et al. (2006). Despite the systematic underestimation of the gust wind speeds the spatial patterns due to the underlying orography are well reproduced by the regional models. Altogether, the regional climate models are able to resolve the local amplifications of wind speeds, e.g. due to orography and land use. This is a big advantage over the coarse resolution of the global models. The underestimation of the gust speeds in the simulations is not relevant in the following, because only relative climate change signals are investigated.

Expected changes of the storm climate are analysed for the gust speeds of a 10-year return period. They vary in the different parts of Germany. The results of the single models show that the storm activity in Northern Germany will increase about 5 – 10% in the future. Also in Central and Southern Germany there is no clear trend, i.e. no

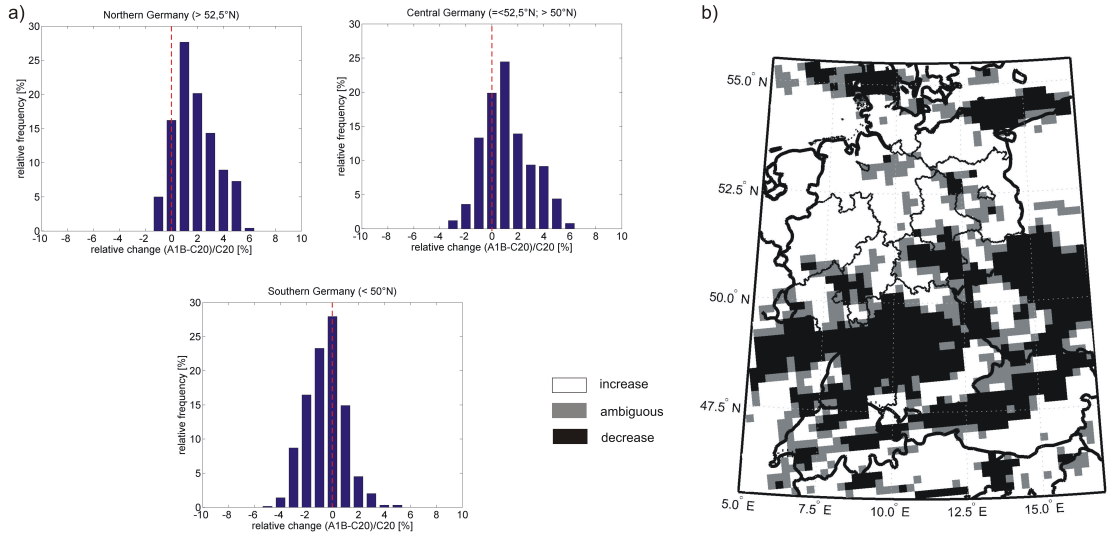

Figure 1: Relative gust wind speeds between the projection and control period relative to the control period for three parts of Germany of a 10-year return period. a) Ensemble mean of the seven regional climate simulations. b) Probable changes larger/smaller than $\pm 0.5\%$ predicted by the majority of the models.

strong changes of storm climate has to be expected. It has to be noted, though, that the changes of the storm climate in regional models greatly depend on the changes in the utilised global model. The ensemble, which is created by seven regional models runs on a uniform grid, confirm the result mentioned before. Figure 1a displays the histograms of relative changes of the gust wind speed for the ensemble mean in different parts of Germany. Furthermore, most likely changes of the storm climate can be identified by the ensemble composite (Fig. 1b). In Northern Germany, the increase of gusts is quite likely. In Central and Southern Germany the trends are indifferent and in some parts even a decrease of the storm activity seems to be possible. It has to be emphasised that such a differentiation between the regions is only possible by means of regional climate models.

4 OUTLOOK

Apart from the data presented here, CLM simulations with a resolution of ~ 7 km are available at our institute. First investigations show that the storm climate in Southern Germany exhibits no clear trend, but an influence of the orography is obvious. In the future, the CLM-7-km data will be also integrated in the ensemble approach.

In addition to the strength of the storms their horizontal extent is an important factor for the loss potential. A so-called storm index, which takes both the strength and horizontal extension of storms into account, is calculated following Della-Marta et al. (2009). First results show no large differences compared to the results of the grid-point analysis. In the future, these results will be linked with the economic losses by the storms.

Acknowledgements:
We thank the Max-Planck-Institute for Meteorology in Hamburg for conducting and providing the ECHAM5 and REMO model data. The REMO simulations were commissioned by the German Federal Environment Agency. The CLM simulations are part of the so-called "Konsortialläufe".

REFERENCES

Della-Marta, P. M., H. Mathis, C. Frei, M. A. Liniger, J. Kleinn and C. Appenzeller, 2009: The return period of wind storms over Europe, *Int. J. Climatol.*, **29**, 437 – 459, doi:10.1002/joc.1794.

Heneka, P., T. Hofherr, B. Ruck and C. Kottmeier, 2006: Winter storm risk of residential structures - model development and application to the German state of Baden-Württemberg, *Nat. Hazards Earth Syst. Sci.*, **6**(5), 721–733.

IPCC, 2007: *Climate Change 2007: the physical science basis: contribution of Working Group I to the Fourth Assessment Report of the Intergovernmental Panel on Climate Change*, [S. Solomon, D. Qin, M. Manning, Z. Chen, M. Marquis, K. B. Averyt, M. Tignor and H. L. Miller eds.], Cambridge University Press, 996 pp.

Palutikof, J. P., B. B. Brabson, D. H. Lister and S. T. Adcock, 1999: A review of methods to calculate extreme wind speeds, *Met. Appl.*, **6**, 119–132.

Ulbrich, U., G. C. Leckebusch and J. G. Pinto, 2009: Extra-tropical cyclones in the present and future climate: a review, *Theoret. and Appl. Climatology*, doi:10.1007/s00704-008-0083-8, published online.

SATELLITE-BASED RETRIEVAL OF GLOBAL RADIATION OVER COMPLEX TERRAIN: A CLIMATOLOGY FOR THE ALPS

Rebekka Posselt[1], Bruno Dürr[2], Reto Stöckli[1], Richard Müller[3], Mark Liniger[1]

[1] Federal Office for Meteorology and Climatology MeteoSwiss, Zürich, Switzerland
[2] Sunergy GmbH, Buchs, Switzerland
[3] Deutscher Wetterdienst DWD, Offenbach, Germany
E-mail: *rebekka.posselt@meteoswiss.ch*

Abstract: Meteosat second generation (MSG) satellite data is used to derive a climatology of surface incoming solar radiation (SIS) over the Alps. Monthly mean SIS maps, as well as the respective anomalies are made available over Switzerland from 2004 to the present. Comparisons with surface based station measurements and climatologies show a very good agreement.

Keywords: *ICAM, surface radiation, satellite,snow*

1 INTRODUCTION

The Satellite Application Facility on Climate Monitoring (CM-SAF, `www.cmsaf.eu`) is part of EUMETSAT's satellite data processing with a special emphasis on the retrieval of climate variables such as cloud parameters, radiative budget and water vapour. The MeteoSwiss contribution to CM-SAF is the validation and improvement of the standard surface incoming shortwave (SIS) radiation product especially over complex terrain such as the Alps. Special attention is drawn to the radiative influence of snow. For this purpose accurate retrieval of clouds over snow is required and the radiative properties of snow have to be considered.

2 DATA AND METHODS

Data from the Meteosat Second Generation (MSG) satellites (Meteosat 8 and 9, in operation since 2004) are used (Schmetz et al., 2002). They provide data in 12 channels covering the visible (VIS) and the infrared (IR) spectra on a horizontal resolution of 3km every 15 min. Additionally, there is a high resolution visible (HRV) channel with a spatial resolution of 1km.

Several IR and VIS channels are used to obtain information about the state of the atmosphere and the surface for each pixel. This information is then used to calculate the cloud index that accounts for radiation reflected from snow in addition to attenuated radiation due to clouds (Dürr and Zelenka, 2009). The SIS is then calculated by scaling the expected clear sky radiation with the cloud index. The clear sky radiation depends on the sun's elevation, surface elevation and the atmospheric turbidity. The latter describes the radiative impact of water vapour, atmospheric aerosols, ozone, etc. on the atmospheric transmission.

Figure 1 shows the monthly mean cloudindex (≤ 0: cloud free, ≥ 1: overcast) for December 2005. The original Heliosat algorithm (upper panel) (Beyer et al., 1996; Hammer et al., 2003) shows a very high cloud index over snowy regions (i.e., in the mountains) which is largely reduced by the new snow detection algorithm (lower panel).

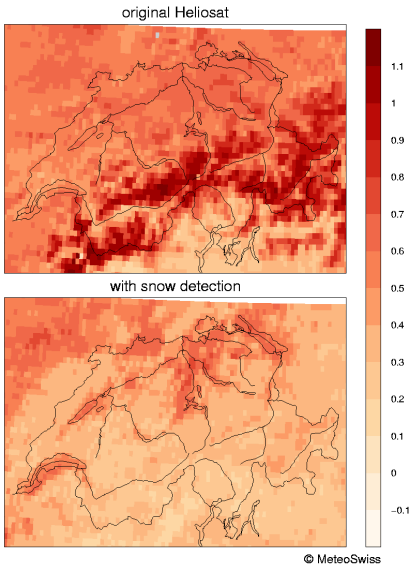

Figure 1: Monthly mean cloud index for Dec 2005 for the original Heliosat and for Heliosat with snow detection

3 RESULTS AND QUALITY ASSESSMENT

A complete 5-year dataset of SIS based on METEOSAT 8 and 9 data is derived. The derived SIS climatology is available as monthly mean SIS and corresponding monthly anomalies over Switzerland for the period 2004-2008. Figure 2 shows the overall mean SIS over Switzerland for the years 2004-2008. The usage of the HRV channel allows for a clear distinction of valleys and mountains. The mountainous regions receive larger amounts of shortwave radiation, amongst others due to snow effects and less foggy/cloudy days (than in the lowlands).

The satellite-retrieved SIS is validated with surface measurements from the Alpine Surface Radiation Budget (ASRB) network in Switzerland. Figure 3 displays two intercomparisons for the hourly mean SIS at the stations Payerne (lowlands) and Jungfraujoch (mountains) for March 2005. In general, the agreement is high with correlation coefficients of 0.94 for Payerne and 0.89 for Jungfraujoch. However, on some occasions the spread is rather large (marked with red points) which is more frequent at the mountainous station than at the lowland

station. The spread results partly from algorithm deficiencies in separating clouds from snow but also from the non-representiveness of comparing local station data to spatially integrated satellite measurements (Zelenka et al., 1999).

For specific climatological events, the physical consistency is further investigated using complementary high-resolution climate monitoring products inferred from surface observations over Switzerland. Figure 4 shows the anomalies of SIS, temperature and sunshine duration (last two: `www.meteoswiss.admin.ch/web/en/climate/climate_today/swiss_anomalies.html`), respectively, for April 2007. This month was characterised extremely high temperatures (more than $5\,^{\circ}\mathrm{C}$ higher than normal for Switzerland). Especially, the lowlands north of the Alps experienced additional radiative input of more than $45\,\mathrm{Wm}^{-2}$ which is consistent with strongly increased sunshine hours in that region.

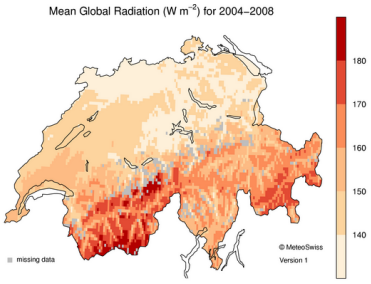

Figure 2: Mean SIS over Switzerland (2004-2008) [Wm^{-2}]

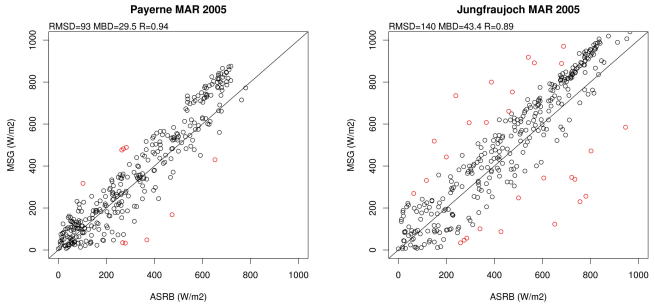

Figure 3: Comparison of SIS from ASRB Stations Payerne and Jungfraujoch to SIS retrieved from MSG satellites for March 2005

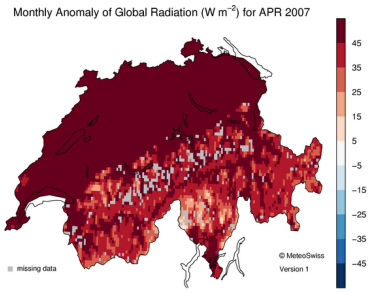

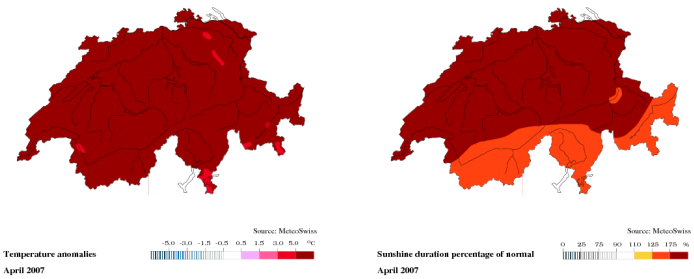

Figure 4: Monthly mean SIS anomaly, temperature anomaly and sunshine duration anomaly for Apr 2007

4 SUMMARY AND CONCLUSIONS

A 5-year climatology for satellite-derived SIS over Switzerland is presented. A new snow detection algorithm helps to distinguish clouds and snow in the alpine region which results in a more accurate estimation of SIS in that regions. There is a high agreement with radiation measurements at the surface, nevertheless, the cause for the partly large spread has still to be investigated. The presented satellite based SIS climatology complements the results and findings of climatologies derived from station based measurements. However, the satellite based climatology allows for a higher spatial resolution and provides information in regions that are not covered by measurement stations. The anomaly maps will be made available soon on `http://www.meteoswiss.admin.ch/web/en/climate/climate_today/swiss_anomalies.html`.

REFERENCES

Beyer, H. G., C. Costanzo, and D. Heinemann, 1996: Modifications of the Heliosat procedure for irradiance estimates from satellite images. *Solar Energy*, **56**, 207–212.

Dürr, B. and A. Zelenka, 2009: Deriving surface global irradiance over the Alpine region from METEOSAT Second Generation data by supplementing the HELIOSAT method. *Int. J. Rem. Sens.*, **(in press)**.

Hammer, A., D. Heinemann, C. Hoyer, R. Kuhlemann, E. Lorenz, R. Müller, and H. Beyer, 2003: Solar energy assessment using remote sensing technologies. *Remote Sens. Environ.*, **86 (3)**, 423–432.

Schmetz, J., P. Pili, S. Tjemkes, D. Just, J. Kerkmann, S. Rota, and A. Ratier, 2002: An Introduction to Meteosat Second Generation (MSG). *Bull. Amer. Meteor. Soc.*, **83 (7)**, 977–992.

Zelenka, A., R. Perez, R. Seals, and D. Renne, 1999: Effective Accuracy of Satellite-Derived Hourly Irradiances. *Theor. Appl. Climatol.*, **62**, 199–207.

Comparison of ground-based UV irradiance measurements with satellite-derived values and 1-D- and 3-D-radiative transfer model calculations in mountainous terrain

J.E. Wagner[1], A. Arola[2], M. Blumthaler[3], M. Fitzka[1], J.P. Gobbi[4], R. Kift[5], A. Kreuter[3], H. Rieder[6], S. Simic[1], A. Webb[5], P. Weihs[1]

[1] Institute for Meteorology, University of Natural Resources and Applied Life Sciences, Vienna, Austria
[2] Finnish Meteorological Institute, Kuopio, Finland
[3] Devision for Biomedical Physics, Innsbruck Medical University, Innsbruck, Austria
[4] Institute of Atmospheric Sciences and Climate, Aerosol Remote Sensing Group, Roma, Italy
[5] Devision for Earth, Atmospheric and Environmental Sciences, University of Manchester, Manchester, UK
[6] Institut for Atmospharic and Climate Science, ETH Zurich, Zurich, Switzerland
E-mail: *jochen.wagner@boku.ac.at*

Abstract: Results from three different calculation methods (satellite retrieval, 1-D- and 3-D-radiative transfer model) for UV radiation in terms of UV-Index, erythemally weighted daily doses and spectrally resolved UV-Irradiance at 305, 310, 324 and 380nm are presented and compared with ground-based high quality measurements. The real case study is performed in very inhomogenous terrain for cloudless situations. 1-D-simulations show the best agreement ($\pm 10\%$) with the measurements whereas 3-D-model simulations and satellite retrieved values often differ much more. Satellite retrieved values significantly underestimate radiation for most stations, while results from 3-D-model calculations mostly overestimate radiation.

***K*eywords:** *UV irradiance, albedo, radiative transfer model, OMI, Grimaldi, Disort*

1 MATERIAL AND METHODS

The ground-based measurements were performed during two measurement campaigns in late summer 2007 and late winter 2008 in Innsbruck and one measurement compaign in May 2008 at Sonnblick.

Satellite-derived UV-values were taken from Ozone Monitoring Instrument (OMI, see LEVELT ET AL. (2006)). For the 1-D-radiative transfer calculations we used the DISORT solver (see DAHLBACK and STAMNES (1991)). The 3-D-radiative transfer calculations were performed with the Monte Carlo Model GRIMALDI (see SCHEIRER and MACKE (2001) and SCHEIRER and MACKE (2003)).

Table 1: *Input parameter for the DISORT model are shown. The mountain stations are modeled as point above a surface with the mean elevation height of the digital elevation model used for the 3-D calculations. α and β stand for the aerosol Angstrom coefficients and sza is the solar zenith angle. The sza varies slightly from station to station (due to different geographic location) and from wavelength to wavelength (due to time differences in the order of one to three minutes of the measurements).*

Measurement site	surface	albedo	o_3	α	β	sza	date	time
Innsbruck	616m	0.01	265 DU	1.1	0.020	58.56°- 58.61	24.02.2008	12:31-12:32 UTC
Lans	833m	0.01	265 DU	1.1	0.016	58.50°- 58.66°	24.02.2008	12:31-12:33 UTC
Hafelekar	1386m	0.01	260 DU	1.1	0.004	58.55°- 58.71°	24.02.2008	12:31-12:33 UTC
Bodenhaus	1296m	0.01	349 DU	1.08	0.022	34.40°- 34.72°	09.05.2008	12:01-12:03 UTC
Kolm-Saigurn	1600m	0.01	349 DU	1.08	0.028	33.09°- 33.37°	09.05.2008	12:01-12:02 UTC
Sonnblick	2059m	0.01	345 DU	1.08	0.0008	34.35°- 34.67°	09.05.2008	12:01-12:03 UTC

2 RESULTS

To compare the results from satellite retrieval and 1-D- and 3-D-radiative transfer models we calculated ratios (measurement/model) shown in figure 1. Results from the 1-model show clearly the best agreement. The values agree always within 10%.

The 3-D-radiative transfer model agrees also very well for Sonnblick section, but there are huge differences at Innsbruck section. We investigate this behavior at the moment. One reason could be a wrong estimation of surface albedo for the Innsbruck section. Other effects, like aerosols, time differences and thus slighly inaccurate solar zenith angles due to the plan-parallel approximation, border effects (periodic border conditions are assumed) and the use of standard profiles for Rayleigh scattering and ozone absorption should contribute to the uncertainty by less than 5%.

Satellite retrieved values mostly underestimates the observed values significant (see figure 1). The agreement for the three stations of the Innsbruck measurement compaign is better than for the Sonnblick region. First of all

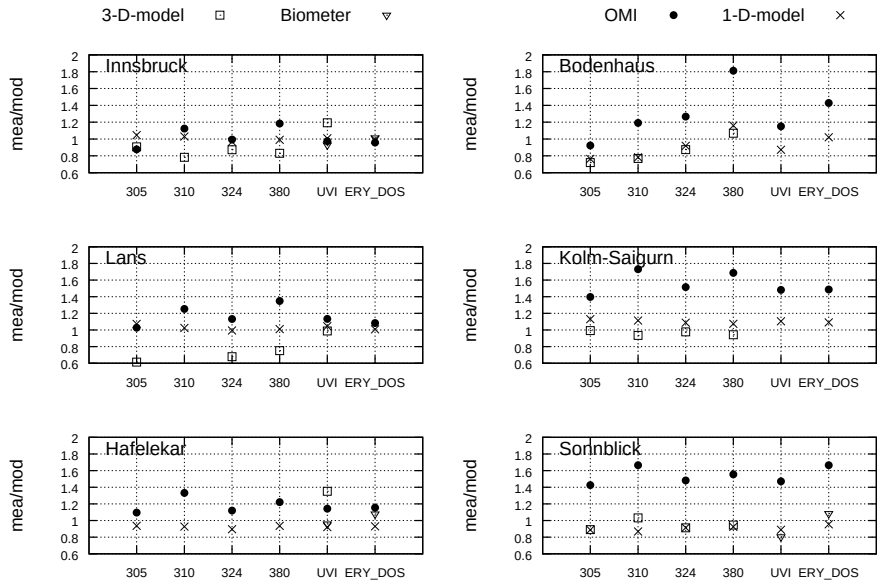

Figure 1: *The ratio of measured and calculated UV radiation (irradiance at 305nm, 310nm, 324nm, 380nm, UV-Index and erythemally weighted daily dose) is shown. Filled circles denote satellite-derived data, crosses denote 1-D-model and squares 3-D-model calculations. In addition triangles show the broadband measurements performed with Biometers. The left column shows results from February 24th 2008 12:30 UTC. The right column shows results from May 7th 2008 12:20 UTC.*

the altitude used in the satellite retrieval differs a lot from the real station height in our area of interest, due to the coarse resolution of the satellite data. Furthermore the cloud detection algorithm misinterprets snowcovered areas as clouds. In this areas the UV-radiation is scaled down.

3 CONCLUSIONS

One-dimensional radiation transfer models are able to reproduce ground-based irradiance measurements in mountainous regions very well. However the good agreement with measurements is very likely due to the compensation of significant effects (restriction of the horizon by the mountains and enhancing the radiation due to reflection at the (snow covered) ground and scattering in the air. To study such effects 3-D-radiative transfer models are indispensable. However the results from 3-D-model in this study are preliminary, since the number of "photons" used for the calculations (10^8) is too low to get the desired accuracy of about 5%. Model runs with 10^9 "photons" are already in preparation. With the current OMI-retrieval algorithm it is very difficult to get very accurate UV-values for ground stations in very mountainous terrain. To improve the algorithm for such areas, one should address issues like station height and cloud detection in (partly) snowcovered terrain.

Acknowledgements:
This work was mainly financed by the Austrian Science Fund (FWF) Projektnumber: P18780-N13.

References

DAHLBACK, A., STAMNES, K., 1991: A new spherical model for computing the radiation field available for photolysis and heating at twilight. Planetary and Space Science **39(5)**, 671–683.

LEVELT, P. F., VAN DEN OORD, G. H., DOBBER, M. R., MIÄLKKI, A., VISSER, H., DE VRIES, J., STAMMES, P., LUNDELL, J. O., SAARI, H., 2006: The Ozone Monitoring Instrument. IEEE Transactions on Geoscience and Remote Sensing **44(5)**, 1093–1101.

SCHEIRER, R., MACKE, A., 2001: On the accuracy of the independent column approximation in calculating the downward fluxes in the UVA, UVB and PAR spectral ranges. Jounal of geophysical Research **106(D13)**, 14,301–14,312.

SCHEIRER, R., MACKE, A., 2003: Cloud inhomogeneity and broadband solar flux. Jounal of geophysical Research **108(D19)**, doi:10.1029/2002JD003,321.

MAP D-PHASE: lessons learned and future developments

Mathias W Rotach[1], Marco Arpagaus[1], Manfred Dorninger[2], Christoph Hegg[3], Andrea Montani[4], Roberto Ranzi[5]

[1] Federal Office of Meteorology and Climatology, MeteoSwiss, Zurich, Switzerland
E-mail: *mathias.rotach@meteoswiss.ch*
[2] University of Vienna, Vienna, Austria
[3] WSL, Swiss Federal Institute for Forest Snow and Landscape Research Birmensdorf, Switzerland
[4] ARPA-SIMC, Bologna, Italy
[5] University of Brescia, Brescia, Italy

Abstract: MAP D-PHASE is a Forecast Demonstration Project of the World Weather Research Programme (WWRP) that is tied to the Mesoscale Alpine Programme (MAP). D-PHASE stands for **D**emonstration of **P**robabilistic **H**ydrological and **A**tmospheric **S**imulation of flooding **E**vents in the Alpine region. Its goal is to demonstrate the ability of reliably and operationally forecasting orographically influenced (determined) precipitation in the Alps and its consequences on the distribution of run-off characteristics. During the D-PHASE Operations Period (DOP) from June to November 2007 an end-to-end forecasting system was operated and a vast amount of data is currently being analysed and evaluated. The present contribution aims at briefly summarising the approach and components of D-PHASE. A number of lessons learned will be drawn from the outcomes. These include consequences concerning the optimal use of the D-PHASE/COPS joint data set as well as open questions and further directions.

Keywords: *Heavy precipitation, flash flood, forecast demonstration, WWRP, high-resolution numerical weather prediction, probabilistic forecast.*

1 INTRODUCTION

A Forecast Demonstration Project (FDP) of the World Weather Research Programme, quite generally, aims at demonstrating the advances an R&D activity has brought to operational atmospheric forecasting. Thus a FDP deals with the forecast of weather with international relevance (high impact weather); demonstrates a clear advance in forecasting capability; provides clear evaluation protocols and is characterized by an expectation of success. D-PHASE is the FDP in relation to the Mesoscale Alpine Programme (MAP, Bougeault et al. 2001) and aims at demonstrating an end-to-end warning system for flood events based on high resolution deterministic probabilistic hydrological and atmospheric modelling in the Alpine region. Some of the D-PHASE essentials are summarized in Table 1. The forecasting system's centre piece was a Visualization Platform (Fig. 1), on which warnings from atmospheric and hydrological models (both deterministic and probabilistic) and corresponding model fields were displayed in uniform and comparable formats. Also, meteograms, nowcasting information and end user communication was made available to all the forecasters, users and end users. From June to August 2007 the COPS (**C**onvective and **O**rographically induced **P**recipitation **S**tudy, Wulfmeyer et al. 2008) mission planning team was among the D-PHASE users. COPS provided high-resolution observational data for a sub-area of the D-PHASE domain that can – from a D-PHASE point of view - be employed for model verification and reliability assessment.

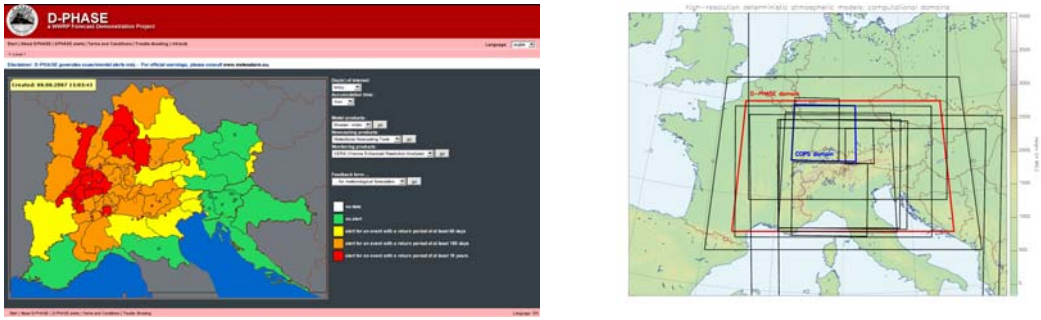

Figure 1. Left: Screenshot of the Visualization Platform (VP) for August 8 2007, level 1 (Alpine vide view); right: model domains for high-resolution atmospheric models including the D-PHASE (red) and COPS (blue) domains. Both from Rotach et al. (2009).

2 RESULTS

Details on D-PHASE, including background, organisation and scientific results can be found in Arpagaus et al. (2009) and Rotach et al. (2009). The more hydrological aspects are summarized in Zappa et al. (2008). Here we only focus on the main achievements and point to directions for further analysis. Just as MAP had proved

the feasibility of atmospheric/hydrological coupling, D-PHASE successfully demonstrated its operational use and extension to ensemble techniques. Judging from preliminary conclusions by atmospheric forecasters (Rotach et al. 2009) this is not only an advance in technical terms, but also helps both communities to take into account the respective other's sphere (hydrosphere vs. atmosphere) in order to improve the decisions and forecasts in one's own. This might be a 'lesson learned' that goes way beyond the present atmosphere-hydrosphere system and should be kept in mind for other applications of atmospheric modelling (such as air pollution dispersion or agro-meteorological applications).

D-PHASE Operations Period (DOP)	June-November 2007	COPS (Jun-to Aug) MAP (Sep-Nov)
D-PHASE area	> 40 catchments across the alps	
Participants	> 30 institutions	Hydro/Met Services Universities Research institutions
Target	Forecasting system for precipitation and flooding in the Alps	End-to-end
Instrument	Visualization Platform	Uniform formats
Approach	Numerical modelling, nowcasting → 30 atmospheric models → 7 different hydrological models → Radar, Satellite and analysis tools	Probabilistic & deterministic

Table 1. Summary of some D-PHASE facts.

Clearly, the single most important factor of success for D-PHASE was the interoperability of all the models: *common formats, common warning levels and common routines* to actually determine the warnings from the model outputs rendered the results comparable and therefore highly valuable. The possibility of comparing objective model verification (deterministic and probabilistic) for a substantial number of models and approaches with subjective evaluation of D-PHASE results (Rotach et al. 2009, for details) makes the D-PHASE data set quite unique.

This available data set together with detailed observations due to COPS will allow to

- systematically demonstrate the additional value of very high-resolution atmospheric modelling;
- investigate the properties and performance of Ensemble Predictions Systems both for atmospheric and hydrological models. Examples can be found in Arpagaus et al (2009) or Zappa et al. (2008).
- study predictability of convection processes and convective initiation using the present model results in connection with the observational results of COPS;
- benchmark models of all types by comparing them with a range of other models of the same category, or even other model types;
- systematically evaluate nowcasting tools such as the position forecast of convective systems in the Thunderstorms Radar Tracking (TRT) tool of MeteoSwiss using the available data, and possibly extend their functionality by introducing model products;
- judge the end user feedback on its own grounds, and compare it to the 'objective' verification results - thus learning even more concerning the improvement of the overall forecasting/warning system.

The D-PHASE data set, in conjunction with the observational data set due to COPS is now available as a testbed for atmospheric convection, in combination with orographic precipitation and coupled to hydrological modelling. The WWRP working group on Meso-scale Weather Forecast Research (WG-MWFR) has recently included the D-PHASE/COPS data set for this purpose in their strategic planning.

REFERENCES

Arpagaus M and 44 co-authors, 2009: MAP D-PHASE: Demonstrating forecast capabilities for flood events in the Alpine region. *Veröffentlichungen der MeteoSchweiz*, **78** (available from http://www.meteoschweiz.admin.ch/web/de/forschung/publikationen/meteoschweiz_publikationen/veroeffentlichungen.html).

Bougeault P, Binder P, Buzzi A, Dirks R, Houze R, Kuettner J, Smith RB, Steinacker R and Volkert H, 2001: The MAP Special Observing Period. *Bull. Amer. Meteor. Soc.*, **82**, 433-462.

Rotach MW and 38 co-authors, 2009: MAP D-PHASE: Real-time Demonstration of Weather Forecast Quality in the Alpine Region. *Bull. Amer. Meteor. Soc*., accepted.

Wulfmeyer V and 27 co-authors, 2008: The Convective and Orographically-induced Precipitation Study: A Research and Development Project of the World Weather Research Program for Improving Quantitative Precipitation Forecasting in Low-mountain Regions. *Bull. Amer. Meteor. Soc*., DOI 10.1175/2008BAMS2367.1.

Zappa M, Rotach MW, Arpagaus M, Dorninger M, Hegg C, Montani A, Ranzi R, Ament F, Germann U, Grossi G, Jaun S, Rossa A, Vogt S, Walser A, Wunram C, 2008: MAP D-PHASE: Real-time demonstration of hydrological ensemble prediction systems. *Atmos. Sci. Let.*, **2**, 80-87, **DOI:** 10.1002/asl.183.

Verification of precipitation forecasts of the D-PHASE data set

Tanja Weusthoff[1], Felix Ament[2], Marco Arpagaus[1], Mathias W. Rotach[1]

[1] MeteoSwiss, Zurich, Switzerland
[2] University of Hamburg, Hamburg, Germany
E-mail: *tanja.weusthoff@meteoswiss.ch*

Abstract: Precipitation forecasts from the Forecast and Demonstration Project D-PHASE are evaluated by means of different verification methods. Standard scores like (relative) bias and probability of detection are utilized for individual catchment regions based on Swiss radar data and the relative value for predefined warnlevels is determined (cost/loss analysis). The forecasts of selected models are additionally Fuzzy verified against Swiss radar data with a focus on a comparison of the performance of the two operational Swiss COSMO models with their different spatial (and temporal) resolutions. The results show a slight advantage for the higher resolution model on all spatial scales, especially at shorter accumulation times (e.g. 3 h).

Keywords: *D-PHASE, precipitation, verification*

1 INTRODUCTION

In the scope of D-PHASE a real-time end-to-end forecasting system for heavy precipitation and subsequent flood events in the Alpine region was set up. Based on probabilistic and deterministic atmospheric and hydrological models, warnings were issued for specific river catchments. The forecast data of the participating numerical models, including high resolution convection resolving models and models with parameterized convection, are stored in a central data archive at the World Data Center for Climate in Hamburg. These data are well suited to investigate the use of atmospheric/hydrological models for flood forecasting in mountainous regions. Various methods are applied to get an objective verification of the model forecasts.

2 VERIFICATION METHODS

2.1 Catchment Verification

The precipitation forecasts for individual catchment areas as shown in Fig. 1 as well as the alerts issued for predefined warning levels are verified against Swiss radar data (raw data and data calibrated by means of rain gauge measurements). The verification results for the full D-PHASE Operations Period (DOP, June - November 2007) will be presented with a focus on seasonal differences. The scores applied include the (relative) bias, probability of detection, temporal correlation, and relative value.

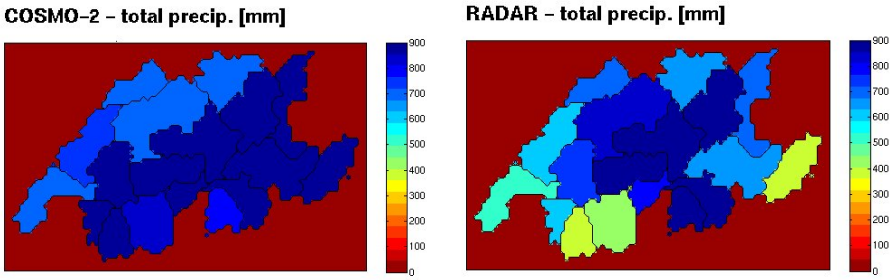

Figure 1: Catchment regions within Switzerland and parts of neighbouring countries. The plot shows total precipitation for each catchment for the whole DOP as forecast by COSMO-2 (left) and measured by radar (right).

2.2 Fuzzy verification

Selected models are additionally evaluated with reference to Swiss radar observations by means of Fuzzy verification methods. While standard verification methods require a point wise match of observation and forecast on the grid scale of the model, Fuzzy verification methods evaluate the forecast on increasing spatial scales by moving window domains of various sizes over the verification domain. An event is identified as e.g. the mean value over the respective window exceeding a given threshold (Upscaling) or the fraction of grid points in the

window exceeding the threshold (Fractions Skill Score). The verification is done on different spatial scales by varying the window sizes and for various thresholds defining an event. The scores are determined for 3 h and 24 h rain accumulations and are then aggregated on different time scales: days, months, and the whole period of 6 months. The robustness of the results is determined by means of a bootstrapping procedure. In addition, the sensitivity of the scores with respect to the rain amount and the dependency of the results on the weather type is investigated.

An example of the Fuzzy verification results for the whole DOP is given in Fig. 2. Each single box represents a specific spatial scale and a certain threshold, for which the respective scores are calculated. The skill of each of the two COSMO models increases with increasing spatial scale and decreases with increasing threshold. In order to compare the two models, the differences of the scores are calculated. The difference plot displayed on the right hand side gives a good impression on which scales the models are comparable and on which scales COSMO-2 outperforms COSMO-7.

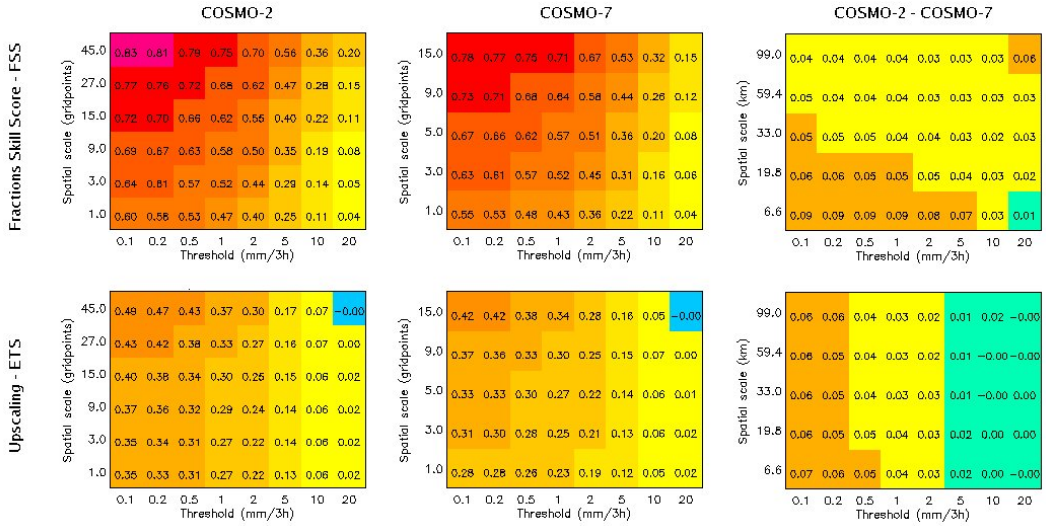

Figure 2: Results of fuzzy verification of COSMO-2 (left) and COSMO-7 (middle) for the whole DOP. Top panels show Fraction Skill Score, lower panels the Upscaling method. On the right hand side, the differences of COSMO-2 minus COSMO-7 are displayed. Positive numbers indicate a better skill of COSMO-2, negative values a better skill of COSMO-7, respectively.

3 RESULTS AND CONCLUSIONS

The data set produced during D-PHASE provides a good possibility to investigate the ability of different models to forecast precipitation for a well defined time period, including summer months with heavy convective rain and the autumn period with less precipitation in the region of interest.

The catchment verification shows no clear signal for a comparison between cloud resolving and convection parameterizing models. However, it reveals differences in the models performance for the two considered seasons. Generally, almost all models overestimate precipitation compared to radar. Adjusting radar data by means of rain gauge measurements results in a reduced overestimation by the models. The relative value calculated for the whole D-PHASE Operations Period on the other hand is larger for high resolution models, which indicates that these models were more useful than the coarser resolution models.

Concerning Fuzzy verification methods, COSMO-2 performs slightly better on all scales for 3 h precipitation accumulations, especially for low precipitation thresholds. In contrast, 24 h accumulations are comparable well forecast by both models in the considered period when using only 00 UTC runs for the comparison. The results show, amongst others, that high resolution convection resolving models generally reveal better skills, especially on shorter time scales and with respect to temporal correlation of precipitation. The statistical significance of the results is evaluated by means of a bootstrapping procedure.

REFERENCES

Arpagaus et al. (2009): MAP D-PHASE: Demonstrating forecast capabilities for flood events in the Alpine region. Report on the WWRP Forecast Demonstration Project D-PHASE submitted to the WWRP Joint Scientific Committee. Published as Veröffentlichung der MeteoSchweiz, 78, 2009, 68pp.

EVALUATION OF OPERATIONAL WEATHER FORECASTS: APPLICABILITY FOR FLOOD FORECASTING IN ALPINE BAVARIA

Uwe Ehret[1]

[1] TU München, Department of Hydrology, Munich, Germany
E-mail: *u.ehret@bv.tum.de*

Abstract: In this study, a range of both deterministic and ensemble rainfall forecast models are evaluated with respect to their applicability for operational flood forecasting in mesoscale alpine catchments in Bavaria. Both continuous and categorical performance measures are applied. In summary, the median of the Cosmo-Leps ensemble forecast outperformed all deterministic forecasts.

Keywords: *rainfall forecast, flood forecast, alpine, deterministic, ensemble, Cosmo-Leps*

1 INTRODUCTION

Flood forecasting in small, alpine head catchments is a difficult task: Due to their size and topographic setting, there are usually neither many upstream river gauges to base the forecast on, nor do forecasts based on river- and rain gauge observations provide lead times of sufficient length. Consequently, weather-, especially rainfall forecasts are needed and heavily influence flood forecast quality.

In this article, a wide range of operationally available rainfall forecasts, both deterministic and ensemble, are evaluated with respect to their quality and applicability for flood forecasting in a range of alpine river catchments in Bavaria. After the introduction, the available data, performance indices used and the set-up of the tests are described in section 2. Based on this, results are presented in section 3, followed by conclusions in section 4.

2 DATA & METHODS

2.1 Rainfall observations

Hourly rainfall observations from over 100 raingauges were used to calculate mean areal rainfall (linear interpolation) in seven (sub-) alpine catchments in and along the Bavarian alps, ranging from 221 km^2 to 1597 km^2. The time series extends from 01.08.2005 to 30.04.2008, excluding the snow-influenced winter months November through March. The time series includes a 300-year flood event in August 2005.

2.2 Rainfall forecasts

Rainfall forecasts were available from both deterministic and ensemble forecasting models (abbreviations in brackets): DWD GME (GME), DWD Cosmo-EU (LME), DWD Cosmo-DE (LMK), NCEP GFS (GFS), Aladin-Austria (ALA), modified MeteoSwiss Cosmo-7 (ALM) forecasts, operationally corrected by a MeteoSwiss meteorologist, Cosmo-Leps (CLE). Also, GME, LME and GFS forecasts were combined to a PEPS (PEP), and a median forecast series from CLE was calculated (CLM). CLE, GME and LME were available for the whole observation period, the others started 01.10.2006.

The forecasts were disaggregated to 1-hour sums (necessary for CLE, GFS and GME) and areal-averaged in the same manner as the rainfall observations. From all forecasts, only the 00:00 and 12:00 runs were used to assure a comparable data base for each forecast model.

2.3 Performance criteria

Continuous and categorical performance criteria were calculated to evaluate the deterministic forecasts: Root Mean Square Error (RMSE), Skill Score (SKSC), Threat Score (THSC) and Heidke Skill Score (HSKS), with the latter two being based on contingency tables. Ensemble forecasts were evaluated by the Briar Score (BRSC).

2.4 Test setup

As not all forecast data were available for the whole period, the performance criteria were calculated for two periods: 01.04.2005-30.04.2008 (only CLE, GME, LME) and 01.10.2006-30.04.2008 (all forecasts).

To account for the increasing forecast uncertainty, rainfall observations and forecasts were aggregated with increasing lead time. This is in accordance with the requirements on weather forecasts in flood forecasting: The

need for high resolution forecasts decreases with increasing lead time. 1/6/12-hour aggregations were used for the forecast ranges 1-9/12-18/24-72 hours, respectively.

To exclude times of no or low rainfall, performance measures were only calculated for areal rainfall observations in the time series exceeding an aggregation-dependent lower limit of 0.1/0.6/1.2 mm/h for 1/6/12-hour aggregations, respectively.

Thresholds for the contingency tables were set specific to each catchment according to the following rule: From all rainfall observations beyond the lower limit take the value with 5% exceedence probability. This was considered an acceptable trade-off between the opposing demands for low thresholds ensuring large enough class occupancies and high thresholds to consider only strong, flood-relevant rainfall events. In the 1-hour aggregation, thresholds were in a range from 1.7 to 3.1 mm/h. This is well below the warning threshold for strong rainfall by the German Weather Service (25 mm/h), which is probably due to the areal averaging.

Calculating 5 performance measures for 7 catchments, 2 period, 9 forecasts, 11 lead times and 3 aggregations led to a huge number of results. In order to condense this amount of information, two approaches were used: Firstly, forecast model performance was ranked for each calculation and averaged over all catchments. The advantage of the rank score is that it is a sharp discriminator and emphasizes even small differences in performance. Secondly, the performance scores were also averaged over all catchments to gain insight in the absolute score values. Investigating the results revealed that, for evaluation, a simple distinction in short- and long-term forecast depths (above or below 12-hours) was sufficient.

Based on the above results, the overall performance evaluation and intercomparison of the different forecasts was based on the manual analysis of condensed score space.

3 RESULTS

Analysing the performance measures in the manner described above, some interesting and surprising results were obtained:

With respect to the overall performance expressed by RMSE, the median of the Cosmo-Leps forecast, which basically is an artificial forecast, clearly outperformed the other models. This was the case for both periods investigated and both rank scores and absolute values. GFS won second place. It seems that the averaging effect of the median smoothes gross over- or underestimations which may occur for single-valued deterministic forecasts.

Results are a less obvious in the case of the threat score THSC, however it is noteworthy that LMK was never among the winners. This is against the assumption that LMK, with short update cycles and lead times should, at least in the short run, outperform the other models but it is in clear accordance with the experience of the flood forecasters of the alpine catchments of rivers Iller and Lech.

Comparing the forecasts to a simple persistence forecast, as expressed by the skill score SKSC and Heidke skill score HSKS again revealed a clear advantage of CLM compared to the other forecasts. Here, too, LMK was always found on the last places. With respect to absolute performance, SKSC of all models was sometimes negative for lead times up to 6 hours, for HSKS only for 1-hour forecasts. This means that in the very short range, a persistence forecast outperforms the others.

From a comprehensive view of all performance measures, some conclusions regarding the quality of the forecast models in the alpine spaces investigated could be drawn: The LMK model showed clear weaknesses. In other parts of Bavaria, however, this was not the case (unpublished study by the author). This indicates that LMK has problems with rainfall processes related to alpine settings. It should be noted, however, that the new version of Cosmo-DE might have overcome this problem.

Further, Aladin-Austria (ALA) performed consistently worse than most of the other models and might therefore be excluded from operational use for flood forecasting.

Apart from the deterministic models, Cosmo-Leps and the self-made PEPS from GME, LME, GFS were compared by means of the Briar score. It should be noted that for both cases, scores were usually quite low (i.e. good), which may indicate domination by large numbers of correct negatives. However, performance differences between the two were obvious and in favour of CLM.

4 CONCLUSIONS

In this study, a range of both deterministic and ensemble rainfall forecast models were evaluated with respect to performance in mesoscale alpine catchments in Bavaria. In summary, the median of the Cosmo-Leps ensemble outperformed all other forecasts. However, it should be investigated whether this artificial forecast exhibits a realistic temporal evolution or whether a single member placed in the centre of the ensemble, would provide similar performance scores plus 'realistic looks'.

Acknowledgements:
The author expresses his gratitude to the Bavarian Environment Agency (LfU) for supplying the data for this work.

A MULTI-MODEL INTERCOMPARISON STUDY FOR QUANTITATIVE PRECIPITATION FORECAST USING THE 6-MONTH MAP D-PHASE DATASET

Stefano Mariani[1], Marco Casaioli[1], Alexandre Lanciani[1], Barbara Lastoria[1], Christophe Accadia[2], Nazario Tartaglione[3]

[1] Institute for Environmental Protection and Research (ISPRA), Rome, Italy
[2] European Organisation for the Exploitation of Meteorological Satellites (EUMETSAT), Darmstadt, Germany
[3] Meteorology and Climate Centre, School of Mathematical Sciences, University College Dublin, Dublin, Ireland
E-mail: *stefano.mariani@isprambiente.it*

Abstract: Demonstrating the benefits in forecasting heavy precipitation and related flooding events in the Alpine region using high-resolution numerical weather prediction (NWP) models, ensemble prediction systems (EPSs), atmospheric-hydrological coupled systems, and real-time nowcasting tools is the purpose of MAP D-PHASE, a Forecast Demonstration Project launched in 2007 in the framework of the WMO WWRP Programme. The present work, performed within the MAP D-PHASE Working Group Verification (WG VER), aims at assessing and quantifying the performance of several NWP models during the entire D-PHASE Operations Period (DOP, from June to November 20007). This intercomparison study is performed by verifying on a daily basis quantitative precipitation forecasts (QPFs) against observational analyses using a multi-method approach based on multi-scale, objective and subjective methods. The combination of different deterministic forecasts, by means of multi-model poor man's ensemble (PME) approaches, is also taken into account for providing multi-model forecasts to be compared against the single deterministic models.

***K*eywords:** *MAP D-PHASE, QPF, multi-model poor man's ensemble, Barnes precipitation analysis, remapping, model intercomparison, verification, categorical scores, object-oriented technique, power spectrum analysis, subjective verification*

1 INTRODUCTION

European institution participating to the MAP D-PHASE project provided during the D-PHASE Operation Period (DOP, from June to November 2007), meteorological simulations modelled by numerical weather prediction (NWP) models and ensemble prediction systems (EPSs) over the D-PHASE and the Convective and Orographically-induced Precipitation Study (COPS) domains. Aim of this work, performed in the framework of MAP D-PHASE Working Group Verification (WG VER), is to evaluate the performance of several deterministic models during DOP and to understand the strengths and weaknesses of these models in forecasting precipitation events over a complex area, such as the Alpine region. Poor man's ensemble (PME) forecasts, obtained by combining the compared deterministic models, are considered within this verification study, as well.

2 FORECAST AND OBSERVED DATA

Several meteorological centers consider the quality of quantitative precipitation forecasts (QPFs) to be a general indicator of the capability of a NWP model to produce a good forecast, because precipitation strongly depends on atmospheric motion, moisture content, and physical processes. For this reason, this verification study is based on a daily intercomparison of QPF data against rainfall analyses, which are obtained by means of non-GTS rain gauge data (see Fig. 1) collected within WG VER from several meteorological services and environmental agencies.

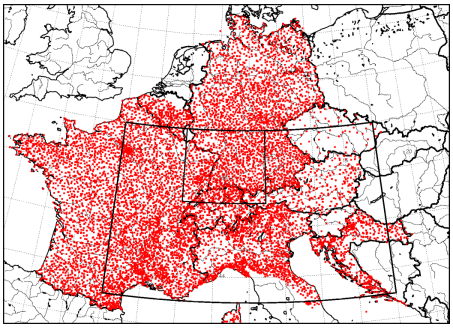

Figure 1: Status of non-GTS data during DOP, with indication of the MAP D-PHASE (large box) and COPS (small box) domains. Courtesy of Theresa Gorgas and Manfred Dorninger (University of Vienna, Austria).

More precisely, since rain gauges provide the more accurate, although localized, estimate of the observed weather, and NWP forecasts should be instead considered, in general, as areal mean quantities, the representativeness of the fields compared need to be addressed before applying any kind of verification method. Consequently, it has been decided to make a selection of the NWP models to be included into this verification work (see Table 1)

Very High Resolution (grid size $\sim$ 2–3 km)	High Resolution (grid size $\sim$ 7–10 km)
	ALADAT (ZAMG)
AROME (Météo France)	ALADFR (Météo France)
COSMOCH2 (Meteo Swiss)	COSMOCH7 (Meteo Swiss)
LAMI28 (ARPA SIM)	LAMI7 (ARPA SIM)
LMK (DWD)	LME (DWD)
LMITA (CNMCA)	LMEURO (CNMCA)
ISACMOL2 (ISAC-CNR)	MESONH8 (Univ. Paul Sabatier)
	QBOLAM11 (ISPRA, ex-APAT)

Table 1: List of the deterministic models selected for the verification study, categorized with respect to the grid size of the native grid. Acronyms and forecast providers as reported in the MAP D-PHASE Implementation Plan.

and to "optimally interpolate" both observations and forecasts at the same scales by means of the Barnes (1964) procedure and remapping (Accadia et al., 2003).

As reported in Table 1, models have been subdivided into two quasi-homogeneous categories, namely the **Very High Resolution**, in which models have a grid horizontal spacing of about 2–3 km, and the **High Resolution**, in which models have instead a grid spacing of about 7–10 km. Each one of these sub-groups can be also considered as a sort of "poor man's ensemble" group. So, according to the PME procedures presented by Ebert (2001), four deterministic forecasts can been obtained: the simple arithmetic ensemble forecast mean (AVE); the ensemble median precipitation forecast (MED); the probability matched forecast based on AVE (PAV); and the probability matched forecast based on MED (PMD).

3 VERIFICATION METHODOLOGY

A verification area, centred over the MAP D-PHASE domain and obtained as intersection of all the selected models' domains, has been considered for the implementation of a multi-method approach based on multi-scale (power spectrum analysis), objective (categorical scores and object-oriented techniques) and subjective methods. Multi-scale methods are a methodological requirement since traditional categorical scores, which measure point-to-point match, are sensitive to small displacement errors. Higher order moments should be studied to evaluate whether the fields to be compared are defined on grids with the same real resolution and whether they have the same amount of small-scale details. Furthermore, objective techniques can provide a quantitative basis to subjective verification, which in turn can suggest physical interpretations to the objective verification findings. Details about this verification methodology can be found in Mariani et al. (2009b).

4 CONCLUSIONS

Some of the verification findings will be illustrated during ICAM 2009, with particular emphasis on the impact of model resolution on the precipitation forecast quality at different scales, the suitability of the PME approaches to provide better forecasts than the single deterministic models, and finally, the helpfulness of the multi-method approach in order to better understand the verification results.

Acknowledgements:
Authors thank MAP D-PHASE partners, which provided NWP data during DOP, and meteorological services and environmental agencies, both at national and at regional level, which have made available non-GTS data for the verification tasks. Our thanks also go to WG VER members for their suggestions and support.

REFERENCES

Accadia, C., S. Mariani, M. Casaioli, A. Lavagnini, and A. Speranza, 2003: Sensitivity of precipitation forecast skill scores to bilinear interpolation and a simple nearest-neighbor average method on high-resolution verification grids. *Wea. Forecasting*, **18**, 918–932.

Barnes, S. L., 1964: A technique for maximizing details in numerical weather map analysis. *J. Appl. Meteor.*, **3**, 396–409.

Ebert, E. E., 2001: Ability of a Poor Man's Ensemble to predict the probability and distribution of precipitation. *Mon. Wea. Rev.*, **129**, 2461–2480.

Mariani, S., A. Lanciani, M. Casaioli, C. Accadia, and N. Tartaglione, 2009: A multi-method approach for quantitative precipitation forecast verification within the MAP D-PHASE project. *Proc. Joint MAP D-PHASE Scientific Meeting – COST 731 mid-term seminar*, Bologna, Italy, 107–115.

USING COPS DATA FOR THE VALIDATION OF THE HIGH-RESOLUTION NWP MODEL COSMO-DE

Kathrin Wapler[1], Axel Seifert[1], Bodo Ritter[1]

[1] Deutscher Wetterdienst (DWD), Offenbach, Germany
E-mail: *kathrin.wapler@dwd.de*

Abstract: The convective and orographically induced precipitation study had the aim to advance the quality of forecasts of orographically induced convective precipitation in complex terrain. The COPS observations, measured at different locations in the Black Forest and Vosges Mountains by a variety of instruments, give information of the boundary layer characteristics and convective initiation. The COPS data set is used for the validation of high-resolution convective-scale NWP simulations of the COSMO-DE model. Comparisons with radar, lidar, radiosonde and surface meteorological observations are performed to study the accuracy of the model in simulating the convective boundary layer.

Keywords: *high-resolution NWP, COSMO-DE, COPS*

1 INTRODUCTION

The convective and orographically induced precipitation study (COPS, Wulfmeyer 2008) took place in the Black Forest and Vosges Mountains from 1 June to 31 August 2007. The aim of this experiment was to advance the quality of forecasts of orographically induced convective precipitation by extensive observations and modelling of its life cycle, thereby identifying the physical and chemical processes responsible for deficiencies in quantitative precipitation forecasts over low mountain regions.

The 35 IOPs during COPS can be distinguished into forced convection, weakly forced convection and high-pressure convection including a variety of conditions, from severe precipitation events to cloud-free days. A variety of observation systems were operated in the area of interest at different locations in valleys as well as on mountain tops. The measurement instruments included radiosondes, Doppler lidar, aerosol Raman lidar, water vapour differential absorption lidar, microwave radiometer, cloud radar, C-Band polarization radar, energy balance stations, GPS receiver as wells as a fleet of research aircraft. The combination of the measurements by these instruments gives information of the boundary layer characteristics and convective initiation. Thus COPS aims to provide a useful data set for the evaluation of numerical models.

Convection initiation is often not adequately reproduced in state-of-the-art NWP models. This results in poor quantitative precipitation forecasts, both in terms of the spatial distribution as well as the temporal evolution of precipitation. An example is shown in Fig. 1. The figure shows the spatial distribution of observed and simulated 24 h accumulated precipitation in the COPS area as well as the diurnal cycle for IOP-1d. Scattered surface-based diurnally induced showers occurred over the Vosges and Black Forest as observed by radar. The precipitation is poorly represented in the operational high-resolution COSMO-DE simulation.

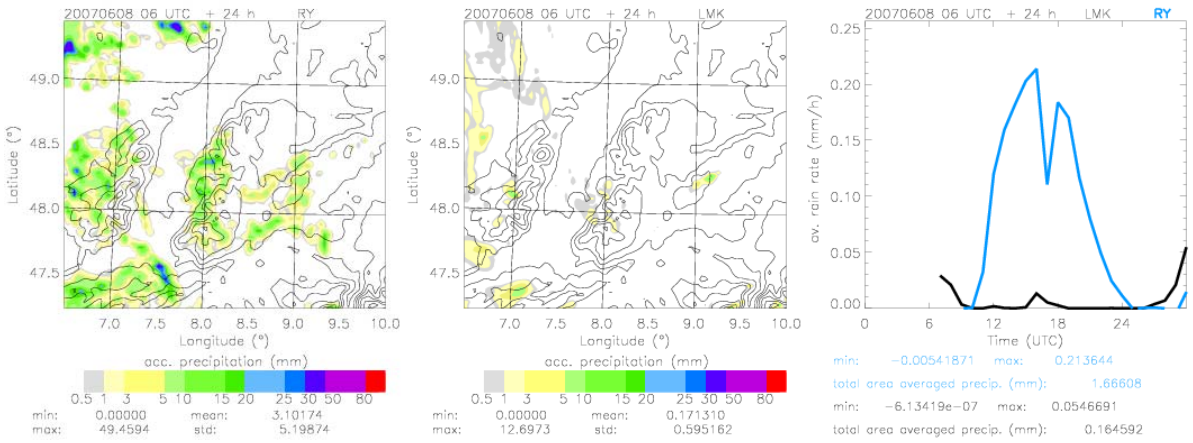

Figure 1. Spatial distribution of 24 h accumulated precipitation in the COPS area for IOP-1d (08.06.2007) from radar observations (left) and operational COSMO-DE simulations (middle); temporal evolution of observed (blue) and simulated (black) area averaged precipitation.

2 MODEL SET-UP

At the German Weather Service (DWD, Deutscher Wetterdienst) a 2.8 km version of the COSMO model, called COSMO-DE (Steppeler et al. 2003, Schättler et al. 2005), formerly known as LMK, is running operationally. Its domain covers Germany, Switzerland, Austria, The Netherlands, Belgium, and most of the Alps. Boundary conditions for the COSMO-DE come from the 7 km COSMO-EU which itself is nested in the global model GME (Majewski et al. 2002), running at a resolution of 40 km.

3 RESULTS

As an example of the evaluation of COSMO-DE using COPS data, comparisons with radiosondes are shown. These have been performed to evaluate the temporal evolution of the boundary layer. Figure 2 (left and middle panel) shows time-height cross-sections of the relative humidity measured by radiosondes launched at supersite R (Rhine Valley, near Achern) during IOP-1c and simulated profiles at the nearest grid point. On this day a few deep surface-based convective showers developed across the southern Black Forest that were not forecasted by the model. The gross features are simulated correctly however the model can't reproduce sharp gradients of relative humidity, e.g. the dry layer at about 3 km, and is too moist near the surface in the evening. The right panel in Fig. 2 shows the difference of simulated and measured temperature. Especially in the afternoon the model is too cold in the lowest 1.5 km and too warm above, thus it is to stable, prohibiting the initiation of convection.

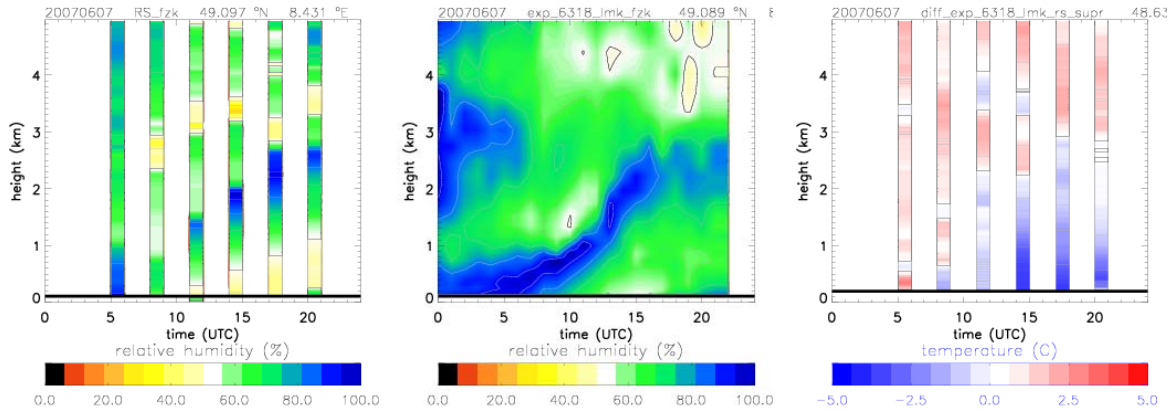

Figure 2. Time-height cross-sections of relative humidity during IOP-1c (07.06.2008) as observed by radiosondes at supersite R (left) and simulated with COSMO-DE at the closest grid-point. Time-height cross-section of the difference between observed and simulated temperatures (right).

4 CONCLUSIONS

High-resolution convective-scale NWP simulations of the COSMO-DE model are evaluated with the COPS data set. The model has shown its ability to forecast deep convection, especially forced convection, e.g. convection that is associated with frontal systems. However, problems occur in the forecast of moist convection in weakly forced conditions, e.g. small-scale orographically-induced deep convection or summertime airmass convection. In these situations explicit convection is often missing in the simulations. This is related to a too stable or too cold boundary layer.

REFERENCES

Majewski, D., D. Liermann, P. Prohl, B. Ritter, M. Buchhold, T. Hanisch, G. Paul, W. Wergen, and J. Baumgartner, 2002: The operational global icosahedral-hexagonal gridpoint model GME: Description and high-resolution test. J. Atmos. Sci. **139** , 319-338.

Schättler, U., G. Doms, and C. Schraff, 2005: A description of the nonhydrostatic regional model LM, Part VII: User's guide. Consortium for Small-Scale Modelling.

Steppeler, C., G. Doms, U. Schättler, H.W. Bitzer, A. Gassmann, U. Damrath, and G. Gregoric, 2005: Meso-gamma scale forecasts using the nonhydrostatic model LM. Meteorol. Atmos. Phys. **82** , 75–96.

Wulfmeyer, V., A. Behrendt, H.-S. Bauer, C. Kottmeier, U. Corsmeier, A. Blyth, G. Craig, U. Schumann, M. Hagen, S. Crewell, P. Di Girolamo, C. Flamant, M. Miller, A. Montani, S. Mobbs, E. Richard, M.W. Rotach, M. Arpagaus, H. Russchenberg, P. Schlüssel, M. König,, V. Gärtner, R. Steinacker, M. Dorninger, D.D. Turner, T. Weckwerth, A. Hense, and C. Simmer, 2008: The convective and orographically induced precipitation study. Bull. Amer. Meteorol. Soc. **89** , 1477–1486.

ASSIMILATION OF WEATHER RADAR REFLECTIVITY IN THE AROME MODEL FOR THE COPS-IOP9

Olivier Caumont[1], Éric Wattrelot[1], Geneviève Jaubert[1], Véronique Ducrocq[1]

[1] CNRM/GAME (Météo-France/CNRS), Toulouse, France
E-mail: *olivier.caumont@meteo.fr*

Abstract: The impact of the 1D+3DVar assimilation of reflectivity data from the French radar network on Arome analyses and forecasts at 2.5 km horizontal resolution is investigated for the Convective and Orographically induced Precipitation Study (COPS) Intense Observation Period (IOP) 9c (20 July 2007). For that, reflectivity data are assimilated in addition to conventional data, and the resulting forecasts are compared with those from a reference experiment assimilating conventional data only. Results show that the assimilation of reflectivity is beneficial, especially for intense precipitation.

Keywords: *radar, reflectivity, data assimilation, COPS*

1 INTRODUCTION

The Arome model is now running operationally at Météo-France since December 2008 at the horizontal resolution of 2.5 km. Within the Arome project, a novel 1D+3DVar assimilation method has been devised to assimilate reflectivity data (Caumont et al. 2008). It is currently heavily tested with a development version (Wattrelot et al. 2008) in order to include it in the next operational release. The present study is part of this series of tests.

The case chosen for this study is that of 20 July 2007, which corresponds to the IOP9c of the COPS campaign (Wulfmeyer et al. 2008). During the morning, pre-frontal convection occurs over central France in a southwesterly flow. Cells are advected and merge to form a squall line that passes over Germany during the afternoon. In the afternoon, precipitation affects France only sparsely, and we therefore focus our study on the morning.

2 EXPERIMENTAL SETUP

In this study, all experiments start at 0000 UTC 20 July 2007 from the latest three-hour 3DVar Rapid Update Cycle (RUC) forecast from the pre-operational Arome system (Brousseau et al. 2008), that assimilates conventional data, i.e., data from radio-sounding, screen-level stations, wind profilers, buoys, ships, aircrafts, satellites, but without radar reflectivity, Doppler velocity, nor Global Positioning System (GPS) data. In experiment 0RAD, only these data are assimilated at 0000 UTC. In 1RAD, reflectivity data from the Sembadel radar, which covers the Massif Central, are assimilated in addition to conventional data. The Sembadel radar was chosen because convective cells that merge into a squall line later in the morning are present over the Massif Central at 0000 UTC. In 11RAD, reflectivity data from all 11 French Metropolitan radars available for assimilation at that time are assimilated in addition to conventional data. In this study, 24-hour simulations with the Arome forecast system are launched from the respective analyses.

3 RESULTS

The 0RAD forecast predicts most convection patterns for the whole day, as shown for instance at 0900 UTC in Fig. 1, but a careful study reveals differences with observations in localized features in terms of intensity and location. Also, the forecast is overall lagging behind observations (compare the location of the leading edge of the mesoscale convective system (MCS) in Fig. 1). The 1RAD forecast is closer to that of 0RAD than to observations. Noticeable differences can be seen, though. For instance, the forecast is not lagging behind observations as much as in 0RAD (see Fig. 1). For 11RAD, the differences with 0RAD are more pronounced and some improvements can be seen in places. In particular, the timing seems to be even better in this simulation (compare the location of the MCS in Fig. 1).

The comparison of observed and predicted 12-hour accumulated precipitation between 0300 UTC and 1500 UTC (Fig. 2) shows that the large band crossing France from southwest to northeast is present in both observations and simulations. It is hard to tell which forecast is best from Fig. 2 only. That is why objective skill scores against raingauges have been computed for the same period (Tab. 1). All scores are improved when reflectivity data from one radar are assimilated, and even more when 11 radars are taken into account. Categorical skill scores for the same period (not shown) prove that most benefits from assimilating reflectivity data are gained for high precipitation thresholds (above 15 mm) in terms of false alarm rate and probability of detection. For lower thresholds, results are rather neutral for 1RAD and slightly positive for 11RAD.

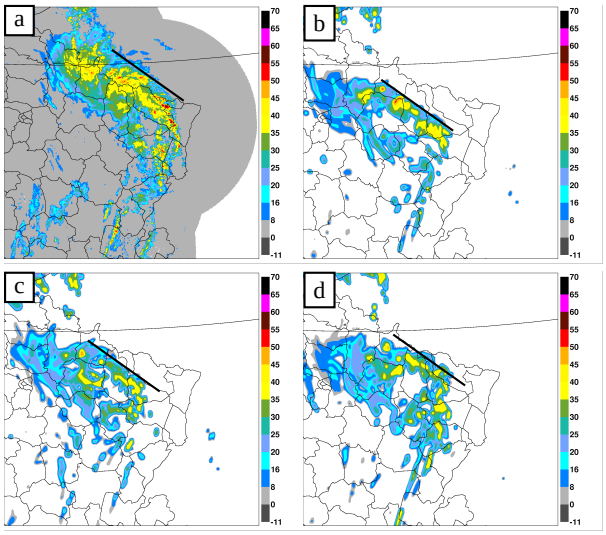

Figure 1: (a) Observed reflectivity (dBZ) composite at 0900 UTC; and simulated reflectivity (dBZ) at 700 hPa for (b) 0RAD, (c) 1RAD, and (d) 11RAD, at the same time. The solid, black line denotes the leading edge of the MCS.

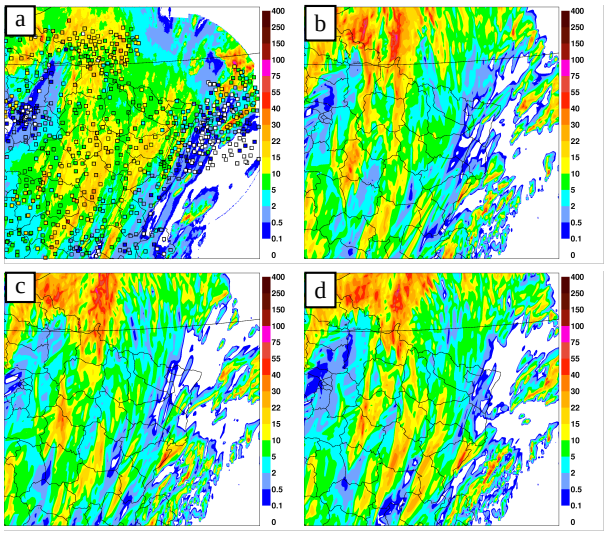

Figure 2: 12-hour accumulated precipitation (mm) between 0300 UTC and 1500 UTC (a) observed by raingauges superimposed on the composite radar estimate (Parent du Châtelet et al. 2006); and predicted by (b) 0RAD, (c) 1RAD, and (d) 11RAD.

Experiment	bias (mm)	RMSE (mm)	R
0RAD	0.21	7.15	0.46
1RAD	−0.09	6.66	0.49
11RAD	−0.05	6.22	0.58

Table 1: Bias, root mean square error (RMSE) and correlation coefficient (R) for accumulated precipitation between 0300 UTC and 1500 UTC (raingauge observations as reference). Data are first averaged over 0.2 °×0.2 ° squares.

4 CONCLUSIONS AND OUTLOOK

This sudy has shown, for a COPS case, that the 1D+3DVar assimilation of reflectivity data into the Arome numerical weather prediction system improved quantitative precipitation forecast over reference forecasts that were already very good. Improvements (e.g., better timing) were noticeable with the assimilation of data from one radar only, and even more with 11 radars. The largest improvements concern intense precipitation.

We plan to carry out the same experiments for the other days of IOP9, and also to study the impact of a rapid update cycle assimilating reflectivity and/or Doppler velocity data.

Acknowledgements: *The COPS campaign and this study benefited from support from the ANR (Agence Nationale pour la Recherche) and the CNRS/INSU (Institut National des Sciences de l'Univers).*

REFERENCES

Brousseau, P. *et al.*, 2008: A prototype convective-scale data assimilation system for operation: the Arome-RUC. *HIRLAM Tech. Rep.*, **68**, 23–30.

Caumont, O., S. Pradier-Vabre, G. Jaubert, and V. Ducrocq, 2008: 1D+3DVar assimilation of radar reflectivities for short-term high-resolution quantitative precipitation forecasts. *International Symposium on Weather Radar and Hydrology (WRaH2008)*, Grenoble and Autrans, France. Abstract no. 02-018.

Parent du Châtelet, J., P. Tabary, C. Gueguen, and B. Fradon, 2006: The Météo-France single-radar and composite QPE operational products. *Proc. 4th European Conf. on Radar in Meteorol. and Hydrol. (Erad 2006)*, Barcelona, Spain. Abstract no. 5.2.

Wattrelot, É., O. Caumont, S. Pradier-Vabre, M. Jurasek, and G. Haase, 2008: 1D+3DVar assimilation of radar reflectivities in the pre-operational AROME model at Météo-France. *Preprints, 5th European Conf. on Radar in Meteorology and Hydrology (ERAD2008)*, Helsinki, Finland.

Wulfmeyer, V. *et al.*, 2008: The convective and orographically-induced precipitation study: A research and development project of the World Weather Research Program for improving quantitative precipitation forecasting in low-mountain regions. *Bull. Amer. Meteor. Soc.*, **89**, 1477–1486.

IMPACT OF GPS DATA ASSIMILATION ON THE CONVECTIVE SCALE PREDICTION OF COPS IOP9

Geneviève JAUBERT [1] , Xin YAN [1], Véronique DUCROCQ [1], Pierre BROUSSEAU [1], Cédric CHAMPOLLION[2], Cyrille FLAMANT[3]

[1] GAME-CNRM, CNRS & Météo-France, 42 Avenue Coriolis, 31057 TOULOUSE Cedex 1, France
[2] UM2/CNRS,Place E.Bataillon, Montpellier, France
[3] LATMOS/IPSL, CNRS-UPMC, Boite 102, 4 Place Jussieu, 75252 Paris Cedex 05, France
E-mail: *genevieve.jaubert@meteo.fr*

Abstract: The impact of assimilating GPS delays in a convective scale NWP system has been studied for IOP9 (18-20 July 2007) of the COPS field campaign over the Black Forest and the Vosges region. The high-resolution temporary GPS receivers network deployed during the COPS campaign provides us a unique opportunity to evaluate the benefit of assimilating such high-spatial GPS data in addition to those from the operational European E-GVAP network. A clear positive impact on the AROME precipitation forecast has been found when the GPS delays are assimilated. The impact is more important on IOP9b (19 July). The comparison with other water vapour measurements performed during the COPS field campaign, such as those from additional soundings and water vapour LIDAR, shows that the tropospheric water vapour field is also improved.

Keywords: *Mesoscale Data Assimilation , GPS zenith delays , COPS*

1 INTRODUCTION

Recent works on the assimilation of high spatial and temporal resolution GPS Zenith Total Delay (ZTD) observations into mesoscale NWP systems suggest that better results can be obtained by increasing the model resolution. The availability of the GPS data from the field campaign COPS (Wulmeyer *et al.*, 2008), associated with the E-GVAP GPS data received operationally at Météo-France provide us an opportunity to verify the impact of GPS data assimilation at the convective scale. The new AROME system, a high-resolution data assimilation system based on non-hydrostatic resolving convection model, running operationally since December 2008 at Météo-France is used for that purpose. The impact has been evaluated on the COPS IOP9. During the three days of this IOP (18-20 July 2007), an elongated frontal zone developed upstream of the COPS region (the Vosges and Black Forest mountains in eastern France and southwestern Germany), associated with deep convection over the COPS region.

2 EXPERIMENTAL SETUP

AROME, the new convective-scale Numerical Weather Prediction system of Meteo-France (Seity et al. 2007), is running at 2.5-km resolution over a domain of 1600 km x 1250 km centred over France. A large part of the software of the AROME suite is common with the Météo-France ARPEGE and ALADIN NWP systems, and the ECMWF system IFS. The AROME dynamics is a non-hydrostatic extension of the limited-area NWP model ALADIN whereas the AROME physical package is extracted from the physical parameterizations of the Meso-NH research model. The AROME 3DVAR assimilation system is based on the ALADIN 3DVAR one.

The GPS ZTD data assimilation follows the ARPEGE and ALADIN GPS data assimilation implementation (Poli et al.,2007, Yan *et al.*, 2009), with slight differences due to higher resolution of the AROME system (Yan 2009). The GPS data which are assimilated come from the GPS network covering the COPS region with 76 stations and from the EUMETNET GPS water vapour program (E-GVAP, http://egvap.dmi.dk/) which provides near-real time GPS ZTD observations over Europe. A total of 316 GPS stations, from the E-GVAP and COPS networks, are included in the Arome domain.

Three AROME assimilation cycle experiments were running according to a 3-hour forward intermittent rapid update cycle: (i) without assimilating any GPS data (REF experiment), (ii) assimilating only the E-GVAP dataset (OPR experiment), and (iii) assimilating the COPS+E-GVAP dataset (COP experiment). In addition, the observations operationally used in the ALADIN-France model are assimilated in the three experiments: observations from radio-soundings, screen-level stations, buoy, ship and aircraft measurements, wind profilers, scatterometers, atmospheric motion vectors (AMS), and some satellites radiances, from METEOSAT/SEVIRI, and NOAA/ATOVS instruments. The REF and COP assimilation experiments start at 21 UTC, 5 July 2007 and the OPR experiment starts from the REF experiment at 00 UTC, 15 July 2007. 30-h AROME forecasts are launched at every 00 UTC on 18, 19 and 20 July from the REF, GPS and OPR analyses.

3 RESULTS

Figure 1a shows the ETS scores for the 12-h accumulated precipitation forecast from 03 to 15 UTC for the three days. The ETS values over the whole AROME domain (France domain) show that both COP and OPR experiments improve the precipitation forecast with respect to the REF one. When looking more specifically over the COPS region (SCOPS domain), the COP experiment performs better than the OPR one for weak precipitation, the both being better than the REF one. Assimilation of the high-spatial COPS GPS dataset in addition to the European E-GVAP dataset has thus a local positive impact.

The COPS data have been further exploited to evaluate the benefit of assimilating GPS ZTD observations on the water vapour field. First, a comparison has been carried out with the COPS additional Nancy soundings, not used in the assimilation cycle (Fig. 1b). This comparison shows that in overall the COP AROME forecasts perform better than the REF ones. This is particularly true for the the 18UTC radiosounding on July, 18: the 18-hour water vapour mixing ratio forecast fits very well with the observation .

The AROME forecasts have been also compared to the water vapour measurements from the airborne differential absorption lidar LEANDRE 2 on-board the French SAFIRE/F20 aircraft. Figure 1c shows the water vapor mixing ratio profiles averaged over the clear air columns along the 10 transects performed between 1224UTC and 1537 UTC during IOP9b for the AROME forecast of the three data assimilation cycle experiments. Three mean observed profiles are shown as observations have been averaged considering the same clear air columns as in the AROME forecast. Figure 1c shows that both COP and OPR runs perform better than the REF one, and that COP performs better than OPR.

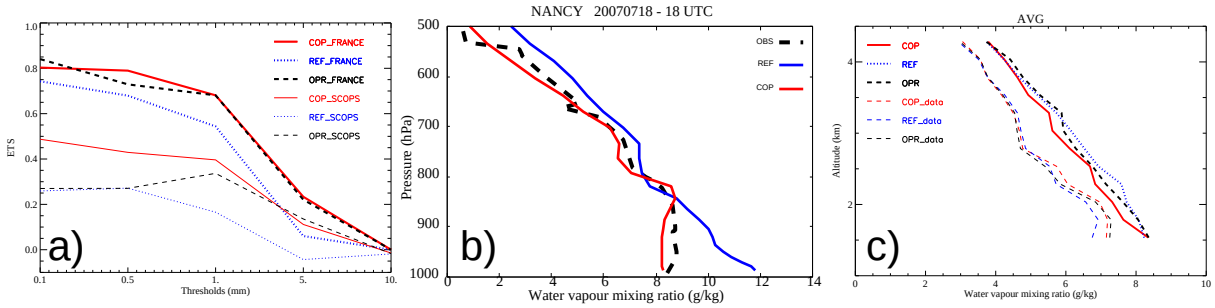

Figure 1: a) Equitable Threat Score (ETS) for 12-h accumulated precipitation forecast against raingauge observations from 03 UTC to 15 UTC, for 18,19 and 20 July 2007 over the FRANCE domain(bold lines) and the Smaller-COPS domain (SCOPS). b) Vertical profile of water vapour mixing ratio (g kg $^{-1}$) from the Nancy sounding at 18 UTC, 18 July 2007 (black dashed lines), and from the 18-h forecast REF (blue) and COPS (red) starting at 00 UTC, 18 July.c) Averaged profiles for the water vapour mixing ratio issued from the COP, OPR and REF AROME forecasts with respect to the LEANDRE 2 derived observations.

4 CONCLUSION

A clear positive impact of the assimilation of a large dataset of GPS ZTD observations in the AROME pre-operationnal suite has been obtained on the COPS IOP9 case study. Assimilation of GPS ZTD improves the short-range precipitation forecast as well as the forecast of the water vapour field. A large part of the impact can be attributed to the assimilation of the near-real time GPS ZTD dataset from E-GVAP. Assimilation of the high-resolution COPS GPS dataset in addition to the E-GVAP one leads to local positive impact on the weak precipitation.

Acknowledgements: *The COPS campaign and this study benefited from support from the ANR (Agence Nationale pour la Recherche) and the CNRS/INSU (Institut National des Sciences de l'Univers).*

REFERENCES

Poli P, Moll P, Rabier F, Desroziers G, Chapnik B, Berre L, Healy SB, Andersson E, EI Guelai FZ. 2007. Forecast impact studies of zenith total delay data from European near real-time GPS stations in Meteo France 4DVAR. *J. Geophys.Res.* **112**

Seity Y, Brousseau P, Malardel S, Masson, Bouttier, Hello 2007. Status of AROME developments, *Aladin Newsletter*, **33:**40-47

Wulfmeyer V *et al.* 2008. The convective and orographically-induced precipitation study: A research and development project of the WWRP for improving quantitative precipitation forecasting in low-mountain regions. *Bull. Amer. Meteor. Soc.* **89(10)**

Yan Xin 2009: Assimilation de donnes GPS pour la prévision de la convection profonde. *PhD*,P.Sabatier Univ. Toulouse France.

Yan X, Ducrocq V, Poli P, Hakam M, Jaubert G, Walpersdorf A. 2009a: Impact of GPS zenith delay assimilation on convective scale prediction of Mediterranean heavy rainfall.*J. Geophys.Res.*, Vol. 114

LONG-RANGE TRANSPORT OF SAHARAN DUST FROM CALIPSO, AIRBORNE AND GROUND-BASED LIDARS, AND A REGIONAL MODEL DURING COPS

J.-P. Chaboureau[1], E. Richard[1], J.-P. Pinty[1], P. Di Girolamo[2], C. Kiemle[3] and C. Flamant[4]

[1] Laboratoire d'Aérologie, Université de Toulouse and CNRS, Toulouse, France
[2] Dipartimento di Ingegneria e Fisica dell'Ambiente, Universita degli Studi della Basilicata, Potenza, Italy
[3] Institut für Physik der Atmosphäre, Deutsches Zentrum für Luft- und Raumfahrt, Oberpfaffenhofen, Germany
[4] Université Pierre et Marie Curie, Service d'Aéronomie/Institut Pierre-Simon Laplace, Paris, France
E-mail: *jean-pierre.chaboureau@aero.obs-mip.fr*

Abstract: A Saharan dust event affected the Rhine valley in southwestern Germany and eastern France on 1 August 2007 during the Convective and Orographically-induced Precipitation Study (COPS) experiment. Prior an episode of intense convection, a layer of dry and clean air capped by a warm and dusty layer was observed using Cloud-Aerosol Lidar and Infrared Pathfinder Satellite Observation (CALIPSO), airborne and ground-based lidar observations from North Africa to Western Europe. The origin of the different layers was investigated using a regional Meso-NH model simulation. Overall, the model reproduces the vertical structure of dust and water vapor. From the simulated Lagrangian back trajectories it is found that the dust was mobilized from Mauritania sources several days before while the dry layer subsided over the north Atlantic. Off Morocco, the dry layer fold down beneath the warm and dusty air and the two-layer structure was advected to the Rhine valley in about two days. As the dry layer can delay the triggering of convection for a few hours, such dusty episodes that occur prior to convective events might be of importance for quantitative precipitation forecasts.

Keywords: *COPS, precipitation, predictability, dust*

1 INTRODUCTION

Long-range transport of mineral dust in the free troposphere is important for many aspects including radiation and cloud microphysics. Such change in thermal structure can affect the skill in forecasts that do not predict dust routinely. For example, Chaboureau et al. (2007) showed an improvement in capturing the observed convective activity over West Africa at the 2-day range by the use of prognostic dust. However the impact on summertime precipitation over Western Europe has received little attention so far. On 1 August 2007 several ground-based lidars observed reaching the COPS area in the afternoon prior a convective event. The dust layer was also observed from airborne lidars in both the COPS area and upstream over the Iberian Peninsula and France. Some days before, CALIPSO observations shows the dust layer off the Moroccan coasts (Figure 1, top right). The long-range transport of dust is investigated using the mesoscale model Meso-NH (Lafore et al. 1998).

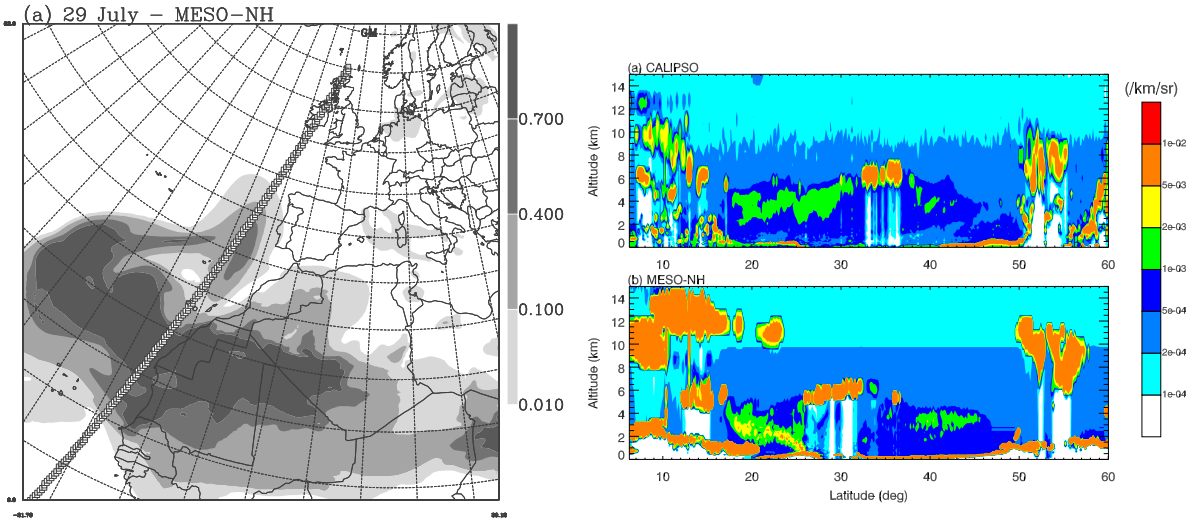

Figure 1: 0300 UTC 29 July 2007. (left) Total aerosol burden (g m^{-2}). The squares indicate the track of CALIPSO. (right) Vertical cross-section of 532-nm attenuated backscattering coefficient (km^{-1} sr^{-1}) along the line shown in left from (a) CALIPSO and (b) Meso-NH.

2 RESULTS

The case was simulated with triply nested models, with a horizontal grid spacing of 32, 8, and 2 km. The case was initialized on 26 July 2007 at 0000 UTC. In a first step it was integrated forward for 4 days using the outer grid only as model spinup for dust and cloud. For keeping the simulation close to the analyzed meteorological conditions, the simulation was nudged towards the ECMWF analyses. At 0000 UTC 1 August 2007 the case was then integrated for 24 hours using the three nested models without any nudging.

An overview of the dust event is given with a snapshot on 29 July (Figure 1). Dust with burden larger than 0.1 μmg was exported out of Africa and almost reached the coasts of the Iberian Peninsula. The good agreement achieved with the aerosol index (AI) obtained from the Ozone Monitoring Instrument (OMI, not shown) allows an assessment of the dust sources in Mauritania and northern Mali. The comparison with CALIPSO observations (Figure 1, right) shows that the model fairly well reproduced the vertical structure of the dust content.

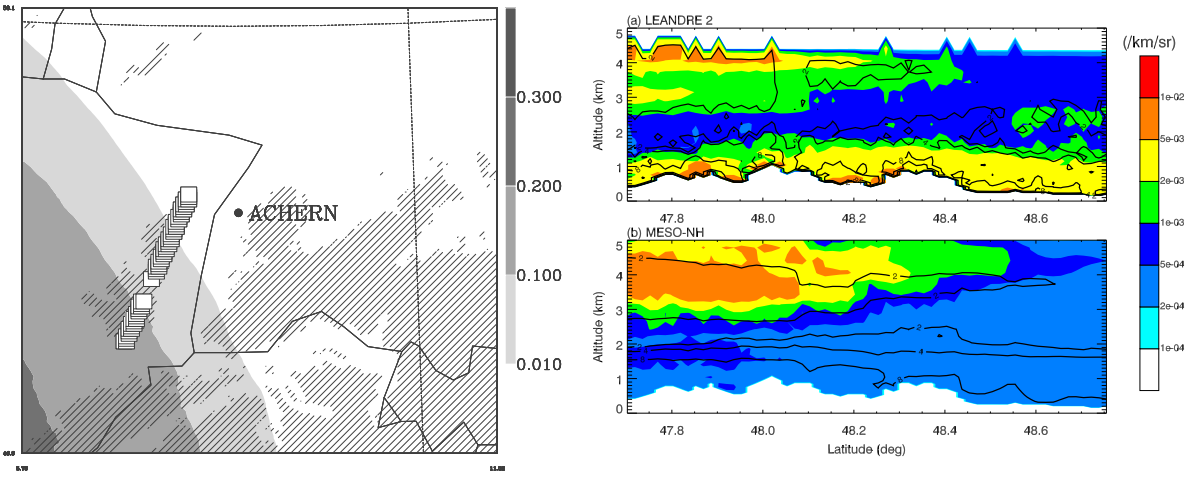

Figure 2: 1200 UTC 1 August 2007. (left) Total aerosol burden (g m^{-2}). The squares indicate the track of the SAFIRE Falcon. The hatch areas are topography above 500 m. (right) Vertical cross-section of 730-nm attenuated backscattering coefficient (shading, km^{-1} sr^{-1}) and water vapor mixing ratio (contours at 2, 4, 8 g kg^{-1}) at along the line shown in left from (a) LEANDRE 2 and (b) Meso-NH.

Another example is shown on 1200 UTC 1 August 2007 when the dust layer reached the COPS area (Figure 2). The LEANDRE-2 lidar sampled the dust layer between 3 and 5-km altitude. The Meso-NH simulation shows remarkable agreement with the observations in capturing the height and arrival time of the dust layer as well as the water vapor content. The lowest layer of high coefficient values is due to background aerosols not simulated by the model. Other comparisons with the DRL WALES airborne lidar and the BASIL Raman lidar operating from Achern confirm the ability of the model to reproduce the transport of dust from Africa to the COPS area.

3 CONCLUSIONS

The dust episode that affected the COPS area on 1 August 2007 is well reproduced by the Meso-NH model as seen with comparison with a set of lidar observations. Sensitivity studies on the predictibaility of precipitation to the dust content are under way.

Acknowledgements:
This study was funded by ANR (COPS France). The CALIPSO data were obtained from the ICARE center. Computer resources were allocated by IDRIS.

REFERENCES

[1] Chaboureau, J.-P., P. Tulet, and C. Mari, 2007: Diurnal cycle of dust and cirrus over West Africa as seen from Meteosat Second Generation satellite and a regional forecast model, *Geophys. Res. Lett.*, **34**, L02822, doi:10.1029/2006GL027771.

[2] Lafore, J.-P., et al., 1998: The Meso–NH Atmospheric Simulation System. Part I: adiabatic formulation and control simulations. Scientific objectives and experimental design, *Ann. Geophys.*, **16**, 90–109.

THE INFLUENCE OF AEROSOL PARTICLE NUMBER AND HYGROSCOPICITY ON THE EVOLUTION OF CONVECTION CLOUD SYSTEMS AND THEIR PRECIPITATION: A NUMERICAL STUDY BASED ON THE COPS OBSERVATIONS ON THE 12 AND 13 AUGUST 2007

Céline Planche, Andrea I. Flossmann, W. Wobrock

Laboratoire de Météorologie Physique, OPGC, CNRS-UBP, Clermont-Ferrand, France
E-mail: *C.Planche@opgc.univ-bpclermont.fr*

Abstract: A 3D cloud model with detailed microphysics for ice, water and aeosol particles (AP) is used to study the role of AP on the evolution of convective clouds and the subsequent precipitation. The model couples the dynamics of the NCAR Clark-Hall cloud scale model (Clark and Hall, 1991) with the detailed scavenging model (DESCAM) of Flossmann and Pruppacher (1988) and the ice phase module of Leroy et al. (2009). The microphysics follows the evolution of AP, drop, and ice crystal spectra. Aerosol mass in drops and ice crystals is also predicted.
The simulated cases are compared with radar observations on 12 and 13 August 2007 (LaMP X-band radar and Poldirad of DLR) over the northern Vosges mountains and the Rhine valley. In order to better understand the role of AP on cloud evolution and precipitation formation several sensitivity studies were performed by modifying not only aerosol number concentration but also their physico-chemical properties.

Keywords: *cloud modeling, detailed microphysics, aerosol particle impact, COPS*

1 INTRODUCTION

The impact of aerosol particles on precipitation formation is only partly understood. In this study we simulate with DESCAM 3D two convective cases observed during the COPS campaign and we examine the impact of the AP particles number and solubility on both the cloud evolution and precipitation formation.

This paper is divided into 4 parts. The model DESCAM 3D is briefly described in the section 2. The results with DESCAM 3D concerning the role of aerosol particles on cloud evolution and precipitation formation over the Vosges Mountains are discussed in section 3.

2 MODEL DESCRIPTION

The 3D model with detailed microphysics couples the 3D non-hydrostatic model of Clark and Hall (1991) with the Detailed Scavenging Model (DESCAM, Flossmann et al., 1988, Leroy et al., 2009) for the microphysical scheme. The microphysics model employs five distribution functions: three of them are number distribution functions for the wet AP, the drops and the ice crystals respectively and the remaining two are mass distributions of AP inside drops and ice particles. Aerosol particles cover the size range from nm to µm while drop and crystal sizes range from 2 µm to 1 cm.
The microphysical processes that have been implemented are: AP growth and activation/deactivation, condensation and evaporation of droplets, coalescance, homogeneous and heterogeneous nucleation, vapor deposition on ice crystals and riming. The model is described in detail in Leroy et al. (2009).

3 COPS CONVECTIVE CLOUD SYSTEMS

3.1 Model setup

The convective cloud systems observed on 12 and 13 August 2007 show quite different characteristics (Hagen et al., 2008) leading to different model setups in order to simulate both events.

For the 12 August case, the model domain covers 130 x 130 km in the horizontal and 16 km high in the vertical. The resolution is 1 km for the horizontal coordinates and 200 m for the vertical one. A second domain with a 250 m grid is nested for the area of interest. The dynamical time step is 3 seconds. The thermodynamic and dynamic conditions are given by the sounding of Nancy, 12 UTC for the 12 August. On 13 August a considerable western wind flow prevailed requiring the use of large scale initialization by means of the ECMWF reanalysis data at 6 UTC. Consequently the outer domain size increased to 384 x 256 km^2 with a horizontal grid of 4 km causing the nesting of two subdomains with 1 km and 0.25 km grid resolution. Figs. 1a and b give 3D views of the spatial location and structure of the convection for the innermost model domains. Convective clouds for both cases reach up to 5 km. On 12 August the precipitating cloud clusters form over the mountains and persists almost at the same place for about one hour. On 13 August, however, clouds and precipitation form on the eastern rime of the Vosges and cross during 1.5 h the entire Rhine valley.

To initialize the microphysics, the AP spectra follows Jaenicke (1988) for a continental air mass. In order to understand the role of AP concentration on cloud evolution and precipitation formation, the number of AP is increased and decreased for polluted and clean environment, respectively. Also, the solubility of AP is modified to understand its role on the rain formation.

a) **b)**

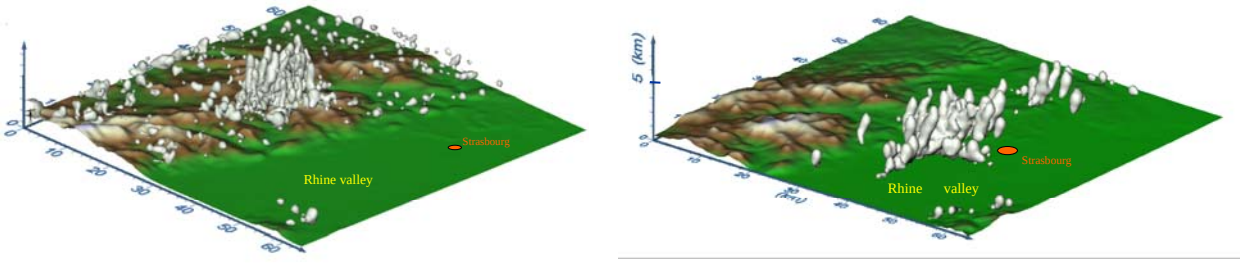

Figure 1. Field of cloud water for 12 August 2007 (a) and 13 August 2007 (b). The white envelope corresponds to 0.1 g/kg.

3.2 RESULTS

Table 1 gives the results of model simulations for the different aerosol number distributions and different particle solubility 60 min after cloud formation starts. Mean rain amount and rain maxima were taken at the surface while data for vertical wind; relative humidity and droplet number were taken at 2 km altitude.

Comparing the results obtained for the continental, clean and polluted cases we can see that the number of rain drops, the rain amount and the relative humidity are quite sensitive to the number of aerosol particles. However, the change of the AP solubility doesn't influence the dynamic or microphysical parameters.

Cases	mean rain amount (mm)	rain max. (mm)	N_{drops} (cm^{-3})	N_{drops} max (cm^{-3})	mean w (m/s)	RH (%)	RH max (%)
Continental	0.63	3.819	30.1	157.7	1.46	100.25	100.6
Clean	0.70	4.114	17.6	88.5	1.34	100.33	100.7
Polluted	0.57	3.264	59.4	405.9	1.40	100.12	100.3
50% soluble	0.63	3.820	30.2	157.6	1.46	100.26	100.6
5% soluble	0.63	3.822	30.1	157.2	1.47	100.25	100.6
$\alpha_c = 0.5$	0.64	3.856	25.8	129.8	1.47	100.22	100.5

Table 1: Rain amount, number of rain drops N_{drops}, vertical wind w and relative humidity RH average values and maxima for the continental, clean, polluted case. In these cases AP were chosen 100% soluble. For the 50 % and 5% soluble cases the continental AP distribution was used, just as for the last case where the sticking coefficient for water vapor was increased from 0.04 to $\alpha_c = 0.5$.

4 CONCLUSIONS

The simulation with our detailed cloud model show good agreement with the cloud and precipitation characteristics observed by our X band Radar and Poldirad of DLR. To understand the role of the AP on cloud evolution and precipitation formation several sensitivity studies were performed by modifying not only aerosol number concentration but also their physico-chemical properties. The numerical results show a strong influence of the aerosol number concentration on the precipitation intensity but little effect of the aerosol particle solubility on the rain formation can be found.

Acknowledgements:
The calculations for this study have been done on computer facilities of IDRIS, CNRS at Orsay and CINES in Montpellier, under the project 940180. The authors acknowledge with gratitude the hours of computer time and the support provided.

REFERENCES

Clark, T. L., and W. D. Hall, 1991: Multi-domain simulations of the time dependent Navier-Stokes equations : benchmark error analysis of some nesting procedure, *J. Comp. Phys.*, **92**, 456-481.

Flossmann, A. I. and. H. R. Pruppacher, 1988: A theoretical study of the wet removal of atmospheric pollutants. Part III : The uptake, redistribution, and deposition of (NH4)2SO4 particles by a convective cloud using a two-dimensional cloud dynamics model. J. Atmos. Sci., 45, 1857-1871.

Leroy, D., W. Wobrock and A. I. Flossmann, 2009: The role of boundary layer aerosol particles for the development of deep convective clouds: a high-resolution 3D model with detailed (bin) microphysics applied to CRYSTAL-FACE , Atmos. Res.; DOI: 10.1016/j.atmosres.2008.06.001

Jaenicke, R., 1988: Aerosol physics and chemistry. In Landolt-Börnstein: Zahlenwerte und Funktionen aus Naturwissenschaften und Technik, V 4b, G. Fischer Editor, Springer, 391-457.

Hagen M., J. VanBaelen and E. Richard, 2008: Orographic influence on life cycle of convection – observations during the COPS. ERAD conference, Helsinki, 2008

INVESTIGATIONS OF THE IMPACT OF AEROSOLS ON A HAILSTORM IN THE BLACK FOREST

Heike Noppel[1], Ulrich Blahak[1], Axel Seifert[2], Klaus D. Beheng[1]

[1] Institut für Meteorologie und Klimaforschung, Karlsruhe Institute of Technology, Germany
[2] German Weather Service, Offenbach, Germany
E-mail: *heike.noppel@kit.edu*

Abstract: Hail storms can cause significant damage to crops, buildings or cars. Therefore, it is of great interest to be able to predict them or to assess the potential to modify them by human activities either inadvertently by air pollution or by intended cloud seeding. To this aim a sophisticated two-moment cloud microphysical scheme has been implemented into the numerical weather prediction model COSMO. A hailstorm in the Black Forest that caused significant damage was simulated with this model system with a horizontal resolution of 1 km. COSMO forecasts with a coarser resolution and the standard one-moment microphysical scheme were used for initialization and boundary conditions. A severe hailstorm that resembles the observations quite well and produces realistic amounts of precipitation and hail at the ground develops with this model system, though some hours late. Sensitivity studies were conducted varying the concentration of cloud condensation nuclei (CCN) and the shape of the cloud droplet size distribution. Results show that both have a significant impact on hail accumulated at the ground and on the size of the hailstones. However, due to the complexity of the storm dynamics and microphysics, general statements whether an increase or decrease in CCN concentration invigorates a hailstorm can not be drawn.

***K*eywords:** *NWP model, hailstorm, aerososl effect, convective clouds, COSMO model*

1 INTRODUCTION

Recent studies of cloud interactions with particulate air pollution, performed mostly on a conceptual level, suggest that pollution aerosols can invigorate convection into severe storms by slowing down the conversion of cloud drops into precipitation. In pristine air rain formation is rather fast, invoking early downdrafts and preventing the lifting of much water to the supercooled levels, so that the cloud dies early with a moderate amount of rainfall. According to the hypothesis that should be tested within the ANTISTORM project, a high concentration of aerosol acting as cloud condensation nuclei (CCN) slows down rain formation and increases the amount of supercooled water in the mature stage of the cloud. This leads to enhanced riming, the production of hail, high precipitation rates and strong downdrafts.

The objectives of the ANTISTORM project were to test this hypothesis, study the impact of aerosols on convective storms in Europe, and "develop models that should help to improve forecasting and even suggest strategies for mitigating storms before disaster strikes" (http://antistorm.isac.cnr.it/).

The numerical model we used for our studies is the COSMO model combined with the 2-moment bulk microphysical scheme by Seifert and Beheng (2006). Some parameters and process descriptions of the 2-moment scheme have been altered to better represent "hail" particles (Blahak, 2008). In order to test the model and to investigate the impact of CCN, the case study described in the following section was chosen.

2 THE HAILSTORM OF JUNE, 28th 2006

On 28/06/2006 the small town of Villingen-Schwenningen (VS) situated in South-West Germany at the eastern edge of the Black Forest was hit by a strong hail storm. Due to the storm more than 100 people got injured and one man drowned. Additionally, many crops, cars and buildings were damaged, mainly by hailstones but also by flooding.

The synoptic situation was characterized by a strong vertical windshear, with northerly to easterly winds at the bottom and a strong wind from West to South-West at levels above 3000 m. According to radio soundings at Nancy and Stuttgart at 12 UTC, lifting condensation level was at about 800 m amsl and temperature at that level about 14 °C . Air temperature near the ground was about 19 °C with a high relative humidity.

In the late afternoon several convective cells could be observed in the vicinity of the Black Forest and the adjacent Rhine Valley. At about 17 UTC one of the cells split close to the crest of the Black Forest and the right cell moved almost perpendicular to the main wind in south-easterly direction. This right mover intensified, developing radar reflectivities of more than 65 dBZ, reached VS at about 17:30 UTC and passed it with the core of the cell situated slightly to the north of the town. After crossing the Swabian Alb, another nearby low montain ridge, the storm finally decayed.

3 MODEL SETUP

For the numerical simulations full orography was used and the model's initial state as well as the boundary values were adopted from operational COSMO-DE forecasts starting at 12 UTC on 28/06/2006. Integration time was 13 hours and the model domain 291 x 291 x 64 gridpoints with a horizontal resolution of 1 km. The COSMO-DE forecasts provided by the German Weather Service had been performed with the standard microphysical one-moment scheme. The output used as boundary conditions was available every hour.

For the nested grid, cloud microphysics was paramterized by an extended version of the two-moment scheme by Seifert and Beheng (2006). Besides modifications concerning hail by Blahak (2008) a new scheme for cloud droplet nucleation based on look-up tables by Segal and Khain (2006) as well as a shape parameter depending on mean diameter for sedimentation and evaporation of raindrops (Seifert, 2008) have been implemented. The scheme was validated for different CCN conditions by comparison to a spectral bin model (Noppel et al., 2008; Seifert et al., 2006).

Four different CCN concentrations leading to different typical maximum cloud droplet concentrations N_{drop} were assumed: (1) low CCN, N_{drop} = 100 cm^{-3}, (2) intermediate CCN, N_{drop} =350 cm^{-3}, (3) high CCN, N_{drop} = 1200 cm^{-3}, (4) very high CCN, N_{drop} = 2100 cm^{-3}. As CCN conditions may also change the size distribution of the nucleated droplets the parameters μ and ν of the assumed generalized gamma-distribution

$$f(x) = Ax^{\nu} \exp(\lambda x^{\mu}) \tag{1}$$

were also varied (x is particle mass). The two other parameters A and λ can be calculated from the predicted bulk mass and number densities (the 0th and 1st moment of the distribution). Three different cloud droplet size distributions (CDSD) were assumed: (a) ν=1/3, μ=2/3, (b) ν=1, μ=1, (c) ν=6, μ=1/3.

4 RESULTS

In all model runs, no convective cells at all develop in the vicinity of the Black Forest during the afternoon. Only at about 20 UTC first convective cells occur. At about 21:30 UTC a right mover occurs whose development is very similar to the observed hail storm. The simulated amount of accumulated precipitation as well in total (up to 51 mm) as for hail only (up to 14.9 mm) seems to be quite realistic and the model produces a significant number of large hailstones (at heights below 2 km amsl up to about 13 particles with more than 2.5 cm in diameter per 1000 m^3). In contrast, simulations with the standard one-moment scheme for microphysics fail to generate a right mover and produce much lower precipitation amounts.

When comparing the results for the different CCN scenarios it becomes evident that CCN concentration as well as the assumed CDSD do have a significant impact on the intensity, lifetime, and dynamics of a convective storm. For example, for scenario 4a (very high CCN concentration, CDSD (a)) the hailstorm is much weaker and passes VS about 15 km further to the North than for scenario 1a (low CCN concentration, CDSD (a)). The consideration of all storms that occur in the model domain shows that a variation in CCN concentration or CDSD may lead to a significant weakening of one hailstorm and at the same time to an invigoration of another one. As the temporal evolution is influenced by CCN concentration and CDSD, the impact of orographical structures also changes.

A closer examination of the dynamics and cloud microphysics of the right moving storm and the comparison of two of the CCN-scenarios reveals how complex the different processes and their interactions within such a storm may be and that it is is almost impossible to predict what will happen if certain microphysical conditions, like aerosol concentrations, change.

REFERENCES

Blahak, U., 2008: Towards a Better Representation of High Density Ice Particles in a State-of-the-Art Two-Moment Bulk Microphysical Scheme. *15th Intern. Conf. on Clouds and Precipitation*, July 7-11, 2008, Cancun, Mexico

Noppel, H., A. Khain, A. Pokrovsky, U. Blahak, K.D. Beheng, 2008: How well can a bulk scheme reproduce the microphysical processes within a convective storm? - Comparisons to a spectral bin model. *15th Intern. Conf. on Clouds and Precipitation*, July 7-11, 2008, Cancun, Mexico

Segal, Y. and Khain, A., 2006: Dependence of droplet concentration on aerosol conditions in different cloud types: Application to droplet concentration parameterization of aerosol conditions. *J. Geophys. Res.*, **111**, D15240, doi:10.1029/2005JD006561

Seifert, A., 2008: On the parameterization of evaporation of raindrops as simulated by a one-dimensional rainshaft model. *J. Atmos. Sci.*, **65**, 3608–3619

Seifert, A., K.D. Beheng, 2006: A two-moment cloud microphysics parameterization for mixed-phase clouds. Part 1: Model description. *M*eteorol. Atmos. Phys., **92**, 45–66.

Seifert, A., A. Khain, A. Pokrovsky and K.D. Beheng, 2006: A comparison of spectral bin and two-moment bulk mixed-phase cloud microphysics. *Atmos. Res.*, **80**, 46–66.

PRECIPITATION DOWNSCALING IN WESTERN NORWAY: TIME-STEP PRECIPITATION INTENSITY

I. Barstad[1], U. Heikkilä[1]and M. Mesquita[1].

[1] Bjerknes Centre for Climate Research, Bergen, Norway
E-mail: *Idar.Barstad@bjerknes.uib.no*

Abstract: High frequency observations from two field campaigns have been compared with time-step precipitation in a numerical model. The numerical model schemes seem not to fully reproduce the observed precipitation. The schemes produce too high level of wetness and the intensities are too low. Typical simulated intensities are about 9mm/hr, whereas the observed values are typically 15mm/hr.
Keywords: *ICAM, time-step precipitation, evaluation, wrf, STOPEX.*

1 INTRODUCTION

The resolution in mesoscale numerical models has increased in the last few years. This has produced higher levels of detail for atmospheric parameters such as precipitation. Evaluating the added improvement in the models is not straight forward. Many goodness measures (e.g. root-mean-square error and Pearson correlation) show reduced skills when the detail level is enhanced (Barstad and Smith, 2005). In this extended abstract we will show how two different microphysical numerical schemes perform at the time-scale of the model time-step.

2 EXPERIMENTS AND RESULTS

The island Stord on the west coast of Norway was chosen as an experimental site for orographic precipitation, STord Orographic Precipitation EXperiment (STOPEX 1; Reuder et al. (2007) and STOPEX 2). Stord has about 600m tall mountains, it is 20km long (north-south) and is 10km wide (west-east). See Figure 1 for geographical information. Southwesterly winds prevail in the area. During autumn 2005 (7 weeks) and 2006 (11 weeks), numerous rain gauges were deployed across the island, and several weather stations (AWS) surveyed the weather situation. The stations used in this study are shown in Figure 1.

The numerical model (WRFV3.0; www.wrf-model.org) was set up with two two-way nested domains (10km-3.3km) and the boundaries were orchestrated by the ECMWF-analysis. A standard set-up was used with 39 vertical layers. Two different microphysical schemes were tested: "mp3" - a simple 3-class scheme (Hong et al. 2004), and "mp10" - a more sophisticated multi-class scheme (Morrison and Pinto, 2006). The model time-step was 20s in the higher resolution domain. An fdda-nudging was used with 6-hour relaxation time outside the planetary boundary layer.

Table 1 shows the performance of the two schemes for 6 stations across the island, from west to east. 'Rain vs. no-rain' cases are shown in % for various accumulation periods and the total accumulated precipitation for Stopex 1 period is indicated. From the table, we find that the simulated 10min cases are too wet, particularly at the upwind flat land station (P1). The mp3-simulation is worse than the mp10 case. Longer accumulation periods camouflage this effect showing better results. The total precipitation amounts show too little simulated precipitation in elevated terrain, too much on the flat land and the mp3-simulation produces the highest values.

Station/measure	Wet (%) – 10min (mp3/mp10)	Wet (%)- 1hr (mp3/mp10)	Wet (%)- 3hr (mp3/mp10)	Wet (%) – 24hr (mp3/mp10)	Total accumulated (mm) (mp3/mp10/**obs**)
P1 upwind-flat land	525/443	285/254	195/183	119/119	787/729/**333**
P3 upwind-slope	360/311	219/203	160/152	110/108	927/766/**768**
P5 top	292/234	192/168	145/138	100/100	856/676/**1120**
P11 leeside-top	256/200	160/137	125/114	98/98	707/640/**1220**
P8 leeside-slope	331/265	208/182	163/154	111/113	804/634/**838**
P9 leeside-flat land	387/324	234/207	169/158	111/113	845/704/**640**

Table 1. Simulated precipitation across Stord island autumn 2005. Wet events (i.e. 100% means as observed) for various accumulation periods (column 2-5) and total accumulated amounts during the campaign (last column). "mp3" and "mp10" refer to two different microphysical schemes used. Underlined values indicate the ones with better skill. See Figure 1 for station locations.

In order to have a closer look at the intensities 'hidden' inside various accumulating periods (10min, 1hr etc.), we turn to tipping bucket measurements and to the comparison with the model time-step precipitation. Figure 2 shows the typical time between each tip (0.2mm amount) observed and simulated. The observed intensity is about 15mm/hr whereas the simulated is closer to 9mm/hr. The mp3-simulation, in particular, shows

too many weak intensity cases (200-400s in Fig.2). This fits with the general picture of a too wet model (Table 1).

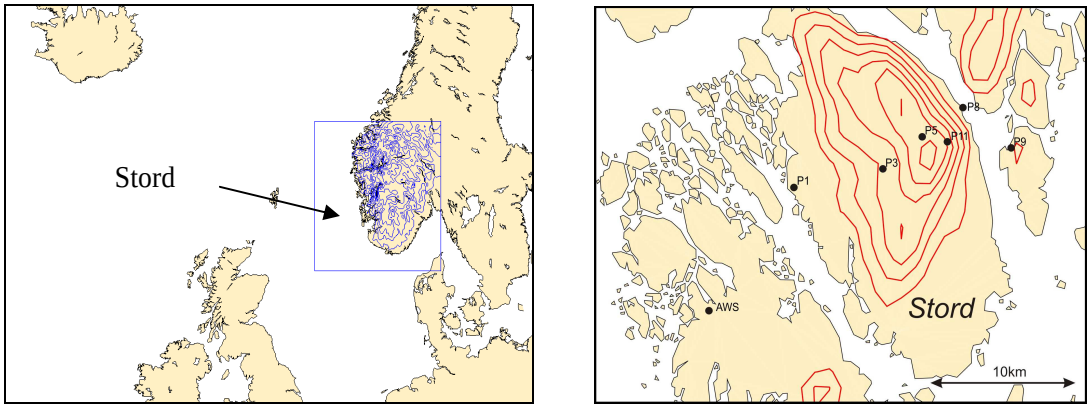

Figure 1. Left: The two nested model domains (10km-3.3km). Right: The terrain (every 100m starting at 100m elevation) is shown by 1km grid. Precipitation stations in Table 1 are indicated.

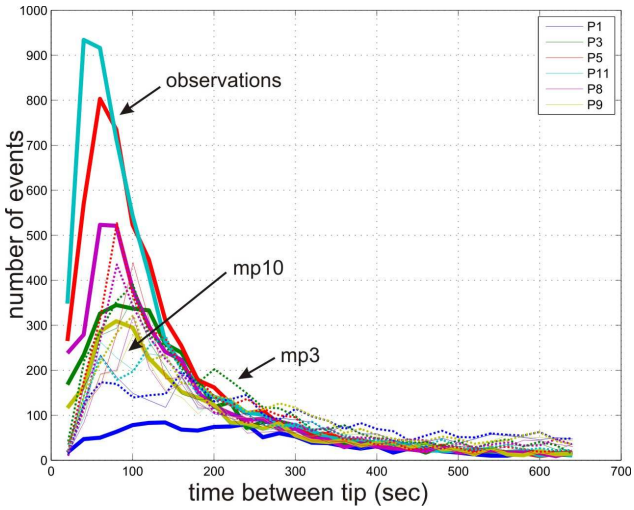

Figure 2. Tipping-bucket vs. modelled values for Stopex 1. 6 stations are shown, cf. Table 1. Heavy solid lines represent the observations, dotted lines the mp3-simulation, and the thin lines the mp10-simulation.

An important case is that of November 5th, 2006. The winds were steadily from the west throughout the day. Some of the rain gauges received as much as 100mm. Simulation of this case with a similar model set up as used in this report, but including an additional 1km nest, shows that the maximum precipitation intensity in a 1km grid was about 15-20% larger than in the 3km grid. This indicates that the precipitation results in the 3.3km grid should ideally be a bit lower than the observed values.

3 CONCLUSIONS

From this investigation, we find that simulation by a mesoscale model with 3.3km grid spacing, has similar problems as the standard problem for numerical models; it rains too often and too little. The simpler scheme used performs better than sophisticated ones in complex terrain, except on the flat land. A case study having higher resolution indicates that higher intensities (15-20% increase) are expected if a 1km grid is nested inside a 3km grid.

Acknowledgements:
Tor de Lange, Joachim Reuder, Geir Ottar Fagerlid, Marianne S. Andersen and Eli Anne Ersdal made valuable contributions in the acquisition of the observational data.

REFERENCES

Barstad, I. and R. B. Smith, 2005: Evaluation of an Orographic Precipitation Model. Journal of hydrometeorology **6**, 85-99.

Hong, S.-Y., J. Dudhia, and S.-H. Chen, 2004: A Revised Approach to Ice Microphysical Processes for the Bulk Parameterization of Clouds and Precipitation. Mon. Wea. Rev. **132**,103–120.

Morrison, H., and J. O. Pinto, 2006: Intercomparison of bulk microphysics schemes in mesoscale simulations of springtime Arctic mixed-phase stratiform clouds. Mon. Wea. Rev. **134**, 1880–1900.

Reuder, J., I. Barstad, G.O. Fagerlid and A.D. Sandvik, 2007: Stord Orographic Precipitation Experiment (STOPEX): An overview of phase I. Hydrology and Earth System Sciences **10**, 17-23.

GRIDDING DAILY PRECIPITATION FROM A SPARSE SURFACE NETWORK IN COMPLEX TOPOGRAPHY — A REDUCED-SPACE OPTIMAL INTERPOLATION APPROACH

Mark A. Liniger, Reinhard Schiemann, Christoph Frei

Federal Office of Meteorology and Climatology MeteoSwiss, Zurich, Switzerland
E-mail: *mark.liniger@meteoswiss.ch*

Abstract: A feasibility study is presented testing the application of reduced-space optimal interpolation for gridding daily precipitation from a sparse gauge network. The results of the study are encouraging, the method clearly outperforms a simpler reference technique and lends itself to the application both in a near real-time and a climate reconstruction context. Including weather-type information does not substantially improve the gridded fields.

***K*eywords:** *ICAM, optimal interpolation, precipitation, gridding, mapping*

1 INTRODUCTION

Operational networks of rain-gauge stations offer dense information on the distribution of precipitation. Yet, only a rather small part of this information is based on automatic measurements available in real-time. Most of the observations are taken manually and are available only weeks to years after the event. Thus, a real-time description of mesoscale precipitation fields is a challenge, in particular in complex topography. In this study, we propose a method to derive quasi real-time fine-scale precipitation fields. The method exploits the statistical relationship between the coarse real-time and dense climatic information. It is rigorously evaluated for daily precipitation fields over Switzerland and it is tested if the inclusion of weather type information yields improved results.

The same method can also be employed to reconstruct precipitation fields in the past when the density of observations was low.

2 METHOD AND DATA

The proposed method is reduced-space optimal interpolation (RSOI; Kaplan et al. 1997). It is normally applied in the context of climate reconstruction and has been used, for example, for reconstructing monthly precipitation totals in the Alps (Schmidli et al. 2001).

RSOI consists of two parts. First, principal component analysis (PCA) is used to obtain a reduced-space description of high-resolution data available during a calibration period. Thereafter, coarse data (available both in the calibration and in a reconstruction period) are used to estimate the principal component scores in the reconstruction period. In this way, the method considers both the temporal evolution of the data in the reconstruction period and the spatial covariance structure known from the high-resolution data.

In the application presented here, the high-resolution data (referred to as "OBS" below) are from a gridded daily precipitation climatology (Frei and Schär 1998, Frei and Schmidli 2006). Figure 1a shows the dense gauge network that forms the observational basis for these grids (red dots) and Figure 1b shows their long-term mean. The coarse data are gauge observations from a sparse network (Figure 1a, blue circles). The calibration period is 1971–1980 and daily reconstructed fields ("RSOI") are derived throughout 2001–2007. As a reference, daily fields created by means of a simpler gridding technique ("SIMPLE") and based on the same sparse gauge network are also taken into account. The study area is Switzerland.

Additionally, RSOI is applied separately for each weather type of two weather type classifications. These classifications are called PCACA (5 types) and SANDRA (22 types), respectively, and are from version 1 of the classification catalogue provided by COST Action 733 (`http://www.cost733.org`).

3 RESULTS

PCA efficiently reduces the dimensionality of the OBS grids. About 93% of the variance in these data can be represented by as few as 10 principal components. Several examples show that RSOI clearly outperforms the simpler gridding technique (e.g., Figure 2abc). A systematic quantitative evaluation of the SIMPLE and RSOI grids through the reconstruction period corroborates this finding (not shown here). The benefit is particularly high in situations of large-scale precipitation. For situations with highly localized precipitation features (e.g., due to thunderstorms) both methods perform at a comparable skill and features not captured by the sparse network cannot be represented satisfactorily (e.g., Figure 2def). Finally, we find that the gain in RSOI reconstruction skill due to the inclusion of weather type information is at best moderate and depends strongly on the weather type.

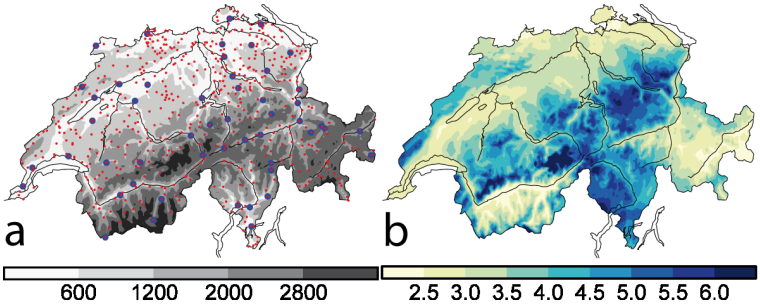

Figure 1: Overview of the study area. (a) Gauges of the sparse network (51 stations; blue circles), the dense network (typically 420 stations on individual days; red dots) and height of topography (shading). (b,c) Long-term mean of daily precipitation (mm d^{-1}).

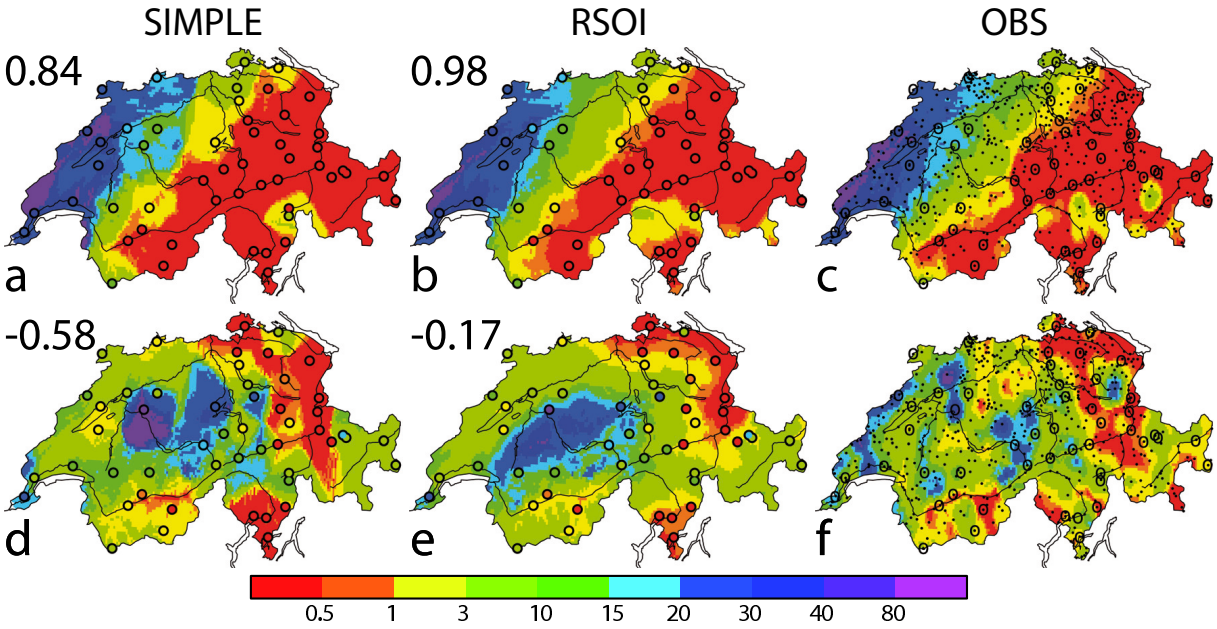

Figure 2: Examples of daily gridded fields (top: 2004-03-13, bottom: 2002-07-30). (a,d) reference method (SIMPLE), (b,e) RSOI, (c,f) high-resolution fields (OBS). Numbers show the mean-squared-error skill score quantifying interpolation quality.

4 CONCLUSION

RSOI is a promising candidate for real-time precipitation gridding. The method presented herein is entirely based on gauge measurements and does not use other sources of data such as radar observations. Therefore, it is attractive as a reference for methods using additional data sources, or in situations when no such additional observations are available. Apart from gridding in a near real-time context, the reconstruction of historical daily precipitation fields is a conceivable application of RSOI.

REFERENCES

Frei, C., and C. Schär, 1998: A precipitation climatology of the Alps from high-resolution rain-gauge observations. *Int. J. Climatol.*, **18**, 873–900.

Frei, C., and J. Schmidli, 2006 (in German): Das Niederschlagsklima der Alpen: Wo sich Extreme nahe kommen. *promet, meteorologische Fortbildung (Deutscher Wetterdienst)*, **32**, 61–67.

Kaplan, A., Y. Kushnir, M. A. Cane, and M. B. Blumenthal, 1997: Reduced space optimal analysis for historical datasets: 136 years of Atlantic sea surface temperatures. *J. Geophys. Res.*, **102**, 27835–27860.

Schmidli, J., C. Frei, and C. Schär, 2001: Reconstruction of Mesoscale Precipitation Fields from Sparse Observations in Complex Terrain. *J. Climate*, **14**, 3289–3306.

HIGH RESOLUTION ANALYSES BASED ON THE D-PHASE & COPS GTS –AND NON-GTS DATA SET

Theresa Gorgas, Manfred Dorninger, Reinhold Steinacker

Department of Meteorology and Geophysics, University of Vienna, Austria
E-mail: *theresa.gorgas@univie.ac.at*

Abstract: A high-resolution data set of surface observations which was set up for the whole year of 2007 in Central Europe is introduced and described. Also availability information for possible users is offered. For the same period and spatial domain an additional set of reanalyses based on the observation data is produced. Methods and examples are presented.

Keywords: *Surface observation data, reanalysis, VERA*

1 INTRODUCTION

In the framework of the programmes MAP D-PHASE and COPS the University of Vienna, collected GTS and Non-GTS data from the national and regional meteorological services for the year 2007 (GOP period) covering a greater Central Europe domain. All surface data are converted to a unique NetCDF format and the precipitation amounts accumulated to 1, 3, 6, 12 and 24 hour values. The data are uploaded to the WDCC (World Data Climate Centre) in Hamburg.

Based on the VERA (Vienna Enhanced Resolution Analysis) method, the GTS and Non-GTS data set is used to create a set of hourly reanalyses for 2007 over Central Europe with a grid-point distance of 8km.

2 THE COPS & D-PHASE GTS AND NON-GTS DATA SET

The MAP D-PHASE and COPS data set of GTS and Non-GTS surface stations involves about eleven thousand Non-GTS and more than thousand GTS stations. Several European national meteorological institutions where asked to provide data from regional operational observation networks, which are not included in the GTS system. As the data collection task concentrated only on operational data the data set does not include data produced during the field campaign of COPS. It is, thus, meant to extend the amount of data available for the COPS and D-PHASE intensive periods and to support continuative work on case studies in a larger area.

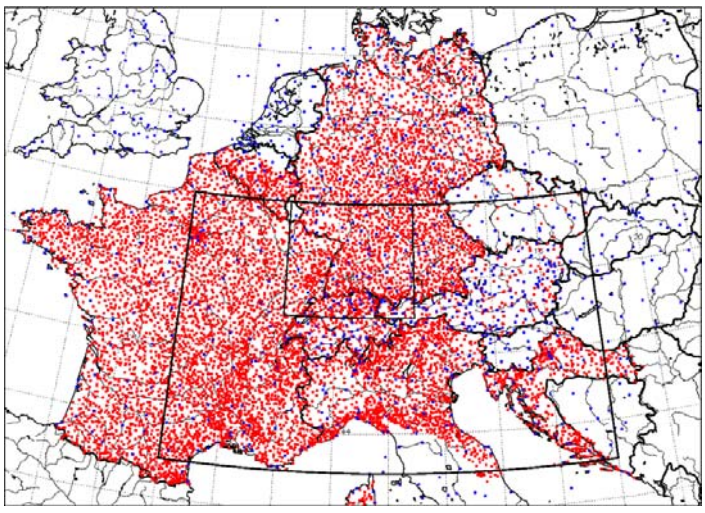

Figure 1. Distribution of all GTS (blue dots) and Non-GTS (red dots) stations. The majority of the latter are precipitation stations. The black frames define the COPS (smaller one) and D-PHASE (larger one) areas.

There is a wide range of parameters which are, if provided by the weather services involved in the data files: Additionally to the "main" parameters like wind, temperature, dew point, pressure and precipitation also other parameters like cloud coverage, present and past significant weather information, gusts, pressure tendency and maximum/minimum temperatures are collected. However, many of the regional observation networks only concentrate on few parameters.

It was always the highest temporal resolution available which was acquired from the providing institutions. Hence temporal resolutions of originally received data range from 5, 6 or 10 minutes to 1-hourly and 3-hourly and up to a maximum of 24-hourly measurements in the case of climatological stations. Especially in the case of precipitation values the variety of accumulation periods poses a problem for the reasonable application of the data.

In order to solve this problem the University of Hohenheim reprocessed the whole data set and produced additional sets, each for the accumulation periods of 1h, 3h, 6h, 12h and 24h. This step enables to the treat the data set as a whole for analysis purposes or other applications.

The data are saved in a unique NetCDF format and in annual files for each observing station, where each file includes all parameters measured by the station. The single files are available as packed files for country, data provider and network. Additional packages are available for each precipitation accumulation period.

3 VERA AND QUALITY CONTROL

VERA has been developed at the Department of Meteorology and Geophysics, University of Vienna. It has already been in use for operational 2D analyses in recent years. The calculation, based on a variational approach, is carried out on a regular 2D grid. Different resolutions (8km for the reanalysis data set, 16km for operational use) and arbitrary target areas can be chosen. For downscaling purposes VERA uses an a priori knowledge on small-scale physical processes over complex terrain, the so called "fingerprint technique", which transfers information from rich to data sparse regions. The hourly reanalyses are performed for following parameters: Equivalent potential and potential temperature, mean sea level pressure, wind and precipitation, the latter for 1h, 3h, 6h, 12h and 24h accumulation periods. In a post processing step also mixing ratio and moisture flux divergence are calculated.

In principle VERA could be defined as "model-independent", which means that it is not necessary to involve an NWP-model's first guess field in the analysis procedure. However, due to the large target area there are data lacking areas at the edge. Therefore grid values of analysis and forecast fields of the global GFS model are employed as bogus stations when there's no other surface observation station near a VERA grid point.

A very important element of the analysis system is the quality control scheme which corrects observational surface data before the analysis procedure. A variational scheme enables weighted correction recommendations for each station value. Wrong and unnatural values or simply stations with too large correction recommendations are sorted out. In the case of very high or highly variable station density - for example by performing analyses of the GTS and Non-GTS data set - partial clustering of stations is possible in order to avoid calculation difficulties.

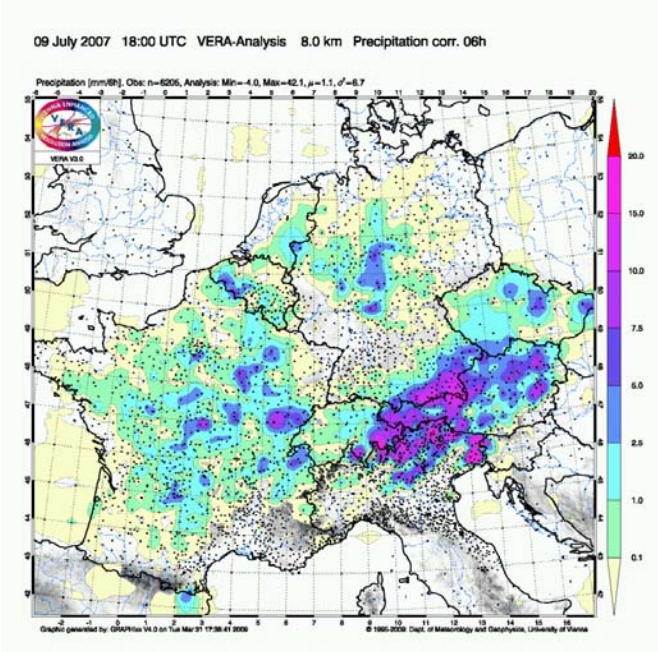

Figure 2. Example of a VERA analysis field for 6-hourly accumulated precipitation.

4 CONCLUSIONS & OUTLOOK

Like the observational data set also the re-analyses of 2007 shall be made available to all users at WDCC. It is intended to serve as a reference for ongoing studies in the framework of COPS and D-PHASE, for example as quick-look for case studies, as a basis for predictability studies or as reference data for verification activities. One of the next working steps concerning the analysis system will be the estimation of analysis errors, important additional information for all possible applications.

We thank all Central European data providers for their support and Thomas Schwitalla from the University of Hohenheim for his efforts concerning the accumulation of precipitation data.
The founding for our activities is provided by FWF (Austrian Science Fund) and DFG (German Research Foundation).

REFERENCES

Steinacker R., M. Ratheiser, B. Bica, B. Chimani, M. Dorninger, W. Gepp, C. Lotteraner, S. Schneider, S. Tschannett, 2006: A mesoscale data analysis and downscaling method over complex terrain. Mon. Wea. Rev., 134, 2758-2771.

Gorgas T. et al., 2008: The GTS and non-GTS data set for COPS and MAP D-PHASE, 7th COPS Workshop, October 27-29, Strasbourg. Presentation available at: https://www.uni-hohenheim.de/spp-iop/7th_COPS_WS/7th_COPS_workshop.html

Rotach, M.W and 38 co-authors, 2009: MAP D-PHASE: Real-time Demonstration of Weather Forecast Quality in the Alpine Region. Bull. Amer. Meteorol. Soc., accepted.

Wulfmeyer V and 27 co-authors, 2008: The Convective and Orographically-induced Precipitation Study: A Research and Development Project of the World Weather Research Program for Improving Quantitative Precipitation Forecasting in Low-mountain Regions. Bull. Amer. Meteor. Soc., DOI 10.1175/2008BAMS2367.1.

NOCTURNAL COLD AIR INTRUSIONS AT ARIZONA'S METEOR CRATER

C. David Whiteman, Sebastian W. Hoch, and Manuela Lehner

University of Utah, Salt Lake City, Utah, USA
E-mail: *dave.whiteman@utah.edu*

Abstract: A persistent nighttime near-isothermal atmosphere inside Arizona's Meteor Crater is produced by cold air inflow into the crater. A regional drainage flow builds up a layer of cold air on the upwind side of the crater and a shallow layer of cold air spills over the 30-60 m high rim and descends partway down the sidewall until reaching its buoyancy equilibrium level. Detrainment of cold air during its katabatic descent destabilizes the basin atmosphere, driving it towards isothermalcy.

Keywords: *ICAM, Meteor Crater, cold air intrusions, basins, katabatic flow, detrainment, atmospheric heat budget*

Arizona's Meteor Crater, 40 km east of Flagstaff, Arizona, is a uniform circular basin that is 1.2 km in diameter and 170 m in depth. The crater rim extends 30-60 m above the surrounding Colorado Plateau, a uniform plain that slopes gently downward from the Mogollon Rim towards the northeast to the Little Colorado River. An unusual nighttime temperature structure evolution occurs in the crater on synoptically undisturbed nights (Whiteman et al. 2008). To our knowledge, such a structure has not been previously reported in other basins. A 30-m-deep, intense inversion forms in the early evening on the crater floor. This is capped by a deep near-isothermal layer that extends to the crater's rim. This vertical temperature structure is maintained as the crater atmosphere continues to cool through the night. The processes responsible for the production and maintenance of the deep, persistent isothermal layer are the subject of this paper.

The isothermal layer was present on synoptically quiescent, clear nights in soundings from 3 tethersondes operated at the valley center, the lower west sidewall and the lower east sidewall. These soundings show that the bulk crater atmosphere is approximately horizontally homogeneous, with weak and variable winds (not shown).

Pseudo-vertical soundings from four lines of temperature data loggers running up the north, east, south and west sidewalls and out onto the adjacent plain were analyzed to visualize the temperatures and temperature gradients during the night in the near-surface layers. The temperature data were combined with wind data from the west, north and east rims and from a 10-m tower 2.5 km southwest of the crater center on the adjacent plain to produce Figure 1.

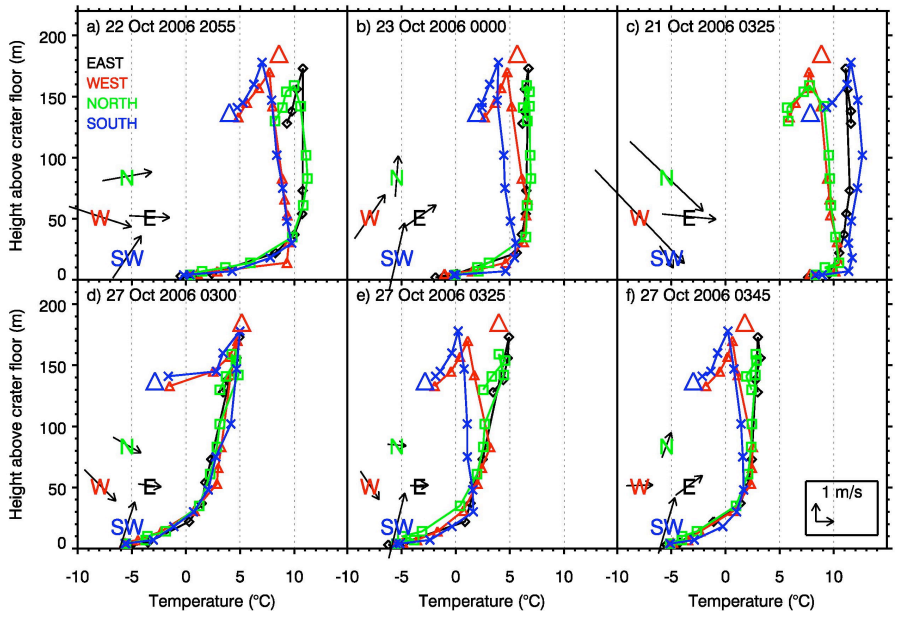

Figure 1. Pseudo-vertical temperature profiles from four lines of temperature data loggers running up the north (green squares), east (black diamonds), south (blue crosses) and west (red triangles) inner sidewalls of the crater to the rim level and out onto the adjacent plain. Vector winds from the 5-m level at the north and east rims, and from the 10-m level at the highest point on the west rim and at the Southwest site on the plain outside the crater are plotted schematically (not to scale) in the lower left part of each subfigure. The red and blue triangles indicate 2-m temperatures at the highest point on the west rim and at the Southwest tower site.

Pseudo-vertical soundings for 2055 MST on 22 Oct are shown in Figure 1a. Temperatures are colder on the south and west rim of the crater than on the north and east rim. Further, temperatures on the outer sidewall of the crater are colder to the south and west than over the plains to the north and east and are colder than temperatures inside the crater at the same height. These first two observations suggest that *cold air is advected to the crater during the night from the southwest*. It is already known (Savage 2008) that a regional-scale drainage or katabatic flow affects the Meteor Crater on undisturbed nights, producing peak winds of 2-4 m/s at heights at or below 50 m. Thirdly, the north and east soundings have an isothermal temperature gradient like that in the

tethersonde profiles, while the south and west lines exhibit a temperature lapse rate of about 15°C/km extending from the rim down into the crater. This observation suggests that *cold air coming over the rim flows down the south and west inner sidewalls of the crater*. The V shaped notch produced by the intersection of the south or west profiles with the north or east profiles occurs at about the same elevation in Figure 1a. But, there are many instances when the apex of the V-shaped notch varies in elevation between the south and west lines (e.g., Figure 1b). This fourth observation suggests that the *notch apex altitude represents the depth to which cold air coming over the rim can penetrate down the slope before reaching its level of buoyancy equilibrium*, where the katabatic current dissipates. When the flow at the Southwest site is predominantly from the south, the coldest air comes over the south rim and the deepest V notch forms on the south sidewall. When the flow is predominantly from the west, the deepest notch forms on the west sidewall (not shown). Thus, if the drainage flow approaching the crater changes direction, this is reflected in a movement of the V notch so that it is maintained on the upwind inner sidewall of the crater. The cold air inflows, which must detrain cold air into the ambient atmosphere as they flow down the sidewall, finally stop when they reach their buoyancy equilibrium level. The detrainment is stronger at higher elevations where steep slopes produce high speeds and where the inflow-ambient air temperature differences are a maximum. The detrainment of the cold air into the crater atmosphere destabilizes it, driving it towards isothermalcy. Figure 1c shows an event where cold air was advected to the crater from the northwest. In that case, the V notch formed on the west and north sidewalls of the crater, rather than on the south and west sidewalls. Finally, Figures 1d,e, and f show a transition from a stable lapse rate (22°C/km) in the crater at 0300 MST 27 Oct 2006 to a near-isothermal lapse rate (5°C/km) at 0345 MST associated with the initiation of a cold air inflow into the crater, as indicated by the formation of the V notches on the west and south sidewalls. Thus, the data support a hypothesis that *the isothermal atmosphere inside the crater is caused by the detrainment and horizontal mixing into the crater atmosphere of cold air that comes over the rim of the crater and flows down the inner sidewall of the crater.* This inflow hypothesis is illustrated in Figure 2.

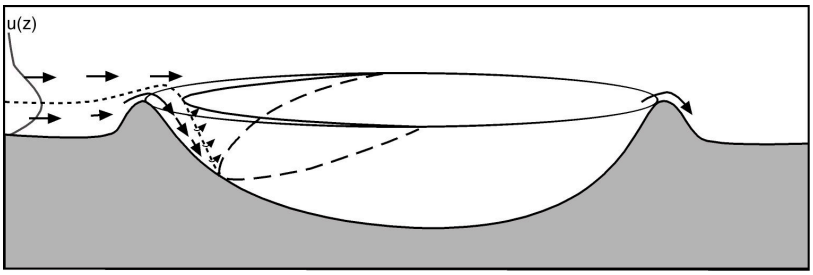

Figure 2. Illustration of the inflow hypothesis. The strongest inflow occurs on the upwind inner sidewall of the crater, with the inflows becomes weaker and penetrating to shallower depths with distance around the crater rim from the upwind direction.

CONCLUSIONS

A mesoscale drainage flow produces an inflow of cold air across the southwest rim of the Meteor Crater. This cold air descends the inner sidewall of the crater as a katabatic current. Detrained cold air from the katabatic current mixes horizontally, destabilizing the crater atmosphere. The horizontal mixing processes are not yet fully investigated, but breaking waves at the upper boundary of the katabatic current may play a role. In future research, a katabatic flow model will be used to simulate the inflow, and we will evaluate turbulence levels in the inflow layer, the effect of the inflow on the crater atmosphere heat budget and the role of the inflow on bulk atmospheric stability inside the crater.

Acknowledgements:
We thank the NCAR ISS and ISFF staff for providing equipment, field support and data processing. Barringer Crater Corporation and Meteor Crater Enterprises, Inc. provided access to the crater. Research was supported by the U. S. National Science Foundation Physical and Dynamic Meteorology Division through grants ATM-0444205 and 0837870 and Army Research Office grant 55900348. Author M .L. was supported by a Doktoratsstipendium aus der Nachwuchsförderung der Universität Innsbruck.

REFERENCES

Savage, L. C., III, S. Zhong, W. Yao, W. J. O. Brown, T. W. Horst, and C. D. Whiteman, 2008: An observational and numerical study of a regional-scale downslope flow in northern Arizona. *J. Geophys. Res.*, **113**, D14114, doi:10.1029/2007JD009623.

Whiteman, C. D., A. Muschinski, S. Zhong, D. Fritts, S. W. Hoch, M. Hahnenberger, W. Yao, V. Hohreiter, M. Behn, Y. Cheon, C. B. Clements, T. W. Horst, W. O. J. Brown, and S. P. Oncley, 2008: METCRAX 2006 – Meteorological experiments in Arizona's Meteor Crater. *Bull. Amer. Meteor. Soc*., **89**, 1665-1680.

ASPECTS OF COLD POOL LIFE CYCLE IN AUSTRIAN SINKHOLES

Manfred Dorninger

Department of Meteorology and Geophysics, University of Vienna, Vienna, Austria
E-mail: *manfred.dorninger@univie.ac.at*

Abstract: Many aspects of cold pool life cycle have been investigated in the recent decades. There have been some indications that the cold pool may oscillate under specific weather conditions. This and the quantification of the cold air outflow through the lowest pass have been addressed in an intense observing period which has been performed in the Gruenloch basin, Lower Austria from October, 19-21, 2008. The basin and the crest line have been equipped with 27 weather stations and one tethersonde at the basin floor. Up to 6 sondes have been operated simultaneously at different heights. Oscillating of the cold air pool is triggered by moderate to strong winds aloft and can only be detected with fast responsing sensors.

Keywords: *cold air pool, basin meteorology, extreme temperature minima, response time*

1 INTRODUCTION

Sinkholes represent an excellent natural laboratory to study formation, the maintenance, fluctuations and dissipation of temperature inversions during fair weather episodes with undisturbed radiative conditions (e.g., Whiteman,et al., 2004). One of the first meteorological observations in history in a basin were made at a place in the Northeastern Austrian limestone Alps, called Gstettner Alm or Gruenloch (Figure 1). It was known from that early observations, that the air temperature at the bottom of the sinkhole may decrease to values some 30 degrees (Centigrade) or more below the ambient temperature at the same level, leading to the lowest temperatures in Central Europe known so far (around –52 deg C, Aigner, 1952). Such extreme temperature minima can only occur when a snow cover is existing, which minimizes the surface heat flux.

Night-time temperature fluctuations at the basin floor during clear sky conditions observed in recent field campaigns indicate that the cold air pool oscillates, however the specific weather conditions have never been really investigated. This is also valid for the origin of the cold air outflow through the lowest saddle. In a field campaign conducted from October, 19-21, 2008, both aspects have been addressed. This paper concentrates on the oscillating aspect.

2 EXPERIMENTAL SET-UP

The station network (Figure 2) was designed to quantify the in- and/or outflow via the crest line including all

Figure 1. Gruenloch basin, view to the northeast from the Kleiner Huehnerkogel (1600 m). Basin floor at 1270 m, lowest saddle at 1320 m (to the left). Diameter at basin floor ~ 300 m, at crest height ~ 1000 m.

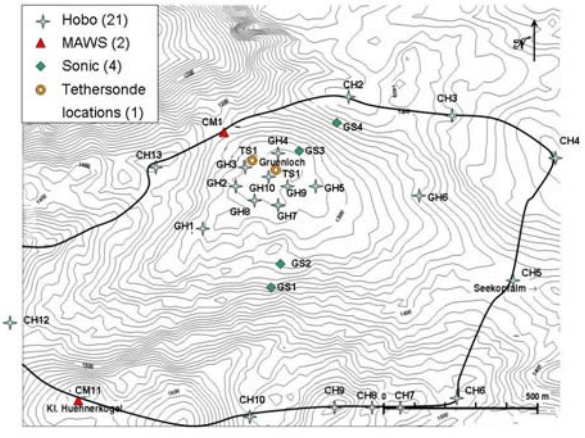

Figure 2. Experimental set-up. Locations of weather stations and tethersonde, 13 stations at the crest line and 14 stations at the basin floor, in operation from October, 19-21, 2008.

mountain peaks and passes and the wind and temperature field at the basin floor. Four weather stations equipped with 3D-sonic anemometers have been deployed at the slopes to investigate a possible cross circulation during daytime.

3 PRELIMINARY RESULTS

The intense observing period lasted from October, 19, 12:00 UTC to October, 21, 12:00 UTC. Figure 3 shows a typical temperature record for a undisturbed weather situation (left). However, during the first night from 19th to 20th a weak upper level short wave trough passed the region leading to moderate winds at crest height from the northwest. This triggered an oscillation of the cold pool indicated by the small temperature fluctuations. The second night was completely undisturbed and has a smoother temperature regime. Data are taken every five minutes which corresponds to the response time of the used temperature sensor in air moving at 1 m/s. On the right hand side the blow-up from the period October, 19, 21:30 to midnight, is depicted. One can recognize a drop in the temperature but hardly an oscillation.

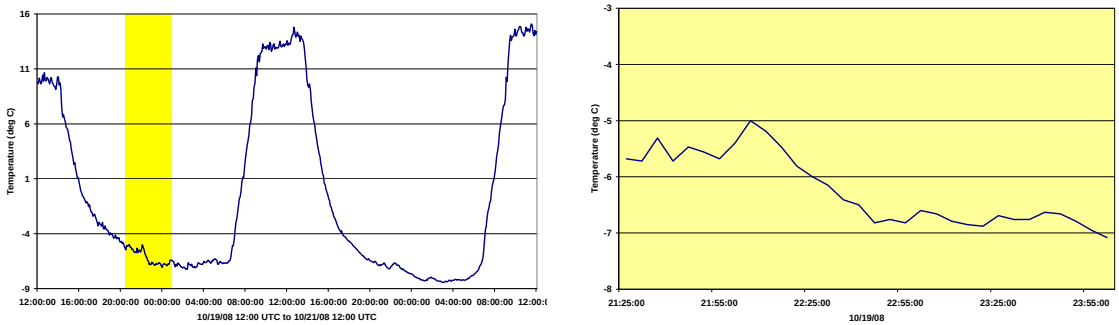

Figure 3. Left: Temperature record from station GH10 (see figure 2) at basin floor for undisturbed and clear sky from October, 19-21, 2008, yellow shaded box: time period, blown up on the right.

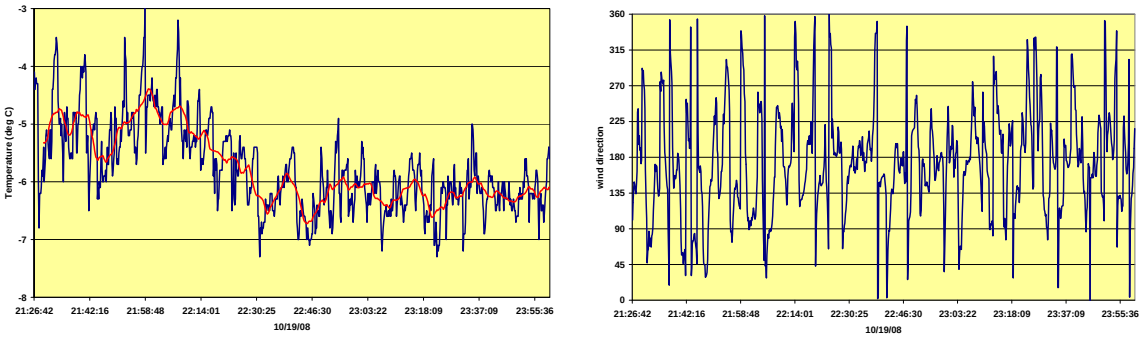

Figure 4. Left: Temperature record from lowest tethersonde for the same period as shown in figure 3, right. Red curve: 5 min gliding mean. Right: wind directions for the same time period.

During the "yellow" time period the height of the tethersonde was kept constant. The lowest sonde was located 1 m above basin floor. The response time of these probes is much faster than for the Hobo weather stations. Short term fluctuations of the temperature in the order of 2 to 3 deg C become evident as shown on figure 4, left hand side (Note: the same temperature scale is used as for figure 3, right, for comparison). These fluctuations are strongly connected to changes in the wind direction (figure 4, right). Wind speeds (not shown) are low with a maximum in the range of 1 m/s. Further evaluations are under way (e.g., characteristic frequency) to understand these fluctuations in detail.

Acknowledgements:
Many thanks due to the students from the University of Vienna for their contributions to the field campaign. Forstmeister P. Kupelwieser is thanked for providing access to the experimental area.

REFERENCES

Aigner, S., 1952: Die Temperaturminima im Gstettnerboden bei Lunz am See, Niederösterreich (The minimum temperatures in the Gstettner basin near Lunz, Lower Austria). *Wetter Leben*, Special Issue **1**, 34-37**.**

Whiteman, C. D., T. Haiden, B. Pospichal, S. Eisenbach, and R. Steinacker, 2004: Minimum temperatures, diurnal temperature ranges and temperature inversions in limestone sinkholes of different size and shape. *J. Appl. Meteor.*, **43**, 1224-1236.

THE ROLE OF SUBSIDENCE IN VALLEY AND BASIN WARMING

Thomas Haiden

Central Institute for Meteorology and Geodynamics, Vienna, Austria
E-mail: *thomas.haiden@zamg.ac.at*

Abstract: The role of thermally driven upslope flows and associated compensating subsidence in the diurnal warming of valley and basin atmospheres is re-investigated. Based on theoretical considerations and illustrated by a simulation of the morning transition during IOP5 of METCRAX it is discussed under what conditions and assumptions the redistribution of heat by the slope flow circulation produces a warming that is different from quasi-horizontal heat input.

Keywords: *valley warming, subsidence*

1 INTRODUCTION

Subsidence in valleys and basins due to thermally driven upslope flows is usually too weak to be measured directly. Its existence has been established by observational studies mostly through a sequence of vertical temperature profiles which show the downward motion of characteristic features, such as inversions. Theoretically, its existence derives from mass-conservation, since air transported upwards by upslope flows at the valley sidewalls must be replaced by downward motion in the valley interior. [Another way of closing the mass budget would be convergence of along-valley flow but observations show that this is not case. During the upslope, up-valley phase there is rather mass divergence along the main valley, mostly due to the branching out of tributary valleys which all develop up-valley flows (Freytag 1987).] The practical relevance of subsidence is that it can suppress mixed-layer growth in the valley and affect the dispersion of pollutants. In order to quantitatively estimate the strength of subsidence in a given topographic setting one needs an estimate of the upslope mass-flux at the valley sidewalls. An upper limit of this mass-flux can be computed based on the concept of 'equilibrium' slope flow.

2 EQUILIBRIUM SLOPE FLOW

The concept of equilibrium slope flow refers to a balance between diabatic heating and along-slope advection in the slope wind layer

$$\frac{\partial \theta_{SL}}{\partial t} = \frac{H}{c_p \rho D} - U \sin\alpha \frac{\partial \theta}{\partial z} \approx 0 , \tag{1}$$

where H is the sensible heat flux, D is the slope wind layer depth, U is the upslope flow speed, and α is the slope angle. From (1) the equilibrium upslope mass-flux is given by

$$\rho D U = \frac{H}{c_p} \left(\frac{\partial \theta}{\partial z} \sin\alpha \right)^{-1} . \tag{2}$$

If such equilibrium is present, it can be shown that the warming of the valley atmosphere due to subsidence corresponds to the sensible heat input at the same height

$$b c_p \rho \left(\frac{\partial \theta}{\partial t} \right)_{SUB} = \frac{H}{\sin\alpha} , \tag{3}$$

where b is half the width of the valley. In the real atmosphere, slope flows are closest to this kind of equilibrium if the slope is steep and homogenous, and the atmospheric stratification strong. If the slope flow strength is less than the equilibrium value by a factor f, where $0 \le f < 1$, then only a fraction fH of the sensible heat input will re-appear as subsidence warming, and the remaining fraction $(1-f)H$ is available for direct horizontal heat transport towards the valley interior. The resulting total valley warming is again the same as in the equilibrium flow case. This insensitivity of valley warming to the actual slope flow volume flux may explain why simple analytical models (Whiteman and McKee 1982, Haiden 1998) can reproduce the observed temperature evolution in valleys without actually modelling the details of the slope flow.

3 COMPARISON WITH METCRAX DATA

Results of a simple numerical model of horizontal heat input and dry-adiabatic adjustment are compared to observations of inversion break-up taken during the Meteor Crater field campaign (METCRAX) conducted in Arizona in 2006 (Whiteman et al. 2008). In real valleys the heat budget of a valley cross-section is influenced by along-valley temperature advection. Also, the mass budget of the upslope flow / subsidence circulation may not necessarily be closed within the two-dimensional cross-section. In closed basins the situation is much more constrained. The upward mass flux across any horizontal plane inside the basin *must* equal the downward mass flux. One has to be careful, however, that external influences such as cold air intrusions or intermittent mixing episodes can be ruled out, or quantified accordingly. During the IOP5 morning transition, the temperature evolution did not show disturbances of such kind.

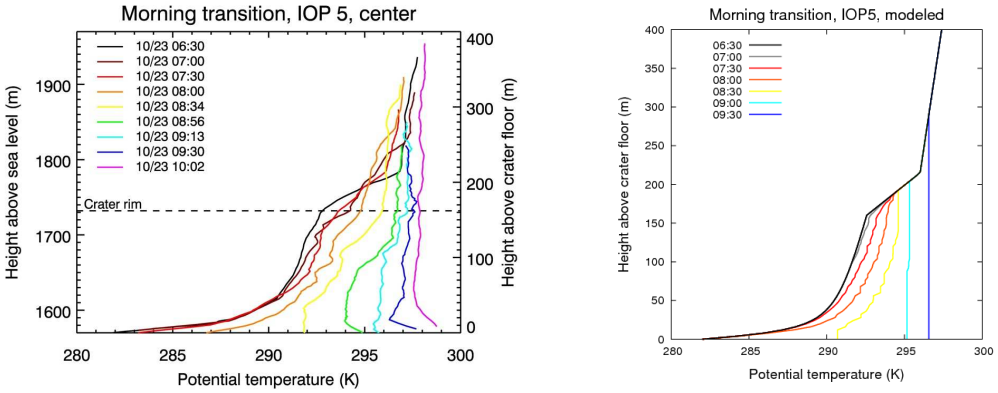

Figure 1. Evolution of potential temperature in and above the meteor crater during the morning transition of IOP5 of METCRAX. Left: observed, right: modelled.

As shown in Figure 1, the simple horizontal heat-input model with dry-adiabatic adjustment captures the main characteristics of the temperature evolution. In the observations, however, there appears to be a downward movement of the more stable layer near crater rim, especially between 07:00 and 08:56. This feature cannot be reproduced by the horizontal heat input method.

4 CONCLUSIONS

To a good approximation, the diurnal warming of valleys and basins can be modelled by horizontal heat transport from the sidewalls to the valley (basin) interior. This does not imply that there is in fact a horizontal transfer of air from the sidewalls towards the interior. It is the result of the organized overturning circulation comprised of upslope flow and subsidence motion. It applies to cases where the sidewalls are sufficiently steep so that the upslope mass-flux is close to its equilibrium value. An important practical consequence is that the warming in such cases can be modelled independently of the slope flows. On the other hand, observations which show a downward movement of stable layers in valley and basin atmospheres indicate deviations from equilibrium slope flow. According to (2) this is to be expected at heights where the stratification changes rapidly because the mass-flux cannot adapt to a different value over arbitrarily short vertical distances.

Acknowledgements:
I would like to thank Dave Whiteman and Sebastian Hoch for providing the METCRAX data and for many inspiring discussions.

REFERENCES

Haiden, T., 1998: Analytical aspects of mixed-layer growth in complex terrain. *Proceedings Eighth Conference on Mountain Meteorology*, Flagstaff, Arizona, 368-372.

Freytag, C., 1987: Results from the MERKUR Experiment: Mass budget and vertical motions in a large valley during mountain and valley wind. *Meteor. Atmos. Phys.*, **37,** 129-140.

Whiteman, C. D., and T. B. McKee, 1982: Breakup of temperature inversions in deep mountain valleys. Part II: Thermodynamic model. *J. Appl. Meteor.*, **21,** 290-302.

Whiteman, C. D., A. Muschinski, S. Zhong, D. Fritts, S. Hoch, M. Hahnenberger, W. Yao, V. Hohreiter, M. Behn, Y. Cheon, C.B. Clements, T. W. Horst, W. O. J. Brown, and S. P. Oncley, 2008: Metcrax 2006 – Meteorological experiments in Arizona's meteor crater. *Bull. Am. Met. Soc.*, **89,** 1665-1680.

ANALYSES OF NEWLY DIGITISED SNOW SERIES OVER THE LAST 100 YEARS+ IN SWITZERLAND

Wüthrich C.[1], Begert M.[1], Scherrer S.C.[1], Croci-Maspoli M.[1], Appenzeller C.[1], Weingartner R.[2]

[1] Federal Office of Meteorology and Climatology MeteoSwiss, Zurich, Switzerland
E-mail: *christian.wuethrich@meteoswiss.ch*
[2] Institute of Geography, University of Berne, Berne, Switzerland

Abstract: In this study a systematic analysis is conducted of 12 Swiss long-term snow series with newly digitised daily measurements since at least 1910. A single snow series even dates back to 1865 and hence belongs to one of the longest and continuous snow series. The 12 surface observation stations are situated in central and eastern Switzerland on altitudes between 450 and 2500 m asl. The trend analyses show an unprecedented decrease of new snow sum in the 1990s and a general reduction of the snow cover over the last 100 years.

Keywords: *Long-term snow series, Switzerland, trend analyses*

1 INTRODUCTION

Snow is on the one hand an important commercial factor especially in the Swiss Alpine region (tourism, hydro-electricity, drinking water) and on the other hand responsible for considerable hazards such as avalanches. In addition, snow can be used as an excellent indicator in detecting climate change. In this respect, high-quality and long-term snow series are crucial for reliable analyses. The objectives of this study are twofold.

In a first step, suitable long-term snow series have been selected, missing data digitised and the entire series quality checked. Therefore snow data from 12 different surface stations with daily measurements since at least 1910 have been selected (situated in central and eastern Switzerland at altitudes between 450 and 2500 m asl). Daily snow data between the beginning of the measurements in the early 20th / late 19th century and the 1940s have been digitised from historical MeteoSwiss paper data. The historically available parameters are a) new snow sum and b) snow depth. Since snow depth data are not available at every station, a reconstruction of this parameter has been undertaken using the method of Brown and Braaten (1998) by combining daily new snow, temperature, precipitation and a melting factor.

In a second step, the long-term snow series have been used for trend analyses over a time period >100 years.

2 LONG-TERM SNOW SERIES

The longest new snow series of Switzerland is dating back to 1865 and was measured in Segl-Maria (1798 m asl) in southeastern Switzerland. An example of the time series of days with snowfall ≥ 1 cm (Figure 1) in Arosa (1892-2008), Chur (1889-2008), Davos (1932-2008) and Segl-Maria (1865-2008) indicates an expected year to year variability and distinct decadal variability. In particular the period from 1940 to 1960 shows signs of fewer days with snowfall, in contrast to the 1970 and the 1980 with generally more days with snowfall. The last two decades mark again a period of fewer days with snowfall, which is in line with previous studies (e.g. Marty, 2008) and the current temperature increase in this region. A similar tendency as for days with snowfall can be indicated for the new snow sum (Figure 2).

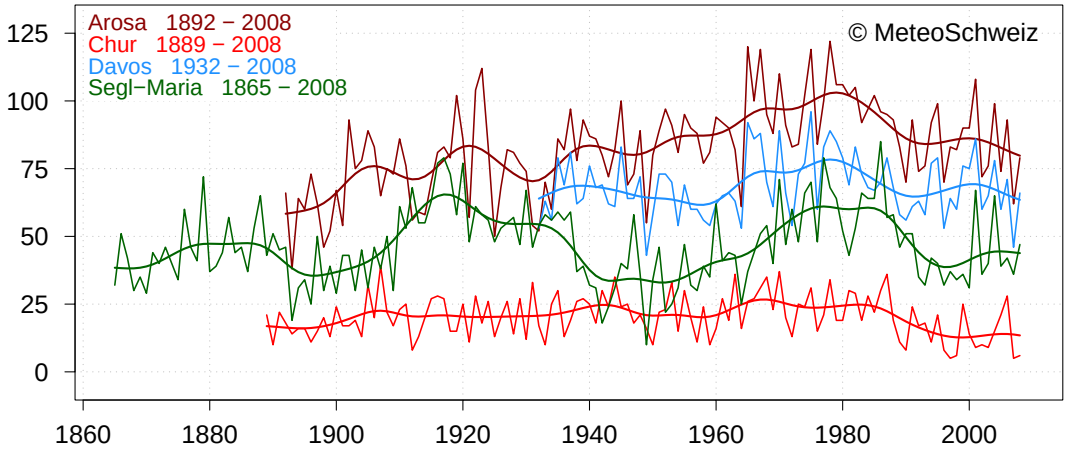

Figure 1. Time series of days with snowfall ≥ 1 cm for stations located in south-eastern Switzerland. Smooth lines indicate a 20-year Gauss filter.

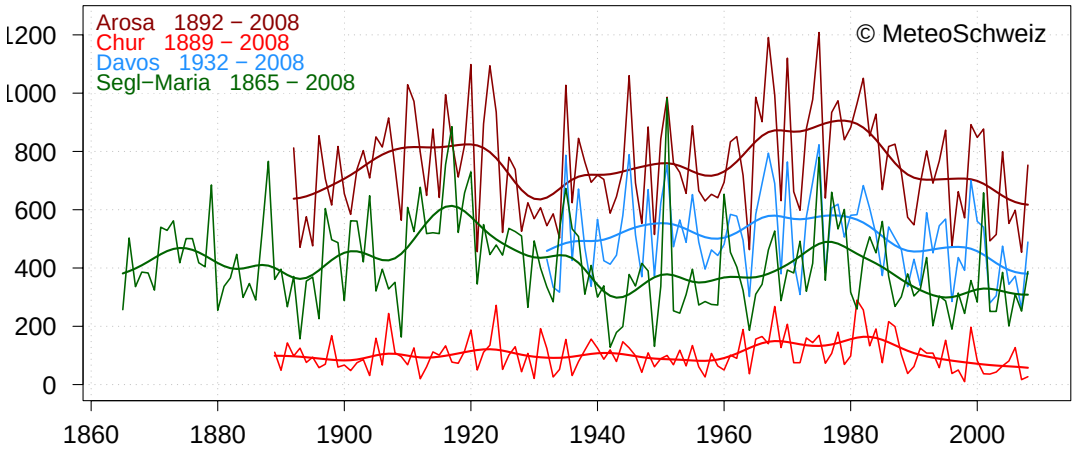

Figure 2. Time series of new snow sum in cm for stations located in south-eastern Switzerland. Smooth lines indicate a 20-year Gauss filter.

3 SNOW TRENDS

The 100 year trend analysis of days with snowfall ≥ 1 cm (not shown) reveals a significant decrease for stations below 800 m asl in the winter season (DJF) and for stations around 1800 m asl in the spring season (MAM). Similar results were found for seasonal new snow sums.

The analyses of the decadal new snow trends (not shown) during the last 100 years shows unprecedented low new snow sums in the winter seasons (DJF) of the 1990s on all highs, but on altitudes < 1500 m asl were already measured low new snow sum in the 1950s and the 1970s. In the spring season (MAM) the decadal snow trends shows as well a decreasing new snow sum in the 1990s. The 1960s shows in contrast to that a once only increasing of the new snow sum in the spring season (MAM) on all altitudes in the last 100 years.

4 CONCLUSIONS

The newly digitized and quality controlled long-term snow series back to the 19th century in Switzerland belongs to the longest continuous snow datasets available (except for very few missing weeks). These long-term snow series show that snow cover is varying substantially on seasonal and decadal time scales. Since snow data series of shorter periods have shown similar trends (e.g. Scherrer and Appenzeller, 2004; Laternser and Scheebli, 2003), our results can be used as a valuable extension. In addition long-term snow series act as useful indicator for climate change studies.

REFERENCES

Brown, R.; Braaten, R.; 1998: Spatial and Temporal Variability of Canadian Monthly Snow Depths (1946-1995); Atmosphere Ocean 36 (1), 37-54.

Laternser, M.; Schneebeli, M.; 2003: Long-term snow climate trends of the Swiss Alps (1931-99). International Journal of Climatology 23: 733 – 750.

Marty, C.; 2008: Regime shift of snow days in Switzerland. Geophy. Res. Lett., 35, L12501

Scherrer, S.C.; Appenzeller, C., 2004: Trends in Swiss Alpine snow days: The role of local- and large-scale climate variability. Geophy. Res. Lett., 31, L13215

DETERMINATION OF SNOW ACCUMULATION IN HIGH MOUNTAINS BASED ON DATA FROM CLIMATE STATIONS

Heidi Escher-Vetter[1], Markus Weber[1,2]

[1] Commission for Glaciology, Bavarian Academy of Sciences and Humanities, Munich, Germany
E-mail: *Heidi.Escher@kfg.badw.de*
[2] Institute of Meteorology and Geophysics, University of Innsbruck, Innsbruck, Austria

Abstract: Local measurements of precipitation are used to validate snow cover model results for Vernagtferner.

Keywords: *glaciers, winter precipitation, measurements and models*

1 INTRODUCTION

Snow accumulation S_a is an important quantity for modelling glacier mass balance and change. S_a is calculated e.g., by the model SURGES (**Su**bscale **R**egional **G**lacier **E**xtension **S**imulator), operated in the framework of the hydrological part of the grid-based DANUBIA system. It was designed to emulate the glacier retreat for global change scenarios runs. This model uses records of meteorological quantities from the operational climate network (ZAMG and DWD), such as air temperature and precipitation intensity p(t). A problem arises from the fact that the network does not extend into regions which are difficult to access. Therefore such series of precipitation event are extrapolated with the help of gradients derived from a cluster of records (Mauser and Bach, 2008). On this basis, the model is able to determine the water equivalent of the snow cover for the whole catchment. By definition, the algorithm enforces the reproduction of the actual records for the stations' locations. But in inaccessible areas a direct validation is not possible unless data are available from scarce storage gauges or snow height measurements, gathered for selected dates at the most. Under favourable conditions, these sparse informations can be used for an estimation of the validity of the model results.

2 PRECIPITATION DATA SOURCES

The basin of Vernagtferner, Oetztal Alps, is a well suited region for the model validation. Table 1 summarizes the usually used methods for measuring precipitation quantities at this site (Braun et al., 2004). The measurement of precipitation in strongly heterogeneous terrain is error prone, and various influences have to be considered. As precipitation can occur in form of rain or snow, not all devices are able to record all quantities. Unheated tipping buckets e.g., only record rainfall events correctly. The deposition of rain into the gauge is obstructed by heavy wind, and this is even worse in the case of snow. Sometimes the snow even covers the complete device. Evaporation and condensation effects are not the same for the devices as for natural surroundings, and misalignment of sonic rangers and stakes reduces the high instrumental accuracy. Only the model is capable to deliver both sums and time series of the water equivalent of the snow cover and of effective precipitation, but it is unable to consider snow redistribution by wind.

Method		**Instrumental Accuracy**	**p(t)**		**P**	
Device	Unit		Snow	Rain	Snow	Rain
Model	[mm w.eq.]	--	+	+	+	+
Tipping bucket	[mm w.eq.]	high		+		
Weighing gauge	[mm w.eq.]	medium	+	+	+	+
Storage gauge	[mm w.eq.]	high			+	+
Sonic ranger S_h	[m]	high	+		+	
Stake S_h	[m]	high			+	

Table 1. Precipitation methods available within the Vernagtbach basin; '+' indicates the capacity to record the quantities.

3 METHODOLOGY

Figure 1 shows the comparison of the modeled time series of water equivalent of the snow cover S_a and the measured snow height S_h. The general structure during the accumulation period is well met, but S_h depicts

additional details, which are caused by processes like settlement and potential redistribution, not considered by the model. The relationship between S_h and S_a is given by eq. 1.

$$S_a(t) = \rho \cdot S_h(t) \qquad \textbf{(1)}$$

The mean density **ρ** of the snow cover increases with time and is not known at this location.

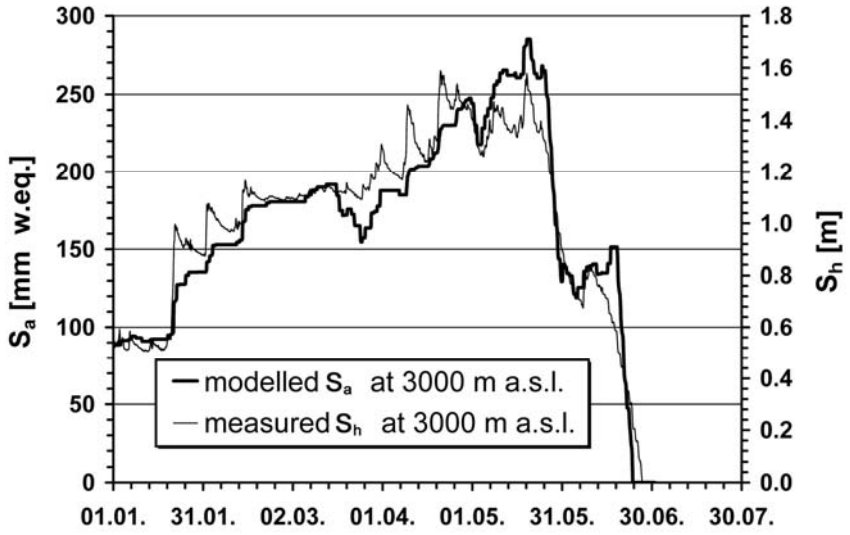

Figure 1. Time series of the recorded snow height of the Vernagtferner sonic ranger and the modelled water equivalent of the snow cover at the same location from 1 January to 31 July 2005.

Storage gauges provide only temporal sums P of the precipitation events over the time span t_0 to t (Eq. 2)

$$P(t) = \int_{t_0}^{t} p(t)dt \qquad \textbf{(2)}.$$

In general, snow height $S_h(t)$ can be calculated from an initial value $S_h(t_o)$ by equation (3)

$$S_h(t) = S_h(t_0) + \frac{r}{\rho} P(t) - M \quad \textbf{(3)},$$

if the local density of the snow cover and the mean portion r of snowfall to the entire precipitation is known, and melt losses M are considered. The records of the storage gauges P can be used in equation (3) for the calculation of S_h for the observation dates. During the winter period, r is close to one and M is negligible. As snow density is typically analyzed for only three to six sites, an average density has to be determined for the total glacier. At the spring survey of 2005, the average density was evaluated to 327 ± 17 kg/m³ (Escher-Vetter et al., 2009). A scale comparison of the series in Fig. 1 however results in a density of 170 kg/m³. This finding suggests that the extrapolated precipitation data have a bias of approx. 150 mm w.eq. to lower values in this case.

Acknowledgements:
Many colleagues helped in this study, and our special thanks go to Monika Prasch, Department of Geography, Ludwig-Maximilians-University, Munich, who provided the model results. Funding from the DFG, BMBF, the GLOWA-Danube project, the Academy Research Programme III.B.1 of the Fed. Rep. of Germany and the State of Bavaria is gratefully acknowledged.

REFERENCES

Braun, L.N.; Escher-Vetter, H.; Heucke, E.; Siebers, M. & Weber, M., 2004: "Experiences with the new ´Vernagtbach' hydro-meteorological station", *in Oerlemans & Tijm-Reijmer: Book of extended abstracts of presentation at the Workshop "Automatic Weather Stations on Glaciers", Pontresina, 28 to 31 March 2004, IMAU, 38 - 44.*

Escher-Vetter, H., M. Kuhn, and M. Weber, 2009: Four decades of winter mass balance of Vernagtferner and Hintereisferner, Austria: methodology and results. Annals of Glaciology 50, 87-95.

Mauser, W., Bach, H. 2008: „PROMET – a Physical Hydrological Model to Study the Impact of Climate Change on the Water Flows of Medium Sized, Mountain Watersheds“, *Submitted to Journal of Hydrology*

THE EXCEPTIONAL METEOROLOGICAL CONDITIONS OF THE DECEMBER 2008 IN THE TRENTINO AREA (NORTH EAST ITALY): SYNOPTIC AND NIVOLOGICAL ANALYSIS AT MESOSCALE

Roberto Barbiero[1], Massimiliano Fazzini[2], Mauro Gaddo[1]

[1]Provincia Autonoma di Trento – Dipartimento Protezione Civile e Infrastrutture.
2 University of Ferrara - Department of Earth Sciences –
Email massimiliano.fazzini@unife.it

Abstract: From the end of November, 2008 and for the whole month of December, 2008, the northern portion of the Mediterranean basin has been interested by a succession of synoptic situations that has brought perturbed weather also on the north east alpine sector of Italy**,** with persistent and snowy phenomenon often till in the Adige Valley. The nivometric data observed in the network of snow manuals fields - active with continuity from the winter season 1980-1981 - and in some automatic stations managed by the Civil Protection of the Autonomous Province of Trento, show "record" values at all the levels. If the analysis is extended to the other winter months, only in January 1986 and locally in December 1981, have been observed similar snow depth measures. The notable frequency of snowy episodes has determined serious and heavy repercussions on the human activities and particularly on the road and railway circulation. Over the 1500 meters of altitude, the heavy snowfalls and the strong winds have determined also the formation of wide frames of snow gust with consequent notable avalanche activity.

Keywords: *Trentino, heavy snowfall, return period, Genoa depression,*

1 INTRODUCTION

The Trentino territory belongs for its totality to the southern sector of the eastern chain of the Alps where the perturbed meteorological situations have origin from intense Mediterranean flows, very recurrent between the end of the autumn and the beginning of the winter. Also the recent winter season has been characterized by such evidence, since the end of the month of November, a succession of synoptic situations that has brought perturbed weather are occurred also in the days of Christmas and the New Year's Eve.

Two exceptionally perturbed phases can be distinguished in this period. The first one started on November 28 and it lasted up to December 1. After some days characterized by conditions of sunny weather for the presence of a high pressure field, on November 28 a centre of low pressure positioned on the upper Tyrrhenian Sea determines unstable flows from southwest on the Alps favouring diffused snowfalls beginning from the morning on the valleys with rains only in the southern valleys. Even if interested by a low centred on the Gulf of Biscaglia, in the following day of November 29 a suspension of the precipitations has been observed for the morning. After some irregular clearing up in the afternoon new precipitations followed in the night, snowy over the 500 - 600 meters about. On November 30 the transit of a front in phase of occlusion on the north Italy (Figure 1) determined moderate precipitations in the night, with snow over the 500 - 600 m. During the day intermittent precipitations still occurred, that have been becoming widespread and more intense from the evening. On the December 1, the transit of a new frontal system determines widespread precipitations, locally very strong, with limit of the snow that goes down until the valleys and then gradually increases up to 800-1200 m in the first morning; in the afternoon an attenuation of the phenomenon occurs with intermittent weak precipitations.

A second intense phase begins on December 10 and it ends on December 17, a week of consecutive precipitations. However the most intense phase interests the first two days. After a period characterized for stable and predominantly sunny weather, with north flows and a fall in minimum temperature values on December 9, from the night of December 10 the arrival of a perturbation (Figure 1) determines snowy precipitations up to low levels in the valleys, in intensification during the day. From the evening an attenuation of the phenomenon has been observed with gradual raising of the limit of the snow level due to the presence of warmer air. On December 11 conditions of perturbed weather persist, with weak or moderate rains in the valleys and with the snow's limit around 800-1000 m on the northern sectors, over the 1000 m on the southern sectors. A new intensification of the precipitations is observed from the evening. Again perturbed weather on December 12 with southeast flows that determine widespread precipitations up to the first afternoon. The limit of the snowfalls is very varying during the day between 1000 and 1500 m, more elevated on the south sectors, with limit decreasing to end of the event.

2. ANALISYS OF NIVOMETRIC DATA

The cumulated snowfall observed during the two phases of perturbed weather has reached exceptional values among 90 cm of the River Adige Valley and 350 cm at the higher levels of Val di Sole valley (Tonale Pass, 1880

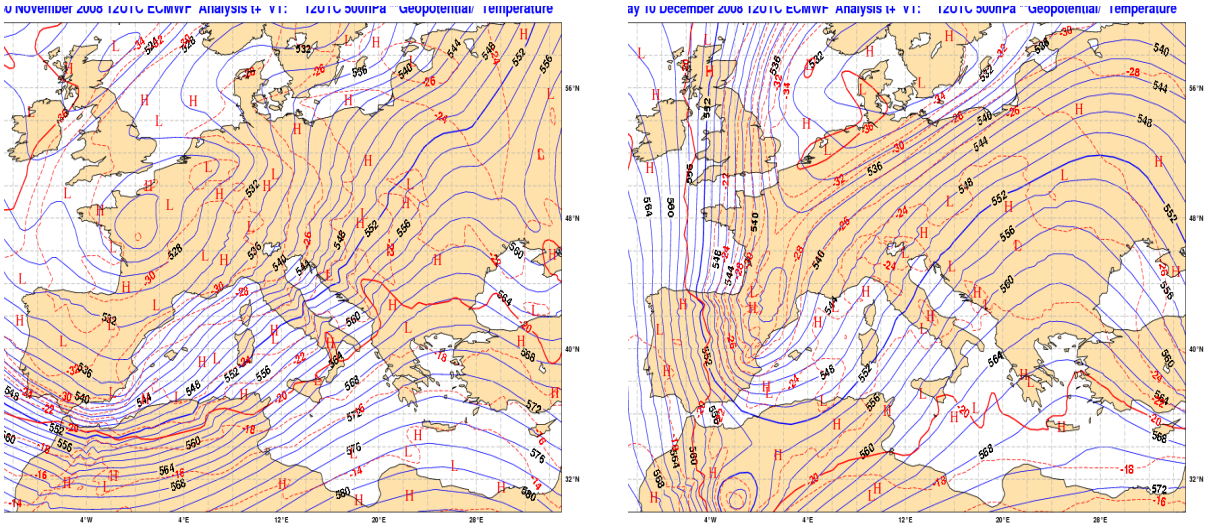

Figure 1 – Geopotential and temperature - 500 hPa – Analysis 30/11/2008 12 UTC (left) and 10/12/2008 12 UTC (right)

m). The monthly cumulated values are decidedly more elevated, considering all the events observed in the period, and vary, that average, from 250 cm at 1500 m level to 450 cm at 2000 m level.

Such values are everywhere double in comparison to the maximum ones observed in the period 1981-2007. Only for the station of Caoria (915 m), the observed data is lower than the maximum historical value of 147 cm recorded in December 1981. On the base of the available data, it has been possible to quantify in about 90 years the return period of a so intense snowfalls. If the analysis is extended to other winter months, it is observed that only in January 1986, in some stations of the Fassa Valley and the Non Valley, the cumulated snowfalls observed are comparable but however lower of about 15-20%.

Such exceptional cumulated snow depth data has been reached also thanks to the numerous other perturbed events observed that have brought weak to locally moderate snowfalls also in the days of Christmas and the New Year's Eve. A first analysis underlines that during and immediately after the two principal snowy events, the index of avalanches danger has reached the degree 4 - strong - on a scale of 5 levels and a number exceptionally high of avalanches have been observed, also of notable dimensions, around 300 events and primarily in the western area (Daone Valley, Giudicarie Valleys, Non Valley) - Meteotrentino, personal communication

3 CONCLUSIONS

The two phases of strongly perturbed weather that have interested the Trentino region derive from a synoptic circulation very recurrent and that determines the higher precipitations with that characterized by the presence of a dynamic depression on the gulf in Genoa (Fazzini et al, 2006, Fazzini 2007). If a cold layer has been formed in the preceding days due to a antyciclonic persistence, the advection of wet and warm air from the Mediterranean Sea determines snowfalls precipitations in the lower levels of the Adige Valley, above all if intensity is heavy (Barbiero et al,. 2007).

Acknowledgements: - *We thank all contributors for all meteorologist and nivologist of PAT - Dipartimento Protezione Civile e infrastrutture*

REFERENCES:

Roberto Barbiero, Massimiliano Fazzini, Mauro Gaddo & Carlo Bisci (2007): Analysis of recent meteorological configurations responsible for substantial snowfalls in the Trentine sector of the Adige valley bottom (eastern italian Alps) *Proc. 29th Intern. Conf. on Alpine Meteorology*, Chambery, France; 312-315

Massimiliano Fazzini, Alessandro Cecili, Alessandro Cinnirella, Mauro Gaddo e Paolo Bolli (2006): Une nouvelle méthode pour la réalisation d'une carte dynamique de l'enneigement du territoire du Trentino (Italie Nord -Orientale) » in Les risques liés au temps et au climat . *Proc. XIX Colloque International de Climatologie*, Gerard Beltrando, Malika Madelin et Hervé Quenol edit.– Epernay – 249-254

Massimiliano Fazzini (2007)**:** Applicazioni della climatologia al "rischio neve": la carta dinamica dell'innevamento della provincia di Trento *Proc. VII congresso di Meteorologia del Friuli Venezia Giulia***.** Regione Autonoma Friuli Venezia Giulia ed, 37-52.

ESTIMATING FOEHN DYNAMICS FROM TRAIN AND CABLE CAR ACCIDENTS

Hans Richner

Institute for Atmospheric and Climate Science, ETH Zurich, Zurich, Switzerland
E-mail: *hans.richner@ethz.ch*

Abstract: Two foehn-related accidents are described: A narrow gauge train was blown from the track and overturned, and a chairlift derailed and ultimately dropped to the ground. The first incident occurred during a strong foehn storm, the second during a moderate foehn. It must be assumed that - particularly in the second case - gustiness played a dominant role.

Keywords: *ICAM, foehn, societal impact, mountainous meteorology, weather-related accidents*

1 INTRODUCTION

Foehn situations can produce violent storms in the lee of mountain ranges. In recent years, in Switzerland, wind speeds in the range of 150 km/h and more were responsible for material damage to fixed structures (such as buildings, piers. etc.), boats, trains, and cable cars. They instigate significant financial losses because transportation systems were delayed or had to be shut down, and - worst of all - they were the cause for severe injuries and even casualties. The two most spectacular incidents happened both in the Jungfrau region: On November 11, 1996, a double motorcoach was used for evacuating a tourist group from the Jungfrau summit to Grindelwald. Despite the fact that the motorcoach was coupled to two heavy snowplows, it was blown from its track. Several passengers suffered light and medium injuries. On January 3, 2008, high winds during a foehnstorm "derailed" the cable of a double chair cable lift. First, the lift stopped, and the cable was caught in the cable catcher, but successive gusts threw the cable out of the catcher, the chairs dropped to the ground. One person died and several were severely wounded. The mean wind speed indicated by the mandatory wind monitoring system was just about at the alarm level.

After the first accidents mentioned here, a rather dense anemometer system was installed in the region, this in addition to the mandatory wind monitoring system required at each cable car. The fact that winds were below the alarm level when the accident happened raises several questions: (i) Are the alarm levels too high? (ii) Are the anemometers mounted at locations which deliver representative values? (iii) Is there sufficient wind information to recognize potentially dangerous situations?

2 OBJECTIVES FOR INVESTIGATIONS BASED ON ACCIDENT ANALYSES

By law, all major accidents with public transportation systems are investigated by an office within the Swiss Federal Department of the Environment, Transport, Energy and Communications (UVEK); the investigation reports are public. In the report of the later accident, the term "gust" appears several times, however, it is never directly dealt with. Quite obviously, neither the wind monitoring system nor the operation procedures deal with gusts in a quantitative manner. The only gust-related parameter which is observed is the peak wind speed.

Any aerial cable car installation is a structure capable to oscillate with many degrees of freedom, and a mathematical treatment of its dynamics is extremely complex. Somewhat simpler is a train on rails. Such a system can in first approximation be treated as a rigid object, in a second step, the rocking (due to the fact that the car is on shock-absorbing springs) can also be considered.

3 THE ANALYSES AND SOME QUALITATIVE CONCLUSIONS

Figure 1 shows the motor coach involved in the incident of November 11, 1996. If mass and dimensions of the car are known, the pressure can be calculated which is needed to balance the gravitational force for a given tilt angle. From this pressure value, the wind speed component perpendicular to the side of the car can be computed with reasonable accuracy.

Assuming stationarity (i.e., a constant, steady wind) a moment calculation (with respect to the downwind rail) should yield the wind speed which was determined as critical in a wind tunnel test. However, since foehn winds are turbulent in general, and even more so near the surface, one must assume that a particularly strong gust overturned the motor coach. The strength of such a gust can be estimated if a certain duration of said gust is assumed. Of course, for a given tilt angle, the strength (or speed) of such a gust would have to be larger than the speed of a steady air stream because it has to overcome the additional inertial force. [Quantitative information will be supplied in the conference presentation.]

Figure 1. The motor coach after being derailed by foehn winds. (© Minirex AG, Schweizerische Eisenbahn-Revue)

Figure 2. Chairlift accident. The cable was caught in the cable catcher, a subsequent gust threw it out. (Source: public UUS report)

As mentioned, the accident with the chair lift (Fig. 2) is much more difficult to treat theoretically. Nevertheless, from the sequence of incidents and from available observations, some conclusions can be made.

Tourists on the chairlift reported that first the cable "derailed". Such an incident causes an emergency stop of the installation. The cable catcher, a device designed to prevent the cable from dropping to the ground, caught the derailed cable. However, subsequent gusts jolted the cable out of the catcher, the cable and the attached chair dropped to the ground.

Because of the 1996 accident described above, the Jungfrau Rail Company installed a wind-monitoring network consisting of ten anemometer sites. From these, from the two anemometers installed at the chair lift, and from two stations run by MeteoSwiss, some wind data is available (the site anemometer data is not recorded). Wind speed was just about reaching the wind alarm level, however, it was not excessive (Fig. 3). Striking is the fact that at least one station exhibited a very regular oscillation of wind speed, however, compared to the natural frequency of the cable (which is in the second range) these oscillations were much slower (period was about 10 … 15 minutes). Hence this observation is most likely irrelevant for the accident. It must be assumed that gusts which were either synchronous to the swinging cable or extremely strong (as one passenger reported) caused the cable to drop. Due to the very steep topography, winds can have significant vertical components, however, because the anemometers measure only in the horizontal plane, these cannot be observed.

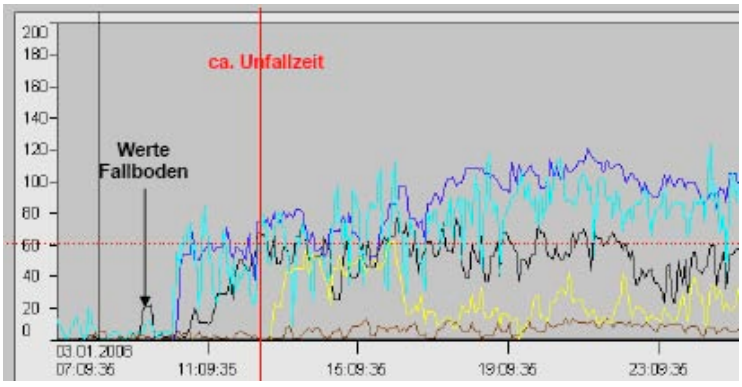

Figure 3: Wind speed recordings of stations in the accident area. The black trace is from the anemometer site closest to the disaster. Note the regular oscillation of the cyan trace. The horizontal red line represents the alarm level. (Source: public UUS report)

4 FINAL REMARK

The dynamics and the turbulent characteristics of strong winds near the surface can, of course, be investigated and analysed much easier with proper instrumentation. Nevertheless, using basic physical laws to investigate accidents as described here gives the numbers found in "scientific" observations immediately a new and also very practical meaning. In addition, a comparison of nearby instrumental measurements with estimations derived from the accidents themselves demonstrates dramatically the fact that it is extremely difficult to make representative observations over complex terrain and/or in turbulent conditions.

Acknowledgements:
The support by the "Unfalluntersuchungsstelle Bahnen und Schiffe" and by the "Jungfrau Railways" is gratefully acknowledged.

TRAPPED LEE WAVE INTERFERENCE IN PRESENCE OF SURFACE FRICTION

Ivana Stiperski[1], Vanda Grubišić[2]

[1] Meteorological and Hydrological Service, Zagreb, Croatia
E-mail: *stiperski@cirus.dhz.hr*
[2] University of Vienna, Vienna, Austria

Abstract: Lee-wave interference over twin peaks in the presence of a frictional boundary layer is investigated by means of idealized high-resolution two-dimensional simulations with the NRL COAMPS model. The interference is examined under linear to highly nonlinear flow regimes. The results show that the pattern of positive and negative interference, evident in the wave amplitude and rotor strength, is consistent with the predictions of linear interference theory. Interference is found to most significantly affect the flow in the lee of the downstream ridge, preventing boundary-layer separation there under conditions of destructive interference and amplifying rotor strength under constructive interference in different flow regimes. Only under strongly nonlinear conditions is the rotor strength amplified by constructive interference beyond that obtained in the lee of a single mountain.

Keywords: *boundary layer separation, critical mountain height, nonlinearity, rotors*

1 INTRODUCTION

Trapped lee waves form downwind of a mountain ridge under conditions conducive to wave energy confinement within the lower troposphere. The study of nonlinear lee-wave resonances over twin ridges under free slip conditions (Grubišić and Stiperski 2009) shows that the resonance is governed by the ratio of the intrinsic trapped lee wave wavelength λ_s and the ridge-separation distance V. The positive and negative interference patterns are evident in the wave amplitudes and total wave drag. In the presence of a frictional boundary layer, the adverse pressure gradients associated with nonlinear, trapped lee waves are expected to lead to boundary layer separation and formation of recirculating regions (or rotors) underneath lee wave crests (Doyle and Durran 2002). Here we investigate the effects of a frictional boundary layer on the lee wave resonance and rotor strength over twin peaks.

2 MODEL SETUP

Two-dimensional numerical simulations were carried out using the nonhydrostatic COAMPS model initialized with an idealized sounding. The surface wind speed is 10 m s^{-1}, vertical wind shear equal to 6 m s^{-1} km^{-1}, and the stability N=0.012 s^{-1} is constant within the troposphere (Fig. 1). Friction at the lower boundary is imposed via a partial-slip condition with surface roughness z_0=0.01m. A set of idealized simulations was conducted for single and double bell-shaped obstacles for mountain heights H=300-1500 m and valley widths V=30-65 km. The mountain half-width is 5 km. The simulations were run for 10 hours during which time a quasi-steady state was reached in the simulations.

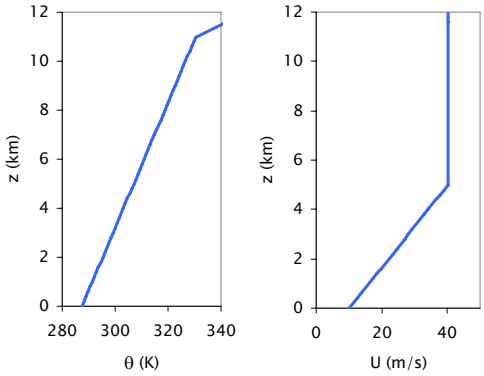

Figure 1. Initial upstream profile of potential temperature (K) and horizontal windspeed (m s^{-1})

3 RESULTS

3.1. Linear regime H< H_c=600 m

For twin peaks lower than H_c the wave interference pattern follows the linear interference theory predictions with constructive and destructive interference occurring, respectively, for V=n*λ_s, and V=(2n-1)/2* λ_s, where λ_s is the intrinsic horizontal wavelength downwind of a single obstacle for the given upstream profile (λ_s=21.8 km) and n>2 is an integer (Fig. 2). The positive and negative interferences are barely evident in the wave amplitudes and horizontal velocity perturbations in the lee of the first obstacle (A_1 and U_1 over the valley), but leave a clear imprint in the lee of the second obstacle, where the wave amplitude and horizontal velocity perturbation (A_2 and U_2) are enhanced or reduced relative to the value in the lee of a single mountain (A_s). The non-dimensional wavelengths cluster around integer values. The flow structure over the downstream obstacle is different under constructive and destructive interference (not shown). Whereas under constructive interference the flow resembles that over a single ridge, for destructive interference the potential temperature and horizontal wind speed are symmetric around the downstream peak. For H>H_s=370 m, the wave-induced adverse pressure

gradients are strong enough to cause boundary-layer separation and rotor formation in the lee of a single obstacle (U_s<0). Within the valley, the rotor strength (U_1) remains equal to U_s for all V, whereas downstream of the secondary obstacle the decrease in amplitude due to destructive interference is strong enough to prevent reversed flow formation, leading to large differences between the flows under constructive and destructive interference.

3.2. Nonlinear regime H_c<H<H_n=1000 m

For H>H_c=600 m the regime becomes nonlinear as the mountains are high enough for flow reversals to occur underneath the first lee wave crests, downstream of both obstacles irrespective of the interference pattern. In the weakly nonlinear regime, H_c<H<H_n=1000 m, the rotors over the valley remain unaffected by the second ridge. The rotors downstream of the second ridge do not attain velocities larger than those downwind of a single ridge, even under constructive interference (not shown).

3.3. Highly nonlinear regime H > H_n

For H≥H_n=1000 m, the nonlinearities start to affect the solutions significantly. Even though the interference still retains its linear pattern of occurrence, it is no longer evident in the variations of total drag (Fig.2), and the V/λ attains also non-integer values. The flow within the valley, unaffected by the secondary obstacle with the linear and weakly non-linear regimes, is weaker than in the lee of a single obstacle and exhibits some variation with V. Also, A_2>A_1 for all V. For H=1000 m constructive interference significantly enhances the rotors developing in the lee of the second ridge, while the rotors within the valley are weaker. For H=1500 m, the enhancement of the rotor circulation is somewhat weaker, possibly due to the nonlinear interaction between the wave field and the PBL flow.

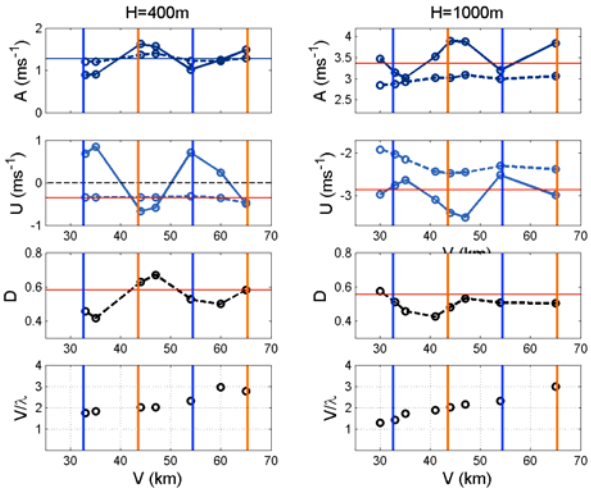

Figure 2. Amplitudes: A_2 (solid), A_1 (dashed); rotor strength U_2 (solid), U_1 (dashed); normalized wave drag (D); non-dimensional wavelength (V/λ), as function of valley width V for H=400 m (left) and H=1000 m (right). Solid red horizontal lines denote values downstream of a single ridge. Vertical lines denote V for which constructive (orange) and destructive (blue) interference is predicted by the linear interference theory.

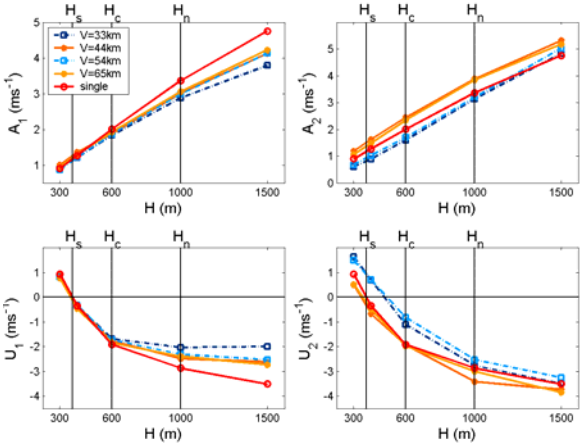

Figure 3. Amplitudes and rotor strength downstream of the first (A_1,U_1) and second (A_2,U_2) obstacle as function of mountain height H. Different V for which constructive (orange) and destructive (blue) interference occurs are indicated, with the values for single ridge in red. Vertical lines denote threshold mountain heights H_s=370 m, H_c=600 m, and H_n=1000 m.

4 CONCLUSIONS

Figure 3 summarizes the influence of mountain height and interference pattern on the wave amplitudes and rotor strength. The significance of the three threshold mountain heights (H_s, H_c and H_n) is best evident in the rotor strength diagrams. Rotors start to form (U_i<0, i=1,2) once the critical mountain height H_s for boundary layer separation is reached. Up to H_c = 600 m, the wave amplitudes and rotor strength increase linearly with H. Within the valley, the U and A values coincide with those for a single ridge, whereas downwind of the second obstacle a clear distinction between constructive and destructive interference is evident in both of these values. Weaker wave amplitudes under destructive interference require a higher critical mountain height for the rotor formation there. In the strongly nonlinear regime, for H>H_c, while the distinction between the interference patterns is becoming more apparent over the valley, where an indication of a limit to the rotor strength is also obtained, downstream of the second ridge the distinction is getting smaller and the rotor strength increases with H reduced.

REFERENCES

Doyle, J.D., and D.R. Durran, 2002: The dynamics of mountain-wave-induced rotors. *J. Atmos. Sci.*, **59**, 186–201.

Grubišić, V., and I. Stiperski, 2009: Lee wave resonances over double bell-shaped obstacles. *J. Atmos. Sci.*, In press.

A NUMERICAL STUDY OF THE COMBINED PROCESSES LEADING TO MEDITERRANEAN QUASI-STATIONARY MCS

Véronique Ducrocq[1], Céline de St. Aubin[1], Emilie Bresson[1], Olivier Nuissier[1], Didier Ricard[1]

[1] GAME-CNRM, Météo-France & CNRS, Toulouse, France
E-mail: *veronique.ducrocq@meteo.fr*

Keywords: *deep convection, heavy precipitation, quasi-stationary mesoscale convective systems*

1 INTRODUCTION

Northwestern Mediterranean regions are frequently affected by torrential rainfall associated with mesoscale convective systems. These systems can stay at the same location during several hours, focusing high-rate precipitation in a specific and limited region. Ingredients favouring the triggering of these events are relatively well-known now (Nuissier et al., 2008; Ducrocq et al., 2008). They include a slow-evolving synoptic environment, conditional convective instability, a low-level moist flow impinging the region, etc. But on the other hand, understanding how these ingredients combine and interact to produce more or less precipitation with different anchored locations is still an open question. The goal of the present study is to address this question based on idealised high-resolution modelling, following the study of Bresson et al. (2009).

2 MODEL SETUP

The effects of the mesoscale atmospheric conditions and of the terrain on the location and intensity of the quasi-stationary precipitating systems are investigated through 2.4-km MESO-NH simulations. Atmospheric conditions are idealized, but not the terrain as we wanted to keep in our simulations the strong topographic component of the region (e.g. sea surrounding by coastal mountain ranges). The idealized atmospheric conditions used as initial and boundary conditions contain the main characteristics of the flow observed during heavy precipitation events over the Cévennes region (Massif Central, see Fig. 2 for location). Indeed, these cases evidence a moist conditionally unstable South-Southeasterly flow over the Mediterranean Sea impinging on the Massif Central Southeastern foothills. With respect to the Bresson et al (2009) study, the simulation domain has been extended southwards and the initial wind fields is now vertically uniform in intensity and direction. Table 1 provides the description of the sensitivity experiments carried out.

Experiments	Max wind U_0	Moisture decrease α	Model terrain
CTRL	20 m s^{-1}	95%	real
WIN10, WIN30, WIN40	10, 30, 40 m s^{-1}	95%	real
ALPS, PYREN, MASC	20 m s^{-1}	95%	Remove the Alps, the Pyrenees, the Massif Central
HUM85, HUM90, HUM100	20 m s^{-1}	85%, 90%, 100 %	real

Table 1. Characteristics of the MESO-NH simulations.

3 RESULTS

The control experiment successes in simulating a quasi-stationary mesoscale convective system with large accumulated rain amounts. Whereas during the initial transition phase, the orographic forcing produces precipitation over the Massif Central foothills, a low-level cold pool progressively forms and pushes the convective system upwind (Fig. 1b). During the stationary phase, the orographic lifting is weaker as the cold pool and the convective system slow down the low-level flow. Two other triggering mechanisms operate. Upstream over the Sea, low-level wind convergence provides the necessary upward lifting for the triggering of new convective cells, whereas more downstream the cold pool facing the low-level moist flow supplies additional lifting. The deflection by the Alps of the flow (Fig. 2b) contributes to increase the both forcing mechanisms.

The set of experiments varying the basic flow speed from 10 to 40 m/s show that the flow speed influences both the location of the precipitating system (Fig. 1) and the occurrence of the cold pool. The weaker the flow speed is, the more upstream the precipitating system is located. Besides, with intense flow, evaporation from the Mediterranean Sea is increased, resulting in nearly saturated lower-levels for experiments with intense flow. Evaporation of falling precipitation is therefore restrained in these experiments and no significant cold pool is formed. The dominant forcing are therefore different according to the flow speed. With low-speed flow, new convective cells are mainly triggered by the low-level convergence over the Sea and by the cold pool. On the

opposite, flow-over regimes are favoured with intense and moist flows and the main mechanism to steadily trigger new cells is orographic lifting in the experiments with high-speed flow. These experiments produce the largest rainfall amounts (Fig. 1cd).

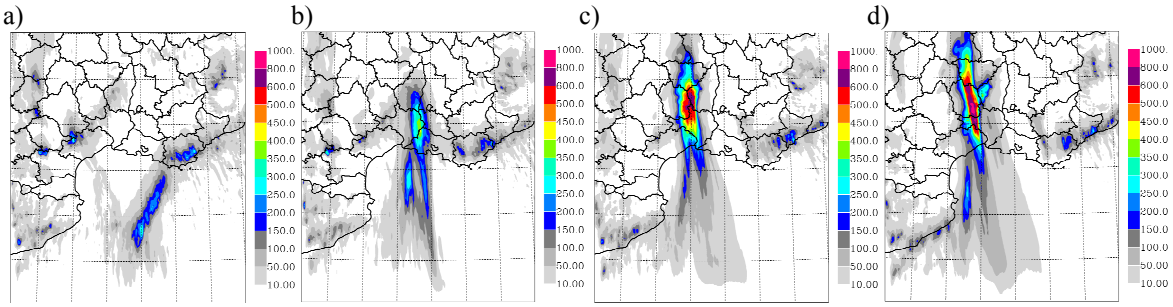

Figure 1. 24-h accumulated surface rainfall (mm) for day 2 of simulation for : a)WIN10; b) CTRL; c) WIN30; d) WIN40.

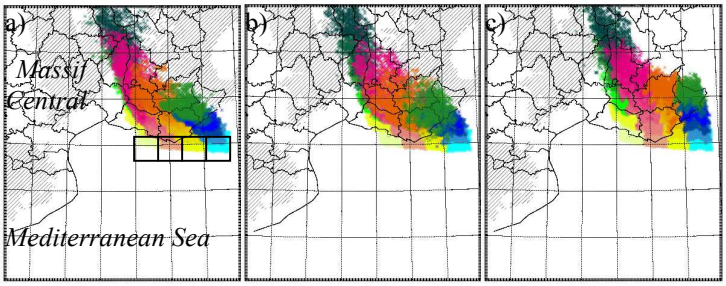

Figure 2. Plumes of Lagrangian parcels that are initially contained in 4 contiguous boxes of 0-500m depth from 42 to 48 h of simulation (by 1 h step) for: a) HUM85; b) CTRL and c) ALPS simulations. The initial parcel boxes are shown in a).

Then, the effects of the mountain ranges have been examined, by alternatively removing them. Even though the mountain ranges are removed, a quasi-stationary convective system is obtained for all the experiments. Removing the Alps helps to highlight the role of this mountain range in deflecting the low-level flow on the eastern side of the domain. The effect of the flow deflection by the Alps is to increase the low-level wind convergence (Fig. 2c). Such deflection of the flow is also evidenced for the Pyrenees although less important than for the Alps. Concerning the Massif Central, it clearly plays a role in blocking the cold pool in the Rhône valley, besides the orographic lifting effect already identified.

Finally, the sensitivity to the environment moisture distribution has been investigated by modulating the moisture apart the axis of maximum flow and humidity. Results of the experiments show that the environmental moisture influences both the location and intensity of the quasi-stationary precipitating system. Indeed, a dryer environment favours a more important deflection of the flow by the Alps as well as a more intense and wider cold pool, pushing the convective system more upstream. The cold pool exerts larger upward lifting, resulting in larger accumulated precipitation than the control experiment. On the opposite, a horizontally homogeneous moist environment reduces the evaporation of precipitation and therefore the cooling beneath the convective system, but supplies larger moisture to produce high precipitation amounts.

4 CONCLUSION

The synthesis of all the sensitivity experiments carried out shows that the location and intensity of the Mediterranean quasi-stationary mesoscale convective systems depend not only on a unique combination of characteristics of the mesoscale environment in which the systems form and evolve (flow speed and direction, moisture distribution, terrain of the region). As instance, the same location of the system can be obtained by varying either the flow speed or the moisture. However, the MESO-NH experiments evidence four main low-level mesoscale forcings which combine or compete to explain the intensity and the location of the system: cold pool forcing, orographic lifting, low-level wind convergence and flow deflection by neighbouring mountains. According to the characteristics of the environment, some of them could be dominant or absent.

REFERENCES

Ducrocq, V., O. Nuissier, D. Ricard, C. Lebeaupin et T. Thouvenin, 2008: A numerical study of three catastrophic precipitating events over southern France. II: Mesoscale triggering and stationarity factors, *Quarterly Journal of the Royal Meteorological Society*, **134**, 131-145.

Nuissier, O., V. Ducrocq, D. Ricard, C. Lebeaupin et S. Anquetin, 2008 : A numerical study of three catastrophic precipitating events over southern France. I: Numerical framework and synoptic ingredients, *Quarterly Journal of the Royal Meteorological Society,* **134**, 111-130.

Bresson, R., D. Ricard and V. Ducrocq, 2009: Idealized mesoscale numerical study of Mediterranean heavy precipitating convective systems, *Meteorology and Atmospheric Physics*, **103**, 45-56.

TOPOGRAPHIC AND DIURNAL EFFECTS ON TROPICAL AND SUBTROPICAL CONVECTION IN SOUTH AMERICA

Ulrike Romatschke[1,2], Socorro Medina[1], Robert A. Houze, Jr[1], Kristen Rasmussen[1]

[1] Department of Atmospheric Sciences, University of Washington, Seattle, USA
[2] Institute for Meteorology and Geophysics, University of Vienna, Vienna, Austria
E-mail: *ulli@atmos.washington.edu*

Abstract: Tropical Rainfall Measuring Mission (TRMM) Precipitation Radar (PR) and National Centers for Environmental Prediction (NCEP) reanalysis data are used to investigate the relation of convective precipitation systems to the topography of South America. Three types of convective radar echo structures are defined: *Deep convective cores* (convective 40 dBZ echo ≥ 10 km in height), *wide convective cores* (convective 40 dBZ echo area ≥ 1000 km²) and *broad stratiform regions* (stratiform echo area ≥ 50,000 km²). Their geographic distribution, diurnal cycles, and relation to the precipitation pattern are studied to gain insight into the mechanisms leading to convection in the vicinity of the Andes. Diurnal heating and capping of the low-level moist flow by dry air flowing over the Andes affects the evening formation of *deep* and *wide convective cores*. Nocturnal downslope flow influences the formation of *wide convective cores* in the early morning. *Broad stratiform regions* appear to be a later stage of mesoscale system development and their locations coincide with the areas of maximum rainfall. The South American low-level jet influences the location of maximum convective activity.

Keywords: *TRMM, South America, convection, diurnal cycle*

1 INTRODUCTION

Since precipitation in tropical and subtropical South America is mostly of convective origin, understanding the mechanisms leading to the development of convective systems is fundamental. Various studies have shown the significant roles of the topography (e.g. Lenters and Cook, 1995), the diurnal heating (e.g. Garreaud and Wallace, 1997), and the synoptic forcing (e.g. Nogués-Paegle and Mo, 1997) in the formation of convection. Data from the satellite-borne Tropical Rainfall Measuring Mission (TRMM) Precipitation Radar (PR) show the location, vertical and horizontal structure, intensity, and nature of convective systems in unprecedented detail. National Centers for Environmental Prediction (NCEP) reanalysis data provide the synoptic context.

In this study we use the summer months of ten years of TRMM PR data to identify three categories of convective radar echo structure: (1) *Deep convective cores* (convective 40 dBZ echo ≥ 10 km in height), which are associated with localized vigorous young convection and often with severe weather. (2) *Wide convective cores* (convective 40 dBZ echo ≥ 1000 km² in horizontal area), which are associated with mesoscale convective systems (MCSs) likely in an early stage of their life cycle. (3) *Broad stratiform regions* (stratiform echo ≥ 50,000 km² in horizontal area), which are associated with MCSs likely in a late stage of their life cycle. This classification allows us to clarify the different convective forcings.

2 DIURNAL HEATING, TOPOGRAPHIC AND SYNOPTIC FORCING OF CONVECTION

Deep convective cores are mainly observed in the subtropics near and to the east of the eastern Andean foothills (Fig. 1a). *Wide convective cores* occur over the same regions and also over the tropical eastern Andean foothills, the Amazon Basin, and the eastern part of the South Atlantic (Fig. 1b). *Broad stratiform regions* are most frequent in the same locations as the *wide convective cores,* however in the subtropical plains they occur to the east of the regions where the *deep* and *wide convective cores* are maximum (Fig. 1c). *Broad stratiform regions* prominently coincide with the regions of maximum surface precipitation (cf. Fig. 1c and d).

The focus of this study is on the eastern Andean foothills and the subtropical plains. In these regions, *deep convective cores* occur preferentially in the afternoon and evening in connection with solar heating. They are observed in an environment of strong directional wind shear where moist low-level easterlies are capped by dry westerlies aloft. This leads to a build-up of extreme instability which is released as the surface flow is lifted over the foothills, similarly to what is observed over the US Great Plains (Carlson et al., 1983) and near the Himalayas (Houze et al., 2007). *Wide convective cores* also peak in the afternoon due to similar mechanisms and also during the morning. Composites of NCEP reanalysis data suggest that the early morning maximum may be associated with nocturnal downslope flow along the foothills, which leads to convergence with the prevailing wind. *Broad stratiform regions* are most frequently observed in the late morning in the same regions as the morning *wide convective cores,* suggesting that they represent similar systems in a later stage of development.

The location of the convection is controlled by the strength of the South American low-level jet (SALLJ), a northerly flow that forms preferentially at night along the eastern Andean foothills. The SALLJ is strengthened as mid-latitude low pressure systems approach from the west. This leads to increased moisture transport from the Amazon Basin to the subtropics and enhanced wind convergence along the subtropical foothills and plains. Hence, the convective activity increases in these regions. As the low pressure systems move further east, anomalous southerly flow along the eastern Andean foothills counteracts the SALLJ and increases moisture and wind convergence to the north, enhancing convection and precipitation along the tropical foothills.

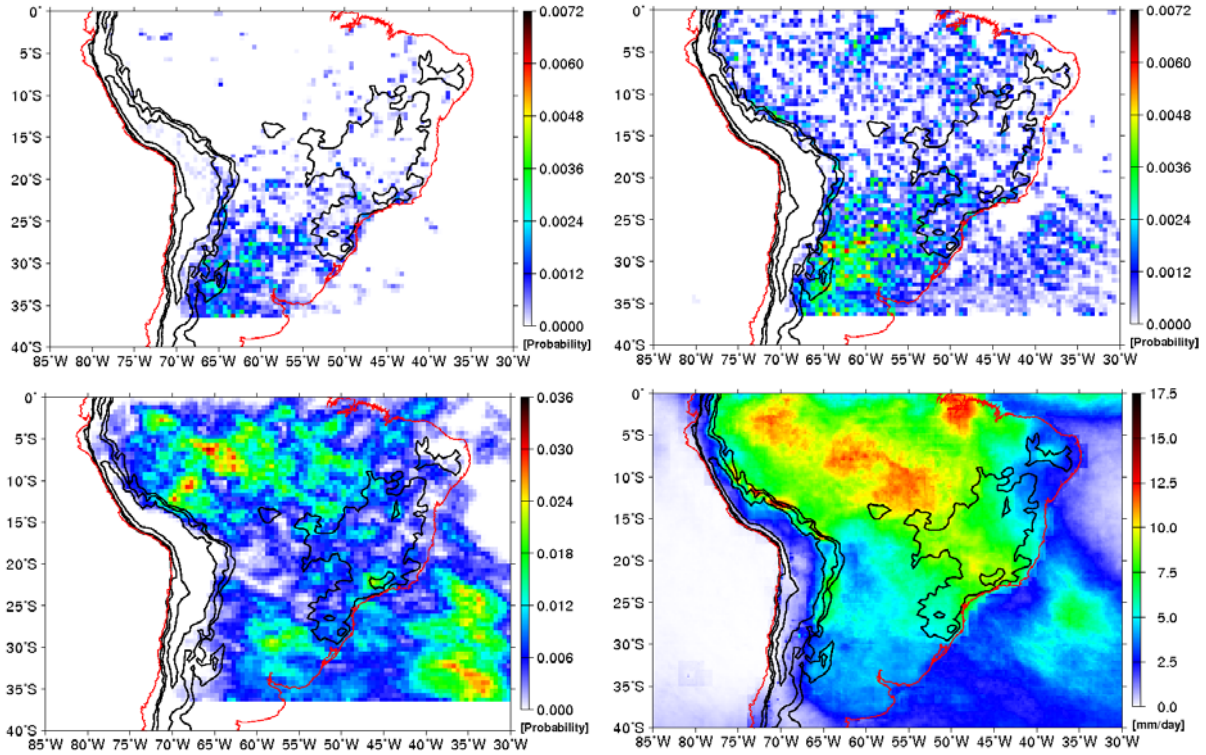

Figure 1. Distribution of the probability of finding (a) a *deep convective core*, (b) a *wide convective core*, and (c) a *broad stratiform region* during summer and (d) summer precipitation climatology from TRMM product 3B43. Orographic contours of 0.3 km, 1.5 km and 3 km are shown in black. Note the different color scales.

3 CONCLUSIONS

Analysis of different types of convective structure highlights how the diurnal heating, the topography and the synoptic forcing play together to develop the convective systems, which predominate in the vicinity of the Andes. Capping of the low-level moist flow by dry air aloft leads, in combination with topographic forcing and diurnal heating, to the formation of *deep* and *wide convective cores* in the evening. Nocturnal downslope flow influences the early morning formation of MCSs containing *wide convective cores* in an early stage and *broad stratiform regions* in a later stage of their life cycle. The locations of occurrence of *broad stratiform regions* coincide with the maximum climatological precipitation. The exact location of the region with maximum convective activity is controlled by the strength of the SALLJ.

Acknowledgements:
Stacy Brodzik and Carol Archambeault assisted in the data processing. This research was supported by the National Science Foundation (ATM-0505739/ATM-0820586) and the National Aeronautics and Space Administration (NNX07AD59G).

REFERENCES

Carlson, T. N., S. G. Benjamin, G. S. Forbes, and Y. Li, 1983: Elevated Mixed Layers in the Regional Severe Storm Environment: Conceptual Model and Case Studies. Mon. Weather Rev., **111**, 1453-1474.

Garreaud, R. D., and J. M. Wallace, 1997: The Diurnal March of Convective Cloudiness over the Americas. Mon. Weather Rev., **125**, 3157-3171.

Houze, R. A., D. C. Wilton, and B. F. Smull, 2007: Monsoon convection in the Himalayan region as seen by the TRMM Precipitation Radar. Q. J. R. Meteorol. Soc., **133**, 1389-1411.

Lenters, J. D., and K. H. Cook, 1995: Simulation and Diagnosis of the Regional Summertime Precipitation Climatology of South America. J. Clim., **8**, 2988-3005.

Nogués-Paegle, J., and K. C. Mo, 1997: Alternating Wet and Dry Conditions over South America during Summer. Mon. Weather Rev., **125**, 279-291.

STRUCTURE OF MID-LATITUDE CYCLONES CROSSING THE CALIFORNIA SIERRA NEVADA AS SEEN BY VERTICALLY POINTING RADAR

Socorro Medina[1], Robert A. Houze, Jr.[1], Christopher R. Willimas[2], and David E. Kingmill[2]

[1] Department of Atmospheric Sciences, University of Washington, Seattle, USA
E-mail: *socorro@atmos.washington.edu*
[2] University of Colorado, Cooperative Institute for Research in Environmental Sciences, and NOAA/Earth System Research Laboratory, Boulder, USA

Abstract: Previous work has shown that a layer of intermittent updraft cells, apparently turbulent in nature, develops as the middle sector of mid-latitude cyclones passes over the Oregon Cascades and that these cells likely contribute to the windward enhancement of precipitation. This study finds a similar layer of cells as the middle sector of extreme extratropical cyclones pass over the Sierra Nevada of California, providing evidence of the repeatability of the signal.

Keywords:, *vertical shear layer, turbulence, orographic precipitation enhancement*

1 INTRODUCTION

Most of the precipitation in the western United States falls during the winter months as mid-latitude cyclones from the Pacific Ocean move inland (Fig. 1, left and center). Previous studies have provided insight into how the precipitation varies from one sector of an extratropical cyclone to another (e.g., Nagle and Serebreny 1962). These studies have focused on the horizontal patterns of cloud and precipitation in the cyclones. However, when these weather systems move over mountainous terrain, the horizontal patterns are affected by the orography and become complex. High temporal and vertical resolution reflectivity and Doppler velocity profiles obtained by vertically pointing (VP) S-band radars (White et al. 2003) provide a better alternative to describe the precipitation processes in different sectors of extratropical cyclones passing over complex terrain. For example, Medina et al. (2007) analyzed the vertical structure of cyclone precipitation over the Oregon Cascades (mbo in Fig. 1), while Kingsmill et al. (2006) focused over the Northern California Coastal Mountains (czd in Fig. 1).

Medina et al. (2007) identified vertical structures that are apparently produced when moist flow impinges upon the terrain. When the middle sector of a storm, characterized by the transition from warm to cold advection, passes over the windward slope, scanning radar observations show that a shear layer often forms on the windward slope. Within the shear layer, the VP radial velocity shows intermittent updraft cells (> 0.5 m s^{-1}). These cells, which are apparently turbulent, are thought to be crucial for enhancing the growth of precipitation particles and for speeding up their fallout over the windward slope (Houze and Medina 2005). This study is part of an investigation aimed at understanding how the complex terrain of the western US modifies the structure of mid-latitude cyclones advancing from the Pacific Ocean. The specific objective of this study is to test the repeatability of the structures observed by Medina et al. (2007) in other west coast locations.

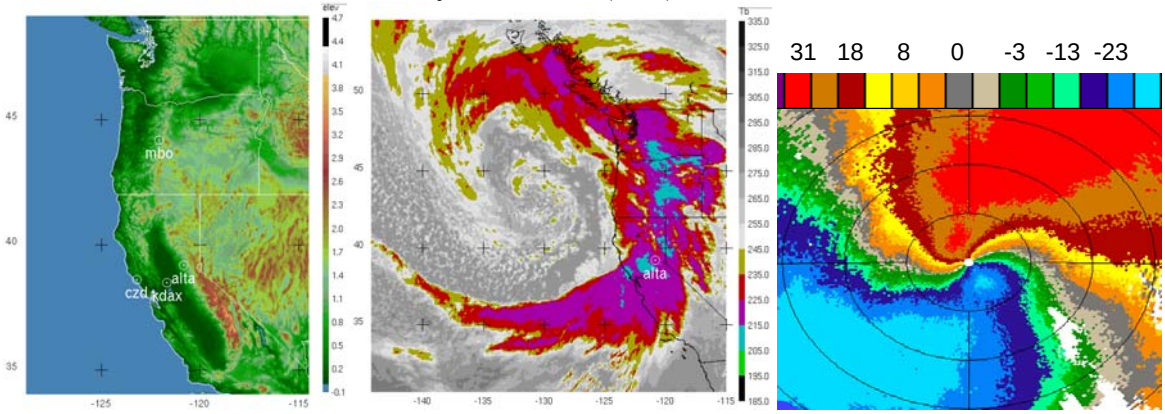

Figure 1. Left: Topography of western US (km) and relevant sites. Center: Infrared satellite temperature (K) during the passage of a mid-latitude cyclone over the area of study (1530 UTC 4 Jan 2008). Right: Radial velocity (m s^{-1}) at 2.4° elevation from the Sacramento radar (kdax, 1457 UTC 4 Jan 2008). Range ring spacing is 25 km. Positive (negative) values indicate flow away from (toward) the radar.

2 DATA

The main dataset for the study is the VP S-band radar data collected as winter storms moved over the western slopes of the California Sierra Nevada. The data was collected during the National Oceanic and Atmospheric

Administration (NOAA) Hydrometeorological Testbed (HMT, Ralph et al. 2005). The VP dataset was collected at Alta (Fig. 1) and Colfax (~17 km southwest of Alta) and it extends over three winter seasons. We use Weather Surveillance Radar (WSR-88D) data and infrared images from the Geostationary Operational Environmental Satellite (GOES) to obtain the larger context of the VP radar structures.

3 RESULTS

The passage of mid-latitude cyclones over the Sierra Nevada is separated by periods dominated by a high pressure offshore of California (i.e., blocking or omega pattern). When this pattern breaks, weather systems are able to penetrate into the region of interest. Preliminary analysis of the VP radar structure suggests that the extreme storms (either by amount of precipitation accumulated and/or by wind intensity) present a layer of intermittent cells in the perturbation radial velocity located above the radar bright band near 2 km (dBZ, left panel; RV', right panel in Fig. 2). RV' was calculated as the residual between the actual radial velocity and the 60 minutes running average radial velocity (Matrosov et al. 1994). The period in Fig. 2 corresponds to the infrared satellite image in the Fig. 1 (center), indicating that the occurrence of the cells coincides with the passage of the middle sector of a storm. The horizontal radial velocity pattern (Fig 1, right) illustrates the strong shear during this case, which was characterized by a south-southeasterly jet at low levels, along the central valley, and strong southwesterlies aloft.

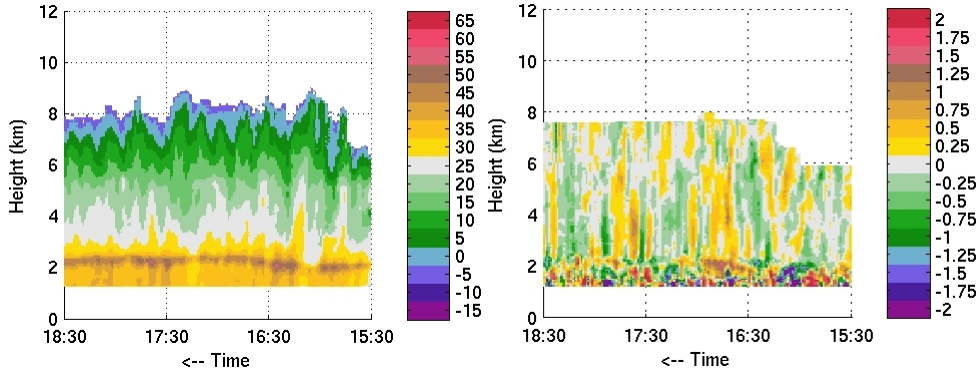

Figure 2. VP radar structure at Alta (4 Jan 2008). Left: reflectivity (dBZ). Right: perturbation radial velocity (RV', m s^{-1}). Positive (negative) values indicate RV' toward (away from) the radar.

4 CONCLUSIONS

This study finds a layer of updraft cells as the middle sector of extreme extratropical cyclones passes over the Sierra Nevada of California, mounting the evidence of the generality of this orographic precipitation signal.

Acknowledgements:
The first and second authors were supported by National Science Foundation grants ATM-0505739 and ATM-0820586. Martin Ralph is acknowledged for his suggestions regarding the analysis the VP radar data. The KDAX data was plotted using NOAA's weather and climate toolkit.

REFERENCES

Houze, R.A., and S. Medina, 2005: Turbulence as a Mechanism for Orographic Precipitation Enhancement. *J. Atmos. Sci.*, **62**, 3599–3623.

Kingsmill, D.E., P.J. Neiman, F.M. Ralph, and A.B. White, 2006: Synoptic and Topographic Variability of Northern California Precipitation Characteristics in Landfalling Winter Storms Observed during CALJET. *Mon. Wea. Rev.*, **134**, 2072–2094.

Matrosov, S.Y., B.W. Orr, R.A. Kropfli, and J.B. Snider, 1994: Retrieval of Vertical Profiles of Cirrus Cloud Microphysical Parameters from Doppler Radar and Infrared Radiometer Measurements. *J. Appl. Meteor.*, **33**, 617–626.

Medina, S., E. Sukovich, and R.A. Houze, 2007: Vertical Structures of Precipitation in Cyclones Crossing the Oregon Cascades. *Mon. Wea. Rev.*, **135**, 3565–3586.

Nagle, R.E., and S.M. Serebreny, 1962: Radar Precipitation Echo and Satellite Cloud Observations of a Maritime Cyclone. *J. Appl. Meteor.*, **1**, 279–295.

Ralph, F.M., R.M. Rauber, B.F. Jewett, D.E. Kingsmill, P. Pisano, P. Pugner, R.M. Rasmussen, D.W. Reynolds, T.W. Schlatter, R.E. Stewart, S. Tracton, and J.S. Waldstreicher, 2005: Improving Short-Term (0–48 h) Cool-Season Quantitative Precipitation Forecasting: Recommendations from a USWRP Workshop. *Bull. Amer. Meteor. Soc.*, **86**, 1619–1632.

White, A.B., P.J. Neiman, F.M. Ralph, D.E. Kingsmill, and P.O.G. Persson, 2003: Coastal Orographic Rainfall Processes Observed by Radar during the California Land-Falling Jets Experiment. *J. Hydrometeor.*, **4**, 264–282.

SOURCES OF UNCERTAINTY EXAMINED BY HIGH-RESOLUTION ENSEMBLE MODELING

Christian Keil and George C. Craig

Deutsches Zentrum für Luft- und Raumfahrt (DLR), Institut für Physik der Atmosphäre
Oberpfaffenhofen, Germany
E-mail: *christian.keil@dlr.de*

Abstract: Forecasts of the high resolution ensemble prediction system COSMO-DE-EPS of Deutscher Wetterdienst (DWD) are used to examine the dominant sources of uncertainty of convective precipitation. A validation with radar data using traditional as well as novel spatial verification measures highlights differences in precipitation forecast performance in differing weather regimes. When the forecast uncertainty can primarily be associated with local, small-scale processes individual members run with the same variation of the physical parameterisation driven by different global models outperform all other ensemble members. In contrast when the precipitation is governed by the large-scale flow all ensemble members perform similarly.

Keywords: *ICAM, predictability, precipitation, COPS*

1 INTRODUCTION

Predictability, or forecast uncertainty, of convective precipitation is influenced by all scales, but in different ways in different meteorological situations. Forced-frontal convective precipitation associated with synoptic weather patterns may be predictable for several days and is primarily governed by lateral boundary conditions in limited area models. Single convective cells developing during air-mass convection situations, which of themselves are predictable only for a matter of hours, are frequently triggered by local, small-scale processes enforced e.g. by mountain ridges and are anticipated to react sensitively to changes in the model physics.

2 TOOLS AND INGREDIENTS

In the *high resolution ensemble prediction system* COSMO-DE-EPS an ensemble of forecasts is generated by combining initial and lateral boundary conditions of four different global models with five variations of physical parameterizations using the COSMO-DE model (dx=2.8km). Forecast quality of all 20 ensemble members is validated using hourly instantaneous *Radar data of the European Composite*. Here the conventional *bias score* is used to provide an integral estimate of the model's behaviour in over- or underpredicting rainfall and the spatial verification measure *DAS* (Keil and Craig, 2009) combining displacement and amplitude errors is applied.

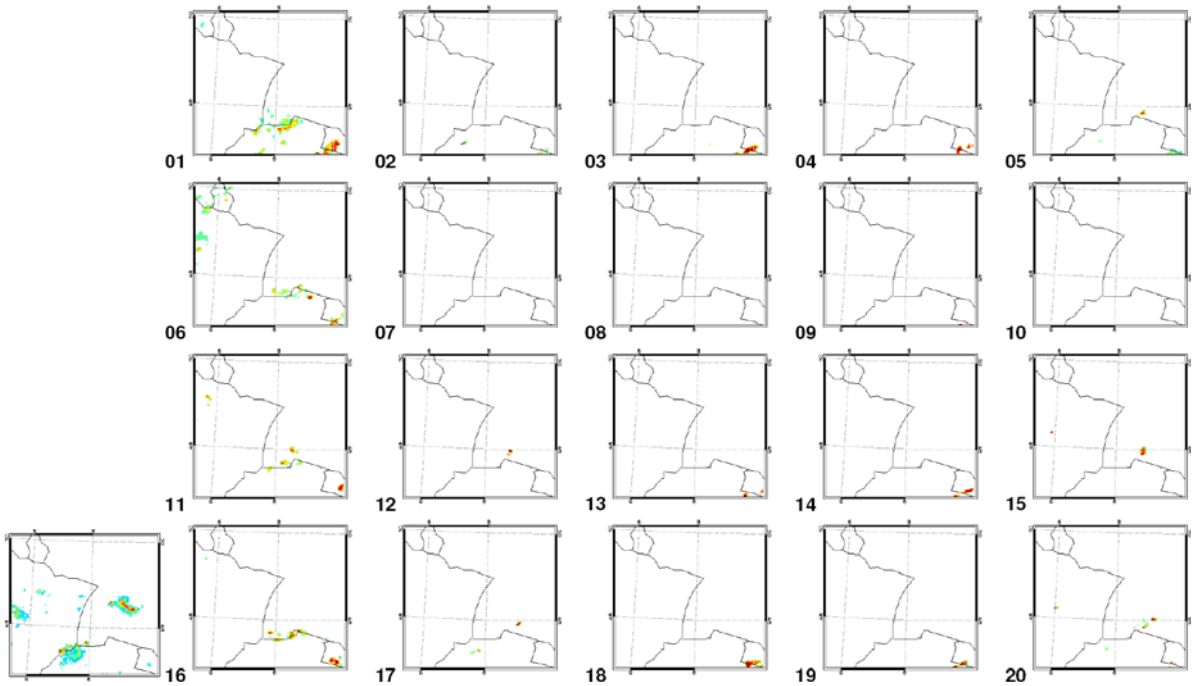

Figure 1. Radar observation (bottom left) and stamp map of forecast synthetic radar imagery displaying all 20 members of COSMO-DE-EPS on 12 August 2007 at 17.15 UTC.

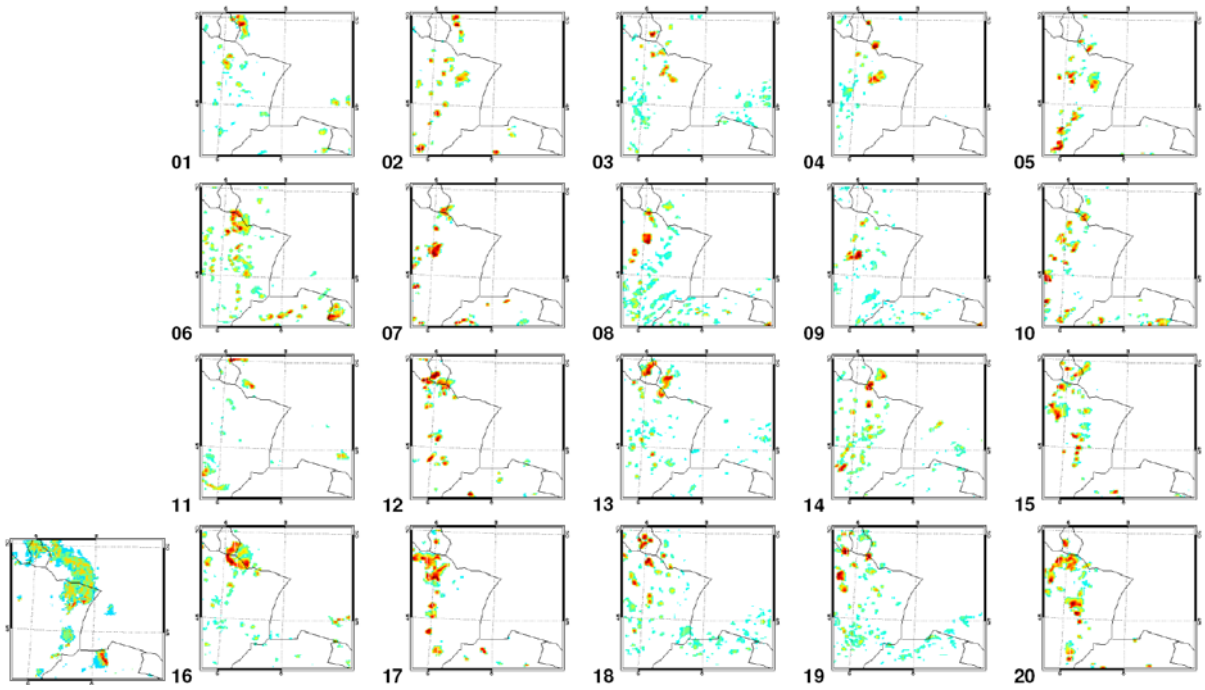

Figure 2. Same as Fig.1 but at 23.15 UTC.

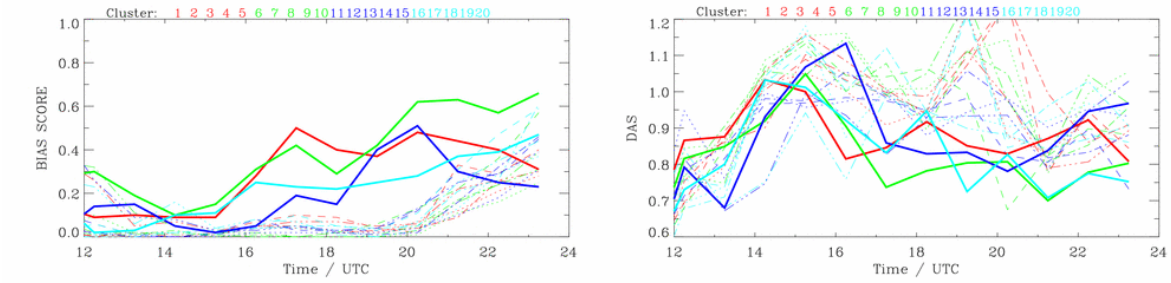

Figure 3. Bias score (left) and DAS (right) for all ensemble members applying a threshold of 19 dBZ on 12 August 2007. Different colours depict different driving global models, solid lines members 1, 6, 11 and 16 with changed entrainment rate.

3 RESULTS

Forecasts of COSMO-DE-EPS are continuously available from 8 to 16 August 2007 covering various meteorological situations during the COPS field experiment. One of the largest spread in bias score occurs during IOP15 on 12/13 August 2007. In the afternoon of 12 August local convection triggered by orography occurred in the COPS region. Members 1, 6, 11 and 16 of the ensemble system outperform the other members generating some convective precipitation along the Swiss-German border at 17.15 UTC (Fig.1). These 4 members are driven by different global models but are run with a modified entrainment rate. In contrast, precipitation along a cold front affects the region at 23.15 UTC. This synoptically forced precipitation is forecast by all members (Fig. 2; not at the correct position, however!) indicating a lower forecast uncertainty, i.e. a higher predictability. Both, the bias score and DAS show the good performance of these 4 individual members and the smaller spread at night when the front enters the COPS region (Fig.3).

4 OUTLOOK

The concept of convective timescale (Craig et al. 2009) will be applied in order to distinguish between different predictability regimes.

REFERENCES

Craig, G. C., C. Keil, and D. Leuenberger, 2009: Constraints on the Impact of Radar Rainfall Data Assimilation on Forecasts of Cumulus Convection**.** Submitted to QJ

Keil, C. and G .C .Craig, 2009: A displacement and amplitude score employing an optical flow technique. WaF, in press.

PROBABILISTIC FORECASTING OF THUNDERSTORMS THROUGH COMBINING NOWCASTING METHODS WITH NWP

Kirstin Kober, George Craig, Christian Keil, Arnold Tafferner

Deutsches Zentrum für Luft- und Raumfahrt, Institut für Physik der Atmosphäre, Oberpfaffenhofen, Germany
E-mail: *kirstin.kober@dlr.de*

Abstract: Short term forecasting of thunderstorms or convective precipitation is an ongoing challenge in atmospheric research. In this work the two different approaches nowcasting and numerical weather prediction (NWP) are applied probabilistically.

Keywords: *probabilistic, thunderstorms, nowcasting, NWP*

1 INTRODUCTION

Nowcasting and NWP are two different methods to address the unsolved problem of short term forecasting of convective precipitation. It is known that nowcasting methods which are based on extrapolation of observations in time perform quite well for very short term prediction (0-1 hour) as in this timeframe the motion of thunderstorms can adequately be described by advection. Physics are included at best very simply and therefore processes like growth and decay are not well described. Hence for longer lead times the skill of the forecasts based on nowcasting decreases quite rapidly. High-resolution NWP is in some cases able to simulate thunderstorms. NWP in general gains skill in forecasting convective precipitation after a certain spin-up time. The inherent uncertainty of the methods and of the meteorological situations requires a probabilistic view to evaluate the skill of the forecasts.

2 DERIVATION OF PROBABILITIES FROM RAD-TRAM AND COSMO-DE-EPS

For the advection based forecasts the radar tracker Rad-TRAM (Kober and Tafferner 2009) is used. Rad-TRAM is upgraded to produce probabilistic forecasts up to 4 hours using the Local Lagrangian method (Germann and Zawadzki 2004). Every 15 minutes a nowcast is provided which forecasts the probability that the threshold of 37dBZ is exceeded (Fig.1).

a) 15 min nowcast for 1700 UTC b) 60 min nowcast for 1700 UTC c) 120 min nowcast for 1700 UTC

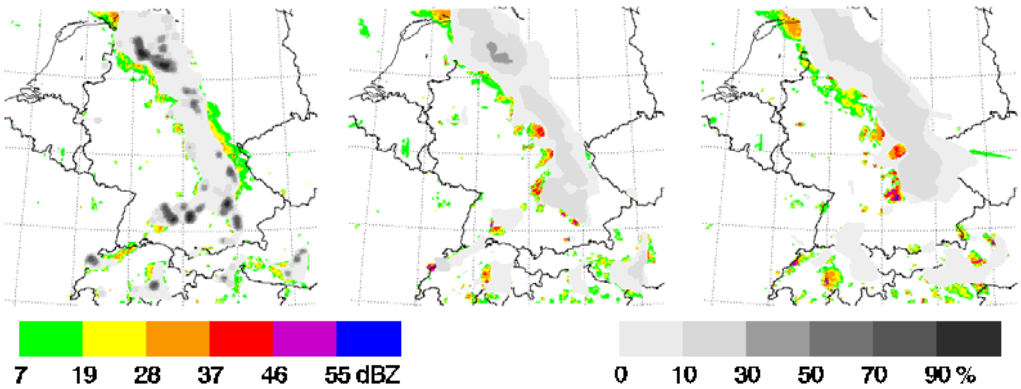

Figure 1: Probabilistic nowcasts with Rad-TRAM-prob for 29.07.2008 at 1700 UTC (a) 15min, b) 60min, c) 120 min). In the background colour-shaded the reflectivities of the European composite at the started time step and grey-shaded the nowcasted probabilities (coloured: www.pa.op.dlr.de/icam2009/extabs).

For the numerical forecasts the experimental, not yet operational, high resolution (2.8km) ensemble of Deutscher Wetterdienst (DWD) is used. Synthetic radar reflectivities are used to forecast the probability that 37dBZ is exceeded. This probability can be derived from the ensemble by two different methods. First, every member can be treated as a deterministic solution and the probability is derived similar to the spatial neighbourhood method (Theis et al. 2005). Second, the entire ensemble is used to derive at each gridpoint the fraction of the members that exceed the threshold. An example for both methods is shown in Figure 2.

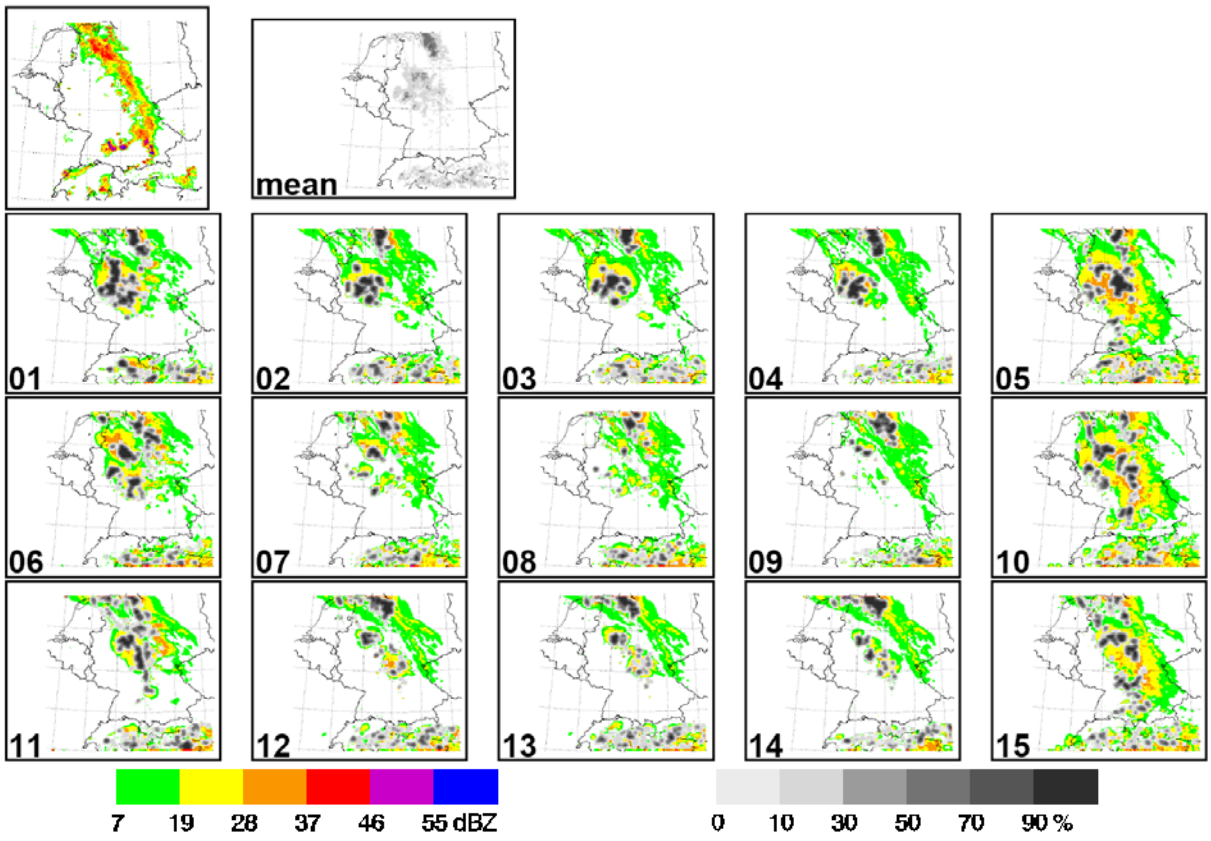

Figure 2: Stamp map of probabilistic COSMO-DE-EPS forecasts showing 15 members and their average (top right) (grey-shaded) for 29.07.2008 at 1700 UTC. In the background the synthetic radar reflectivities and the observed radar reflectivity (top left) is colour shaded (coloured: www.pa.op.dlr.de/icam2009/extabs).

3 FORECAST QUALITY

The forecast skill of Rad-TRAM and COSMO-DE-EPS probabilistic forecasts is calculated with the standard quality measures for the verification of probabilistic forecasts of dichotomous predictands: the Brier Score and its decomposition, reliability diagrams, and ROC curves (Wilks 2006). Furthermore the Conditional square root of ranked probability score (CSRR) is calculated (Germann and Zawazdki 2004). With these scores the development of quality with lead time and on average is calculated for both forecast sources for selected episodes (not shown). First results show that especially short nowcasts have more reliability and resolution than the NWP forecasts.

4 FUTURE

The next step will be to calculate to development of forecast skill in different synoptic situations. With this knowledge methods to combine the two forecast sources can be investigated. Weighting functions for example could be the probabilistic step to be included into the system 'Wx-FUSION' (Weather Forecast User oriented System Including Object Nowcasting) currently under development at DLR. Wx-FUSION will generate forecasts of different weather hazards relevant for applications in airport environments.

REFERENCES

Germann, U., I. Zawadzki, 2004: Scale dependence of the Predictability of Precipitation from Continental Radar Images. Part II: Probability Forecasts. *J. Appl. Meteor*. **43**, 74 - 89.

Kober, K., A. Tafferner, 2009: Tracking and nowcasting of convective cells using remote sensing data from radar and satellite. *Meteorol. Z.* **1**, 75-84.

Theis, S. E., A. Hense, U. Damrath, 2005: Probabilistic precipitation forecasts from a deterministic model: a pragmatic approach. *Meteorol. Appl*. **12**, 257-268.

Wilks, D.S., 2006: Statistical Methods in the Atmospheric Sciences. San Diego, London: Academic Press, 282pp.

ENSEMBLE METEOROLOGICAL FORECAST FOR THE UPPER RHONE RIVER BASIN

Javier Garcia Hernandez[1], Paul Sirvent Gimenez[1], Frédéric Jordan[2], Jean-Louis Boillat[1], Anton Schleiss[1]

[1] Laboratoire de Constructions Hydrauliques (LCH), Ecole Polytechnique Fédérale de Lausanne.
EPFL-ENAC-ICARE-LCH Station 18, CH-1015 Lausanne, Switzerland,
E-mail: javier.garciahernandez@epfl.ch
[2] e-dric.ch eau énergie environnement ingénieurs conseils,
Grand-Chemin 73, CH-1066 Epalinges, Switzerland

Abstract
A semi-distributed hydrological model was developed for the Upper Rhone River basin in Switzerland. It is currently operational for a real-time flood forecast in the Rhone Valley. It simulates the snow and glacier melt, soil infiltration and run-off processes, flood routing in rivers as well as hydropower scheme operations.

For the computation of flood prediction, the numerical meteorological forecasts COSMO-LEPS, COSMO-7 and COSMO-2, provided by MeteoSwiss, have been assimilated. The forecast errors are analyzed by comparing the performance on different time periods, regarding the observed and the predicted rainfall and temperature over the entire catchment area as well as in punctual locations. The influence of the lead time is described with the aim of providing an estimation of the forecast error. A performance evaluation is achieved considering indexes like Brier Score and Relative Operating Characteristic.

Keywords: *Deterministic and ensemble meteorological forecast, Brier Score, Relative Operating Characteristic*

1 INTRODUCTION

Forecasting precipitation is a complex task because the formation of precipitation involves interactions between many different types of processes related to synoptic-scale, mesoscale dynamics, boundary conditions, etc. Further complexity occurs in mountainous regions where the topography influences in an important way the cloud dynamics and the precipitation microphysics.

Ensemble prediction system (EPS) is a feasible way to complete deterministic forecasts with an associated occurrence (Buizza & al., 2005). The existing uncertainty about the current state of the atmosphere is taken into account by calculating different forecast scenarios with an associated probability. EPS constitutes one of the most promising avenues in the meteorological research (Demeritt & al., 2007).

COSMO-LEPS is the limited-area EPS (Ensemble Prediction System) developed within the COSMO consortium (Consortium for Small-scale Modeling) since 2002. This system combines the benefits of the ensemble approach with the high-resolution of the limited-area model integrations. The COSMO-LEPS system provides daily ensemble forecasts with high resolution (horizontal mesh-size of 10 km) based on a 16-member ensemble for central and southern Europe with a lead time of 132 hours. Initial and boundary conditions are representative members of the global ECMWF (European Centre for Medium-Range Weather Forecasts) ensemble. The purpose of COSMO-LEPS is the improvement of the early and medium-range predictability of extreme and localized weather events, particularly when orographic and mesoscale-related processes play a crucial role (Marsigli & al., 2007).

Deterministic forecasts COSMO-7 and COSMO-2 are complementary to COSMO-LEPS. The regional COSMO-7 is driven by the global model of ECMWF and covers most of western and central Europe. It is calculated twice daily for 72 hours lead time on a grid spacing of about 6.6 km. The local COSMO-2, driven by COSMO-7, covers the Alpine region with Switzerland at the center and is computed on a grid spacing of about 2.2 km. It is provided 8 times daily for 24 hours lead time. Both COSMO-2 and COSMO-7 offer the benefit of the nowcasting and short range forecasting.

Meteorological predictions are finally used as input for the hydrological model, created with Routing System (García & al., 2007), producing hydrological ensemble forecasts as well as deterministic forecasts for the flood prediction in the Upper Rhone River basin (Jordan, 2007).

2 METEOROLOGICAL INDEXES

Indexes like the intensity or temperature bias and volume or average temperature bias for different time periods as well as indexes commonly used in meteorology such as the Brier Score (BS) and the Relative Operating Characteristic (ROC) are used to evaluate the forecast performance.

The bias represents the report between the predicted and observed values. The BS allows comparing the forecast probability of an event and its occurrence (Brier, 1950). It depends on three factors: reliability, resolution and uncertainty. The ROC curve defines the ability of a probabilistic forecast system to distinguish between situations predicting the occurrence and the non-occurrence of an event (Mason & Graham, 1999). It is frequently applied to assess the ability of ensemble forecast systems to discriminate between the occurrence and non-occurrence of precipitation accumulations over a specific threshold.

3 RESULTS

The proposed indexes allow the comparison of deterministic COSMO-7 (C7) and COSMO-2 (C2) and probabilistic COSMO-LEPS (CL) forecasts for different time periods.

Bias indicators show a big dispersion in the precipitation intensity for the deterministic forecasts as well as for the weighted average of the probabilistic one. Besides, an overestimation of the precipitation is in general produced which increases by a long way the forecast period.

Temperatures are usually rather well predicted and similar in all the forecasts. The hourly error is around 2.5°C and the daily average error around 2°C.

BS commonly show values smaller than 0.4 for all studied forecasts (Figure 2, left). Forecasts are generally better than the persistence (prolongation of the first day measured observation). However, a severe assessment is necessary for higher rain intensities. This will be possible as soon the re-simulations of past events (September 1993 and October 2000) from MeteoSwiss will be achieved.

The ROC index proves that the probabilistic forecast is better for the prediction of an event exceeding a threshold (Figure 2, right). Thresholds of 5 to 50 mm/24h have been studied, being the performance of the probabilistic forecasts higher for smaller thresholds, as well as for deterministic meteorological forecasts. Although, re-simulations will also be required for heavier precipitation data. Regarding the Correct Alarm Ratio and the Miss Ratio (Mason & Graham, 1999), probabilistic forecasts provide also better results.

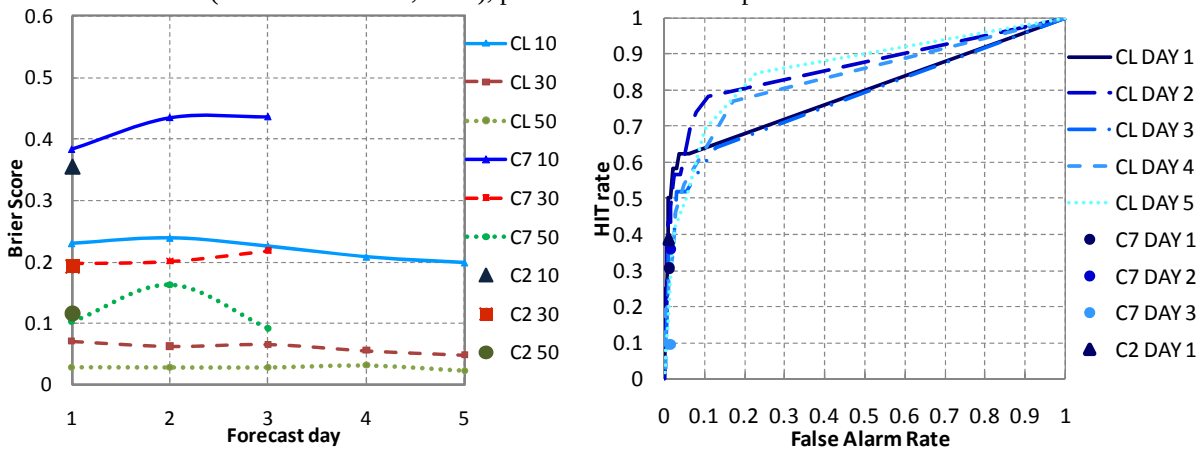

Figure 1: Left: Brier Score for different thresholds (10, 30 and 50 mm/24h), forecasts from 01.07.2008 to 02.28.2009. Right: ROC for the 30mm /24h threshold, forecasts from 01.07.2008 to 02.28.2009.

4 CONCLUSIONS

The indexes used to evaluate the forecast performance show the improvements of the EPS in the meteorological area. The results provided decrease the uncertainty in the flood forecasting domain, where the methods of risk analysis have taken more importance during the last years, allowing the decision-makers to know the rationality of their decisions.

More events of extreme precipitations are necessary for the assessment of high thresholds in order to have a large sample providing representative results. That is the motivation of events re-simulations by MeteoSwiss.

Acknowledgements:

The present research is part of the MINERVE project, funded by the Swiss Federal Office for Environment (FOEV), the Canton of Valais and the Canton of Vaud. Meteorological data are provided by the Swiss Weather Services (MeteoSwiss).

REFERENCES

Brier, G. W. (1950). Verification of forecasts expressed in terms of probability. *Monthly Weather Review*, Vol. 78, 1, 1-3.

Buizza, R., Houtekamer, P.L., Toth, Z., Pellerin, G., Wei, M. and Zhu, Y. (2005). A comparison of the ECMWF, MSC and NCEP global ensemble prediction systems. *Monthly Weather Review* Vol. 133, 1076–1097.

Demeritt, D., Cloke, H., Pappenberger, F., Thielen, J., Bartholmes, J. and Ramos, M.H. (2007). Ensemble predictions and perceptions of risk, uncertainty and error in flood forecasting. Environmental Hazards 7, 115-127.

García Hernández, J., Jordan, F., Dubois, J., Boillat, J.-L. & Schleiss, A. (2007). Routing System II: Flow modelling in hydraulic systems, *Communication du Laboratoire de Constructions Hydrauliques N°32*, ed. A. Schleiss, EPFL, Lausanne.

Jordan, F. (2007). Modèle de prévision et de gestion des crues - optimisation des opérations des aménagements hydroélectriques à accumulation pour la réduction des débits de crue. PhD Thesis N°3711, Ecole Polytechnique Fédérale de Lausanne.

Marsigli, C., Montani, A. and Paccangnella, T. (2007). Ensemble activities at ARPA-SIM: the COSMO-LEPS and COSMO-SREPS systems. *Proceedings, 29th International Conference on Alpine Meteorology*, 4.-8. June 2007, Chambéry.

Mason, S.J. and Graham, N.E. (1999): Conditional probabilities, relative operating characteristics, and relative operating levels. *Weather Forecasting*, Vol 14, Issue 5, 713-725.

THE CANADIAN HIGH-RESOLUTION NWP SYSTEM FOR THE 2010 WINTER OLYMPICS

Jason Milbrandt[1], Ron McTaggart-Cowan[1] and Jocelyn Mailhot[1]

[1] Numerical Weather Prediction Research Section, Environment Canada, Montreal, Canada
E-mail: *Jason.Milbrandt@ec.gc.ca*

1 INTRODUCTION

The 2010 Winter Olympics and Paralympics will be held near Whistler/Vancouver, Canada during January-March, 2010. In support of the operational forecasting during the events and as a testbed for NWP systems in Canada, Environment Canada will be running a high-resolution limited-area mesoscale model, twice daily. The main objectives are to improve the forecast of precipitation quantities and types, winds, and temperatures in this coastal region of complex orography. The influence of steep terrain surrounding the venues is clearly one of the greatest challenges associated with numerical modelling in the Whistler/Vancouver region. This complexity is enhanced by the presence of the Burrard Inlet, the Strait of Georgia, and the Pacific "data void" in the vicinity of the forecast region. In order to provide accurate forecasts in a region so strongly influenced by forcings on the broad range of scales from cyclones in the Gulf of Alaska, through frontal windstorms, to terrain-induced flows, the high-resolution modelling system will use a triply-nested model grid, with horizontal spacings of 15 km, 2.5 km and 1 km. The inner nest is shown to be capable of resolving many of the orographic features in the Whistler/Vancouver area and of producing realistic simulations of channelled and orographically-perturbed flows.

One important component of a cloud-resolving atmospheric model is the cloud microphysics parameterization. A cloud scheme affects the model dynamics through latent heat release due to phase changes of water as well through changes to buoyancy; it interacts with the radiation scheme through its production of hydrometeor fields; and it is responsible for the prediction of precipitation phase, type, and quantity. In the Canadian high-resolution forecast system, a detailed six-hydrometeor-category double-moment bulk scheme will be used. To our knowledge, this will be the first time that a fully double-moment bulk scheme will be used for an operational forecast system such as this one. In addition to optimizing the scheme for operational use, a new approach to explicitly forecasting the solid-to-liquid ratio of precipitating snow using information provided by the microphysics scheme is being explored.

2 PROGNOSTIC SNOW DENSITY FROM THE MICROPHYSICS SCHEME

The microphysics parameterization is a modified version of the multi-moment bulk scheme described in Milbrandt and Yau (2005). The scheme was originally designed as a research tool for cloud-resolving models. It has since been adapted for operational purposes. The single-moment version of the scheme has been running in the quasi-operational Canadian 2.5-km limited-area model since April 2008 with the double-moment version being tested in the current (2009) prototype of the 2010 Winter Olympics high-resolution forecast system. Several of the modifications made to the original scheme pertain to the treatment of the snow category. To reflect a modern understanding of the proper representation of ice crystal categories, the exponent in the mass diameter relation for snow has been changed from 3 to 2, with corresponding changes to the coefficients (e.g. Mitchell, 1996). A physical implication of this is that the bulk density of snow is not longer a prescribed constant as with the previous representation of snow, as spherical particles with a constant density, but rather the density is inversely proportional to the maximum particle dimension. This is consistent with ground-based distrometer measurements (Brandes et al., 2007).

For the quantitative prediction of the depth of accumulated snowfall, most NWP systems predict the liquid-equivalent solid precipitation and then multiply it by an assumed solid-to-liquid ratio. In the current microphysics scheme, we exploit the new aspect of the representation of snow that its bulk density is a variable function of size to provide an estimate of the instantaneous solid-to-liquid ratio of precipitating snow. This quantity is equal to the ratio of the volume flux to the mass flux at the surface. With a constant bulk snow density, the fluxes are simply proportional to each other by a factor of the assumed density. Thus, for a snow density of 0.1 g cm^{-3}, for example, the solid-to-liquid ratio will be exactly 10-to-1. With a variable density, on the other hand, the ratio increases with the mean-mass diameter of the snow distribution. Thus, we are exploiting

both the variable density with the new mass-diameter relation plus the fact that a double-moment scheme can provide a better estimate of the mean-mass diameter than a single-moment scheme, since it can explicitly include processes such as aggregation and size-sorting. Estimates of the densification of snow during melting are made. For the calculation of the instantaneous solid-to-liquid ratio, we also apply the precipitation flux ratio for graupel, mass-weighted with that of snow. The effect of this is that the solid-to-liquid ratio can change with the environmental conditions. For example, if riming becomes important during a snowfall event, which is often the case in the mountainous coastal regions of the Vancouver area, there will be a shift from snow to graupel in the model which will be reflected by a decrease in the instantaneous solid-to-liquid ratio.

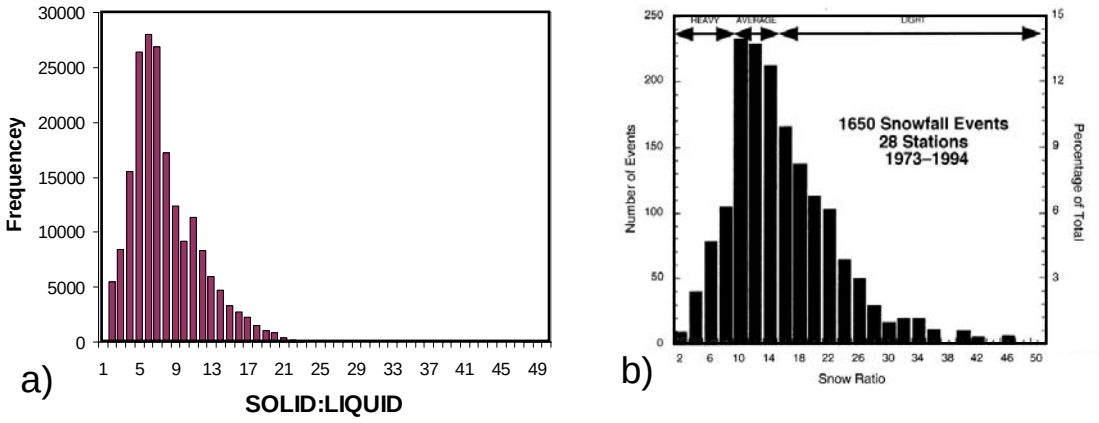

Figure 1. a) Frequency of the grid-point values of the solid-to-liquid ratio of the accumulated 12-h solid precipitation for a 2.5-km simulation of a heavy snowfall even in eastern Canada. b) Histogram of the number of observed values of a given solid-to-liquid ratio for 1650 snowfall events over 28 stations in the north-east United States during 1973-94. Reproduced from Roebber et al. (2003).

Although this work is preliminary and more comparison to observations is required to evaluate the method, the proposed approach for the prognostic solid-to-liquid ratio appears to produces a realistic range of values. For example, for a heavy snowfall even in eastern Canada, Fig. 1a shows the number of grid points with specific values of the solid-to-liquid ratio for the accumulated snowfall. For a qualitative comparison only, Fig. 1b shows the frequency of values for 21 year period over the north-east United States. Note that such observations vary with geographical location. Modification to the scheme have been made since the above simulation, such as imposing a lower limit on the slope of the snow size distribution, and the method now generally produces higher values than shown in Fig. 1a.

3 CONCLUSION

An overview of the Canadian high-resolution forecast system for the 2010 Winter Olympics will be presented along with some results from the 2009 winter practicum. This season has shown that there is indeed added value to the forecast with the high-resolution (2.5-km and 1-km) grids. The new approach for the prognostic solid-to-liquid ratio produces a realistic range of values. Comparisons of specific cases to observations will be presented.

REFERENCES

Brandes, E. A., K Ikeda, G. Zhang, M. Schonhuber, R. M. Rasmussen, 2007: A statistical and physical description of hydrometeor distributions in Colorado snowstorms using a video distrometer. *J. Applied Meteor. and Climatology.* **46**, 634-650.

Milbrandt, J. A. and M. K. Yau, 2005: A multimoment bulk microphysics parameterization. Part II: A proposed three-moment closure and scheme description. *J. Atmos. Sci.*, **62**, 3065-3081.

Mitchell, D. L., 1996: Use of mas- and area-dimensinoal power laws for determining precipitation particle terminal velocities. *J. Atmos. Sci.*, **53**, 1710-1723.

Roebber, P. J., S. L. Bruening, D. M. Schultz, and J. V. Cortinas Jr., 2003: Improving snowfall forecasting by diagnosing snow density. *Wea. and Forecasting*, **18**, 264-287.

Part B

Extended Abstracts of

Poster presentations

The order is in topical blocks as in the programme (pages *x-xvii*)
and within them numbered consecutively (nn = 01, ..., max):

Pnn	for	Precipitation Processes
Cnn	for	Climate Aspects
Bnn	for	Boundary Layer Processes
Dnn	for	Dynamical Aspects
Snn	for	Snow Pack

Observations of convection initiation and development from the Doppler on Wheels radars and comparison with high resolution WRF simulations

Lindsay J. Bennett[1], Alan M. Blyth[1,2], Tammy M. Weckwerth[3]

[1] School of Earth and Environment, University of Leeds, Leeds, UK
[2] National Centre for Atmospheric Science, UK
[3] Earth Observing Laboratory, National Center for Atmospheric Research, Boulder, Colorado, USA
E-mail: *l.j.bennett@leeds.ac.uk*

Abstract: Observations and model simulations are presented of convection initiation on IOP15a, 12 August 2007.

***K*eywords:** *convection initiation, mobile radar, WRF*

1 INTRODUCTION

Two mobile X-band Doppler on Wheels (DOW) radars were operated during the Convective and Orographically-Induced Precipitation Study (COPS). Their objectives were to (1) provide high resolution wind fields in regions not covered by the operational radar network, (2) observe areas of convergence and determine their role in the initiation of convection, and (3) observe the evolution of convective cells and the influence of the terrain on their propagation.

Observations from the DOWs during IOP15a, 12 August 2007 are presented and compared with simulations using the Weather and Research Forecasting (WRF) model. Early results show that the model simulations of the timing and location of precipitation compare well with the observations and suggest that the clouds formed as a result of converging upslope flows.

2 DATA

The location of the DOW radars are shown in Fig. 1 along with the COPS supersites, the POLDIRAD radar and the main river valleys. DOW2 was located at Hohbuhn in the Rhine Valley, whilst DOW3 was located at Schopfloch on the eastern side of the Black Forest.

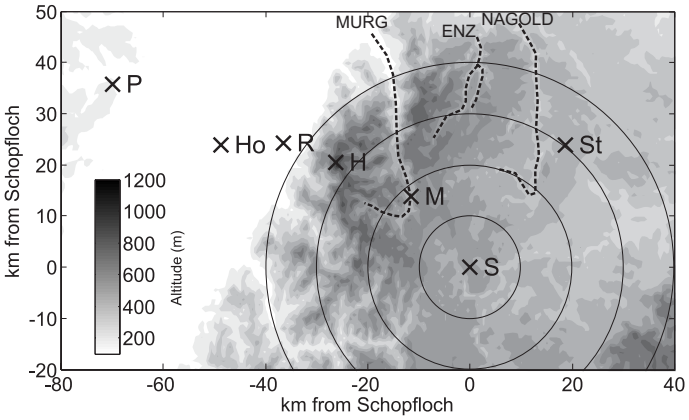

Figure 1: Map showing Black Forest topography (grey scale contours), major river valleys (black dashed lines) and site locations (crosses): Poldirad (P), Hohbuhn (Ho), Schopfloch (S), Achern (R), Hornisgrinde (H), Murg (M) and Stuttgart (St).

The Advanced Research WRF (ARW) model Version 3.0 was used to simulate this case study. The model was run with an outer domain and two higher resolution nests. The horizontal resolution of the domains were 6.3, 2.1 and 0.7 km respectively. The inner domain was centred over the COPS region. The model was run with 121 vertical levels, initialised at 0000 UTC and run for 18 hours, and the outer domain was driven by either 1°GFS or 0.25° ECMWF analyses, updated every 6 hours.

3 EARLY RESULTS

Sequences of PPI scans from DOW3 showed that small convective cells began to develop between 10 and 30 km north of the radar from approximately 1000 UTC. Larger cells developed from about 1130 UTC and examples of

these are shown in Figs. 2a and b. Satellite images reveal that shallow convective clouds were widely distributed across the northern Black Forest, but the locations of the first echoes observed by DOW3 (Fig. 2c) indicates that precipitating clouds only occurred on the eastward facing slope, between the Murg and Nagold valleys.

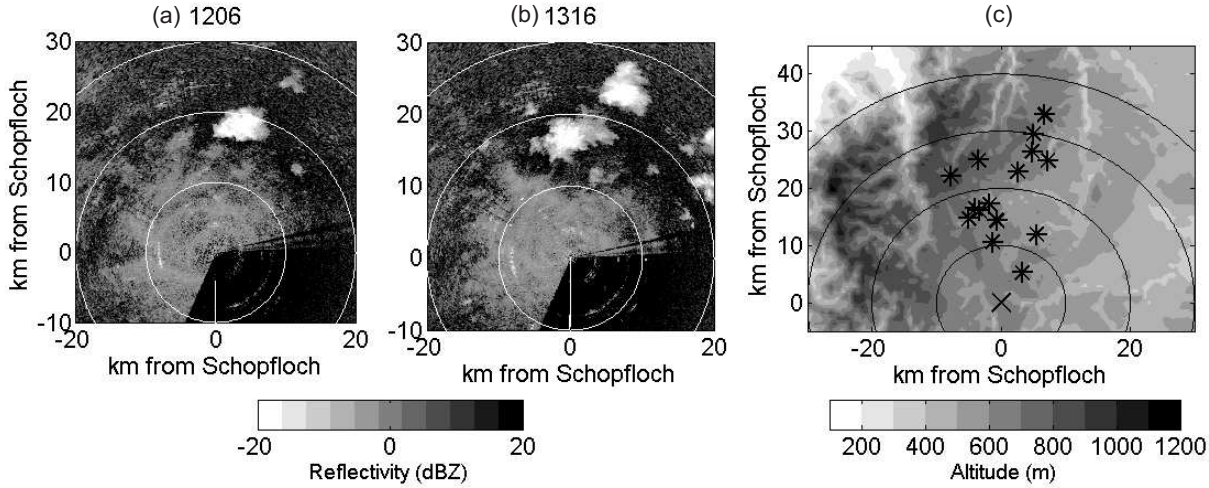

Figure 2: Examples of convective cells observed by DOW3 at (a) 1206 and (b) 1226 UTC. The location of the first precipitation echoes of all significant cells is shown in (c).

Figure 3 shows examples of simulated 10 m horizontal wind vectors overlaid on orography. At 0700 UTC down-valley and down-slope winds are occurring. The wind direction is southerly along the Murg and Nagold valleys and south-westerly along the Enz and down the eastward facing slope. By 0900 UTC, the wind direction has shifted 180 degrees to a northerly flow along the centre of the valleys and to an upslope north-easterly or north-westerly along the valley sides. These flows lead to areas of convergence that results in the development of clouds by 1000 UTC. Clouds develop widely across the northern Black Forest but those that precipitate are confined to the eastern slope (not shown).

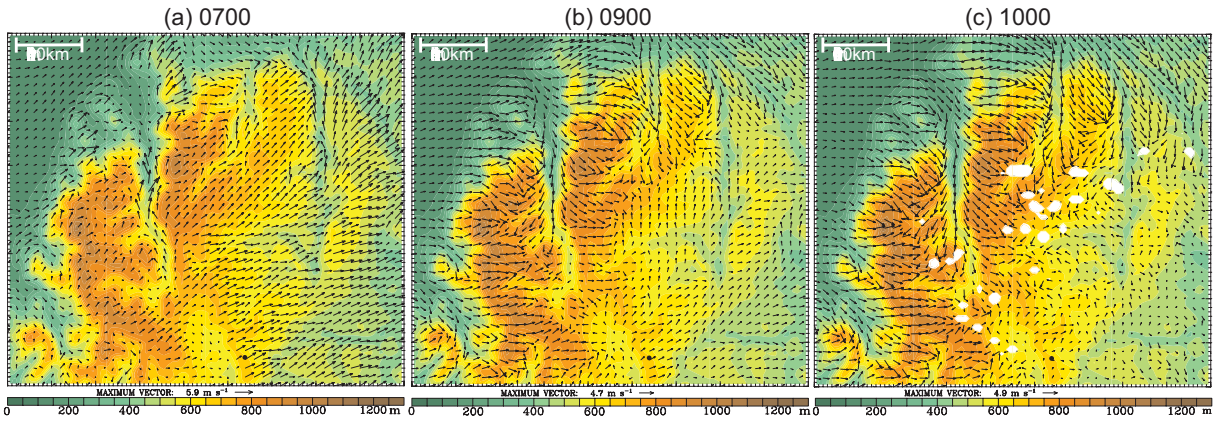

Figure 3: Output from model runs initialised with GFS analyses. A subsection of the inner domain is shown at (a) 0700, (b) 0900 and (c) 1000 UTC. The contours show orography and the vectors are the 10 m horizontal wind. The black dot marks the location of DOW3.

4 FUTURE WORK

Investigations are under way into the processes creating the convergence zones on the eastern slope. In particular, the influence of topographic shading and differential heating will be evaluated. Comparisons will also be made between the DOW observations on several other days and WRF runs to examine the ideas found in this study that the convergence lines produced by the valley flows are responsible for the initiation of precipitating convection.

CHARACTERIZATION OF THE CONVECTIVE ACTIVITY IN THE EASTERN IBERIAN RANGE, SPAIN

Samuel Buisán [1], Francisco Espejo [1], Gerardo Sanz[1]
Francisco Cortés[2], Cristina Lafragüeta[2]

[1] State Meteorology Agency (AEMET), Aragón Regional Office, Zaragoza, Spain
E-mail: *sbuisan@inm.es*
[2] SODEMASA – Environmental Department, Aragón Regional Government, Spain

Abstract: Mediterranean climates are characterized by dry summers. However, this work presents a region which, despite its being close to the Mediterranean Sea, shows a different precipitation pattern that presents a maximum between May and September. This is mainly due to the high convective activity developed in this area. The main contributing factors are the geographical situation, favourable to the appropriate synoptic weather conditions, the elevated altitude, and the convergence of two different air masses, the first one characterized by a continental dry and hot air from the central plateau of the Iberian Peninsula and the second one by cool and humid air from the sea. All these factors lead to the remarkably high number of violent storms reported.

Keywords: *Altitude, Mediterranean Sea, severe weather, mountainous area, Iberian Range*

1 INTRODUCTION

The Eastern Iberian Range, shown in Figure 1, is located in the Northeast of Spain roughly aligned in a NW-SE direction along some 400 Km. Our area of interest lies on its easternmost part, the closest one to the Mediterranean Sea, covering a surface of around 7000 km^2 in the Spanish province of Teruel, in the region of Aragón. It is a plateau-like morphology with a mean elevation of around 1500 m, reaching 2020 m at the Javalambre peak. The distance to the Mediterranean Sea is on average 50 km along its eastern side.

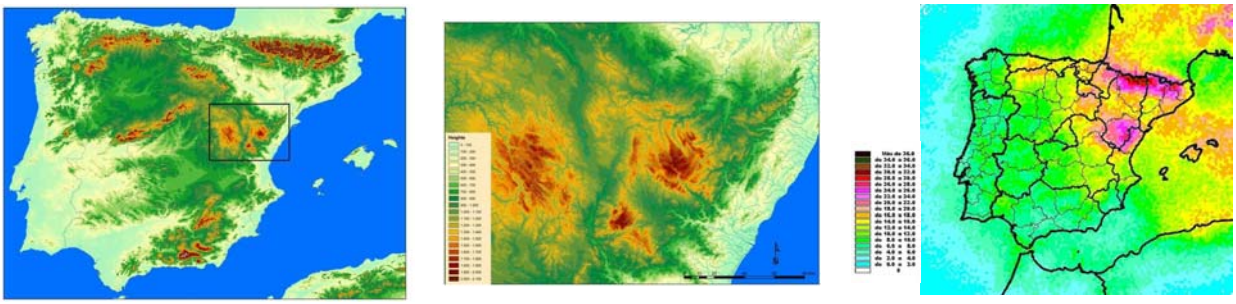

Figure 1. A and B) Eastern Iberian Range, characterized by its elevation and closeness to the Mediterranean Sea. C) Average thunderstorm days per year (2000 – 2007 period), from [1].

2 DESCRIPTION OF CONVECTIVE ACTIVITY

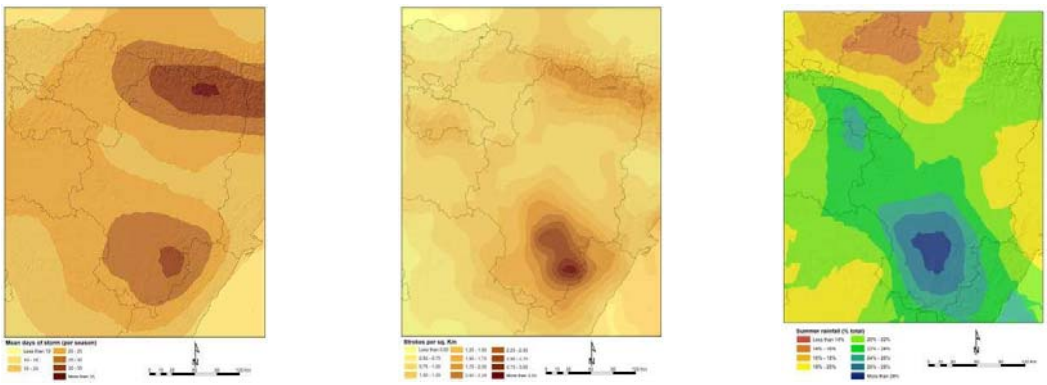

Figure 2. A) Average thunderstorm days during warm season (Apr.-Sep./2002-08) B) Flash rate density per square kilometre during the warm season (Apr.-Sep./2002-08) C) Percentage of summer rainfall from the annual mean.

This area is characterized by a significant high number of storms as shown on Figure 1C) with around 30 thunderstorm days per year, these figures are only exceeded on the Pyrenees. Most of these days are concentrated in the spring and summer months with an average of 5 thunderstorm days per month, Figure 2A). The study area is the first one in flash rate density in Spain recording an average of more than 3 cloud-to-ground flashes per km2, Figure 2B), during the warm season (Apr.-Sep.). Taking into account the number of strokes per flash, the real number of strokes could well double these figures. Comparing Figure 2A) and Figure 2B) it is clear how, in spite of the lower number of thunderstorm days on the Eastern Iberian Range, their severity is higher, fact that is also confirmed by forecasting experience. The focus of convective activity is found in the Sierra del Rayo (Lightning's Sierra), a great example of accuracy in traditional toponymy.
Finally, Figure 2C) shows how the precipitation during the summer months (JJA) accounts for around 30 percent of the annual precipitation.

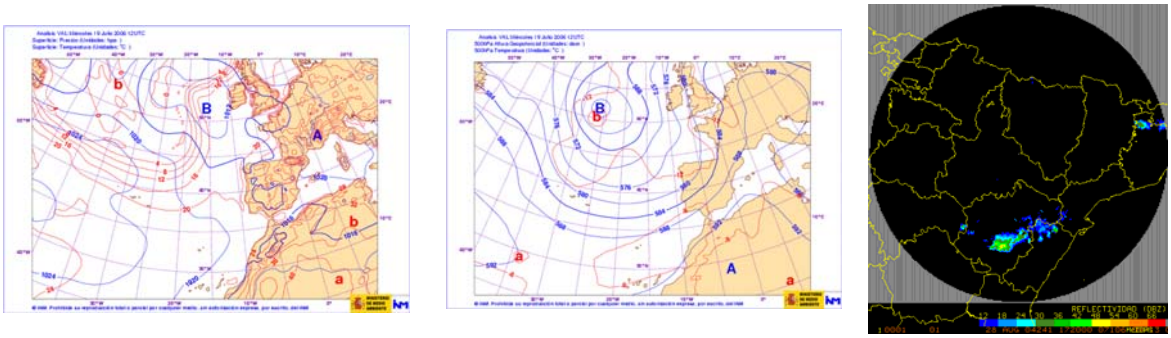

Figure 3. Typical synoptic conditions associated with severe weather. A) Surface pressure and temperature at 12 UTC (19.07.06) B) 500-hPa geopotential height and temperature at 12 UTC (19.07.06) C) Radar observed supercell (28.08.04)

Intensive heating during the warm season produces a thermal low, Figure 3A), in the centre of the Iberian Peninsula, which together with the high altitude of the region facilitates the convection. This relative low pressure enhances the ascending southeast humid low level flow from the sea providing moisture and wind shear. When midlevel instabilities and/or dynamical forcing are present, Figure 3B), all the ingredients are then favourable for severe weather to develop.

Numerous episodes of severe weather including severe thunderstorms, supercells, Figure 3C), and mesoscale convective systems, occur each season. Severe hail has been frequently observed during these episodes. Moderate and significant tornadoes have been reported, including some severe F3 tornadoes such as those of the Sierra del Rayo in 1999, near the town of Alcañiz in 2003, and Corbalán in 2004.

Flash floods are also frequent especially during cut-off low conditions over the Mediterranean Sea, particularly at the end of summer and the beginning of autumn.

3 CONCLUSIONS

This part of Spain is sparsely populated and for this reason numerous episodes of severe weather have not been reported. The expansion of human activities due to the opening of new motorways and tourism makes this area a new focus of interest, apart from the mere fact that this is probably one of the regions of Europe more prone to severe weather events. The weather forecast office of the Spanish State Meteorology Agency (AEMET) in Aragón must provide timely and accurate forecasts and must watch for severe weather giving the appropriate warnings, including fire alerts, which are issued to local emergency management and public safety officials. A deeper study of these phenomena is currently carried out in order to better understand these processes.

Acknowledgements:
Evelio Álvarez, Francisco Pérez Puebla, César Zancajo, Ramón Vazquez and Margarita Palmer (AEMET).
All the current and former staff at the weather forecast office of the Spanish State Meteorology Agency (AEMET) in Aragón.

REFERENCES

[1] Francisco Pérez Puebla y César Zancajo Rodríguez: El carácter tormentoso del año 2008 en España, 6º Simposium do APMG, Lisboa - Portugal

THE IMPACT OF CONVERGENCE ZONES ON THE INITIATION OF DEEP CONVECTION: A CASE STUDY FROM COPS

B. Adler[1], N. Kalthoff[1], Ch. Barthlott[1], U. Corsmeier[1], S. Mobbs[2], S. Crewell[3], K. Träumner[1], Ch. Kottmeier[1], A. Wieser[1], V. Smith[4]

[1] Institute for Meteorology and Climate Research, Karlsruhe Institute of Technology (KIT), Karlsruhe, Germany
E-mail: *bianca.adler@imk.fzk.de*
[2] National Centre for Atmospheric Science, Leeds, United Kingdom
[3] Institute for Geophysics and Meteorology, University of Cologne, Cologne, Germany
[4] Institute for Climate and Atmospheric Science, University of Leeds, Leeds, United Kingdom

Abstract: During the 'Convective and Orographically-induced Precipitation Study' (COPS) performed in summer 2007, deep convection developed on July 15, although convective available potential energy was only moderate and convective inhibition was high. Data analysis revealed that the convection was triggered by the optimal superposition of a mesoscale and an upslope-wind induced convergence zone.

Keywords: *boundary layer, slope winds, convection indices, convective inhibition, updraught*

1 INTRODUCTION

Development of moist convection requires some kind of instability and a trigger mechanism like i.e. mid- and upper-tropospheric lifting or forcing by planetary boundary-layer (PBL) processes. Convergence zones of different origin are important PBL phenomena which initiate deep convection (Wilson et al., 1992).

The "Convective and Orographically-induced Precipitation Study" (COPS) was performed in summer 2007 in south-western Germany (Black Forest) and eastern France (Vosges). The case study reported here deals with the interaction of different low-level convergence zones and their impact on the initiation of deep convection on July 15, 2007. To investigate the different mechanisms which were responsible for triggering convection data analysis based on radiosondes, standard meteorological instruments, aircraft measurements, and remote sensing systems was carried out.

2 SYNOPTIC CONDITIONS AND DEEP CONVECTION ON JULY 15, 2007

The COPS area was located in the transition zone between an eastern European ridge stretching from the Mediterranean Sea to Poland and a high-amplitude eastern Atlantic trough. The large-scale forcing resulted in weak lifting concentrating on the western part of the domain. Near the surface, the investigation area was in the transition zone between a surface low in the west and a surface high in the east accompanied by convergence in between. Consequently, low-level SE wind dominated in the COPS domain in the morning (Fig. 1 left). While the surface low was approaching, the area with convergence moved towards the east, such that SW wind prevailed in the PBL of the whole COPS area in the afternoon (Fig. 1 right).

The atmosphere was characterised by warm, but dry air masses which did not favour atmospheric instability. A PBL-capping inversion, a weak inversion at about 2200 m asl, and some minor mid-tropospheric inversions existed. In the Rhine valley, CAPE was small and CIN rather high. East of the Black Forest crest at Heselbach, CAPE and CIN reached moderate values. LFC was higher than 3200 m asl at all sites.

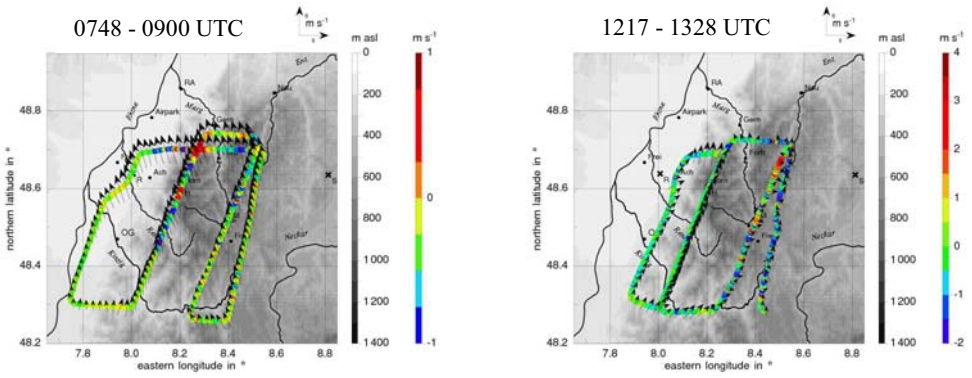

Figure 1. Horizontal wind vectors and vertical wind (colour code) as measured by the Dornier 128 aircraft on July 15.

First cumulus clouds formed over the Black Forest at about 1115 UTC. At about 1230 UTC shallow clouds were detected by satellite over the Vosges. Until 1400 UTC two cloud bands had developed over the Black Forest. During the next hour three isolated deep convective cells developed from the cloud bands. The cell southeast of Freudenstadt even developed into a mature cumulonimbus. At 1730 UTC all clouds in the COPS area had disappeared.

3 INITIATION OF CONVECTION BY BOUNDARY LAYER PROCESSES

Thermally induced wind systems developed over the Vosges and Black Forest. The resulting vertical wind of the two upslope wind systems at the western and eastern slope of the Black Forest crest, based on the continuity equation, was about 0.1 m s^{-1} at the top of the convergence zone above the Black Forest crest between 0830 and 1130 UTC. Thermally induced upvalley winds developed within the valleys of the northern Black Forest. Based on the wind profile in the Kinzig valley a rough estimate of the mean vertical wind at the top of the valley wind layer at the valley head was performed. Maximum values of about 0.5 m s^{-1} were reached between 1100 and 1300 UTC. Thus, slope and valley winds were too weak to overcome the CIN and trigger convection on this day.

To elaborate the characteristics of the mesoscale flow structure the local change of the horizontal wind was analysed: At Meistratzheim (V) and Achern (R) change of the low-level wind from SE to SW was completed at 1000 UTC and at 1030 UTC, respectively, which indicated the end of the passage of the convergence zone (Fig. 2 left). At Oberkirch (OBE) and the Hornisgrinde (H) the convergence zone had passed at 1100 UTC (Fig. 2). During its passage over the mountain crest, it optimally superimposed on the convergence zone generated by the stationary slope winds. Consequently, strong upward motion occurred which penetrated the capping inversion at 2100 m asl (Fig. 2 right) and roughly reached the LFC. The strong updraughts were accompanied by a change in the wind direction from SE to W and an increase in humidity. At Barongartenhütte (BAR), the convergence zone had passed at 1330 UTC and at Igelsberg (IGE) and Heselbach (M) at about 1400 UTC, respectively (Fig. 2 left). The humidity and temperature profiler at Heselbach showed that during the passage of the convergence zone an increase in humidity occurred up to about 4.5 km asl. Applying the continuity equation to the Heselbach wind profiler data, a mean vertical wind speed at the top of the convergence zone of 1.2 m s^{-1} resulted. The Dornier 128 aircraft measurements between 1317 and 1328 UTC revealed updraughts of about 3.5 m s^{-1} below individual convective cells within the convergence zone (Fig. 1 right).

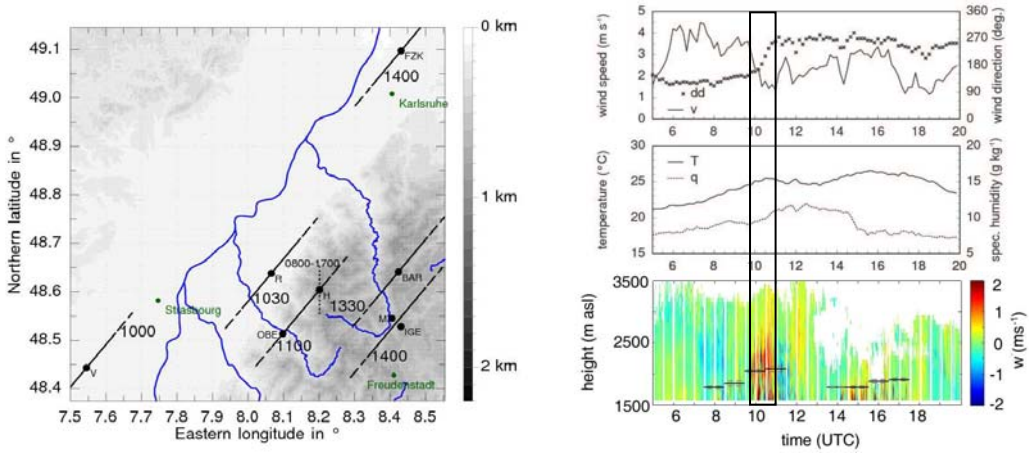

Figure 2. Left: Position and end of passage time of the mesoscale convergence zone (solid dashed lines) and duration and position of the upslope wind-induced convergence zone (dotted line). Right: Surface measurements and vertical wind speed profile measured by the wind lidar at Hornisgrinde.

4 SUMMARY

Deep convection developed on July 15, 2007 over the Black Forest. The analysis showed that an optimal superposition of an eastward moving mesoscale and a stationary upslope wind-induced convergence zone over the mountain crest initiated the convection (Kalthoff et al., 2009).

REFERENCES

Kalthoff, N., B. Adler, C. Barthlott, U. Corsmeier, S. Mobbs, S. Crewell, K. Träumner, C. Kottmeier, A. Wieser, V. Smith, P. Di Girolamo, 2009: The impact of convergence zones on the initiation of deep convection: A case study from COPS. Atmos. Res. doi: 10.1016/j.atmosres.2009.02.010.

Wilson, J.W., G.B. Foote, N.A. Crook, J.C. Fankhauser, C.G. Wade, J.D. Tuttle, C. Mueller, 1992: The role of boundary-layer convergence zones and horizontal rolls in the initiation of thunderstorms: a case study. Mon. Wea. Rev. **120**, 1785 – 1815.

INFLUENCE OF LOCAL OROGRAPHY ON FORECAST OF PRECIPITATION IN CASE OF FLASH FLOODS IN SLOVENIA ON SEPTEMBER 18, 2007

Vanja Kovač[1], Jure Cedilnik[1], Nedjeljka Žagar[2], Mark Žagar[2]

[1]Environmental Agency of the Republic of Slovenia, Ljubljana, Slovenia
[2]University of Ljubljana, Faculty of Mathematics and Physics, Chair of Meteorology, Ljubljana, Slovenia
E-mail: vanja.kovac@gmail.com

Abstract: The influence of the Slovenian orography on the ALADIN model forecasts is studied in flash flood case which occurred on September 18, 2007. Various modifications of model orography were tested, resulting in amplitude of the differences in the 24-hour accumulated rainfall around ±30 % of the precipitation amounts in the reference experiment over the same area.

Keywords: *numerical weather prediction, ALADIN model, orography modelling, extreme precipitation*

1 INTRODUCTION

On September 18, 2007 heavy precipitation occurred across the northwestern Slovenia causing severe flash floods with a death toll of 6 and the damage about 250 million Euros. Extreme precipitation was measured at many stations across the country and 24-hour cumulative amounts locally exceeded 400 mm. Precipitation occurred ahead of the cold front related to the intense low-level moisture advection from the southwest and a relatively strong vertical wind shear over the Slovenian region. The operational forecasts, while able to predict heavy rains sufficiently well so that the weather service issued the flash flood warnings, systematically underestimated the amounts of precipitation and failed to provide details of the spatial distribution.

The purpose of this study is to estimate the influence of the local orography on the operational forecasts of the mesoscale model ALADIN-SI. The emphasis is on the intensity and spatial distribution of the simulated precipitation. In order to gain a quantitative estimate of the orography impact, several sensitivity studies with altered orography are carried out and preliminary results are presented. Since the ALADIN applications used operationally in neighbouring countries had a few differences compared to the operational ALADIN-SI at the time of the flash flood event, they can be studied as a limited area ensemble; we show some results of the comparison of several ensemble members.

2 COMPARISON OF OPERATIONAL ALADIN RESULTS

We choose to present the precipitation forecast from simulations which mimic the operational ALADIN applications in Slovenia (ALADIN-SI), Croatia (ALADIN-HR) and Slovakia (ALADIN-SK). Their only difference is the horizontal resolution and the domain size. In each case the model orography was prepared using the variational approach of Bouteloup (1995). Resulting topographic features of Slovenia had somewhat different shape and height of orographic peaks. The cumulative precipitation distributions showed to be strongly correlated with the underlying orography. In each case the distribution of 30-hour cumulative precipitation resembles the models' orography (not shown). Precipitation maxima differ significantly: from 90 mm in ALADIN-SI to 107 mm in ALADIN-HR and 165 mm in ALADIN-SK (Fig. 1). Forthcoming work aims at studying in more detail methods for preparing the mesoscale model orography.

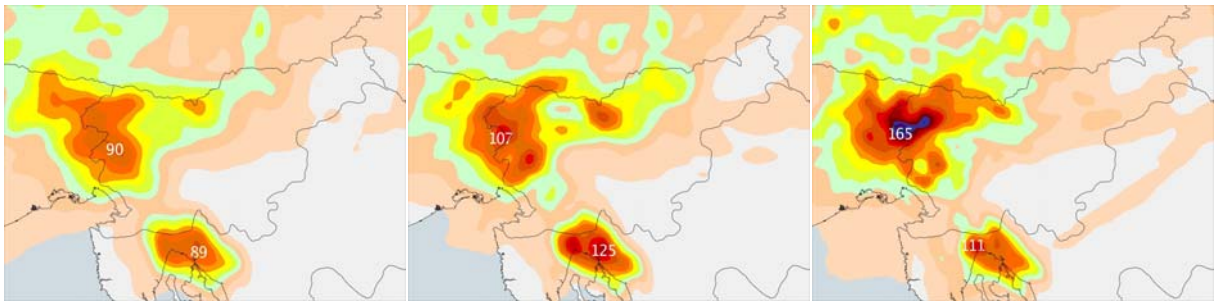

Figure 1. 30-hour accumulated precipitation at 18 UTC September 18, 2007 (contour intervals 10 mm). Left: ALADIN-SI, middle: ALADIN-HR and right: ALADIN-SK.

3 SENSITIVITY STUDIES ON THE IMPACT OF SLOVENIAN OROGRAPHY

Sensitivity studied performed 30-hour simulations starting on September 17, 2007, 12 UTC. Various experiments tested the impact of different mountains across the northwestern Slovenia. For these experiments, we

applied a more recent, ALARO version of ALADIN model, which includes a set of new physical parametrizations. Sensitivity experiments varied from removing or lowering down selected mountains to removing the whole mountain system such as the Kamnik Alps. The reference orography and two examples of the orography used in sensitivity simulations, denoted NO_JKA and NO_KA, are presented in Fig. 2.

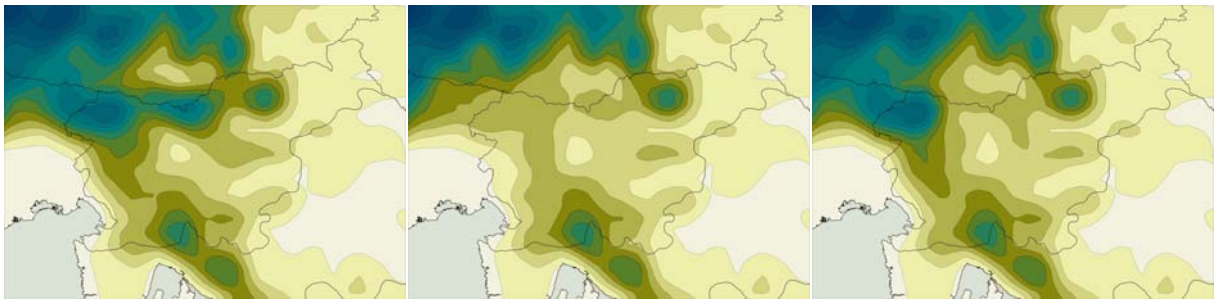

Figure 2. Examples of the orography used in sensitivity experiments (contour intervals 200 m). Left: reference orography (REFR), middle: experiment in which the Julian and the Kamnik Alps were removed (NO_JKA), right: experiment without the Kamnik Alps (NO_KA).

As expected, results show that the orography considerably impacts the moist and potentially unstable flow in the lower troposphere and so the location and amounts of precipitation. The position and strength of the low-level convergence zone ahead of the front are defined by the orography. The spatial distribution of the differences between the reference and sensitivity experiments agrees well with the changes in the terrain (Fig. 3 versus Fig. 2). When the terrain is raised the airflow slows down, and in the opposite case, when new gaps open the airflow accelerates. In the former case the precipitation increases on the windward side while in the latter case more moisture reaches areas behind the original terrain. Compared with the REFR experiment which produced up to 135 mm of rain within 24 hours, the precipitation in the NO_KA experiment changed between -40 mm to +22 mm. In the NO_JKA experiment the change with respect to REFR varied between -33 mm and +43 mm. The orography impact on the precipitation distribution is limited to the surroundings of the modified terrain (Fig. 3).

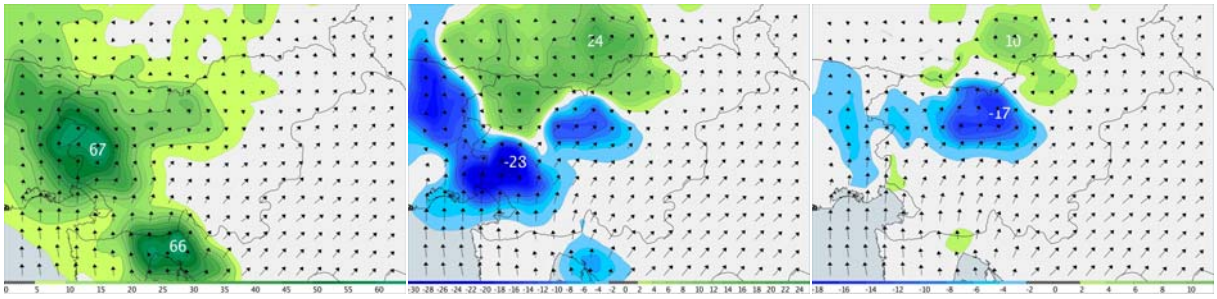

Figure 3. 10 m wind field and 18-hour accumulated precipitation at 12 UTC September 18 for three experiments: REFR (left), NO_JKA (middle) and NO_KA (right). For experiments NO_JKA and NO_KA the precipitation difference with respect to reference (REFR) is shown. The largest arrows represent wind speed of 12 m/s.

4 OUTLOOK

We are working on additional experiments at higher resolution to perform more in-depth study of the model sensitivity to the details of the terrain representation.

REFERENCES:

Bouteloup, Y., 1995: Improvement of the spectral representation of the earth topography with a variational method. Mon. Wea. Rev. **123,** 1560–1574.

Kovač, V., 2008: The influence of local orography on the precipitation forecast with ALADIN for 18 September 2007. Bsc Thesis, University of Ljubljana (In Slovenian), 58 pp.

Piriou, J.-M., Redelsperger, J.-L., Geleyn, J.-F., Lafore, J.-P. and Guichard, F., 2007: An Approach for Convective Parameterization with Memory: Separating Microphysics and Transport in Grid-Scale Equations. J. Atmos. Sci. **64**, 4127-4139.

Žagar, M., 2008: Analysis of causes and numerrical modelling of heavy precipitation on 18 September 2007. Ujma **22**, 101-104.

THE OROGRAPHIC IMPACT ON PATTERNS OF EMBEDDED CONVECTION DURING THE AUGUST 2005 ALPINE FLOOD

Wolfgang Langhans[1], Alexander Gohm[2], Günther Zängl[3]

[1] Institute for Atmospheric and Climate Science, ETH Zurich, Switzerland
[2] Institute of Meteorology and Geophysics, University of Innsbruck, Austria
[3] DWD, Offenbach, Germany
E-mail: *wolfgang.langhans@env.ethz.ch*

Abstract: Convective precipitation structures during a heavy Alpine precipitation event in August 2005 are investigated utilizing a mesoscale non-hydrostatic numerical model and observational data. The focus is on the mechanism of convective initiation during the very beginning of the event, when organized cellular updrafts enhanced the precipitation. A set of sensitivity experiments with systematically modified topography is conducted in order to investigate the role of single topographic obstacles in initiating and arranging convection.
***K*eywords:** *banded convection, August 2005 Alpine flood, orographic precipitation*

1 INTRODUCTION

The August 2005 heavy precipitation event has been selected for investigations, as it features a period of intense embedded convective precipitation, which resulted in locally intensified rainfall. The convective cells are embedded in the northeasterly low-level jet and cause heavy precipitation over the low-mountain terrain in southern Germany and northern Alpine slopes during an early stage of the event. Furthermore, observations and simulations suggest that these downstream propagating convective cells become aligned in a banded manner (Langhans, 2008). Previous studies highlighted the potential of convective bands to enhance precipitation in mountainous regions (e.g., Cosma et al., 2002; Fuhrer and Schär, 2007; Kirshbaum et al., 2007). In this study the mechanisms of convective initiation during the period of interest are determined, whereby special attention is also given to the influence of topographic obstacles. Therefore, numerical experiments with partly removed or flatened orography and others with additional idealized orographic obstacles are performed.

2 EXPERIMENTAL SETUP

The Weather Research and Forecasting modeling system (WRF) is used for numerical simulations. Three two-way nested model domains are used with a horizontal mesh size of 30 km, 10 km, and 2 km, respectively. The innermost domain encloses the Alpine area, i.e., Switzerland, Austria, and the German Alpine foreland. Convective clouds are treated explicitly within this model domain. The initial and boundary conditions are obtained from the European Centre for Medium Range Weather Forecasts (ECMWF) operational analysis. Several sensitivity simulations are conducted using modified topography. The reference run (REF) uses a 30" orography in the innermost domain. The influence of individual mountain ridges is explored by the experiments NOBF and NOSA, in which the Bavarian Forest and the Swabian Alb, respectively, are removed. Within the NOALPS run the terrain elevation in the innermost Alpine domain is limited to 500 m, which completely removes the Alpine arc. Idealized ridges are added to the flatened NOSA topography in two experiments: with respect to the Swabian Alb, in the ADDRIDGE1 run the ridge is located slightly further north, whereas in the ADDRIDGE2 simulation the ridge is right at its original location. The simulated precipitation fields are validated against a dense network of daily rain gauge measurements and the CERAD (Central European Weather Radar Network) radar composite.

3 RESULTS

Two precipitation bands are observed by the CERAD radar measurements (not shown) over the northern Alpine foreland. Also rain gauge records indicate these banded regions of relatively high daily accumulated precipitation (see Fig. 1a). The REF run reproduces these patterns over southwestern Germany very well (see Fig. 1b). Compared to the radar product the REF simulation shows a qualitatively similar development of precipitation structures. Convective cells become aligned and form two flow-parallel bands during the afternoon of 21 August. The REF simulation reveals the presence of two low-level convergence lines, which are the driving mechanism for initiating the cells in this banded manner. The northern band is located over the Swabian Alb, while the southern band seems to trail downstream of the Bavarian Forest. However, removing specific mountain ranges (NOBF, NOSA) results in small modifications of the spatial distribution and intensity of daily accumulated precipitation and the

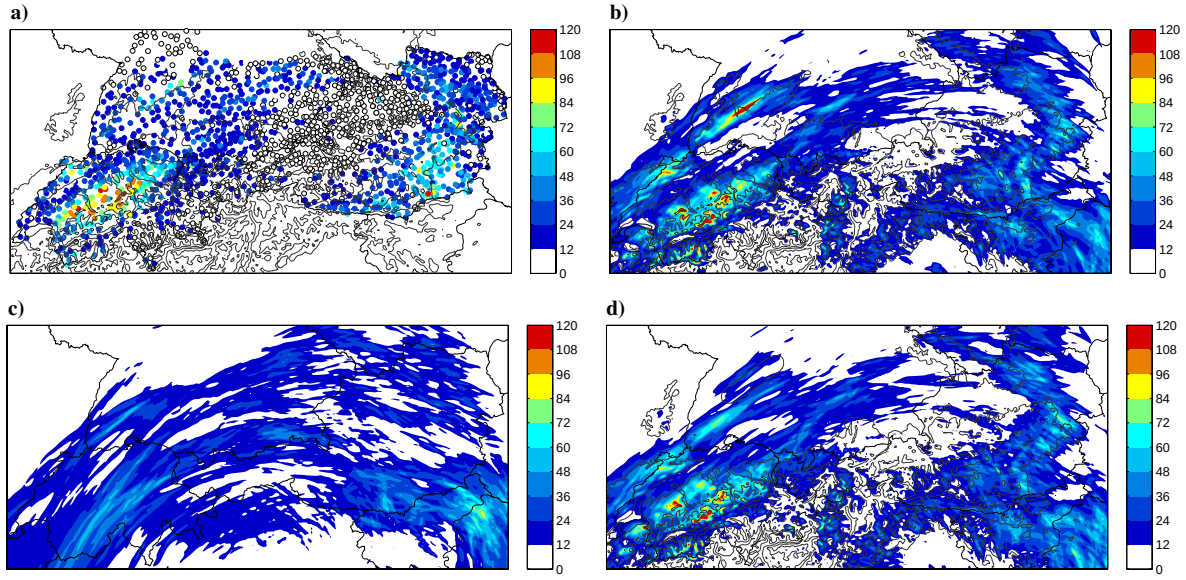

Figure 1: Daily accumulated precipitation (mm) over the northern Alps between 0600 UTC 21 August and 0600 UTC 22 August 2005 from (a) rain gauge measurements, (b) REF, (c) NOALPS, and (d) ADDRIDGE1. Orography is indicated every 1000 m.

arrangement of the cells appears even more banded. Only the NOALPS simulation (see Fig. 1c) shifts the position of both convergence lines, thereby modifying the regions of convective updrafts.

Further knowledge about the impact of the Swabian Alb on the convective initiation in the northern convergence line is gained from ADDRIDGE1 and ADDRIDGE2. The former, in which the convergence line is positioned slightly to the south of the ridge, produces much higher convective inhibition, that results in less continuous triggering in the convergence zone, scattering and weakening of convective updrafts (see Fig. 1d). ADDRIDGE2, in which the position of the ridge is in phase with the position of the convergence line, retains the banded shape and intensity of convection.

4 CONCLUSIONS

A primary mechanism for both the initiating and aligning of convective cells over the northern Alpine foreland during the afternoon of 21 August 2005 is given by the presence of two synoptically forced low-level convergence lines. A sensitivity study reveals no significant influence of mountains, as the primary mechanism consistently triggers moist convection at the same locations. However, the experiments show that the orography (e.g., Swabian Alb) constitutes a secondary mechanism for triggering convection. Enhancement (weakening) of the alignment of convective cells is achieved, when the convergence line is located above (next to) a ridge.

Acknowledgements: *Rain gauge data was provided by the national weather services ZAMG, DWD, MeteoSwiss, and by the Austrian hydrological service HZB. Thanks to all weather services contributing to the CERAD product, especially to Kurt Zimmermann (ZAMG). The Central IT Services (ZID) as well as the High-Performance-Computing (HPC) Consortium of the University of Innsbruck are acknowledged for access to their Linux Compute Clusters.*

REFERENCES

Cosma, S., E. Richard, and F. Miniscloux, 2002: The role of small-scale orographic features in the spatial distribution of precipitation. *Quart. J. Roy. Meteor. Soc.*, **128**, 75–92.

Fuhrer, O., and C. Schär, 2007: Dynamics of orographically triggered banded convection in sheared moist orographic flows. *J. Atmos. Sci.*, **64**, 3542–3561.

Kirshbaum, D.J., G. Bryan, and R. Rotunno, 2007: The triggering of orographic rainbands by small-scale topography. *J. Atmos. Sci.*, **64**, 1530–1549.

Langhans, W., 2008: Cloud-resolving simulations of the August 2005 Alpine flood: the sensitivity to microphysics parameterizations. Master's thesis, University of Innsbruck, 114 pp.

ANALYSIS OF DIFFERENT ALADIN FORECAST RUNS FOR THE FLASH FLOOD CASE IN SLOVENIA, 18 SEPTEMBER 2007

Jože Rakovec[1], Rahela Žabkar[1] and Mark Žagar[1,2]

[1]University of Ljubljana, Faculty of Mathematics and Physics, Chair of Meteorology, Ljubljana, Slovenia
E-mail: *joze.rakovec@fmf.uni-lj*
[2]Vestas Wind Systems A/S, Randers, Denmark; and part time with UL FMF

Abstract: The strong precipitation case of September 18th, 2007 in Slovenia is analyzed as regards the different forecast lead times. Relevat characteristics for strong precipitation are studied along the trajectories leading to the location of the event.

Keywords: *precipitation, convection, orographic enhancement, flash flood*

On the 18 September 2007 extreme prefrontal precipitation in Julian Alps, extending also to Kamnik Alps, caused severe floods in Slovenia. Heaviest rainfall occurred ahead of the cold front passing Slovenia in the evening of that day. The 24-hours precipitation accumulation, measured with rain gauges exceeded 300 mm (Figure 1). Radar measurements offered information that strong prefrontal convection was repeatedly forming at the upslope side of the orographic obstacles in the impinging SW flow (Figure 2): the main reasons for strong precipitation were constant inflow of moist and conditionally unstable air from southeast, wind shear in higher atmospheric layers, and the terrain complexity.

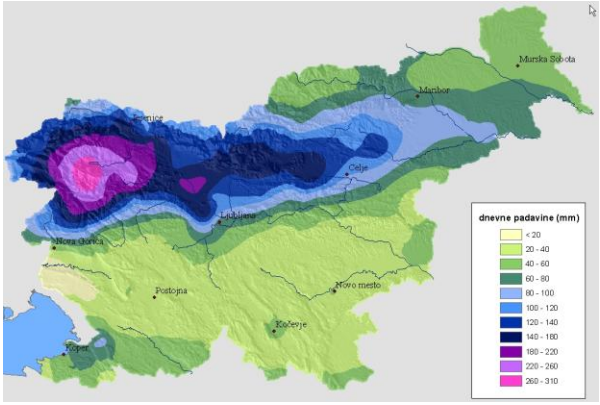

Figure 1 The 24-hour precipitation accumulation measured with rain gauges.

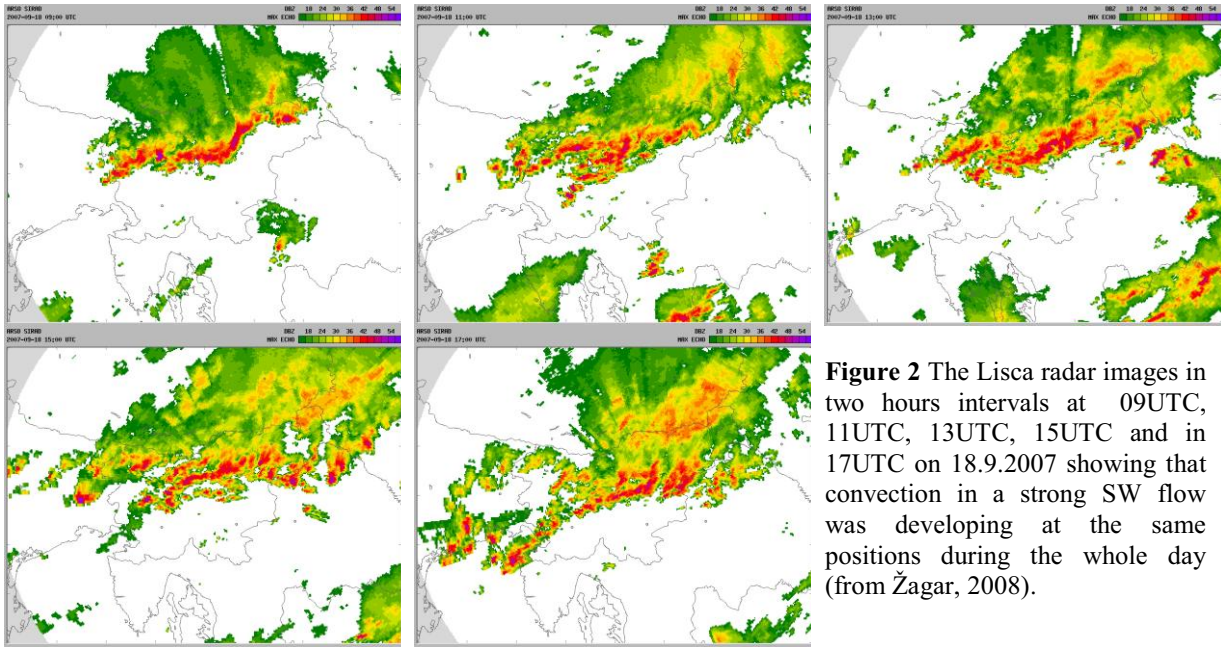

Figure 2 The Lisca radar images in two hours intervals at 09UTC, 11UTC, 13UTC, 15UTC and in 17UTC on 18.9.2007 showing that convection in a strong SW flow was developing at the same positions during the whole day (from Žagar, 2008).

The operational limited area hydrostatic model ALADIN at Environmental Agency of Republic of Slovenia with 9 km resolution forecasted the precipitation occurrence for September 18 well, but not its quantity and the intensity. The rate of precipitation underestimation varied from one model's run to another, reaching 200 mm for the 24 hours precipitation accumulation.

In the present study we evaluate and compare forecasts with different lead-time (+72, +60, …, +12 hours ahead) of operational ALADIN model for the September 18 (Figure 3). With comparison of 3D trajectories calculated for different forecast runs we focus on relation between the accuracy of precipitation forecast and representation of moist air advection in numerical prediction (Figure 3).

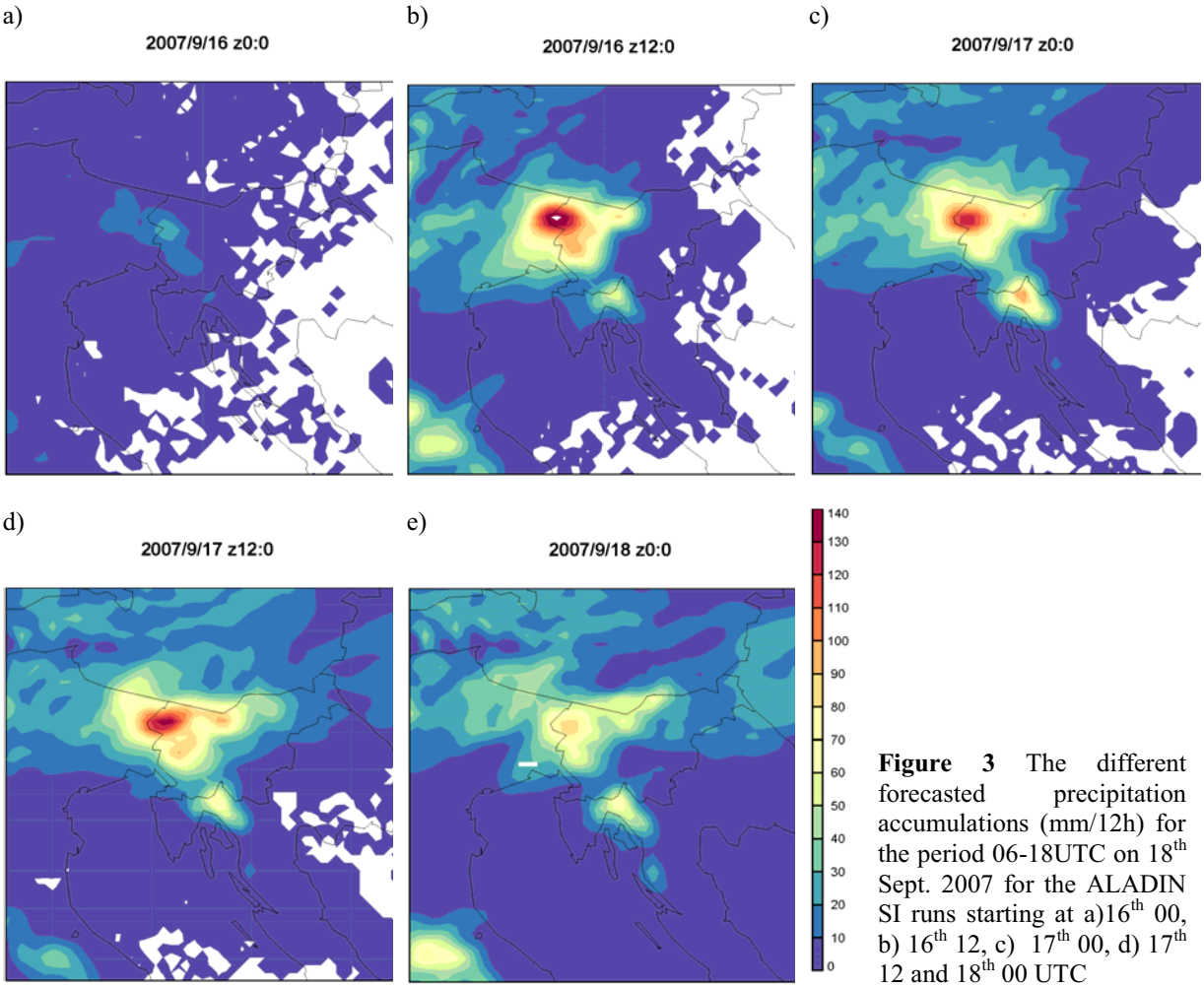

Figure 3 The different forecasted precipitation accumulations (mm/12h) for the period 06-18UTC on 18th Sept. 2007 for the ALADIN SI runs starting at a)16th 00, b) 16th 12, c) 17th 00, d) 17th 12 and 18th 00 UTC

The moisture divergence, equivalent potential temperature, CAPE etc. at different levels along these trajectories reveal the main differences between the forecasts, and so contribute to the explanation of different forecasts of precipitation amount by different forecast runs. These results (more details in poster) we evaluate in the light of the other possible sources of different lead-time forecast error and compare them with some other sources of uncertainties, e.g. representation of orography in the model (Kovač, 2008).

REFERENCES

M. Žagar, 2008: Analiza vzrokov in numerično modeliranje močnih padavin 18. septembra 2007 = Analysis of causes and numerical modelling of heavy precipitation on 18 September 2007. *Ujma (Ljublj.)*, **22**, 101-104.

V. Kovač: The influence of local orography on the precipitation forecast with ALADIN for 18. Sept. 2007, (Diploma work at UL FMF, supervisor: N. Žagar, in Slovenian), 58 pp.

THE IMPACT OF MULTI-SCALE SYSTEMS ON FREEZING RAIN AND SNOW STORMS OVER SOUTHERN CHINA

Jianhua SUN and Sixiong ZHAO
Institute of Atmospheric Physics, Chinese Academy of Sciences, Beijing，China
Email: sjh@mail.iap.ac.cn

Abstract: Synoptic weather patterns, quasi-stationary fronts, surface conditions, and stratification associated with severe freezing precipitation and snow storms during January-February 2008 are diagnosed in this paper. The impact of multi-scale systems on freezing rain and snow storms over southern China are obtained.

Keywords- *quasi-stationary front, freezing rain, stratification*

1 INTRODUCTION

Freezing precipitation, including freezing drizzle (FZDZ), freezing rain (FZRA), and ice pellets (IPE) (Carrière et al., 2000; Bernstein, 2000), is a major hazard that impacts many economic and social activities. During 11 January – 2 February 2008, record damage (since 1950) from snow and freezing precipitation occurred over southern China. Four periods of heavy snowfall and freezing precipitation occurred continuously over southern China: 0000 UTC 11 – 0000 UTC 17 January, 0000 UTC 18- 0000 UTC 22 January, 0000 UTC 25 – 0000 UTC 30 January and 0000 UTC 31 January – 0000 UTC 02 February. The persistent of snowfall and freezing precipitation affected transportation, electric power, communication, agriculture, and forestry seriously. In paper, we will try to get some answer for following questions. What kind of large-scale circulation is responsible for sustaining freezing precipitation? What are the impacts of the quasi-stationary front on the formation of freezing precipitation and the snow storm? What is favorable surface and stratification for the formation of freezing precipitation in southern China.

2 RESULTS

2.1 The synoptic weather pattern for the four periods

The long period anomaly of the atmospheric circulation is one of the important reasons for the freezing precipitation and snow storms. For example, the blocking high pressure (BHP) in the middle latitudes was located near west Siberia for more than 20 days, and also the west Pacific Subtropical High (WPSH) was to the north and west of its normal position. There was a transverse trough between the BHP and WPSH, which is very favorable to the southward invasion of cold air from North China. The BHP and trough in middle latitudes existed from the lower to upper troposphere, and could be found clearly even at 200hPa. The trough (disturbance) in the south branch (TSB) of the westerlies stayed for a long period and was very active. The southwest current ahead the TSB can transport very rich moisture to the Chinese continent. Cold/dry air from the north and warm/moist air from the south converged toward each other, and then the favored environment for snowfall and freezing rain could appear in different areas at different stages.

2.2 The quasi-stationary front

The east-west oriented quasi-stationary front (or shear line) located in southern China was the most important system producing freezing rain and the snow storms. This kind of quasi-stationary front has hardly been observed before during wintertime. The position of the stationary front is, to some extent, similar to that of the Meiyu front in summer. The denser isolines of pseudo-equivalent potential temperature and higher temperature of inversion were in the west part of front, thus, of the conditions of west front was more favorable for the formation of freezing precipitation. The strongest moisture convergence occurred ahead of the front at low levels and then climbed slantwise along the front to the middle troposphere.

2.3 The surface conditions and the stratification associated with freezing precipitation

The formation of freezing rain was very sensitive to some key influencing factors. The preferred ground surface temperature for freezing rain was from - 1 to - 3℃. The warm layer and inversion existed while freezing rain occurred, and at the same time, the formation of freezing rain was sensitive to both the thickness of the warm layer and the near surface frozen layer. The incomplete melting of snowflakes in the warm layer may be the mechanism of ice pellet formation. In addition, the warm rain and melting processes could be the mechanisms of freezing rain formation.

Finally, one kind of the conceptual model for multi-scale systems that sustain freezing precipitation has been proposed (Fig.1), including the synoptic conditions, details of the quasi-stationary front, and the sounding profiles associated with freezing rain and ice pellets.

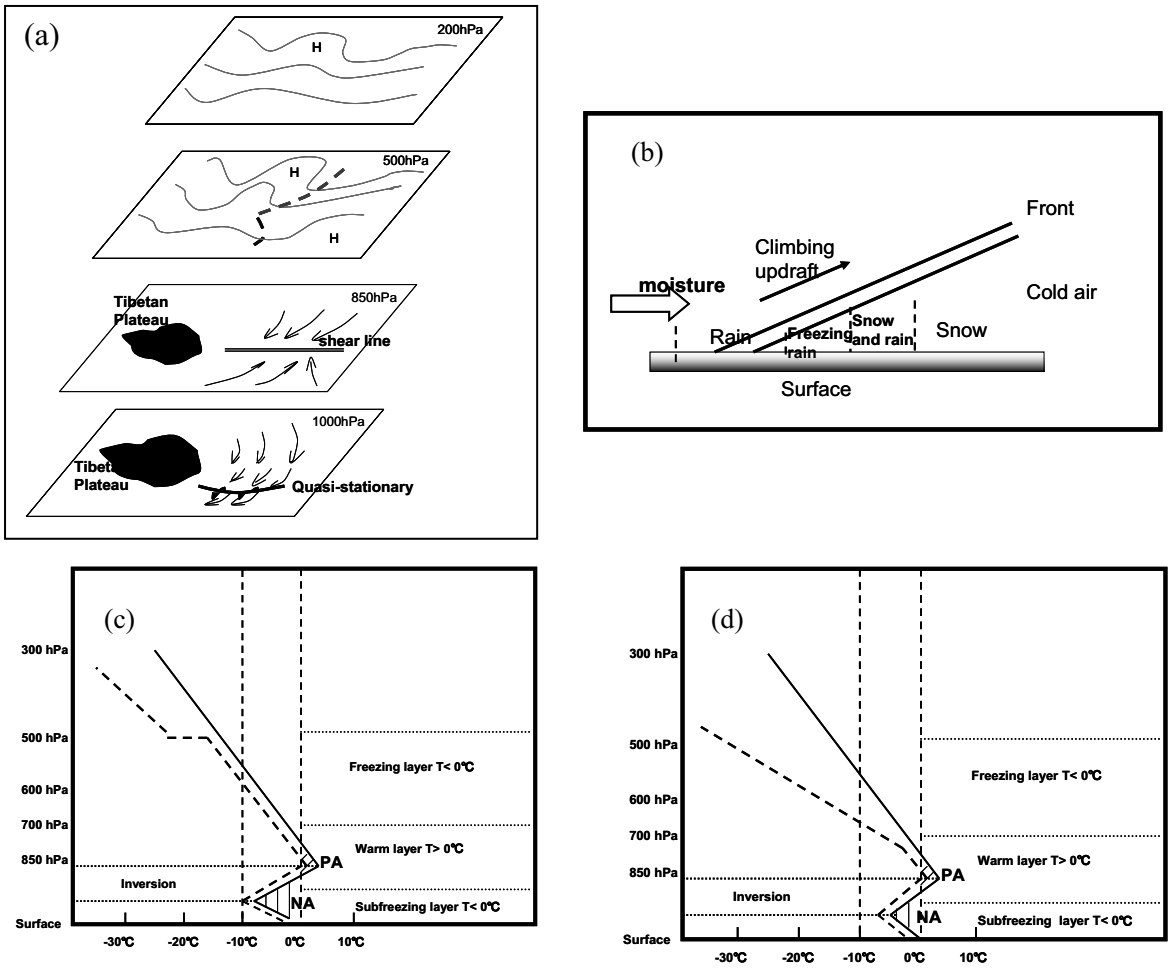

Fig.1 The multi-scale conceptual model for sustaining freezing precipitation in southern China: (a) The synoptic weather pattern, (b) the structure of quasi-stationary front, (c) the stratification condition for ice pellet and for (d) freezing rain

3 CONCLUSION

A long duration of freezing precipitation was caused by stationary and anomalous synoptic weather patterns, such as a blocking high pressure system and the trough in the south branch of westerlies, which induced the meeting of cold air from the north and warm, wet air from the south in southern China.The conditions of west part of front were very favorable for the formation of freezing precipitation. The moisture convergence occurred ahead of the front at low levels and then lifted slantwise along the front up to the middle levels. Favorable conditions at the ground surface for freezing precipitation occurred with temperature at about - 1 ~ - 3℃ and weak wind. The warm layer and inversion layer existed while freezing rain occurred.

Acknowledgements: *This research was supported by the National Natural Science Foundation of China under Grant No. 40875021 and 40605016, and foundation of Institute of Heavy Rain, China Meteorological Administration, Wuhan*.

REFERENCES

Bernstein, B. C., 2000: Regional and local Influences on freezing drizzle, freezing rain, and ice pellet events. *Wea. Forecasting*, **15,** 485–508.

Carrière, J. M., C. Lainard, C. Le Bot, and F. Robart, 2000: A climatological study of surface freezing precipitation in Europe. *Meteorol. Appl.*, **7,** 229–238.

MISREPRESENTATION OF THE SEEDER-FEEDER MECHANISM BY KESSLER-TYPE AUTOCONVERSION SCHEMES

Günther Zängl, Axel Seifert

Deutscher Wetterdienst, Offenbach, Germany
E-mail: *Guenther.Zaengl@dwd.de*

Abstract: Idealized simulations of moist flow over narrow isolated mountains have been conducted to investigate the ability of various autoconversion schemes to adequately represent the seeder-feeder effect, which in particular requires that no significant amounts of rainfall are generated in the absence of seeding. From the considered schemes, the Kessler scheme is found to have the largest deficits in this respect.

***K*eywords:** *Orographic precipitation, seeder-feeder mechanism, cloud microphysics*

1 INTRODUCTION

The seeder-feeder mechanism, i.e. local intensification of larger-scale (frontal) precipitation within orographic clouds, is known to be one of the most important mechanisms of orographic precipitation. The relevance of the ambient precipitation lies in the different microphysical time scales for autoconversion and accretion. Autoconversion, i.e. initiation of rain due to the coalescence/collision of cloud drops, has a typical time scale of 15–30 min depending on the cloud water density and the number concentration of cloud droplets. In comparison, precipitation growth due to accretion of cloud water by rain or frozen precipitation particles is a much faster process. This implies that for given ambient conditions, narrow mountain ridges may not receive significant precipitation amounts in the absence of ambient precipitation, but experience a marked local rainfall intensification when seeding is present. To obtain realistic simulated precipitation amounts at very high resolution ($\Delta x \lesssim 1$ km), it is thus important to reasonably discriminate between the microphysical timescales of autoconversion and accretion. Here, we focus on idealized simulations of moist flow over isolated mountains, investigating the precipitation amounts occurring in the absence of seeding. Ideally, these should exhibit a marked dependence on the mountain width, getting very small when the advective timescale for the flow over the mountain is smaller than the microphysical conversion time.

2 MODEL SETUP

The simulations presented here have been conducted with the Penn State/NCAR mesoscale model MM5, using (depending on the mountain width) three or four interactively nested model domains with a finest horizontal mesh size of 2250 m and 750 m, respectively. The model topography consists of four isolated mountains with a height of 400 m, 800 m, 1200 m and 1600 m, respectively, and a base-to-base width of about 36 km (12 km) in the wide-mountain (narrow-mountain) case. The atmospheric conditions assumed in the simulations involve a weakly moist stable ridge-normal flow with positive shear from 12.5 m s^{-1} at sea level to 25 m s^{-1} at tropopause level, and constant wind speed higher above, and a nearly saturated moisture field up to a pressure of 400 hPa. Two weakly moist stable temperature profiles are considered with freezing levels at 2300 m (denoted as T1) and 1500 m (T2), respectively. Thus, the ice phase does not play a significant role in precipitation initiation. Taking into account some upstream deceleration, the time required for the flow to cross the windward slope of the mountain is about 30 min (10 min) in the wide-mountain (narrow-mountain) case, so that only small amounts of precipitation should be generated in the latter one. The simulations use a PBL parameterization to account for surface friction and a mixed-phase microphysics scheme including graupel (Thompson et al., 2004). By default, this scheme uses the Berry and Reinhardt (1974) parameterization for autoconversion, which is based on the stochastic collection equation. Sensitivity tests consider the simple Kessler-type parameterization implemented in older versions of this scheme and the more recent Seifert and Beheng (2001) parameterization, in which both autoconversion and accretion are derived from the stochastic collection equation. In the simulation acronyms used in the following, we will use BR, KES and SB to refer to these parameterizations.

3 RESULTS

The results of our simulations are presented in Fig. 1. Apart from a general precipitation increase with mountain height, all cases considered here exhibit higher precipitation maxima for the wide mountains than for the narrow mountains. The latter is opposite to the respective dependence of the condensation rate, which is proportional to the slope (and thus inversely proportional to the mountain width) at least at low levels where gravity-wave

effects are weak. This implies that for all microphysical schemes considered here, the dependence of the simulated precipitation amounts on the mountain width has the expected sign.

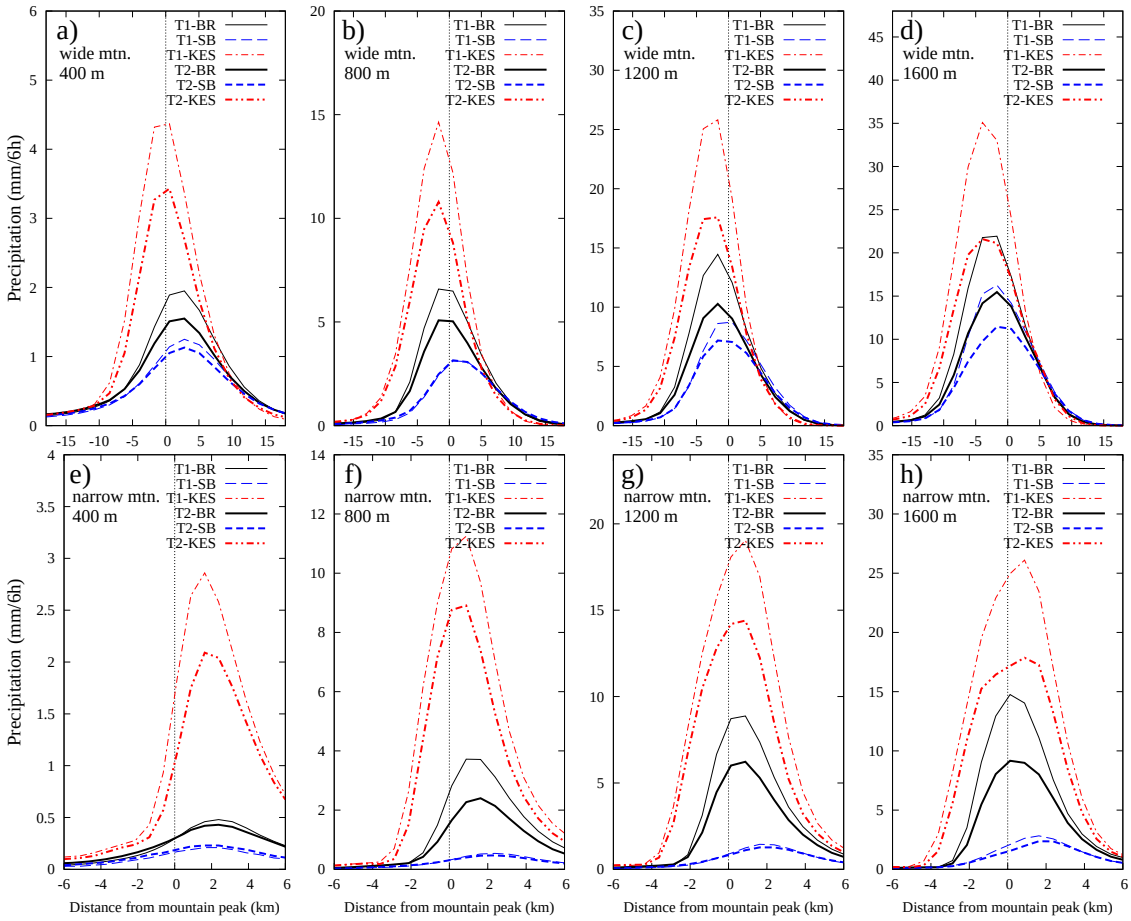

Figure 1: 6h-accumulated precipitation for wide (top) and narrow (bottom) mountains with a height of (a,e) 400 m, (b,f) 800 m, (c,g) 1200 m and (d,h) 1600 m. See text for explanation of simulation acronyms.

Nevertheless, there are tremendous differences between the autoconversion schemes, which in turn depend on the mountain width and height. While the KES scheme always produces the highest rainfall amounts, the more physically based BR and SB schemes are reasonably close together for the wide mountains. In that case, the relative difference between the two latter schemes does not show a clear dependence on mountain height. However, the additional precipitation produced by the KES scheme is, in relative amounts, largest for the lowest mountain (Fig. 1a). For the narrow mountains, the discrepancies between the autoconversion schemes become even more pronounced. The rainfall amounts obtained with the KES scheme now exceed those produced by the SB scheme by roughly one order of magnitude. The differences between BR and SB are now also much larger than for the wide mountains, with a clear tendency to increase with increasing mountain height.

4 CONCLUSIONS

As a conclusion, we note that the KES scheme does not appear to be suitable for simulating the seeder-feeder effect, because it still produces unrealistically large amounts of rain in the absence of seeding and thus does not allow for a proper discrimination between the seeding and no-seeding regimes.

REFERENCES

Berry, E. X., and R. L. Reinhardt, 1974: An analysis of cloud drop growth by collection: Part IV. A new parameterization. *J. Atmos. Sci*, **31,** 2127–2135.

Thompson, G., R. M. Rasmussen, and K. Manning, 2004: Explicit forecasts of winter precipitation using an improved bulk microphysics scheme. Part I: Description and sensitivity analysis. *Mon. Wea. Rev.*, **132,** 519–542.

Seifert, A., and K. D. Beheng, 2001: A double-moment parameterization for simulating autoconversion, accretion and selfcollection. *Atmos. Res*, **59-60**, 265–281.

WATER VAPOR FIELDS RETRIEVE WITH TOMOGRAPHY SOFTWARE

Mathieu Reverdy[1], J. Van Baelen[1], A. Walpersdorf[2], G. Dick[3], M. Hagen[4], E. Richard[5]

[1] Laboratoire de Météorologie Physique, Aubière, France
E-mail: *m.reverdy@opgc.univ-bpclermont.fr*
[2] Laboratoire de Géophysique Interne et Tectonophysique, Grenoble, France
[3] GeoForschungsZentrum-GFZ, Potsdam, Germany
[4] DLR Oberpfaffenhofen, Wessling, Germany
[5] Laboratoire d'Aérologie, Toulouse, France

Abstract**:** As part of the COPS campaign, a GPS project as collected data during the summer period of 2007 to study water vapor in Rhine valley. An initial GPS network has been deployed with 50 GPS stations (including a dense area of 16 GPS stations) to study water vapor density through a GPS tomography software. In addition, rain data were provided by two different radar.

Keywords: *ICAM, Water vapor, tomography, GPS, inverse problem*

1 INTRODUCTION

Water vapor is a very important parameter in atmospheric sciences. However, due to the spatial and temporal variability of water vapor, it is a parameter which is difficult to estimate with classical methods. Since few decades, this quantity can be estimated using remote sensing technologies as for example radio sounding, spectrometers, lidars, radiometers, and so on. Since the early 90's, researchers have focused on the study of the water vapor using the Global Positioning System. Indeed, the GPS offers an autonomous, all-weather and continuous system for the restitution of the water vapor. With such a technology we can retrieve the IWV (Integrated Water Vapor) over an area. This quantity has been validated by means of comparisons with other measurements and is now tested for assimilation in numerical weather prediction models. In addition, when a dense network of GPS stations exists, we can use the GPS to perform tomography in order to retrieve the 3 dimensional distribution of water vapor density. Tomography is a powerful mathematical tool of inversion which is used to retrieve information based on distant data.

As part of the COPS (Convective and Orographically-induced Precipitation Study), a project dedicated to the study of precipitation occurrences and the formation of convective systems in Rhine valley, a GPS project as collected data during the summer period of 2007. An initial GPS network has been deployed with 50 GPS stations (including a dense area of 16 GPS stations) to study water vapor.

To do so, collected GPS data has been used in tomography software to retrieve the 3 dimensional repartition of the density of water vapor over the studied area. Tomography allow us to study water vapor with very good precision (order of g/m^3) regarding to spatial and temporal variability of water vapor.

In addition, rain data were provided by two different radar. Poldirad radar working in C band and a X-band radar. The resulting data display the rain reflectivity over the same area that a part of the GPS network for comparison and further correlation.

2 SOFTWARE METHOD

The tomography algorithm is based on SIWV inputs: the IWV along the receiver to satellite baselines. The principle of the tomography is as follow: the volume above the GPS network is divided into voxels. The height of the voxels is function of the altitude in order to provide a better resolution in the low layers of the atmosphere where the water vapor is concentrated. Then, an algorithm looks at the repartition of each SIWV through the voxels. Using this repartition, *a priori* solution as initialization and weighted matrix, the mathematical inversion is done to retrieve the 3 dimensional distribution of water vapour as shown in equation 1.

$$m = m_0 + W_m^{-1} \times G^t \times \left(G \times W_m^{-1} \times G^t + \alpha^2 \times W_e^{-1}\right)^{-1} \times \left(d - G \times m_0\right) \quad (1)$$

Where m are the density of water vapor in g/m^3; m_0 are the *a priori* solution, G is the matrix of the SIWV repartition, d are our data (in our case the SIWV) and W_x and *alpha* are the weighted matrix. Another method based on direct STD (Slant Total Delay) as been tested on COPS campaign.

3 RESULTS

Among all the GPS and radar data, we will focus on an event which took place in August the 12th and 13th. A convective system passed over the GPS network (Figure 1 left), allowing us to study the role of the water vapor in the formation and maintain of convective cells (Figure 1 right).

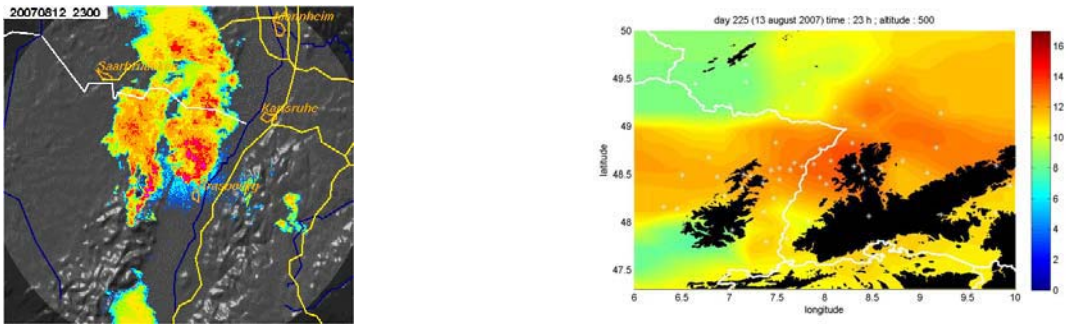

Figure 1. Left: radar precipitation from POLDIRAD during COPS-2007; right: tomography result of the water vapour density (g/.m^3). Horizontal cut at 500m.

This case is of great interest since the area is part of the Vosges and black-forest region allowing us to study water vapor structures with strong orographic effects through vertical cut (Figure 2).

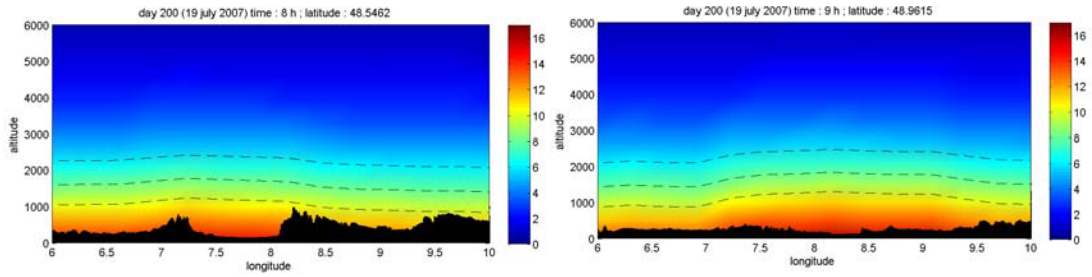

Figure 2. Water vapour density in g/m^3. East-West and North-South over the GPS network. Dashed lines correspond to isolines 10, 8 and 6 g/m^3.

In addition, we will also present preliminary results for some different cases which took place in June and July 2007. Those periods are really different from the first one regarding to the reflectivity map and the water vapor distribution.

4 CONCLUSIONS AND OUTLOOKS

The next step of this work will be to do inter-comparison with GFZ-Potsdam tomography results using different inversion methods. Likewise, comparison with model outputs as well as lidar measurements, balloon sounding, etc, will also be done to study the accuracy of the GPS tomography. In addition, water vapor density retrieval will be performed over a smaller area where the dense GPS network is available. The algorithm will use SIWV passing entirely through the voxel as well as the SIWV coming from GPS stations outside the voxels area.

REFERENCES

Flores A., Ruffini G., Rius A., (2000), 4D tropospheric tomography using GPS slant wet delays, *Annales Geophysicae, 18,* 223–234.

Reverdy M., Van Baelen J., (2007), Estimation des paramètres atmosphériques à partir des signaux GPS, CNES contract n°04/CNES/1928-5.

Van Baelen, J., J-P Aubagnac, A. Dabas (2005), Comparison of near real-time estimates of integrated water vapor derived with GPS, radiosondes, and microwave radiometer, *J. of Atmosph. Ocean Techn., 22*, 201-210.

Walpersdorf A., Bock O., Doerflinger E., Masson F., Van Baelen J., Somieski A., Bürki B., (2004), Data analysis of a dense GPS network operated during the ESCOMPTE campaign: first result, *Physics and Chemistry of the Earth, 29, 201-211.*

SIMULTANEOUS X-BAND AND K-BAND STUDY OF PRECIPITATION TO DERIVE SPECIFIC Z-R RELATIONSHIPS

F. Tridon, J. Van Baelen, Y. Pointin

Laboratoire de Météorologie Physique, UMR CNRS/UBP 6016,
24, avenue des Landais, 63177 Aubière cedex, France
E-mail: *F.Tridon@opgc.univ-bpclermont.fr*

Abstract : Using a simple scanning X-band radar and a vertically looking K-band radar, we show the need in using several specific Z-R relationships to improve the rain estimates by taking into account the high variability of rain regimes within the precipitations systems. To determine these specific Z-R relationships, we propose some simple classification schemes based on the trend of the reflectivity intensity.

***K*eywords :** *ICAM, radar, Z-R relationship, drop size distribution, precipitation estimation*

1 INTRODUCTION

During more than 50 years of development, ground-based weather radar became a tool fitted to quantitative rainfall measurements. The major source of errors lie in the conversion of the radar reflectivity factor Z ($mm^6\ m^{-3}$) to rain rate R ($mm\ h^{-1}$). These two parameters are related to each other via the raindrop size distribution (DSD) which cannot be inferred by conventional weather radar measurements. Hence, it has been common practice to take a simple power law relationship between Z and R, like the well known Marshall-Palmer relationship. DSD is extremely variable in time and space even within a single precipitating event. Thus, many of these relationships have been proposed, nevertheless, in most of the cases, a unique relationship is used for one precipitating event.

The aim of this work is to categorize the different rain regimes that might occur even within individual precipitation cells to derive the corresponding specific relationships. Then we will confront the rain estimates with these specific relationships to the classical approach using one single relationship in order to investigate their potential for improve rain estimation. To do so, we analyse the simultaneous measurements of a scanning X-band radar and a vertically pointing K-band radar in their common volume.

In section 2, we will describe the radars and data. In section 3, we will present the methods and their performances. Finally, we will outline some conclusions and perspective for future developments.

2 EXPERIMENTAL SET-UP

During the summer of 2007, for the international COPS (Convective and Orographically induced Precipitations Study)(Wulfmeyer et al., 2008) campaign, the X-band radar was installed on a small hill at the foot of the Vosges mountains in order to overlook a largely instrumented site where we had installed the K-band radar.

The K-band (24.15 GHz) radar is a Micro Rain Radar (MRR) : it is a FMCW system which provides Doppler spectra with 64 lines over a range of 0.8–12.2 m/s in 30 range gates of 100 m with a typical time resolution of 10 s. Under the assumption of zero vertical wind, profiles of DSD are derived using the relation between the drop diameter and the terminal fall velocity. These profiles of DSD allow to correct for the rain attenuation, and to derive reflectivity factor and rainrate. Further details are described in Peters et al. (2005).

The X-band (9.41 GHz) radar is scanning at a fixed elevation of 5° with a time resolution of 30 s, a range resolution of 60 m up to a maximum range of 20 km, and an azimuth resolution of 2° with a beam width of 2.4°. Furthermore, attenuation correction was also taken into account by applying the classical Hitschfeld and Bordan (1954) method to the X-band radar reflectivity measurements. Finally, we performed a statistical cross calibration between the X-band and MRR reflectivity wich allow a relative comparison of rain rate between the two systems.

An example of the resulting reflectivity measured by the two systems during the night of August 07 2007, is presented in figure 1 (right). The reflectivities correspond very well and show very similar features. However, one can notice slight differences which could be attributed to the differences between the sampling strategies and the two volumes sounded by the radars. Indeed, the geometrical dimensions of the radar beams are noticeably different with a volume ratio close to 100 (see figure 1 (left)). Thus, the X-band radar volume can include parts of the precipitating system not seen by the MRR.

3 RAIN REGIMES CLASSIFICATION AND PRECIPITATION ESTIMATION

The figure 1 (right) gives us confidence in using observations from common volume in order to investigate the Z-R relationships to be applied to the X-band reflectivity field. In a first step, we will focus on this common

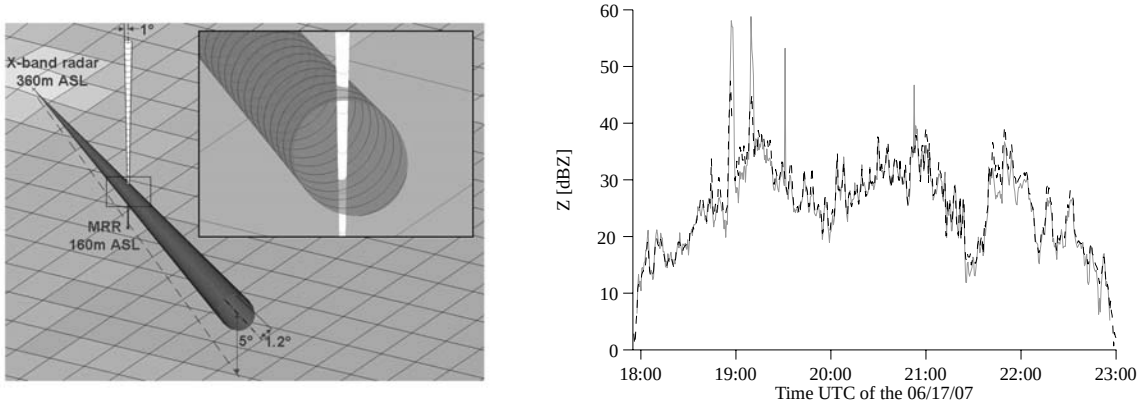

FIG. 1: Left : Representation of the X-band radar and MRR common volume. Right : Time series of the reflectivities of the MRR (dash line) and the X-band radar (solid line) for the precipitating event of June 17, 2007.

volume only. Our objective is to find simple techniques to categorize rain regimes from the X-band reflectivity. We propose different schemes based on the trend of this reflectivity intensity (increasing, decreasing, stagnating) or on its intensity itself. The MRR measured reflectivity and estimated rain-rate are used to derive the corresponding Z-R relationship which is then applied to the X-band radar reflectivity measurements in order to calculate a corresponding rain-rate which, in turn, is compared to the MRR derived value. This procedure is biased towards the MRR estimation which we will use as a reference, but the goal at this point of the project is to evaluate candidate rain regime selection scheme to later improve rainfall estimates.

The table 1 presents the results of the two methods in terms of total accumulated rainfall for the entire COPS campaign data set. It shows that the classification based on intensity degrades precipitation estimation whereas the increasing-stagnating-decreasing classification slightly improves it. Thus, this results give us confidence in using this last method in order to determine the specific Z-R relationships.

MRR	single Z-R relationship	Increasing, stagnating and decreasing intensity classification	Rain intensity classification
73.51	68.23 (-7.18%)	68.67 (-6.58%)	65.04 (-11.52%)

TAB. 1: Total rainfall (in mm) estimated by the different methods, and difference (%) from the MRR reference.

4 CONCLUSIONS AND PERSPECTIVES

We have shown the need in using specific Z-R relationships to account for the high variability of rain regimes within the precipitations systems. To determine these specific Z-R relationships, the classification scheme based on the trend of the reflectivity intensity (increasing, stagnating, decreasing) shows great promises for improvement of the rain estimation.

We are still working on the improvement of this classification scheme in order to extend and validate this study by rainfall comparisons with a network of raingages over the domain covered by the X-band radar.

Acknowledgements:
Participation to the COPS campaign was made possible with the support of the French ANR research grant BLAN06-3_136575 and INSU LEFE funding.

REFERENCES

Hitschfeld W. and J. Bordan, 1954: Errors inherent in the radar measurement of rainfall at attenuating wavelengths. *J. of the Atmos. Sci.*, **11**, 58–67.

Peters, G., B. Fischer, H. Münster, M. Clemens, A. Wagner, 2005: Profiles of Raindrop Size Distributions as Retrieved by Micro Rain Radars. *J. Appl. Meteorol.*, **44**, 1930-1949.

Wulfmeyer, V. and co-Authors, 2008: The Convective and Orographically-induced Precipitation Study: A Research and Development Project of the World Weather Research Program for improving quantitative precipitation forecasting in low-mountain regions. *Bull. Amer. Meteor. Soc.* **89**(10), 1477–1486, DOI:10.1175/2008BAMS2367.1.

Environmental conditions and radar observations of organized thunderstorms

Helge Tuschy[1, 2, 3], Martin Hagen[1], Georg J. Mayr[2]

[1] Deutsches Zentrum für Luft-und Raumfahrt (DLR) Oberpfaffenhofen, Germany
[2] University of Innsbruck, Innsbruck, Austria
[3] European Severe Storms Laboratory, ESSL
E-mail: *Helge.Tuschy@dlr.de*

Abstract: Different cases of organized thunderstorms are reviewed: a bow echo, a mesoscale convective system, a supercell and a hailstorm. The high resolution COnsortium for Small-Scale MOdelling (COSMO) model of the German weather service (DWD) is utilized to calculate the parameters for severe weather. In addition, the polarization diversity doppler weather radar (POLDIRAD) at DLR, Oberpfaffenhofen is used to detect the storms and to gain more detailed information about their structure. Finally several significant severe weather outbreaks in central Europe are included into this study (03 August 2008 eastern France, 25 June 2008 Czech Republic and 15 August 2008 southwest Poland).

***K*eywords:** *deep moist convection, wind shear, tornado, radar, COSMO*

1 INTRODUCTION

Despite the rapid enhancement of models' resolution and the increase in the calculating capacity, forecasting the initiation or the future tracks of thunderstorms remains difficult. Several organized thunderstorms, like bow echoes, mesoscale convective systems, supercells and hail storms are studied and the efficiency of the model is assessed by means of the calculation of forecasting parameters for severe thunderstorms (e.g. convective available potential energy (CAPE), directional and speed shear, convective inhibition (CIN) ...). Additionally, parameters like the significant tornado parameter (STP), the energy helicity index, or the SWEAT index are calculated to compare those results with studies from Switzerland (e.g. Huntrieser,1996 or Houze Jr.,1993) and North America (e.g.Craven,2002, Edwards et al.(2000, 2004)). To get a better insight in the structure of thunderstorms, the POLDIRAD was used, where not only rotation but also precipitation distribution and different type of precipitation can be analyzed.

2 SETUP

POLDIRAD operates at C-band (5.5027 GHz, 5.45cm). Research measurements are performed either in operational mode (radar range:120km) or in surveillance mode (radar range:300km). A subjective study of special features like hail spikes or hook echoes is carried out for the extensive archive of the POLDIRAD. 9 cases were selected for the final study, six occurred over southern Germany and 3 of them over NE-France, the Czech Republic and SW-Poland, respectively.
Data assimilations from the high resolution model of the national German weather service (DWD), the COSMO-DE, are used for those case studies. It is a high resolution version of the non-hydrostatic weather forecasting model of the COSMO community. The model domain contains 421x461 grid points, spaced 2.8km apart with 50 vertical levels. Severe thunderstorm forecast parameters are computed from model level data to achieve a better vertical resolution. The intent is to describe the imminent environment where thunderstorms evolve with the most effective/latest weather model and to see how the model assimilation performs different situations. There is also the chance to get a unique insight into those thunderstorms, which moved nearby the polarimetric radar station where hail cores or concentrated swaths of damaging wind became visible. The parameters are compared with studies of North America or Switzerland.

3 FIRST RESULTS

On the 15 August 2008, COSMO-DE performed well in highlighting the area of interest over southwest Poland (Fig.1, 2), where a regional tornado outbreak occured. In comparison to GFS (calculated at the European Storm Forecast Experiment (ESTOFEX, http://www.estofex.org/), COSMO-DE had strong hints in the parameter fields (e.g. the significant tornado parameter was above 3 just around the region, where tornadoes evolved).
The investigation of the radar already procured numerous interesting features like intense hail spikes, persistent bounded weak echo regions or hook echoes. The evolution of long lived outflow boundaries can be examined, which are a focus for thunderstorm initiation later-on and serve as an area, where wind shear increases significantly and hence enhances the potential for severe thunderstorm events.

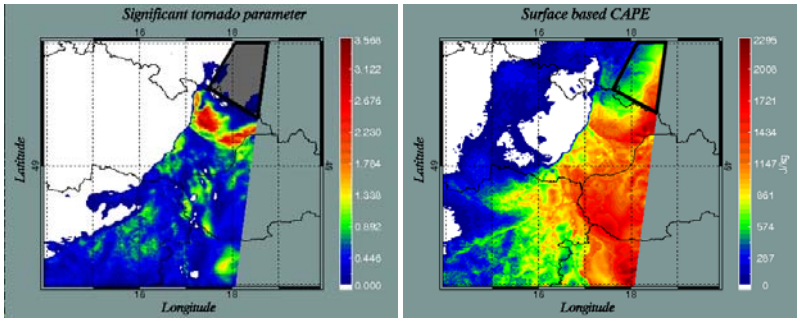

Figure 1: 15 August 2008, both at 15UTC: The significant tornado parameter (Edwards et al.2004) (left) and surface based convective available potential energy (J/kg) (right). Tornadoes evolved in the highlighted area between 15Z-19UTC. (coloured: http://www.pa.op.dlr.de/icam2009/extabs/)

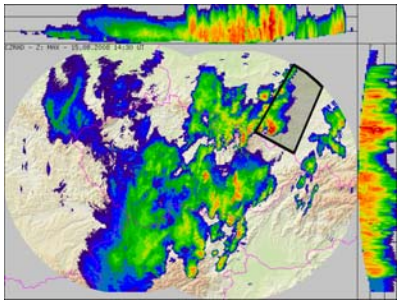

Figure 2: 15 August 2008, at 14.30UTC: The maximum radar reflectivity composed from radars Brdy and Skalky (source: CHMI). Tornadoes evolved in the highlighted area between 15Z-19UTC. (coloured: http://www.pa.op.dlr.de/icam2009/extabs/)

4 FUTURE WORK

The remaining cases are investigated in more detail and the parameters are compared to results from studies in Switzerland and North America in order to find out similarities or geographical differences. Of special interest are the F4 tornado at Hautmont in northeast France on 3 August 2008 and the significant derecho over the Czech Republic on 23 June 2008.

Acknowledgements:
The authors want to thank Meteo France, the Institut Royal Météorologique (KMI), the Institute of Meteorology and Water Management (IMGW), the Czech Hydrometeorological Institute (the Radar Department and the Satellite Department, CHMI), the European Organisation for the Exploitation of Meteorological Satellites (EUMETSAT) and the German weather service (DWD) for the provision of data.

REFERENCES

Craven, J.P. et al., (2002): *Baseline climatology of sounding derived parameters associated with deep, moist convection. Preprints, 21st Conf. Severe Local Storms, San Antonio*

Edwards, R. et al., (2000): *RUC-2 Supercell proximity soundings, Part II: An independent assessment of supercell forecast parameters. Preprints, 20th Conf. Severe Local Storms, Orlando FL*

Edwards, R. et al., (2004): An update to the supercell composite and significant tornado parameters. Preprints, 22nd Conf. Severe Local Storms, Hyannis MA

Huntrieser, H. et al., (1996): *Comparison of traditional and newly developed thunderstorm indices for Switzerland. Weather and forecasting, volume **12**, 108–125*

Houze, R.A. et al., (1993): Hailstorms in Switzerland: Left movers, right movers and false hooks. Monthly weather review, volume **121**, 3345–3370

MODIFICATION OF ATMOSPHERIC PARAMETERS BY DEEP CONVECTION OVER COMPLEX TERRAIN DURING COPS

Holger Mahlke, Ulrich Corsmeier, Christoph Kottmeier

Institut für Meteorologie und Klimaforschung (IMK), Karlsruhe Institute of Technology (KIT), Germany
E-mail: *holger.mahlke@imk.fzk.de*

Abstract: The goal of the study is to investigate the interactions between deep convection events over complex terrain (e.g. cumulonimbus development) and their atmospheric environment based on observational data obtained during the COPS field campaign in summer 2007.

Keywords: *ICAM, COPS, deep convection, low mountain area*

1 INTRODUCTION

Not all aspects of how deep convection interacts with its atmospheric environment are understood in detail, especially over complex terrain. Deep convection is a complex four dimensional process, governed by scale dependent interactions of numerous factors such as the vertical distribution of the meteorological parameters, the cold outflow causing gust fronts, the shading by the storm's anvil cloud, and the cooling of evaporating hydrometeors. Another important factor is the orographic structure of the underlying terrain, since often secondary flows develop over mountainous regions during the day which can trigger deep convection (Barthlott et al., 2005). These processes need to be understood in detail for improved forecasts of convective events that can strongly affect societal living (risk of wind storms, flash flood events, hail damages etc). A suitable way is to perform case studies based on measurements and simulations.

2 DATA AND METHOD

The Convective and Orographically Induced Precipitation Study (COPS) field campaign (Wulfmeyer et al., 2008) in summer 2007 in the Black Forest, the Rhine valley, and the Vosges mountains, provided the opportunity to investigate the above interactions due to temporally and spatially dense data obtained from various measurement platforms (remote sensing systems, ground stations, radiosondes, research aircraft etc.) and by performing of numerical simulations. Multiple data sets were obtained of days with deep convection present.

One of the measurement systems used was a mobile radiosonde system developed at IMK (Kottmeier et al., 2001). During COPS, 78 of these balloon-borne sondes were launched simultaneously by up to 4 mobile teams that were sent to different sites in the northern Black Forest, where convection was expected. The aim was to get "snapshots" of the convective development by measuring prior to, during and after convective cells passed the aerological stations.

Based on data derived from these soundings and measurements made by other instruments case studies are composed on COPS days where deep convection occurred and interacts with its environment. The results are compared to respective numerical simulations using the COSMO-DE model (resolution: 2.8 km).

3 EXAMPLE

On 20 July 2007, some thunderstorms and showers developed around noon across the northern Black Forest in front of a shortwave trough which triggered a mesoscale convective system (MCS) over eastern France (Fig. 1). The showers were mainly a result of the gust front of the MCS. The model forecast by COSMO-DE did not capture the development adequately, since no precipitation was simulated before 16:30 UTC.

Comparisons between the model output and radiosonde profiles from Hornisgrinde Mountain, close to where the initiation of a first convective cell took place, showed that: 1. The passage of the gust front was correctly forecast by the model, but the model was prior to the passage of the front and even more after the passage distinctly too warm (~10 K, Fig. 2). 2. A significant increase in specific humidity (~3 g kg^{-1} at 8 UTC) in the boundary layer a few hours before the initiation of convection was underestimated by the model (Fig. 3). Probably this was the reason why the model did not simulate the initiation of deep convection.

High values of boundary layer humidity were also observed at the mobile radiosonde site Dornstetten (Fig. 4) about 15 minutes before two convective cells passed the site. Thirty minutes later, during the second cell's passage, another radiosonde showed within the convective cell and in its vicinity lower values of temperature below 2 km, higher air temperature in the upper two thirds of the troposphere, and an increase of humidity in heights above the boundary layer depth. The boundary layer cooling was also observed in profiles from radiosondes released some time after a cell passage. Afterwards there was only little further convective activity

in the northern Black Forest until the evening due to the reduced amount of convective available potential energy (CAPE; e.g. 17 J kg^{-1} at Hornisgrinde Mountain at 14:05 UTC, ~0 J kg^{-1} in Dornstetten 16:14 UTC).

4 CONCLUSIONS AND OUTLOOK

A measurement strategy using mobile radiosondes teams proved to be a good approach to investigate deep convection processes if they are embedded in the framework measurements of a field campaign. Subject of future work will also be to analyse whether the temporal and spatial variability of the parameters going along with the convective development is well represented in the COSMO-DE model.

REFERENCES

Barthlott, Ch., U. Corsmeier, C. Meißner, F. Braun and Ch. Kottmeier, 2005: The influence of mesoscale circulation systems on triggering convective cells over complex terrain, *Atmos. Res.* **81**, 150-175.

Kottmeier, C., Reetz, T., Ruppert, P., and N. Kalthoff, 2001: A New Aerological Sonde for Dense Meteorological Soundings, *J. Atmos. Oceanic Technol.*, **18**, 1495-1502.

Wulfmeyer, V., A. Behrendt, and H.-S. Bauer, Ch. Kottmeier, U. Corsmeier, A. Blyth, G. Craig, U. Schumann, M. Hagen, S. Crewell, P. Di Girolamo, C. Flamant, M. Miller, A. Montani, S. Mobbs, E. Richard, M.W. Rotach, M. Arpagaus, H. Russchenberg, P. Schlüssel, M. König,, V. Gärtner, R. Steinacker, M. Dorninger, D.D. Turner, T. Weckwerth, A. Hense, and C. Simmer, 2008: The Convective and Orographically-induced Precipitation Study: A Research and Development Project of the World Weather Research Program for improving quantitative precipitation forecasting in low-mountain regions. *Bull. Amer. Meteor. Soc.* **89**, 1477-1486.

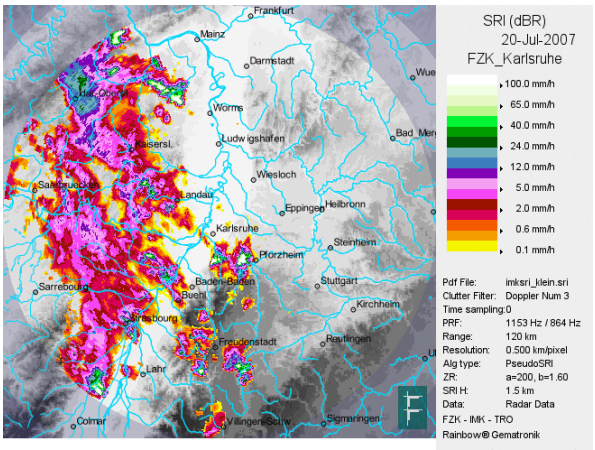

Figure 1. Convective precipitation rate derived from IMK-C-band rain radar on 20 July 2007, 10:30 UTC. Courtesy of Jan Handwerker.

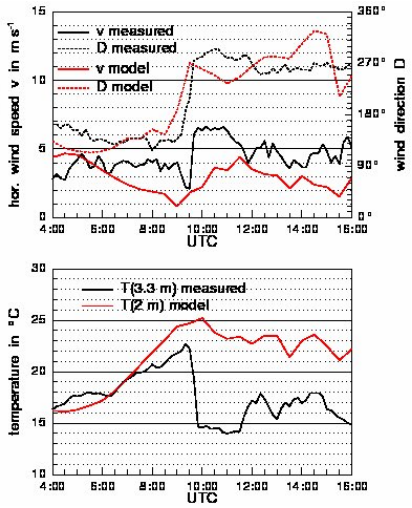

Figure 2. Wind speed (D) and direction (v, above) and temperature (below) measured by ground station at Hornisgrinde and forecast by COSMO-DE model, on 20 July 2007. Courtesy of Christian Barthlott and Norbert Kalthoff.

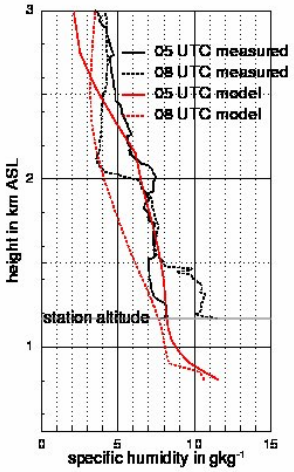

Figure 3. Comparison of specific humidity measured by radiosondes at Hornisgrinde Mountain and forecast by COSMO-DE model, on 20 July 2007.

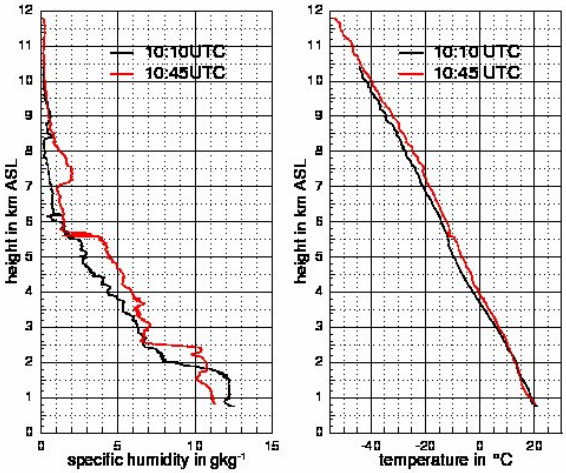

Figure 4. Specific humidity (left) and temperature (right) above height of two radiosondes at Dornstetten on 20 July 2007, 10:10 UTC (black) and 10:45 UTC (red).

CONVERGENCE INDEX: A NEW PERFORMANCE MEASURE FOR THE JUMPINESS OF OPERATIONAL RAINFALL FORECASTS

Uwe Ehret[1]

[1] TU München, Department for Hydrology, München, Germany
E-mail: *u.ehret@bv.tum.de*

Abstract: The degree of jumpiness of a sequence of rainfall forecasts strongly influences the end-users perception of its reliability. To objectively evaluate forecast convergence, a new performance measure termed 'convergence index' is proposed. It is applied on areal-averaged rainfall observations and forecasts of several numerical weather models in the mesoscale alpine catchment of the river Iller/Germany. It is shown that in combination with the root mean square forecast error, the convergence index allows useful evaluation of forecast quality: From the models used (Median of Cosmo-Leps, GME, Cosmo-EU, Persistence), the Median forecast scored highest.

Keywords: *rainfall forecast, convergence index, jumpiness, Cosmo-Leps*

1 INTRODUCTION

Rainfall forecasts serve as important prerequisite for many aspects of disaster management. In flood management for example, this ranges from the pre-flood drawdown of reservoir water levels to the preparation of protective measures such as the publication of warnings or timely evacuation.

In this context, the inevitable jumpiness of deterministic rainfall forecasts, which is partly even a positive sign of a models flexibility and ability to capture the full spectrum of atmospheric states, is distracting as firstly, many decisions in flood management are threshold-dependent and require forecasts consistently above (or below) the threshold and secondly, repeated switches from warning to all-clear erodes credibility in the eyes of non-expert users and the public. Consequently, for flood managers, evaluation of a rainfall forecasts jumpiness is useful. However, to date objective evaluation criteria are rare.

In this work, a new method termed 'convergence index' to evaluate a forecasts convergence is proposed. The work is structured in three parts: The first (Data & Methods) introduces the convergence index and the test data set used. The second (Results) displays results of its application on the test data set. In the third part (Conclusions), conclusions are drawn and the usefulness of the new performance measure is critically evaluated.

2 DATA & METHODS

2.1 Rainfall observations

Hourly rainfall observations from 26 raingauges were used to calculate mean areal rainfall (linear interpolation) in the alpine catchment of the river Iller/Germany up to Kempten (area: 954 km^2). The timeseries extends from 01.08.2005 to 30.04.2008, excluding the snow-influenced winter months November through March. The timeseries includes a 300-year flood event in August 2005.

2.2 Rainfall forecasts

The following rainfall forecasts were used (abbreviations in brackets): GME (GME), Cosmo-EU (LME), Cosmo-Leps Median (CLM), and, as reference, a simple persistence forecast (PER).

The forecasts were disaggregated to 1-hour sums (necessary for Cosmo-Leps and GME) and areal-averaged in the same manner as the rainfall observations. From all forecasts, only the 00:00 and 12:00 runs, cut to a maximum forecast depth of 48 hours were used to assure comparability. Accordingly, persistence forecasts were also generated only for the same initial times and forecast depths.

2.3 Convergence index

Based on a set of forecasts for a given observation, ordered by decreasing lead time, the convergence index (KONV) sums up the instances where the values, from on forecast to the next, do not approach the observed value (divergence) and the instances where forecasts switch from over- to undershooting (oscillation). The sums are divided by the maximum of possible occurrences and thus normalized to [0,1], where 0 means perfect convergence without oscillation.

To suppress the influence of small changes, a tolerance range, expressed in percent of the actual rainfall observation value, is applied. Times where forecast fluctuations are within the tolerance range are not

considered. Also, divergence and oscillation occurrences are inversely weighted by the forecast lead time to reduce the influence of poor (and less relevant) forecasts with long lead time.

However, KONV only expresses how good a series of forecasts approaches the observation in relative terms and even a series which is far off in absolute values may attain high scores. Therefore, KONV should be evaluated in combination with a measure that expresses forecast quality in absolute terms. Here, the root mean square error (RMSE) of the forecast series for each observation, also inversely weighted by lead time, was calculated.

2.4 Test setup

KONV and RMSE were calculated for each areal rainfall observation in the timeseries exceeding a threshold of 2.4 mm/h, which delineates the upper 5% of rainfall observations above a detection limit of 0.1 mm/h. Thus, only strong, flood-relevant rainfall events were considered. The tolerance range of KONV (as explained in 2.3) was set to 5%. From all values of KONV and RMSE, the mean was calculated (shown in Figure 1).

3 RESULTS

The main results (as shown in Figure 1) are: i) The persistence forecast exhibits the highest RMSE and ii) the lowest KONV, which indicates that it shows poor absolute values but good convergence. While the first result is in accordance with intuition, the latter is not. Further, iii) the Cosmo-Leps Median forecast shows the best overall performance (indicated by the smallest distance from the graphs point of origin), followed by GME and Cosmo-EU. The latter three iv) differ mainly with respect to KONV, not to RMSE.

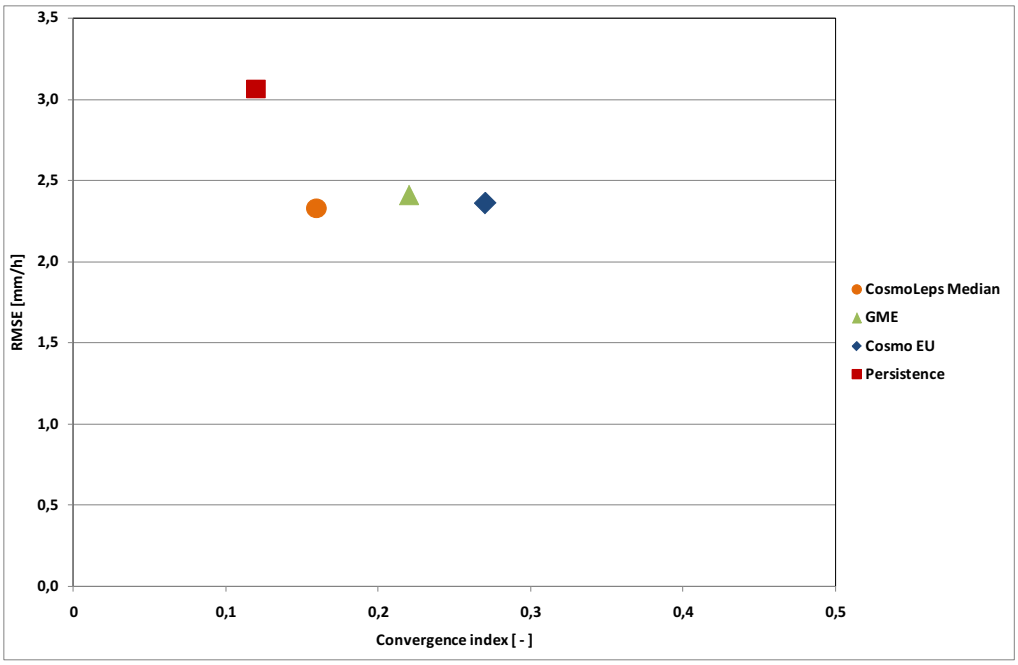

Figure 1. Performance of different forecasts with respect to Convergence index (0=optimal) and RMSE (0=optimal). Shown are mean values of the time series 01.08.2005-30.04.2008.

4 CONCLUSIONS

A new method to quantify the jumpiness of forecasts was proposed and applied on a series of areal rainfall observations and forecasts in a mesoscale alpine catchment. From the forecasts investigated, the Cosmo-Leps Median performed best. These findings are in accordance with other investigations by the author (not shown here), assessing rainfall forecast quality in alpine regions, where the Cosmo-Leps Median forecast often outperformed deterministic forecasts.

In combination with a measure that expresses forecast quality in absolute terms (here: RMSE), the convergence index may be useful for flood managers to find the most reliable rainfall forecast.

Acknowledgements:
The author expresses his gratitude to the Bavarian Agency for the Environment (LfU) for supplying the data for this work.

HYMEX, AN EXPERIMENTAL PROGRAM DEDICATED TO THE HYDROLOGICAL CYCLE IN THE MEDITERRANEAN

Véronique Ducrocq[1], Philippe Drobinski[2], Piero Lionello[3] and the HyMeX ISSC

[1] GAME-CNRM, Météo-France & CNRS, Toulouse, France
E-mail: veronique.ducrocq@meteo.fr
[2] IPSL-LMD, CNRS, Palaiseau, France
[3] Department of Science of Materials, University of Lecce, Italy

Keywords: *Mediterranean, water cycle, high-impact events, coupled processes*

1 INTRODUCTION

The Mediterranean basin has quite a unique character that results both from physiographic conditions and historical and societal developments. The region features a nearly enclosed sea surrounded by very urbanized littorals and mountains from which numerous rivers originate (Fig. 1). This results in a lot of interactions and feedbacks between ocean-atmosphere-land processes that play a predominant role on climate and on high-impact weather. The Mediterranean area concentrates indeed the major natural risks related to water cycle, which include heavy precipitation and flash-flooding during the fall season, severe cyclogenesis associated with strong winds and large sea waves during winter, and heat waves and droughts accompanied by forest fires during summer. The capability to predict such high-impact events remains weak because of the contribution of very fine-scale processes and their non-linear interactions with the larger scale processes.

Water resource is a critical issue for a large part of the Mediterranean basin. Freshwater is rare and unevenly distributed in time and space with few short duration heavy precipitation and long drought periods. Moreover, this happens in a situation of increasing water demands and climate change. The Mediterranean region has been indeed identified as one of the two main "hot-spots" of climate change, which means that its climate is especially responsive to global change. Large decrease in mean precipitation and increase in precipitation variability during dry (warm) season are expected as well as large increase in temperature. There are still, however, large uncertainties on the future evolution of the climate in the Mediterranean. Progress has to be made in the monitoring and modelling of the Mediterranean coupled climate system (atmosphere-land-ocean) in order to quantify the on-going changes and to better predict their future evolution in order to provide guidelines for development of adaptation measures.

These societal and science issues motivate the HyMeX (HYdrological cycle in the Mediterranean Experiment, http://www.hymex.org/) program, which is an experimental program aiming at a better quantification and understanding of the water cycle in Mediterranean - with emphases on intense events.

2 HYMEX SCIENCE OBJECTIVES

HyMeX proposes to monitor and modelling the Mediterranean coupled system (atmosphere-land-ocean), its variability (from the event scale, to the seasonal and interannual scales) and characteristics over one decade in the context of global change (2010-2020). In particular, HyMeX aims at addressing key issues related to (1) the water budget of the Mediterranean basin, (2) the continental hydrological cycle and related water resources, (3) heavy precipitation and flash-flooding and (4) intense air-sea exchanges produced by severe regional winds and cyclogenesis. HyMeX aims also at monitoring vulnerability factors and adaptation strategies developed by different Mediterranean societies to accommodate the impacts of climate change and intense events. The reader is referred to the HyMeX White book (Beranger et al, 2008) for a comprehensive description of the science issues addressed in HyMeX.

Figure 1 illustrates one of the coupled phenomena addressed in HyMeX. The Mediterranean Sea is characterized by several key-spots of intense air-sea exchanges associated with very strong winds, which are caused by the orographic response to the large scale forcing (e.g. Mistral, Bora, Sirocco, Tramontana, etc), deep cyclogenesis (e.g. Genoa cyclogenesis, etc) and high/low pressure patterns. These successive intense air-sea exchange events and the associated sea surface cooling affect considerably the heat and water budget of the Mediterranean Sea with formation of dense water and deep ocean convection during winter and early spring. Modifications of the ocean mixed layer in their turn influence the atmospheric boundary layer.

3 HYMEX OBSERVATION STRATEGY

A three-level nested observation strategy is proposed:

• *A long-term observation period* (LOP) lasting about 10 years to gather and provide additional observations of the whole coupled system in order to analyze the seasonal-to-interannual variability of the water cycle and to estimate the water budget. It is proposed that the LOP consists in enhancing the current operational observing systems and existing long-term observatories in hydrology, oceanography and meteorology, not excluding the setup of new networks. There is a general agreement that the LOP will have to cover the whole Mediterranean basin, developing and maintaining the acquisition of the long-term time series required to study its seasonal and interannual variability.

• *An enhanced observation period* (EOP) for both budget and process studies. The Enhanced Observation Period is envisaged lasting for at least 4 years, embracing the SOP periods. However, EOP may cover only part of the year, i.e. activities may be restricted for some aspects to specific periods (e.g. autumns for heavy precipitation, extending to winter for severe cyclogenesis and strong winds).

• *Special observation periods* (SOP) lasting several months, which will aim at providing detailed and specific observations to study key processes of the water cycle in specific Mediterranean regions. A first series of SOPs will take place in Northwestern Mediterranean in order to document heavy precipitation systems during fall and intense air-sea fluxes and dense water formation at the end of winter. The first HyMeX SOP over Nortwestern Mediterranean is now foreseen for September-October 2012.

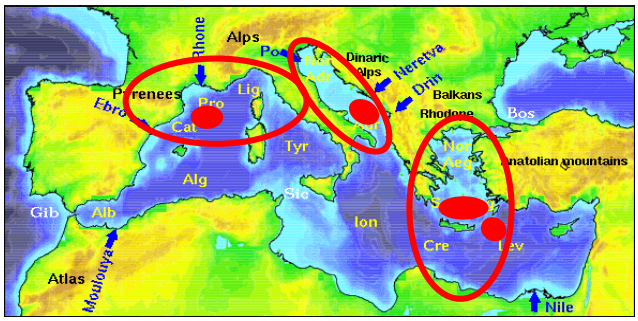

Figure 1. The four major sites of dense water formation (red line) and of deep ocean convection (red spots) over the Mediterranean basin.

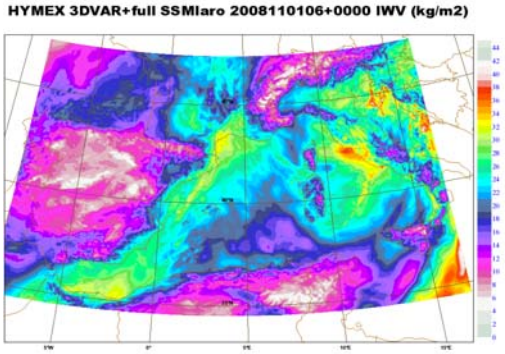

Figure 2. Integrated Water Vapour (mm) simulated by the 2.5-km AROME –WMED model (Courtesy: G. Jaubert).

4 HYMEX MODELING STRATEGY

The modelling strategy associated with the observation strategy includes :

- The development of regional coupled systems (ocean-atmosphere, atmosphere-land, ocean-land-atmosphere) to reduce uncertainties of the future regional projections. Validation of these systems includes measuring their skill in accurately simulating the Mediterranean water budget by using the HyMeX multidisciplinary databases.
- The development and improvement of high-resolution deterministic or ensemble modelling systems to improve the prediction capabilities of extreme events. Some of these systems will run in real-time during the SOPs to serve as guide for the deployment of dedicated instrumentation. Figure 2 illustrates one of this system currently developed for real-time application during the HyMeX SOPs. The AROME-WMED model is a version of the AROME NWP system running its own 3-hourly rapid update assimilation cycle at 2.5 km over the western Mediterranean. Such high-resolution large domain allows to include the major mountain ranges of the western Mediterranean region (Atlas, Pyrenees, Alps, Massif Central, etc) and to describe their influence on the atmospheric circulation .
- The development of new process modelling, parameterization development, novel data assimilation systems for the different Earth compartments. For example, improvement of air-sea flux parameterizations or development of data assimilation in cloud and precipitation systems are major objectives of HyMeX and part of the observation strategy is designed to serve these objectives.

REFERENCES

Béranger K., Braud I., Carlotti F., Chanzy A., Claud C., Delrieu G., Doerenbecher A., Despiau S., Drobinski P., Ducrocq V., Dulac F., Durrieu de Madron X., Elbaz-Poulichet F., Escadafal R., Estournel C., Giordani H., Guieu C., Guiot J., Hallegate S., Kageyama M., Jacob F., Lachassagne P., Lang M., Li L., Martin E., Médail F., Noilhan J., Moussa R., Perrin J.L., Plu M., Prieur L., Ricard D., Rinaudo J.C., Radakovitch O., Roux F., Lutoff C., Somot S., Taupier-Letage I., 2008: HyMeX (Hydrological cycle in the Mediterranean Experiment): Towards a major field experiment in 2010-2020. Eds. P. Drobinski, V. Ducrocq, available at http://www.cnrm.meteo.fr/hymex/, version 1.3.2, February 2008, 124 pp.

OPERATIONAL PERFORMANCE OF DISCHARGE PREDICTION IN ALPINE REGIONS

Frédéric Jordan[1], Javier Garcia Hernandez[2], Alexandre Gal[3]

[1] e-dric.ch, Le Grand-Chemin 73, CH-1066 Epalinges, Switzerland
E-mail: *fred.jordan@e-dric.ch*
[2] Ecole Polytechnique Fédérale Lausanne, Dept. of Civil Engineering, Station 18, CH-1015 Lausanne, Switzerland
[3] Groupe E, Route de l'Abbaye, CH-1025 Posieux, Switzerland

Abstract: The Groupe-e is an electricity provider, operating 6 dams with large reservoirs located in the Saane river basin in Switzerland. The 1800 km^2 Saane river basin is an alpine catchment area, with elevations from 450 m a.s.l. (Laupen) to 3200 m a.s.l. (Wildhorn). Due to its specific electricity market, the Groupe e company is able to self-produce only a moderate part of its electricity sales, the remaining part has to be bought on the spot electricity market. For this reason, it is of highest importance to predict the future inflows in the reservoirs in order to adjust the hydroelectricity production and the electricity trades on the spot market.

During 2007 and 2008, a hydrological prediction model was developed, including the functioning of the 6 existing hydropower schemes. In this semi-distributed conceptual model, the Saane river basin is decomposed into 43 sub-basins. Each one is cut into 300m elevation bands in order to take into account the temperature-driven processes (snow melt, glacier melt, rainfall-snow separation, PET).

Different deterministic numerical weather prediction models are used in the system, such as ECMWF, COSMO-7 and COSMO-2 models. The system was able to provide relevant information during 2008, such as high flows and small floods due to snow melt and summer storms. The 2008 operational performance of the whole system is presented below, comparing the different predicted inflow models. The results are compared with persistence, continuous simulation based on observations and updated continuous simulation.

Keywords: *Hydrology, Discharge prediction, Flood*

1 INTRODUCTION

Discharge prediction is a powerful tool for hydroelectricity production. However, the uncertainty associated to the inflow forecasts is important, depending on particular meteorological situations. For this reason, ensemble discharge forecasts are now used by researchers in order to quantify the related uncertainty. For daily use of inflow forecasts, the ensemble forecasts are of complicated use and do not suit yet for operational systems. The aim of this contribution is to present the operational performance of the RS3.0 system (Garcia et al., 2007), a discharge prediction system after its first year of operational use.

2 MODEL DESCRIPTION

The Saane river is located in the North side of the Alps in Switzerland (Fig. 1, left). Its 1800 km^2 catchment area is mountainous with snow covered areas during 4 months per year including a small glacier. The basin has elevations from 450 to 3200 m a.s.l. The Groupe-e company is owner of 6 hydropower schemes with 2 large reservoirs located in this catchment area. In the simulation model (Fig. 1, right), the catchment area is divided into 43 sub-basins with 40 km^2 of average area. Each sub-basin is divided into 300 m elevation bands to take into account the temperature effects. The computed hydrological processes are separation between solid and liquid precipitation, snow melt, glacier melt, real evapo-transpiration, soil infiltration, surface runoff and river routing. The model computes hydraulic schemes as well (Jordan, 2007).

3 SIMULATION

The performance analysis compares continuous simulation results, filtered simulation results and forecast results. The simulation results (continuous and filtered) are obtained with observed meteorological input data, while forecast results are obtained with predicted meteorological input data from the COSMO-7 model of Meteoswiss. The performance is evaluated with the Nash indicator computed on a whole year simulation period. The continuous simulation is obtained by a direct hydrological simulation during the period. The filtered simulation is obtained by updating the initial conditions of the model every 12 hours. The updating procedure allows comparing simulated and observed discharges at every discharge measuring gauge. Finally, the forecasts

are computed by using 2 numerical weather forecasts per day during the same year period. Different lead times are analyzed, from 0-12 h to 60-72 h ahead.

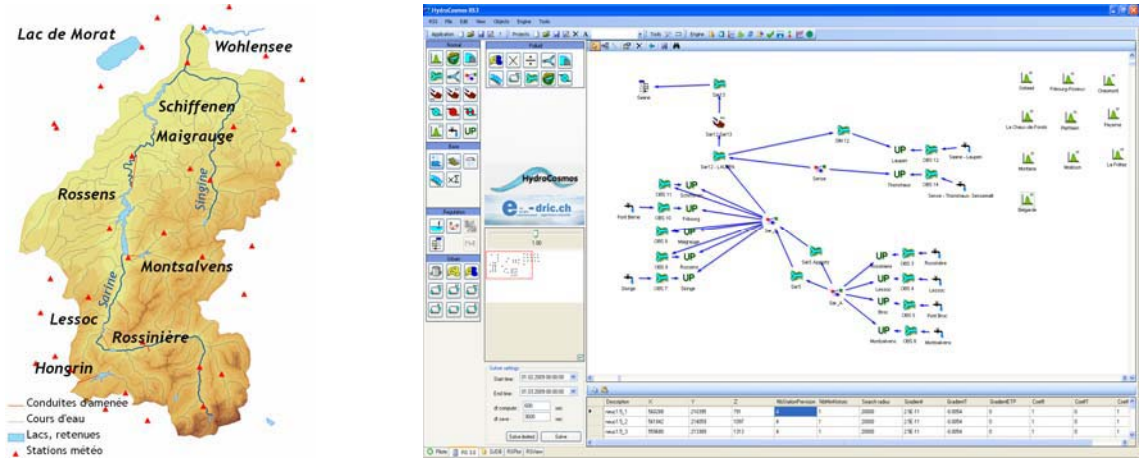

Figure 1. Map of the Saane river basin (left) with the sub-catchments, rivers, reservoirs and meteorological measuring stations. Corresponding RS3.0 model (right) with the main user interface.

4 PERFORMANCE OF THE MODEL

Fig. 2 presents the whole year forecasts at Rossinière dam for 24h lead time (left). The good correlation between observed and predicted discharge is due to good quality 24h meteorological forecasts and a relatively long 12 h response time of the basin. Systematic simulation and forecasts results show 3 different elements (Fig. 2, right). First, the filtered simulation provides a much better performance that the continuous simulation, which is expected. For this reason, the filtered simulation provides the operational initial conditions of the hydrological forecast. Second, the average forecast performance is lower than the one of the filtered simulation. Nevertheless, it can be better than the continuous simulation one, at least for lead times lower than 48 hours. Finally, the forecast performance (COSMO7) strongly decreases for lead times higher than 36 hours, and the persistence theoretical model (PERS) provides in average better Nash values.

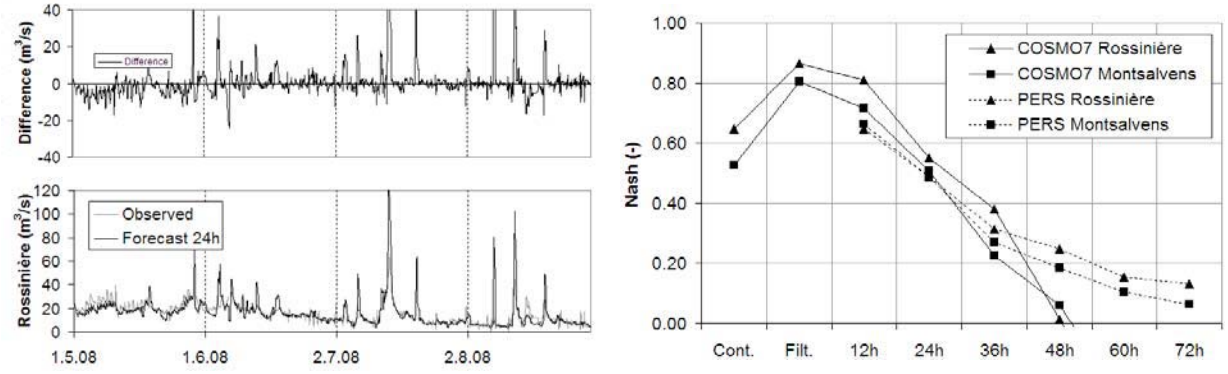

Figure 2. Comparison between observed and predicted inflows 24h ahead at the Rossinière dam (left). Differences (prediction minus observation) are also presented. Synthetic analysis of Nash coefficients computed during the year 2008 (right). Cont. = continuous simulation ; Filt. = filtered ; 12h – 72h = lead times.

A detailed analysis will provide useful information in order to assess the part of the uncertainty due to the hydrological model and the part due to the meteorological forecast. These results illustrate the difficulties to predict discharges more than 48h ahead with the COSMO7 deterministic model.

REFERENCES

García Hernández, J., Jordan, F., Dubois, J., Boillat, J.-L. & Schleiss, A. (2007). Routing System II: Flow modelling in hydraulic systems, Communication du Laboratoire de Constructions Hydrauliques N°32, ed. A. Schleiss, EPFL, Lausanne.

Jordan, F. (2007). Modèle de prévision et de gestion des crues - optimisation des opérations des aménagements hydroélectriques à accumulation pour la réduction des débits de crue. PhD Thesis N°3711, Ecole Polytechnique Fédérale de Lausanne.

ANALYSIS OF PRECIPITATION PATTERNS ON MOUNT BALDO (ITALY)

Giacomo Poletti[1], Massimiliano de Franceschi[1,2], Alberto Bellin[1], Dino Zardi[1]

[1] Dipartimento di Ingegneria Civile e Ambientale, Univesità di Trento, Trento, Italy
E-mail: *Dino.Zardi@ing.unitn.it*
[2] Seminario Maggiore, Diocesi di Bolzano-Bressanone, Bressanone, Italy

Abstract: Preliminary results are shown from a research work aiming at retrieving and organising in a dataset precipitation data from 16 stations disseminated on Mount Baldo, in order to produce a climatological analysis of precipitation in the area. The final dataset covers an overall 90 year span (1919-2008), although the various stations have been operated very discontinuously in it. The analysis of the 11 most representative time series provides an overview of typical annual and seasonal mean values along with their trends. Correlation analysis between total monthly precipitation data shows that stations located on the same side of the mountain are better correlated with respect to other lying closer, but on the opposite side. Suitable mapping through Kriging techniques allows to infer the spatial distribution of precipitation under various seasonal and typical weather patterns. 100 precipitation events have been classified into 7 typical meteorological scenarios, identified on the basis of patterns from ECMWF reanalysis. Specific features of each scenario are evaluated and discussed.

Keywords: *orographic lifting, precipitation, mountain, rain gauge, Kriging.*

1 INTRODUCTION

The mountain chain of Mount Baldo, in the southern Prealps, lies between the Lake Garda and the Lagarina Valley (Figure 1). Ranging from 65 m a.m.s.l. of the mountain feet at the shore of Lake Garda up to about 2200 m a.m.s.l. of its main crests, Mount Baldo displays a remarkable variety of local microclimates, geographical characters and ecosystems, in particular flora (since it received the name of *Hortus Europae*, i.e. Europe's Garden). Precipitation over Mount Baldo originates both from evaporation and up-slope advection of water vapour, especially from the side of Lake Garda, and from the lifting of moist airflows, especially from south. These effects may variously occur and interact under different meteorological scenarios.

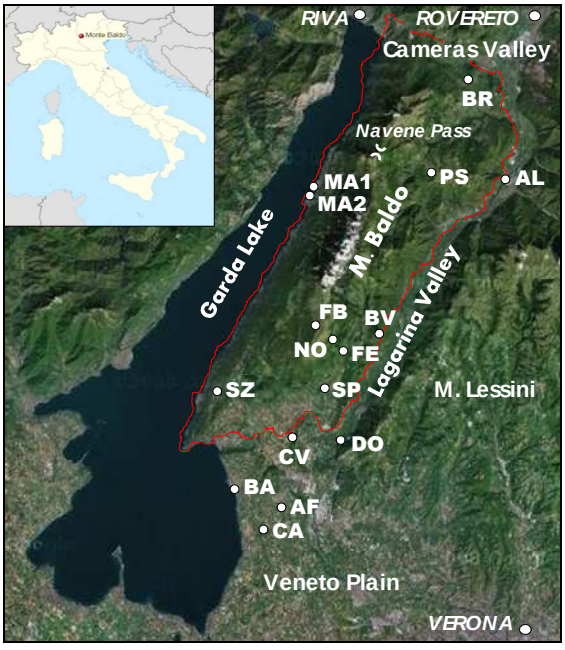

Figure 1. Map of Mount Baldo with the precipitation measuring stations: Affi (AF), Ala (AL), Bardolino (BA), Brentonico (BR), Belluno Veronese (BV), Calmasino (CA), Caprino Veronese (CV), Dolcè (DO), Ferrara di Monte Baldo (FE), Rifugio Fiori del Baldo (FB), Malcesine (MA1, MA2), Prà da Stua (PS), Spiazzi di Monte Baldo (SP), San Zeno di Montagna (SZ).

2 DATASET

The dataset collected for the present analysis includes data from 16 weather stations disseminated on the mountain (Figure 1) and covers an overall period of 90 years (1919-2008). Since the various stations have been operated very discontinuously, the analysis focused on the 11 most representative time series and provides an

overview of typical annual and seasonal mean values along with their trends. Correlation coefficients between total monthly precipitation data (Table 1) show that stations located on the same side of the mountain are better correlated with respect to other lying closer, but on the opposite side.

	AL	BV	BR	CA	CV	DO	FE	MA	PS	SZ	SP
AF	0.805	0.783	0.744	0.947	0.897	0.784	0.790	0.713	0.797	0.770	0.787
	AL	0.854	0.860	0.818	0.854	0.738	0.847	0.876	0.893	0.783	0.813
		BV	0.795	-	0.853	0.712	0.889	0.824	0.855	0,762	0.794
			BR	0.795	0.805	0.731	0.792	0.794	0.901	0.728	0.774
				CA	-	0.870	-	-	-	-	-
					CV	0.840	0.848	-	-	0.746	0.826
						DO	0.750	0.624	0.745	0.637	0.753
							FE	-	-	0.690	0.797
								MA	0.856	0.736	0.774
									PS	0.823	0.776
										SZ	0.759

Table 1. Correlation coefficients *r* between monthly total precipitation (orange: $r > 0.85$, yellow: $0.75 < r < 0.85$, white $r < 0.75$). Dashes denote 11 couples displaying no overlapping periods so that correlation coefficient could not be evaluated.

3 PRECIPITATION MAPPING AND ANALYSIS

Suitable mapping through Kriging techniques allowed to infer the spatial distribution of precipitation under various seasonal and typical weather patterns. In an area characterized by various weather conditions, 100 precipitation events were classified into 7 typical meteorological scenarios, identified on the basis of patterns from ECMWF reanalysis. Specific features of each event are evaluated and discussed (an example in Figure 2).

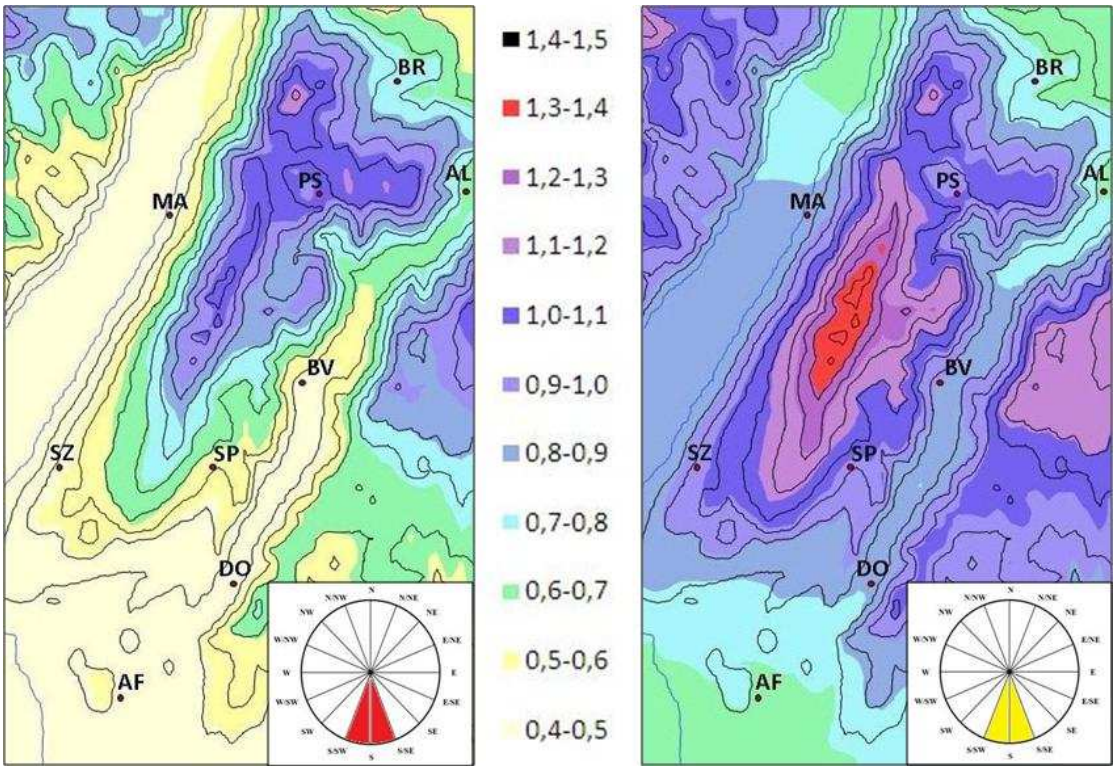

Figure 2. Average distribution of precipitation for two events with strong (left) and moderate (right) southerly flows. Scale is normalised to the maximum measured total precipitation value. Height contours every 250 m.

ASSIMILATION OF LEANDRE2 WATER VAPOR OBSERVATIONS WITH THE AROME 3D-VAR CYCLE FOR COPS

Matthias Grzeschik[1], Genevieve Jaubert[2], Cyrille Flamant[3], Evelyne Richard[1]

[1] Laboratoire d'Aérologie, CNRS and University of Toulouse, Toulouse, France
[2] Centre National de Recherches Météorologiques, Météo-France, Toulouse, France
[3] Service d'Aéronomie, CNRS and University Pierre et Marie Curie, Paris, France
E-mail: *Matthias.Grzeschik@aero.obs-mip.fr*

Abstract: This study is investigating the sensitivity of forecast quality on initial conditions with respect to the water vapor field and the possible contribution of high resolution lidar measurements to an improvement of precipitation forecast. The airborne Leandre2 Differential Absorption Lidar (DIAL) system was measuring water vapor profiles during the Convective and Orographically-induced Precipitation Study (COPS) in mattress patterns to observe the 3D distribution of water vapor. This quasi volume information of the water vapor field promises a positive impact on the quality of the modeled humidity field and also improvements of the precipitation forecast can be expected. The observations was assimilated with the AROME 3D-Var cycle and the impact was studied by comparing short range forecasts from analysis with and without additional water vapor information.

***K*eywords:** *ICAM, data assimilation, water vapor, airborne, lidar, DIAL*

1 INTRODUCTION

Leandre2 measures water vapor profiles with a high spatial and temporal density. The data collected during the COPS IOPs of July 2007 represent a total of 22 hours. The outstanding property of these data is the high resolution of $20\,\mathrm{m}$ vertically and $5\,\mathrm{sec}$ in time. Since the water vapor was observed along the aircraft track, while it was flying mattress patterns, the measurements give good information about the spatial distribution of water vapor in the boundary layer. These data set is to be used to investigate the role of the distribution of water vapor on the initialization of convection by forcing the model towards the observed humidity field.

2 DATA PROCESSING

The Leandre2 data were provided as water vapor mixing ratios together with estimated observation error in netCDF format. These data were prepared to be used with the AROME 3D-Var system.

For the assimilation, it had to be assured, that no bad data are used. Therefore, the dataset was first cleaned by removing data with an absolute error larger than $1.5\,\mathrm{g/kg}$, a relative error larger than $50\,\%$, and a relative error smaller than $2\,\%$. Further data were removed after inspecting the data by human eye.

The water vapor profiles were averaged in horizontal to profiles with a minimum distance of $20\,\mathrm{km}$ and with a temporal interval not larger than two minutes. In vertical, the profiles were roughly averaged to the AROME model levels. The resulting super observations, see figure 1, were furthermore used for the screening.

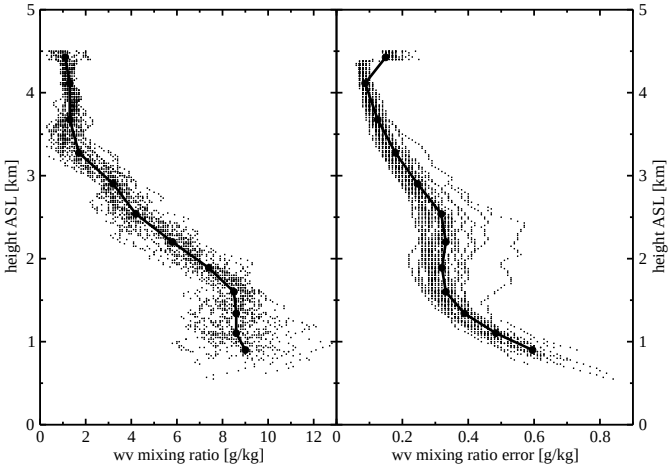

Figure 1: Result of thinning for an example of one super observation profile. The left panel shows the water vapor mixing ratio observation and the right panel shows the corresponding measurement error. The raw observation are represented as small dots, while the super observation are marked as larger dots, connected by lines.

During the screening, all available super observations were compared with AROME $3\,\mathrm{h}$ forecasts of the corresponding observation time. The resulting statistics of Leandre2 observations for July 2007 are shown in figure 2. This comparison yielded to a dry bias at the bottom of the profiles of about $0.5\,\mathrm{g/kg}$ and a RMS of about $1.5\,\mathrm{g/kg}$. The distribution of deviations can be roughly assumed to be gaussian after removing the bias of panel one of figure 2.

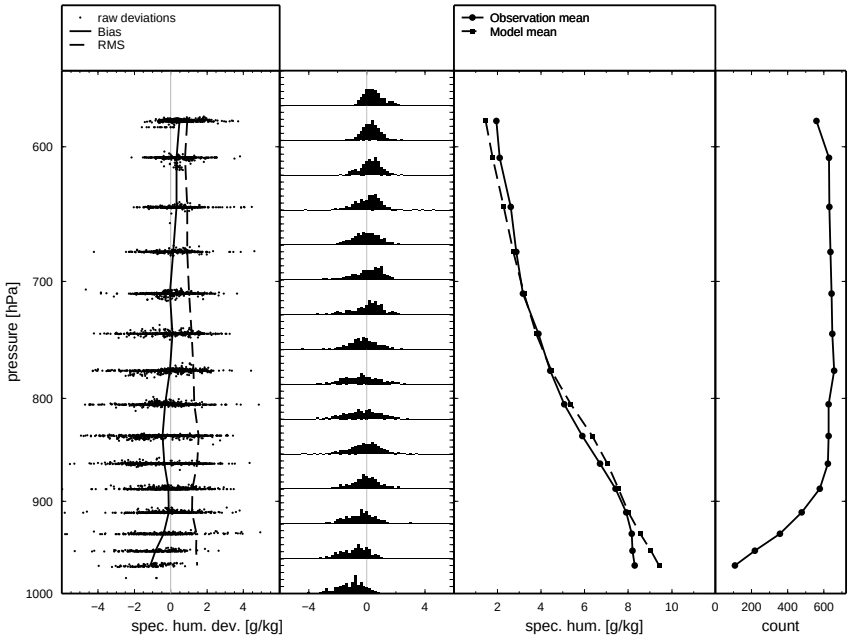

Figure 2: Statistics of all Leandre2 observations against AROME forecasts. The first panel shows the deviation Leandre2 - AROME of specific humidity for each super observation as dots. The solid line is the mean of the deviation and represents the bias, while the dashed line is the RMS. The second panel shows the histogram of the deviations for each level, while the third panel shows the mean of the absolute specific humidity for the observation and AROME. At last, the fourth panel shows the number of observations for each level over the whole period.

3 ASSIMILATION

In a next step the super observations were introduced in the AROME assimilation cycle every three hours, with the 3D-Var technique in a resolution of 2.5 km. Figure 3 shows the difference of water vapor in 2 km height for the analysis at 12 UTC, while additional observations were already assimilated at 9 and 12 UTC. A clear impact of the order of 3 g/kg is visible in the cops region.

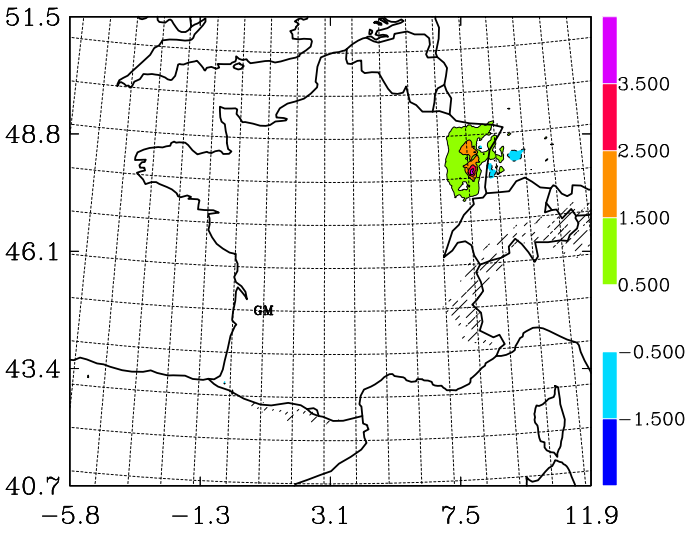

Figure 3: Water vapor differences (with Leandre2 minus the control experiment) at 2 km height for 14 of July, 12 UTC after assimilating Leandre2 observations at 9 UTC and at 12 UTC.

4 OUTLOOK

The impact of these data should be further investigated. How does it evolve in the further assimilation cycle? Is the influence of Leandre2 on the forecast positive, compared with other observations as TEMP, AMDAR, and so on? Does the modification of the water vapor field yield to an improved forecast in terms of convection and precipitation and the reasons for this change in the water vapor field.

Additionally is currently in development the assimilation of DIAL data from the DLR Falcon system, which provided similar data during COPS.

Acknowledgements:
Christoph Kiemle, DLR, Institut für Physik der Atmosphäre for providing DLR Falcon DIAL data.

PROPOSAL OF A NEW METHOD TO SELECT THE REFERENCES SERIES: FIRST RESULTS

Fiorella Acquaotta[1], Simona Fratianni[1]

[1] Department of Earth Science University of Turin, Turin, Italy
E-mail: *fiorella.acquaotta@unito.it*

Abstract: Most techniques used to adjust daily climatological time series for reconstruction the missing values and for inhomogeneities require a reference series obtained from neighbouring stations. In many cases, the selection of reference series is obtained using only statistical methods and neglecting the climatological peculiarities of the meteorological station.
In this study we have tried to estimate the importance of climatological features compared with the statistical methods. We have studied the maximum and minimum daily temperatures series of the Piedmont (NW Italy). We have selected the candidate series (to reconstruct or to homogenize) and the neighbouring series. For each selected station we have carried out a climate analysis and we have applied the statistical tests in the period 1998-99. The methods have allowed to assess which reference series "better represent" the candidate series.

Keywords: *References series, maximum and minimum temperatures, statistical tests, climate indexes.*

1 INTRODUCTION

The techniques for the reconstruction of the missing values or to create homogeneous reference series are becoming more important in the international field (Della Marta et al. 2006) in order to estimate the real climate changes of a region. However, in many cases, the reference series selection is obtained using only statistical methods and neglecting the climatological peculiarities of the meteorological stations (Peterson et al. 1994, Eischeid et al. 1995).

In this paper we have tried to use both methods, statistic and climate, so to consider all the factors that cause the state of a meteorological variable.

2 DATA AND METHODS

We have used an objective method to select, from a set of neighbouring stations, the reference series more suitable to reconstruct the missing values or to homogenise a candidate series.

We have chosen as candidate series the minimum (Tn) and maximum (Tx) daily temperatures of Turin, for the period 1998-1999. Then we have been selected the neighbouring series (Tab. 1) that were operating continuously in the considered period.

For each station we have carried out a climate analysis using climate indexes. For the minimum daily temperature we have used the frost day (Tn<0°C), day with Tn>10°C and tropical nights (Tn>20°C), while for the maximum daily temperatures the summer day (Tx>25°C), day with Tx>10°C and ice day (Tx<0°C). To quantify the "climate differences", for each climate index, we have calculated the difference in day between the values obtained from the candidate series and the neighbouring series for each month.

Subsequently, for each month, we have made a statistical analysis. We have identified and excluded the outliers (between 2nd and 98th quantiles), and evaluated the maximum, the minimum, the median, the average and the standard deviation. On each set of values we have applied the Shapiro-Wilk test to assess whether the data assume a normal distribution and, thank to results of this test, we have applied the Student test, parametric test, or the Wilcoxon signed-rank test, nonparametric test, to evaluate if the two series, candidate and neighbouring, have the same average. The Kolmogorov-Smirnov test, nonparametric test, has been applied in order to estimate if the two series have the same distribution and then the correlation coefficient has been calculated.

The results obtained from climate indices and statistical tests have been classified by appropriate conversion tables that allow us to highlight the best results (Tab. 2). The values obtained by the division into classes of the comparison methods have been added to detect, for each month, the four best neighbouring series suitable to interpolate the candidate series.

3 RESULTS

The analysis on the minimum daily temperatures series has revealed the low possibility to use the daily values of neighbouring series to reconstruct or to homogenise the series of Turin. In fact, in many months, we have not identified the reference series because the sum of the results had low scores (Tab. 3). It was possible to identify only an exception, in October, for the meteorological station of Luserna S. Giovanni.

Good results were obtained from the maximum daily temperatures series (Tab. 3). In each month, except August, we have found at least one reference station. In the months of February and May most of neighbouring stations are suitable to interpolate the daily values of the candidate station.

Stations	E [m]	Latitude	Longitude
Torino	240	45°04'49"	7°40'25"
Varallo	470	45°49'14	8°16'30"
Lucerna	475	44°48'50"	7°14'32"
Asti	117	44°53'09"	8°12'48"
Vercelli	135	45°19'32"	8°23'26"
Cumiana	327	44°57'53"	7°23'31"
Pino T.se	608	45°02'32"	7°45'58"
Lanzo	580	45°17'23"	7°29'38"
Piverone	230	45°25'53"	8°02'04"
Verolengo	163	45°11'10"	8°00'43"

Table 1. Geographical localization of the meteorological stations analyzed, E = elevation.

Climate indexes		Statistical tests	
Difference (days)	**Score**	**Results**	**Score**
0	6	1	6
±1	5	0.96-0.99	5
±2	4	0.92-0.95	4
±3	3	0.88-0.91	3
±4	2	0.84-0.87	2
±5	1	0.80-0.83	1
≥±6	0	<0.80	0

Table 2. Classification of the results obtained from climate indices and from statistical tests. We have assigned a score equal to 6 for the best result climbing up to 0 for the worst results.

M	Jan	Feb	Mar	Apr	May	Jun	Jul	Ago	Sep	Oct	Nov	Dec
1	5/0.55	8/0.87	8/0.89	7/0.80	6/0.72	10/0.68	5/0.58	2/0.76	3/0.84	6/0.85	2/0.85	4/0.61
2	8/0.68	7/0.82	3/0.79	0/0.53	1/0.83	0/0.70	0/0.40	0/0.75	0/0.79	4/0.62	4/0.81	6/0.71
3	5/0.73	14/0.90	7/0.93	2/0.86	13/0.86	2/0.85	5/0.70	2/0.81	6/0.86	7/0.85	5/0.86	7/0.81
4	5/0.72	15/0.92	15/0.94	11/0.86	10/0.88	2/0.84	4/0.75	3/0.90	5/0.87	8/0.92	7/0.87	3/0.62
5	10/0.91	10/0.94	8/0.95	12/0.93	10/0.93	3/0.90	3/0.84	3/0.91	7/0.94	8/0.94	4/0.92	8/0.87
6	8/0.81	10/0.94	6/0.95	8/0.92	11/0.96	5/0.90	3/0.85	4/0.93	8/0.96	8/0.94	8/0.91	11/0.63
7	6/0.80	10/0.93	6/0.95	9/0.93	4/0.95	3/0.89	1/0.82	3/0.91	9/0.92	8/0.91	10/0.90	5/0.76
8	10/0.88	19/0.94	10/0.95	3/0.90	18/0.91	5/0.88	12/0.84	7/0.92	12/0.94	9/0.96	4/0.93	9/0.89
9	8/0.85	21/0.92	17/0.95	8/0.88	13/0.93	3/0.88	5/0.85	3/0.91	7/0.95	8/0.95	19/0.94	8/0.88
m	**Jan**	**Feb**	**Mar**	**Apr**	**May**	**Jun**	**Jul**	**Ago**	**Sep**	**Oct**	**Nov**	**Dec**
1	1/0.50	3/0.88	6/0.71	0/0.76	0/0.58	0/0.73	0/0.32	0/0.71	1/0.80	0/0.79	5/0.91	0/0.78
2	0/0.54	5/0.91	5/0.77	0/0.62	6/0.56	3/0.84	0/0.52	0/0.69	0/0.67	16/0.84	9/0.89	0/0.76
3	0/0.29	2/0.84	6/0.55	0/0.56	0/0.34	1/0.51	0/0.42	0/0.62	0/0.70	3/0.82	6/0.83	0/0.71
4	0/0.22	1/0.83	6/0.50	4/0.56	0/0.59	6/0.76	2/0.41	0/0.56	0/0.60	4/0.71	5/0.77	5/0.71
5	0/0.74	4/0.94	9/0.89	3/0.89	4/0.68	3/0.84	0/0.39	0/0.75	0/0.78	2/0.84	8/0.88	2/0.87
6	4/0.39	6/0.79	4/0.74	3/0.86	5/0.66	4/0.91	0/0.56	0/0.79	3/0.75	2/0.70	5/0.79	0/0.48
7	0/0.49	3/0.88	9/0.88	3/0.90	0/0.67	2/0.84	0/0.43	0/0.74	1/0.80	2/0.85	6/0.91	0/0.70
8	0/0.51	3/0.88	6/0.79	1/0.75	6/0.64	6/0.85	0/0.68	1/0.80	3/0.73	4/0.84	8/0.87	1/0.83
9	0/0.21	3/0.90	6/0.55	0/0.55	0/0.35	0/0.73	0/0.27	0/0.50	0/0.66	0/0.72	5/0.77	0/0.71

Table 3. Results obtained by comparison of the maximum (M) and minimum (m) temperatures series and corresponding correlation coefficient; Stations: 1= Varallo, 2= Luserna S. Giovanni, 3= Asti, 4= Vercelli, 5= Cumiana, 6= Pino T.se, 7= Lanzo, 8= Piverone and 9= Verolengo.

4 CONCLUSIONS

The results obtained by this first pilot methodology on the minimum and maximum daily temperatures series have allowed to highlight that, in many cases, the simple presence of neighbouring stations with a good correlation coefficient is not enough to affirm that the series are "similar". The climate peculiarities play a key role in the climate determination because their features can create important effects on the trends of the meteorological variables, even for some periods of the year.

REFERENCES

Della Marta P., H. Wanner, 2006: A method of homogenizing the extremes and mean of daily temperature measurements, Journal of Climate, Volume **19**, 4179-4197.

Eischeid, J., C. Baker, T. Karl and H. Diaz, 1995: The quality control of long-term climatological data using objective data analysis, Journal of Applied Meteorology, Volume **34**, 2787-2795.

Peterson T., D. Easterling, 1994: Creation of homogeneous composite climatological reference series, International Journal of Climatology, Volume **14**, 671-679.

A quality control and bias correction method developed for irregularly spaced time-series of observational pressure- and temperature-data

Stefan Sperka[1], Dieter Mayer[1], Reinhold Steinacker[1]

[1] Department of Meteorology und Geophysics, University of Vienna, Vienna, Austria
E-mail: *stefan.sperka@univie.ac.at*

Abstract: Within the creation of the MESOCLIM-dataset (3 hourly MSLP, potential- and equivalent potential temperature VERA-analyses for a 3000 times 3000 km_2 area centered over the Alps from 1971-2005) a method to detect and correct occurring biases in the observational raw data had to be developed. The method is based on an automated variational algorithm that minimizes second spatial derivates in meteorological fields.

***K*eywords:** *MESOCLIM, Bias correction, MSLP-analyses*

1 INTRODUCTION

There are many reasons for a change of a measurement site's performance, for example a change in the instrumentation, a slight modification of the location or a different way of data processing (pressure reduction). For the creation of a 3 hourly MSLP, potential- and equivalent potential temperature VERA-analyses-dataset, a method to estimate these artificial influences was developed, using an automated variational algorithm that minimizes second spatial derivates in meteorological fields and calculates deviations for each observation (Steinacker (2000)). These deviations were calculated for each station at each time, using a piecewise functional fitting approach that considers the stations primary and secondary neighbours. The resulting timeseries of deviations were then used to estimate a bias correction for each meteorological parameter at each measurement site. Additionally, the data was checked for gross errors by comparing it to ERA-40 gridded data.

2 Bias Correction: Theory

The output of the automated quality control algorithm was checked for inhomogeneities, that could be caused by artificial shifts in the stations records, with a Standard Normal Homogeneity Test (SNHT). The variant of the SNHT used here was developed by Haimberger (2007) for testing analysis feedback data of radiosonde temperatures and is defined as:

$$T_k = (\frac{N}{2}(\mu_{1k} - \mu)^2 + \frac{N}{2}(\mu_{2k} - \mu)^2)/\sigma_k \quad (1)$$

$\frac{N}{2}$ denotes the sample length, μ_{1k}, μ_{2k} and μ the mean deviations in interval one, two and over both of them and σ_k is the standard deviation. Synthetic timeseries were generated to test the tests capability to detect inhomogeneities of different sizes, and to determine the significant threshold level for the SNHT values. The results suggest that it is possible to detect breaks $\geq 2\sigma$, while smaller breaks can be lost in the noise. Once the assumed artificial breaks are determined, the median of the deviations between breaks is used as bias correction estimate.

3 Results

In the top panel of figure 1 the deviation timeseries of station 11022 (Retz, Austria) is shown in black and the red vertical lines indicate detected breaks. To correct these inhomogeneities the median of the deviations between two breakpoints was used as correction estimate. The middle and bottom panels of figure 1 show the uncorrected and corrected MSLP timeseries of the same station and their trends. Considering that the long term trend of MSLP should be rather close to zero, the correction seems to have a good effect on the timeseries.

4 Conclusions

In general the bias correction reduces the standard deviation of the stations trends and helps to produce smoother fields. Most MSLP-trends of stations with long records, that were differing from zero, could be reduced by the bias estimates. For potential and equivalent potential temperature the standard deviation of trends from stations with records longer than 20 years could be reduced by 10 percent.

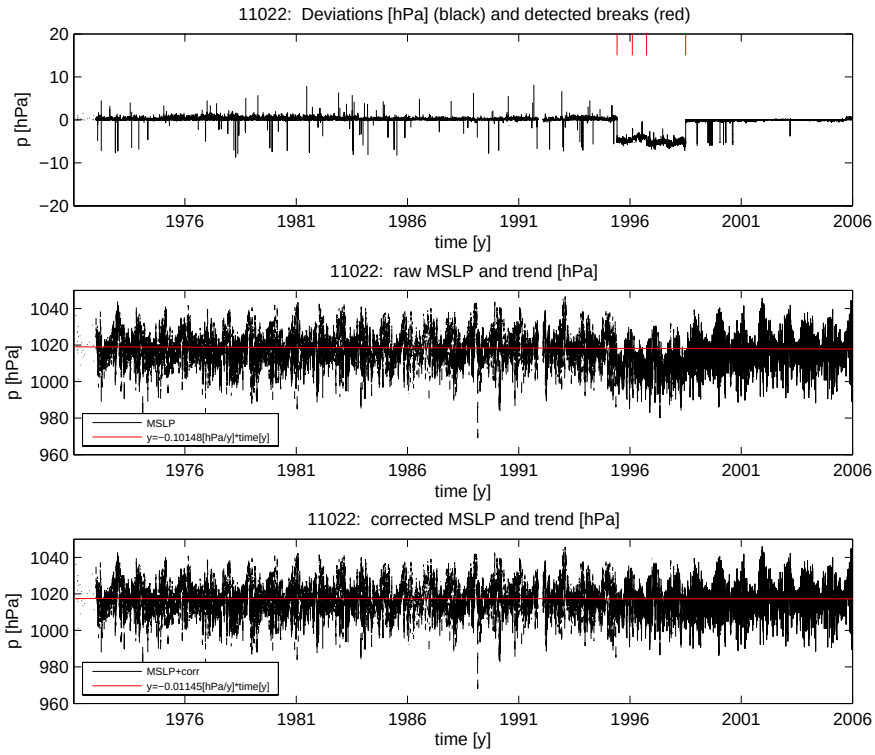

Figure 1: Deviations, uncorrected and corrected MSLP

REFERENCES

Haimberger, L. 2007. Homogenization of radiosonde temperature timeseries using innovation statistics. *Journal of Climate*, **20**(7), 1377–1403.

Steinacker, et al. 2000. A Transparent Method for the Analysis and Quality Evaluation of Irregularly Distributed and Noisy Observational Data. *Monthly Weather Review*, **128**(7), 2303–2316.

RADAR-BASED HAIL CLIMATOLOGY OF EASTERN SLOVENIA

Mark Žagar[1,2] and Benedikt Strajnar [2]

[1] University in Ljubljana, Faculty for mathematics and physics
[2] Environmental Agency of the Republic of Slovenia, Ljubljana, Slovenia
E-mail: *Benedikt.strajnar@rzs-hm.si*

Abstract: Several hail diagnostic and detection methods were applied on the three-dimensional radar reflectivity data. Nominal resolution of the data was 1km in the horizontal as well as in the vertical direction. Most methods use a certain value of the reflectivity as a threshold and combine the information of the temperature profile of the atmosphere to assess the depth of the column with freezing temperatures, an important parameter in the detection algorithms. The temperature profile was taken from the radiosonde data. We have produced a map, showing the 5 year average number of events with probable hail fall over each of 1 km squares covering the NE Slovenia. When sufficiently long data series is used to prepare the climatology it can also be used to provide the probability of hailstorm events in the future. The hail probability estimate based on this study should be used with caution, but can nevertheless present valuable additional information to ease decision making in case of crop and vines insurance and physical protection with nets.

Keywords: *ICAM, radar hail detection, hail climatology*

1 INTRODUCTION

Agriculture largely depends on meteorological and climatic conditions. Extreme weather phenomena comprise spring and summer thunderstorms with hail, which is one of the most limiting factors in agriculture in eastern and north-eastern parts of Slovenia. Lack of sufficiently dense traditional (surface) hail observational network calls for alternative approaches for creation of spatially complete hail climatology. The weather radar is an obvious choice, even though the presence of complex terrain with hills up to 1500 m high does present a certain difficulty for the region of eastern Slovenia due to occultation.

2 DATA AND METHODS

Data used were the 3-dimensional radar reflectivity maps from Slovenian C-band single-polarization weather radar, located at Mt Lisca. In our case only 5 seasons (May-August, 2002 - 2006) were used, primarily due to suboptimal quality of the radar system at Mt. Lisca prior to year 2002. Three methods were designed and applied, mainly following the hail detection algorithms used at other national weather services (e.g. Holleman, I., 2001) and in literature. The method based on the data from Grossversuch hail suppression experiment (Waldvogel et al., 1979; Federer, B., 1986) calculates the probability of hail p using polynomial expression

$$p = -1.20231 + 1.00184 \cdot \Delta h_0 - 0.17018 \cdot \Delta h_0^2 + 0.01086 \cdot \Delta h_0^3 \qquad (1)$$

where Δh_0 is the difference between 45 dBZ echo-top and freezing level height in km. Modified version requires continuous reflectivity exceeding threshold. Another methodology, used at Austrian meteorological service (Gmoser H. et al., 2006), examine columns of 5 km depth with sufficiently high radar reflectivity.

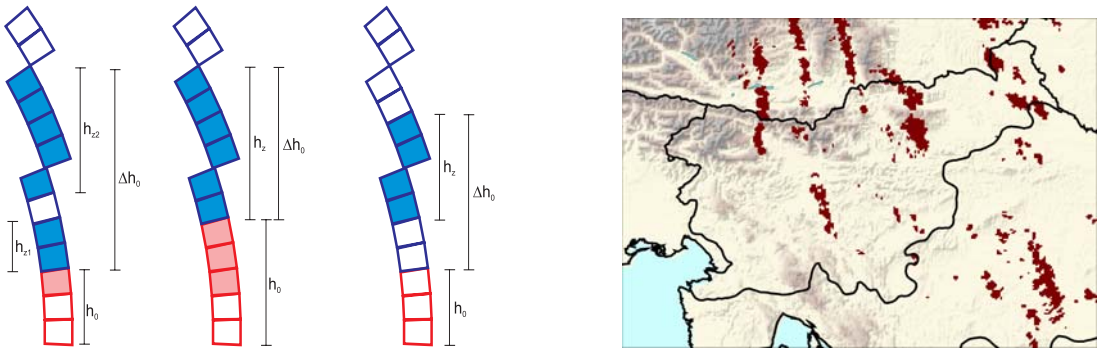

Figure 1. Left: illustration of hail detection. Depending on the method, actual height and extent of high reflectivity columns (solid rectangles) in cold parts of the cloud (blue colours) are parameters which determine hail probability; right: hail occurrence in the stormy day (August 9th, 2004). Daily contributions are summed up to give the climatology maps.

To estimate the freezing level height, Ljubljana radiosoundings (or, if missing, Zagreb or Udine) were used. Verification was performed subjectively from case to case, hail detection products was compared to some available ground measurements and damage reports from newspapers, civil protection etc.

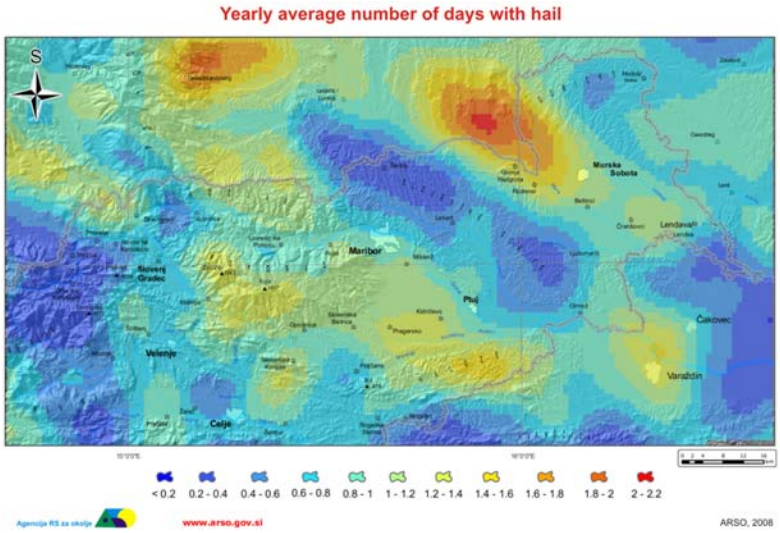

Figure 2. A map of spring and summer hail fall frequency for the period of 2002-2006. The raw map is smoothed by a spatial filter.

3 RESULTS

The results of the radar data analysis are spatial maps of yearly days with occurrence of hailstorms. An example of the product (average over both) is shown in Fig. 2, representing the average number of days in a year a hailstorm occurs over a geographic location of SE Slovenia. In this figure, the results are smoothed by a 5 km filter for reducing noise, i.e. preventing the end users from assuming that the spatial resolution of the product of 1 km is anywhere relevant.
Results show significant spatial distribution of detected hailstorm frequency. While the average is about 1 per year per square kilometer, we also observe values from 0.2 to around 2. These values agree quite well with climatological frequencies in the vegetation period on some Slovenian climatological stations (Dolinar, 2005). Maximums are located over the Drava and Mura river basins and lowlands and regions close to the line connecting them (e.g. Pohorje mountain range). This can be explained by more moisture available for convection. Minimums occur over the hilly regions in between.

4 CONCLUSIONS

The remote sensing derived climatology of hail has many potential sources of error, especially those originating from radar technology, and because it is indirect. But it can help us understand the spatial distribution of hail events. Because of large data set, we decided to focus only on the time period of most frequent hail. There are for sure some missed hail events, especially in September and rarely in other months of the year.
The hail frequency maps are typically meant to enter further algorithms, such as various decision trees in order to obtain a scientifically based estimation of potential economical impact of hail to unprotected crops. Successively, cost of protecting crops (e.g. hail nets or insurance) can be compared to potential damage.
Using also the newest data, this product could for sure be significantly improved in the future.

Acknowledgements
The authors would like to thank Anton Zgonc from Environmental agency of Slovenia for help in preparing radar dataset. This study was supported by Slovenian research agency project no. CRP V4-0359.

REFERENCES

Dolinar M., 2005: Prostorska in časovna analyze neviht in toče v vegetacijskem obdobju (1961-2004). Environmental agency of the Republic of Slovenia, Ljubljana.

Federer, B., A. Waldvogel, W. Schmid, H. Schiesser, F. Hampel, M. Schweingruber, W.Stahel, J. Bader, J. Mezeix, N. Doras, G. D'Aubigny, G. DerMegreditchian, and D.Vento, 1986: Main Results of Grossversuch IV. *J.Appl.Meteor.*, **25**, 917–957.

Gmoser H., Zwatz-Meise V., 2006: Warning System of ZAMG for Austria - Concept and Applications. Subgroup on Regional Aspects of Public Weather Services, Bucurest, 4. – 7. December 2006.

Holleman, I., 2001: Hail Detection using Single-Polarization Radar, KNMI Scientific Report, WR-2001-01.

Strajnar B. and Žagar M., 2007: A radar-based hailstorm climatology for Slovenia. 4th European Conference on Severe Storms, Trieste, 10-14 September 2007.

Waldvogel, A., B. Federer, and P. Grimm, 1979: Criteria for the Detection of Hail Cells. *J. Appl. Meteor.*, **18**, 1521–1525.

An Enhanced Hail Detection Algorithm for the WSR-88D. *Wea. Forecasting*, **13**, 286–303.

SPATIAL VARIABILITY AND TRENDS OF HAILSTORM FREQUENCY AND THE RELATION TO ATMOSPHERIC CHARACTERISTICS IN SOUTHWEST GERMANY

Michael Kunz, Marc Puskeiler

Institute for Meteorology and Climate research (IMK), Universität (TH) / Forschungszentrum Karlsruhe, Germany
E-mail: *kunz@kit.edu*

Abstract: By combining radar reflectivity data with loss data from a building insurance company, hail streaks between 1997 and 2007 are determined for a region that covers most parts of Baden-Württemberg (southwest Germany). In the mean, the hail patterns exhibit a high spatial variability that can be attributed to triggering or amplification mechanisms for convection by orographic features. In the last three decades, hail days and total hail damage have increased significantly due to changes in static stability. Several convective indices that depend upon surface temperature and moisture reveal a positive trend regarding both the annual extreme values and the number of days above/below specific thresholds.

***K*eywords:** *hail, hail damage, climate change, convective indices, low mountain ranges*

1 INTRODUCTION

Severe thunderstorms and associated extreme events, like heavy rainfall, gusts, or hail, pose a significant threat to modern societies and their assets. In the federal state of Baden-Württemberg (southwest Germany), almost a quarter of the total damage on residential buildings is related to large hail, yielding a mean annual loss of around 26.9 Mio €. In the past, single severe hailstorms caused up to 100 Mio € damage to buildings in this region. Loss prevention and risk management purposes require information about the local probability of occurrence of severe hail storms as well as identification of possible trends related to climate change.

2 DATA AND METHODS

Due to their small horizontal extent, convection-related phenomena like hail are usually not captured accurately by one single conventional observation system (Houze, 1993). Therefore, data sets from different observation systems are used to supplement this study: data from a building insurance company (Sparkassenversicherung) to determine hail days and affected regions, radar data to identify hail streaks and to estimate the intensity, and convective indices derived from radiosonde observations (Stuttgart) at 12:00 UTC to assess long-term changes of the convective potential of the atmosphere.

By applying the cell tracking algorithm TRACE3D (Handwerker, 2002) on 3D radar reflectivity data between 1997 and 2007, individual storm tracks are identified for a region that covers most parts of Baden-Württemberg. From this sample, damage-related hail streaks are separated using the insurance loss data that are available for five-digit postal code zones. These streaks are projected on a 10×10 km^2 grid in order to quantify hail track density. By statistical modelling of extremes, a cumulative distribution function (generalized Pareto distribution) is estimated, which relates radar reflectivity and probability of occurrence.

From the Stuttgart soundings between 1974 and 2003, various convective indices are derived that allow to quantify the thunderstorm potential of the atmosphere. In order to estimate long-term changes, different percentiles of the annual frequency distribution (90th, 95th, and 99th percentiles) as well as the number of days per year above/below appropriate thresholds of the indices according to the study of Kunz (2007) are calculated.

3 RESULTS

The identified hail streaks show a significant spatial variability in the occurrence probability that is supposed to be due to orographic influences (Fig. 1, left). Lowest probabilities are found over the rolling terrain in the north as well as over the elevated terrain of Black Forest and Swabian Jura. Between the two mountain ridges, the probability of hail streaks to occur is highest. One may assume that air masses that partly goes around the mountains in cases of southwesterly flow directions favour the development of convergence zones downstream of Black Forest. Also a flow deviation at the upstream border of the Swabian Jura, indicated by a sharp gradient of the hail streaks, may facilitate the formation of convergence zones in this area. Note that the high number of storm tracks behind the northern Black Forest mountains in radial direction to the radar location is an indication that beam shielding at the mountains does not substantially modify the results.

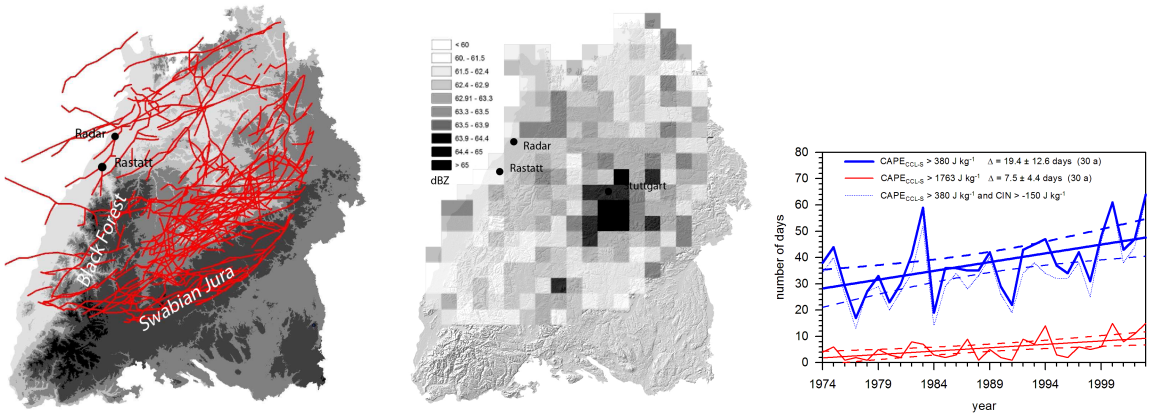

Figure 1: Damage-related hail tracks according to IMK-radar data for a radar reflectivity of $\geq$ 55 dBZ (left) and radar reflectivity for a return period of 1 year (middle), both between 1997 and 2007. Number of days per year with a CAPE above two specific thresholds (solid lines) and for a combination of CAPE and convective inhibition (CIN; thin dotted line) (right).

Considering not only the number but also the intensity of severe thunderstorms in terms of radar reflectivity for specific return periods, does not substantially change the spatial distribution of the hail patterns (Fig. 1, middle). The highest intensities are well correlated with the highest track densities. Again, the lowest values occur over the mountains of Black Forest and Swabian Jura.

By examining atmospheric stability in a 30-year perspective, it is found that most of the commonly used convective indices that depend upon near-surface temperature and moisture reveal a positive trend regarding both the annual extreme values and the number of days above/below specific thresholds. An example is shown in Fig. 1 (right) for the convective available potential energy (CAPE) as integrated from the convective condensation level (CCL) to the equilibrium level (EL) and assuming a surface-based parcel (S) that was lifted. A relationship can be established between the indices and the annual number of hail damage days, yielding correlation coefficients between 0.65 and 0.80 (Kunz et al., 2009). In contrast to this, indices derived from temperature and moisture at higher levels exhibit either a negative or no significant trend. The trend directions of the indices can be attributed to different temperature and moisture stratification in the various atmospheric layers. The significant positive trends of both surface temperature and water vapour can be concisely expressed by an increase in wet-bulb potential temperature. This indicates the presence of warmer parcels throughout the whole troposphere during convection.

4 CONCLUSIONS

Although it is impossible to deduce a direct relationship between orography and hail frequency, local effects like flow channelling or orographically induced wind systems are certainly decisive for the spatial variability of hail streaks. In particular for hot spots as identified in this study, it is very important to know whether severe thunderstorms will further increase in intensity and/or probability in the light of global warming. Even if our analysis provides an indication for an increase of severe thunderstorms in the past decades due to an decrease of static stability, these trends cannot be projected into the future. Hence, the next steps are to apply the methods to reanalysis data and to regional climate simulations to quantify possible changes of the hailstorm potential in the next decades. Both data sets are available at IMK at the very high resolution of approx. 7 km.

Acknowledgements: *We thank the Sparkassenversicherung (SV) for the provision of detailed loss data, Jan Handwerker for providing the radar data and the tracking algorithm TRACE3D, and the German weather service for the provision of the radiosonde data.*

REFERENCES

Handwerker, J., 2007: Cell tracking with TRACE3D, a new algorithm. *Atmos. Res.*, **61**, 15–34.

Houze, R. A., Jr. 1993: *Cloud dynamics, International Geophysics series*, volume **53**. Academic Press. 573 pp.

Kunz, M., J. Sander and Ch. Kottmeier, 2009: Recent trends of thunderstorm and hailstorm frequency and their relation to atmospheric characteristics in southwest Germany. *Int. J. Climatol.*, DOI: 10.1002/joc.1865.

Kunz, M., 2007: The skill of convective parameters and indices to predict isolated and severe thunderstorms. *Nat. Hazards Earth Syst. Sci.*, **7**, 327–342.

ANALYSIS OF SNOW COVER CHARACTERISTICS CHANGE IN SLOVAKIA

Pavol Faško[1], Milan Lapin[2], Jozef Pecho[1] and Katarína Mikulová[1]

[1]Slovak Hydrometeorological Institute, Bratislava, Slovakia, e-mail: pavol.fasko@shmu.sk
[2]Faculty of Math, Phys. and Informat., Comenius Univ., Bratislava, Slovakia, e-mail: lapin@fmph.uniba.sk

Abstract: Snow cover information is very frequently used. For many people it is in the centre of interest during all winter season. On the other hand snow cover is one of the mostly impacted due to ongoing climate change. Recently some increase in winter precipitation has been registered, mainly in the northern Slovakia. This resulted in significant increase of new snow in the high mountain localities at some extreme events (above 1300 m a.s.l.). Such examples are well known not only in Slovakia, but also at many sites in the Alps (the newest events occurred in the 2008/2009 winter). On the other side significant decrease of snow cover days was observed in the lowlands.

There are about 700 precipitation gauges in Slovakia every year since 1951 and some lower number since 1921. In 1980 the Slovak Hydrometeorological Institute decided to create precipitation database, including all snow data (climatologic database is ready for 1961-2008). Altogether 600 station data are complete in 1981-2008. In spite of shorter 30-year period, it is considered long enough to identify principal changes in snow cover during current climate change. This snow cover series is very valuable also for future analysis in some years or decades. In the paper the new and the total sow cover data observed once a day are analyzed. The elaboration brought plenty of characteristics, never issued in Slovakia up to present. Because of existence of limited snow characteristics for the period 1921-2000, some comparisons are included as well. Limited area in the paper enables to present selected information only.

The analysis presented here is focused mainly on the changes in annual regime and territorial distribution of snow cover due to warming of climate and change in precipitation. Very important is the dividing line between the influence of rising temperature and increasing winter precipitation. It is considered that currently it lies about 900 m a.s.l. and it tends slowly to increase. Below this boundary decrease of snow is observed and above it some increase. Finally some extreme events with high new and total snow cover depth are listed. Snow cover analysis is highly important also in prevention of dangerous avalanche events occurring in Slovakia every year.

Keywords: *snow cover regime changes in Slovakia, statistical analysis of snow cover characteristics, long-term changes of liquid, solid and mixed precipitation rate, fresh snow cover depth chages and extremes*

1 INTRODUCION

Analysis of snow cover regime changes within the territory of Slovakia represents the essential goal of this contribution. Snow cover characteristics, such as snow cover depth as well as snow water equivalent, play an important role in different climatological and hydrological analyses and they are widely used in operative meteorological service, particularly during the winter season.

Liquid, solid and mixed precipitation proportion of total precipitation value is considered to be relevant characteristic indicating sufficiently noticeable the long-term changes of temperature as well as precipitation conditions. More precisely the change of regime of particular precipitation state (liquid, solid and mixed) could be used as significant indicator of climate change evidence in specified region. Recently the snow cover extreme events, particularly calamitous flurries of fresh snow are occurring more frequent and theirs impact on society activities are becoming more obvious and serious in Slovakia. Regarding this fact we have decided to prepare a statistical analysis of selected characteristics of snow cover emphasizing the fresh snow cover extremes at particular meteorological stations in Slovakia within the 1951-2009 period.

2 RESULTS AND CONCLUSIONS

The analysis of long-term series of precipitation state ratio (liquid, solid and mixed) at selected meteorological stations has confirmed the existence of positive trend in the case of annual liquid and mixed precipitation rate and on the contrary the negative trend of annual solid precipitation rate in the south as well as north part of Slovakia, including mountain regions (e.g. the High Tatras; Figure 2). Analogous or even more expressive trends of proportion of particular precipitation state have been revealed for individual months as well as for period when solid and mixed precipitation predominate (in the cold half-year). Similarly the results of fresh snow cover depth analysis have shown an expected increase at considered meteorological stations in Slovakia in the winter (e.g. Oravská Lesná, Figure 1). The fresh snow cover depth maxima raking and its temporal occurrence support an exceptional status of the values recorded in the last decade of the 20th century and in the first decade of the 21st century, as well. In the case of n-days sum maxima (particularly 3-, 4- and 5-days sum) of fresh snow cover depth as well as the number of days with higher values of fresh snow cover depth the statistical analysis have preliminarily detected a significant positive trend for the most of territory of Slovakia in the winter (Figure 1).

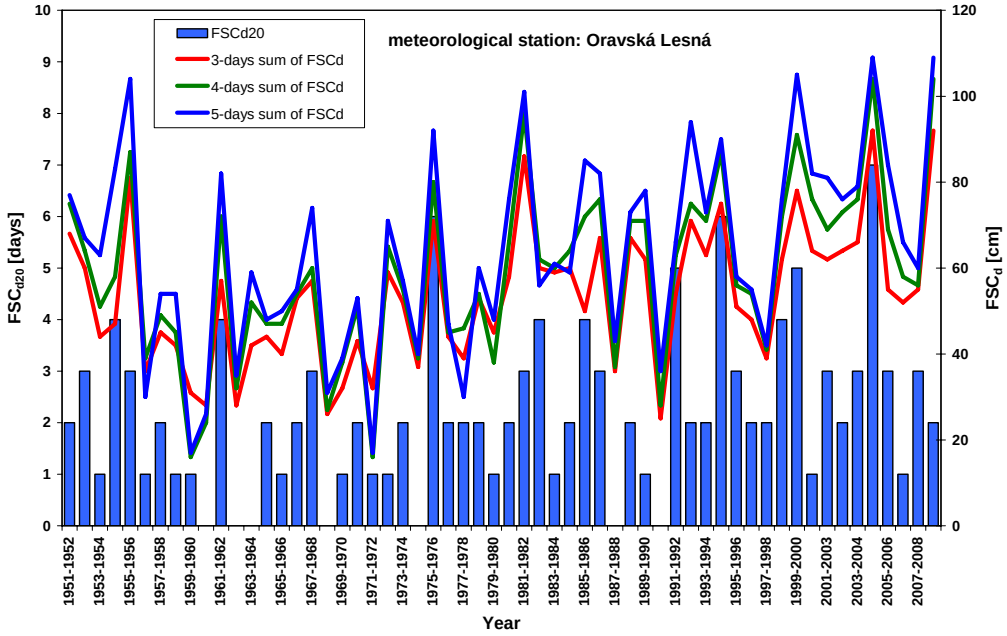

Figure 1. Number of days with fresh snow cover depth ≥ 20 cm (FSC_{d20}) and n-days sum of fresh snow cover depth (FSC_d) at mateorological station Oravská Lesná (780 m a.s.l.) in the 1951/1952-2008/2009 winter.

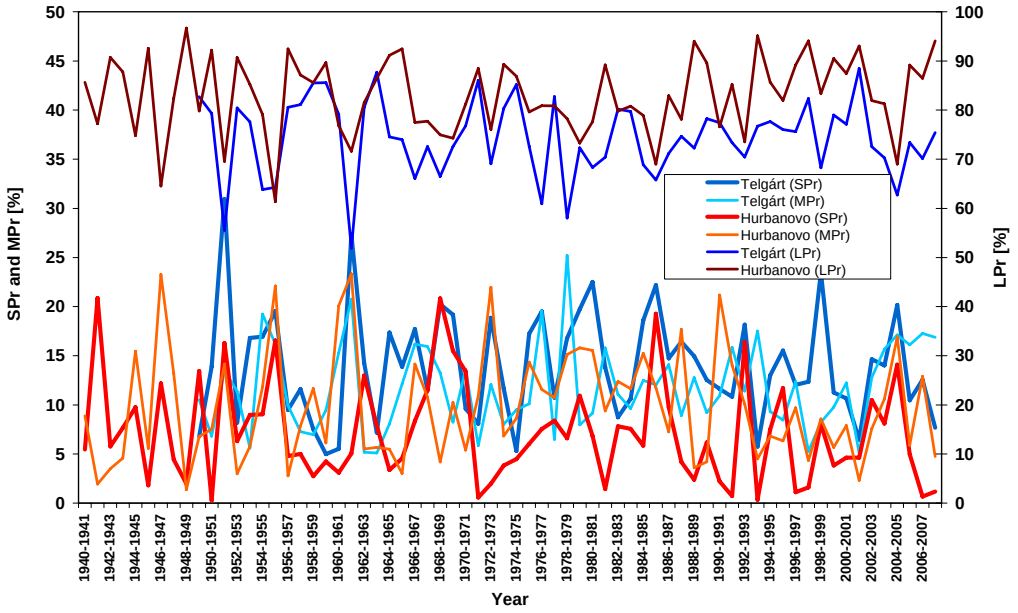

Figure 2. Liquid (LPr), solid (SPr) and mixed (MPr) precipitation rate at meteorological stations Hurbanovo (115 m a.s.l.) and Telgárt (901 m a.s.l.) in the 1941/1942-2008/2009 winter.

Acknowledgements: *We thank all contributors for their cooperation on the paper.*

REFERENCES

Faško, P., Handžák, Š., Lapin, M., 1997. Selected snow cover characteristics change in the Low Tatras region (Slovakia) in 1921-1995. In: National Climate Programme of the Slovak republic. Vol. 7, Slovak Ministry of the Environment and Slovak Hydrometeorological Institute, Bratislava 1997, p. 47-67.

Lapin, M., Faško, P., Pecho, J., 2007. Snow Cover Variability and Trends in the Tatra Mountains in 1921-2006. In: Proceedings of the 29th International Conference on Alpine Meteorology, Chambéry, France, 4.-8.6.2007.

Lapin, M., Melo, M., Faško, P., Pecho, J. (2007): Snow Cover Changes Scenarios for the Tatra Mountains in Slovakia. In: Proceedings of the 29th International Conference on Alpine Meteorology, Chambéry, France, 4.-8.6.2007.

Vojtek, M, Faško, P., Šťastný, P., 2003. Some selected snow climate trends in Slovakia with respect to altitude. In: Acta Meteorologica Universitatis Comenianae 32; p. 17-27.

15 YEARS OF SPECTRAL UV-MEASUREMENTS AT SONNBLICK OBSERVATORY: INVESTIGATION OF SHORT- AND LONG-TERM CHANGES AT AN ALPINE HIGH ALTITUDE STATION

Michael Fitzka, Stana Simic, Philipp Weihs, Helga Kromp-Kolb

Institute for Meteorology, University of Natural Resources and Applied Life Sciences, Vienna, Austria
E-mail: *michael.fitzka@boku.ac.at*

Abstract: Monitoring of spectral UV radiation and total ozone at Sonnblick observatory (3,106 m a.s.l.) is performed since 1994, representing the longest available time series of spectral UV in Austria. A current goal is to quantitatively understand the influence of clouds, ozone and surface albedo on spectral UV. Continuous measurements are examined alongside model calculations (SDISORT). The increases in surface UV during the last decades are calling for more detailed investigations. Long-term trends in UV irradiance are investigated based on clear sky measurements using trend tests. Results from Simic et al. (2008) show significant downward trends for several combinations of solar zenith angle and wavelength, which are apparently caused by an increase in sunshine duration during periods of high values of total ozone. Due to large variations and the serious dependence on various atmospheric parameters, detection of significant trends is notably hampered.

Keywords: *ICAM, UV radiation, ozone, albedo, short-term changes, trend detection, radiation transfer model*

1 INTRODUCTION

Surface UV levels are influenced by the concentration of total ozone and by clouds, surface albedo and aerosols. Knowledge of spectral UV radiation and its dependence on these parameters, which may change in the course of a changing climate, are prerequisites to quantitatively understand and estimate future UV radiation.

Increase of UV radiation during the last decades is reported where a decrease of stratospheric ozone has been observed (Bartlett and Web 2000). The magnitude of this change and their causes are, however, uncertain, calling for more detailed investigations of the influence of clouds, albedo, and other atmospheric parameters (Bais and Lubin et al. 2007). Monitoring of spectral UV exists since the beginning of the 1990ies. Thus, studies on long-term changes are hampered by the limited lengths of available data series (Glandorf et al. 2005).

The present study aims at estimating the impact of changing cloud cover, total ozone and surface albedo on spectral UV irradiance at Sonnblick observatory, using continuous measurements of spectral UV and radiation transfer model calculations. Additionally it is attempted to analyze the measurements of spectral UV irradiance for potentially underlying trends over the measurement period (Simic et al. 2008).

2 DATA & METHOD

Spectral UV irradiance and total ozone are being measured with a Brewer spectrophotometer at Sonnblick observatory since 1993 and an additional Bentham DM150 spectroradiometer since 1997. Brewer data were used for both short- and long-term investigations. Data from the Bentham spectroradiometer were employed in ancillary analysis (e.g. influence of changing snow-line). Cloud observations are regularly performed by the Austrian Weather Service, providing the input data for estimating cloud effects. A semi-empirical algorithm for the reconstruction of albedo based on snow observations was developed and deployed (Simic 2006).

The analysis of short-term changes in surface UV levels is based on a combination of measurements and model calculations (Arola et al. 2003). First off, actual measurements were reconstructed using the radiation transfer model SDISORT. A second data-set was created using a combination of daily climatological means of the model input data along with actually measured data. The variation of UV irradiance due to a specific parameter X (e.g. ozone, albedo, clouds) was then estimated as the ratio of modeled UV using the actual value of parameter X and climatological data of the *remaining* variables to modeled UV using climatological data of *all* variables, including parameter X. The amplitude was calculated as the spread of ratios divided by the mean ratio on a daily and on a monthly basis. The amplitude can then be regarded as the maximum variability due the specific parameter during a day respectively a month.

Long-term changes in surface UV levels were investigated for several combinations of wavelength and solar zenith angle in the time series of monthly deviations from the 13-year climatological mean values of UV irradiance under clear-sky conditions. Trends were identified through the use of regression models (R^2, Theil-Sen estimate) and tested for significance through various trend tests.

3 RESULTS

Throughout the year, ozone is the dominating parameter influencing surface UV levels. On a daily basis, ozone can cause variability of more than 200%, the highest values are found during late winter and spring, the period of the strongest interannual variation in stratospheric ozone. Enhanced cumulus convection surpasses the effect of ozone during summer, daily variability of more than 150% can be reached. Cloud influence is notably reduced during the rest of the year. Additionally, due to the station's high altitude, cloud-layer thickness is smaller, reducing the influence of clouds compared to lower altitude stations (Arola et al. 2003). Albedo has its greatest influence in April. This is the period of snow-melt, causing the snow-line height and therefore albedo to change rapidly. Variability due to albedo can reach a maximum of 32% on a daily basis. On a monthly time-scale, despite being significantly reduced in magnitude, variations show the same behavior throughout the year.

Due to the relatively short time-series and the strong variations therein, only few trends could be reliably identified. Most of the significant changes were found at a solar zenith angle of 55°, representing the data selection criteria yielding the greatest number of available measurements. Trends were only found at wavelengths of 305 nm and higher, as variations are distinctly increasing with decreasing wavelength. Unexpectedly, the significant trends display decreases, rather than increases. This would suggest an increase in stratospheric ozone, but no significant changes were found in the time series starting in 1994.

The decreases my therefore be explained by increasing sunshine duration during spring and summer over the period of investigation: At a solar zenith angle of 55°, an increase of almost 19% per decade is present in the number of available clear-sky spectra over the whole period. At the same time, the increase during January to June is almost 45%/dec. This may explain the observed highly significant downward trends, since more measurements of UV irradiance during higher total ozone concentrations were included in the latter parts of the investigation period. The same behavior is found at different zenith angles, although less pronounced and significant. Tab. 1 summarizes the calculated trends.

SZA	305 nm	310 nm	315 nm	324 nm
45°	-9.5 $^{+}$	-11.1 $^{+}$	-10.5 $^{+}$	-9.8 $^{+}$
55°	-23.9 *	-19.9 *	-15.6 *	-14.4 *
65°	-3.8 $^{-}$	-5.7 $^{+}$	-4.6 $^{+}$	-6.0 $^{+}$

Table 1. Linear trends in relative departures of UV radiance from climatological monthly mean values, trends given in percent per decade, symbols to the right indicate trend significance (-: insignificant, +: significant, *: highly significant).

4 CONCLUSION

Surface UV levels show strong dependencies from the influencing factors ozone, clouds and albedo on different time scales. Seasonal variations in the influencing factors also lead to distinctly varying seasonal impacts on surface UV levels. The knowledge of the factors' contributions to UV variability is a prerequisite for the estimation of surface UV levels and the assessment of UV induced risks for human health, as well as the estimation of future UV levels in the course of a changing climate.

Investigations focusing on long-term changes in spectral UV radiation are still notably hampered by the high variations in the relatively short time-series. Despite being based on one of the longer time-series available today, only precautious statements regarding actual trends in surface UV levels can be given at a decent level of resilience. Longer time-series are a crucial basis for further assessments.

Acknowledgements:
This work has been funded by the Austrian Ministry of Agriculture, Forestry, Environment and Water Management and by the Commission of the European Communities, project "Stratosphere-Climate Links with Emphasis on the UTLS, Scout-03".

REFERENCES

Arola, A., Lakkala, K., Bais, A., Kaurola, J., Meleti, C., and Taalas, P.: Factors affecting short- and long-term changes of spectral UV irradiance at two European stations, J. Geophys. Res., 108(17), 9, 1–11, 2003.

Bais, A., Lubin, D., Arola, A., Bernhard, G., Blumthaler, M., Chubarova, N., Erlick, C., Gies, H., Krotkov, N., Lamtz, K., Mayer, B., McKenzie, R., Piacentini, R., Seckmeyer, G., Slusser, J., Zerefos, C., Feister, U., Fioletov, V., Gröbner, J., Kyrö, E., and Slaper, H.: Surface ultraviolet radiation: past, present and future, Scientific assessment of ozone depletion: 2006, 7(21), 1 – 54, 2007.

Bartlett, L. M. and Webb, A. R.: Changes in ultraviolet radiation in the 1990s: Spectral measurements from Reading, England, J. Geophys. Res.-Atmos., 105(D4), 4889–4893, 2000.

Glandorf, M., Arola, A., Bais, A., and Seckmeyer, G.: Possibilities to detect trends in spectral UV irradiance, Theor. Appl. Climatol., 81, 33–44, 2005.

Simic, S.: Investigations on the transfer of ultraviolet radiation on the Hoher Sonnblick, doctoral thesis, BOKU Vienna, 2006

Simic, S., Weihs, P., Vacek, A., Kromp-Kolb, H., and Fitzka, M.: Spectral UV measurements in Austria from 1994 to 2006: investigations of short- and long-term changes. Atmos. Chem. Phys., 8, 7033-7043; ISSN 1680-7324, 2008.

SATELLITE REMOTE SENSING ASSESSMENT OF CLIMATE RISKS AND IMPACTS ON ROMANIAN MOUNTAIN FORESTS

Maria Zoran

National Institute of R&D for Optoelectronics
Bucharest Magurele, 409 Atomistilor Street, MG 5, 077125 Romania
E-mail: *maria@dnt.ro*

Abstract: During last years, due to anthropogenic and climatic stressors, most Carpathian Mountain forests in Romania had experienced environmental degradation. As in mountain areas, climate changes rapidly with height over relatively short horizontal distances, mountain forests represent unique areas for the detection of climatic change and the assessment of climate-related impacts. Mountain forest landscape pattern and the biogeophysical variables controlling observed patterns can be addressed through time series remote sensing satellite imagery, which provide useful information on spatial variations in physiological characteristics, productivity, successional patterns, forest structure and decline. Multispectral, multiresolution and multitemporal satellite imagery is used to classify and map various forest and/or land-use types. The specific aims of this paper are to: 1) quantify the changes and rates of change between 1990 and 2008 in vegetative composition across a forest landscape in Romanian Carpathians on Prahova Valley using Landsat TM and ETM, MODIS data; 2) examine the changes in landscape structure in relation with climatic changes and extreme events; 3) assess the climate risks and their potential impact on Romanian mountain forests; 4) investigate and discuss the spatio-temporal changes observed in the landscape composition, pattern and structure o in the context of forest management activities and other disturbances. The preservation and enhancement of mountain forest vegetation cover in natural, semi-natural forestry ecosystems is an essential factor in sustaining environmental health and averting natural hazards. In order to decrease the risk for socio-economic impacts, long-term adaptive strategies in modern silviculture seem necessary.

Keywords: *Satellite remote sensing, climate change,. extreme events, Carpathian Mountain forests, Romania*

1 INTRODUCTION

The continuing and accelerating rate of global climate change and its potentially severe impacts on nature and mountain forest ecosystems addresses scientific and policy responses for possible help adaptation to the partly inevitable consequences. Monitoring the vegetation dynamics of the Carpathian Mountains forests in Romania is important for understanding the consequences of climate-driven changes in these areas. The transitional height regions of the mountain forests is expected to be sensitive to even small changes in environmental variables and thus it can offer early insight into potential changes in forest vegetation driven by climate and anthropogenic changes. Climate change is likely to change existing forest systems, as changes in phenology, length of growing season and northwards shift of forest species can be related to climate change (Olesen et al., 2007;IPCC, 2007). The anticipated increase in both climate variability and extreme events may influence forest health and biomass production (Leckebusch et al., 2007). In spite of the potential of adaptive capacity of forest systems to adjust to climate change (Schar, et al., 2004), an increase in the number of hot days, changes to potential evapotranspiration and more frequent occurrence of drought periods will have a direct impact on mountain forest condition. Climate impacts are of increasing concern to societies, particularly in regions with high climatic variability in context of local, regional and global climatic changes.

2 SATELLITE REMOTE SENSING IN FOREST RESEARCH

Satellite remote sensing, based on building spectral databases, global large datasets, refining validation, calibration procedures in multi-source, multi-temporal environment is an important investigation tool of land vegetation and forest cover monitoring at regional, national, and global scales. In order to estimate climate and anthropogenic impacts on forest vegetation, during the last years, satellite imagery has been used for the analysis of bio-geophysical parameters of forest ecosystems as well as for assessment of the soil moisture content, CO_2 (carbon dioxide), O_3 (ozone) and NO (nitrogen oxide) concentrations in forest ecosystems.
As forests act as sinks for carbon dioxide, these play a fundamental role in mitigating climate change, being very vulnerable to changes in meteorological variables as temperature, precipitation and extreme weather events, which can have destructive impacts and reduce the carbon sequestration potential of the forest. On the other hand, forest fires events have an even more negative effect since destroying the forest increases the amount of carbon dioxide in the atmosphere.

3. RESULTS

To evaluate the climate risk and impacts of the management practice on biophysical properties of the mountain forest system, a set of biophysical variables have been estimated from time series Landsat TM ,

ETM+ and MODIS data over 1990 - 2008 period. The data included vegetation indices, surface broadband albedos. To study climatic and anthropogenic impacts , have been done several classifications of forest vegetation (evergreen, mixed , decidous) over tested area- Prahova Valley, located in Southern Carpathian Mountains (Figure 1). Image pairs of the same vegetation index, for subsequent years, were subtracted producing continuous maps indicating areas of change. Statistical analysis was carried out to see if there is a correlation between the two sets of output. The analysis of different classifications over selected test area have shown mountain forest changes due to high levels of atmospheric pollution mainly close of main road traffic air masses dynamics at regional level as well as due to deforestation for land-use conversion.and disease epidemics.

The relationship between phenological development of mountain forests and climate variability is a critical element in understanding current and future impacts of global climate change. Based on Normalized Difference Vegetation Indices (NDVI) derived from satellite data , phenological changes observed in Crapathian temperate forest are strongly related to global climate change. Figure 2 represents NDVI map from MODIS TERRA 16/08/2007 image for Prahova Valley, Carpathian mountain forest test area.Some conclusions have been obtained : average satellite phenology is scalable from fine (IKONOS) to coarse (Landsat) satellite sensors scales, but important fine-grain distinctions (such as microclimates) are lost at coarser scales; interannual phenological variability recorded from MODIS satellites data has a great potential to be used in spectral/climatic models in synergy with in-situ monitoring data of biogeophysical parameters. Based on time series satellite data, continued analyses of interannual phenology will be an effective tool for monitoring mountain forest responses to global-scale climate variability as well as for assessment of climate risks and its impact on mountain environment. Forest cover has also a great impact on local mountain climate.

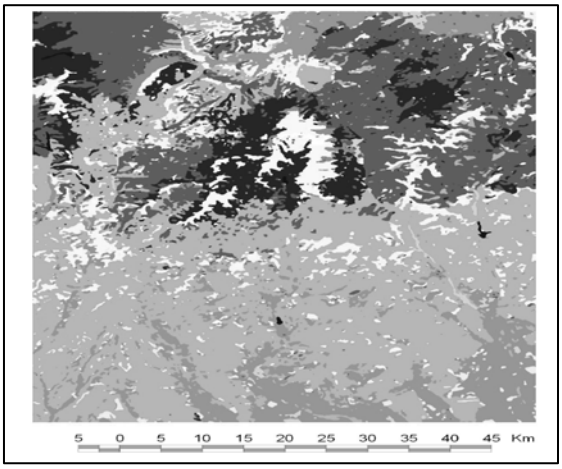

Figure 1. Forest vegetation classification on Landsat ETM+ 16/08/2007 for test area.

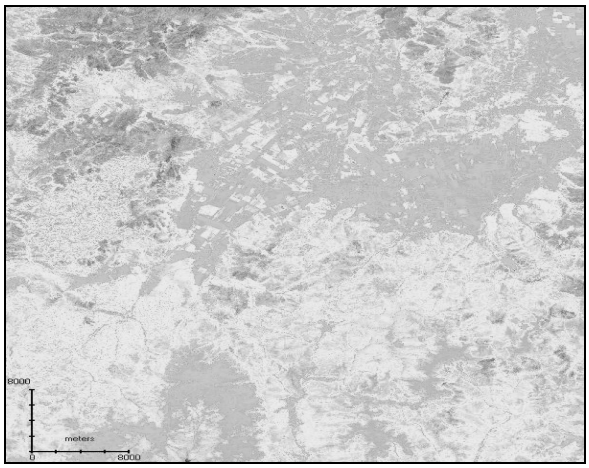

Figure 2. NDVI map from MODIS TERRA 16/08/2007 for Prahova Valley, Carpathian mountain forest test area

4 CONCLUSIONS

As a result of global climate change, there is a growing evidence that some of the most severe weather events could become more frequent in Romania over the next 50 to 100 years. In the case of Carpathian mountain forests, winter storms and heat waves are considered key climate risks, particularly in prealpine and alpine areas. Effects of climate extremes on forests can have both short-term and long-term implications for standing biomass, tree health and species composition. The preservation and enhancement of mountain forest vegetation cover in natural, semi-natural forestry ecosystems is an essential factor in sustaining environmental health and averting natural hazards. Romanian mountain forest system is under continuous influence of characteristic meteorological-climatic fluctuations of continental climate. For a better management and decision making is important to be performed medium and long term changes forecasting.

REFERENCES

Olesen, J., Fronzek, S., Heidmann, T., et al., 2007: Uncertainties in projected impacts of climate change on European agriculture and ecosystems based on scenarios from regional climate models. Climate Change **81**, 123–143.

IPCC (2007): Intergovernmental Panel on Climate Change Working Group II. Climate Change 2007: Impact, Adaptation and Vulnerability. IPC Working Group II [http://www.ipcc.ch].

Leckebusch, C.G., Ulbrich, U., Fro¨ hlich, L., Pinto, J.G., 2007: Property loss potentials for European midlatitude storm in a changing climate. Geophysical Research Letters 34, 05703.

Schar, C., Vidale, P.L., Lu¨ thi, D., Frei, C., Ha¨ berli, C., Liniger, M., Appenzeller, C., 2004: The role of increasing temperature variability in European summer heat waves.Nature 427, 332–336.

EEA Report No 4/2008, Impacts of Europe's changing climate - 2008 indicator-based assessment.

TRENDS IN HEAVY PRECIPITATION IN MOUNTAINOUS AND LOWLAND AREAS IN CENTRAL EUROPE: ARE THE DIFFERENCES RELATED TO CHANGES IN CIRCULATION?

Jan Kysely[1]

[1] Institute of Atmospheric Physics AS CR, Prague, Czech Republic
E-mail: *kysely@ufa.cas.cz*

Abstract: Trends in winter-time indices of heavy precipitation are evaluated at rain-gauge stations covering the Czech Republic over 1961-2005. The study focuses on differences between mountainous and lowland areas and other regional patterns. For all characteristics of heavy precipitation, spatially coherent increasing trends are identified; they are more pronounced in the western than eastern part of the country, with relative magnitudes mostly between +20 and +30% over the 45 years. The increases in heavy precipitation are generally stronger at sites in higher-elevated and mountainous regions that are windward in prevailing southwestern to northwestern flows, which points to the fact that changes in the frequency and intensity of zonal circulation play important roles in governing changes in precipitation extremes. The analysis partly supports an emerging global picture of prevailing positive trends in precipitation extremes over the mid-latitudinal land areas of the Northern Hemisphere in winter. However, the differences between mountainous and lowland regions and the cut-off between the western and eastern parts of the Czech Republic indicate that (i) the observed trends are to a large extent driven by changes in zonal circulation, and (ii) the pattern of changes becomes more complex and less coherent in regions where the changes in zonal circulation play less important role.

Keywords: *heavy precipitation, trend analysis, atmospheric circulation, central Europe*

1 INTRODUCTION

Trends towards higher frequency and intensity of winter-time precipitation extremes have been found in many extratropical regions of the world, including western and central Europe (e.g. Moberg and Jones 2005; Hundecha and Bardossy 2005; Schmidli and Frei 2005). The present study evaluates regional patterns of trends in various indices of heavy precipitation, and differences between mountainous and lowland areas, using high-quality dataset from rain-gauge stations covering the Czech Republic. For details concerning quality of the data, methodology used, results for other seasons and their interpretation refer to paper in *International Journal of Climatology* (Kyselý 2009).

2 DATA AND METHODS

Daily precipitation totals measured over 1961-2005 at 175 stations are used as an input dataset. The altitudes of stations range from 150 to 1322 m a.s.l. There were no significant station displacements during 1961-2005, and the daily series of precipitation records are uninterrupted.

Common indices are selected to characterize various aspects of the intensity of heavy precipitation events in winter (DJF); they include maximum seasonal *k*-day precipitation amounts, 'rain intensity index' (RII), defined as the mean precipitation amount per wet day, and percentage of total precipitation falling on days above long-term seasonal 90th and 95th percentiles of daily amounts (%P90, %P95).

Non-parametric Kendall's tau is used to estimate linear trends; statistical significance of the trends is evaluated by the Mann-Kendall test.

3 RESULTS

Increasing trends dominate over the western part of the Czech Republic in all indices of heavy precipitation in winter (Fig. 1). The trends are positive at about 90% of stations, and approximately one third of them are significant at p=0.10. For rain intensity index (RII), the positive significant trends appear at 50%/36% of sites if evaluated at p=0.10/0.05. Relative magnitudes of the trends are usually between 3 and 10% per 10 years, but they exceed 10% per 10 years at about one tenth of sites for the *k*-day winter maxima, and at one fifth (two fifths) of sites for the percentage of precipitation occurring on days above the long-term seasonal 90th (95th) percentiles (%P90, %P95). In most characteristics, the positive trends are more pronounced and spatially more uniform in the south (the Vltava river basin) than the north areas (the Elbe river basin) of the western region. For some of the indices (e.g. R5, %P90), relatively large areas appear in the southwest where all (or nearly all) locations posses increasing trends that are significant at p=0.10.

Over the eastern part of the Czech Republic, increasing trends are more frequent than decreasing ones for most indices of heavy precipitation (except for RII), but they are insignificant and spatially incoherent. The fraction of positive trends significant at p=0.10/0.05 does not exceed 12%/9% in any characteristics of extremes.

Increases prevail in the mountainous and highland areas while decreases or trends close to zero in the lowland regions, mainly in the eastern part of the country. This appears to be related to the enhanced influence of windward slopes under

more frequent and intense zonal circulation in winter (cf. Jacobeit et al. 2001). The spatial pattern of trends in heavy precipitation in winter is also linked to trends in mean precipitation which are increasing in the western part of the country while there is no clear trend (with decreases being more frequent) in the eastern region (Kyselý 2009).

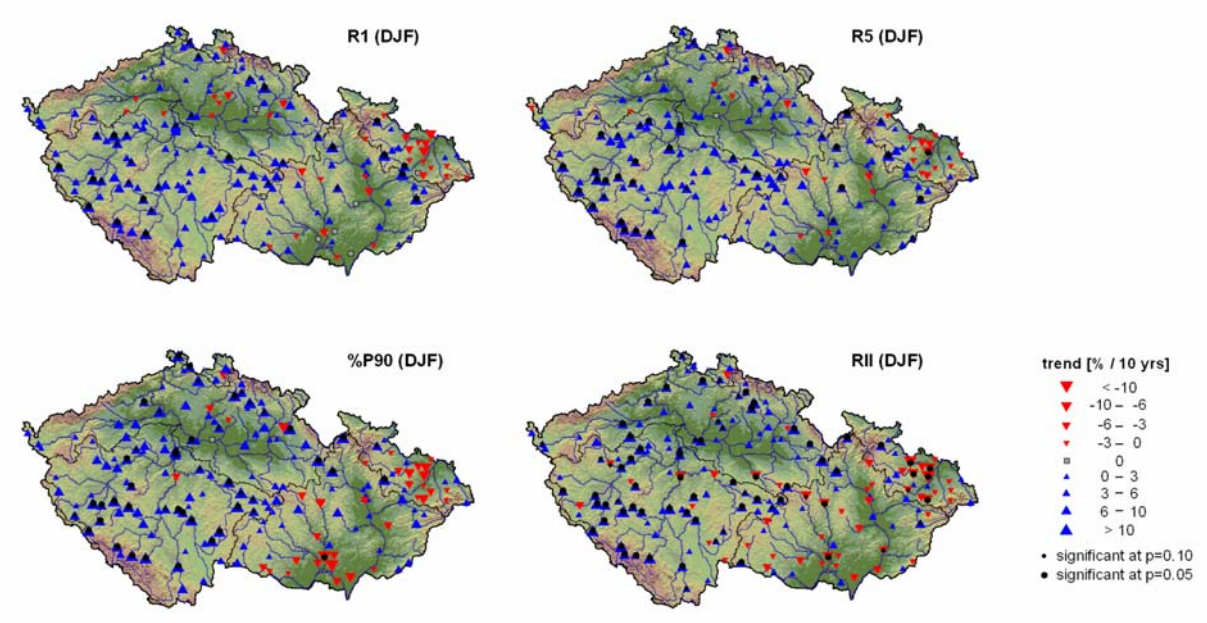

Figure 1. Trends in characteristics of heavy precipitation in winter. Increasing (decreasing) trends are marked by ▲(▼).

4 CONCLUSIONS

Spatially coherent and statistically significant increasing trends have been identified for all indices of winter-time heavy precipitation in the western part of the Czech Republic. This finding is in accord with results for relatively nearby regions in Germany (Hundecha and Bardossy 2005), Switzerland (Schmidli and Frei 2005) and northern Italy (Brunetti et al. 2001). The mean rise of 21-26% over the 45 years for 1-day to 20-day winter maxima (averaged over the stations), and 30-35% for the fraction of precipitation falling on days exceeding the long-term 90th and 95th percentiles is relatively large compared e.g. with the centennial increases in high quantiles and the seasonal 1- to 10-day extremes in Switzerland, which were between 10 and 30% in winter (Schmidli and Frei 2005). However, this change is the only widespread and spatially uniform trend in heavy precipitation over all seasons, and it is not clearly observed in the eastern part of the Czech Republic where Mediterranean influences play more important roles in producing heavy precipitation events. The trends are generally more pronounced in the western than eastern parts of the country and in mountainous than lowland sites, which suggests that the increases are linked to the modes of the North Atlantic climate variability (e.g. the North Atlantic Oscillation) and changes in the intensity of the zonal circulation.

Acknowledgements: *The study was supported under project B300420801 of the Grant Agency of AS CR. Thanks are due to O.Halásová, Czech Hydrometeorological Institute, Hradec Králové, for drawing the maps, and P.Štěpánek, Czech Hydrometeorological Institute, Brno, for providing the daily precipitation dataset and performing quality checks.*

REFERENCES

Brunetti M, Maugeri M, Nanni T. 2001. Changes in total precipitation, rainy days and extreme events in northeastern Italy. *International Journal of Climatology* **21**: 861-871

Hundecha Y, Bardossy A. 2005. Trends in daily precipitation and temperature extremes across western Germany in the second half of the 20th century. *International Journal of Climatology* **25**: 1189-1202

Jacobeit J, Jönsson P, Bärring L, Beck C, Ekström M. 2001. Zonal indices for Europe 1780-1995 and running correlations with temperature. *Climatic Change* **48**: 219-241

Kyselý J. 2009. Trends in heavy precipitation in the Czech Republic over 1961-2005. *International Journal of Climatology*, doi: 10.1002/joc.1784.

Moberg A, Jones PD. 2005. Trends in indices for extremes in daily temperature and precipitation in central and western Europe, 1901-99. *International Journal of Climatology* **25**: 1149-1171

Schmidli J, Frei C. 2005. Trends of heavy precipitation and wet and dry spells in Switzerland during the 20th century. *International Journal of Climatology* **25**: 753-771

SCENARIOS OF AIR HUMIDITY AND SATURATION DEFICIT CHANGE FOR SLOVAKIA

Milan Lapin and Martin Kremler

Faculty of Mathematics, Physics and Informatics, Comenius Univ. in Bratislava, Slovakia
E-mail: lapin@fmph.uniba.sk, kremler@fmph.uniba.sk, Web: www.dmc.fmph.uniba.sk

Abstract: About 30 meteorological stations in Slovakia have complete and good quality observations since 1951 (1961). Most of them well represent important sub-regions, like the Danubian lowland and area round the Tatra mountain. The paper presents detail daily air humidity and daily saturation deficit analysis from 6 stations in 1961-2008, including some information on air temperature and humidity (5 of those stations lie in the Tatra mountains, Hurbanovo in the lowland). In 2007 the newest Canadian CGCM3.1 model with daily data outputs have been analyzed (IPCC emission scenarios SRES-A2 and B1 applied). Based on the CGCM3.1 outputs the scenarios of daily data in 1961-2100 are presented for selected stations.

Keywords: *measured air humidity, Canadian GCM3.1 outputs, modeled humidity data, modeled evapotranspiration.*

1 INTRODUCTION

Temperature increase by 1.6°C and precipitation decrease by 25 mm (3.1%) was registered in Slovakia in the 1881-2008 period. On the other hand annual relative air humidity means decreased in the lowlands by 5% since 1901. This decrease was less significant in the mountains. Water vapor pressure had insignificant trend in 1901-2008 in all year round with some lower values in 1976-1993. Significant increase in air temperature and changes in precipitation occurred in Slovakia predominantly after 1985. These changes influenced regime of air humidity, potential (E_o) and actual (E) evapotranspiration, soil moisture and runoff mainly in southern Slovakia. For example, E_o increased at Hurbanovo (lowland, 115 m a.s.l.) by 17.5% in 1951-2008.

2 METHOD AND RESULTS

Saturation deficit (d) enables to calculate monthly E_o sums by several methods (Lapin et al. 2008). A common formula can be expressed as $E_o = k.d$, where k is a coefficient different for any month and any region. The CGCM3.1 based scenarios of E_o were are calculated using simple Zubenok formula and saturation deficit (d – difference between saturated and actual water vapor pressure). Selected data and humidity scenarios from the CGCM3.1 outputs downscaling for Slovakia are in Tables 1 and 2.

Modeled d means will increase up to 2100, both at A2 and B1 scenarios. More intense increase is modeled for A2 scenario (Table 2), in the April to September season (Growing season – GS) 2071-2100 up to 20% compared to period 2001-2030 (up to 40% trend in 1961-2100), and only by 8% at the B1 scenario (up to 17% trend in 1961-2100). If the A2 scenario will fulfill, the increase in E_o can reach even 25-30% in the GS compared to 1951-1980 averages. The d and E_o increase will be less significant in the mountains (Table 2 and Figure 1).

Because of insignificant change in precipitation totals is supposed (some small decrease is more probable in the lowlands), it is expected a decrease in soil moisture up to 25% and runoff decrease up to 25% in Slovakia. The presented method of water balance related variables calculation can be applied also for other Slovak localities with sufficiently reliable data on air humidity and temperature.

Acknowledgement:
Some parts of this paper are based on the results of project VEGA No. 1/4033/07 and the observed SHMI data.

Table 1. Deviations of Growing Season (GS = April to September) mean values in selected periods between SRES A2 and SRES B1 scenarios and between SRES A2 scenario and measured averages in 1961-1990 (T – air temperature, e – water vapor pressure, U – relative humidity, Hurbanovo, 115 m a.s.l., Strbske Pleso, 1360 m a.s.l.).

Station	Element		1961-1990	1991-2020	2021-2050	2051-2080	2071-2100	1996-2025	2016-2045	2061-2090
Hurbanovo	T (A2-B1)	[°C]	0.0	0.2	0.0	1.1	1.7	0.2	0.2	1.0
Hurbanovo	T (A2-M)	[°C]	0.0	0.7	1.8	2.8	3.9	1.0	1.7	3.2
Hurbanovo	e (A2-B1)	[hPa]	0.0	0.0	0.1	0.8	1.5	0.0	0.0	1.0
Hurbanovo	e (A2-M)	[hPa]	0.1	0.6	1.5	2.5	3.5	0.7	1.3	2.9
Strbske Pleso	U (A2-B1)	[%]	0.0	-0.9	0.0	-0.9	-1.0	-0.6	-0.9	0.0
Strbske Pleso	U (A2-M)	[%]	0.6	0.4	-0.2	0.5	-0.2	0.0	-0.5	0.7
Hurbanovo	U (A2-B1)	[%]	0.0	-1.1	0.2	-0.6	-0.7	-1.2	-0.8	0.2
Hurbanovo	U (A2-M)	[%]	-1.0	-1.8	-1.5	-1.4	-1.6	-2.1	-1.9	-0.9

Table 2. Mean values of Growing Season (GS) saturation deficit *d* [hPa] in selected periods (Mean – average of daily $d = e^* - e$; MeMax – average of GS maxima in daily *d*; e^*, *e* – saturated and actual atmospheric water vapor pressure 2 m above ground; M1961-1990 – based on measurements, other columns – modified CGCM1.3 SRES A2 model values, A2-B1 – difference of *d* between Mean SRES A2 and Mean SRES B1, selected periods represent the scenarios frames used in Slovakia).

Station Altitude	*d* [hPa]	M1961-1990	1961-1990	1991-2020	2021-2050	2051-2080	2071-2100	1996-2025	2016-2045	2061-2090
Poprad	Mean	**4.0**	**4.1**	**4.4**	**4.8**	**4.9**	**5.3**	**4.5**	**4.9**	**5.0**
695 m	MeMax	11.3	11.2	12.4	13.9	14.2	14.4	13.0	14.0	14.4
	A2-B1		0.0	0.2	0.1	0.5	0.6	0.1	0.2	0.4
Telgart	Mean	**3.0**	**3.2**	**3.4**	**3.8**	**3.9**	**4.2**	**3.5**	**3.8**	**3.9**
901 m	MeMax	9.2	9.7	10.6	12.4	12.4	12.5	11.3	12.3	12.5
	A2-B1		0.0	0.2	0.1	0.5	0.5	0.1	0.2	0.3
Lipt. Hradok	Mean	**4.3**	**4.5**	**4.7**	**5.2**	**5.3**	**5.7**	**4.9**	**5.2**	**5.4**
640 m	MeMax	12.9	12.4	13.4	15.2	15.1	15.5	14.2	15.2	15.2
	A2-B1		0.0	0.2	0.1	0.5	0.7	0.2	0.2	0.4
Strbske Pleso	Mean	**3.1**	**3.2**	**3.4**	**3.8**	**3.9**	**4.2**	**3.5**	**3.8**	**3.9**
1360 m	MeMax	11.1	11.3	12.4	14.0	14.7	14.5	13.0	14.1	14.8
	A2-B1		0.0	0.2	0.0	0.4	0.6	0.1	0.2	0.3
Sliac	Mean	**5.0**	**5.2**	**5.5**	**6.0**	**6.2**	**6.6**	**5.7**	**6.0**	**6.3**
313 m	MeMax	13.2	13.2	14.3	15.7	16.1	16.4	14.9	15.8	16.0
	A2-B1		0.0	0.2	0.1	0.6	0.8	0.2	0.3	0.5
Hurbanovo	Mean	**6.5**	**6.6**	**7.1**	**7.6**	**8.0**	**8.7**	**7.3**	**7.7**	**8.2**
115 m	MeMax	17.6	17.1	18.1	19.8	21.8	22.0	18.9	19.9	21.8
	A2-B1		0.0	0.4	0.0	0.7	1.1	0.3	0.2	0.7

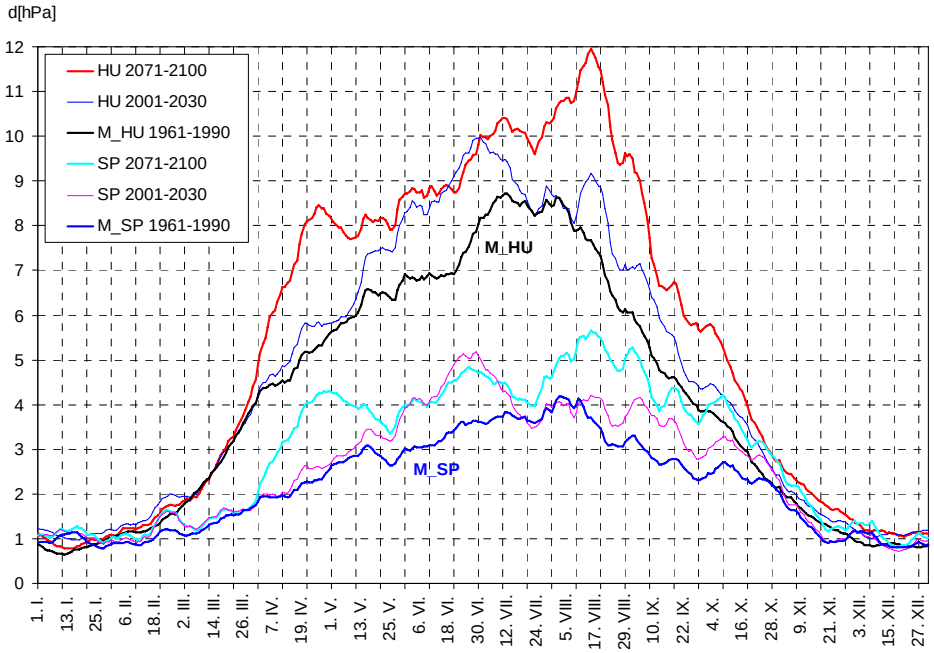

Figure 1: Annual patterns of mean saturation deficit *d* [hPa] at Hurbanovo (HU 115 m a.s.l.) and Strbske Pleso (SP 1360 m a.s.l.), measured (M) in 1961-1990 and modeled in 2001-2030 and 2071-2100 (modified CGCM3.1 SRES A2 model outputs), all 11-day running means, significant d increase is supposed mainly in the April to September season (GS).

REFERENCES

Boer, G. J., Flato, G. & Ramsden D., 2000: A transient climate change simulation with greenhouse gas and aerosol forcing: Projected climate to the twenty-first century. Climate Dynamics, 16: 427–450.

Halmova, D., Melo, M., 2006: Climate change impact on reservoir water supply reliability. IAHS – AISH Publication, Wallingford, 308, 407-412.

Lapin, M., Drinka, R., Kremler, M., Tomlain, J., 2008: Scenarios of Air Humidity and Potential Evapotranspiration Change for Hurbanovo, 16 pp. In: CD Proc. of the XXth Czecho-Slovak Bioclimatological Conference, Mikulov, Czech Republic.

Recommendation on calculation of evaporation from the continent surface 1976. Utverzhdeny GUGMS, Min. melioracii i vodnogo khozyajstva SSSR, Min. seljskogo khoz. SSSR. Gidrometeoizdat, Leningrad. (in Russian)

Étude de l´Impact de la Variabilité du Climat et des Changements Climatiques sur la Guinée-Bissau.

Cherno Luis Mendes

Direction Générale de la Météorologie Nationale de la Guinée-Bissau
E_mail: Cherno_lm@yahoo.fr;

Resumé

Les changements climatiques (augmentation de température, réduction de pluviométrie) qui puissent affecter directement la régénération naturelle des forêts ou les facteurs anthropiques persistants comme le feu de brousse abusifs des aires forestières il aura par conséquent une réduction du revêtement végétal, ce qui obligera les autorités à prendre des mesures de réduction ou de suspension de licences de sciage qui à la fois réduira la production des sciages, menant par conséquent à la réduction de la production des charpenteries et la disparition de certains. Compte tenu de l'évolution de la dégradation du moyen naturel comme conséquence des changements climatiques au niveau national, les entreprises forestières verront certainement leur aires d'exploitation (abattages) réduites à un pourcentage drastique ou à 50 %, ou encore dans une situation de crise majeure de dégradation de forêts voir leur licences supprimés.

1. Introduction

Les services météorologiques nationaux doivent orienter ses actions dans une perspective d´appui au développement socio-économique et coopération international, pour permettre sauver la vie humaine et des biens matériels, la défense civil et l´appui à une large spectre des activités économiques, tels que la agriculture et la production alimentaire, la navigation aérienne, la pêche, et la navigation maritime, la gestion des ressources hydriques, l'industrie, l´énergie, le tourisme et la gestion et protection de l´environnement etc. Les observations climatiques qui permet de caractériser les éléments du climat sont : la température, l'humidité relative, la précipitation l'insolation, le vent etc.

2. La vulnérabilité des secteurs et les impacts des changements climatiques sur ces secteurs, surtout dans les systèmes de production.

Pour ce que concerne la température, et selon le même rapport, les projections pour l'horizon 2100 se traduit dans une augmentation de 2 °C, avec des intervalles de variations de 0,1 à 8,2 °C.

En se basant sur la connaissance del' écologie et les limites de tolérance de certains cultures plus pratiquées dans le pays, on a constaté qu'une augmentation de la température et de pluviométrie qui dépassent les limites de tolérance de ces cultures entraînant des altérations significatives dans la floraison, rendement, odeur, goût, etc. selon les cas. Pour ce qui est de la température, et si on considère que les maximum atteint les entre 32 à 39 °C (mars/mai) et les minimum 20 à 24 °C (décembre à février), une augmentations de 2 °C à l'horizon 2100 déchaînerait possiblement des augmentations de l'ordre de 34 à 41 °C, dans les mois chauds, et 22 à 26 °C pour les mois moins chauds.

Dans ces circonstances, les cultures d'acajou et les horticoles seraient dans des conditions adverses de développement, puisqu'ils dépasseraient les limites de tolérances hydrique et environnementale, parce que la floraison et récolte de acajou devraient coïncider avec les mois de mars, avril et mai. La production horticole serait aussi menacée pourvu qu'elle commence dans les mois novembre jusqu'à mai et juin. De ce fait, la culture serait la plus affectée avec des altérations des températures prévues pour l'horizon 2100, suivie de celle de l'horticole.

3. Température

Les conséquences de l'augmentation des concentrations des gaz à effet de serre les températures moyennes globales ont été obtenues à l'aide du GCM MAGIC/SCENCE. Pour la projection des réchauffements globaux pour les latitudes de la Guinée-Bissau pour l'horizon 2050 et 2100, toutes les sensibilités ont présenté des graduations de valeurs positives dans des conditions du scénario de l'émission IS92a par rapport à la valeur normale 1961-1990. En utilisant les sensibilités 1, 5, 2,5 et 3,5 °C pour l'horizon 2050, le model prévoit une augmentation de température de l'ordre de 1,1 à 1,5 °C et pour l'horizon 2100 une augmentation de 2 °C avec intervalles de variations 0,1 à 2,8 °C.

4. Precipitation

En Guinée-Bissau il a été remarqué une baisse de la pluviométrie, passant de 6 à 5 mois dans l'année (juin à octobre), au contraire des années précédentes. Actuellement, les pluies presque accompagnées de vents forts engendrent des dégâts dans les plantations et cultures. Selon les informations obtenues à partir du service météorologie nationale, les niveaux attendus de diminution de pluviométrie pour l'horizon 2100 seraient d'environ 11,7 %.

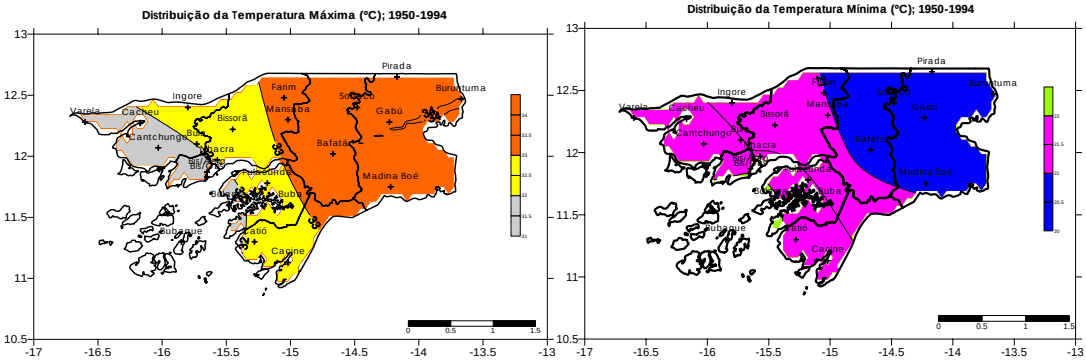

Fig. 1 (a) : Distribution de la température maximale et minimale pour la Guinée-Bissau (période 1950-1994)

Par rapport à ce paramètre climatique, il serait possible d'observer deux situations : notamment des situations des valeurs minimales et maximales. Les spéculations sont faites à partir des valeurs moyennes considérées plus basses. Dans cette situation, une diminution de 11,7 % de pluviométrie produirait une diminution des valeurs minimales de 117 mm dans la zone nord et centre et 176 mm pour la zone sud et les îles. Cela implique que les pluies passeraient de 1000 mm pour 883 mm dans la zone nord et centre, et de 1500 mm pour 1325 mm pour la zone sud et les îles. Si on suit le raisonnement, même, pour les valeurs maximales de 1500 et 2000 mm, il y aurait de même, une diminution de pluviométrie de 1500 pour 1583 mm dans la zone nord et centre, et de 2000 par 1825 mm pour la zone sud et les îles. Donc, la pluviométrie projetée pour l'horizon 2100, malgré sa tendance de diminution, ne posera pas de danger en termes quantitatifs dans le secteur de l'agriculture. De même pour un scénario plus pessimiste, les valeurs estimées se situeront entre 883 et 1383 mm, quantités valables pour une production agricole, dans les conditions d'une bonne distribution du point de vue spatio-temporelle.

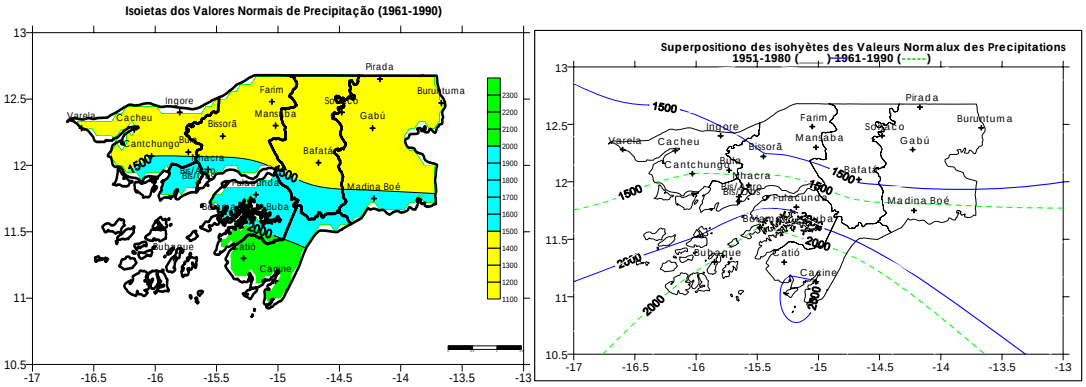

Fig. 2 (b) : Graphiques de la distribution de la pluviométrie et de sa décalage vers le sud de la Guinée-Bissau (période : 1961-1990)

5. Conclusion

Malgré la grande pression dont les forêts guinéennes sont cibles, elles représentant une importante source de séquestration du CO2 atmosphérique, dont la valeur est calculée à 11.288.401 kilotonnes. L'étude de cas, dans le cadre de l'option de mitigation dans le secteur forestier, pour une petite superficie d'une peu plus de mille kilomètres carrés, illustre bien cette capacité de séquestration, la quantité de carbone séquestrée, suite à l'atténuation est estimé à 883.207.649 tonnes (huit cents quatre vingt trois millions, deux cents sept mille et six cents quarante neuf tonnes), en 40 ans d'application des mesures d'atténuation (2005-2044).

D'une manière générale, les données de l'inventaire des GES prouvent que la Guinée-Bissau est loin d'être un pays polluant et émetteur de ces gaz, ce qui laisse conclure que sa part dans l'échauffement global est dérisoire, cela, dans les conditions où les facteurs socio-économiques responsables par les émissions ne s'aggravent pas, ce qui suppose l'adoption des mesures qui tendent à limiter ces émissions.

6. Bibliographie

2006 : Communication Nationale Initiale de la Guinée-Bissau sur les Changements climatiques pp-220.

MODELLING OF NOCTURNAL DRAINAGE WINDS AT METEOR CRATER, ARIZONA USING KLAM_21

Meinolf Kossmann[1], Sebastian W. Hoch[2], C. David Whiteman[2], Uwe Sievers[1]

[1] Deutscher Wetterdienst, Offenbach am Main, Germany. E-mail: *meinolf.kossmann@dwd.de*
[2] Department of Meteorology, University of Utah, Salt Lake City, UT, USA

Abstract: Nocturnal airflow conditions at Meteor Crater, AZ are simulated with the single-layer drainage wind model KLAM_21 to support interpretation of field observations taken during the METCRAX 2006 campaign. A heat budget analysis is conducted to estimate the contribution of intrusions on the bulk nocturnal heat loss inside the crater.

Keywords: *meteor crater, drainage winds, flow splitting, cold air pooling, heat budget*

1 INTRODUCTION

The single-layer cold air drainage model KLAM_21 of the Deutscher Wetterdienst (Sievers, 2005; Kossmann and Sievers, 2007) is used to simulate nocturnal drainage winds at Arizona's Meteor Crater. Results are compared with observational data gathered during the METCRAX 2006 field campaign (Whiteman et al., 2008), which included frequent vertical soundings inside and outside of the crater. The crater is located on the Colorado Plateau about 40 km east-southeast of Flagstaff, AZ. In the vicinity of the crater, the Colorado Plateau is inclined from southwest (Mogollon Rim) to northeast (Little Colorado River) and mostly covered by rocks and bare soil. The depth and the diameter of the crater at the rim are approximately 170 m and 1.2 km, respectively. The crater rim is about 30 to 60 m above the level of the surrounding Colorado Plateau.

Model simulations for idealised nights with no ambient wind have been carried out in a 75 km x 75 km domain with a grid resolution of 50 m in the 10 km by 10 km inner grid and a 250 m resolution outside the inner grid (Fig. 1). Prescribed, spatially and temporally constant local heat loss rates of 30, 20, and 15 W/m^2 were used to account for variations in nocturnal cloud cover.

2 RESULTS

In agreement with observations (Savage et al., 2008), the model simulates the development of regional scale southwesterly drainage winds down the Colorado Plateau, although modelled wind speeds are somewhat lower than those observed. Due to the terrain elevations of the crater rim, these southwesterly drainage winds are deviated around the crater, which is associated with flow deceleration due to blocking and flow splitting on the windward side and flow convergence on the leeward side, while flow acceleration is found on the northwestern and southeastern sides of the crater (Fig. 2). Under cloud-free conditions (30 W/m^2 run) the depth of the southwesterly drainage winds exceeds rim height about 2.5 hours after sunset. The resulting flow of cold air over the rim into the crater generates jet winds above the rim and disturbs the previously decoupled conditions inside the crater (Fig. 2). The 20 and 15 W/m^2 runs simulate the onset of inflow about 3.5 and 5 hours after sunset, due to a slower growth of the depth of the regional southwesterly drainage winds.

Inside the crater the results for all model runs show downslope winds converging towards the crater bottom and a continuously growing cold air lake with extremely weak winds. After the onset of inflow the single-layer physics of KLAM_21 causes all cold air crossing the crater rim to subside into the crater, leading to an accelerated growth of the cold air lake inside the crater. In contrast, observations inside the crater show the development of a two-layer thermal structure early in the night, which is characterised by a strong, approximately 30 m deep temperature inversion at the crater bottom and an almost isothermal layer aloft which extends to rim level (Fig. 3). During the course of the night this two-layer structure is maintained while the crater atmosphere is cooling continuously and a temperature jump develops at rim level. The maintenance of the near-isothermal layer in the crater is indicative to the presence of turbulent mixing processes in the upper part of the crater atmosphere throughout the night. This mixing possibly results from wind shear near rim level and from drainage wind detrainment at the crater sidewalls (Whiteman at al., 2009).

The total nocturnal heat deficit and associated heat loss rates in the crater were estimated from both, model outputs and observations. While the prescribed local loss rates are of similar magnitude as those estimated by Hahnenberger (2008) from vertical temperature soundings outside the crater, it appears that the advective contribution of inflow to the total heat loss inside the crater is clearly overestimated by the model KLAM_21. This finding supports the indirect conclusion that a significant amount of cold air crossing the crater rim is flowing over the crater, while only a fraction of this air actually subsides into the crater, thereby contributing to heat loss in the crater (Fig. 3).

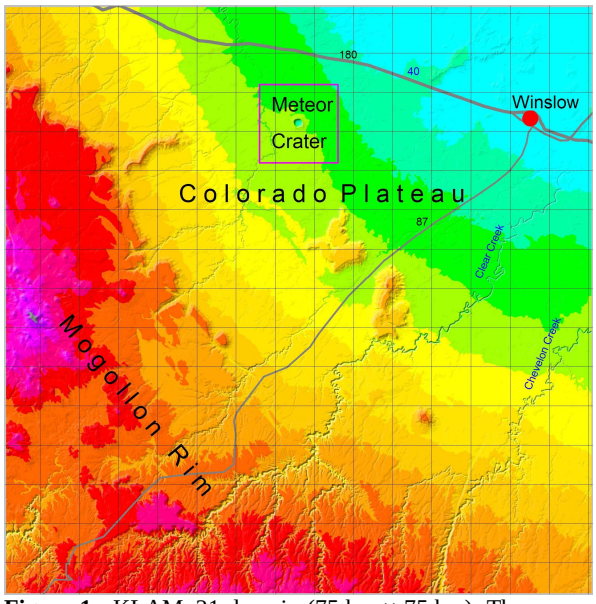

Figure 1. KLAM_21 domain (75 km × 75 km). The square shows the 10 km × 10 km nested high resolution area centred at the crater. Colour shading indicates terrain height with 75 m height intervals.

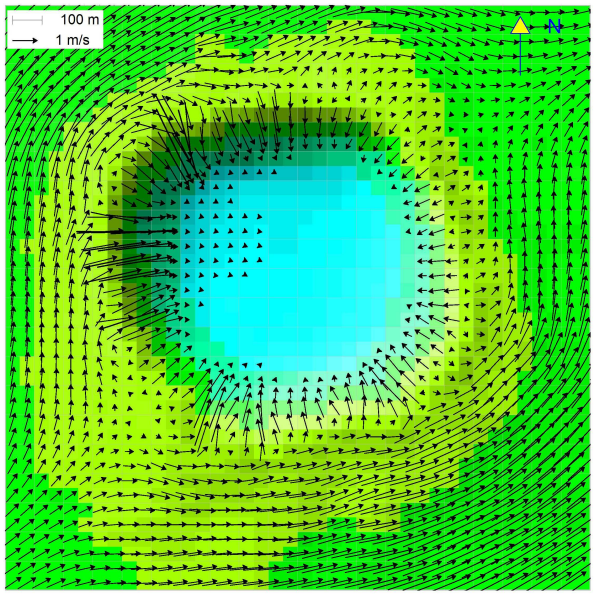

Figure 2. Mean wind vectors in the cold air layer at 3h after onset of surface cooling (30 W/m^2 run). 'Sun shading' is superimposed on the colour shading of the terrain elevation (50 m height intervals) to enhance relief visualisation.

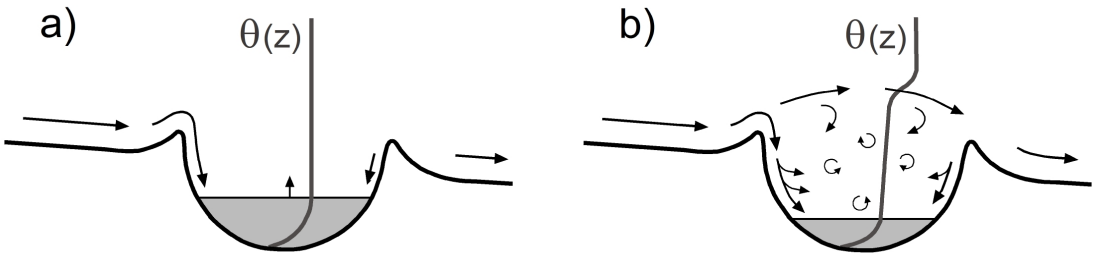

Figure 3. Influence of regional drainage wind intrusions on boundary layer structure and heat loss in the Meteor Crater. The schematic representations illustrate results from KLAM_21 (a) and a hypothesised real world behaviour (b).

3 CONCLUSIONS

Regional southwesterly drainage winds approaching the Meteor Crater and favourite locations of intrusions into the crater are well captured by the KLAM_21 simulations. However, the simulation of the multi-layer structure observed inside the crater is beyond the capabilities of the single-layer drainage wind model KLAM_21. A bulk heat budget analysis of the crater atmosphere suggests that the contribution of inflow to the total heat loss inside the crater is overestimated by KLAM_21. It is therefore hypothesised that a significant fraction of the cold air crossing the crater rim is flowing over the crater and not contributing to heat loss inside the crater. To test this hypothesis, future work will include the evaluation of vertical wind profiles observed within and above the crater and conduction of model simulations with ambient winds of varying speed and direction.

Acknowledgements:
We thank all contributors to METCRAX 2006 for their engagement in the field campaign and data evaluation.

REFERENCES

Hahnenberger, M., 2008: *Topographic effects on nighttime cooling in a basin and plain atmosphere*. MSc thesis, Department of Meteorology, University of Utah, 87 pp.

Kossmann, M. and U. Sievers, 2007: KLAM_21 drainage wind modelling of wintertime air pollution events in Christchurch, New Zealand. *Proc. 29th International Conference on Alpine Meteorology*, Chambery, France, 29–32.

Savage, L.C., S. Zhong, W. Yao, W.O. Brown, T.W. Horst, and C.D. Whiteman, 2008: An observational and numerical study of a regional-scale downslope flow in northern Arizona. *J. Geophys. Res.* 113, D14114, doi:10.1029/2007JD009623.

Sievers, U., 2005: Das Kaltluft-Abfluss-Modell KLAM_21. Theoretische Grundlagen, Anwendungen und Handhabung des PC-Modells. *Berichte des Deutschen Wetterdienstes* 227.

Whiteman, C.D., et al., 2008: METCRAX 2006 – Meteorological experiments in Arizona's Meteor Crater. *Bull. Amer. Meteor. Soc*. 89, 1665-1680.

Whiteman, C.D., S.W. Hoch, and M. Lehner, 2009: Nocturnal cold air intrusions at Arizona's Meteor Crater. *Proc. 30th International Conference on Alpine Meteorology*, Rastatt, Germany.

MINIMUM TEMPERATURES CLASSIFICATION AT THE PYRENEES AREA USING EMPIRICAL ORTHOGONAL FUNCTIONS (EOF)

Josep Ramon Miró, Meritxell Pagès

Meteorological Service of Catalonia, Barcelona, Spain
E-mail: *jrmiro@meteo.cat*

Abstract: In order to forecast temperature in complex terrain areas is important to determine the most likely areas to have Cold Air Pool (CAP) formation. In this work Empirical Orthogonal Functions (EOF) were used to determine the spots where the temperature trends to cool more than the surroundings.
The EOF decomposition is applied to the minimum temperature time series obtained from Automatic Weather Stations (AWS) located in different altitudes along the Segre Valley in the Pyrenees. The EOF decomposition separates the original time series among its variation patterns, which is useful to separate the different sources of variation.

Keywords: *Complex terrain temperature, Empirical Orthogonal Functions, Cold Air Pool, Valley*

1 INTRODUCTION

The idea is to classify the different valleys in order to understand the mechanisms of Cold Air Pool (CAP) formation that are related with the shape and the drainage of these valleys (Eisenbach et al, 2003). The EOF is used to determine where in a valley CAP formation is likely to have (Lundquist et al, 2008). Decomposing the temperature time series among the EOF, it explains the principal variability patterns of the minimum temperatures across the time and the space. As a first work the Segre Valley is analyzed here; this valley has several zones with different shapes and it's very interesting to explore the different temperature behaviour. Moreover, in this valley there are an enough number of temperature sensors that provide us a good knowledge of the temperature behaviour in it.

2 DATA AND METHODOLOGY

2.1 Location

Pyrenees range extents longitudinally 435 km, from Biscay Gulf in the Atlantic Ocean to the Mediterranean Sea, of which 220 km belong to Catalonia in the eastern area where the study takes place. Pyrenees separate the Iberian Peninsula from the rest of Europe, supposing a barrier to advections, especially those from the north. The Segre Valley was chosen due to this valley has different basins and is surrounded by high peaks.

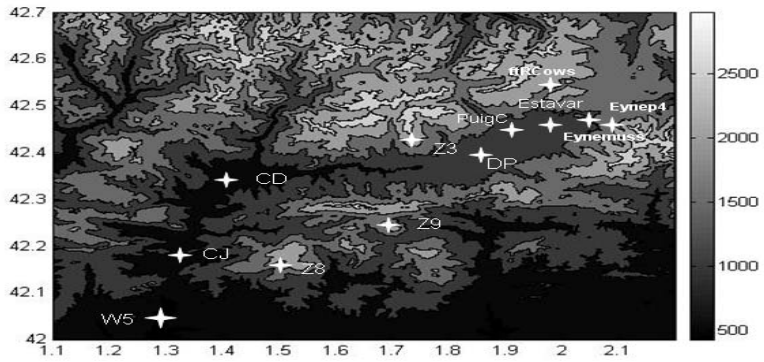

Figure 1. The Segre Valley. The crosses represents the AWS

2.2 Data

The data used was the daily minimum temperatures of different automatic weather stations located both in the top of the mountain and in the floor of the valley (Table 1).

Puigc.	DP	CJ	W5	CD	Z3	Z9	Z8	Estavar	Eyne4p	EyneMus	FtrCows
1210	1097	566	506	849	2310	2149	2300	1268	2305	1559	2111

Table 1. Most Name of the AWS and its height above sea level.

The data was provided by AWS: DP (Das), CJ (Organyà), W5 (Oliana), CD (La Seu d'Urgell), Z3 (Malniu), Z9 (Cadí Nord) and Z8 (Port del Compte), by a Manual Weather Station: Puigc (Puigcerdà) and data recorded by Hobos in an experimental campaign in the Pyrenees: Estavar (Estavar), Eyne4p (Eyne), EyneMus (Eyne) and FtrCows (Font Romeu) (Pepin and Kid, 2006). The data used was from November 2003 until May 2005.

2.3 Methodology

According to (Lundquist et al, 2008), the minimum temperature was decomposed in:

$$T(\vec{x},t) = \overline{T}(\vec{x}) + \overline{T'}(t) + \tilde{T}(\vec{x},t) + \varepsilon \qquad (1)$$

Where $\overline{T(\vec{x})}$ is the mean annual temperature, $\overline{T'}(t)$ is the temporal deviations through measurements and $\tilde{T}(\vec{x},t)$ the local variations through time. $\tilde{T}(\vec{x},t)+\varepsilon$ was decomposed in EOF applying Singular Value Decomposition (SVD). The first EOF is related with days likely that have likely have cold air pools and inversions. Then to discriminate between CAP zone, no-CAP zone or no signal, we choose an adequate threshold for the different spatial weights obtained from the first EOF.

3 RESULTS

A map indicating likely CAP regions, no-CAP regions and no-signal regions are obtained across de Segre Valley (Fig 2)

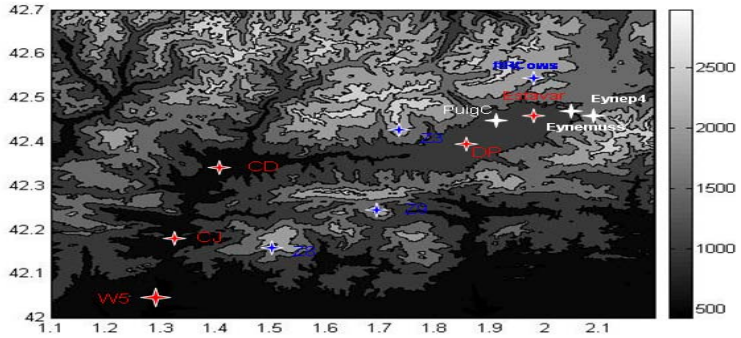

Figure 2. Classification of CAP (red crosses), no-CAP (blue crosses) and no-signal (white crosses)

4 CONCLUSIONS

The results obtained are good and self consistent, but more future works is needed to determine the relationship between the valley shape and the CAP formation. The future work will focus the characterize the CAP with GIS techniques and to relate it to the results obtained with EOF.

Acknowledgements: *We thank Nicholas Pepin and Jessica Lundquist for help us in developing our study and to provide us all we needed. Also we thank Jordi Cunillera, for his support in carrying out our study. Also we want to thank Mònica Herrero, Marc Prohom, Jessica Amaro, Laura Barberia for help us in obtain the data stored in the Meteorological Service of Catalonia.*

REFERENCES

Eisenbach, S., B. Pospichal, C. D. Whiteman, R. Steinacker, and M. Dorninger. 2003. "Classification of Cold Air Pool Events in the Gstettneralm, a Sinkhole in the Eastern Alps." Presented at the International Conference on Alpine Meteorology and MAP, May 18-23, 2003, Brig, Switzerland

Whiteman, C. D., 2000: Mountain Meteorology. Fundamentals and Applications. Oxford University Press.

Lundquist, J.D., N. Pepin, and C. Rochford, 2008. Automated algorithm for mapping regions of cold-air pooling in complex terrain, J. Geophys. Res., 113, D22107

Pepin, N., and D. Kidd (2006), Spatial temperature variation in the eastern Pyrenees, Weather, 61, 300– 310

Lundquist, J.D., N. Pepin, and C. Rochford, 2008. Automated algorithm for mapping regions of cold-air pooling in complex terrain, J. Geophys. Res., 113

FOG WATER COLLECTION WITH SFC DURING THE PERIOD 2000-2008

Marina Mileta

Meteorological and Hydrological Service of Croatia
E-mail: *mileta@cirus.dhz.hr*

Abstract: The highest meteorological station in Croatia, Zavizan (1594 m a.s.l.), is equipped with SFC (standard fog collector). Zavizan is situated on the Velebit Mountain which is the natural boundary between maritime and continental climate. The methodology used was described in Schemenauer and Cereceda (1994). Fog water collection started in the summer 2000. The paper discusses the daily fog water amounts collected during the warm part of the period 2000-2008. Fog water collected in days without precipitation are analysed separately. .Maximum one day – value was 27.8 l / m² while the highest daily rate in days without rain was 19.0 l/m². The maximum highest rates are collected in October, month with maximum days with fog.

Keywords: ICAM, *fog water, mountainous area ,Croatia*

1 INTRODUCTION

The highest mountain meteorological station in Croatia, Zavizan was located on Northern Velebit with a very severe climate. The results of meteorological data from Zavizan included fog water and detailed discussion on the problem of measurements was published in a meteorological monograph (2003), celebrating the 50th anniversary of the weather station. The measurements of fog water in Croatia using Grunow type of fog collector (for the 30-year period) and using the standard fog collector SFC were presented by Mileta (1998, 2003). This paper presents the results of fog water collection by SFC for the period 2000-2008 during the warm part of the year.

2 EXPERIMENT PROCEDURE

2.1 Measurement site and setup

The weather station Zavizan equipped with the SFC was located at the foot of Vucjak Hill on Northern Velebit, 1594 m above sea level (45°49' N, 14°59' E). According to the distribution of wind directions, east is the most frequent wind direction at Zavizan. This wind is a strong bora wind as a consequence of postfrontal cold air advection. The methodology used was described in Schemenauer and Cereceda (1994), and is based on the use of a standard fog collector (SFC) of 1 m² of polypropylene mesh. The results presented here are the daily fog water amounts collected during different long periods in the warm part of 9-year period (2000-2008). The measurements lasted until the air temperature became negative.

3 RESULTS

The daily fog water amounts in the period 2000-2008 during the warm part of the mentioned years have been measured. The data were obtained between July 27 and November 10 in 2000, May 16 and September 27 in 2001, June 26 and October 25 in 2002, July 3 and October 10 in 2003, during June and September (13-24) in 2004, between May 1 and August 31 in 2005, and June 2 and October 17 in 2006, between May 29 and October 12 in 2007 and between May 14 and September 16 in 2008. Maximum daily collected fog water was at the end of October and November, months with maximum days with fog. The maximum one-day value was 27.8 l/m² on October 8, 2003. The highest daily collection rate in days without rain was 19.0 l/m² on October 16, 2002. Synoptic situation on October 7, 2003 was characterised by west upper air current with advection of moist air from Atlantic and on October 16, 2002 was southwest upper current with advection of moist air from Mediterranean.

Tab. A	MAJ			JUN			JUL			AUG			SEP			OKT			NOV		
	SFC	H	%	SFC	H	%	SFC	H	%	SFC	H	%	SFC	H	%	SFC	H	%	SFC	H	%
2000							0,3	1,9	15,8	1,4	7,0	20,0	80,0	247,4	32,3	177,7	278,3	63,9	102,5	211,5	48,5
2001	24,5	36,2	67,7	37,4	153,6	24,3	34,5	67,3	51,3	8,2	10,4	78,8	87,8	241,9	36,3						
2002				14,3	43,5	32,9	21,0	56,0	37,5	99,8	370,4	26,9	128,5	409,4	31,4	165,9	102,1	162,5			
2003							9,0	16,4	54,9	16,6	17,3	96,0	78,2	114,5	68,3	88,2	95,7	92,2			
2004				61,5	104,3	59,0	-			-			44,9	168,8	26,6						
2005	77,1	168,1	45,9	17,4	44,0	39,5	46,9	86,1	54,5	92,1	267,9	34,4									
2006				36,9	97,5	37,8	22,3	80,9	27,6	75,3	247,5	30,4	-			27,1	10,8	250,9			
2007	27,6	47,1	58,6	46,3	130,8	35,4	16,6	26,8	61,9	50,8	193,9	26,2	94,9	258,2	36,7	38,4	12,9	297,3			
2008	46,9	108,1	43,4	41,6	139,5	29,8	10,6	47,6	22,3	18,1	33,1	54,5	32,5	22,8	142,5						

Tab. B	MAJ	JUN	JUL	AUG	SEP	OKT	NOV
	SFC	SFC	SFC	SFC	SFC	SFC	SFC
2000			0,1	.	5,7	32,0	-
2001	7,5	1,2	4,4	2,2	1,2		
2002		4,0	4,4	2,3	5,4	35,5	
2003			0,8	0,3	7,3	7,2	
2004		0,9	-	-	1,0		
2005	0,9	1,6	3,4	10,8			
2006		1,6	0,4	0,5	-	24,9	
2007	.	3,1	2,7	2,6	2,2	2,6	
2008	2,3	1,4	2,5	2,1	0,6		

Table 1. **A** The amounts of fog water collected with standard fog collector (SFC), amounts of precipitation collected with the Raingauge (H) and fog water contribution with respect to rain (%). **B** The amounts of fog water in days without rain.

3 CONCLUSION

The fog water collection on the Velebit Mountain shows that there is a great potential of fog water resource. These results represent opportunities for the restoration of the degraded vegetation after a forest fire. The highest amounts of fog water were collected in autumn when maximum of precipitation occurs. It is caused by the cyclonic activity in this part of the year. The maximum one-day value was 27.8 l / m² on October 8, 2003. The highest daily collection rate in days without rain was 19.0 l/m² on October 16, 2002. Synoptic situation on October 7, 2003 was characterised by the west upper air current with advection of moist air from Atlantic and on October 16, 2002 was the southwest upper current with advection of moist air from Mediterranean.

At the meteorological stations on the Adriatic cost are installed the dew condensers. It is interesting to note that, even in dry conditions such as during the summer 2003, dew continues to provide a consistent (and sometimes only available) amount of water. The installation of dew condenser at the mountain station Zavizan has been planning which could reveal more information about potential of atmospheric water resource.

REFERENCES

Mileta, M., 1998: Fog precipitation on the mountain in Croatia, First International Conference on fog and fog collection, Vancuver, 20-24 July 1998, 413-416.

Mileta, M., 2003: Special Measurements of precipitation and fog water, Zavižan among snow, wind and sun. Meteorological Monography (in Croatian with English summary), Zagreb, 181-190.

Mileta, M., 2004: Results from fog water collection on Mt. Velebit in Croatia, 3rd International conference on fog, fog collection and dew. Cape Town 11-15 October 2004, H4.

Schemenauer, R.S., Cereceda, P., 1994: A proposed standard fog collector for use in high elevation region. Journal of Appl. Meteo., 33, 1313-1322.

THE APPLICATION OF THE COUPLED MODEL IN THE NUMERICAL SIMULATION OF THE LOCAL RADIATION FOG

Lin-lin QI, Xiao-dan WANG and Jian-hua SUN

Institute of Atmospheric Physics, Chinese Academy of Sciences, Beijing, China
E-mail: *niceqll@mail.iap.ac.cn*

Abstract: Fog occurrence is one of the most important events that can lead to low visibility and thus cause casualties and the loss of properties. An effective forecasting method rests upon a perfect initial field and a comprehensive model of the phenomena. The 3D fog model coupling with the MM5 is used to simulate the local winter radiation fog in Chongqing and Changsha respectively. The results show that the unilaterally coupled model can reproduce the circulation and the heavy radiation fog. Especially, the occurrence, location, dissipation and concentration of fog are in accordance with observation. So it is feasible to apply the 3D fog model, coupling with the MM5, in the forecast of fog.

Keywords: *fog, mesoscale model, 3D fog model, unilaterally coupling*

1 INTRODUCTION

Reinforcing the research on the genesis mechanism and structural feature of fog and improving the detection and forecast of fog have become a very urgent task of meteorologic department. Previous studies show that the three-dimension fog numerical model considers the impacts of more factors, adapts to simulate small-scale fog in complicated terrain, approximately describes fog law, needs a relatively short runtime, and thus becomes a good tool to forecast microphysical characteristics of small-scale or single-point fog. However, the model is designed for local fog, and needs the information of atmospheric stratification to run in fixed-point region. Currently, spatial and temporal scales of sounding data used to reflect the information of atmospheric stratification are too sparse, which can not satisfy real-time forecast of local fog. At the same time, a large number of studies (Dong Jianxi et al., 2006; Zhou Mei et al., 2006) show that with the development of mesoscale model, it has also been widely applied to regional fog forecasting. But due to the generality of model, most forecasts provided by mesoscale model are regard to the characteristics and evolution of regional fog. It does not apply to local and rapid, fixed-point forecast of fog. It can be seen that the method coupling fog model with mesoscale model can not only provide the initial field of higher spatial and temporal scales for mesoscale model, but also take the advantages of fog model in the physical mechanism and feedback mechanism of fog. It will be an important direction of development to promto the ability of fog forecasting. Therefore, in the paper we attempt to conduct the research on fog forecasting coupling the MM5 with the three-dimension fog model in order to discuss the feasibility of the application in fog forecasting. It can further provide a basis for operational forecast.

2 BRIEF INTRODUCTION OF MODEL AND SCHEME DESIGN

We simulate the radiation fogs in Chongqing and Changsha, carry out the study of fog forecasting using the MM5 coupling with the three-dimension fog model. Specific simulation program design is as follows: (1) Mesoscale model MM5 uses two-way interactive nested grid. In the experiments, two domains with a grid spacing of 18 and 6 km are nested. The center of model in Chongqing is (29.52°N，106.49°E), the one in Changsha is (28.1°N，113°E). The initial-boundary value uses 1 ° × 1 ° NCEP reanalysis data corrected objectively by the ground and upper-air data. The simulated times respectively are 0000UTC 22 January 2003 ~ 0000UTC 23 January 2003 (Chongqing) and 0000UTC 12 December 2003 ~ 0000UTC 13 December 2003 (Changsha), output frequency is 6 hours.(2) The fog model uses 30 by 30 point staggered grid, grid spacing is 5 km. To reduce effects of lateral boundary, 3 horizontal grids close to the boundary are as extensional grids of model. There are 19 layers in the vertical direction, they are respectively 0, 2, 6, 15, 30, 50, 75, 100, 125, 150, 200, 250, 350, 450, 550, 700, 900, 1200, 1500 m.(3) The initial fields, terrain and standing vegetation of the fog model are from the output of the MM5 domain 2 in order to couple the MM5 with the fog model in one-way mode. The simulated times of Chongqing and Changsha respectively are 1200UTC 22 January 2003 ~ 1200UTC 23 January 2003 (Chongqing) and 1200UTC 12 December 2003 ~ 1200UTC 13 December 2003 (Changsha), output frequency is 30 minutes.

3 RESULTS AND ANALYSIS

Previous studies have indicated that it is regarded as foggy generation when liquid water content reaches 0.01 gkg-1(Shi Chune et al., 1997), therefor, in the paper liquid water content is applied to analyse the simulated fog formation and evolution. According to figure 1, at 1330UTC 22 January 2003, fog first formed in eastern region, the scope was small. At 1500UTC, fog scope expanded and covered most of the simulated region, the contour of eastern region was more intensive, fog concentration was slightly strong. At 2100UTC, mist developed to dense fog, the maximum value of liquid water content in the highlands of eastern region reached 0.63 gkg-1. High value areas of liquid water content were almost consistent with that of topographic contour. Liquid water content of the central region was relatively small, which may be related to urban heat island effect. At 0000UTC 23, liquid water content of the whole region continued to rise, but marginally, when fog developed to the strongest phase. After 0000UTC, solar radiation caused the ground to start warming, with the rise in the

ground temperature, the ground relative humidity decreased, droplet evaporated and the ground fog began to disperse. At 0230UTC 23, radiation fog cleared off entirely, the residual existed in the form of low cloud. From the vertical cross-section for the simulated temperature, relative humidity and liquid water content, we can see that during the development stage, near-surface temperature inversion layer had taken shape, the ground and near-surface layer atmospheric temperatures decreased. In the middle of the region the drop range of temperature was smaller, in the north and south were significant. High value areas of relative humidity were located in southeastern region, corresponding to the one of topographic contour. Relative humidity below 10m reached over 85%, according with observation and helpful to form radiation fog. However, fog thickness was quit thin, only several meters. At the advanced stage, the ground and near-surface layer atmospheric temperatures continued to decrease, relative humidity increased clearly, the air below 30m had been close to saturation, in the central part of the middle and upper layers relative humidity was smaller. Fog developed rapidly in the south. Fog thickness in the highlands was great, about 100m, in the middle was small, less than 40m. With the previous observations that fog thickness in Chongqing is normally 200 ~ 400m, we find that the simulated fog thickness is far less than reality and significantly small.

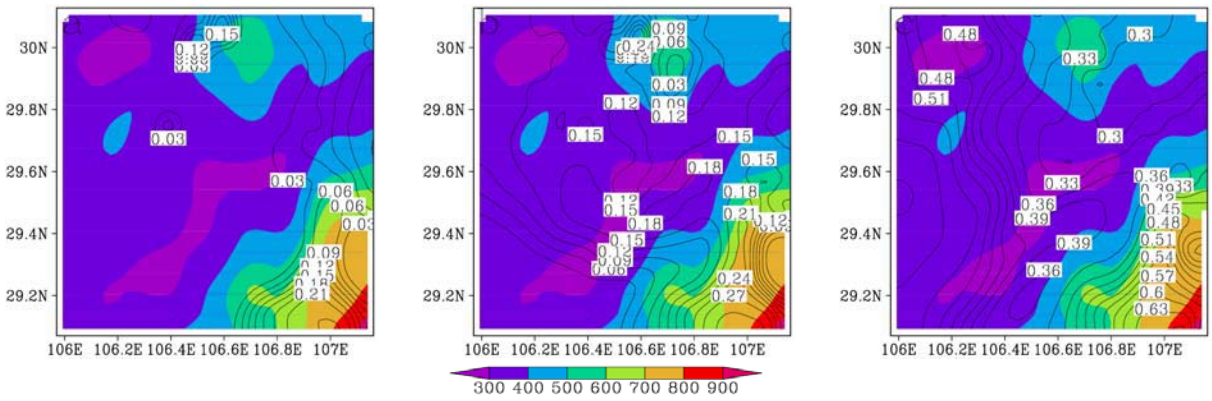

Figure 1. The simulated liquid water content at surface and topography at (a) 1330 UTC 22, (b) 1500 UTC 22,(c) 2100 UTC 22 Jan 2003(contour: liquid water content, units：g kg^{-1}; shaded: topography)

Thus, it does follow that the fog in Chongqing is divided into four stages: (1) formation stage (1330UTC 22 January 2003 ~ 1500UTC 22 January 2003). Because of radiation cooling, the air reached saturation point. Radiation fog came out in the highlands of eastern region at first, then expanded into the central and western region, and basically covered all the simulated zone at 1500UTC. (2) development stage (1500UTC 22 January 2003 ~ 2100UTC 22 January 2003). The air kept cooling, fog concentration and thickness increased, and mist developed into dense fog. (3) maturity stage (2100UTC 22 January 2003 ~ 0000UTC 23 January 2003), the ground temperature stopped decreasing, liquid water content rised, but little, fog top lifted. (4) dissipation stage (0000UTC 23 January 2003 ~ 0200UTC 23 January 2003). The ground temperature went up after the sun came out. To sum up, except for the simulated fog dissipating ahead of reality and fog thickness smaller, the method coupling the MM5 with the three-dimensional fog model can siumulate the macroevolution of fog formation, development, mature and dissipation as well as microstructural characteristics of fog.

Analysis of Changsha case is left out.

4 CONCLUSIONS

At present, there is important significance to enhance fog forecasting. In the paper, the 3D fog model coupling with the MM5 is used to simulate the local winter radiation fog in Chongqing and Changsha respectively. The results show that the unilaterally coupled model can reproduce the evolution, location, dissipation and concentration of heavy radiation fog, especially in complex geographical environments simulation capacity is stronger. Although there is still a certain lack for the simulation of fog thickness and dissipation that need further improve physical mechanisms of model, generally speaking, it is feasible to apply the 3D fog model coupling with the MM5 in fog forecasting. In addition, what deserves special mention here is that fog simulation with the two-way coupled model considering the feedback mechanism of fog will be the focus of our next study.

REFERENCES

Dong Jianxi, Lei Hengchi, Hu Zhaoxia, et al. 2006: Numerical simulation and diagnosis of a dense fog in Beijing and its penumbra.*Climatic and Environmental Research* (in Chinese), **11** (2) : 175 ~ 184.

Zhou Mei, Yin Yan, Wang Weiwei. 2006: A numerical study on the long-lasting wide spread dense fog event during December 24—27, 2006. *Journal of Applied Meterological Sciense* (in Chinese), **19** (5) : 602 ~ 610.

Shi Chune, Cao Bimin, Li Zihua, et al. 1996: umeical simulation of 3D local cirrculation over complicated terrain[J]. *Journal of Nanjing Institute of Meteorology* (in Chinese), **19** (3) : 320 ~ 328.

AERODYNAMIC ROUGHNESS LENGTHS OF SNOW

Christof Gromke[1], B. Walter[1], C. Manes[2] , M. Lehning[1]

[1] WSL Institute for Snow and Avalanche Research SLF, Davos, Switzerland
E-mail: *gromke@slf.ch*
[2] Politecnico di Torino, Department of Hydraulics, Transport and Civil Infrastructures, Torino, Italy

Abstract: Aerodynamic roughness lengths z_0 of snow surfaces have been determined from wind velocity measurements in a boundary layer wind tunnel. Complementary, surface characteristic length scales have been deduced from photographs of these snow surfaces by means of digital image processing and statistical analyses. Both sets of data are confronted in order to reveal possible correlations between the geometric properties of snow surfaces and the associated aerodynamic roughness lengths z_0. The current dataset generally shows increasing roughness lengths z_0 with increasing characteristic length scales.

Keywords: *aerodynamic roughness length, boundary layer velocity profile, structure function, characteristic length scales*

1 INTRODUCTION

The aerodynamic roughness length z_0 is a crucial parameter in the log-law formulation of the boundary layer wind profile and therefore in most model formulations of land-atmosphere interaction. It accounts for the effects of surface roughness on the flow. However, choosing the correct value of the roughness length for diverse surfaces remains a difficult task. Regarding snow surfaces and their corresponding values of z_0, a great lack of knowledge exists. A wide range of values for z_0 spanning two orders of magnitude can be found in literature, making it difficult to choose the appropriate value in model applications.

This work suggests an idea to link the aerodynamic roughness lengths of fresh-snow to characteristic lengths scales of its surface obtained by digital image processing and statistical analyses.

2 METHODS

In the SLF atmospheric boundary layer wind tunnel (situated on 1650 m a.s.l. in Davos, Switzerland) flows over snow covered surfaces and atmosphere-cryosphere interaction processes are studied. The experiments are performed with naturally fallen snow which is collected in custom-made trays positioned outside the wind tunnel facility in a wind sheltered area. The snow laden trays are placed in the wind tunnel providing an 8 m long natural fetch of snow on which a boundary layer develops. Air from outside the wind tunnel facility with ambient temperature is sucked in and the wind tunnel ceiling is adjusted to achieve a vanishing pressure gradient in order to guarantee natural flow conditions.

By measuring vertical profiles of mean horizontal wind velocity using 2D Hot-Wire-Anemometry (HWA) and subsequent curve fitting analysis to the logarithmic velocity profile

$$u^+(z) = \kappa^{-1} \ln\left(\frac{z-d}{z_0}\right), \tag{1}$$

aerodynamic lengths z_0 of snow covered surfaces were determined (approach (i)). For the experiments, the wind tunnel flow velocities were kept small to prevent snow drift and to maintain unaltered snow surface structures during the course of an experiment.

In a complementary procedure (approach (ii)), photographs of the naturally fallen snow surfaces were taken before and after the wind tunnel experiments. The photographs were processed by digital image analysis resulting in contour lines of the snow-air interface to which length co-ordinates of vertical height z and horizontal distance x were assigned (Fig. 1). Based on the contour line co-ordinates, second order spatial structure functions $D_2(r)$, with r horizontal lag, were calculated according to

$$D_2(r) = \left\langle [z(x+r) - z(x)]^2 \right\rangle . \tag{2}$$

The obtained structure functions $D_2(r)$ shown in a double logarithmic chart exhibit 3 distinct regions (Fig. 1). Applying multivariate statistical analysis to fit the second order structure functions by three regression curves yields a total of four characteristic length scales; two horizontal length scales, the crossover length l and the saturation length L, and their corresponding vertical length scales $[D_2(l)]^{1/2}$ and $[D_2(L)]^{1/2}$ (Manes et al. 2008).

The aim of this investigation is to reveal correlations between the aerodynamic roughness lengths z_0 obtained from approach (i) and the surface characteristic length scales obtained from approach (ii).

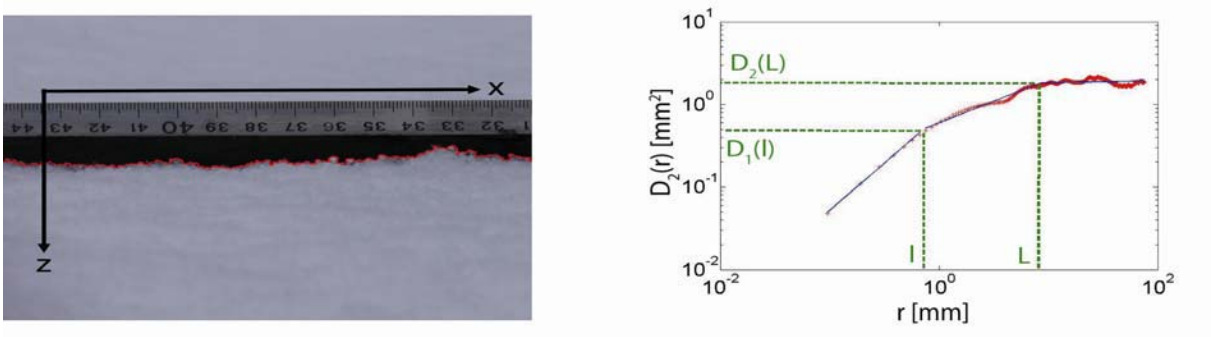

Figure 1. Photograph of snow surface with snow-air interface contour line (left) and diagram of second order structure function $D_2(r)$ with characteristic length scales (right).

3 RESULTS

In January and February 2008/09 five experiments with freshly fallen snow have been performed. Tab. 1 lists the aerodynamic roughness lengths z_0 obtained by approach (i) and the corresponding surface characteristic length scales obtained by approach (ii).

z_0	l	$[D_2(l)]^{1/2}$	L	$[D_2(L)]^{1/2}$
0.01	0.34	0.21	2.82	0.43
0.05	0.55	0.34	9.24	0.91
0.06	0.53	0.43	13.63	1.63
0.07	0.49	0.40	12.62	1.29
0.19	0.71	0.43	4.12	0.80

Table 1. Aerodynamic roughness lengths z_0 and surface characteristic length scales l, $[D_2(l)]^{1/2}$, L, $[D_2(L)]^{1/2}$ sorted by increasing z_0 (units: mm).

4 DISCUSSION AND CONCLUSION

The aerodynamic roughness lengths found are in overall agreement with the results of Clifton et al. (2006) and Andreas et al. (2004) who deduced z_0-values from wind tunnel experiments and field studies in the Arctic and Antarctic, respectively, and provide values $0.01\text{mm} < z_0 < 0.1\text{mm}$.

Analysing Tab. 1 generally shows increasing characteristic length scales with increasing roughness length, except for the roughest case where the length scales associated with the saturation region, L and $[D_2(L)]^{1/2}$, do not fit with this pattern. The data suggest a degressive increase of the characteristic length scales with increasing z_0. Values of z_0 and the crossover length scales l and $[D_2(l)]^{1/2}$ are mostly within one order of magnitude, whereas the saturation length scales usually exceed the roughness lengths by two orders of magnitude. However, the existing data set is still not sufficient to allow for more detailed and universal conclusions.

Moreover, it has to be noted that the roughness Reynolds number criterion $z_0^+ = z_0 u_* / \nu > 2.5$ is not strictly fulfilled for all the measurements. Calculations of the roughness Reynolds number resulted in $z_0^+ = 0.1$, 0.8, 0.9, 0.9 and 3.3 according to the sequence of cases listed in Tab. 1. This indicates that only in the last case an aerodynamically rough regime with a flow independent z_0 is present, whereas otherwise aerodynamically smooth or transitional regimes with z_0 slightly depending on the flow prevail.

The final goal of this work is to bring both approaches, (i) and (ii), together and to constitute a relationship between the aerodynamic roughness length and the characteristic length scales according to

$$z_0 = f\left(l, [D_2(l)]^{1/2}, L, [D_2(L)]^{1/2}\right). \quad (3)$$

However, in order to constitute a functional relationship, a larger dataset of z_0-values and characteristic length scales obtained from wind tunnel measurements and digital image processing/statistical analysis is required.

REFERENCES

Andreas, E. L., R. E. Jordan, P. S. Guest, P. O. G. Persson, A. A. Grachev and C. W. Fairall, 2004: Roughness Lengths over Snow, Proc. 18th Conf. on Hydrology of the American Meteorological Society, Seattle, WA, 11-15 Jan. 2004, pp. 8.

Clifton, A., J. D. Ruedi M. and Lehning, 2006: Snow saltation threshold measurements in a drifting-snow wind tunnel, Journal of Glaciology **52**, pp. 585-596.

Manes, C., M. Guala, H. Löwe, S. Bartlett, L. Egli and M. Lehning, 2008: Statistical properties of fresh snow roughness, Water Resources Research **44**, W11407, doi:10.1029/2007WR006689.

MONITORING THE ATMOSPHERIC BOUNDARY LAYER IN THE ARCTIC (MABLA) - THE GUFUSKÁLAR PROJECT

Haraldur Ólafsson[1,3,4] , Ólafur Rögnvaldsson[2,4], Joachim Reuder[4], Hálfdán Ágústsson[1,2]
Guðrún Nína Petersen[3], Halldór Björnsson[3], Trausti Jónsson[3] and Jón Egill Kristjánsson[5]

[1] Háskóli Íslands (University of Iceland)
[2] Reiknistofa í veðurfræði (Institute for Meteorological Research), Iceland
[3]Veðurstofa Íslands (Icelandic Meteorological Office)
[4]Geophysical Institute, University of Bergen
[5]Institute of Geosciences, University of Oslo
E-mail: *haraldur68@gmail.com*

Abstract: A new project of meteorological observations in a 412 m high mast in the vicinity of Snæfellsjökull Glacier in W-Iceland is described. The project is expected to provide data on various types of orographic disturbances, including corner winds, wakes, blockings and downslope windstorms.

Keywords: *MABLA, Gufuskálar, W-Iceland, mast, boundary-layer monitoring, Arctic, turbulent fluxes*

1 INTRODUCTION

Climate change, new challenges in fine-scale weather forecasting and unanswered questions on the nature of the atmospheric boundary-layer and mountain meteorology have motivated a new project, Monitoring of the Atmospheric Boundary-Layer in the Arctic (MABLA). The first goal of this project is to establish a monitoring of the atmospheric boundary-layer in a more than 400 m high mast at Gufuskálar at the west coast of Iceland (Fig. 1).

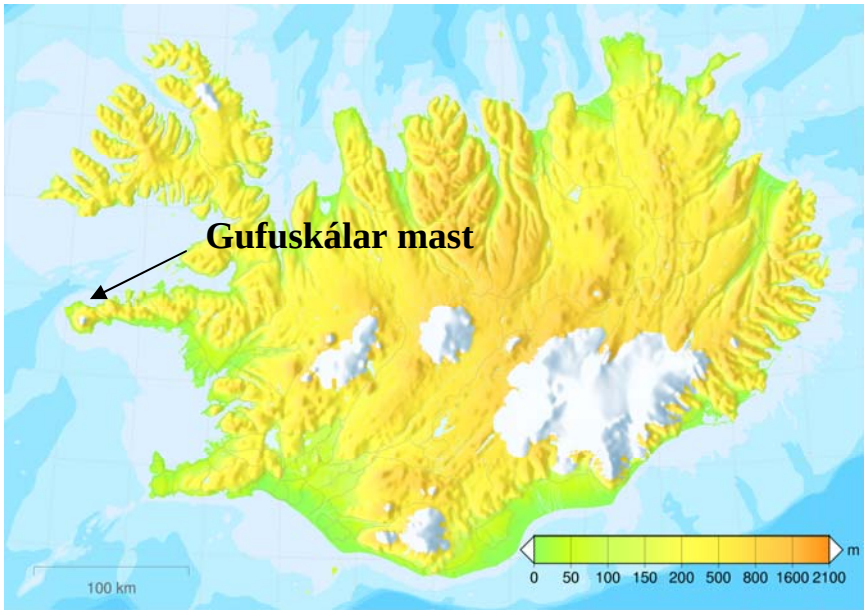

Figure 1. Location of the Gufuskálar mast at the west coast of Iceland.

2 OBSERVATIONS IN THE GUFUSKÁLAR MAST

The Gufuskálar mast is situated at the tip of the Snæfellsnes peninsula, a short distance northwest of the almost 1.5 km high, but rapidly melting Snæfellsjökull Glacier. A manned weather station was operated at Gufuskálar 1970-1994 and an automatic weather station has been operated there since 1994. The Stykkishólmur weather station that has a temperature series dating back to the middle of the 19th century is only a little more than 50 km to the east of Gufuskálar. The main mast of Gufuskálar is 412 m high, while a smaller 40 m high

mast is nearby. The taller mast was erected in 1963 and is currently used for transmitting long wave radio signals. The observations in the masts will consist of automated weather stations recording winds, temperature and humidity at roughly 10, 40, 100, 200 and 400 meters every 10 minutes. In addition, there will be high-frequency observations to assess turbulent fluxes of heat and momentum at 10 and 100 meters and observations of short- and long-wave radiation. Measurements at 10 and 40 metres started in the fall of 2008 and installation of instruments at the remaining levels will be completed during the summer of 2009.

3 SCIENTIFIC OBJECTIVES

The Gufuskálar observations serve a multiple purpose. They are expected to provide a description of the atmospheric boundary-layer inside a corner wind in northeasterly flow, an upstream blocking in northwesterly flow and in wakes or downslope windstorms in southeasterly flows. From a forecasting perspective, the data on turbulent transport of momentum down to the surface of the earth during windstorms is expected to give guidance for tuning of parameterization schemes with the aim of improving forecasts of surface mean winds and surface wind gusts (e.g. Ágústsson and Ólafsson, 2009; Rögnvaldsson et al., 2009). From a climatic perspective, future observations from Gufuskálar are expected to complement the exceptionally long Stykkishólmur time-series of temperature. The Gufuskálar project is a long-term investment. The measurements are expected to monitor a plausible climate change associated with the predicted global warming and the retreat of the sea ice north of Iceland. Being located at the shoreline, observations from Gufuskálar can be expected to be useful in describing the marine boundary-layer and for validating algorithms of remotely observed winds over the sea.

Figure 2. Installation of equipment in one of the two masts at Gufuskálar, W-Iceland in August 2008.

Acknowledgements:
MABLA is supported financially by the the Icelandic Research Fund (RANNÍS) and the Norwegian Research Fund through the THORPEX-IPY project. The access to the Gufuskálar mast is provided by the National Radio Company (RÚV).

REFERENCES

Ágústsson, H. and H. Ólafsson, 2009: Forecasting wind gusts in complex terrain. Meteorology and Atmospheric Physics, in press.

Rögnvaldsson Ó., J.-W. Bao, H. Ágústsson and H. Ólafsson, 2009: Downslope windstorm in Iceland – WRF/MM5 model comparison. Atmos. Chem. and Phys., in revision.

MIXING IN THE STABLE ATMOSPHERE OF AN IDEALIZED ALPINE VALLEY

Yann Largeron[1], Chantal Staquet[1], Charles Chemel[2], Jean-Pierre Chollet[1]

[1] Laboratoire des Ecoulements Géophysiques et Industriels (LEGI), CNRS, Grenoble, France
[2] University of Hertorfdshire, Hatfield, UK
E-mail: *yann.largeron@hmg.inpg.fr*

Abstract: The nocturnal radiative cooling of a sloping ground surface often induces katabatic flows. These natural self-generated flows may account for the major part of the observed atmospheric dynamics over a complex terrain by stable conditions and weak synoptic forcing. One may wonder about the ability of these flows to increase the transport properties of the atmosphere, a necessary step to characterize the dispersion of pollutants in a valley. The aim of the present study is to analyse these transport properties by the computation of a turbulent mixing coefficient, and to propose a parameterization of this coefficient. For this purpose, we perform LES numerical simulations with the ARPS meteorological code and adapt the analysis of mixing of Winters and d'Asaro (1996) to the present configuration.

***K*eywords:** *stable atmosphere, alpine valley, katabatic wind, turbulent diffusivity, ARPS code*

1 INTRODUCTION

In the absence of a strong synoptic forcing, the atmospheric flow in a valley is mainly created by thermal circulations due to the cooling or warming of the ground. For instance, the nightime radiative cooling of the ground leads to a downslope wind (refered to as a katabatic wind). In the present paper we consider the situation of a nocturnal katabatic wind in an idealized valley in which the ground cools by infra-red emission. We also focus on a stably stratified atmosphere.

Our aim is to analyze the turbulent mixing induced by the katabatic wind and we perform LES numerical simulations for this purpose. Our estimate of mixing relies on a method derived by Winters and d'Asaro (1996) which leads to an exact expression for the vertical turbulent mixing coefficient (more precisely, for the turbulent mixing coefficient normal to the isotherms). When adapted to our LES approach, this expression becomes :

$$\kappa_{t_{LES}} = -< \kappa_x \left(\frac{\partial\theta}{\partial x}\right)^2 + \kappa_y \left(\frac{\partial\theta}{\partial y}\right)^2 + \kappa_z \left(\frac{\partial\theta}{\partial z}\right)^2 >_{z_*} \cdot \left(\frac{d\theta}{dz_*}\right)^{-2} \tag{1}$$

in which $(\kappa_x, \kappa_y, \kappa_z)$ is the subgrid scale turbulent mixing coefficient computed by the code; $\theta(\overrightarrow{x}, t)$ is the (virtual) potential temperature field; and $z_*(\overrightarrow{x}, t)$ is the equilibrium altitude of a particle being at $\overrightarrow{x}$ at time t and is constant over an isothermal surface. The coefficient $\kappa_{t_{LES}}$ characterizes the turbulent heat flux resulting from the scales larger than the grid scale (explicitely resolved by the code) but also includes the subgrid contribution to turbulence.

2 SETUP OF THE SIMULATION

The simulations are performed with the "Advanced Regional Prediction System" (ARPS code) which is a non-hydrostatic atmospheric mesoscale model used here as a LES code. The turbulence closure scheme is the classical turbulent kinetic energy scheme (so-called TKE$^{1/2}$). In the simulations, the topography of the valley follows the analytical profile of Rampanelli et al. (2004). The length is 20 km and the width is 1240 m with summits rising at 1700 m. By this way, the valley resembles the Chamonix valley located in the French Alps.

We model a 3 hour long nocturnal episode starting at 22 h. In order to study the influence of a katabatic wind in a stable atmosphere for weak synoptic conditions, we impose no velocity field at initial time. The vertical profile of the potential temperature at $t = 0$, denoted $\theta_{amb}(z)$, increases linearly with height, being equal to $\theta_0 = 271$ K at the bottom of the valley. The Brunt-Väisälä frequency $N_{amb} = \sqrt{g/\theta_0 \left(d\theta/dz\right)_{amb}}$ is therefore constant. We perform different simulations for various values of N_{amb}. We also impose the ground to be colder by 3 K than the adjacent air and use the two-layer soil model of Noilhan and Planton (1989).

Open lateral boundary conditions are applied in both horizontal directions. The velocity field satisfies a no-slip condition at the ground and a Rayleigh damping layer is imposed at the top of the domain. At the ground, thermal fluxes are prescribed by the soil model every time step. The temperature of the soil surface then decreases with time, consistently with real soil behavior.

The horizontal resolution is 200 m and the vertical resolution starts at 5 m and slowly increases with height until 7000 m. The associated number of grid points is then $121 \times 103 \times 140$ and the time step is 0.25 s. We ran 10 differents simulations.

3 RESULTS

We focus upon the value of the turbulent mixing coefficient averaged over the layer of air associated with the katabatic wind. We denote this average by $<>_s$. The turbulent mixing coefficient $< \kappa_{t_{LES}} >_s$ thus obtained is comprised between 0.01 and $2\ m^2/s$ depending on the stability of the atmosphere and the time considered. Very few measurements are available in the litterature but those made in Antartica (Brost and Wyngaard (1978)) gave values between 0.01 à $0.6\ m^2/s$ in the katabatic layer, consistently with what we obtain. In a convective situation by contrast, $\kappa_{t_{LES}}$ typically varies between 1 and $700\ m^2/s$.

Figure 1a displays the temporal evolution of $< \kappa_{t_{LES}} >_s$ during the 3 hours of simulation for different values of the stability parameter N_{amb}. Each profile is quasi-linear for $t \geq 40$ suggesting to scale $< \kappa_{t_{LES}} >_s$ by $\alpha \cdot t$ (with $\alpha = 8.87 \cdot 10^{-3}$ given by a linear regression). The result is displayed versus N_{amb} for different times in Figure 1b. Surprisingly, a unique behavior is observed for $t > 40$.

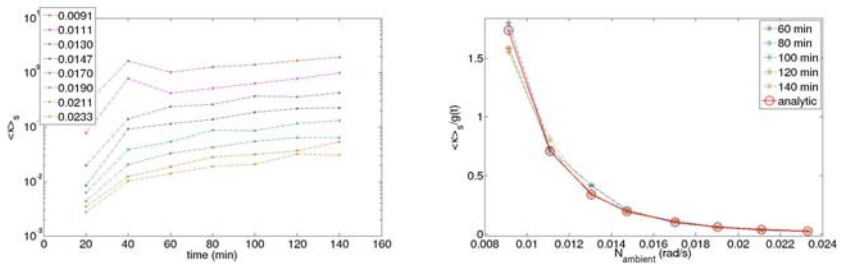

(a) (b)

Figure 1: (a) Evolution of $< \kappa_{t_{LES}} >_s (t)$ for different values of N_{amb}. (b) Colour crosses : Numerical values for $< \kappa_{t_{LES}} >_s (N_{amb})$ scaled by αt (see text). Red circles : Analytical function (2).

As an attempt to understand this behavior, we replaced $\kappa_x = \kappa_y$ and κ_z by their expression from the subgrid scale model. With a few assumptions, the result can be expressed as:

$$< \kappa_{t_{LES}} >_s \approx \frac{A}{N_{amb}^4} + \frac{B}{N_{amb}^5} \tag{2}$$

and is displayed with a red curve on Figure 1b. The curve fits remarkably well the numerical data.

In order to address the dependence of the mixing coefficient upon the subgrid scale model, we ran simulations with another subgrid scale model (the first order Smagorinski-Lilly closure scheme). We observed the same type of dependence of $< \kappa_{t_{LES}} >_s$ upon N_{amb} and found the same order of magnitude for the mixing coefficient (a ratio about 1.5 is found between the two cases). Two different conclusions can be drawn from this result. One may either conclude that the subgrid scale turbulence is correctly parameterized by each subgrid scale model or that the mixing coefficient does not depend upon the subgrid scale model. In both cases, this result ensures that a turbulent mixing coefficient can be estimated from LES.

4 CONCLUSIONS

We computed a mixing coefficient in the katabatic layer from the method of Winters and d'Asaro (1996). This coefficient was found to vary between 0.01 et 2 m^2/s, decreases with the stability of the atmosphere (as $\approx A \cdot N_{amb}^{-4} + B \cdot N_{amb}^{-5}$) and increases almost linearly with time. Most importantly, the mixing coefficient was found not to depend upon the subgrid scale turbulence model, for the two models we considered.

Acknowledgements:
Y.L. is supported by a grant of the région Rhône-Alpes. Computations have been performed on the computers of Joseph Fourier university in Grenoble (Mirage clusters) and on the clusters of the Institut du Développement et des Ressources en Informatique Scientifique (IDRIS).

REFERENCES

Brost, A. and Wyngaard, J., 1978, A model study of the stably stratified planetary boundary layer, *J. Atmos. Sci.*, **35**, 1427-1440

Noilhan, J. and Planton, S., 1989, A simple parameterization of land surface processes for meteorological models, *Mon. Weather Rev.*, **117**, 536-549

Rampanelli, G. and Zardi, D. and Rotunno, R., 2004, Mechanism of up-valley winds, *J. Atmos. Sci.*, **61**, 3097-3111

Winters, K.B. and D'Asaro, E.A., 1996, Diascalar flux and the rate of fluid mixing, *J. Fluid Mech.*, **317**, 179-193

High resolution atmospheric modelling for mountain and valley stations and its applications to complex dispersion conditions

D. Arnold[1], I. Schicker [2], P. Seibert[2], A. Vargas[1]

[1] Institut of Energy Technologies, Technical University of Catalonia, Barcelona, Spain
[2] Institute of Meteorology, University of Natural Resources and Applied Life Sciences, Vienna, Austria
E-mail: *delia.arnold@upc.edu*

Abstract: High resolution modelling with resolutions lower than 1 km is needed when complex topography is involved. Two case studies have been carried out at a valley and a mountain station with MM5V3.7 to evaluate three important topics: the influence of different boundary layer and soil schemes on the results, influences of the orographic shadowing option and the influence of using SRTM 3" satellite topographic data instead of the GTOPO 30" data used by default in MM5.

***K*eywords:** *ICAM, MM5, high resolution modelling, Inn Valley.*

1 INTRODUCTION

Numerical modelling in complex topographical areas is still challenging due to local meteorological phenomena which may lead to very poor air quality conditions. Therefore, high resolution modelling with resolutions lower than 1 km, both in the meteorological and dispersion fields, is needed. In this context, and within a newborn project of the BOKU-Met and the INTE research groups, an analysis of the improvements in the modelling results when using high resolution satellite topography data and land-use data, and better soil initial conditions, has started. First case studies have been carried out for two stations: Penhas Douradas, located on the slope of a mountain ridge in Portugal, and Innsbruck, located in the Inn Valley, Austria. Modelling has been done using the mesoscale meteorological model MM5V3.7 (PSU/NCAR) (Dudhia 1993) with G. Zängl's extensions for Alpine simulations (Zängl 2003) at both stations to evaluate three specific topics. First, the influence of different boundary layer and soil schemes. Second, influences of the orographic shadowing option which is currently not implemented in the distributed memory version of MM5. And third, improvement of the results using SRTM 3" satellite topographic data instead of the, as highest resolution available, GTOPO 30" data used by default in MM5.

2 MODEL SET-UP

MM5 was driven with the 6-hour ECMWF analyses and 3-hour forecasts at 1x1 degrees and standard model levels. The outermost domain was nudged every three hours towards the meteorological input to avoid drifting of the model. Sensitivity tests were performed changing one parameter at a time. A subset of the Innsbruck runs is presented here with MRF and ETA PBL schemes, Noah and 5-layer soil schemes, with and without SRTM 3" data and with and without orographic shadowing (Tab. 1). In all simulations 35 vertical layers and 2-way nesting interaction were used.

MM5run	S1	S2	S3	S4
Domain configuration	50x70, 85x94, 124x142, 115x14, 88x169 64.8 km, 21.6 km, 7.2 km, 2.4 km, 0.8 km			
BL scheme	ETA/MRF	ETA	MRF	ETA
Soil scheme	Noah	Noah/5-layer	Noah	5-layer(IRS)
Oro. shadow.	Yes	Yes	Yes/No	Yes
SRTM3" in D5	No	No	No	Yes/No

Table 1: Specification of configurations of the four sensitivity runs (labelled S1,2,3,4) in Innsbruck.

3 RESULTS

Modelled temperatures for each of the 4 sensitivity runs are compared with the measurements (Fig. 1). In agreement with previous results (Schicker and Seibert 2009) the ETA BL scheme gives in general better results but with too warm nights. The MRF scheme damps the diurnal temperature range. Soil schemes also make a difference in the temperature simulations. Both Noah and 5-layer soil schemes smooth out the diurnal cycles, but maxima temperatures are better simulated with the first one. Orographic shadowing create colder boundary layers. It has also been noticed, that it depends significantly on the BL scheme used in the simulation (not shown here). Additional tests for Penhas Douradas station and other similar locations have shown that those ones located on

mountain slopes are not as much affected as the ones located in the valleys regarding the BL scheme used and the orographic shadowing. However, the shadowing from the valley below may affect the development of thermally driven flows and further studies are being done.

SRTM 3" elevation data has only been tested in Innsbruck. Although during the first period of the run the simulations are in better agreement with the measurements than the ones using GTOPO 30", after some time, the simulations perform clearly worse. Additional work to asses this problem is currently ongoing.

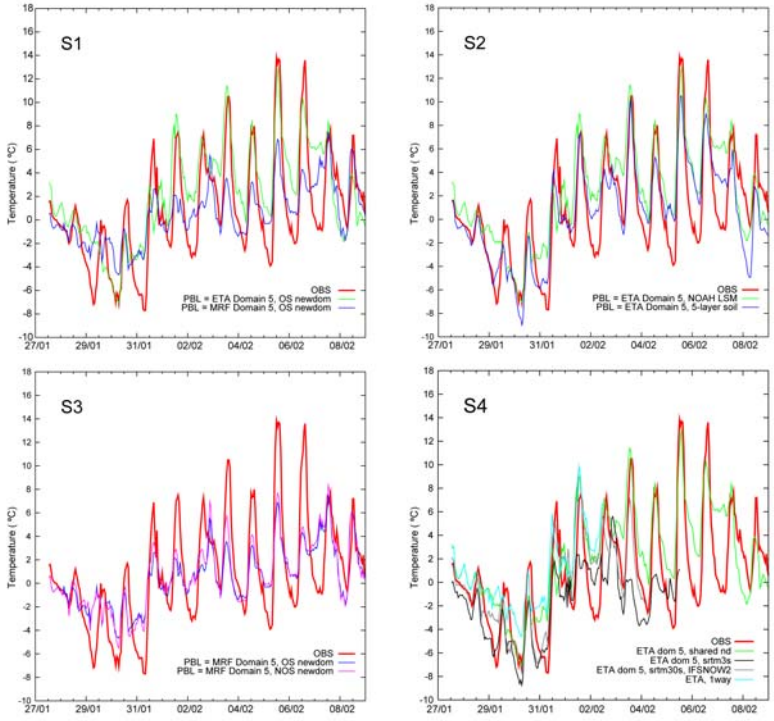

Figure 1: Comparison of the modelled and measured 2 m temperature in Innsbruck for the four runs.

4 CONCLUSIONS

MM5 simulations have been carried out for stations with complex topography and with different configurations and parametrisations. The parametrisations selection strongly influences the modelled results. In Alpine regions, ETA and 5-layer soil model give more realistic results. Orographic influence and the modifications introduced when using satellite elevation data are still under study and need further work. The final implications on the dispersion of radon and CO are currently studied with the Lagrangian particle dispersion model, MM5v3.7-FLEXPARTv6.2, developed specially to work with MM5 output and thus able to simulate complex dispersion conditions specially in the short range.

Computational costs must be considered too, not only regarding storage demands, but also computing time. To downscale from the global fields to such small grid sizes, typically six domains will be needed and thus more storage capacity should be available. Moreover, increasing resolutions in the horizontal and the vertical require small time steps to be numerically stable. This increases significantly the amount of time needed to run the simulation even in HPC.

Acknowledgements:

We thank the EMS for the financial support to assist this conference through a YSTA. We acknowledge the EU-FP6 Network of Excellence ACCENT. ECMWF ERA-40 data used in this study was provided by ECMWF through the Special Project MOTT.

REFERENCES

Dudhia, J., 1993: A non-hydrostatic version of the Penn State-NCAR Mesoscale Model: validation tests and simulation of an Atlantic Cyclone and cold front. *Mon. Wea.Rev.*, **121**, 1493-1513.

Schicker, I., and Seibert, P., 2009: Simulation of the meteorological conditionrs during a winter smog episode in the Inn Valley. *MAP*, **103** (1-4), 211 – 222.

Zängl, G., 2003: A generalized sigma coordinate system for the MM5. *Mon. Wea.Rev.*, **131**, 2875–2884.

MOUNTAIN WAVE RELATED TURBULENCE DERIVED FROM SONIC ANEMOMETERS AND AN ELASTIC BACKSCATTER LIDAR

Željko Večenaj[1], Stephan F.J. De Wekker[2] and Vanda Grubišić[3]

[1]Department of Geophysics, Faculty of Science, Zagreb, Croatia
E-mail: *zvecenaj@gfz.hr*
[2]Department of Environmental Sciences, University of Virginia, USA
[3]Department of Meteorology and Geophysics, University of Vienna, Austria

Abstract: A case study of mountain wave related turbulence during the Terrain-induced Rotor EXperiment in the Owens Valley is presented. Large spatial and temporal variability in aerosol backscatter was observed in the valley atmosphere associated with mountain wave activity. The corresponding turbulence structure along and across the valley was investigated using data collected by three 30 m NCAR towers equipped with 6 levels of ultrasonic anemometers. Time series of turbulent kinetic energy (*TKE*) show much higher levels of *TKE* in the valley center than on the sloping western part of the valley. An analysis of the *TKE* budget shows that mechanical production of turbulence is dominant and balanced by turbulent dissipation in central parts of the valley. The data and analysis from this case study can be used to evaluate and improve turbulence parameterization schemes in atmospheric numerical models.

Keywords: T-REX experiment, turbulent kinetic energy, budget equation, dissipation rate

1 INTRODUCTION

Terrain-induced Rotor Experiment (T-REX) was conducted during spring 2006 in Owens Valley, California. During the Intensive Observation Period 1 (IOP 1) from 0000 UTC on 02 March to 1500 UTC on 03 March 2008 a transition occurred from a quiescent to a disturbed boundary layer accompanied by large spatial inhomogeneities in the aerosol backscatter (De Wekker and Mayor, 2009).The turbulence structure near the surface during these transitions is poorly known and potentially important for the modification of mountain wave activity and the generation of rotors and subrotors on the lee-side of mountains.

Turbulent kinetic energy (*TKE*) is produced and destructed by various processes that are explained by the different terms in the *TKE* budget equation (e.g. Stull, 1988). One of the terms is the eddy dissipation rate (ε) which is parameterized in numerical models (e.g. Mellor and Yamada, 1974) and used in turbulence nowcasting at the airports (e.g. Frech, 2007). By quantifying both the *TKE* and ε, parameterization schemes that are used in these models can be evaluated and potentially improved.

2 FIELD EXPERIMENT, INSTRUMENTATION AND DATA

Data from three towers from the Integrated Surface Flux Facility (ISFF) installed by NCAR and from the Raman-shifted Eye-safe Aerosol Lidar (REAL) are used in this study. Figure 1 shows the map of the site with the towers and REAL indicated.

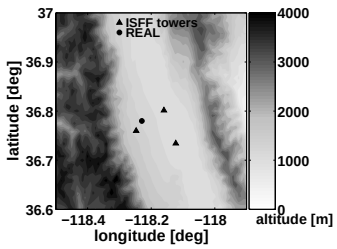

Figure 1. The map of the area of interest together with the locations of the towers and the lidar.

The western tower (WT) was located on the alluvial slope on the western side of Owens Valley. The central tower (CT) and the south tower (ST) were located along the valley's central axis extending from NNW to SSE. Each tower was 35 m tall and instrumented with CSAT3 ultrasonic anemometers collecting data with a sampling rate of 60 Hz at heights of 5, 10, 15, 20, 25 and 30 m. REAL was installed between WT and CT on the alluvial slope providing an undisrupted view in all directions within its range. Vertical and horizontal scans were made using REAL (De Wekker and Mayor, 2009).

3 RESULTS

In Cartesian system, the *TKE* is defined as a sum of variances of all three wind components:

$$TKE = \frac{1}{2}\left(\overline{u'^2} + \overline{v'^2} + \overline{w'^2}\right) \quad (1)$$

The *TKE* budget equation is expressed as (e.g. Stull, 1988):

$$\underbrace{\frac{\partial TKE}{\partial t}}_{I} = \underbrace{\frac{g}{\Theta_v}\left(\overline{w'\theta_v'}\right)}_{II} \underbrace{-\overline{u'w'}\frac{\partial U}{\partial z}}_{III} \underbrace{-\frac{\partial\left(\overline{w'TKE}\right)}{\partial z}}_{IV} \underbrace{-\frac{1}{\rho}\frac{\partial\left(\overline{w'p'}\right)}{\partial z}}_{V} \underbrace{-\varepsilon}_{VI} \qquad (2)$$

Term *I* represents a local storage of *TKE*. Term *II* is the buoyant production/consumption term depending on the sign of the heat flux ($\overline{w'\theta_v'}$). Term *III* denotes mechanical (shear) production term. Term *IV* describes the turbulent transport of *TKE* by the vertical velocity *w* of turbulent eddies. Term *V* is a pressure correlation term that shows how pressure perturbations redistribute *TKE* in the vertical. Finally, term *VI* represents the dissipation of *TKE* by molecular viscosity into heat.

Between 2345 UTC on 02 March and 0115 UTC on 03 March REAL detected interesting features that indicated presence of high levels of turbulence (De Wekker and Mayor, 2009). ISSF towers reveal that *TKE* indeed is strong along the valley (ST, Fig. 2c and CT; Fig. 2b) due to the influence of strong south-easterly flows along the valley. However, *TKE* is considerably weaker at WT (Fig. 2a). REAL data shows that downslope advection of stable stratified air occurs near the western tower leading to the low levels of turbulence there. The *in-situ* measurements do not capture the increased mixing above ~ 1 km revealed by REAL. REAL indicated that this increased mixing is caused by the interaction of the downslope flow and the SE flow along the valley. From Fig. 3 it is obvious that the mechanical term and ε are predominant and almost in balance at all mid-levels at the CT (Fig. 3b) and ST (Fig. 3c). In general, the values at WT are approximately 5 times smaller than at CT and ST, confirming that the turbulence is suppressed at WT. However, ε is noticeable larger than the sum of *TKE* production terms, i.e. mechanical shear and buoyancy, at WT. This indicates that the *TKE* was not produced locally but advected from elsewhere by the downslope flows.

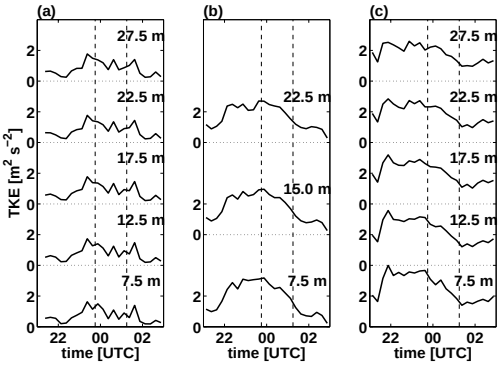

Figure 2. Temporal evolution of the *TKE* evaluated at various mid-levels at WT (a), CT (b) and ST (c). The heights of the various mid-levels are indicated in the figure. Vertical dashed lines depict the period of interest.

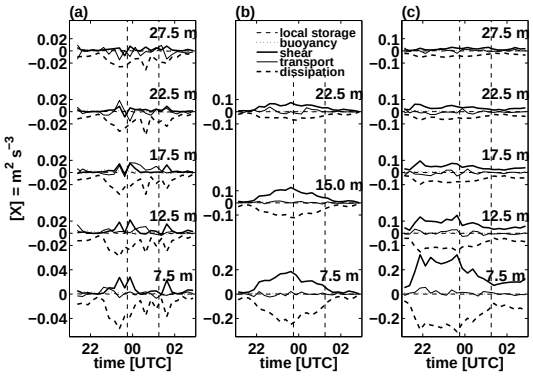

Figure 3. Temporal evolution of the terms from the *TKE* budget equation (equation 2 in text) evaluated at the mid-levels at WT (a), CT (b) and ST (c). The heights of the mid-levels are indicated in the figure.

4 SUMMARY

During T-REX IOP 1, a transition from a quiescent to a disturbed boundary layer is accompanied by large variability in space and time of aerosol backscatter and turbulent kinetic energy. Stably stratified downlope flows suppress the *TKE* on the western side of the valley while the *TKE* is enhanced in the central part of the valley, where a strong interaction between downlope flows, channelled along-valley flows and mountain waves occurs. At the along-valley locations locally produced shear-driven turbulence is balanced by turbulent dissipation while advection effects play an important role at the western slope location. This study exemplifies the benefit of combined in-situ and remote sensing measurements in providing an improved understanding of temporal and spatial turbulence variability in complex terrain.

Acknowledgements:
This study is partially supported by the Croatian Ministry of Science, Education & Sports, projects BORA No. 119-1193086-1311. This work was started while ZV was a visiting student at the University of Virginia.

REFERENCES

De Wekker S.F.J. and S.D. Mayor, 2009: Observations of atmospheric structure and dynamics in the Owens Valley of California with a ground-based, eye-safe, scanning aerosol lidar. J. Appl. Meteor. Climat.In press.

Frech, M., 2007: Estimating the turbulent energy dissipation rate in an airport environment. Boundary-Layer Meteorol. **123**, 385–393.

Mellor, G.L. and T. Yamada, 1974: A hierarchy of turbulence closure models for planetary boundary layers. J. Atmos. Sci. **31**, 1791-1806.

Stull, R.B., 1988: An Introduction to Boundary Layer Meteorology, Kluwer Academic, 666 pp.

ALONG-COAST FEATURES OF THE BORA RELATED TURBULENCE

Željko Večenaj[1], Danijel Belušić[1], Vanda Grubišić[2] and Branko Grisogono[1]

[1]Department of Geophysics, Faculty of Science, Zagreb, Croatia
E-mail: *zvecenaj@gfz.hr*
[2]Department of Meteorology and Geophysics, University of Vienna, Austria

Abstract: The mesoscale bora structure in the along-coast direction (normal to the mean bora flow) is featured by an interchange of jets and wakes related to mountain gaps and peaks. Here we examine the along-coast, off-shore turbulence structure of the bora that occurred on 7 November 1999 during the Mesoscale Alpine Program (MAP) Intensive Observation Period 15. We use the aircraft and dropsonde data measured along the lee side of the Dinaric Alps over the Adriatic by the NCAR Electra aircraft. The results are compared with the output from the WRF ARW numerical model.

Keywords: MAP, bora wind, turbulence, turbulence kinetic energy, dissipation rate, WRF ARW model

1 INTRODUCTION

Along the eastern Adriatic coast, a downslope wind called bora is a common occurence. Bora blows from the northeastern quadrant and is most frequent during the winter season. Bora mean wind speed can surpass 20 m s^{-1} and due to its gustiness can reach speeds in excess of 60 m s^{-1} (e.g. Belušić and Klaić, 2006). During such events, there is strongly developed turbulence in the lee of the coastal mountains.

The mesoscale bora structure in the along-coast direction (normal to the mean bora flow) is featured by an interchange of jets and wakes related to mountain gaps and peaks as documented in Grubišić (2004) for a bora event over northern Adriatic that occurred on 7 November 1999 during the Mesoscale Alpine Programme (MAP) Intensive Observation Period 15. We present here a study of turbulence in the early stage of this bora event. The study is based on the aircraft data measured along the lee side of the Dinaric Alps over the Adriatic by the NCAR Electra aircraft. The data includes two vertically separated flight legs (lower at ~ 370 m, higher at ~ 680 m) and six dropsonde measurements along the legs. The results are compared with the output from the WRF ARW numerical model for this event.

2 OBSERVATIONAL DATA ANALYSIS

During IOP 15, two 216 km long coast-parallel flight legs were flown by the NCAR Electra, one at ~680 m ASL flying SE to NW, and the other at 380 m ASL from NW to SE. High-resolution aircraft data was obtained at the frequency of 25 Hz. The aircraft flew at the mean velocity of 100 m s^{-1}. Two hours ealier, nine dropsondes were released by the aircraft from a 4200 m ASL leg above the low-level flight legs. The area of interest, together with the horizontal wind along the lower flight leg, and the coordinates of the dropsondes, are shown in Fig. 1.

The coordinate system is rotated counter clockwise with the x-axis perpendicular to the flight legs and pointing SW. The y-axis is parallel to the flight legs and points toward SE. The crosspectrum and spectrum analyses of the heat and momentum flux from the aircraft data for both flight legs show the energy gap (e.g. Metzger and Holmes, 2008) at the wave number that corresponds to the wavelength of 120 m. This impelled us to filter the aircraft data using the Moving Average (MA) of 120 m. Consequently, we neglect all of the phenomena on scales greater then this MA. The flight legs are divided into 100 segments of 2160 m. For each segment the turbulent kinetic energy (*TKE*) and *TKE* dissipation rate (ε) are calculated. The latter is calculated using the inertial dissipation method provided by Kolmogorov's 1941 theory (?) (e.g. Večenaj et al., 2007). The *TKE* values are used as the control parameter for the evaluation of ε (Figs. 2a-c). Bulk Richardson number, R_B, (e.g. Stull, 1988) calculated from the aircraft data is compared with the one calculated from the dropsonde data (Fig. 2d).

3 COMPARISON OF MEASUREMENTS AND MODEL RESULTS

This bora event was simulated using the WRF ARW model. While u wind speed component is reproduced successfully along the flight legs, the agreement with the v component, potential temperature (θ) and *TKE* is poorer (Fig. 3). With respect to the aircraft data, the model significantly overestimates v along the entire flight legs while it underestimates θ on the northern part and *TKE* on the southern part of the legs. There is a good agreement between the aircraft and dropsonde data along the flight legs (Fig. 4). Comparison of the modelled with the dropsonde data shows a good agreement with u and θ, while v shows more deviation both in magnitudes and in vertical structure.

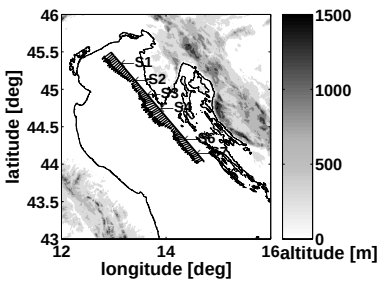

Figure 1. Area of interest together with a lower flight leg (height of 370 m), wind vectors (1600 m means) and positions of dropsondes.

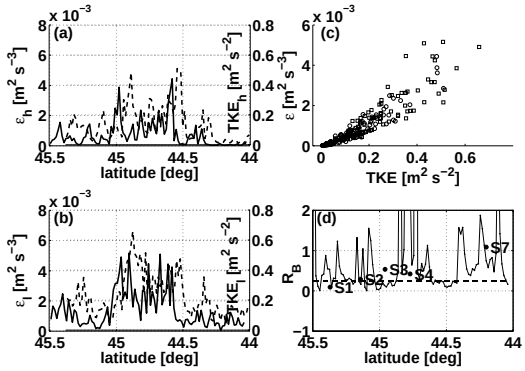

Figure 2. ε (solid line) and *TKE* (dashed line) on (a) higher (b) lower flight leg. (c) ε vs. *TKE* on higher (circles) and lower (squares) flight leg. (d) R_B between flight legs from aircraft data (solid line) and from dropsonde data (diamonds).

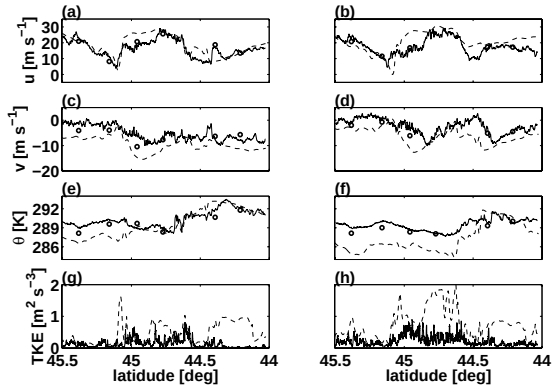

Figure 3. Aircraft (solid line), dropsonde (circles) and modelled data (dashed line) along the higher (a, c, e, and g) and the lower (b, d, f, h) flight leg.

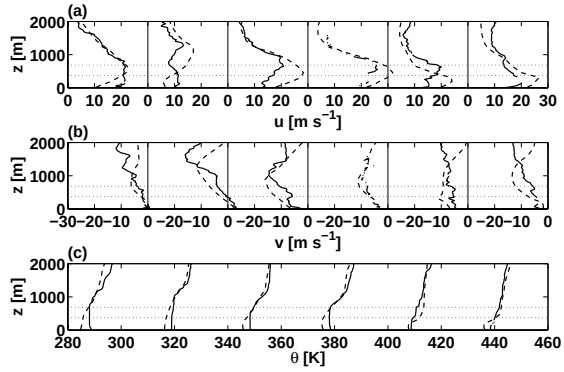

Figure 4. Six dropsonde along flight legs (solid line) and modelled (dashed line) data of (a) u and (b) v. (c) θ is consecutive shifted for 30 K.

4 SUMMARY

A significant spatial variability of *TKE* and ε along the flight legs is revealed in this bora case associated with mesoscale phenomena that are part of bora such as mountain waves, wave breaking, jets and wakes, shear zones, where the jets, wakes and the shear zones are closely related to the terrain complexity of the eastern Adriatic coast.

Variations of *TKE* time series closely follow those of ε which gives the information about robustness and consistency of the ε estimation. As expected, a scatter plot shows that ε increases with *TKE*. The empirical relation between these two variables is yet to be examined.

In general, aircraft in situ data agrees well with the dropsonde data which points out to the degree of measurements reliability. The WRF ARW model reproduces the *u* wind speed component along the flight legs well, while the *v* component and θ are overestimated and underestimated, respectively. Also, *TKE* is well simulated at the northern part of the legs, while it is overestimated at the southern part. As for the vertical range, *u* and θ are reproduced more successful than *v*.

Acknowledgements:
This study is supported by the Croatian Ministry of Science, Education & Sports, projects BORA No. 119-1193086-1311.

REFERENCES

Belušić, D. and , Z.B. Klaić, 2006: Mesoscale dynamics, structure and predictability of a severe Adriatic bora case. Meteorol. Z. **15**, 157-168.

Grubišić, V., 2004: Bora-driven potential vorticity banners over the Adriatic. Q. J. R. Meteorol. Soc. **130**, 2571-2603.

Metzger, M. and H. Holmes, 2008: Time scales in the unstable atmospheric surface layer. Boundary-Layer Meteorol. **126**, 29-50.

Stull, R.B., 1988: An Introduction to Boundary Layer Meteorology, Kluwer Academic, 666 pp.

Večenaj, Ž., D. Belušić, and B. Grisogono, 2007: Estimation of turbulence kinetic energy dissipation rate in a bora event. *Proc. 29th Intern. Conf.on Alpine Meteorology*, Chambery, France, 745-748.

ANALYSIS OF SECOND ORDER MOMENTS OF SURFACE LAYER TURBULENCE IN AN ALPINE VALLEY

Dino Zardi[1], Massimiliano de Franceschi[1,2], Mauro Tagliazucca[3], Francesco Tampieri[3]

[1] Gruppo di Fisica dell'Atmosfera, Università di Trento, Trento, Italy
E-mail: *Dino.Zardi@ing.unitn.it*
[2] Seminario Maggiore, Diocesi di Bolzano-Bressanone, Bressanone, Italy
[3] Istituto di Scienze dell'Atmosfera e del Clima, Consiglio Nazionale delle Ricerche, Bologna, Italy

Abstract: Results from the analysis of field measurements in the atmospheric surface layer in the Adige Valley, south to the city of Bolzano/Bozen in the Alps, are presented. Values of drag coefficient, displacement height and roughness length are similar to those reported in the literature about surface layer turbulence over plain uniform terrain. All the nondimensional standard deviations of wind velocity components are well reproduced with just one Monin-Obukhov similarity relationship. The analysis of temperature fluctuations results in distinct behaviours in the stable and unstable regimes respectively, which require suitable expressions such as those already proposed in the literature. In the present case the coefficients for near neutral conditions are lower than generally reported. The importance of using an appropriately formulated recursive filter to separate low frequency unsteadiness of the mean flow from turbulence signal is also shown.

Keywords: *surface layer turbulence, valley, second order moments*

1 INTRODUCTION

Many recent studies on boundary layer turbulence investigate areas with nonhomogenous terrain, testing appropriate extensions of concepts valid for flat uniform terrain. The present paper focuses on the stability dependence of wind velocity and temperature variances and aims at exploring the applicability of MOST in the central region of a valley floor.

Standard deviations of the three wind components and of air temperature are a basic information concerning the intrinsic statistical properties of surface layer turbulence. Moreover they are required for appropriate parameterization of diffusion processes into the atmosphere. The vertical structure of velocity standard deviations within MOST has been examined by various authors (Doran et al., 2002; Rotach and Zardi, 2007), who explored a rather wide group of situations, including some cases of complex terrain. However so far only few results are available in the literature for the case of mountain valleys and their similarity scaling.

2 DATA AND METHODS

Results are based on turbulence measurements performed in July 1999, under various weather conditions, with a sonic anemometer in the middle of the valley floor (so as to be minimally affected by sidewall effects), in a locally plain and almost horizontal area (down-valley slope everywhere less than 0.2%), rather regularly surrounded by uniformly high apple tree orchards (de Franceschi et al., 2009).

Besides the techniques commonly adopted in the field of micrometeorology (Lee et al., 2004), special care was devoted to the appropriate design parameters of the digital recursive filter used to separate turbulent fluctuations from the mean flow (de Franceschi and Zardi, 2003), as well as to evaluation of the rotation angles required for streamwise alignment (de Franceschi, 2004). Furthermore the analysis of wind velocity standard deviations is based on the well known expression that Panofsky and Dutton (1984) proposed for the vertical component (only) under unstable conditions. In particular, in the present work the following expression

$$\frac{\sigma_i}{u_*} = \alpha_i \left(1 + \beta_i |\zeta|\right)^{1/3} \tag{1}$$

has been assumed as test function for the three wind components (u, v and w) and both stability ranges. Furthermore, for the temperature fluctuations two different expressions have been tested, namely

$$\frac{\sigma_i}{|\theta_*|} = \begin{cases} \alpha_\theta \left(1 - \beta_\theta \zeta\right)^{-1/3} & \zeta \le 0 \\ \alpha_\theta \left(1 + \beta_\theta \zeta\right)^{-1} & \zeta \ge 0 \end{cases} \tag{2}$$

3 RESULTS

The analysis of data from nondimensional standard deviations allows to adopt, for all the wind components, the same Monin-Obukhov similarity relationship in the form of equation (1), thus extending its applicability to the case of winds over a valley floor under slowly varying situations. The best-fit coefficients α_i and β_i are

reported in Table 1. The latter also shows the benefit in terms of reduced scatter around the best fit curve following a correct definition of the design parameters for the digital filter (de Franceschi and Zardi, 2003).

	$\zeta < 0$								
	α_u	β_u	R^2	α_v	β_v	R^2	α_w	β_w	R^2
unf.	2.02±0.07	5.14±0.96	0.29	2.09±0.08	4.81±1.06	0.20	1.06±0.02	6.48±0.56	0.70
McM	1.85±0.05	5.50±0.89	0.40	1.85±0.06	5.80±1.10	0.31	1.13±0.01	4.94±0.32	0.77
dFZ	1.80±0.02	0.78±0.05	0.71	1.63±0.02	1.32±0.10	0.74	1.27±0.01	2.82±0.14	0.97
	$\zeta > 0$								
	α_u	β_u	R^2	α_v	β_v	R^2	α_w	β_w	R^2
unf.	2.02±0.09	22.50±3.92	0.64	2.21±0.10	16.60±3.06	0.50	1.12±0.02	1.42±0.16	0.35
McM	2.01±0.06	12.80±1.63	0.67	1.98±0.09	16.10±2.69	0.57	1.17±0.01	1.48±0.15	0.41
dFZ	1.92±0.02	1.01±0.06	0.69	1.71±0.02	1.68±0.12	0.69	1.32±0.01	0.88±0.06	0.64

Table 1: Best-fit coefficients for eq. (1) for the along-valley wind directions ["unf." = values obtained without any filtering procedure; "McM" = McMillen's (1988) procedure; "dFZ" = de Franceschi and Zardi (2003) correction].

As to temperature variance, two different behaviours are met in the stable and unstable regimes respectively: the expressions (2) seem to reproduce well the data, though with lower coefficient values (Table 2) than commonly reported for near neutral conditions.

	$\zeta < 0$				$\zeta > 0$		
	α_θ	β_θ	R^2		α_θ	β_θ	R^2
unf.	1.47±0.11	21.0±8.82	0.25		1.73±0.05	0.17±0.07	0.07
McM	1.19±0.11	19.0±9.59	0.20		1.55±0.04	0.01±0.02	$6\ 10^{-3}$
dFZ	1.15±0.11	16.9±8.34	0.29		1.21±0.02	$3\ 10^{-3}$±$7\ 10^{-3}$	$1\ 10^{-3}$

Table 2: Best-fit coefficients for eq. (2) for the along-valley wind directions ["unf." = values obtained without any filtering procedure; "McM" = McMillen's (1988) procedure; "dFZ" = de Franceschi and Zardi (2003) correction].

4 CONCLUSIONS

The analysis of turbulence data from a field measurement campaign in an Alpine valley, thanks to suitable data-treatment (de Franceschi and Zardi, 2003) which proved to be effective in filtering out the short-period nonstationarities, allowed a reliable estimation of best-fit parameters for similarity functions.

The results presented here give a new perspective on the behaviour of second order moments in the Surface Layer turbulence in an mountain valley, especially about the validity of MOST over all stability ranges and wind velocity components, for which a single similarity function provides simpler but well reliable description.

Acknowledgements:
This work has been partly supported by: the Bolzano Municipality under the contract "Evaluation of the pollutant dispersion in the Bolzano area"; the Environmental Protection Agency of the Province of Trento under the contract "Study of the Boundary Layer processes in the Adige Valley"; the Italian National Institute for the Scientific and Technological Research on the Mountain (INRM) under the research contract "Study of atmospheric dynamics in Alpine valleys".

REFERENCES

Doran, J.C., J.D., Fast, J. Horel, 2002: The VTMX 2000 Campaign. Bull. Amer. Meteor. Soc., **83**: 537–551.

de Franceschi, M., Investigation of Atmospheric Boundary Layer in Alpine Valleys. Monographs of the School of Doctoral Studies in Environmental Engineering. Università di Trento, 2004. ISBN 88-8443-052-6, 135 pp (http://www.ing.unitn.it/dica/eng/monographs/)

de Franceschi, M., D. Zardi, 2003: Evaluation of cut-off frequency and correction of filter-induced phase lag and attenuation in eddy covariance analysis of turbulence data. Boundary-Layer Meteorol., **108**: 289–303.

de Franceschi, M., D. Zardi, M. Tagliazucca, F. Tampieri, 2009: Analysis of second order moments in the Surface Layer turbulence in an Alpine valley, Q. J. R. Met. Soc., *submitted*

Lee, X., W. Massman, B. Law, 2004: Handbook of Micrometeorology. A Guide for Surface Flux Measurement and Analysis. Kluwer Academic Publishers, Dordrecht.

McMillen, R.T., 1988: An eddy correlation technique with extended applicability to non-simple terrain. Boundary-Layer Meteorol., **43**: 231–245.

Panofsky, H. A. and Dutton, J. A. 1984 Atmospheric Turbulence. Models and methods for engineering applications. Wiley and Sons Inc., New York

Rotach, M., D. Zardi, 2007: On the boundary layer structure over highly complex terrain: key findings from MAP. Q. J. R. Met. Soc., **133**: 937–948.

VALIDATING THE TURBULENCE PARAMETERIZATION SCHEMES OF A NUMERICAL MODEL USING EDDY DISSIPATION RATE MEASUREMENTS IN A TERRAIN-DISRUPTED AIRFLOW

Pak Wai Chan

Hong Kong Observatory, Hong Kong, China
E-mail: *pwchan@hko.gov.hk*

Abstract: A number of turbulence parameterization schemes are available in the latest version (6.0) of the Regional Atmospheric Modelling System (RAMS). Chan (2009) studied the performance of these schemes by simulating the eddy dissipation rate (EDR) distribution in the vicinity of the Hong Kong International Airport (HKIA) and comparing with the EDR measurements of remote-sensing instruments at the airport. For the e-l (turbulent kinetic energy – mixing length) scheme considered in that study, the mixing length is assumed to be a constant. This assumption is removed in the present paper and simulations of EDR fields are repeated for terrain-disrupted airflow in the vicinity of HKIA. It is found that, with a variable mixing length, the performance of the e-l scheme is greatly improved. With suitable choice of the empirical constants in the turbulence closure, the accuracy of the EDR profile (in comparison with LIDAR and wind profiler measurements) is found to be comparable with that predicted by the Deardorff scheme. A study on the sensitivity of the simulation results to these empirical constants has also been performed.

Keywords: *RAMS, turbulence parameterization, e-l scheme*

1 INTRODUCTION

The Hong Kong International Airport (HKIA) is situated in the vicinity of complex terrain. To its south is the mountainous Lantau Island with peaks rising to about 1 km above mean sea level (AMSL) and valleys as low as 400 m in between. The airport is surrounded by sea in the west, north and east. To its northeast, at a distance of 10-12 km, there are a couple of mountains with a height of 500-600 m. Airflow disturbances arising from terrain disruption may bring about significant turbulence to aircraft landing at or departing from HKIA. Following the requirement of the International Civil Aviation Organization (ICAO), the turbulence intensity in aviation is quantified in terms of the cube root of eddy dissipation rate (EDR), ε. Forecasting of $EDR^{1/3}$ by numerical weather prediction (NWP) models would be useful in the provision of turbulence alerting services to aircraft.

Chan (2009) demonstrated that the forecasting of $EDR^{1/3}$ in typical cases of terrain-disrupted airflow around HKIA was possible by running the Regional Atmospheric Modelling System (RAMS) version 6.0 at high spatial resolution. The innermost model domain has a horizontal resolution of 50-200 m. The forecasting results had been shown to depend very much on the choice of the turbulence parameterization scheme. It turns out that the Deardorff scheme appeared to have the best performance in the selected cases. In RAMS 6.0, there are also a couple of new turbulence parameterization schemes available, such as the e-l (turbulent kinetic energy [TKE] – mixing length) scheme of Trini Castelli et al. (2005). However, this scheme is found to give too much turbulence near the ground and $EDR^{1/3}$ drops too rapidly with altitude in comparison with the other turbulence schemes and actual measurements.

The default setting of RAMS 6.0 adopts a constant mixing length for e-l scheme. In the present study, a variable mixing length is applied to two different wind regimes, namely, southwest monsoon in the summer and northeast monsoon in the winter over southern China.

2 E-L SCHEME AND NUMERICAL MODEL SETUP

In e-l scheme, the diffusion coefficient of momentum K_m is determined as:

$$K_m = c_\mu e^{1/2} l \tag{1}$$

where c_μ is a closure empirical constant. Following Xu and Taylor (1997), it has a value of 0.41. This constant is in turn related to the corresponding empirical constant of dissipation term of TKE $\varepsilon_\mu = c_\mu^3$. In the present study, c_μ is made variable and the resulting $EDR^{1/3}$ field is compared with the actual measurements to find out a suitable value for this empirical constant.

The model setup is similar to that in Chan (2009). The initial and boundary conditions for RAMS are obtained from a mesoscale regional spectral model of the Hong Kong Observatory (HKO). Only three nested domains are employed in the present study of RAMS, namely, at spatial resolutions of 4 km, 800 m and 200 m. In the second and third domains, terrain data of Hong Kong at 100 m horizontal resolution is used in order to resolve the major topographical features around HKIA.

3 MODEL SIMULATION RESULTS

A moderate southwest monsoon case is studied. The LIDAR measurements around HKIA at that time are shown in Fig. 1. The model-simulated wind field is found to be generally consistent with the LIDAR data (not shown).

The model-simulated $EDR^{1/3}$ profile at Siu Ho Wan (location in Fig. 2) and the actual measurement by a 1299-MHz wind profiler at that location are compared in Fig. 3. It can be seen that the results from e-l scheme and Deardorff-scheme are rather close to the actual measurements in the first 1 km or so AMSL, whereas Mellor-Yamada (MY) scheme gives rather small $EDR^{1/3}$ values. The root-mean-square difference between model simulated and actual data (at all heights) as a function of c_μ for e-l scheme is given in Fig. 4, which shows that a c_μ value of about 0.45 gives the smallest difference. This is consistent with the results in the literature (between 0.40 and 0.55). Using the e-l scheme with $c_\mu = 0.45$, the simulated $EDR^{1/3}$ field is given in Fig. 2. The turbulence intensity is larger at areas just downstream of the mountains of Lantau Island and decreases gradually several kilometres downstream. The results for a northeast monsoon case near HKIA are basically the same (not shown).

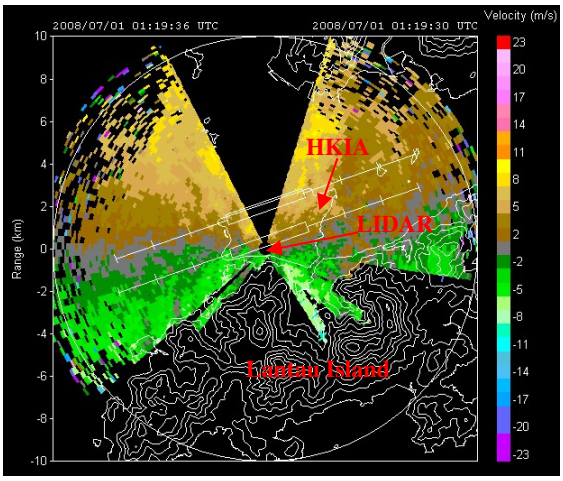

Figure 1. LIDAR velocity image at 3.2-degree conical scan at 01:19 UTC, 1 July 2008.

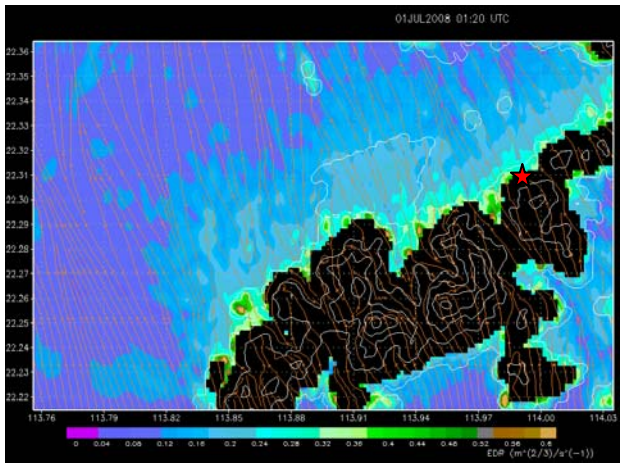

Figure 2. Model simulated $EDR^{1/3}$ field at 50 m AMSL at 01:20 UTC, 1 July 2008. The location of Siu Ho Wan wind profiler is indicated by the star.

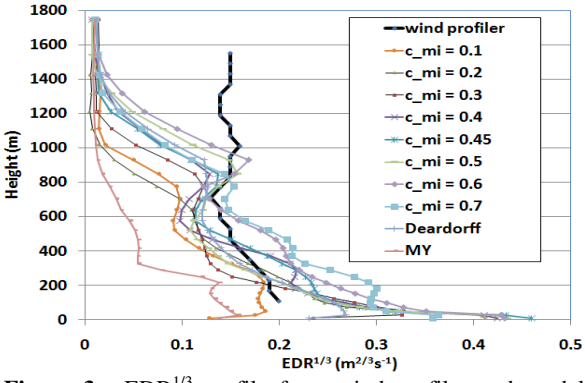

Figure 3. $EDR^{1/3}$ profile from wind profiler and model simulations of different turbulence parameterizations for 1 July 2008 case.

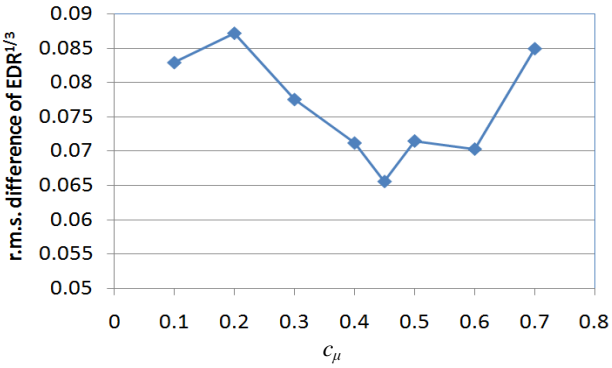

Figure 4. Root-mean-square difference of $EDR^{1/3}$ values as a function of c_μ for 1 July 2008 case.

4 CONCLUSIONS

It has been found that the use of a variable mixing length in e-l scheme in RAMS simulation gives $EDR^{1/3}$ fields comparable with those obtained with Deardorff scheme. The optimal c_μ value (0.45) for model simulation is consistent with those reported in the literature.

REFERENCES

Chan, P.W., 2009: Atmospheric Turbulence in Complex Terrain: Verifying Numerical Model Results with Observations by Remote-sensing Instruments. Meteorol. Atmos. Phys., **103**, 145-157, DOI: 10.1007/s00703-008-0342-3.

Trini Castelli, S., E. Ferrero, D. Anfossi, and R. Ohba, 2005: Turbulence closure models and their application in RAMS. Environmental Fluid Mechanics, **5**, 169–192.

Xu, D., and P.A. Taylor, 1997: On Turbulence Closure Constants for Atmospheric Boundary-Layer Modelling: Neutral Stratification. Boundary-Layer Meteorology, **84**, 267-287.

ESTIMATING AND TESTING THE TOPOGRAPHIC AMPLIFICATION FACTOR USING GIS AND CLIMATE DATA FROM THE WESTERN U.S.

Sharon Zhong, Jessica Van Deusen, Yi Chen, Ashton Shortridge

Department of Geography, Michigan State University
E-mail: *zhongs@msu.edu*

Abstract: High resolution DEM data and GIS tools are employed to identify basins in Western U.S. The value of Topographic Amplification Factor (*TAF*) is estimated for each basin and the usefulness of *TAF* to explain the observed differences in diurnal temperature variations among these basins are explored using climate data.

Keywords: *Topographic Amplification Factor, diurnal temperature range in basins, Western U.S. basins*

1 INTRODUCTION

The Topographic Amplification Factor, or *TAF*, has been used to explain why air in a valley or basin heats or cools more than air over adjacent plains (Steinacker 1984; Whiteman 1990). *TAF* is defined as

$$TAF = \frac{A_{xy}(h)/V_{valley}}{A_{xy}(h)/V_{plain}}$$

where A_{xy} is the horizontal area through which energy enters or leaves the top of the volumes at height *h* above valley floor or plain, and V_{valley} and V_{plain} are the volumes of atmosphere subject to heating or cooling in the two regions, respectively. An elementary integration of first principles of thermodynamics links *TAF* to the differential temperature variations between a valley and a plain. Because the heated or cooled air volume is smaller in a valley than above the plain, the same heating or cooling provides larger increase or decrease of temperature within the valley. Due to its simplicity and intuitiveness, the *TAF* concept has been used to interpret lower minimum temperatures in basins and sinkholes as well as valley wind development.

Using GIS and high resolution DEM data, we have identified basins and sinks in the western United States and estimated their *TAF* values. We have also obtained climate data for a number of basins to examine how well the *TAF* concept may be used to explain the differences in the observed diurnal temperature ranges among the basins.

2 APPROACH

2.1 Finding the basin and estimating *TAF*

To identify basins and estimate *TAF*, we used 1 arc second DEM data and GIS software. Many steps are involved in delineate a basin and determine its *TAF* and the flow chart below outlines the major steps. The basins identified in Western U.S. are shown in Figure 1 and the *TAF* values estimated are listed in Table. 1.

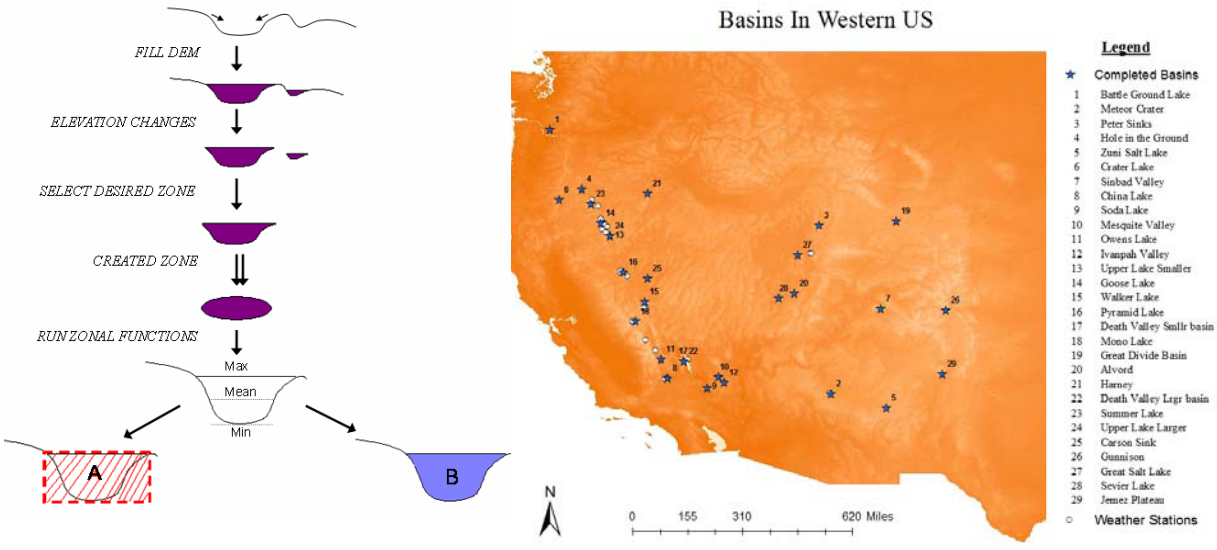

Figure 1. Flow chart (left) showing the major steps in identifying basins in Western U.S. (right). *TAF* is calculated as the ratio B/A. Also shown on the terrain and basin map are locations of weather stations used in the analyses.

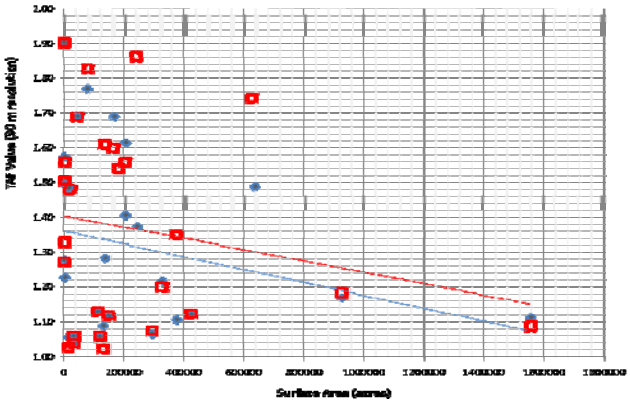

Figure 2 shows *TAF* values as a function of surface area of the basins. As expected, *TAF* value tends to decrease as the surface area of a basin increases. But for small basins, *TAF* values are more sensitive to the slope and shape of the sidewalls.

Figure 2. *TAF* as a function of surface area. The red squares are *TAF* values calculated using 30-m resolution data and the blue diamonds are *TAF* using 90-m data.

Basin Name	TAF	Basin Name	TAF	Basin Name	TAF
Battle Ground Lake	1.270	Mesquite Valley	1.688	Great Divide Basin	1.557
Meteor Crater	1.558	Owens Lake*	1.826	Alvord	1.861
Peter Sinks	1.901	Ivanpah Valley	1.128	Harney	1.073
Hole in the Ground	1.504	Upper Lake (small)	1.057	Death Valley (large)	1.199
Zuni Salt Lake	1.328	Goose Lake	1.022	Summer Lake*	1.349
Crater Lake	1.025	Walker Lake*	1.610	Upper Lake (large)*	1.120
Sinbad Basin	1.478	Pyramid Lake*	1.116	Carson Sink	1.741
China Lake*	1.059	Death Valley (small)*	1.599	Gunnison	1.181
Soda Lake	1.037	Mono Lake*	1.539	Great Salt Lake*	1.086

Table 1. Estimated *TAF* values for basins in Western United States. The * indicates basins having climate data.

2.2 Diurnal temperature range of *TAF*

Climate data are used to determine whether *TAF* or the "volume effect" can be used to explain some of the differences in the maximum and especially the minimum temperature observed in these basins. Because majority of these basins are located in remote areas, only a third of them have climate data available (stared in Table 1). Data from these basins range from 20-30 years and most stations only have temperature and precipitation records which prevented a selection of ideal days with clear sky and weak winds when the volume effect is most prominent. To avoid the errors associate with simple height adjustment in comparing maximum and minimum temperature which may overwhelm the effect of *TAF*, the mean diurnal temperature ranges are compared.

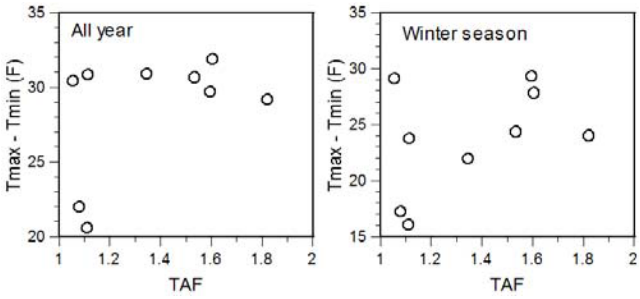

Figure 3. Mean diurnal temperature range and TAF

Figure 3 shows the diurnal temperature variation averaged over days without precipitation as a function of *TAF*. There is no clear relation between the diurnal range and *TAF*. For winter season, there appears to be an indication that larger diurnal range corresponds to larger *TAF* values, but the correlation is weak. Adjustment for density differences did not improve the correlation. The lack of correlation in the current analysis is likely due to other complicating factors affecting energy budget, such as cloudiness, winds, solar radiation, humidity, and vegetation, which could not be controlled in the current analyses. Synoptic maps and output from North American Regional Reanalysis are being used to help better control these factors.

Acknowledgements:
We thank Diane Barach for helping with identifying and downloading climate data. This research is supported by the U.S National Science Foundation through Grants No. ATM 0837860 & ATM 0640206.

REFERENCES

Steinacker, R. 1984: Area-height distribution of a valley and its relation to the valley wind. Contrib. Atmos. Phys. **57**, 64–71.
Whiteman, C.D. 1990: Observations of thermally developed wind systems in mountain valleys, in Atmospheric Processes over Complex Terrain. W. Bluemen ed. Meteorological Monograph, American Meteorological Society, 323 pp.

Winter High Pressure - Mater of mixing air in the Belluno Pre-alpine basin

Robert-Luciani Thierry, Marigo Gianni
E-mail: *tluciani@arpa.veneto.it*
Avalanches Centre of Arabba, ARPA Veneto, Italy

Keywords: synoptic, mixing air, wind, boundary layer, Alps' basin

INTRODUCTION

During winter, High pressures can be present for several days on the Alps with problem of mixing air in the valleys, especially in the Pre-alpine basin like Belluno depression. Normally in this area winds are often very weak, especially during winter, when air viscosity (member of Reynolds) increases appreciably and laminar and stratify flow tends to deposit and almost immovable, without micro-turbulences, so when winds are strong on top of mountains, including in certain situation of Foehn. The absence or long periods of calm of wind without any exchange and strong stagnation of the same air mass in the lower level generate serious problems on the air quality due to high concentration in pollutants (pm10)

DATA AND METHODS

The first step consists to recognize each synoptic configuration observed on meteorological charts at 500, 700, 850 and 950 hPa. In this way to compare the situation in height (free atmosphere) and the same thing at low or ground level (planetary boundary layer) with the aim to create a synoptic database. The complete synoptic classification retains nine different types of weather, but only the first tow type shows principally problems of air mixing. So criteria of the synoptic classification consider wind factor in the low level basin, presence of inversion temperature (Sodar profile), daily temperature range and vertical air motion…

The second step consists to join synoptic situation with wind parameters (speed and direction) in the low layers (six automatic monitoring stations with wind speed and direction at five and ten meters level measurements situated in different and significant point of basin bottom for the needs of present study, added data Sodar in the central part of the basin to evaluate vertical temperature configuration in the first 900/1000 m).

The data of wind have a frequency of 24 mean values/day for the speed and the direction, added value of the strongest gust (max wind speed/24h) registered during all day.

The analysis covers a period of five years 2001-2005, and an other years (2006) with elevated winds analysis and vertical atmospheric data.

Without forgetting a study of cloud cover from HVR and Infrared images of Meteosat8 (2006) to define certain type of day about solar radiation, using 12 images for each day on the Italian oriental Alps.

RESULTS

In Belluno basin 30% of winter period presents problem of mixing air due to very important temperature inversion stratification, absence of wind and no air turbulences in the lowest layers. The weakness of the ventilation associated with the stable situations is a normal fact, but more surprising when anafront arrives with a strong increase of relative humidity and absolute blocking of winds. Paradoxically the situation is more critical within hours which precede the passage of anafront structure. The biggest concentrations of pollutants in the air are observed when temperatures is very cold in the lower levels, with very high humidity and when there is a very important increasing temperatures inversion when warm front reaches Alps.

The worse air mixing conditions correspond in the saturated and cold air or better when there intense and persistent fog in the basin. This last one creates a full-size thermal spatial and vertical homogeneity, preventing any air mixing in the first 50 /100 first meters above ground, thus one almost immobility of air. The moderate movements are of the order of 400 - 600 m/h (speed wind around 0.01, 0.02 m/s) with very high concentration of pm10 at Belluno and Feltre (two biggest city of this Basin)

Another peculiarity of Belluno basin is the absence of winds while on nearest top mountains speed of winds are sometimes strong: 30/50 km/h, but it seems that there are no exchanges between free atmosphere laminar flow

and cold air stratification in the air basin low level. So that it can have a mixing air, is needed vertical dynamics like front crossing or intense Foehn conditions to remove the low layer of cold air. Otherwise the air flow remains very weak, especially during the night, with bad air quality.

The poor quality of air for insufficient ventilation is more often exceeded to Belluno and Feltre than not in Milan. Colder, more humidity and more viscosity determine high stagnation of air with consequent problems, especially in the closed orographic basin, where the erosion of Planetary Boundary layers happens only in case of very dynamical flow conditions.

CONCLUSION

The wind in Valbelluna introduces characteristics of extreme weakness aerologic flow during the stable winter synoptic situation, so during the first phase of disturbance weather. Everywhere in this orographic basin, it possible to observe a very limited dynamic of winds in all the seasons and particularly during the cold semester from October to March, especially in the southern sector where the basin is more closed, with high frequency of fogs or low stratus and high deficit of solar radiation. So during the first phases of wintry disturbance weather, which often appears the worse condition with very high humidity, rather strong temperature inversion and absolute air stagnation. To attended a real remixing of the air, it ‘s necessary to wait the front crossing or Foehn conditions on the Belluno Basin.

REFERENCES

Blackadar A. K. (1957) Boundary layer wind maxima and their significance for growth of nocturnal inversion. Bull. Am. Meteorol. Soc. n° 38, pag . 283-290

Demoor G. (1983); Les théories de la turbulence dans la couche limite atmosphérique. Cours et manuels. Météo-France

Demour G. e Veyre P. (1999). Les bases de la météorologie dynamique. Cours et manuels. Météo-France.

James I. N. (1994); Introduction to circulating atmosphere. Cambridge University Press.

Malardel S. (2005). Fondamentaux de Météorologie, l’école du temps, ed. Cépaduès. Météo-France.

Malardel S. (2005). La couche limite, description e bref aperçu théorique. Cours et Manuel Météo-France

Robert-Luciani Th. (1991). Capitolo sulle situazioni sinottiche sul Nord-Est Italia, pagg. - Tesi di Dottorato

Trom M. (1996) Un’esercitazione di fisica con il foehn, Nimbus 13-14: 99-103

Stull, R. B. (1988). An introduction to Boundary layer Meteorology. Kluwer Academic.

WRF-CHEM STUDY OF THE HIGH OZONE EPISODE DYNAMICS OVER THE COMPLEX TERRAIN OF SLOVENIA

Rahela Žabkar and Jože Rakovec

University of Ljubljana, Faculty of Mathematics and Physics, Chair of Meteorology, Ljubljana, Slovenia
E-mail: *rahela.zabkar@fmf.uni-lj.si*

Abstract: Characteristics of temporal and spatial dynamics of high ozone episodes in Slovenia have been analyzed with the help of a coupled meteorological-photochemistry WRF/Chem model. The ability of model to represent the meteorological conditions and the ozone evolution over the complex terrain of Slovenia has been evaluated.

Keywords: *WRF-Chem model, complex terrain, tropospheric ozone*

1 INTRODUCTION

In Slovenia the highest frequency of exceedances of ozone threshold values during the warm months of the year is usually related to the south-western part of the country, separated from central Slovenia with the Alpine-Dinaric mountain ridge. The rest of Slovenia generally experiences lower ozone daily maxima with occasionally exceeded thresholds.

In the present research we study the temporal and spatial dynamics of high ozone episodes in Slovenia with a coupled meteorological-photochemistry WRF/Chem model. The main purpose is to understand and explain some observed characteristics of the high ozone episodes, e.g. the higher observed ozone maxima in Mediterranean south-western Slovenia (especially during the first part of the episodes) and higher ozone levels in central Slovenia related to the south-western air masses origin (Žabkar et al., 2008), as well as to identify potential direct impact of Po River Basin emissions on ozone levels in Slovenia.

2 METHODOLOGY

Among 50 days in years 2003 to 2005 with ozone daily maxima above 165 μg/m^3 at least at one air quality station, we focus on three episodes (example of measured ozone during one episode shown in Figure 1) for which we explore the characteristics of episode dynamics with a 2.2 version of the WRF/Chem model. Simulations in 27 km, 9 km and 3 km domains (Figure 2) and with 51 vertical levels were performed using a coupled one-way nesting strategy. The initial and boundary meteorological conditions were taken from ECMWF analysis archive data with the 0.25º horizontal resolution and the temporal resolution of 6 hours.

The modelling results were evaluated with ozone measurements from 12 ground level air quality stations and 15 meteorological stations spread over the complex terrain of Slovenia, while vertical structure of atmosphere was compared to radiosounding observations in Ljubljana, Udine and Zagreb.

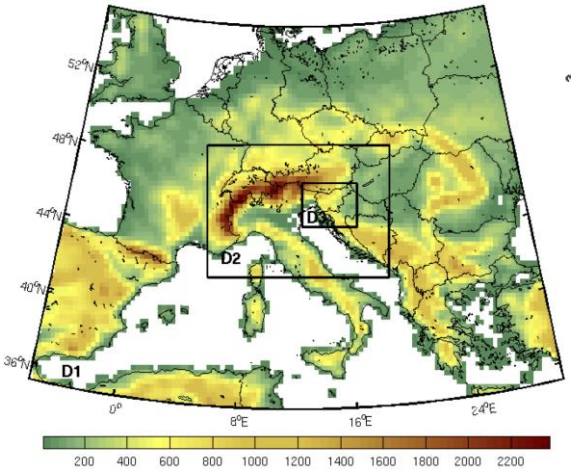

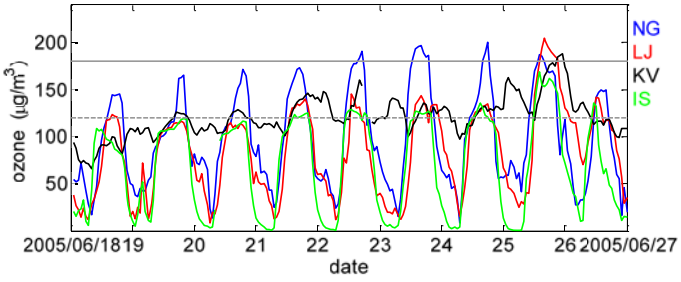

Figure 1. (Above) Measured ozone levels during one of three analyzed episodes at Mediterranean Nova Gorica (NG), elevated Krvavec (KV), rural Iskrba (IS) and urban Ljubljana (LJ) station.

Figure 2. (Left) Configuration of model domains with 27 km (D1), 9 km (D2) and 3 km (D3) resolution. Shown is 27 km orography.

3 RESULTS AND CONCLUSIONS

According to model results all three discussed episodes express a similar temporal evolution, which in general consists of three phases, closely related to the synoptic situation. During the first phase the distinctive air

(re-)circulations, characteristic for the northern Adriatic Sea and its coastal regions (land-sea breezes coupled with thermal mountain winds) enable significant pollutant accumulations in the re-circulating air in the Mediterranean region. Together with favourable meteorological conditions (warm weather, a lot of sunshine and lack of precipitations) this accumulated pollution explains high ozone levels in the south-western Slovenia during the first phase of the episodes, as well as the ozone "jump" at the non-Mediterranean stations during the second phase, when this polluted Mediterranean air is with south-westerly flow advected over Slovenia.

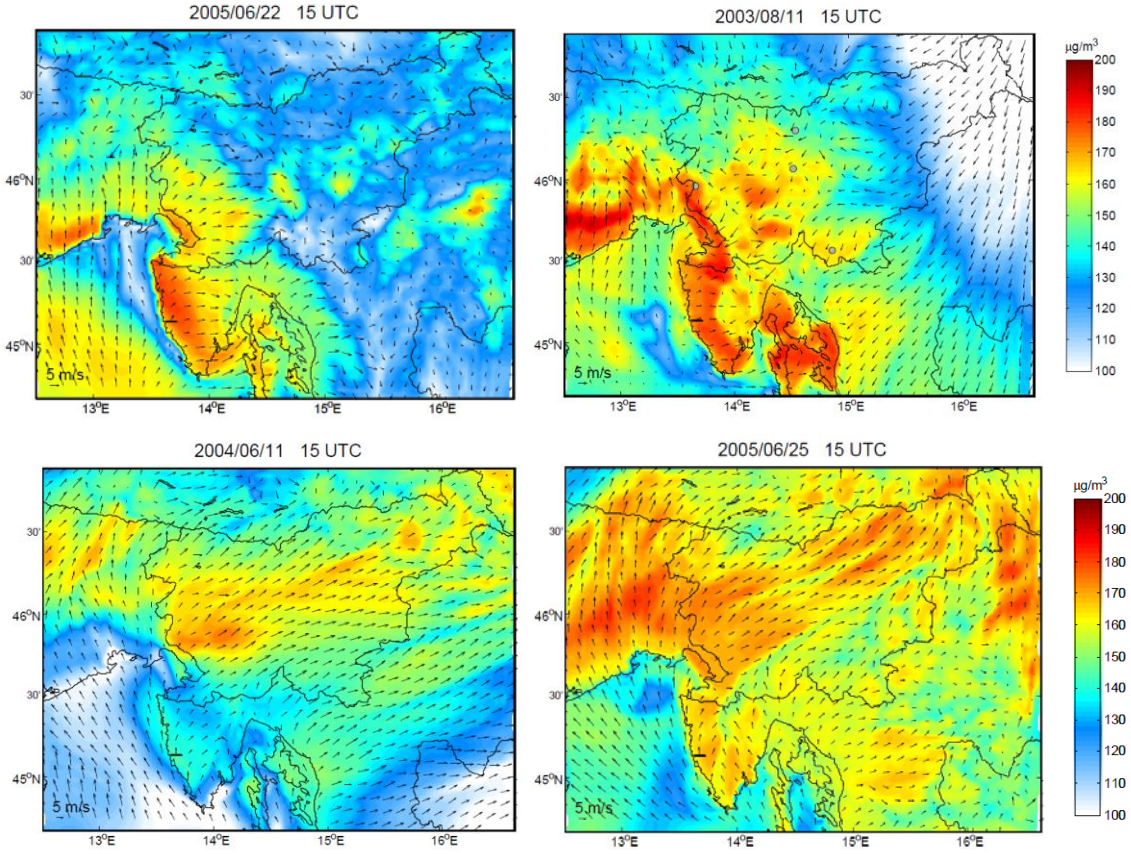

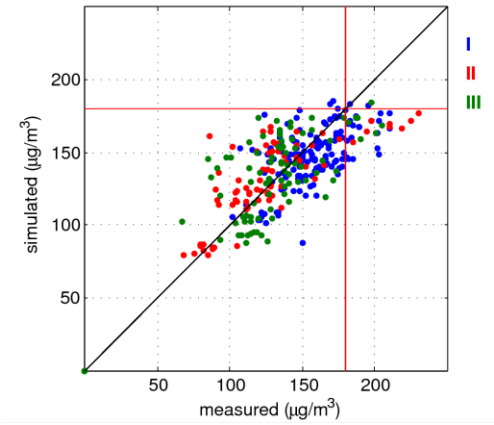

Figure 3. (Above) Examples of simulated near ground ozone and 10 m wind. Upper two panels: during the first phase of the episodes, when near ground ozone levels over coastal areas are significantly higher than over central Slovenia. Lower two panels: during the second phase, when the Mediterranean pollution is with south-westerly flow advected over Slovenia.

Figure 4. (Left) Scatter plot comparing measured and simulated hourly ozone levels for 12 Slovenian stations during three analyzed episodes. Red lines indicate 1-hourl warning threshold value 180 µg/m^3.

With the model we were able to represent the principal characteristics of the episode evolutions, while the accurate representation of location, duration and extension of the highest ozone levels was usually not feasible. The selection of some model parameterization schemes (especially PBL scheme and land surface model) played a significant role in simulated planetary boundary layer meteorological conditions and consequently influenced simulated ozone levels.

REFERENCES

Žabkar R., J. Rakovec, S. Gaberšek, 2008: A trajectory analysis of summertime ozone pollution in Slovenia. *Geofizika*. Volume **25**, 179–202.

HEAT WAVES IN THE ROMANIAN CARPATHIANS DURING THE COLD SEASON

Dana M. Micu [1], Sorin Cheval [2], Mădălina Baciu [2]

[1] Institute of Geography, Romanian Academy, Bucharest, Romania
E-mail: *d_a_n_a_art@yahoo.com*
[2] National Meteorological Administration, Bucharest, Romania

Abstract: Heat waves are a representative index frequently used to analyse the incidence of extreme temperature in a given area. A study was undertaken on the frequency and duration of such phenomena in the Romanian Carpathians during the cold season (September 30-May 31). The STARDEX heat wave definition used reads that: there should be at least five consecutive days with daily maximum temperature deviations higher than 5°C from the multiannual average of the day taken into consideration. Investigations had in view the mountain weather stations located >1,000 m above sea level (27 locations) over the 1961-2007 period. Regional patterns of heat waves were expressed by comparing their severity in terms of persistence for the weather stations located both in the alpine, sub-alpine and forest vegetation belts. The results indicated significant increasing frequency trends of heat wave duration associated to the high temperature anomalies recorded during the cold season, especially in the last quarter of the 20th century and after 2000. Low altitude mountain sites are generally most affected by heat wave occurrence.

Keywords: *heat waves, maximum temperature, Romanian Carpathians*

1 INTRODUCTION

The climate warming process affects the Romanian Carpathians by increased climate variability and extreme events. Even small changes in the means and variations of the key climate variables (temperature and precipitation) might be considered as signals of this process in areas less exposed to a significant temperature increase at high altitude.

Previous studies, focused on the temperature regime and extremes in the Romanian Carpathians at over 1,000 m altitude (Baciu et al., 2004; Cheval et al., 2004; Micu and Micu, 2006 etc.), indicated that highest values were recorded in summer months, while winter and spring warming comes second in terms of statistical significance. In this context, the present study focuses on the temporal and spatial distribution of heat waves during the extended cold season in the Romanian Carpathians. According to the study, the extended cold season is considered to last from September 30 to May 31. Investigations looked at the links between heat wave frequency and duration on the one hand, and the local geographical setting and the atmospheric circulation patterns, on the other.

2 DATA AND METHODS

The study was conducted based on two heat wave indicators defined by the STARDEX project (heat wave duration index and the 90th percentile of heat wave duration). Daily maximum temperature data from 27 weather stations covering the entire Carpathian range and some intra-Carpathian depression areas were analysed in this study over the 1961-2007 period (Fig. 1). The Mann-Kendall and Pettitt statistical tests were applied in order to estimate the trends and detect the shifting years in the cold season time series. The selection of the significance of the corresponding trends and threshold years consider the ≥95% significance level threshold.

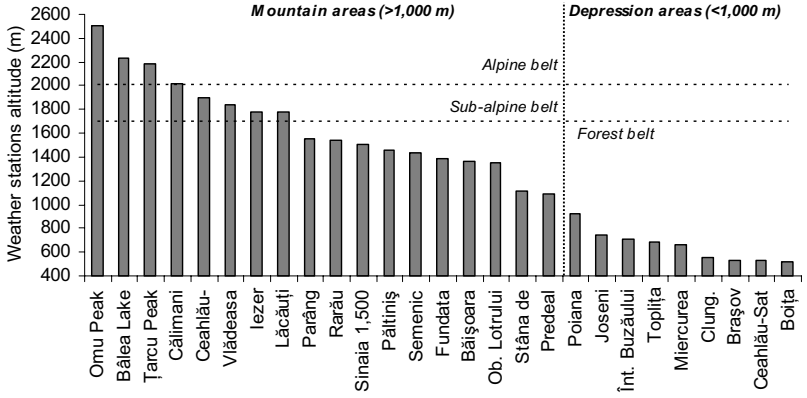

Fig 1. Altitudinal distribution of the 27 weather stations in the Romanian Carpathians, located both in mountain and depression areas.

3 RESULTS

The variability of maximum temperatures in the Romanian Carpathians highlights the heterogeneous character of mountain climate patterns. It is obvious that altitude and the general atmospheric circulation play a very important role in the distribution of temperature values shaping cold season characteristics.

Generally, the Eastern Carpathians show the lowest frequency of heat waves, mainly in the northern part and on their eastern slopes, due to exposure to the circulation of Arctic air masses from the North-Eastern and Northern sectors, causing severe winters and early and prolonged air freeze intervals. It was noticed that heat waves usually cumulated less than 10 days over the entire cold season (47-85% frequency), while durations of 11-20 days count for 9 to 29% over the analysed period. According to statistical tests returns and to these atmospheric circulation patterns, most of the weather stations located in this Carpathian branch showed no significant trends in the variability of heat wave duration over the 1961-2007 period.

The Southern Carpathians and Curvature Carpathians, as well as the Banat Mountains (part of the Western Carpathians) on their western, south-western and southern slopes, are as a rule very much exposed to heat wave duration due to the warm Mediteraneean air mass circulation associated with cyclonic activity. It is worth noting that heat waves in these locations cumulate less than 10 days/season (55-65% frequency) or 11-20 days/season (24-30%).

In terms of the multiannual mean duration of such phenomena the values between the three branches are comparable (Fig. 2).

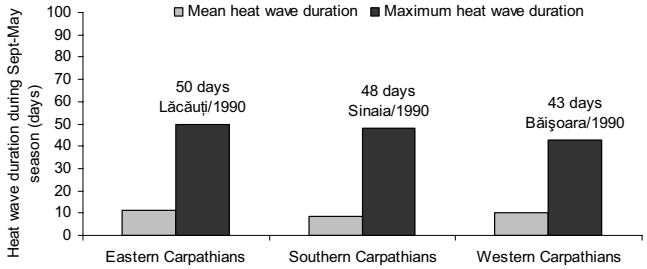

Fig 2. Mean and maximum heat wave durations in the three Romanian Carpathians branches during the cold season.

The data of many forest belt locations in the Western Carpathians (Semenic, Stâna de Vale and Băişoara stations) and in the Southern Carpathians (Parâng, Sinaia 1,500 m and Păltiniş stations) also revealed a higher sensitivity to the climate warming process over the September-May interval. Less visible/or absent even, such influences appeared particularly in the alpine sites, especially those situated above 2,200 m (except for Bâlea Lake where heat waves duration showed increases mostly visible after 2000).

As several climatological studies have already suggested, the Romanian Carpathians recorded higher heat waves frequency during the cold season in most of the studied locations, especially in the last quarter of the 20th century. This finding is also indicated by the Pettitt statistical test to the effect that higher frequency of the shifting years in the heat wave duration occurred during the cold season, after 1990 (66%), than before 1990 (34%).

A low frequency of significant heat waves durations was determined over the late 1960s and the early and mid 1970s, with 11 to 20 days/season at most of the weather stations (especially in the Eastern Carpathians). A better-defined interval of climate warming was delimited starting with 1990 (a record year in terms of maximum heat wave duration in the Romanian Carpathians) particularly since 2000, when most locations (especially the forest belt ones) registered heat waves of 11 to 30 days/season, due to noticeable increase trends of maximum temperature values for most of the mountain areas.

4 CONCLUSIONS

The study has shown that the winter maximum temperature regime of the Romanian Carpathians is clearly influenced by the climate warming process. There is an evident spatial simultaneity in heat waves occurrence especially during the warmest years (e.g. 1990, 2002, 2007). These findings are particularly relevant for forest belt weather stations (located below 1,700-1,600 m), while alpine and sub-alpine sites still maintain their severe winter characteristics. Altitude and the general atmospheric circulation play a very important role in the distribution of temperature values shaping cold season characteristics.

REFERENCES

Baciu, M., Busuioc, A., Breza, T., 2004: Spatial and temporal variability of meteorological phenomena frequency in the cold season, Romanian Journal of Meteorology, **6** (12), 27–39.

Cheval, S., Baciu, M, Breza, T., 2004: The variability of climatic extremes in the Romanian Carpathians, Annals of Western University of Timisoara, Geography series, **XIV**, 59–78.

Micu, D., Micu, M., 2006: Winter temperature trends in the Romanian Carpathians – a climate variability index, Annals of Western University of Timisoara, Geography series, XVI, 141–158.

CASE STUDY OF BURA OF 1ST AND 3RD FEBRUARY 2007

Martina Tudor[1]

[1] Croatian Meteorological and Hydrological Service, Zagreb, Croatia
E-mail: *tudor@cirus.dhz.hr*

Abstract: Two cases when the operational forecast seriously underestimated the wind speed maxima are analysed. The first one in the night between 1st and 2nd February 2007 and the second one in the evening of 3rd February 2007.

Keywords: *bura,*

1 INTRODUCTION

The operational forecast is performed using hydrostatic Aladin model with 8 km horizontal resolution on 37 vertical levels using digital filter initialization (DFI, no data assimilation), semi-Lagrangian horizontal diffusion (SLHD) and prognostic TKE scheme. That forecast is operationally further dynamically downscaled to 2 km horizontal resolution using the procedure described in Ivatek-Šahdan and Tudor (2004).

2 DATA AND METHODS

2.1 General situation

On 1st February 2007, the NW jet-stream moved SW across Croatia. Its edge reached the eastern Adriatic coastline around 12 UTC. Then the direction of the jet stream changes, from NW to NE as the jet strengthens and moves SE along the coast. On 3rd February, at 9 UTC another NW jet-stream reaches Croatia, strengthens and changes the wind direction from NW to NE as it reaches further SE by the evening of the same day. The high level wind is first perpendicular to the Dinaric Alps, but later in the 2nd episode it is parallel to the mountains on eastern Adriatic coast.

2.2 Observed weather

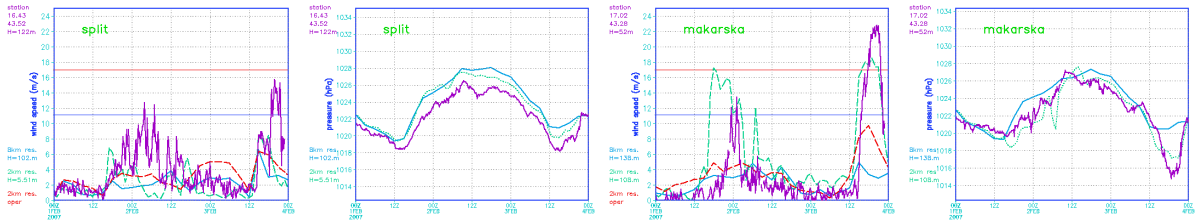

Figure 1. Forecast in 8 km resolution (blue line), 2 km dynamical adaptation (red dashed) and 2 km resolution full run (green dashed) and 10 minute measurements (purple) of 10 m wind and pressure reduced to mean sea level for Split (left) and Makarska (right) locations. The longitude and latitude of the measuring station locations as well as height are also shown.

During the evening and night on 1st and 2nd February 2007, measured 10 m wind speed significantly exceeded the forecast one (Figure 1). Average 10 minute wind speed significantly changed from one interval to the next one. Vertical sounding data (Figure 2) show two temperature inversions, at 850 and at 700 hPa, but the upper one is barely noticeable in the Zadar sounding. The second bura episode, in the evening of 3rd February 2007 was characterized by much stronger and more steady 10 m wind. There were also two temperature inversion layers, one at 900 and 700 hPa.

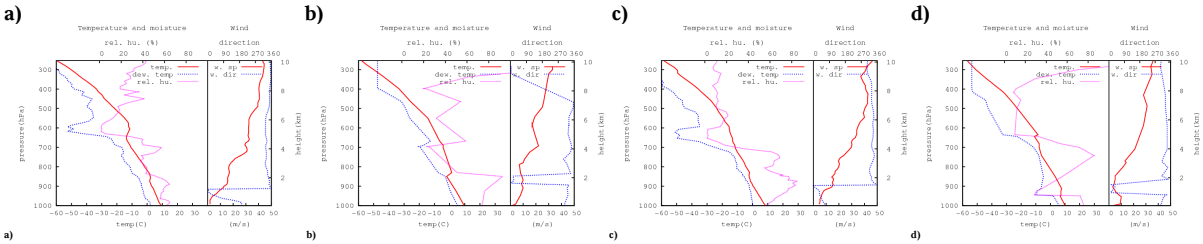

Figure 2. Measured vertical profiles of temperature and wind for Zagreb (a and c) and Zadar (b and d) locations for 12 UTC on 1st (a and b) and 3rd (c and d) February 2007.

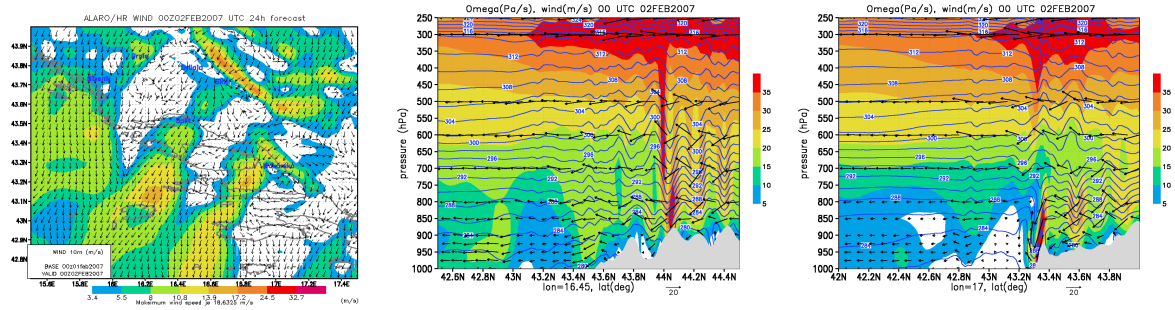

Figure 3. Forecast of wind 10 m above ground (left) and meridional vertical cross-sections through Split (center) and Makarska (right) for 00 UTC 2nd February 2007. Vertical cross-sections show potential temperature in blue lines and arrows show the direction of vertical velocity component.

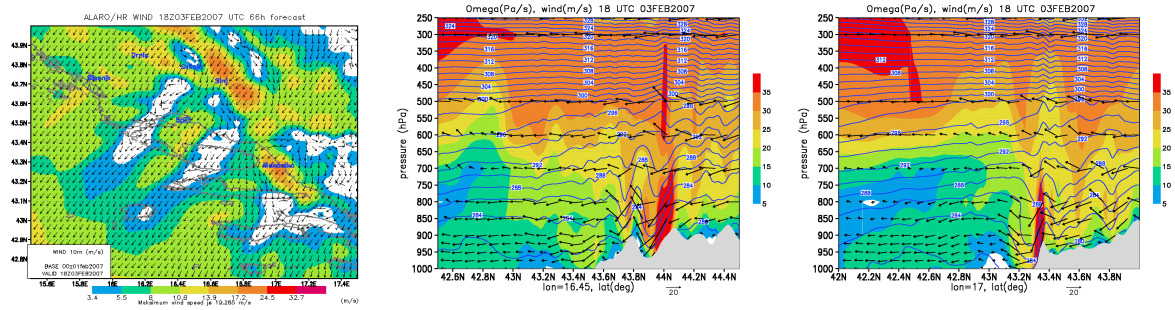

Figure 4. As Figure 3 for 18 UTC 3rd February 2007.

3 MODEL SETUP

The full 2 km resolution forecast alone instead of the operational dynamical adaptation did not improve the forecast, but the full forecast run was used to test the impact of other processes in the model. The possibility that the digital filter initialization (DFI) removed part of the energy of the high-frequency waves from the initial conditions was explored, but the run without DFI did not improve the simulated wind field. There are two horizontal diffusion schemes used simultaneously in the operational model. One is the "standard" 4th order numerical diffusion (ND), and the other is the semi-lagrangian horizontal diffusion (SLHD) scheme. When the intensity of the ND was reduced by a factor of 100, high amplitude waves developed which were responsible for development of the windstorm. Unfortunately not on all locations that were hit by this bura episode.

The first bura episode is characterized by a stable layer above mountains below 700 hPa and less stable layer above (Figure 3) while in the second one the layer up to 500 hPa was far less stable than the one above (Figure 4). In both cases, the high amplitude wave developed on the lee side of Biokovo mountain (right panel of Figures 3 and 4) as well as Dinara mountain upstream of Split (center panel of Figures 3 and 4) but the windstorm is too weak in the Split area (for lat=43.5 in the center panel of Figures 3 and 4).

4 CONCLUSIONS

Usage of non-hydrostatic (NH) dynamics did not improve the 10m wind forecast but it had a positive impact higher in the atmosphere, where usage of SLHD and NH dynamics reduces the TKE as well as values of extreme PV suggesting that removal of those two mechanisms forces other, like vertical turbulent diffusion, to compensate.

Acknowledgements: *The author wishes to thank Ivana Stiperski for advice, literature and for being the patient listener.*

REFERENCES

Ivatek-Šahdan, S. and M. Tudor, 2004: Use of High-Resolution Dynamical Adaptation in Operational Suite and Research Impact Studies. Meteorologische Zeitschrift, 13, No. 2, 1-10

THE COMPLEX BORA FLOW IN THE LEE OF SOUTHERN VELEBIT

Ivana Stiperski[1], Branka Ivančan-Picek[1], Vanda Grubišić[2]

[1] Meteorological and Hydrological Service, Zagreb, Croatia
E-mail: *stiperski@cirus.dhz.hr*
[2] University of Vienna, Vienna, Austria

Abstract: The complex flow structure in the lee of the Southern Velebit is investigated by means of very high-resolution numerical simulations carried out with the NRL COAMPS model. The focus is placed on a wintertime severe bora episode. The spatially complex and temporally highly variable 3D flow structure is characterized by a hydraulic jump over the lee slope and a pronounced wake over the Zadar area. The wake structure appears very sensitive to the upstream flow evolution and is highly non-stationary. The reversed flow along the wake centerline as well as flow separation and rotor formation are observed during different stages of the bora evolution. Sensitivity experiments show the height of Velebit exerting a strong influence on the flow structure, including the onset and strength of the bora flow and the structure of the wake. The terrain of the Zadar peninsula, although significantly lower than that of Velebit, is shown to influence the characteristics of the fully developed bora flow.

Keywords: *bora, critical level, orography, rotors, upstream conditions, wake*

1 INTRODUCTION

The strong bora winds are a common occurrence along the eastern mountainous Adriatic coast, especially in wintertime. The most severe Bora is found in the foothills of Southern Velebit, characterized by significant horizontal and vertical wind speed variability over a relatively small area (e.g. Grubišić, 2004; Belušić and Klaić, 2006). The highest bora windspeed ever recorded in Croatia (69 m/s) was measured in the lee of the southern tip of Velebit. Located only a short distance away, in the lee of one of the highest Velebit peaks (1757m), the area of the city of Zadar (ZD) (Fig. 1) is characterized climatologically by winds considerably weaker compared to its surroundings. In this study we investigate small-scale characteristics and spatial variability of the severe Bora flow in the wider Zadar area with the aim of identifying reason for the "Zadar calm". A severe bora event of 20 December 2004 is examined during which a sodar system was operated at the Zadar Zemunik (ZZ) airport.

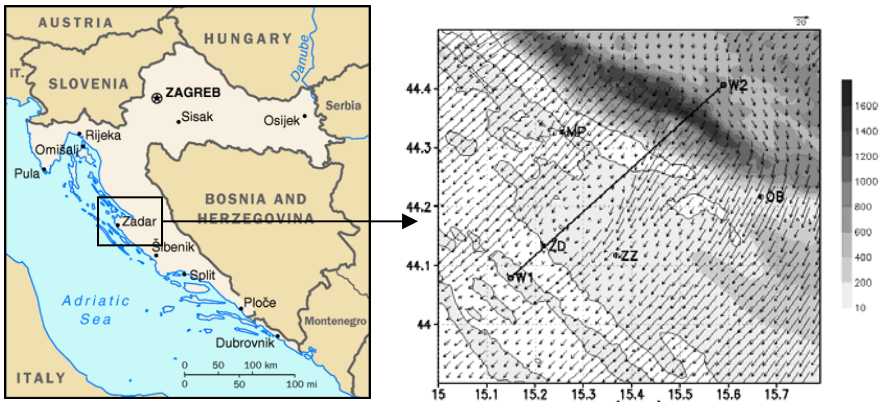

Figure1. Location of Southern Velebit with broader Zadar area (left) and the innermost model domain (right). Letter codes in the right panel indicate stations Zadar (ZD), Zadar airport (ZZ), Obrovac (OB), and Pag Bridge (MB). W1-W2 marks the baseline of the vertical cross section through the wake.

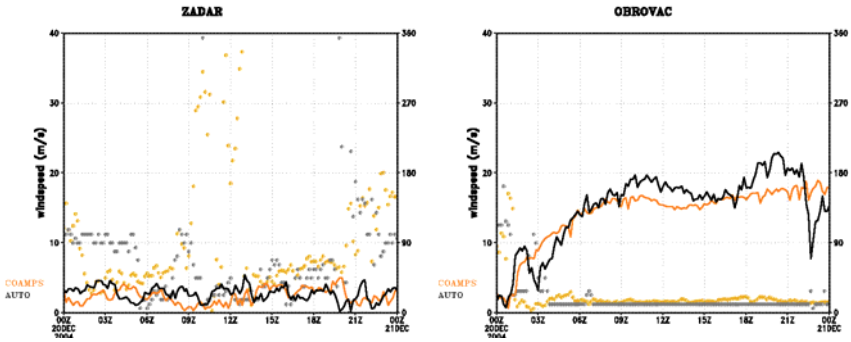

Figure 2. Time series of the measured (grey) and modeled (orange) 10-minute wind speed (solid) and wind direction (dotted line) at Zadar (ZD) and Obrovac (OB).

2 BORA OBSERVATIONS AND MODEL SETUP

The examined bora event developed under the influence of a lee cyclone in the Gulf of Genoa and a high-pressure system over central Europe. The upstream flow impinging on the Velebit was characterized by a synoptically induced critical level at 3.2 km and several inversions with the bases at 0.6, 1.3 and 2.3 km. The bora flow showed significant spatio-temporal variability as seen by comparing the winds measured at the automatic weather stations Pag Bridge and Obrovac with those at Zadar, where the wind was distinctly weaker (Fig. 2). The simultaneous sodar measurements at ZZ reveal a weak low-level flow and the maximum bora speeds above 300 m MSL (Ivančan-Picek et al. 2007). The analysis of the

spatial and temporal bora flow variability was facilitated by real-data three-dimensional numerical simulations, carried out with the nonhydrostatic NRL's COAMPS model with 6 nested domains. The horizontal resolution in the innermost domain was 333 m. In addition to the baseline run, two sensitivity experiments were conducted, one with the reduced Velebit height (rhV), and the other in which the topography of the Zadar peninsula was removed (nZ).

3 RESULTS

The numerical results shown in Fig. 3 show a hydraulic jump over the steep lee slopes of the Velebit, followed further downstream by a pronounced wake over the city of Zadar and beyond. The wake is spatially and temporally highly variable (Gohm et al. 2008). It is especially well developed in the initial stages of the bora development (Fig. 3 left and center), when a reversed flow is present along the wake centerline (Schär and Smith 1993). The reversed flow at the ground is also present towards the end of the examined period (from 21-23 UTC; Fig. 4), with trapped lee waves and weak and shallow lee-wave rotors over the Zadar peninsula (Hertenstein and Kuettner 2003), suggesting a possibility of the lee wave resonance (Grubišić and Stiperski 2009). The reduction of the Velebit height leads to the disappearance of the wake; instead the high-speed flow at low levels extends far downstream (Fig. 3 right). The removal of the Zadar peninsula affects most strongly the flow separation and the rotor zone (Fig. 4 right), with the reversed flow that is both stronger (> -5ms^{-1}) and higher reaching.

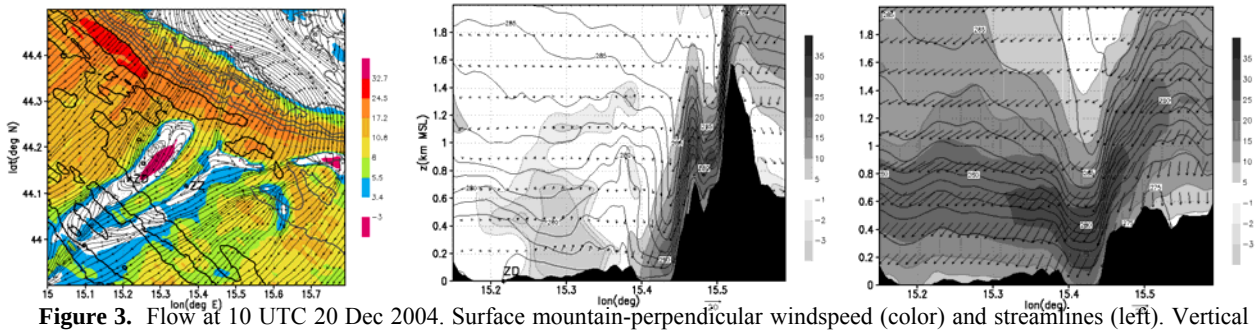

Figure 3. Flow at 10 UTC 20 Dec 2004. Surface mountain-perpendicular windspeed (color) and streamlines (left). Vertical cross-sections of mountain-perpendicular windspeed (gray shade), potential temperature (lines) and horizontal wind direction (arrows) along W1-W2 for the baseline run (center) and the rhV run (right).

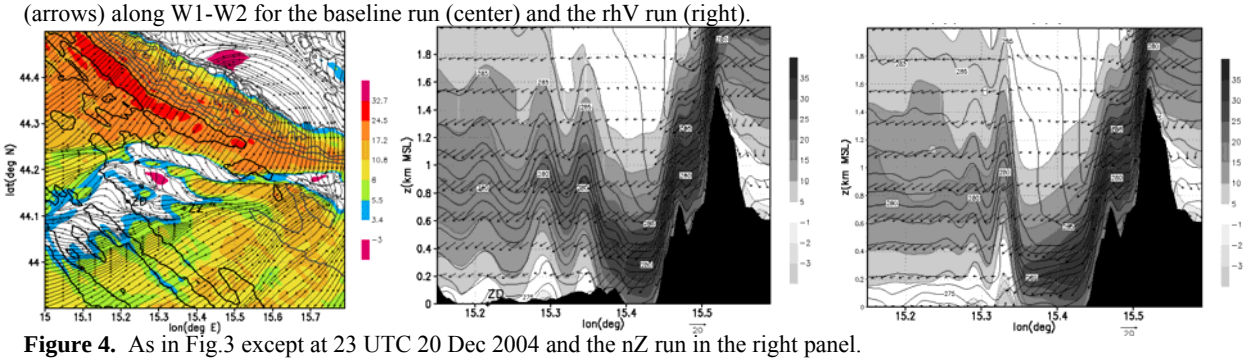

Figure 4. As in Fig.3 except at 23 UTC 20 Dec 2004 and the nZ run in the right panel.

4 CONCLUSIONS

The new observations and numerical simulations of the flow in the lee of Southern Velebit provide an insight into the nature of the "Zadar calm", which lies within the wake of the highest terrain. The wake is strongly influenced by the upstream flow evolution and shows high spatio-temporal variability. Both the terrain of the Southern Velebit and the low-elevation Zadar peninsula were found to exert a strong control of the wake flow.

REFERENCES

Belušić, D., Z. B. Klaić 2006: Mesoscale dynamics, structure and predictability of a severe Adriatic bora case. *Meteorol. Z.*, **15**, 157–168.

Gohm, A., G. J. Mayr, A. Fix, and A. Giez, 2008: On the onset of bora and formation of rotors and jumps near a mountain gap. *Quart. J. Roy. Meteor. Soc.*,**134**, 21-46.

Grubišić, V., 2004: Bora-driven potential vorticity banners over the Adriatic. *Quart. J. Roy. Meteor.Soc.,* **130**, 2571-2603.

Grubišić, V., and I. Stiperski, 2009: Lee wave resonances over double bell-shaped obstacles. *J. Atmos. Sci.,* In press.

Hertenstein, R.F., and J.P. Kuettner, 2003: Rotor types associated with steep lee topography: influence of the wind profile. *Tellus*, **57**, 117-135.

Schär, C., and R.B. Smith, 1993: Shallow-water flow past isolated topography. Part I: vorticity production and wake formation. J. Atmos. Sci. **50**, 1373-1400.

Ivančan-Picek , B., V. Grubišić, I. Stiperski, M. Xiao, and A. Bajić, 2007: "Zadar calm" during severe bora. *Proc. 29th Intern. Conf. on Alpine Meteorology*, Chambery, France, 261–264.

OROGRAPHIC ENHANCEMENT OF SEVERE WINDSTORMS IN THE AUSTRIAN ALPS: TWO CASE STUDIES

Florian Pfurtscheller[1], Alexander Gohm[1]

[1] Institute of Meteorology and Geophysics, University of Innsbruck, Innsbruck, Austria
E-mail: *Florian.Pfurtscheller@student.uibk.ac.at*

Abstract: This study investigates two different types of windstorms that occurred in winter 2008. The analysis is based on observations from an operational network of automatic weather stations and high-resolution numerical simulations with the mesoscale model RAMS. The study shows the similarities and differences between the two windstorms regarding the wind speeds on the northern and southern side of the Alps and demonstrates the ability of RAMS to simulate the storms in a regional scale.

***K*eywords:** *winterstorms, RAMS, north foehn*

1 INTRODUCTION

Mid-latitude windstorms in wintertime, associated with intense cyclones and jet streams, are among the natural hazards that cause the greatest damage to vegetation, infrastructure, and human life. For example, the windstorm Kyrill that occurred in January 2007 was responsible for 49 fatalities and insured losses over 2.4 billion of US dollars in central and northern Europe (Munich Re Group, 2008). Over flat terrain such storms often cover large areas influencing many countries. In complex terrain such as the Alps the wind field is modified by the orography and the severity of the associated winds decreases or even enhances depending on the location. Our goal is to analyze two windstorms, which occured in the winter 2008, to investigate the performance of a mesoscale numerical model to simulate the intensity and pattern of the wind field in regional and local scale.

2 DATA AND MODEL

The data consists of measurements from automatic weather stations (AWS) of the Austrian national weather service ZAMG and several avalanche warning services, as well as from SYNOP-stations. The numerical model used for the analysis is the Regional Atmospheric Modeling System RAMS (Cotton et al., 2003). The model domain consists of three nested grids with horizontal grid spacing of 32, 8 and 2 km. The outermost grid covers whole Europe while the innermost grid covers the area of the Eastern Alps including Austria (Fig. 1). Sensitivity simulations were conducted with an additional fourth grid with horizontal grid spacing of 0.7 km (see black boxes in Fig. 1a–b)

3 RESULTS

Our first case, the windstorm Paula, occurred between 18 UTC 26 January and 06 UTC 28 January 2008 and was associated with a jet stream that caused northerly winds over eastern Europe. The eastern parts of the

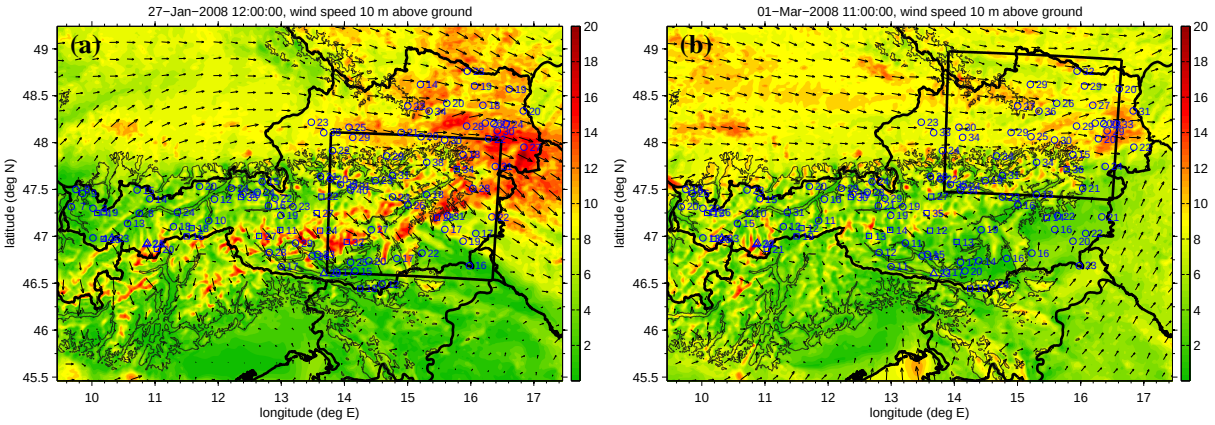

Figure 1: RAMS simulated wind speeds (m s^{-1}) and wind vectors of model domain three at 10 m above ground at (a) 12 UTC 27 January 2008 with observed maximum wind gusts on 27 January 2008 and at (b) 11 UTC 01 March 2008 with observed maximum wind gusts on 01 March 2008

Austrian Alps were most affected by the windstorm. Sustained wind speeds at mountain stations typically exceeded 30 m s^{-1}, with gusts up to 64 m s^{-1}. In valleys and over flat areas sustained winds typically exceeded 20 m s^{-1}. The simulation and observations (Fig. 1a) of the first case show that the highest wind speeds were caused by flow channelling in the Danube River Valley (northwestern Austria), by a corner jet at the eastern edge of the Alps and by north foehn in the valleys on the southern side of the Alps. Stations affected by the north foehn measured exceptionally high wind gusts of up to 40 m s^{-1} in the valleys between eastern Tirol and Burgenland (12-17°E). The time series of Graz (Fig. 2) shows that the RAMS simulation with four grids is able to capture the breakthrough of the north foehn. However, both simulations have problems to reproduce the low-level cooling during the calm conditions in the night before, which is associated with a very strong, only 400 m thick, surface inversion. The radiosonde of Graz at 03 UTC (not shown) reveals a strength of this inversion of more than 12°C . With the turbulence parameterization of Deardorff (Deardorff, 1980) the wind speeds in the four-grid simulation better agree with the observed gusts, while the surface winds in the simulation with three grids and with the turbulence parameterization of Mellor-Yamada (Mellor and Yamada, 1982) are closer to the observed sustained wind speeds. The second case occurred between 00 UTC 01 March and 06 UTC 03 March 2008. It can be separated into two windstorm events: Emma and Fee. Our focus is on Emma, and in contrast to Paula, this storm affected greater parts of central and northwestern Europe. The synoptic scale flow was from northwesterly directions. Fig. 1b shows that in contrast to Paula the strongest winds exceeding 30 m s^{-1} occurred north of the Alps. The highest wind speeds were also caused by flow channelling in the Danube River Valley and a corner jet at the eastern edge of the Alps, while the southern side was partly sheltered by the Alpine barrier. With the approach of an intense cold front and thunderstorms, winds on the northern side of the Alps increased. With the passage of front north foehn was reported in some valleys on the southern side of the Alps.

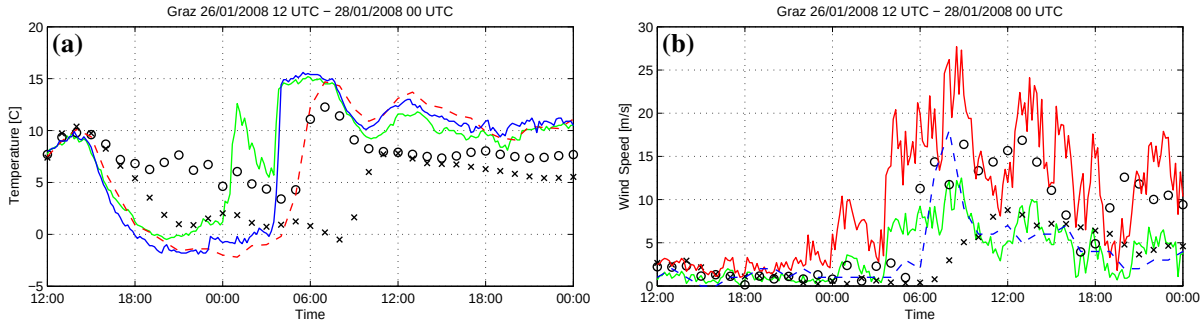

Figure 2: (a) Time series of temperature of two AWS at the town of Graz (solid green and blue line) and of the SYNOP-station at the airport of Graz (dashed) compared with the three-grid simulation (crosses) and four-grid simulation (circles). (b) Time series of wind speed (green) and gusts (red) at the 'green' AWS shown in (a) and the wind speed at the airport of Graz (dashed) compared with the wind speeds of the three-grid simulation (crosses) and four-grid simulation (circles), respectively.

4 CONCLUSIONS

The RAMS simulations are able to capture the wind speeds at a regional scale, but have problems in a local scale. Both events are characterized by wind modification and enhancement by flow channeling in the Danube River Valley and by a corner jet at the eastern edge of the Alps. In contrast to the first case Paula, Emma did not cause severe winds and gusts at the mountains and in the valleys on the southside of the Alps.

Acknowledgements: *We thank Manuela Lehner for her support in conducting the simulations and the ZAMG and several Austrian avalanche warning services for providing the observations.*

REFERENCES

Cotton, W.R., R.A. Pielke, R.L. Walko, G.E. Liston, C.J. Tremback, H. Jiang, R.L. McAnelly, J.Y. Harrington, M.E. Nicholls, G.G. Carrio, and J.P. McFadden, 2003: RAMS 2001: Current status and future directions. *Meteor. Atmos. Phys.*, **82**, 5–29.

Mellor G.L., T. Yamada, 1982: Development of a turbulence closure model for geophysical fluid problems. *Rev. Geophys. Space Phys.*, **20**, 851–875

Deardorff J.W., 1980: Stratocumulus-capped mixed layers derived from a three-dimensional model. *Bound. Layer Meteor.*, **18**, 495–527

Munich Re Group, 2008: *Highs and lows–Weather risks in central Europe.* Munich Reinsurance Company, Munich, 58 pp. http://www.munichre.com/pulications/302-05482_en.pdf, accessed 08 April 2009

FOEHN DIAGNOSIS AND MODEL VERIFICATION

Klaus Burri[1], Bruno Dürr[2], Thomas Gutermann[3], Christian Häberli[4], Patrick Hächler[4], Alfred Neururer[5], Hans Richner[6], and Richard Werner[7]

[1] Working Group Foehn-Research Rhine Valley/Lake Constance
E-mail: *knburri@swissonline.ch*
[2] Sunergy GmbH, Buchs, Switzerland
[3] formerly MeteoSwiss, Zurich, Switzerland
[4] MeteoSwiss, Zurich, Switzerland
[5] Central Institute for Meteorology and Geodynamics (ZAMG), Regional Office for Tyrol and Vorarlberg, Innsbruck, Austria
[6] Institute for Atmospheric and Climate Science, ETH Zurich, Zurich, Switzerland
[7] Salzachwind GmbH, Dornbirn, Austria

Abstract: The strong foehn case of December 8, 2006 is analysed and used as testbed for the mesoscale model COSMO-2. The investigations are a joint effort of Austrian, German and Swiss researchers and focus on the Rhine Valley and Lake of Constance.

Keywords: *ICAM, foehn, case study, model verification, forecasting, climatology*

1 INTRODUCTION

The "Working Group Foehn-Research Rhine Valley/Lake Constance" (AGF, Arbeitsgemeinschaft Föhnforschung Rheintal/Bodensee) collects and archives meteorological parameters and investigates foehn phenomena in the Rhine Valley since the early 1970's. The main task of the Working Group is to find plausible criteria and methods for a more reliable foehn forecast.

At present, a report is being prepared which studies in detail the foehn case of December 8, 2006. This foehn case produced high wind velocities and was reaching quite far; it was one of the rare cases when foehn was observed north of Lake of Constance.

2 WHAT IS FOEHN?

Despite the fact that even professional meteorologists believe that foehn can be identified unambiguously, there are uncertainties when defining a particular weather pattern as "synoptic foehn situation". Similarly, there are no generally accepted criteria for foehn-typical parameters such as cross-ridge pressure gradient, wind direction and speed, temperature, and humidity that would give a clear YES or NO decision for foehn at a specific location. Because different meteorologists use different definitions, a comparison of foehn statistics is difficult, sometimes impossible.

An objective, computer-based method for determining foehn at a given station has recently been developed. The criteria are based on data supplied by the automatic network Swissmetnet (formerly ANETZ). Threshold values for the various parameters are station-specific; they were determined by using elaborate statistical methods. As a test, the automatic method was compared to the most careful, subjective classifications of the weather situation for the two primary foehn stations Altdorf and Vaduz, this for the period January to November 2008. For Altdorf, the objective method yielded 70, the subjective one 69 foehn incidents, however, they agreed only on 67; hence, objectively there were 3, subjectively 2 additional – but different! – incidents. For Vaduz, the methods agreed on 58 incidents, the objective one produced 3, the subjective one 6 additional unrelated foehn incidents. Details of the objective classification procedure are to be published soon.

3 THE FOEHN CASE OF DECEMBER 8, 2006

Fig. 1 shows the synoptic situation at the surface for December 8, 2006. In the previous week, cold air intrusions between Newfoundland and Greenland caused the formation of troughs over the Atlantic. On their leading edge, large regions of Europe were in a mild southwesterly flow. Repeatedly, there were strong cyclogeneses between Iceland and Great Britain. On December 7, steered by a low over Scotland, cold polar air moved southward. On December 8, the low had moved over the North Sea, and over the Benelux a secondary low formed which must be regarded as the trigger for the strong foehn situation over the Alps. As can be seen in the surface analysis (Fig. 1), the eastward moving, associated cold front was retarded by the formation of a wave. The surface pressure difference between Locarno-Monti and Vaduz increased to 13.3 hPa at 09 UTC, between Bozen and Innsbruck to 8.5 hPa at 12 UTC.

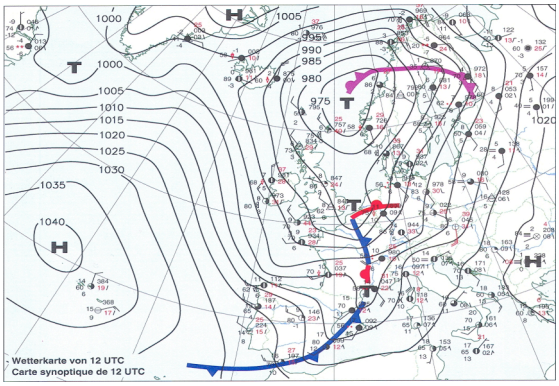

Figure 1. Synoptic surface chart for December 8, 2006. (Provided by MeteoSwiss)

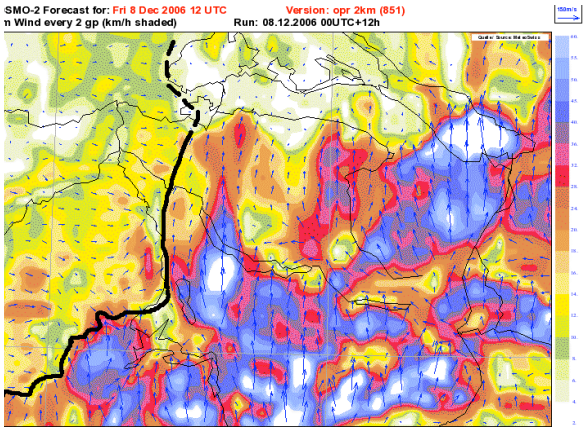

Figure 2. COSMO-2 forecast for the Rhine Valley region.

4 MESOSCALE ANALYSES

A significant event as this foehn case offers a perfect possibility to test forecasting procedures. For 12 UTC of December 8, VERA analyses were produced for the parameters pressure, potential temperature, surface wind direction and speed, and equivalent-potential temperature (VERA: Vienna Enhanced Resolution Analysis). Subsequently, the 12-hour forecast of the COSMO-2 model of MeteoSwiss (Fig. 2) was compared to actual observations at specific stations and to the detailed analysis.

In general, the model produces the main features on the larger scale quite well; fields for pressure, temperature, humidity, and wind do show the major characteristics. Wind speed over the Alpine ridge is reasonable. The (too) high wind speeds east of Lake of Constance are most likely caused by underestimating friction over the smooth water surface, and possibly by the fact that the model assumes a slightly higher temperature of the water. This increases the instability, making it easier for the air mass to penetrate the surface boundary layer.

When it comes to details, several shortcomings of the forecast must be noted: Despite the 2-km resolution, features that are induced by the topography are not represented satisfactorily. In particular, the specific representation of winds in valleys (lack of channelling and too low wind speed, important issues for forecasting a foehn storm) and of the diffluence of the flow at the valley exits (wind speeds over the Lake of Constance are unrealistically high) is inadequate.

Cloudiness and relative humidity fields exhibit the classical pattern for a prefrontal foehn: clouds over the Alpine ridge, frontal cloudiness from the Jura Mountains to the Black Forest. Relative humidity over the Swiss Plateau is – as consequence of the penetrating foehn air – below 50 percent (Fig. 3).

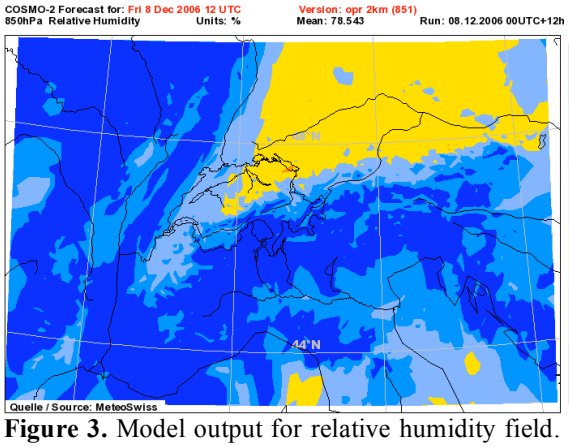

Figure 3. Model output for relative humidity field. Yellow indicates humidity below 50 percent.

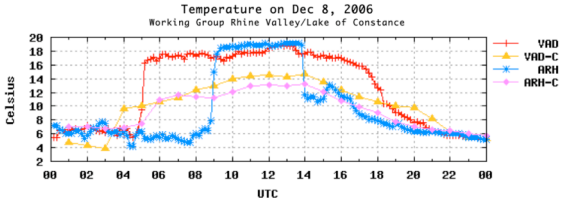

Figure 4. Observed and forecast temperature for Vaduz (VAD) and Altenrhein (ARH). The forecast values are labelled with VAD-C and ARH-C, respectively.

A time series analysis (Fig. 4) shows that the model is not (yet) capable to forecast the onset and breakdown of foehn at a specific location. The change of the air mass, expressed by significant changes in wind, temperature, and humidity is represented unsatisfactorily; the changes occur too early and are much too small.

Acknowledgements:
We thank MeteoSwiss for supplying the data used in our study. In particular, we are indebted to Emanuele Zala (MeteoSwiss) who provided the model data for the comparisons.

LABORATORY EXPERIMENTS ON MOUNTAIN INDUCED ROTORS

Christoph Knigge[1], Dieter Etling[1], Alexandre Paci[2], Olivier Eiff[3]

[1] Institut für Meteorologie und Klimatologie, Leibniz Universität Hannover, Hanover, Germany
[2] Centre National de Recherches Météorologiques Toulouse, Météo-France, Toulouse Cedex, France
[3] Institut de Méchanique des Fluides de Toulouse, Université de Toulouse, Toulouse, France
E-mail: *knigge@muk.uni-hannover.de*

Abstract: We present laboratory experiments on stratified flows over isolated obstacles which were aimed at the simulation of atmospheric rotors. An elevated density inversion above the obstacle height, which seems to favour the development of mountain induces rotors, was introduced compared to the classical tank experiments. In fact our experimental setup was guided by the simulations of Vosper (2004), which provided systematically the upstream conditions under which mountain rotors are expected. We were able to confirm the results from these numerical simulations over a wide range of parameters.

***K*eywords:** *Rotor, inversion, lee wave*

1 INTRODUCTION

The problem of mountain-induced rotors has received considerable interest in recent years, which cumulated in the large international field experiment T-REX (Grubisic et al, 2008). Also several numerical simulations on the formation of rotors have been published recently (e.g. Vosper 2004, Doyle and Durran 2007). Although much insight into the rotor problem has been gathered through these activities, some additional information might be provided by laboratory experiments in stratified towing tanks. This kind of research has been used frequently with respect to the lee wave problem (e.g. Eiff and Bonneton 2000), but not many systematic laboratory experiments on the rotor problem have been performed.

The mayor finding of recent numerical simulations that an elevated inversion above the mountain greatly supports the rotor formation has motivated our experimental work because this kind of stratification profile has not been used very often before.

2 EXPERIMENTAL SET UP

The experiments have been performed in the fluid dynamical facilities of Météo-France/CNRM at Toulouse consisting of two towing tanks. The dimensions of the tanks are: length: 22 m, width: 3 m; height: 1 m (large tank) and 7 m x 0.8 m x 0.7 m (medium tank). In both tanks we used a bell-shaped obstacle of 13 cm respectively 3.5 cm height. The stratification was set up as guided by the simulations of Vosper (2004): A neutral bottom layer below a density jump $\Delta\rho$ at the height z_i (inversionheigth) followed by a linear density profile above ($N > 0$). In practice, inversion height and density jump were not as sharp as in the principle schematic. The simulations by Vosper have shown, that rotor formation depends on the non dimensional mountain height H/z_i and the inversion Froude number F_i defined as:

$$F_i = \frac{U}{\sqrt{g\frac{\Delta\rho}{\rho_0}z_i}} \,. \tag{1}$$

The experiments were run for different combinations of F_i and H/z_i by varying the towing speed U, the inversion height z_i and the density jump $\Delta\rho$.

The documentation of the experiments was performed by different cameras making photos and videos of the flow field. The velocity fields within lee waves and rotors were obtained by a PIV method. To get a quantitative impression of the flow, streak line photos were made. Due to the differences in the used laser systems (continuous laser in the large tank and pulsed laser in the medium tank), streakline photos could only be made in the large tank.

3 RESULTS

53 experiments in the medium tank and 26 experiments in the large tank have been performed for various combinations of the inversion Froude number F_i and the non-dimensional obstacle height H/z_i. The former were mainly used for checking the parameters under which rotors can be observed in the laboratory experiments and also helped us in preparing the experiments in the large tank, which were more complex to set up.

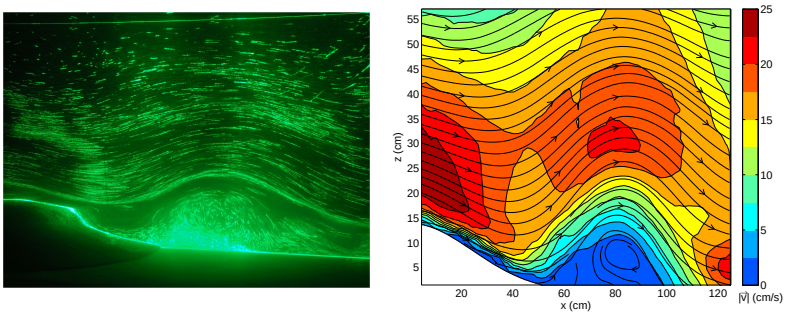

Figure 1: Observations of a Rotor case for $H/z_i = 1.1$ and $F_i = 0.90$ showing part of the lee wave and rotor below the crest. Flow is from left to right. Left: Streak lines; right: Streamlines and velocity field.

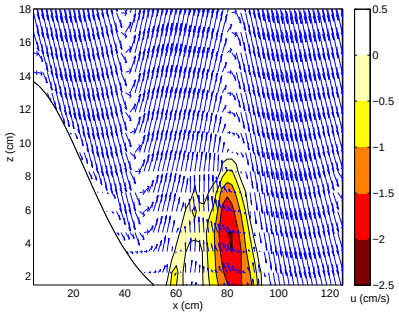

Figure 2: Close-up of the velocity field of the rotor case shown in Fig. 1. The area of backward flow towards the obstacle is shaded.

Here we present detailed analyses of the rotors flows only for the large towing tank, where streakline photos could be made. All flow phenomena described in the simulations by Vosper (2004) have been found in the laboratory, which are lee waves, hydraulic jumps and rotors.

We define a rotor as a flow situation where there is a counter-rotating vortex behind the obstacle beneath the first wave crest. In the strict sense there should be also a near surface flow toward the obstacle (full rotor) but a stagnant fluid in this region might be also termed as rotor. Figure 1 shows a rotor case for $F_i = 0.9$ and $H/z_i = 1.1$. A vortex structure under the wave crest can clearly be seen as indicated by somewhat chaotic behaviour of the streak lines (Fig. 1, left). This is also evident in the velocity field as obtained by a PIV (Fig. 1, right). A clear flow towards the obstacle can be observed in the layer close to the surface, which is even more evident in the zoom in Figure 2, where the velocity vectors are shown and only the flow component backwards toward the obstacle is coloured.

All observed flow phenomena are summarised in Fig. 3. Compared to the results obtained by Vosper (solid and dashed lines in Fig. 3) the boundaries of the observed rotor cases do not coincide exactly.

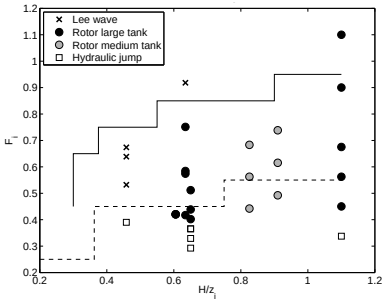

Figure 3: Flow regimes as observed in the experiments as depending on F_i and H/z_i. The flow regimes as obtained in the numerical simulations of Vosper (2004) are also indicated as follows: Solid line separates lee waves from rotors, dashed line separates rotors from hydraulic jumps.

Nevertheless the experiments have captured the main physics of the rotor simulation that an elevated inversion above the mountain top is favourable for rotor formation.

4 CONCLUSIONS

Our experiments guided by recent numerical simulation of Vosper (2004) confirm, that an elevated inversion is supporting the formation of rotors in the lee side of mountains, as was already indicated in numerical simulations mentioned above. A flow regime diagram as in Vosper (2004) is showing the dependence of the observed phenomena (lee wave, rotor and hydraulic jump) of the relevant flow parameters F_i and H/z_i.

Acknowledgements:

The experiments have been performed within the EU framework HYDRALAB III under grant 022441(RII3). We thank B. Beaudoin, J-C. Boulay, J.-C. Canonici, M. Morera, S.-L. Pigat and H. Schaffner of the Météo-France/CNRM fluid mechanics laboratory for their kind support during the experiments.

REFERENCES

Doyle, J.D. and D.D. Durran, 2007: Rotor and sub-rotor dynamics in the lee of three-dimensional terrain. *J.Atmos.Sci.*, **64**, 4202–4221.

Eiff, O. S., F. Huteau, J. Tolu, 2005: High Reynolds-number orographic wave-breaking experiments. *Dyn. Atmos. Oceans*, **40**, 71–89.

Grubisic, V. and coauthors, 2008: The terrain-induced rotor experiment: A field campaign overview including observational highlights. *Bull. Amer. Metor. Soc.*, **89**, 1513–1533.

Vosper, S. B., 2004: Inversion effects on mountain lee waves. *Quart. J. Roy. Meteor. Soc.*, **130**, 1723–1748.

THE CAPE TOBIN JET

Haraldur Ólafsson[1,3,4] , Hálfdán Ágústsson[1,2]
Melvyn A. Shapiro[4,8], Jón Egill Kristjánsson[5], Idar Barstad[6] and Andreas Dörnbrack[7]

[1] Háskóli Íslands (University of Iceland), [2] Reiknistofa í veðurfræði (Institute for Meteorological Research), Iceland, [3]Veðurstofa Íslands (Icelandic Meteorological Office), [4]Geophysical Institute, University of Bergen [5]Institute of Geosciences, University of Oslo, [6]Bjerknes Centre for Climate Research, Bergen, [7]Deutsche Luftfahrts und Raumforschung (DLR), Oberplaffenhofen, Germany, [8]NOAA/CIRES, Boulder, USA
E-mail: *haraldur68@gmail.com*

Abstract: A case of strong northerly winds close to Cape Tobin in E-Greenland is discussed with the help of dropsondes and a numerical simulation. Winds of about 45 m/s are observed at only 900 hPa, in a very stably stratified air mass. The jet extends about 200 km away from the coast of Greenland. When the jet impinges the high topography of E-Greenland, parts of the low-level cold air is lifted and mixed with the warm air above, leading to a "cold föhn" at levels close to 850 hPa on the downstream side.

Keywords: *IPY, THORPEX, GREENEX, Cape Tobin, East-Greenland, low-level jet,*

1 INTRODUCTION

When easterly flow impinges the mountains of Greenland, north of approximately 69°N, strong winds along the E-Greenland coast are generated. These winds blow into the Denmark Strait, north of NW-Iceland and form a jet that we choose to call the Cape Tobin Jet. As a part of the IPY-THORPEX and GREENEX programmes, a case of a Cape Tobin Jet was explored with dropsondes on 9 March 2008. This short paper describes the observations and a few details of the flow as simulated numerically.

2 THE CAPE TOBIN JET

Figure 1 shows the simulated surface winds and two-metre temperatures on 9 March 2008 at 12 UTC. There is strong acceleration at the coast of Greenland and strong flow into the Denmark Strait. The low-level air mass in the jet is very cold, which corresponds with the fact that the area is mostly covered with sea ice. Figure 2 shows the temperature profiles of the northernmost (upstream) and the westernmost (downstream) dropsondes shown in Fig. 1. Upstream, there is a very strong inversion close to 900 hPa, while downstream of the approximately 3000 m high topography, the air mass is close to neutral up to about 800 hPa. The upstream winds below the inversion are about 22 m/s, and the winds are stronger inside the inversion. The 800-850 hPa layer is much colder downstream than upstream. Figure 3 shows that the jet has a maximum of about 45 m/s inside the stable layer at about 900 hPa. The flow has been simulated with the numerical model WRF with boundary conditions from the ECMWF and horizontal resolution of 9 km. Figure 4 shows two cross sections of the simulated flow, one along the flow, across the E-Greenland mountains and one across the jet off the coast of Greenland. The cross section along the flow shows that some of the low-level dense air is lifted across the mountains and ends up in a downslope windstorm. The cross section across the flow shows that the jet is indeed confined to the inversion layer and that it extends about 200 km away from the mountains of E-Greenland. Apart from weak observed winds in the wake of the E-Greenland topography (a wake), the simulation is in quite good agreement with the observations.

3 DISCUSSION AND CONCLUSIONS

Both the observations and the simulations show extreme winds at only about 600 metres above the sea in the Cape Tobin Jet. As these winds appear not to reach down to the surface, they can not be detected with the QuikSCAT technology, and even if they did, such data would probably not be reliable because of extensive sea-ice cover in the region. Indications of very strong winds in this region have however been presented by Moore and Renfrew (2005) and Kolstad (2008). Winds of this kind present a challenge for calculations of turbulent transport of horizontal momentum in numerical models, and they may presumably be brought down to the surface by turbulent mixing, as the air mass flows over open sea and becomes less stable.

The trajectory of the air mass impinging the E-Greenland topography is a little unusual: in most cases, air at low levels does not climb 3000 m high mountains. The kinetic energy of the flow is so great that some of the

low level cold air is able to climb the mountains and mix with warmer air above. Consequently, the downslope flow at levels above the upstream inversion is relatively cold. This could be called a "cold föhn".

Further work with the Cape Tobin Jet will consist of dynamic analysis of the forces at stake, the role of the sea ice and the variability of the jet in past climate and future climate projections. From a forecasting perspective and development of numerical tools, the jet will provide a testbed for vertical mixing of momentum.

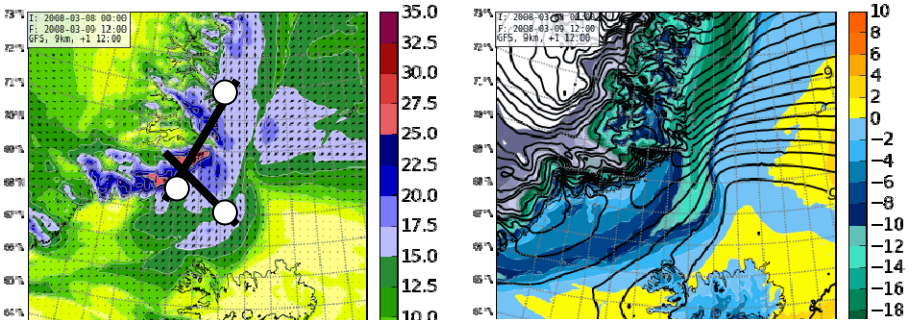

Figure 1. Simulated surface wind speed (left) in m/s and two-metre temperature (right) in °C. The approximate position of the dropsondes in Figs. 2 and 3 and the cross sections in Fig. 4 are shown on the left panel.

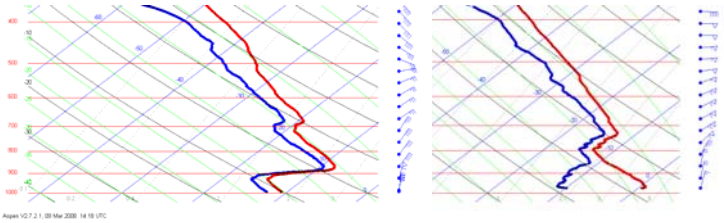

Figure 2. Vertical profiles from dropsondes upstream of the E-Greenland mountains (left) and downstream of the E-Greenland mountains (right)

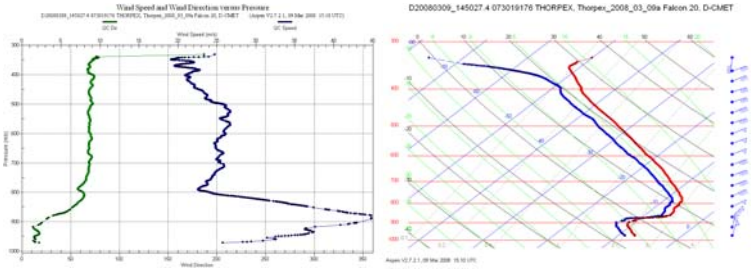

Figure 3. The vertical profile of winds (left), temperature and humidty (right) from the southernmost dropsonde shown in Fig. 1. The peak winds are 45 m/s

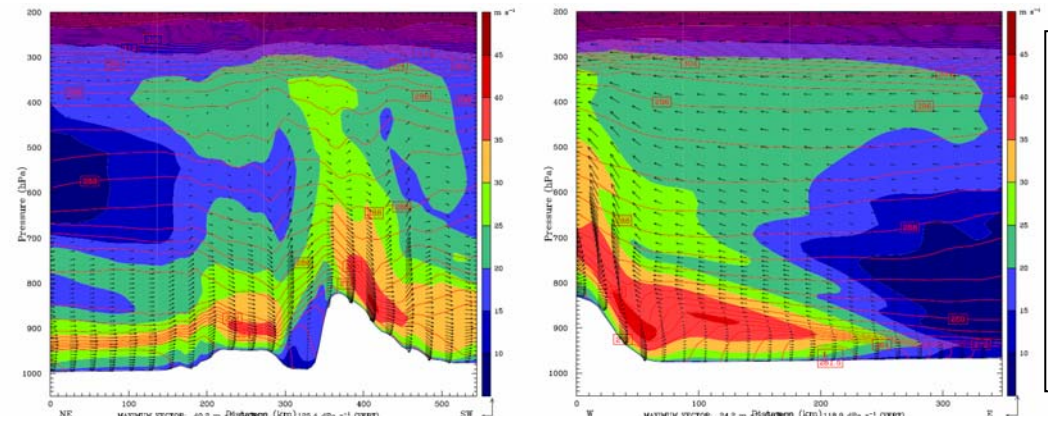

Figure 4. Simulated vertical profiles along the flow from the NE to the SW (left) and across the flow, from the NW to the SE (right), showing wind speed (m/s) and potentital temperature (K). The positions of the sections are shown in Fig. 1.

Acknowledgements:
The observations presented here were provided with support from EUFAR, within the framework of GREENEX and with support from the Norwegian Research Fund (IPY-THORPEX).

REFERENCES

Moore, G. W. K. and I. Renfrew, 2005: Tip jets and barrier winds: A QuikSCAT climatology of high wind speed events around Greenland. *J. Climate*, **18,** 3713–3725

Kolstad, E. W., 2008: A QuikSCAT climatology of ocean surface winds in the Nordic seas: Identification of features and comparison with the NCEP/NCAR reanalysis, *J. Geophys. Res.*, 113, D11106, doi:10.1029/2007JD008918.

SIMULATIONS OF MESOSCALE FLOW OVER AN ARCTIC FJORD

Tiina Kilpeläinen[1,2], Haraldur Ólafsson[2,3]
[1] The University Centre in Svalbard, Norway
E-mail: *tiina.kilpelainen@unis.no*
[2] University of Bergen, Norway
[3] University of Iceland, Iceland

Abstract: **Mesoscale flow over Isfjorden, Svalbard, was simulated applying the Weather Research and Forecasting (WRF) model. The direction of the large scale flow affects local wind-, temperature- and humidity fields as well as the spatial distribution of the turbulent fluxes. Spatial differences are largest when the large scale wind is blowing along the fjord.**

Keywords: *Arctic fjord, mesoscale simulation, topographical effects*

1 INTRODUCTION

Fjords, narrow and deep inlets of the sea, are features of mountainous regions and are distributed at high latitudes in both hemispheres. The local meteorological conditions in fjords are affected by surrounding complex topography, possible sea ice and oceanographic phenomena. The atmospheric boundary layer over fjords is poorly understood and many processes occur on spatial scales that cannot be resolved by climate and weather prediction models. This study addresses the spatial variability of wind, temperature and humidity, and its effect on the turbulent fluxes over an Arctic fjord.

2 SIMULATIONS

The Weather Research and Forecasting (WRF) model, initialized with ECMWF operational analysis data, was used to simulate spatial variability over Isfjorden, Svalbard (Fig. 1). The model system consists of three polar stereographic domains at horizontal resolution of 9 km, 3 km and 1 km. Three real cases, representing different large scale flow directions, were chosen: 19/02/2008 northwesterly wind, 13/02/2008 northeasterly wind and 26/02/2009 southeasterly wind. Isfjorden was ice-free apart from the innermost parts of the fjord, and the sea surface temperature in the ice-free area was set to constant. Simulated temperature and wind speed show fairly good agreement with weather mast measurements performed on the southern coast of Isfjorden.

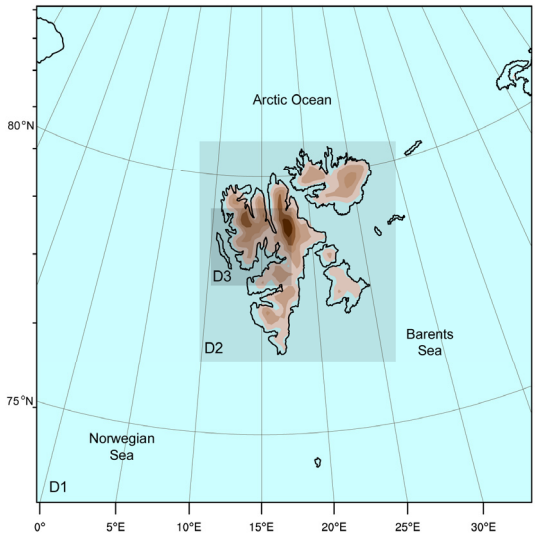

Figure 1. The three domains used in WRF model.

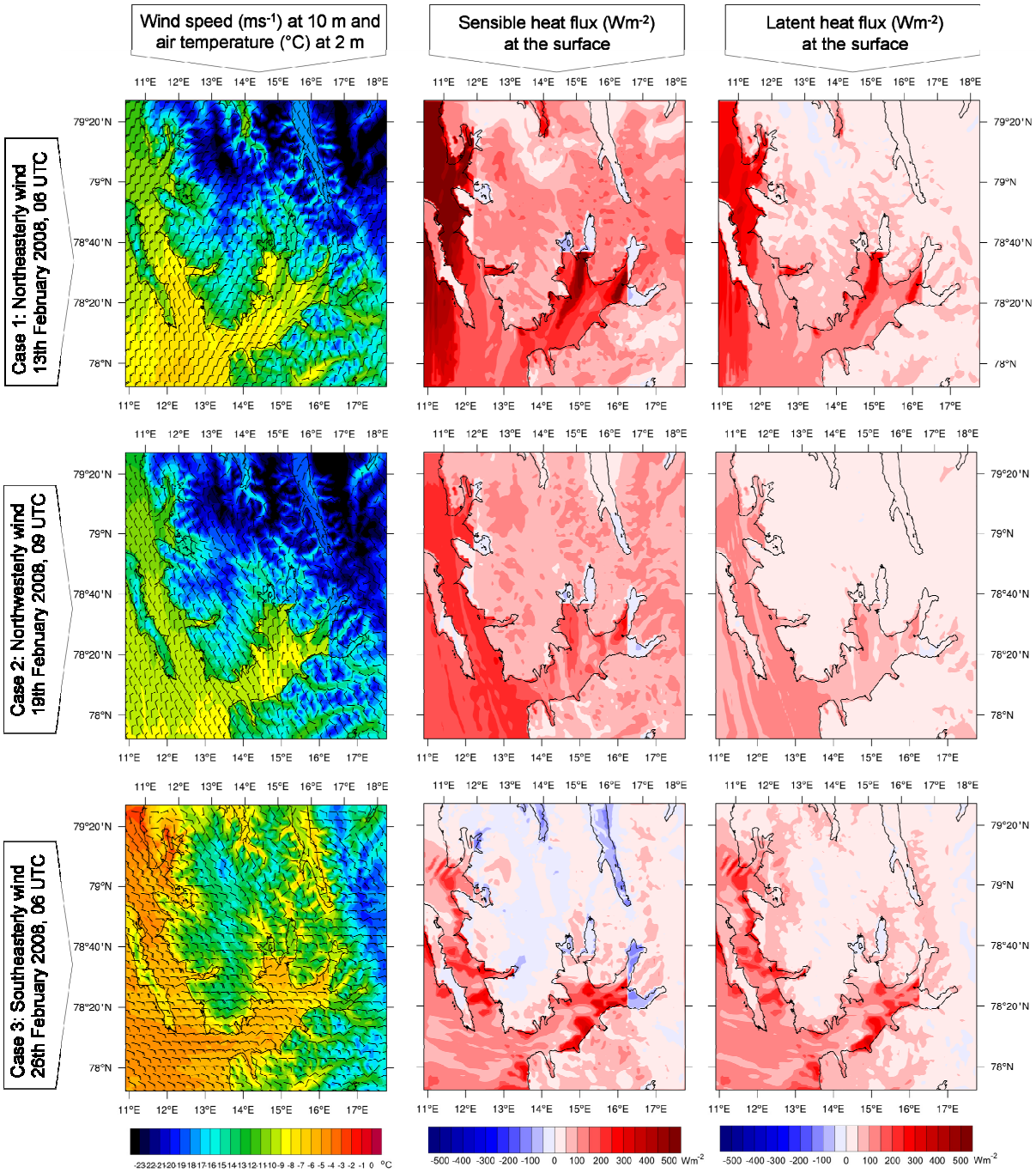

Figure 2. The left panel shows horizontal wind vectors at 10 m level and temperature at 2 m for domain 3. The sensible heat flux and latent heat flux are shown in the middle panel and the right panel, respectively.

3 SPATIAL VARIABILITY

The simulations indicate that the direction of the large scale flow has an influence on the spatial distribution of wind speed, air temperature and humidity over Isfjorden, especially on the location of maxima and minima, and as a consequence of these also the spatial distribution of the turbulent fluxes is largely influenced (Fig. 2). When the wind has a northerly component, cold air is transported over the fjord through the valleys in northeast, creating pronounced local minimum of air temperature and maxima of wind speed and the turbulent fluxes. Local differences within the ice-free area of Isfjorden, caused by the topography, can exceed 400 Wm^{-2} for sensible heat and 350 Wm^{-2} for latent heat flux. The spatial differences are largest when the large scale wind is blowing along the fjord.

SEVERE TURBULENCE IN THE WAKE OF SOUTHEAST-ICELAND

Hálfdán Ágústsson[12], Haraldur Ólafsson[134]

[1] Háskóli Íslands (University of Iceland), Iceland
E-mail: *halfdana@gmail.com*
[2] Reiknistofa í veðurfræði (Institute for Meteorological Research), Iceland
[3] Veðurstofa Íslands (Icelandic Meteorological Office), Iceland
[4] Bergen School of Meterology, Geophysical Institute, Bergen, Norway.

Abstract: On 18 November 2008 a commercial aircraft encountered severe turbulence while flying in westerly flow across the wake of SE-Iceland. The situation is simulated with horizontal resolutions down to 1 km. The simulations show a type 1 rotor (Hertenstein and Kuettner, 2005), which is in agreement with the vertical profile of wind and temperature. Very strong shear-turbulence is reproduced in the lee-wave and inside the rotor. The lee-waves and the turbulence patterns are not stationary and as the upstream vertical windshear increases, the lee-wave becomes less steep, but the turbulence increases. From a forecasting perspective, this event could have been foreseen quite accurately, but not with the NWP tools that are currently in use for aviation forecasts. Their resolution is typically of 9 to 27 km and even more, and that is not adequate. This event underlines the urgency of delivering products from fine-scale simulations over complex terrain to pilots.

Keywords: *Wake, severe turbulence, rotor, complex orography, ICAM, Iceland*

1 INTRODUCTION

There is mounting evidence in the scientific literature that turbulence aloft may be successfully forecasted using fine-scale numerical simulations of weather. Observations of such turbulence are currently limited to large experiments using specialized aircraft, e.g. as in the Greenland Flow Distortion Experiment (Renfrew et al., 2008) or to aviation incidents where commercial airplanes accidentally fly into regions of severe turbulence. One such incident is described in Ólafsson and Ágústsson (2009), where an international flight encounters severe turbulence and breaking waves in easterly flow over Greenland. In this case the incident could presumably have been avoided as fine-scale simulations reproduced the turbulence which reached up to the tropopause.

Here we investigate an incident where a domestic flight along the south coast of Iceland encounters severe turbulence in the wake of Southeast-Iceland in the afternoon of 18 November 2008. The airplane first encounters the turbulence at 8.000 ft east of Mt. Öræfajökull and the severe turbulence continues for 5-7 min. while the airplane descends towards Höfn. There was no warning, i.e. SIGMET, for this region until after the incident. Winds were strong and westerly in the troposhere (Fig. 1), and the Keflavik sounding (SW-Iceland) shows a forward vertical windshear and an inversion at 900 hPa at 12 UTC (not shown). At 12 UTC a downslope windstorm was initiated at Kvísker on the eastern side of Mt. Öræfajökull with winds increasing suddenly from 5 m/s to 40 m/s and a significant warming and drying of the air. Kvísker is close to the track of the airplane through the wake and the previous study of Ágústsson and Ólafsson (2008) shows that the current situation is in fact characteristic for downslope windstorms and a turbulent wake of Southeast-Iceland.

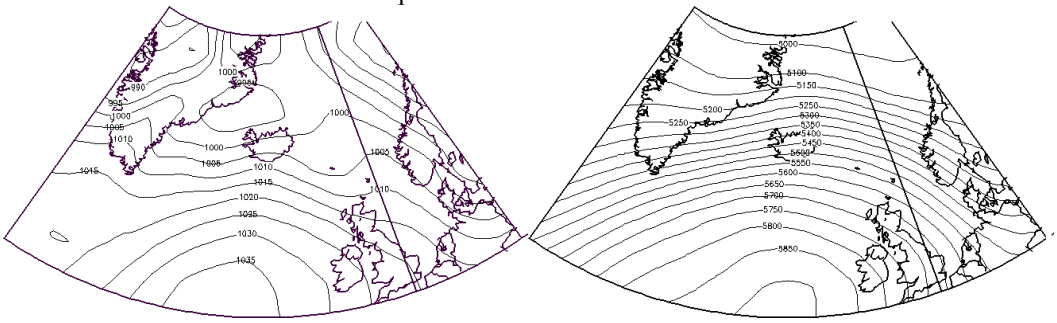

Figure 1. Analysis from NCEP/NCAR provided by NOAA/ESRL physcial science division. The figures are valid at 18 UTC on 18 November 2008 and show the mean sea level pressure [hPa] (left) and the 500 hPa geopotential height [m] (right).

2 RESULTS

The atmospheric situation is reproduced using the WRF-model (Skamarock et al., 2005) with three nested grids using a resolution of 9, 3 and 1 km and 40 sigma-layers. The model was forced using the ECMWF-analysis on model levels. Apart from the 1 km grid, the setup is similar to what is used for operational forecasting at Veðurstofa Íslands and published online at: "http://belgingur.is", by Reiknistofa í veðurfræði.

The simulated wind field in Southeast-Iceland reveals a great dependence on the horizontal resolution of the model (Fig. 2). A resolution of at least 3 km is necessary to reproduce the leeside windstorm and the wave pattern in the wake. The model successfully reproduces the observed winds and temperature at a resolution of 1 km at Kvísker while the agreement is worse at coarser resolutions (not shown). The winds at 950 hPa reveal the same wave pattern and patches of strong turbulence in the wake while section A across Mt. Öræfajökull and into the wake reveals a series of large amplitude waves with large values of turbulence kinetic energy (TKE) in the region of strong wind shear below the waves (Fig. 3). This wave pattern is not stationary and the waves become less steep and the turbulence increases as the upstream vertical windshear increases (not shown).

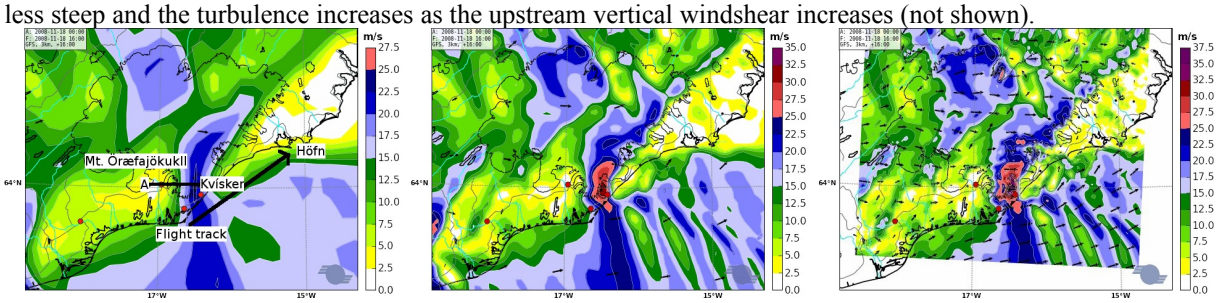

Figure 2. Simulated surface winds [m/s] at a horizontal resolution of 9 km (left), 3 km (middle) and 1 km (right) in Southeast-Iceland at 16 UTC on 18 November 2008. Also shown are locations mentioned in the text, the track of the airplane and section A.

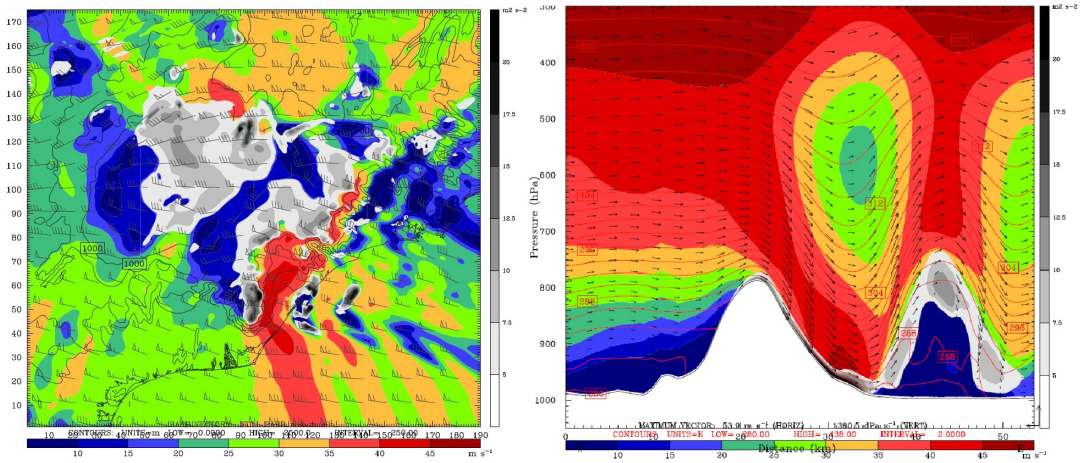

Figure 3. Simulated winds [m/s], turbulence kinetic energy [J/kg] and potential temperature [K] at 950 hPa (left) and in section A (right) at 16 UTC on 18 November 2008. The section only shows the first wave in a series of lee waves.

3 CONCLUSIONS

In this paper, a case of a type 1 rotor as classified by Hertenstein and Kuettner (2005) is presented. The structure of the rotor is in agreement with the upstream vertical profile of wind and temperature. There is strong shear-turbulence in the lee-wave and inside the rotor. It is evident that this event could have been forecast quite accurately, but not with the NWP tools currently used in aviation forecasts. Their horizontal resolution is typically 9 to 27 km or even coarser, which is simply not adequate. This study underlines the urgency of delivering products from fine-scale simulations over complex terrain to pilots.

Acknowledgement:
We thank the pilot, Aðalsteinn Marteinsson for providing detailed information on the turbulence incident.

REFERENCES

Ágústsson H. and H. Ólafsson, 2008. Variability in the Kvísker downslope windstorms. *Proc. Amer. Meteorol. Soc. Conf. Mountain Meteorology*, Whistler, Canada.

Hertenstein, R. F. and J. P. Kuettner, 2005. Rotor types associated with steep lee topography: influence of the wind profile. Tellus 57A, pp. 117-135.

Ólafsson H. and H. Ágústsson, 2009: Gravity wave breaking in easterly flow over Greenland and associated low level barrier- and reverse tipjets. In press, Meteorology and Atmospheric Physics, March 2009.

Renfrew, I. A., G. W. K. Moore, J. E. Kristjánsson, H. Ólafsson, S. L. Gray, G. N. Petersen, K. Bovis, P. R. A. Brown, I. Føre, T. Haine, C. Hay, E. A. Irvine, A. Lawrence, T. Ohigashi, S. Outten, R. S. Pickart, M. Shapiro, D. Sproson, R. Swinbank, A. Woolley, and S. Zhang, 2008. *Bulletin of the American Meteorological Society,* 89 (9), pp. 1307–1324.

Skamarock, W. C., J. B. Klemp, J. Dudhia, D. O. Gill, D. M. Barker, W. Wang and J. G. Powers 2005. A description of the Advanced Research WRF version 2. Technical Report NCAR/TN-468+STR, National center for atmospheric research.

GREENLAND AND EXTREME NORTHERLY WINDS IN THE NORDIC SEAS

Beathe Tveita[1], Haraldur Ólafsson[3,4], Anne Dagrun Sandvik[5] and Berit Hagen[2]
[1]Storm Weather Centre, Bergen, Norway
[2]Norwegian Meteorological Institute
[3]Háskóli Íslands (University of Iceland)
[4]Bergen School of Meteorology, Geophysical Institute, University of Bergen
[5]Institute for Marine Research, Bergen, Norway
E-mail: *beathe.tveita@storm.no*

Abstract: A study of the impact of Greenland on the atmospheric flow in the Nordic Seas in the case of an extreme northerly windstorm north of Iceland is presented. Removing Greenland leads to much warmer air at low levels east of Greenland, a much weaker frontal jet north of Iceland and no jet at Cape Tobin. The surface pressure is much higher everywhere over the Nordic seas north of ca. 69N when Greenland is present. The wake area at the east coast of Greenland, west of Iceland is much colder when Greenland is not present.

Keywords: *Greenland, Cape Tobin Jet, Wake, damming, extreme winds, Nordic Seas, WRF, QuikSCAT.*

1 INTRODUCTION

Several authors have elaborated on the role of Greenland in the play of weather and climate on different time scales. Kristjánsson and McInnes (1999) studied how Greenland contributed to the Icelandic Trough when a synoptic cyclone moved to the northeast between Iceland and Greenland. Petersen et al. (2004) showed that on a climatological time scale, Greenland contributes to a positive pressure anomaly at its east coast, extending across the N-Atlantic towards Scandinavia.

In this study, a case of an extreme northerly windstorm is simulated with and without Greenland. The flow is initialized at 18 UTC on 4 March 2000 and the fields are compared 24 hours later. The simulations are carried out with the WRF model with boundaries from the ECMWF and horizontal resolution of 9 km. More details on this case are given in Tveita et al., (2009).

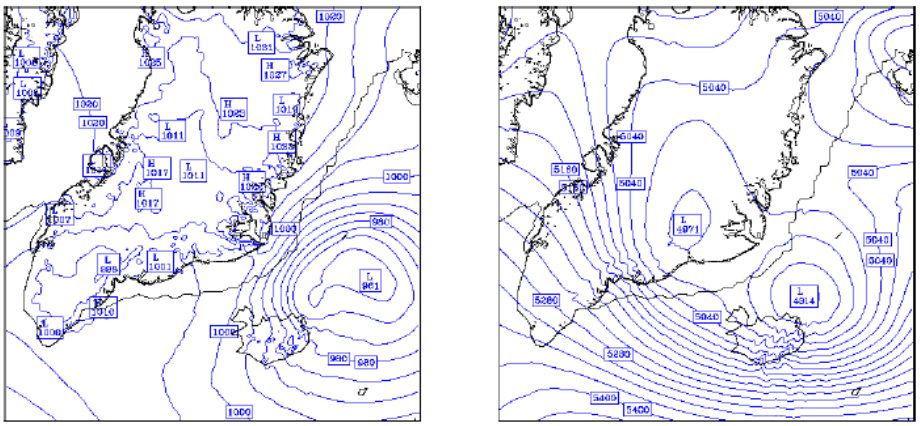

Figure 1. MSLP (left) and geopotential height at 500 hPa (right) valid at 18 UTC on 5 March 2000. The simulation is initialized 24 h earlier.

3 RESULTS

The results are presented in Figures 1-3 and schematically in Fig.2 (right). The main features when Greenland is present are i) cold air damming east of Greenland and a positive surface pressure anomaly extending very far to the east, ii) a warm wake at the coast of Greenland, west of Iceland, extending to the east of Iceland, iii) very strong winds in a frontal zone north of Iceland and also close to Cape Tobin, but weak winds in the wake of Greenland further south.

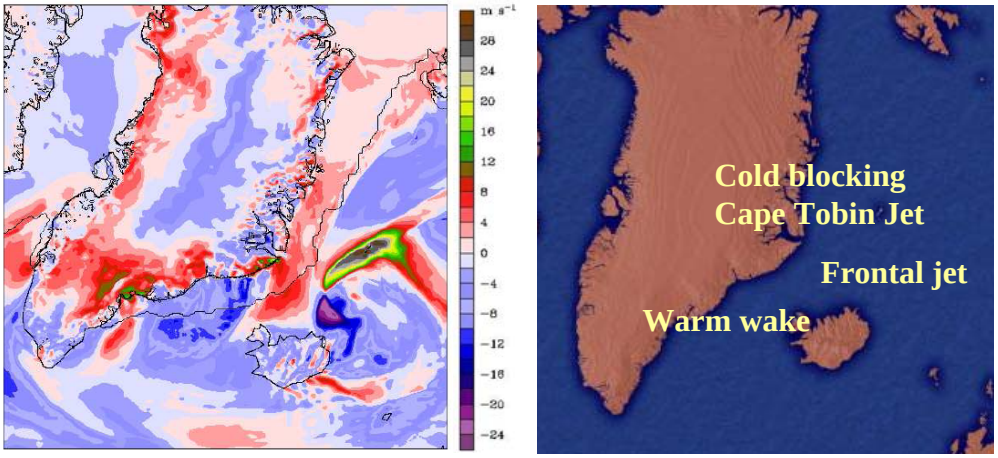

Figure 2. Surface wind speed in the NOGREEN simulation subtracted from the CONTROL simulation (left) and a schematic overview of the main features of the fields of difference between NOGREEN and CONTROL.

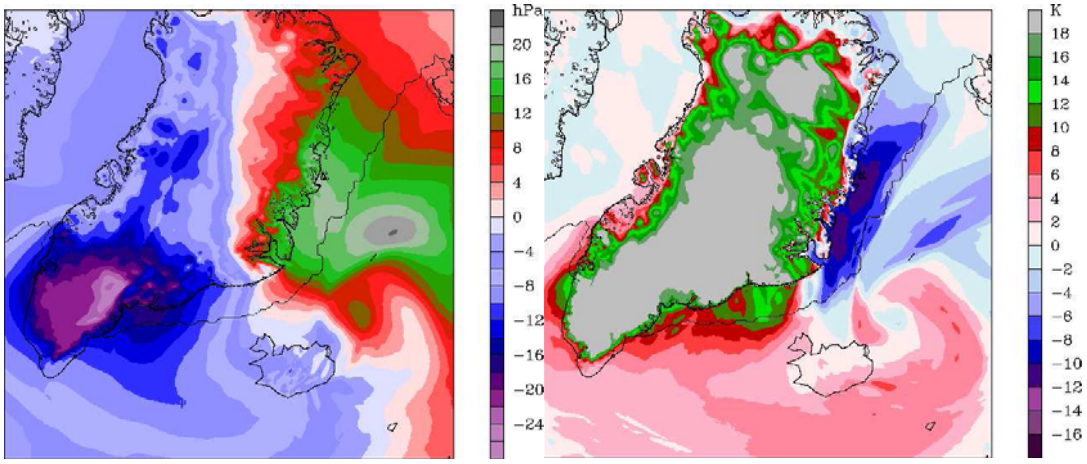

Figure 3. Difference fields (CONTROL-NOGREEN). Left: MSLP (hPa); Right: Temperature at 850 hPa (K) at 18 UTC on 5 March 2000.

3 DISCUSSION

None of the key features described in the previous section are surprising, except perhaps the magnitude and the extent of the sea level pressure difference north of Iceland. It does however correspond to the climatological study by Petersen et al. (2004). As expected, Greenland has in a case like this a very strong positive effect on the surface winds in the vicinity of Cape Tobin, and a negative effect in the wake area further south. The greatest impact is however in the frontal zone, further to the east where the cold dammed air meets warmer air in the southeast. A difference in wind speed of 25-30 m/s between the two simulations (CONTROL-NOGREEN) gives a solid foundation for stating that the extreme windstorm was indeed generated by Greenland.

REFERENCES

Kristjánsson, J. E., McInnes, H., 1999: The impact of Greenland on cyclone evolution in the North Atlantic. Quarterly Journal of the Royal Meteorological Society, 125(560), 2819-2834.

Petersen, G. N., J. E. Kristjánsson and H. Ólafsson, 2004: Numerical simulations of Greenland´s impact on the Northern Hemisphere winter circulation. Tellus 52A, 102-111.

Tveita, B., H. Ólafsson, A. D. Sandvik, B. Hagen, 2009: A numerical study of an extreme windstorm in the Greenland Sea. Submitted to Meteorology and Atmospheric Physics.

FORECASTING EXTREME WINDS IN THE NORDIC SEAS - THE GREENLAND DAMMING

Berit Hagen[1], Haraldur Ólafsson[2,3], Anne Dagrun Sandvik[4] and Beathe Tveita[5]
[1]Norwegian Meteorological Institute
[2] Háskóli Íslands (University of Iceland)
[3]Bergen School of Meteorology, Geophysical Institute, University of Bergen
[4]Institute for Marine Research, Bergen, Norway
[5]Storm Weather Centre, Bergen, Norway
E-mail: *berit.hagen@met.no*

Abstract: A study of QuikSCAT data reveals that a large proportion of extreme wind cases in the Nordic Seas appear to be linked to damming of low-level dense air east of Greenland. Forecasts with different lead times of one Greenland-damming windstorm and three extreme windstorms that were not influenced by Greenland are compared and the Greenland-damming storm forecast has the best skill. Simulations of all the four cases suggest little sensitivity of the extreme winds to parameterization of the PBL and horizontal resolution in the range from 3 to 27 km.

Keywords: *Greenland, damming, extreme winds, Nordic Seas, WRF, QuikSCAT.*

1 INTRODUCTION

Accurate forecasting of extreme winds is of utmost importance, both for security and economic reasons. In recent years, continuous wind observations have been made available by the QuikSCAT remote sensing system. Here, cases of extreme winds in the Nordic Seas, recorded by QuikSCAT are studied. A case where Greenland plays a strong role through damming of low-level air is compared to cases where such effects are not important. Details on the QuikSCAT data processing and the numerical simulations are given in Hagen et al. (2009).

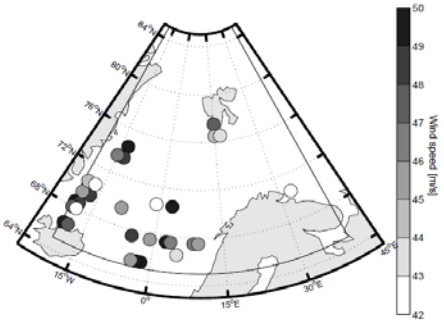

Figure 1. Position of the most severe wind events in the Nordic Seas 2000-2006, detected by QuikSCAT.

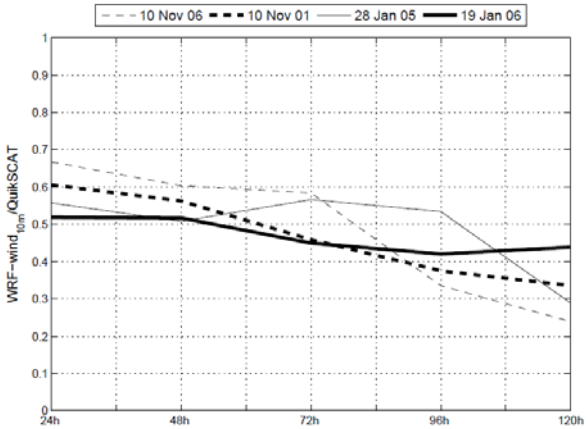

Figure 2. Forecast skill in 4 of the cases in Fig. 1, simulated with different lead time with initial conditions and boundaries from the ECMWF and horizontal resolution of 9 km.

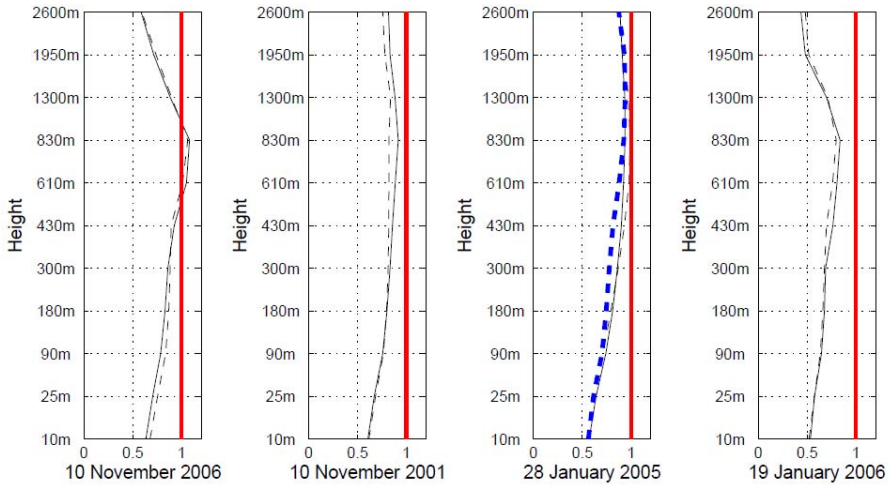

Figure 1. Simulated wind profiles in four cases of extreme surface winds, normalized with the observed QuikSCAT value at the surface. Solid lines show results when using the MYJ PBL scheme, while dotted lines show results from the YSU scheme. A bold dotted line indicates results from a simulation with 65 vertical levels (instead of 33 levels as in all the other simulations).

2 RESULTS

Figure 1 shows the distribution of the 30 strongest wind cases 2000-2006. There is a large concentration of cases just east of Greenland. These cases are linked to damming of low-level dense air, leading to very strong northerly surface winds in reverse vertical wind-shear situations. Four of the extreme wind cases are simulated, with the WRF model and boundaries from the ECMWF. One of the cases is a Greenland-damming case (10 November 2006), while the three other cases are not. Figure 2 shows the skill of the forecasts of the extreme winds at different lead times. All the forecasts underestimate the winds, giving typically about 30 m/s while the QuikSCAT indicated about 45 m/s. Of all the four forecasts, the Greenland-damming case has the best skill at lead times of 24, 48 and 72 hours. There was not much sensitivity of the forecasts to horizontal resolution of the simulations (not shown).

Figure 3 shows the wind profiles from 24 h forecasts of the four cases. While in all of the cases, the surface winds are underestimated, the simulated winds at typically 600-800 meters height do come close to the observed surface winds. In the Greenland-damming case, the simulated winds exceed the observed surface winds at these levels. There is quite limited sensitivity to the two parameterization schemes that were tested, as well as to the vertical resolution.

4 DISCUSSION AND CONCLUSION

The fact that the orographic windstorm has the best forecast skill has of course no statistical significance, but from a dynamic standpoint, this is not entirely surprising, since the damming of cold air by Greenland is quite a straightforward process to simulate, provided that the topography and the surface fluxes are reasonably correct. From this study, one may state that there is an indication that extreme winds associated with cold-air damming by Greenland may be better forecasted than extreme winds associated with “ordinary” extratropical cyclones. Although all the short-range forecasts do predict a strong windstorm, the skill of the forecasts is far from outstanding. There are several possible reasons for this. Firstly, the simulated cyclones may be to shallow or the pressure gradients not as steep as in reality. Secondly, the vertical mixing of horizontal momentum may be underestimated by the models. The parameterization schemes are not tuned for extreme winds and there are quite limited observations of vertical profiles in extreme situations. Such observations are planned (Ólafsson et al., 2009). Finally, the QuikSCAT procedures may overestimate the surface wind speed.

REFERENCES

Hagen, B., H. Ólafsson, A. D. Sandvik, B. Tveita, 2009: Forecasting wind extremes in the Nordic Seas. Submitted to Meteorology and Atmospheric Physics.

Ólafsson, H., Ó. Rögnvaldsson, J. Reuder, H. Ágústsson, G. N. Petersen, H. Björnsson, T. Jónsson and J. E. Kristjánsson, 2009: Monitoring the atmospheric boundary-layer in the arctic (MABLA) – the Gufuskálar project. An extended abstract in this issue.

"UP-HILL EFFECT" ON WINDS AT THE HONG KONG INTERNATIONAL AIRPORT IN STRONG NORTHERLY WINDS ASSOCIATED WITH TROPICAL CYCLONES

Pak Wai Chan[1] and T.C. Cheung[2]

[1] Hong Kong Observatory, Hong Kong, China
E-mail: *pwchan@hko.gov.hk*
[2] Chinese University of Hong Kong, Hong Kong, China

Abstract: The Hong Kong International Airport (HKIA) is built on a reclaimed island surrounded by complex terrain from the E to SW directions. It is however exposed to the Pearl River Estuary to the N and NW. Given this geographical setup, it may be expected that, in northwesterly airflow, the effect of the complex terrain in the vicinity of HKIA would be insignificant and the winds over the airport would be rather uniform. Nevertheless, uneven wind distribution on the airfield has been observed in strong northwesterly winds associated with tropical cyclones. For instance, the winds at the north runway were found to be stronger than those over the south runway by as much as 10 – 15 knots. The uneven wind distributions over HKIA in strong northwesterly winds associated with tropical cyclones are studied in this paper. They appear to arise partly from an "up-hill effect" when winds are forced to climb over the mountainous Lantau Island to the south of the airport. High-resolution numerical simulation is performed using the Weather Research and Forecasting (WRF) model version 2.2. The model successfully reproduces the wind speed difference between the north and the south runways of the airport.

Keywords: *up-hill effect, tropical cyclone, WRF*

1 INTRODUCTION

The Hong Kong International Airport (HKIA) is situated to the north of the mountainous Lantau Island. It is exposed to the Pearl River Estuary to the north and northwest. With this geographical setup, airflow disturbances are expected to appear in the airport area due to terrain disruption when east to southwesterly winds prevail, whereas more uniform winds may occur over the airport for north to northwesterly airflow. However, rather uneven wind distribution is observed over HKIA for strong northwesterly winds associated with tropical cyclones or winter monsoon. The winds at the two runways of the airport (locations in Fig. 1) may become very different in those situations. The wind speeds measured at the anemometers over the north runway were found to be larger than those over the south runway by as much as 10-15 knots. This could have significant implications for aircraft operation. For instance, the crosswind at the north runway may be too strong for aircraft to land. As such, the aircraft may need to land at the south runway, which is closer to the terrain. This may render the wind more turbulent.

The uneven wind distribution over the airport in northwesterly winds associated with tropical cyclones is presented in this paper. Its cause is studied by high-resolution numerical simulation.

2 UNEVEN WIND DISTRIBUTION IN TYPHOON NURI

In the morning of 22 August 2008, Typhoon Nuri was situated to the southeast of Hong Kong bringing gale force north to northwesterly winds to the territory. The wind distribution around HKIA at about 10 a.m. on that day is shown in Fig. 1. It can be seen that there is quite significant wind difference between the two runways of the airport. The north runway recorded north-northwesterly gales of about 35-40 knots. On the other hand, the south runway had strong winds of only about 25 knots. Normally, aircraft would land at the north runway of HKIA. However, because of the gale-force crosswind at that runway, they could only opt to land at the south runway from the west. The airflow turned out to be quite turbulent near the threshold of the south runway (cube root of eddy dissipation rate of about 0.4 $m^{2/3}s^{-1}$, as determined by onboard flight data, indicating moderate turbulence) for the aircraft to operate. After a couple of hard landing events, it was decided to stop the aircraft operation until the wind subsided or changed direction.

The time series of the anemometer data at the two runways of HKIA in Typhoon Nuri case (22 and 23 August 2008) are shown in Fig. 2. The measurements from the pair of anemometers at the eastern end, near the middle and at the western end of HKIA are compared. It could be seen that, for wind directions of about 300 to 360 degrees, the wind speed difference between each pair of anemometer becomes larger. In general, this difference is more pronounced for the anemometer pair at the western part of the airport. These anemometers are closer to the terrain of Lantau Island (Fig. 1) and it seems that the wind difference may be related to terrain effect on the airflow in *northwesterly* winds.

3 OTHER TROPICAL CYCLONE CASES WITH STRONG NORTHWESTERLY WINDS

The wind data of other tropical cyclone cases since HKIA opened in 1998 have also been reviewed to see whether or not the wind difference as noted in Section 2 above occurred only in the case of Typhoon Nuri. Two

other strong northwesterly wind cases due to tropical cyclones were identified, namely, Typhoon Sam and York in August and September 1999 respectively. The wind records for Typhoon Sam are shown in Fig. 3. It could be seen that, similar to Typhoon Nuri, wind speed differences between the anemometer pairs were the largest in north to northwesterly winds. Moreover, this difference was slightly larger for anemometers near western end of HKIA.

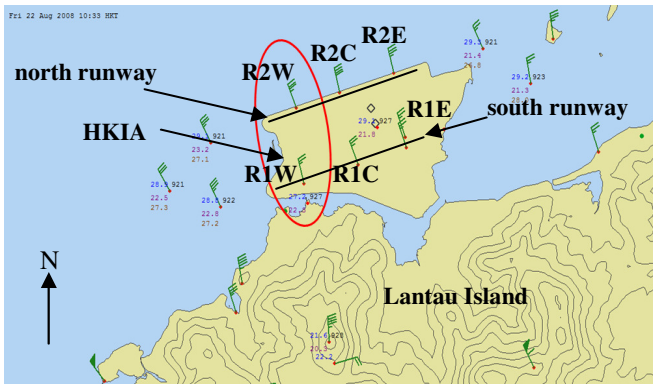

Figure 1. Surface wind distribution around HKIA at 10:33 a.m., 22 August 2008. Runway length: about 4 km.

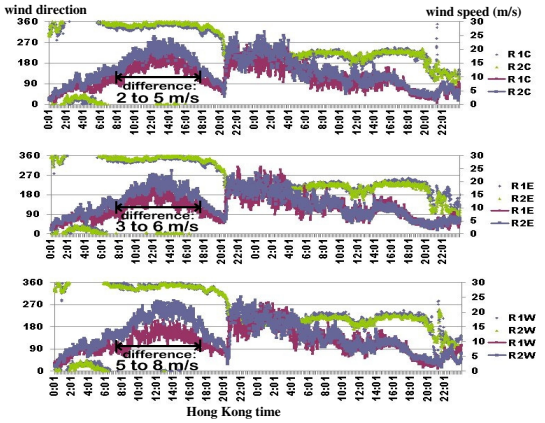

Figure 2. Time series of HKIA anemometer readings on 22-23 August 2008 during the passage of Typhoon Nuri. Anemometer locations: see Fig. 1.

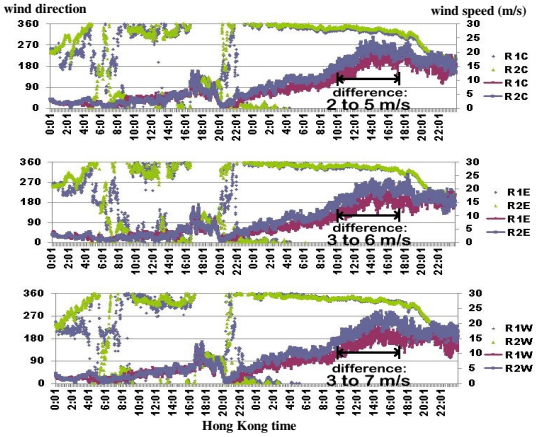

Figure 3. Time series of HKIA anemometer readings on 21-22 August 1999 during the passage of Typhoon Sam.

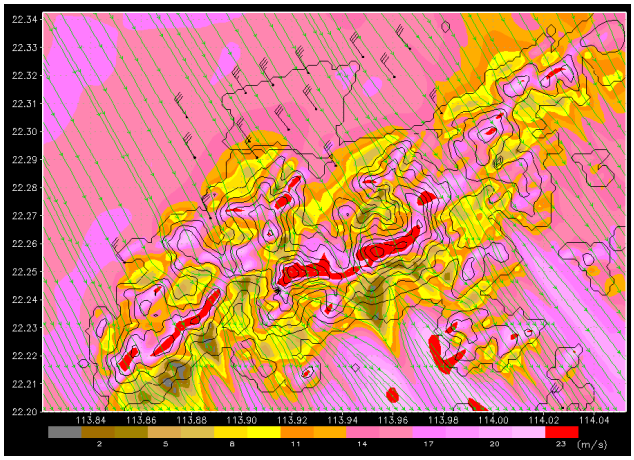

Figure 4. WRF-simulated wind speed distribution at the surface at about 02 UTC, 22 August 2008.

4 NUMERICAL SIMULATION

The uneven wind distribution over HKIA is studied numerically using the Weather Research and Forecasting (WRF) model version 2.2. Three nested domains are used, from southern China to areas around Lantau Island. The innermost domain has a spatial resolution of 200 m. The Typhoon Nuri case is considered and the winds near the airport in gale-force north to northwesterly wind condition are shown in Fig. 4. It could be seen that the wind speed differences between the two runways, viz. about 10 knots at the western end and about 5 knots for middle and eastern end, are reasonably reproduced. A sharp gradient of surface wind speed is successfully simulated near the foothill of Lantau Island, which covers the southern part of the airport. The model simulation results suggest that the wind speed difference could be due to "up-hill effect" on the airflow when the winds start to climb up the mountains of Lantau Island. Similar "up-hill effect" has been discussed in the literature (e.g. Stull (2004)).

5 CONCLUSIONS

Uneven wind distribution between the two runways of HKIA is observed in the strong northwesterly wind cases associated with tropical cyclones in Hong Kong. The difference is in the order of 10-15 knots and could have significant implication to aircraft operation. Based on WRF simulation results, it could be related to "up-hill effect" as the winds start to climb over the mountains of Lantau Island.

REFERENCES

Stull, R. B., 2004: An Introduction to Boundary Layer Meteorology, Kluwer, 670 pp.

ARE TORNADOES POSSIBLE ALSO IN SLOVENIA? CASE STUDY OF AN EXTREME EVENT OF 13 AND 14 JULY 2008

Uroš Strajnar

Environmental Agency of the Republic of Slovenia, Ljubljana, Slovenia
E-mail: *uros.strajnar@gov.si*

Abstract: Extreme convective events also appear frequently in Slovenia, but tornadoes are very unlikely. In the paper the most catastrophic convective event in year 2008 is discussed, when the damage to the houses and forests was similar to tornado's.

Keywords: *extreme event, tornado, downburst*

1 INTRODUCTION

It is well known that tornadoes can occur in most European countries. Rough estimation based on survey of average tornadic activity in Europe conducted among the participants of the European Conference on Severe Storms 2002 (Dotzek, 2003) is more than 300 tornadoes per year in Europe.

Even in the Alps tornadoes sometimes form, especially at the eastern flanks. In Slovenia's neighbouring countries Austria, Italy, Hungary and Croatia, there is significant occurrence of tornadoes very close to the Slovenia border. According to Holzer (2000) the tornado density in the period from 1946 to 1971 in South-Eastern Austria is 0.9 tornadoes per 10000 km² per year, while Giaiotti's (2005) statistics for the period from 1991 to 2000 for Eastern Italy (Friuli) is roughly 10 tornadoes per 10 years. In Hungary average number of tornadoes is 3 to 5 per year (Sárközi, 2005).

On the other hand there is no official statistics for Slovenia and there are only a few tornado occurrences, despite that this region has one of the highest number of thunderstorms in the Alps. The most reliable estimation based on number of volunteer observed tornadoes between 2000 to 2007 (European Severe Storms Laboratory, http://www.essl.org/research/tornado/) is 0 to 0.3 tornadoes per 10000 km² per year. Because a tornado is unusual phenomenon in Slovenia and the major threats are hail, heavy precipitation and downburst winds, there are only volunteer organised observation and no official tornado warning system is in operation.

The case of 23 August 1986 is known as a strongest tornado, when estimated wind speed reached 60 m/s. At that time there was no synoptic observation of tornado and the wind speed estimation and the synoptic diagnose of that event was made from the damage caused by tornado. The last evidences of tornadoes near Slovenia are pictures of waterspouts over the Trieste bay on 8/8/2008 and Piran bay on 28/5/2007.

2 DISCUSSION

In the paper an extreme event of 13 and 14 July 2008 is discussed when several heavy thunderstorms developed and produced large hail, heavy precipitation and heavy winds, which caused damage similar to the tornado's. On 13/7/2008 a deep and quite intense, quasi-stationary upper long-wave trough was covering the western parts of Europe, slowly beginning to evolve into an upper cut-off cyclone over the Alpine regions late in the period. In the lower levels there were warm and moist south to south-westerly winds, which blew ahead of the cold front which has reached the region during the night. A deep layer shear (0 to 6 km) was present with values higher than 25 m/s and lifting condensation level 690 m which is favourable for supercell development. After the cold front passage there was a slight stabilisation of atmosphere, but during the 14/7/2008 upper trough again destabilised the air mass.

The most intense event during this period was a pre-frontal storm from 10:00 to 14:00 UTC 13/7/2008 which travelled from west to north-east Slovenia. Figure 1 shows radar images for the period when the most damage was done are presented. At 12:10 UTC the most developed convective system was in centre of Ljubljana plane in Medvode with reflection more than 57 dBZ and the shape close to the hook. There was rather weakly argumented observation of tornado sent to European Severe Weather Database (http://www.essl.org/ESWD/), some damage to the buildings, but no images of tornado. Nevertheless, this case is now verified as tornado. On a zoomed picture of radar measured radial velocities field (Fig. 2 right) in the centre of white circle there are some pixels changing from 15 m/s to -15 m/s which could indicate some rotation.

Afterwards system travelled to the mountain region of Gozd where several large forest areas were destroyed. According the nearest automatic reporting station the wind gusts exceeded 23 m/s. Unfortunately the most affected regions have not been covered by the reporting network. On the basis of aerial photos and the pattern of destroyed trees there was a strong scientific and public debate about possibility of tornado, but officially it was

deduced that the most probable reason for the destruction was a downburst. There was no photo or any other direct evidence of tornado cloud. At 13:10 UTC the system travelled to the east and the maximum precipitation rate 33 mm per 15 minutes was measured in Celje with return period of 100 years.

Considering radar maximum echoes and radial velocities the possibility of tornado on Ljubljana flatland at 12:10 UTC could not be denied, on the other hand the radar vertical cross-section through the storm (Fig 2. left) shows that instead of hook echo two separate cells are more likely.

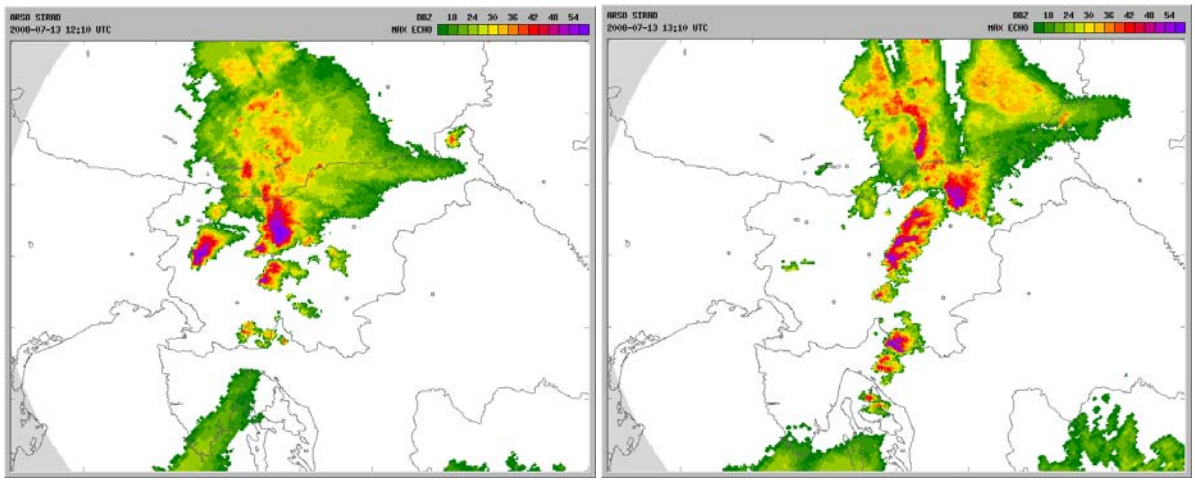

Figure 1. Maximum echoes from Lisca radar (Slovenia) for 13/7/2008 12:10 and 13:10 UTC.

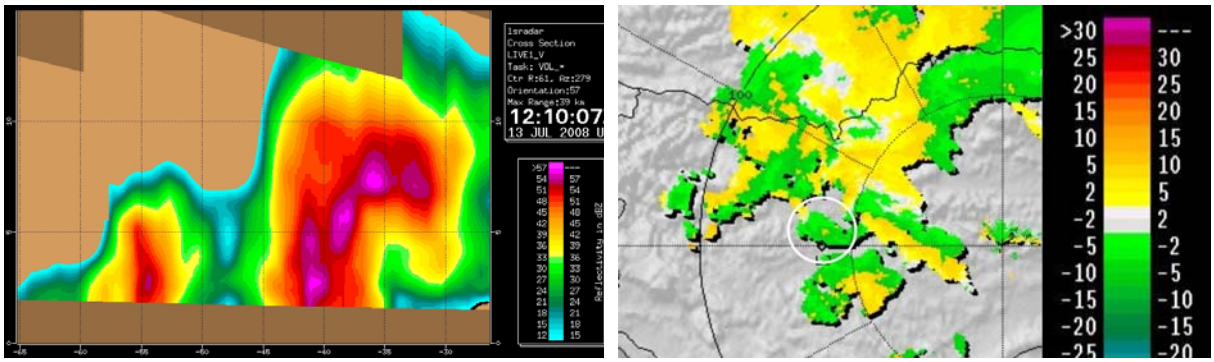

Figure 2. Left: Radar (Lisca) echoes vertical cross-section in SW–NE direction trough the centre of the white circle on the right figure for 13/7/2008 12:00 UTC; right: radar radial velocities at 4 degrees elevation on 13/7/2008 12:10 UTC. The scale is in m/s.

3 CONCLUSIONS

Although the climatology of neighbour countries shows that tornadoes are possible in the area, there was no case in Slovenia with a photo or record found till now. The possible reason for such small number of tornadoes comparing with neighbouring countries is that terrain in Slovenia is unfavourably shaped and complex with few and not extensive flatlands.

The presented case showed that the possibility of tornado at 13/7/2008 12:10 could not be denied. For the further work detailed analysis of storm relative mean radial velocities will be done, which is at moment as operational product not available. It would, besides the limitation in complex terrain and resolution, give better description of the dynamics of the extreme event.

REFERENCES

Giaiotti, D. B., M. Giovannoni, A. Pucillo, F. Stel, 2005: The climatology of tornadoes and waterspouts in Italy. Atmos. Res. **83**, 534–541.

Holzer, A. M., 2000: The Tornado climatology of Austria. Atmos. Res. **56**, 203–211.

Sárközi, Sz., 2005: A systematic approach to synoptic tornado climatology of Hungary for the recent years (1996–2001) based on official damage reports. Atmos. Res, Chambery, France, 263–271.

Dotzek, N., 2003: An updated estimate of tornado occurrence in Europe. Atmos. Res. **67-68**, 153–161.

Sioutas, M. V., A. G. Keul. 2007: Waterspouts of the Adriatic, Ionian and Aegean Sea and their meteorological environment. Atmos. Res. **83**, 542–557.

TRANSPORT AND CHEMICAL CONVERSION IN CONVECTIVE SYSTEMS ABOVE COMPLEX TERRAIN

W. Wilms-Grabe[1], U. Corsmeier[1], W. Junkermann[1], Ch. Kottmeier[1], F. Holland[2], H. Geiss[2] and B. Neininger[3]

[1]Institute for Meteorology and Climate Research, Karlsruhe Institute of Technology (KIT)
E-mail: *Walburga.Wilms-Grabe@imk.fzk.de*
[2]Institute of Chemistry and Dynamics of Geosphere, Research Center Jülich [3]MetAir Switzerland

Abstract: The COPS-TRACKS campaign of summer 2007 was focussed on the transport and chemical conversion of air pollutants under convective conditions. In this context the Karlsruher city plume was investigated, applying several airborne platforms. The results show a positive correlation between O_3 and CO in remote parts of the plume, which is an indicator for longer-distance transport and underlines the importance of the terrain structure for local trace gas distributions.

Keywords: *TRACKS, complex terrain, air pollution, O_3/CO correlation, transport processes, convective boundary layer*

1 INTRODUCTION

In July 2007, the COPS-TRACKS campaign (Transport and Chemical Conversion in Convective Systems) was carried out in southwestern Germany in order to study the transport of atmospheric trace gases and aerosols under convective conditions. One focus of this experiment was to investigate the dilution of air pollutants due to dynamical and chemical processes above complex terrain. Therefore, the dispersion of the plume of Karlsruhe, a city with moderate anthropogenic emissions, has been detected by coordinated measurements of ground based stations and different airborne platforms, namely three aircraft and a zeppelin.

2 MEASUREMENT PERFORMANCE

Karlsruhe is located in the upper Rhine valley between the Palatine mountains and the Black Forest. The transport of air masses is deeply influenced by this orographical situation (fig. 1). The day of measurement is the 25/07/2007. The weather conditions in the upper Rhine valley are characterized by a high pressure situation with occasionally 1/8 cloudiness and a maximum ground temperature of about 24 °C. The wind arises from westerly directions and ranges between 3 and 8 m/s during the measurement time period. The 25/07/2007 represents a frequently occurring summer situation with medium-sized convective conditions. The anthropogenic emissions of air pollutants mainly result from traffic and industry and also represent typical conditions of a usual summer day in the region of Karlsruhe.

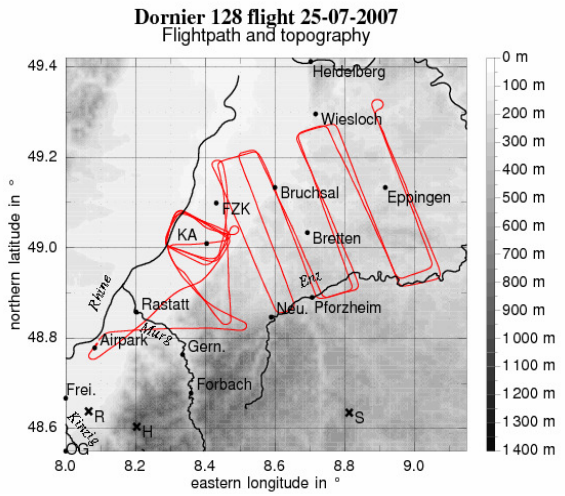

In the lee of Karlsruhe, three aircraft – *Dornier* (IMK Karlsruhe), *Dimona* (MetAir) and *Ultralight* (IMK Karlsruhe/Garmisch-Pat.) – and the *Zeppelin NT* (Jülich) flew between 13:20 UTC and 17:40 UTC inside the convective boundary layer in order to detect the city plume in different distances to Karlsruhe. Each aircraft chose a special flight pattern (example fig. 1). The measured components comprised meteorological variables as well as standard trace gases and aerosols. Ground based monitoring stations of LUBW completed the measurements.

Figure 1. Two-dimensional view on the flight patterns of Dornier in the lee of Karlsruhe. The abbreviation '*KA*' symbolizes *Karlsruhe*, '*FZK*' denotes the *Research Center of Technique and Environment Karlsruhe*.

3 RESULTS

Some selected results are presented in the following analyses, concerning the relationship between O_3 and CO. Usually, near to industry emissions one would expect enhanced CO-concentrations (because of uncomplete combustion) and low ozone concentrations at the same time. However, special situations can lead to positive correlations of both species, for example biomass burning plumes in the boundary layer (*Takegawa et al., 2003*) or the impact of remote pollution sources (*Ancellet et al., 2009*).

Fig. 2 shows the ozone concentration, measured by the Dornier aircraft in the lee of Karlsruhe, in a three-dimensional view of the mattress pattern, one leg around 750 m height and a second leg in 1000 m height above sea level. Both legs reveal moderate ozone concentrations about 53 ppb above the city area of Karlsruhe and in the direct easterly neighbourhood of the city, i.e. downstream of the wind direction. This occurs due to the reduction of background ozone mainly by NO_x-emissions. With increasing distance to Karlsruhe, ozone is enhancing up to 60 ppb as result of the common photochemical production of O_3 by NO_x-, VOC- and CO-chemistry. Also in the north-south direction the measurement shows a gradient in the O_3-distribution with higher concentrations up to 63 ppb at the borders and lower concentrations inside the mattress pattern, likely reflecting the shape of the Karlsruhe city plume, directly crossed by the aircraft.

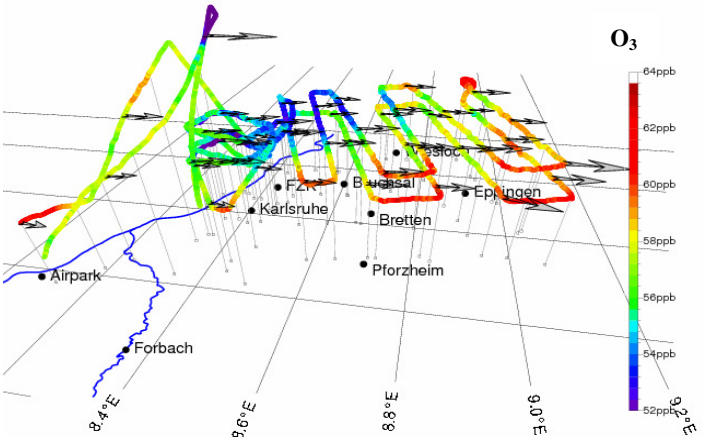

Figure 2. Ozone distribution, measured by the Dornier at 25/07/07 between 13.22 UTC and 16.55 UTC. The arrows specify the wind.

The Dornier measurements of CO (not shown here) offer moderate concentrations between 100 ppb (background concentration) and 124 ppb, but indicate the same principle distribution pattern as O_3: lower values inside the mattresses, higher values at the leg borders. Fig. 3 demonstrates the correlation of O_3 and CO for the data obtained in the remote lee area of Karlsruhe, at least 20 km away from the city emission sources. The $\Delta O_3/\Delta CO$ ratio is found to be 0.46 which is higher than the biomass burning $\Delta O_3/\Delta CO$ ratio (= 0.12) calculated by *Takegawa et al. (2003)*. The coefficient of determination amounts to 0.71, therefore the positive correlation is noteworthy and possibly gives a hint on transport mechanisms from remote emission sources.

In contrary, for the region directly bordering to the city of Karlsruhe the O_3/CO-correlation (not shown here) is unassigned, the coefficient of determination comes to only 0,26. This discrepance in the O_3/CO-correlation as function of the distance between city plume and emission source area provides an indicator for possible long-distance transport of air pollutants from remote emissions.

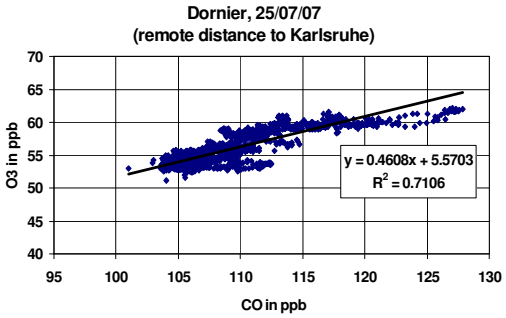

Figure 3. Correlation of O_3 and CO in the remote lee area of Karlsruhe.

4 CONCLUSIONS

On 25/07/07, the city plume of Karlsruhe was transported easterly in the Kraichgau region. The positive correlation between O_3 and CO in the lee area remote of Karlsruhe gives a hint, that the measured concentrations derive not only from the city plume itsself, but are considerably determined by mesoscale transport processes in the existing complex terrain formation and by the accompanying chemical conversion conditions. To gain more detailed information about the significance of the different dynamical and chemical interactions, a study with a regional transport model can provide essential understanding. Especially OH-radicals, which are important in the O_3- and CO-chemistry but which have not been measured during TRACKS, have to be taken into account.

This study addresses not to extreme atmospheric conditions, but to an ordinary summer situation with moderate anthropogenic emissions, a frequently occurring situation. The results help to determine the general significance also of vertical transport of trace gases during a whole summer season and to estimate human exposure to air pollutants under common summer conditions in the upper Rhine Valley.

REFERENCES

Ancellet, G., J. Leclair de Bellevue, C. Mari, P. Nedelec, A. Kukui, A. Borbon, and P. Perros, 2009: Effects of regional-scale and convective transports on tropospheric ozone chemistry revealed by aircraft observations during the wet season of the AMMA campaign. Atmos. Chem. Phys., 9, 383-411.

Kottmeier, Ch., N. Kalthoff, U. Corsmeier, et al., 2008: Mechanism initiating deep convection over complex terrain during COPS. Meteorol. Z., 17 (6), 931-948.

Takegawa, N., Y. Kondo, M. Ko, M. Koike, K. Kita, D. R. Blake, W. Hu, C. Scott, S. Kawakami, Y. Miyazaki, J. Russell-Smith, and T. Ogawa, 2003: Photochemical production of O_3 in biomass burning plumes in the boundary layer over northern Australia. Geophys. Res. Let., vol. 30, n°10, pp. 7.1-7.

DYNAMICAL AND PHYSICAL PROCESSES CHARACTERIZING UPPER-LEVEL CUT-OFF LOWS IN WINTER

Andrea Buzzi[1], Lorenzo Catania[2]

[1] Institute of Atmospheric Sciences and Climate (ISAC-CNR), Bologna, Italy
E-mail: *A.Buzzi@isac.cnr.it*
[2] ARPA-Piemonte (ext. collab.), Torino, Italy

Abstract: Upper level cut-off lows are cold-core cyclonic vortices, associated with positive potential vorticity anomalies in the upper troposphere – lower stratosphere, that are conducive to severe convection in summer and cold spells and snowfalls in winter. In the latter season, especially when travelling over continents, they can survive for many days and sometimes exhibit intensification even while migrating at relatively low latitudes, away from the main polar vortex from which they originate. Their maintenance and possibly intensification are explored using real and idealized numerical simulations. The presence of significant IR radiative cooling in a moist and cloudy troposphere, lying just under the lowest tropopause and surmounted by very dry stratospheric air, is found to significantly contribute in reinforcing the vortex strength, due to intensification of the lower portion of the positive PV anomaly.

Keywords: *Cut off low, upper level vortex, potential vorticity anomaly, atmospheric radiation*

1 INTRODUCTION

Upper level cut-off lows (ULCL's), detached from the arctic polar vortex and wandering for several days over mid-latitude belts, have been recognized as distinct from usual cyclones. They can convey important weather phenomena, like sudden snowstorms and convection, in the case they migrate over warmer surfaces. ULCL's are characterized by a tropospheric cold temperature anomaly, often without a clear signature in the m.s.l.p. field. ULCL's are associated with a sharp positive anomaly of potential vorticity (PV) in the upper troposphere, due to a downward protrusion of stratospheric air, superimposed on the tropospheric cold pool. The dynamical structure of ULCLs, including the implications of the PV distribution and of the related patterns of wind and potential temperature, has been the subject of numerous studies (for example, Eliassen and Kleinschmidt, 1957; Thorpe, 1985).

The problem of maintenance and intensification of ULCL's by radiative transfer processes is considered here, after the ULCL has acquired a quasi-circular symmetry, away from the region of formation. The working hypothesis is that atmospheric radiation contributes significantly to increase the PV maximum in the upper troposphere by means of vertical differential heating. A few case studies of ULCL's events that affected Europe in winter, moving with an east-to-west component from north-eastern Europe to southern Europe and the Mediterranean (Catania, 2008), indicate that the ULCL's can get reinforced, in terms of PV maximum, temperature minimum and circulation strength, in the mid-upper troposphere, well after their formation stage, while travelling over land in a latitude belt comprised between about 45°-60° N. Satellite imagery and meteorological analyses indicate that such ULCL's are characterized by the presence of rather compact cloud layers lying just below the dynamical tropopause, the latter being typically situated around 400-500 hPa. The combined presence of almost saturated air and clouds below the tropopause and very dry air above it (typically less than 10% of relative humidity) favours a strong radiative cooling of a layer embracing the cloud top and the base of the PV anomaly, favouring a growth of the PV maximum where the vertical derivative of diabatic heating is higher, according to the equation:

$$\frac{d\,P}{d\,t} = \frac{\vec{\zeta}}{\rho} \cdot \nabla\,\dot{\theta} \qquad (1)$$

where P is the Ertel PV, $\vec{\zeta}$ is the absolute vorticity vector, $\dot{\theta}$ is the diabatic heating/cooling and ρ is air density. In the case considered here, in the vortex core, the horizontal and vertical velocity is small, therefore $dP/dt \approx \partial P/\partial t$ and both $\vec{\zeta}$ and $\nabla\,\dot{\theta}$ are approximately vertical.

Previous studies of the impact of radiative transfer in atmospheric phenomena that bear some similarity with ULCL's, namely PV filaments (Esler et al, 1999; Forster and Wirth, 2000) and formation of arctic air masses (Emanuel, 2006), have documented its relevance on the evolution of such systems, including destabilization and convective mixing of the saturated air.

2 DATA, METHODS AND MODEL

The real ULCL events of 10-14 Dec. 2001 and 13-16 Dec. 2007 (Fig. 1) have been studied using ECMWF analysis fields, both for direct diagnostics and for running numerical experiments with the limited area BOLAM

model at a resolution of 0.25°x0.25° (Catania, 2008). Various sensitivity experiments were performed with full physics, with or without radiation (the BOLAM model uses a combination of Morcrette, 1991, Ritter and Geleyn, 1992, and Mlawer et al, 1997, radiation schemes), with or without precipitation processes, surface fluxes etc. In addition, a model based experimental approach has been undertaken by simulating idealized ULCL's structures, using the same BOLAM model with fixed or periodic lateral boundary conditions and with a horizontal grid distance of 20°x20°. The ULCL structures have been prescribed by defining a dipolar (in the vertical) Gaussian temperature anomaly (cold in the troposphere and warm in the stratosphere), superimposed on a horizontally uniform atmosphere with a tropopause, as suggested by the observed thermal structure of ULCL's (Fig. 1). A gradient wind balance, taking into account the thermal wind relationship, has been prescribed, imposing a lower condition of vanishing wind and geopotential perturbation. Most experiments have been run with constant Coriolis parameter, in which case a quasi steady state can be easily obtained in quasi inviscid conditions. The model humidity field has been defined in order to have a saturated cloudy layer in the tropospheric part of the ULCL and very dry air above, where PV attains stratospheric values. Experiments have been performed in which radiation, moisture, microphysics, horizontal and vertical diffusion have been prescribed in various manners in order to evaluate mainly the contribution of the IR radiative transfer.

3 RESULTS

The analysis of numerical experiments on real cases has revealed an important role of radiation, if combined with the presence of moist air and clouds in the cold dome. Since removal of radiation has important effects also far away from the ULCL, it is preferable to consider idealized simulations in which only the IR radiation fluxes *anomalies* are considered, after subtracting the far field radiation. In this way the effects of radiation due only to the particular temperature and moisture anomalies associated with the baroclinic vortex are isolated, as shown in Fig. 2. Relative cooling prevails near and just below the cloud top, situated at 440 hPa, and warming above, while PV increases by about 5 PV units in a layer between 400 and 450 hPa and decreases around 300-350 hPa, in agreement with eq. 1.

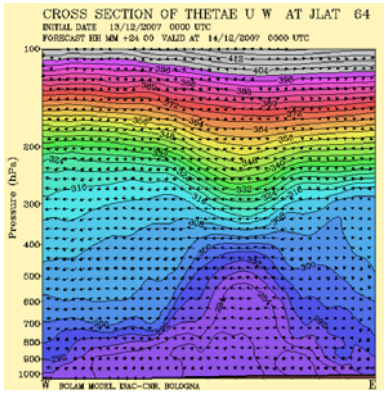

Figure 1. Vertical cross-section of equivalent potential temperature and wind vector (u, w) on the same plane across the ULCL of Dec. 2007, over eastern Europe.

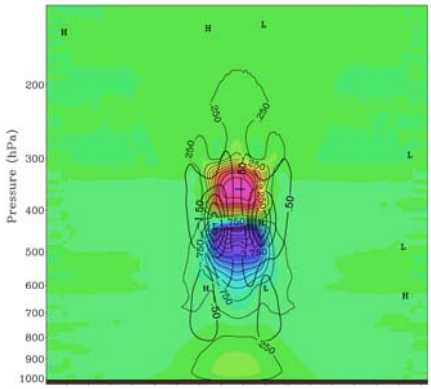

Figure 2. Vertical cross-section of radiative heating/cooling (thin lines and red/blue colours) in the ideal ULCL, and related changes of the normal velocity field (thick lines), after 4 days.

4 CONCLUSIONS

Simulations of real and idealized ULCL's indicate that the radiative transfer in the anomalous profiles of temperature and moisture can sustain and even reinforce the ULCL strength, by augmenting the amplitude of the PV anomaly and of the cyclonic flow in a thick layer situated in the upper portion of the cold pool.

REFERENCES

Catania, L., 2008: Processi radiativi e dinamici di mantenimento di vortici freddi in quota alle medie latitudini. Dissertations (*Tesi di Laurea*) in Physics. University of Bologna.

Esler, J. G., L. M. Polvani and R. A. Plumb, 1999: On the mix-down times of dynamically active potential vorticity filaments. *Geophys. Res. Lett.*, **26**, 2953-2956.

Emanuel, K., 2008: Back to Norway: an essay. *Synoptic-Dynamic Meteorology and Weather Analysis and Forecasting - A Tribute to Fred Sanders.* L. F. Bosart and H. B. Bluestein Ed., American Meteorological Soc., Boston, 87-96.

Eliassen, A., and E. Kleinschmidt, 1957: Dynamic Meteorology. *Handbuch der Physik*, **48**, 1-154.

Forster, C., and V. Wirth, 2000: Radiative decay of idealized stratospheric filaments in the troposphere. *J. Geophys. Res*., **105**, 10,169-184.

Mlawer, E. J., S. J. Taubman, P. D. Brown, M. J. Iacono, and S. A. Clough, 1997: Radiative transfer for inhomogeneous atmospheres: RRTM, a validated correlated-k model for the longwave. *J. Geophys. Res.*, **102D**, 663-16, 682-16.

Morcrette, J.-J., 1991: Radiation and cloud radiative properties in the ECMWF operational weather forecast model. *J. Geophys. Res.,* **96D**, 9121-9132.

Ritter, B. and J.F. Geleyn, 1992: A comprehensive radiation scheme for numerical weather prediction models with potential applications in climate simulations. *Mon. Wea. Rev.*, **120**, 303-325.

Thorpe, A. J., 1985: Diagnosis of balanced vortex structure using potential vorticity. *J. Atmos. Sci*., **42**, 397-406.

VERY HIGH RESOLUTION MODELLING OF FLOW OVER STEEP OROGRAPHY USING A TERRAIN-INTERSECTING MESH

A. Gadian[1], S. Lock[2], A. Coals[1], S. Mobbs[1]

[1] NCAS, University of Leeds, LS2 9JT, UK
[2] ICAS, University of Leeds, LS2 9JT, UK
E-mail: *alan@env.leeds.ac.uk*

Abstract: This poster presents results for idealised orographic stratified flows generated in a Microscale Model with a cut-cell representation of orography, resulting from a terrain-intersecting mesh. Comparisons with analytical solutions and other orographic models show promising results for the accuracy of the method. Further results demonstrate the potential of the cut-cell approach for steeper and more complex terrain.

Keywords: *Cut-cells, terrain-intersecting grids, modelled orographic flows*

1 INTRODUCTION

A generation of numerical atmospheric models has developed based on terrain-foll owing vertical coordinate systems due to their computational simplicity — of o perating on a rectangular grid regardless of the shape of the underlying orograp hy; of the lowest vertical level always coinciding with the orographic surface; and of the lowest few vertical levels being naturally positioned for application of a boundary layer scheme.

However, many studies (e.g. Sundqvist (1976) and Janjic (1989)) have demonstrated problems associated with the terrain-following approach — the generation of spurious winds in the vicinity of hills, and instabilities associated with distorted grid-cells near steep orographic gradients.

Massive growth in computing capacity and the resultant move to finer grid-resolu tions means the errors and instabilities associated with terrain-following grids above steep gradients are becoming an unavoidable hindrance. As grid resolutio ns increase, steeper and more complex gradients in the underlying orography are being resolved by the model grid. The numerical schemes in high-resolution mode ls must be capable of reliably and accurately solving flows over those steep gra dients.

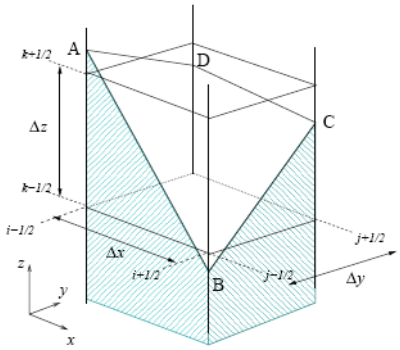

Figure 1: An example cut-cell in a terrain-intersecting model: $ABCD$ repr esents the orographic surface that intersects the model levels

2 METHODS

There has recently been some investigation of the potential for terrain-*in tersecting* grids, where the vertical levels remain horizontal throughout the do mian. In the presence of uneven orography, the vertical levels intersect the lo wer boundary resulting in some grid-cells that are *cut* by the orography. Figure 1 illustrates an example cut-cell within a terrain-inter secting model domain.

To solve the flows through irregularly-shaped cut-cells, Adcroft et al. (1997) explor ed the use of a finite-volume approach in an incompressible ocean model, where t he ocean-bottom topography was represented with cut-cells. The cut-cell method was seen to produce smooth solutions, where more rigid step-representations of o rography had failed. The method was extended and further explored in Bonaventura (2000), Steppeler et al. (2002), and Steppeler et al. (2006), resulting in a cut-cell method being implemented in the high-resolution numerical weather prediction model at the Deutscher Wetterdienst — the COSMO-DE model.

This work explores the potential for the cut-cell method in a very high resolution model. The Microscale Model is designed for exploring dynamics and moist processes at grid resolutions of $\Delta x < 100$m, with a particular focus on flows over steep gradients.

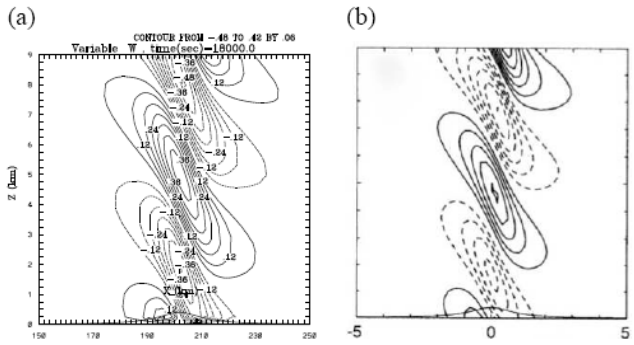

Figure 2: Results for stratified flow over a 2D bell-shaped hill, with half-width 10km, as described in Gallus et al. (2000): plots show the vertical velocity field, with a contour interval of 0.1 from (a) the Microscale Model; and (b) the analytical solution reproduced from Gallus et al. (2000)

3 RESULTS AND CONCLUSIONS

Results from the model compare well with linear solutions for well-studied idealised test cases (see Figure 2). At higher resolutions, resolving steeper gradients, the results for dry inviscid flows over orography look promising and will be presented here. In addition, routines for computing latent heat exchange between water vapour and liquid water have been implemented and tested. Current work is focusing on exploring the potential of the cut-cell Microscale Model for moist orographic flows.

REFERENCES

Adcroft, A., Hill, C., and Marshall, J., 1997: Representation of topography by shaved cells in a height coordinate ocean model. *Mon. Wea. Rev.*, **125**.

Bonaventura, L., 2000: A Semi-implicit Semi-Lagrangian Scheme Using the Height Coordinate for a Nonhydrostatic and Fully Elastic Model of Atmospheric Flows. *J. Comp. Phys.*, **158**.

Gallus, W. and Klemp, J., 2000: Behavior of flow over step orography. *Mon. Wea. Rev.*, **128**.

Janjic, Z. I.,1989: On the pressure gradient force error in σ-coordinate spectral models. *Mon. Wea. Rev.*, **117**.

Steppeler, J., Bitzer, H., Minotte, M., and Bonaventura, L., 2002: Nonhydrostatic Atmospheric Modeling using a z-Coordinate Representation. *Mon. Wea. Rev.*, **130**.

Steppeler, J., Bitzer, H.-W., Janjic, Z., Schättler, U., Prohl, P., Gjertsen, U., Torrisi, L., Parfinievicz, J., Avgoustoglou, E., and U. Damrath, 2006: Prediction of Clouds and Rain Using a z-Coordinate Nonhydrostatic Model. *Mon. Wea. Rev.*, **134**.

Sundqvist, H., 1976: On vertical interpolation and truncation in connection with use of sigma system models. *Atmosphere*, **14**.

THE SUMMER OF COPS-2007: MULTI-SCALE DYNAMICS VISUALIZED BY VARIABLE-SPEED TIME-LAPSE SATELLITE IMAGERY

Hans Volkert

Deutsches Zentrum für Luft-und Raumfahrt, Institut für Physik der Atmosphäre, Oberpfaffenhofen, Germany
E-mail: *Hans.Volkert@dlr.de*

Abstract: Some 9000 Meteosat images at 15' intervals span the full 3 months of the COPS field phase. Their display in variable-speed time-lapse loops provides an intuitive and persuasive synopsis of generation, motion and decay of cloud systems of differing horizontal scale and at distinct atmospheric levels.

Keywords: *ICAM, Meteosat, cloud motions, synoptic meteorology*

1 INTRODUCTION

Atmospheric dynamics focus on the interplay of the acting forces, mainly in the horizontal direction, e.g. the pressure gradient force in approximate balance to the Coriolis force on the rotating globe, modulated by friction and resulting individual acceleration of air parcels. Physical processes like cloud generation induced by the significantly smaller vertical motions (due to buoyancy forces) can eventually lead to the fall-out of precipitation. Synoptic, i.e. combined-view, horizontal charts at various levels are still the standard medium when insights about the evolving state of the atmosphere are sought, be it directly from observations or from computer generated analysis or forecast fields. Vertical sections provide an upright perspective, but tend to overemphasize height over distance and along-section motions to perpendicular ones.

Since more than 40 years satellite imagery has been providing an additional perspective. In an early study, Warnecke et al. (1968) combined multi-wavelength composite imagery by polar orbiting satellites with conventional observations to investigate the life cycle of a tropical cyclone. Since the late 1960s, weather satellites in geosynchronous orbit allow through their fixed relative position the direct production of time-lapse loops (short films). At the poster we present for the COPS field phase (June-August 2007) a 3-month-long sequence from multi-channel SEVIRI images obtained from Meteosat-8 at 15' (or 900") intervals on a stereographic weather map projection with overlaid geographical grid.

2 THE COPS-2007 CLOUD MOTION LOOP

Multi-spectral data of the SEVIRI instrument on the Meteosat Second Generation satellites are regularly received and processed by DLR-IPA, e.g. for the detection and tracking of convective cells over central Europe (Zinner et al., 2008). For all regular scan scenes from Meteoat-8 (15' intervals) a 3-channel (high resolution visible and two infrared channels) colour composite was created on a weather map projection (10ºE as vertical meridian) resulting in 8832 images for the COPS field phase from 1 June to 31 August 2007. They are online available for scientific users under password protection from www.pa.op.dlr.de/cops/msg_vis_archive.html which is linked to the general site www.cops-2007.de branch "operational products / satellite products / MSG imagery".

But only when combined to a video-clip with standard image frequency of 25 frames/s and displayed at relative speeds of 0.5, 1.0, 2.0 the full "drama of weather" (Shaw, 1933; admirable juxtaposition of atmosphere and antique theatre) becomes evident for the high-speed viewing system of human eyes and brain. The considerable time-lapse factors ('speed-ups') of 11250-, 22500- (=25x900"), and 45000-fold provide a breath-taking impression of ceaseless motions, much more rotational than translatory, under the quick successions of longer day-light and shorter dark night periods. Opposing motion directions at low and high elevations are frequent. The full three-month clip has 402 MB and can be run at variable speeds with, e.g., MS-MediaPlayer.

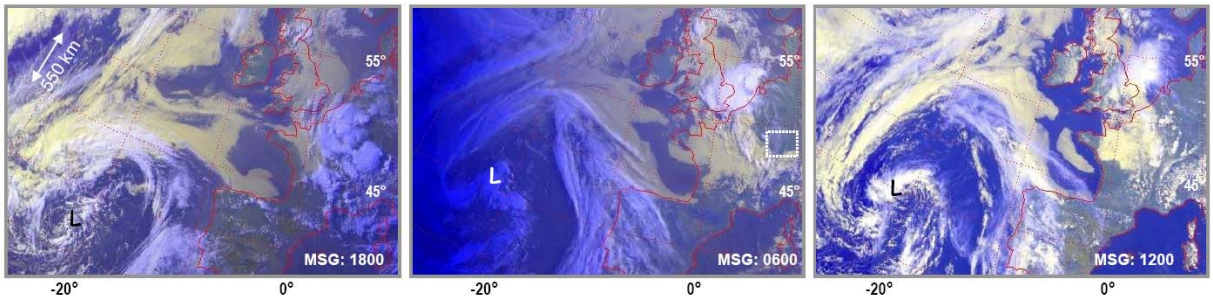

Figure 1. Three snapshots of spiralling cloud bands around a cyclone (L: low pressure centre) west of Portugal on 7 (18 UT) and 8 June 2007 (06, 12 UT). Three channel composite of SEVIRI sensor aboard Meteosat-8, transformed on a stereographic weather map projection (5º x 10º lat./lon. dotted grid; 10ºE vertical). The small dotted frame indicates the inner COPS area.

3 GLIMPSES TO A FEW "STILL LIFES"

While the moving dynamics of the atmosphere over Europe and the east Atlantic during summer 2007 can only be inferred from the video-clip, we present here two examples in a sequence of single frames.

During four days (6-9 June) a cyclone 'danced' west of Portugal sending its frontal cloud bands onto the continent (cf. Fig. 1 for three glimpses during the central period) before a following larger low pressure system covered the ocean area around 20º–10ºW for full five days (10-14 June). Sequences of fast moving high-level cirrus bands indicate frequent streamers, most likely connected with stratospheric intrusions (Appenzeller and Davies, 1992).

The end of June saw an impressive '*pas de deux*' of two cyclones over the eastern Atlantic and the North Sea, respectively, linked by an elongated, curved cloud band as if they were holding hands (Fig. 2). The detailed cloud structures and their vertical extent become best visible during the hours when the sun is rising or setting over Europe. Inspection of close-ups from rapid scans (at 5' minute intervals) allow during daylight periods the detailed identification of embedded convection. After a parallax correction their position can be precisely located.

4 CONCLUSION

Short sequences of cloud motions are regularly presented in TV weather forecasts, both observed during the previous hours and pre-determined from short-range NWP model output. Web-based access to Meteosat loops is also available for schools (cf. Dudek, 2009).

However, it is felt that the research community does not sufficiently use video technology combined with satellite data and classical synoptic experience. A regular archive of temporal complete, spatially well resolved and navigated multi-channel satellites scenes, put together in overlapping month-long loops for both normal (15') and rapid (5') scans over carefully selected areas has a huge potential *(i)* of inspiring researches; *(ii)* of educating students, teachers and pupils; and *(iii)* of impressing the public at large regarding the true nature of the weather producing atmosphere and the astonishing daily successes of providing skilful forecasts for the seemingly chaotic medium, at the ground of which we spend our days.

Discussions are sought with participants of ICAM-2009 during and after the conference. The video-clip COPS-Jun JulAug2007.avi is available from the author for non-commercial usage.

Acknowledgements:
I want to thank my colleagues Luca Bugliaro and Hermann Mannstein for their efforts to process and archive the multi-channel SEVIRI data obtained from EUMETSAT. Bernhard Mayer kindly assembled the videoclip in avi-format. The inspiration to look at extended loops of satellite imagery stems from my student days in the late 1970s with Prof. Günter Warnecke (FU Berlin), who extensively used the then novel loops from geostationary satellites for his undergraduate courses.

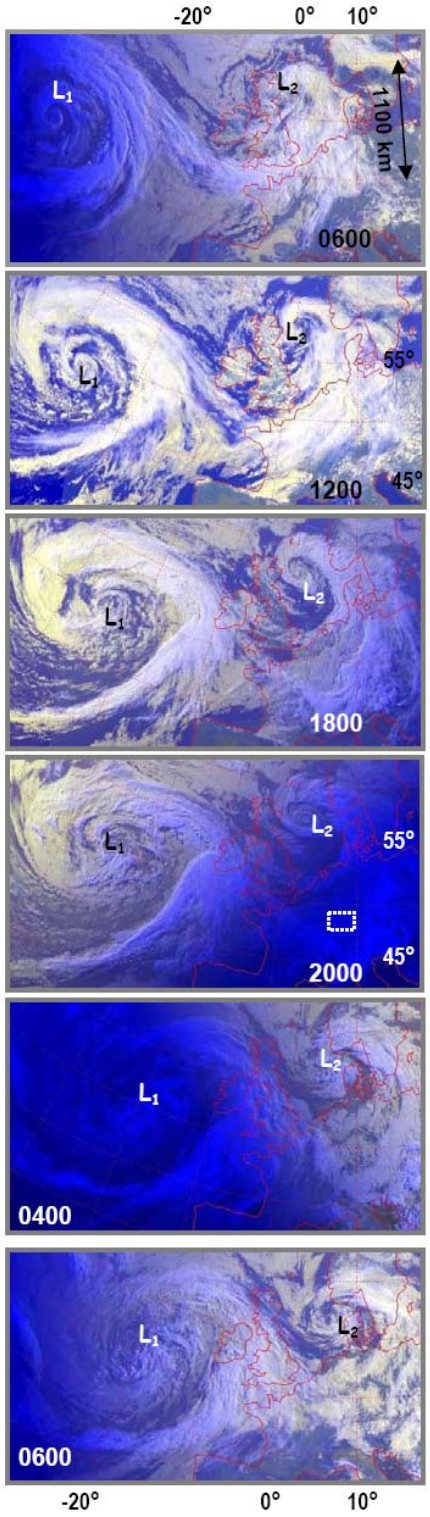

Figure 2. Top to bottom: Cloud band developments around two cyclones over eastern Atlantic (L_1) and North Sea (L_2) on 29/30 June 2007. Details analogous to Figure 1.

REFERENCES

Appenzeller, C. and H.C. Davies, 1992: Structure of stratospheric intrusions into the troposphere, *Nature* **358**, 570–572.

Dudek, P., 2009: Website "http://sat-sh.lernnetz.de/wetterfilme/msg/ " ,Weather films for schools (in German; accessed April 2009)

Shaw, N., 1933: *The drama of weather*. Cambridge University Press, Cambridge, UK, xiv + 269 pp.

Warnecke, G., L.J. Allison, E.R. Kreins and L.M. McMillin, 1968: A satellite view of the typhoon Marie 1966 development. NASA Technical Note TN D-4757, 94 pp.; online available from http://ntrs.nasa.gov/ (search for "typhoon Marie").

Zinner, T., H. Mannstein, A. Tafferner, 2008: Cb-TRAM: Tracking and monitoring severe convection from onset over rapid development to mature phase using multi-channel Meteosat-8 SEVIRI data. *Meteorol. Atmos. Phys.* **101**, 191–210.

Relationship between morphology PARAMETERS and duration of snow cover at microscale: preliminary study in several major ski areas of the territory of Trentino (Italian Eastern Alps)

Massimiliano Fazzini[1], Mauro Gaddo[2],
[1] Università di Ferrara – Dipartimento di Scienze della Terra
E-mail: *massimiliano.fazzini@unife.it*
[2] Provincia Autonoma di Trento - Ufficio Previsione ed Organizzazione

Abstract: The duration of stay of snow on the ground in areas of medium and high Alpine mountains, is very uneven and depends on many morphological variables, starting from the altitude and the exposure to hillside. A special case concerns the valley, the highlands and karst areas where the thermal effect together with that of the "sky wiew factor" difficult to determine hardly modelling situations. In this study, it was decided to consider the longest continuous period during which snow remains on the ground at the different exposure finding a relationship with the exposure itself and to hillside, in three sample areas identified in extended ski areas, located in different areas of the Alps Tridentine: thus district of Pampeago-Latemar, San Martino di Castrozza-Passo Rolle and Passo Tonale. Statistical reports, researched by a simple and a multiple linear regression analysis of the forward kind, show results in some respects surprising and very useful for climatological-tourism applications in ski areas.

Keywords: *Snow duration, exposition, microscale, ski district*

1 INTRODUCTION

Beginning from the ’80, we witness a strong decrement of seasonal fresh snow quantities, that can vary, depending on geographical area and altitude, from 3 to 5 cm per season (Fazzini *el al*., 2004). This signal, together with an evident increment of winter average temperatures, that can be quantified, in the same period, between 0.3 and 0.5 °C, comes from a proportional decrement of days with snowfalls. Consequently, a decrement of days with snow on the ground can be observed. All that gives rise to strong repercussion on the skiability of middle and low altitude ski areas, and the alpine ski tracks facing South are feasible for a limited number of days (Fazzini, 2008; Fazzini e Bisci, 2008). Trento Province relies, since winter 1981-1982, on a well organized nivometeorological network; moreover, a recent Provincial Law on avalanche sites control in ski areas, promoted a higher density of such measuring sites. Thanks to the relative abundance of data, their remarkable quality and their geographical positioning, including all main aspects, in important ski areas, it is possible to attempt a microscale climate study that can better clear the existing relationships between morphology and snow parameters in a territory.

Figure 1. Study areas position

2. DATA AND METHODS

A climatological analysis has been carried out on a series of nivometric data belonging to 2005-2006, 2006-2007, and 2007-2008 seasons for those measuring sites located in Pampeago – Ski Center Latemar and San Martino di Castrozza – Passo Rolle (Pale di San Martino Group) ski areas. In the Passo Tonale area, nivometric data are available for the season 2007-2008 only, so results have not been considered since they were not comparable with those of the two other study areas. In the Pampeago area - situated in Val di Fiemme and representative of the Dolomites - data have been sampled at altitudes ranging from 1,750 to 2,100 m a.s.l in the four major aspects. In San Martino di Castrozza, representative of the south Dolomites, data are relative to altitudes between 1450 and 2050 m a.s.l for all major aspects. For all the stations listed in this work, data from the current, extremely snowy season, are being collected. As soon as snow will melt on all sites, new data will be integrated and analyzed with the existing ones. Up till now, nivological daily data, man measured at 8.00 am, have been analyzed. For each measuring site, monthly and seasonal fresh snow contributions have been calculated, as well as the summation of days characterized by snow coverage of the ground, continuous (*Len cont*) and total (*Len tot*). Only *Len cont* values have been used. At the same time, to try describing quantitatively the environment surrounding each site, 16 measures, both morphometrical and topographic, have been calculated, to be correlated with the nivological

variable. A stepwise type multiregressive statistical analysis has been performed, considering the nivological variable as a dependent, and the morphological measures as independent ones. Angular parameters have been linearized using *sinus* and *cosinus*.

AREA SAN MARTINO	Elev	Expos	Slope	Htot	Len tot	Len cont
S.MARTINO DI C.ZZA	1461	47	2	342	130	123
PASSO ROLLE	2004	214	6	448	179	174
CALAITA	1602	14	5	344	137	129
VAL CIGOLERA	1878	106	13	425	148	144
COL VERDE	1879	221	18	375	129	116
AREA PAMPEAGO	Elev	Expos	Slope	Htot	Len tot	Len cont
PAMPEAGO VILLAGE	1780	147	20	275	137	134
GARDONE'	1675	94	9	229	129	124
MONSORNO	2000	195	14	342	153	152
AGNELLO	2065	345	13	387	171	170

Table.1 – Topographical and nivological parameters for the sites used in the analysis: Elev: elevation above sea level – m; Expos: Aspect of slope °; Htot: average of seasonal fresh snow, cm; Len tot: duration of total snow cover, days; Len cont: duration of continuous snow cover, days.

3 RESULTS

From the analysis of nivological data, comes into sight that, at the same altitude, San Martino di Castrozza area is more snowy than Pampeago one, because of its location, more external in regard to Alpine range, and for the arrangement of the valleys. The Pale di San Martino group is actually more exposed than the Latemar group to Mediterranean currents that, statistically, bring the heaviest snowfalls (Fazzini et al 2005); the mouth of San Martino valley (Val Cismon) faces south, favouring the entrance of mild advections, which afterwards undergo a heavy convergence - uplift process at the head of the valley. Nevertheless, due to a higher thermal continentality of Pampeago area, no substantial differences can be observed with regards to the duration of snow on the ground. On Passo Tonale area, measures made at the same altitude of 1880 m a.s.l. on N and S aspects showed a difference of 23 days in the persistence of the snow on the ground. The analytical relationship between altitude and snow persistence results to be found only in Pampeago area (R^2 = 0.93), with an increase of snow coverage of 10,8 days/100 meters of altitude increase. The corresponding values for San Martino area are R^2 = 0.43 and 6,7 days/100 meters. The multiple linear regression analysis raised the level of explained variability to 0.98 in Pampeago area, thanks to the statistical contribution of site aspect and the gradient ratio of the slope overhanging the site. Similarly, the explained variability of San Martino area reached values of 0.93 thanks to statistical contribution of site aspect, the *sinus* of the azimuth of the valley axis, and the *cosinus* of slope steepness.

4. CONCLUSIONS

With the analysis of the statistical relationship of multivariate type between morphological parameters and continuous presence of snow cover, flattering results have been obtained. Using the data of current season, and therefore using the data from Passo Tonale area too, the model could be further improved; using the information coming from morphological measures used in the study areas, a regionalization of the model could be tried.

Acknowledgements: *We thank Enrico Filaferro for an critical rewiew of analisys and PAT and ITAP - Pampeago nivologist.*

REFERENCES

Massimiliano Fazzini., Simona Fratianni, Augusto Biancotti, & Paolo Billi, 2004: "Skiability condition in several skiing complexes on Piedmontese and Dolomitics Alps. Meteorologische Zeitschrift, Gerard Borntraeger ed, Berlin, Stuttgard Volume .**13.3**, 253-258

Fazzini M., Giuffrida A., Frustaci G., 2005: Snowfall analisys over peninsular Italy in relationship to the different types of synoptic circulation: first results – *Proc. 28th conference on Alpine Meteorology, Zadar*, Croatian Meteorological Journal, Volume **40**, 650-653.

Massimiliano Fazzini and Carlo Bisci, 2008: Alpine climatology and touristic application of a skiability index in Paneveggio-Pale di San Martino park area (easter trentino region, italian Alps - Studia Crescent, Volume **2-2008**; 41-49.

Massimiliano Fazzini, 2008: Impact du changement climatique sur l'enneigement dans les Pré-Alpes du Trentino: le cas de Folgaria – *Proc XXI colloque Internationale AIC Montpellier*, 234-239

SNOW PRECIPITATION VARIABILITY IN THE WEST ALPS IN ITALY: EVALUATION OF AN ALGORITHM FOR THE SURVEY OF SNOW COVER THROUGH SATELLITE IMAGES

Terzago S.[1], Cassardo C.[2], Cremonini R.[3], Fratianni S.[1]

[1] University of Torino, Department of Earth Science, Torino, Italy
E-mail: 315697@*studenti.unito.it*
[2] University of Torino, Department of Physics, Torino, Italy
[3] Regional Agency for Environmental Protection, Torino, Italy

Abstract: Snow cover greatly influences the climate in the Alpine region and it is one of the most important factors in the analysis of the climate change because of its interconnections with other phenomena: the different distribution and amount of snow precipitation during the winter season influence energy, radiation and hydrologic budgets, as well as atmospheric circulation.
In this paper the results of the analysis of snow precipitations in North-West Italy in the period 2000-2009 are presented: nivometric measurements performed in 10 automatic meteorological stations of ARPA Piemonte Network were used. In the studying of Alpine climatology satellite data can be exploited to achieve information on temporal and spatial variability of snow cover extent: for this purpose MSG's SEVIRI snow cover algorithm was evaluated for 19 cases of study in the period 2007-2009 using at-ground stations.

Keywords: *snow, climate, MSG snowcover algorithm, Alps*

1 INTRODUCTION

Snow cover over Alps influences climate both at large and local scale as snow reflects most of the solar radiation, varying surface radiation, energy and hydrologic budgets. Ground-based meteorological stations and satellite data can provide complementary information on snow cover: the first ones about the nivometric statistical parameters and the climate trends for local scale, the second ones about the extension of snow cover, the snow line and the reflectance of snow covered areas on large scale. The analysis of snow precipitation variability through these two different point of view will allow to achieve a global understanding of snow processes and dynamics in the Alpine Region.

In this paper the first results of the analysis of 10 ground-based stations measurements in the South-West Piedmont Alps in the period 2000-2009 are presented: time series are continuous and homogeneous in this period so the results can be compared.

For a future exploitation of satellite data in climatological studies, the quality of satellite snow cover products need to be assessed and improved: daily SEVIRI snow cover was generated for 19 clear-sky days in the period 2007-2009 and validated with 111 at-ground measurements in Piedmont and Aosta Valley. It was quantified the snow product accuracy in presence of fresh snow, for different snow depths and different seasons.

2 DATA

Snow depth measurements performed in the automatic meteorological stations have been considered to evaluate the monthly mean snow depth over the period 2000-2008 and the results are reported in Table 1. The standard deviation is generally high for the strong annual variability of snow precipitation. Fresh snow depth records have been used to determinate the number of snowy days per month which shows little fluctuations. In Figure 1 the monthly-averaged snow depth and the number of snowy days for the Acceglio station are represented: as in all the other stations, the highest peak for snow depth corresponds to the last snow season (2008-2009), when heavy snowfalls occurred over Piedmont. In January 2009 the monthly mean snow depth is 112 cm, in February it is 124 cm: in both cases the values exceed two standard deviations the month average, however, in order to classify them as anomalous events, they should be compared to the mean value of a 30-years time series.

At-ground snow depth and fresh snow depth measurements have been used for the validation of SEVIRI snow cover product which discriminates snow covered and snow free areas. The quality of the SEVIRI snow cover has been determinated using contingency tables and statistical indices, as reported in Table 2: the probability of a correct classification of snow covered areas is CSI=0.74 and the probability of overestimation of snow cover (FAR=0.17) is comparable to the probability of underestimation (BIAS=1.04). Further analysis show that the quality of snow cover is higher in Winter than in Spring, when snow is overestimated. It was observed

that the accuracy of the snowcover product is very high in presence of fresh snow or if snow depth higher than 30 cm (CSI=0.95). When snow depth is lower than 10 cm the probability of misclassification increase.

Station	Elevation a.s.l. [m]	UTM_x	UTM_y	Mean Snow Depth [cm]					
				Nov	Dec	Jan	Feb	Mar	Apr
Acceglio	1610	339567	4927939	13±13	39±29	41±27	45±30	31±23	3±2
Argentera	1680	335978	4918048	16±15	57±36	60±37	63±39	50±35	8±5
Boves	575	385442	4910296	1±2	9±11	10±8	8±6	2±3	0±0
Castelmagno	1755	354208	4918133	17±15	52±29	49±32	55±36	42±28	10±8
Paesana	1265	362370	4947015	8±12	19±26	21±14	27±19	22±19	2±1
Piaggia	1645	398488	4880823	4±4	29±33	36±36	46±47	34±37	8±7
Pian delle Baracche	2135	351816	4934725	30±21	73±43	73±38	84±38	85±41	72±30
Pontechianale	1575	345555	4941889	11±12	29±25	19±16	21±15	13±9	3±3
Rifugio Mondovì	1760	398757	4894142	15±11	56±38	59±41	73±47	73±47	49±36
Valdieri	1390	361709	4896272	18±18	67±37	79±48	97±48	89±55	31±27

Table 1. Monthly mean snow depth and standard deviation calculated over the period 2000-2008 for 10 ARPA Piemonte ground stations.

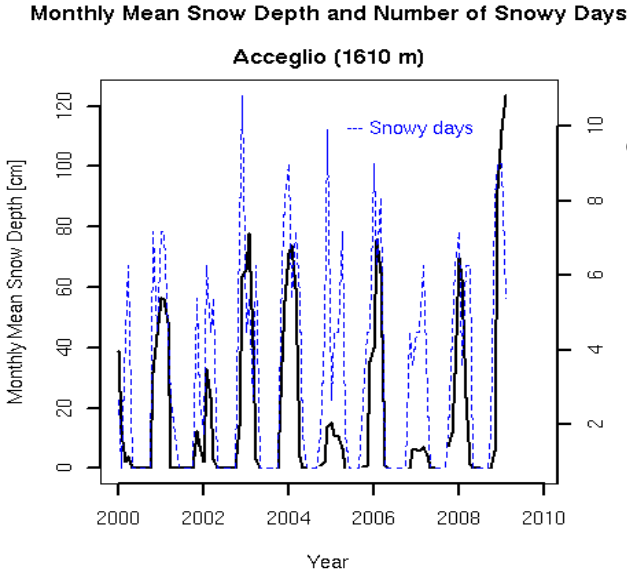

Figure 1. Monthly-averaged snow depth and number of snowy days in the period from January 2000 to February 2009.

GROUND STATIONS	SEVIRI no snow	SEVIRI snow
no snow	413 (correct negatives)	110 (false alarms)
snow	85 (misses)	550 (hits)

$$POD = \frac{hits}{hits+misses}$$

$$CSI = \frac{hits}{hits+false\ alarm+misses}$$

$$FAR = \frac{false\ alarm}{hits+false\ alarm}$$

$$BIAS = \frac{hits+false\ alarm}{hits+misses}$$

POD = 0.87
CSI = 0.74
FAR = 0.17
BIAS = 1.04

Table 2. Validation of SEVIRI snow cover with in-situ measurements: contingency table and statistical indices.

3 CONCLUSIONS

A first analysis on snow precipitation features over Alps in North-West Italy has identified the monthly mean snow depth during the period 2000-2008 in 10 at-ground stations: a strong variability in the abundance of snow has been pointed out. Longer time series are necessary to determinate climate trends and to investigate on the heavy snowfall of the 2008-2009 winter.

The quality of SEVIRI snow cover product is better in Winter than in Spring when snow cover is overestimated, probably due to the stronger solar illumination: snowcover algorithm test threshold should be optimised to have a constant accuracy during the snow season. Deep snow and fresh snow are correctly identified while shallow snow should be detected with a more liberal test threshold.

REFERENCES

Kidder S. Q., Vonder Haar T. H., 1995: Satellite Meteorology: an introduction. Academic Press.

Parajka J., Bloschl G., 2006: Validation of MODIS snow cover images over Austria. Hydrology and Earth System Sciences, 10.

Schmetz J., Pili P., Tjemkes S., Just D., Kerkmann J., Rota S., Ratier A., 2002: An introduction to Meteosat Second Generation (MSG). Bulletin of American Meteorological Society.

Using polar-orbiting weather satellite data to estimate the snowline of central-European mountains

Ralf Becker[1], Peter Bissolli[2], Thomas Reich[3]

[1] Deutscher Wetterdienst, Remote Sensing Division, Offenbach
E-mail: ralf.becker@dwd.de
[2] DWD, Dept. Climate and Environment, Offenbach,[3] DWD, Dept. Hydrometeorology, Berlin

Abstract: The utilization of atmosphere and surface parameters derived from satellite remote sensing is of increasing importance to describe status and changes of weather, climate and the regarded processes in the biosphere. Even in regions with good coverage concerning ground based measurements satellites contribute to fill temporal and spatial gaps. Imaging radiometers provide information on surface snow and ice based on multispectral algorithms with a spatial resolution from 500 m to 3000 m. Verification with respect to ground based measurements shows very good results.

Keywords*: snowline, mountains, satellite remote sensing, AVHRR, MODIS*

INTRODUCTION

Snow and glacier ice play an important role in the description of the hydrological cycle by acting as a reservoir for water. The real-time monitoring of snow cover contributes to improve the water management. In the mid-latitudes of central Europe this is of special interest in and near the Alps and highlands like the Black forest and the Bavarian forest. Standard methods to detect and monitor snow cover are based on synoptical data as input and kriging techniques to handle the heterogeneous spatial distribution of stations and orographic effects. In orograpical structured area there is a lack of accuracy of such methods.

DATA AND METHODS

Observations of operational satellite systems namely Meteosat second generation, Noaa/MetOp AVHRR and Terra/Aqua MODIS have the potential to provide snow products on a daily basis with spatial resolution comparable or better than grid increment of the hydrological models. The work presented here shows the applicability of an automatic scheme evaluating AVHRR and MODIS data to determine the snowline in mountainous areas. A well-established algorithm, developed within the framework of the Satellite Application Facility for Nowcasting (NWCSAF, Dybbroe et.al. 2005), is used to detect snowy pixels in the AVHRR imagery. For MODIS a dedicated algorithm was set up: a multi-spectral thresholding of calibrated radiances is applied to separate clear land and sea from cloudy and snow-covered scenes. It is independent of other non-static data like numerical model forecasts and outputs a combined snow/cloudmask that is finally convoluted with background topography information (GIS), allowing for the calculation of snowlines. The core snow and ice detection is mainly based on a NDSI module (*normalised difference snow index*, Hall et.al. 2001). The first processing step separates pixels that can be classified for sure by its spectral features as snow meanwhile the others remain uncertain. The second, box-based step analyses the neighborhood of these pixels to catch pixels with mixed spectral features. A set of regions has been defined to cover low mountain ranges, like Thuringian forest in the middle and Black forest in the southwest of Germany, as well as parts of the Alps. In a postprocessing step an automatic quality assessment is conducted. It checks whether cloud coverage of the scene is tolerable in terms of absolute coverage as well as vertical distribution of snowy pixels.

COMPARISON AND VERIFICATION

A comparison study of MODIS to Nowcasting SAF software results - the validated PPS algorithm - is enabled by setting up a processing with preprojected data on a spatial scale of 500 m. The data ranges from May 2007 to August 2008. According to that the results for MODIS are in a good agreement facing a correlation of .94 but systematic overestimation of MODIS vs. AVHRR snowline of about 200 m is considered. A verification was carried out for the same time range by taking into account all European synoptical and climatological snow measurements with snow heights of at least 1 cm. The scores show a clear seasonal cycle with PODs of .2 in summer (both) and .86 (AVHRR) and .82 (MODIS) in winter months. Bad figures during summertime can be explained by more mixed pixels with less snow contribution over central Europe at this time.

APPLICATIONS

The hydrological model SNOW is simulating the snow cover evolution up to 72 hours lead time. Additional initial data on snow cover extent based on AVHRR and MODIS are feeded into the model to improve some critical aspects of conventional snow assimilation like melting phase heterogeneity (neighborhood of snowy and snowfree picture elements) and insufficient correlation with terrain height as exploited by kriging techniques. First results of adjustment examples using AVHRR snowmask show that the speed of melting is accelerated considerably. The goal of the project SnowClim is to build a European snow climatology to serve as input for touristical applications, regional climate monitoring, water management and traffic a.o. In a first step the satellite based values shall help to identify wrongly coded data of snow cover in the synop database and to compare the duration times of snow cover especially in regions with less dense ground based measurements.

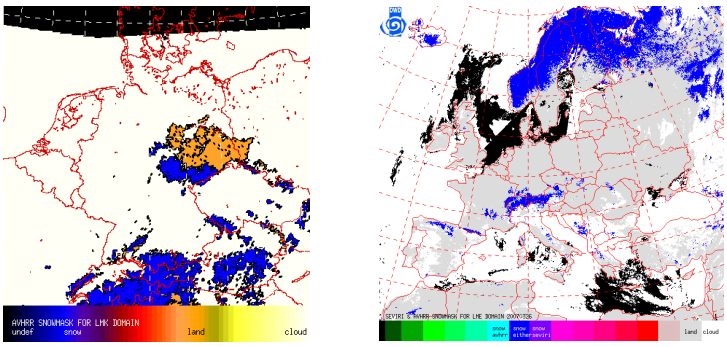

Figure 1: Sample AVHRR snowmask mapped for the domain of COSMO-DE model at 2.8 km scale (left, valid for 20071225, snow=blue, cloud=white). Input are two NOAA-17 midmorning overpasses (8:00 to 10:30 UTC), processed on 1 km scale using NWCSAF/PPS software. Merged AVHRR and SEVIRI snowmask for the COSMO-EU domain (right). Higher importance of polar orbiter data given at higher latitudes due to decreased applicability of SEVIRI data north of 60 degrees.

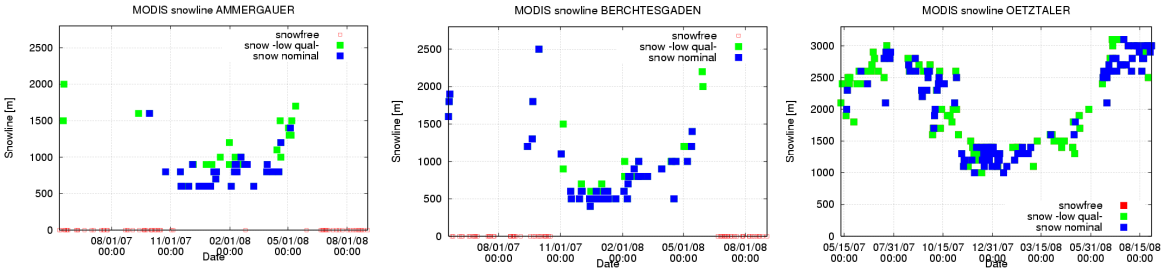

Figure 2: Snowline evaluations covering the winter season 2007/08 based on MODIS for some selected regions – the Ammergau and Berchtesgaden mountains as examples for the northern Alps and Oetztal as part of the central Alps. Blue squares are associated with nominal quality referring to almost cloudfree conditions and near-nadir viewing geometry. Green squares mark evaluations that lack one of these boundary conditions, still usable but larger error bars. If there was no snow detected an open red square is drawn. Note that results of a central alpine area characterized by permanent snow and glaciers (right panel valid for Oetztal, time range here from May 15, 2007 to Aug 15, 2008) do reflect the seasonal variation of snowline.

OUTLOOK

The very promising results enable the utilization of a merged (MODIS/AVHRR/SEVIRI) snowmask in the assimilation scheme of the SNOW model on a 1 km scale, maintained by the department of hydrometeorology of DWD. In the context of the DWD-project SnowClim (European snow climatology) the satellite-based evaluation shall be used as comparison and potential correction regarding a climatological derivate like duration of snow cover with respect to its height dependency.

REFERENCES

Droz, M. and S. Wunderle, 2002. Snow line analysis in the Alps based on NOAA/AVHRR data spatial and temporal patterns for winter and springtime in 1990, 1996 and 1999, Proceedings of the EARSeL-LISSIGWorkshop: Observing our cryosphere from space, Bern (CH) March 11-13

Dybbroe, A., K.G. Karlsson and A. Thoss, 2005. AVHRR cloud detection and analysis using dynamic thresholds and radiative transfer modelling – part one: Algorithm description. J. Appl. Met., 41(1):3954.

Hall, D.K., G.A. Riggs and V.V. Salomonson, 2001. Algorithm Theoretical Basis Document (ATBD) for the MODIS Snow and SeaIce Mapping Algorithms. http://modis-snow-ice.gsfc.nasa.gov/atbd.html

A NEW DEVICE FOR ACCURATE MEASUREMENTS OF METEOROLOGICAL PARAMETERS IN A SNOW RICH ENVIRONMENT

Manfred Dorninger

Department of Meteorology and Geophysics, University of Vienna, Vienna, Austria
E-mail: *manfred.dorninger@univie.ac.at*

Abstract: A deep snow pack, remote locations, no external power supply and very low temperatures are often the main ingredients when it comes to the deployment of meteorological stations in mountainous terrain. WMO recommendations concerning distance of the sensors to the surface are hardly fulfilled especially due to the varying snow depths. The accurate position of the sensor related to the snow surface is normally not known since a daily inspection is not possible. Even worse, the sensor might be completely snow-covered. The paper introduces the so called "METLIFT" which has been developed at the department recently. A snow height sensor measures the distance to the snow surface. If certain limits are exceeded the whole station is adapted accordingly. The lift can deal with a snow depth of up to 4 m. Accumulators recharged by solar panels guarantee the internal power supply. Data transfer is possible via radio transmission and/or GSM.

Keywords: *WMO, snow depth, mountainous terrain, meteorological instruments*

1 INTRODUCTION

WMO recommends a height between 1.2 m and 2 m above ground level for the measurement of air temperature and humidity (WMO, 2008). The height above ground level is specified to take care of the possible strong vertical temperature and humidity gradients at the lowest layers in the atmosphere. Especially in snow rich and remote locations it may be hardly possible to follow this advice. Therefore most of the meteorological stations in mountainous terrain are situated at mountain tops where strong winds will blow off the snow or in valleys where a daily inspection of the sensors is possible. In other unpopulated mountainous areas, e.g. basins, plateaus, the distance of the sensor to the snow surface is not known or the sensor will be snow-covered. Figure 1 shows two examples of our Gruenloch basin experience from recent winter campaigns.

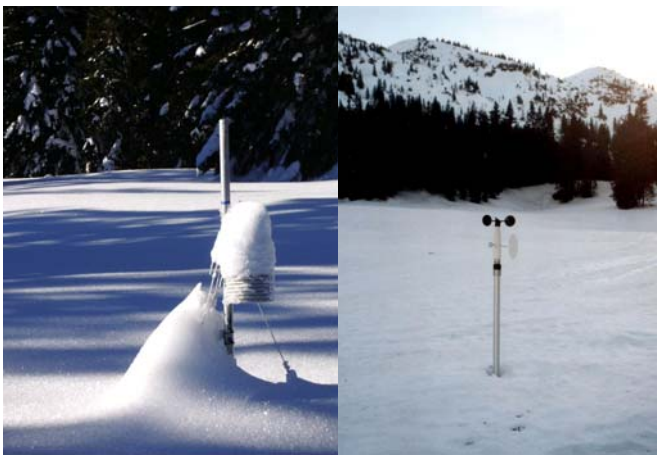

Figure 1. Snow cover in Gruenloch area; left: Temperature/Humidity sensor about 50 cm above snow surface; right: weather station almost completely snow-covered. In both cases: snow depth about 3 m.

2 METLIFT

In close cooperation with the technical high school in Waidhofen/Ybbs, Lower Austria, a new device was developed to guarantee the sensor height above surface within the WMO limits in harsh and remote environments. An ultrasonic snow height sensor measures the distance to the snow surface. If it exceeds certain limits due to snow accumulation or snow melt the lift adapts its height accordingly.

2.1 Overall set-up

Figure 2 shows the prototype of METLIFT. The lift is 6 m high and can pull out for another 4 m. Sensor arms are mounted every meter to allow the connection of additional sensors or to measure a profile of a certain

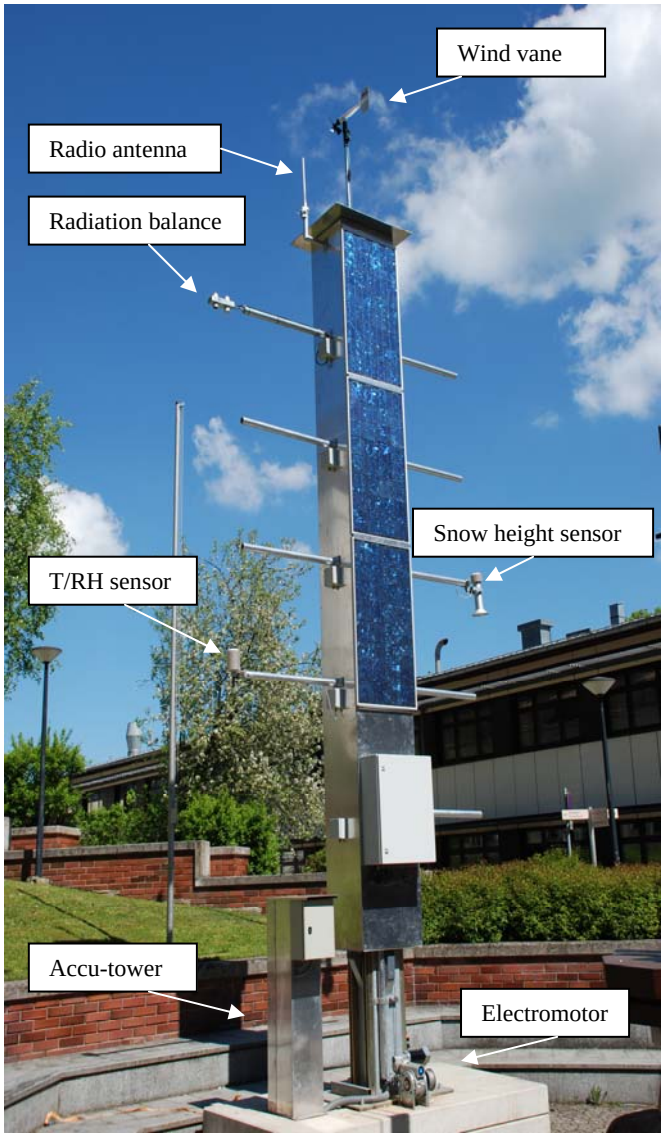

Figure 2. Prototype of METLIFT. Protective housing for the electromotor and for the accu-tower will be added in the final set-up.

parameter of the lowest 5 m above surface. Sensors can be added easily since cable wiring is provided to each sensor arm. Horizontal winds are measured at 7 m height above surface.

2.2 Some technical details

METLIFT is independent of external power supply. Three lead gel accumulators (12V, 85Ah) recharged by three solar panels provide the energy necessary for the sensors, the data loggers, the data transmission components and for the electromotor to lift the system. It has to be ensured that the temperature in the accu-tower stays within the operation temperature limits of the accumulators to avoid a loss of power or even worse a destruction of the accumulators. The accu-tower is insulated and a heat pipe provides additional energy to the interior of the accu-tower to keep the temperature high enough. METLIFT is energy optimised to keep the energy consumption at low levels.

The components of the lift device consist of a 12V electromotor with a worm gear with a transmission rate of 2856:1. This means that the lift moves extremely slow. The lifting is realized via a winch, a steal rope and a return shaft.

Basins represent very often dead zones for GSM signals. Therefore, METLIFT is equipped with a radio transmission system. The radio signal is sent to a nearby mountain station and then converted into a GSM signal.

All electronic units are checked for temperatures down to -70 degree Celsius.

3 SYSTEM CHECKS

Several tests have been performed during the winter season 2008/2009. The data transmission check verified the data flow from the logger via the radio signal and GSM signal to a server and the real-time availability on a webpage. The power consumption of each sensor, of the logger, of the data transmission system and of the control unit for the lift has been measured and optimized in the energy consumption check. Icing conditions have been simulated by sprinkling the tower during very cold days.

4 FURTHER OUTLOOK

METLIFT will be brought into the field in the upcoming summer season in the Dachstein region in Austria. Due to the very remote location all components have to be transported via helicopter. First field data are expected in autumn 2009.

REFERENCES

WMO, 2008: Guide to Meteorological Instruments and Methods of Observation. WMO-Nr. **8**, 681pp.

EXTENDED ABSTRACT TEMPLATE FOR ICAM-2009: A CASE-STUDY OF VOLUNTARY COOPERATION (12 PT BOLD CENTRED)

Hans Volkert [1] and Günther Zängl [2] (10 pt centred)

[1] Deutsches Zentrum für Luft-und Raumfahrt, Institut für Physik der Atmosphäre, Oberpfaffenhofen, Germany
E-mail: *Hans.Volkert@dlr.de*

[2] Deutscher Wetterdienst, Forschung und Entwicklung, Offenbach, Germany (10 pt centred)
Email: *Guenther.Zaengl@dwd.de*

Abstract: This example presents all layout details for an easy production of a two-page Extended Abstract for each oral and poster presentation which was accepted for the 30th International Conference on Alpine Meteorology (ICAM) to be held in Rastatt, Germany, from 11-15 May 2009. The abstract should briefly summarize the main contents of your contribution. Recommended maximum size 10 lines using Times new roman 9pt. The sample is reproduced here as it may be useful at future occasions.

Keywords: *ICAM, group dynamics (9 pt in italics)*

1 INTRODUCTION (headline in CAPITALS, 10 PT BOLD)

The extended abstracts will be gathered in the preprint volume for the 30th International Conference on Alpine Meteorology. In order to have similar format for all abstracts of the conference volume, this document gives some recommendations to the authors when elaborating their extended abstract. The extended abstract should be formatted **in A4 format** (210 mm x 297 mm) with page margins of 25 mm on the left and right sides and 25 mm on the top and bottom. The **maximum allowed size is 2 pages**. Pages **must not** be numbered as the pagination will be done during the final editing process.

The first page must begin with the paper title in capital letters centred. All authors' names and affiliations appear just below the title. The email address is only necessary for the first author. An abstract and keywords directly follow directly.

The text should be divided in several sections, e.g. INTRODUCTION, DATA AND METHODS (or MODEL SETUP for numerical modelling papers), RESULTS and CONCLUSION. The title of each section should be in capital letters. Sections can be divided in sub-sections with subtitles. The text must be in a **single column format**. For the body, the text must be single-spaced and justified, using preferably Times new Roman font. Sizes are specified at various locations. It should be structured in paragraphs, new paragraphs begin indented without an empty line. The paper should be written in English. SI units should be used.

References will appear at the end of the extended abstract. List citations alphabetically in the reference section. Three examples of citations are given in this document (Bougeault et al. 2001, Houze 1993, Schwitalla et al. 2007). Acknowledgements is an optional item placed just before the references section.

2 TABLES, FIGURES AND EQUATIONS

2.1 Tables and figures (10 pt bold)

A caption must be provided for each table and figure. Captions should be below the figures/tables and must be numbered (Tab. 1; Fig. 1). Figures may be provided in colour, but should also be readable when printed in greyscale, because the printed Extended Abstract Volume will not contain colour figures. However, colour figures will be available in the online version of the extended abstracts.

2.2 Equations

Equations should be marked with numbers at the right side, equation (1) is an example:

$$ax + b = c \tag{1}$$

Presentation type / Session topics	BoundLayer	Climate	Dynamics	Num.Wea.Pred.	Precipitation	Snow
Oral (#talks, #sessions)	18 in 3	6 in 1	14 in 3	12 in 2	34 in 7	6 in 1
Poster	31	17	27	–	24	7

Table 1. Distribution of presentations in topical groups (cf. programme on pp. ii-xvii; as of 15 April 2009) – Example of a table with columns and lines filled with some quantitative information (entries in 10 pt; caption in 9 pt).

Figure 1. Two versions of the ICAM-2009 logo. Left: towering cumulus above the Black Forest as viewed from Baden Airpark during COPS-2007; right: view from the northern Black Forest heights into the Rhine valley under the cover of high cirrus (9 pt).

Figure 2. View of the venue of ICAM-2009. Right: Spacious foyer, where some of the poster boards will be placed; middle: lecture hall with large elevated screen; the outside garden next to the river Murg invites for informal discussions and relaxing moments during breaks.

3 SUBMISSION OF EXTENDED ABSTRACT

The extended abstract should be produced with MS-Word or LaTeX. For both formats, templates are provided *(ICAM-ExtAbsTemplate.doc* and *ICAM-ExtAbsTemplate.tex)* on the ICAM-2009 web page (www.pa.op.dlr.de/icam2009/downloads/). Of course, other word processing systems can be used as well, in that case, the authors are encouraged to follow the recommendations given in this example. The file should be converted in **pdf-format before submitting your abstract** to **icam2009@dlr.de**. When pdf conversion is not possible, a MS-Word (.doc) or a postscript file (.ps) is also acceptable.

Please submit your extended abstract not later than 3 April 2009. **Note that if you do not submit an extended abstract, your contribution will not appear in the Volume of Extended Abstracts.** Please use the following naming convention to help us producing the Volume of Extended Abstracts:

`ICAM-Name_of_first_author-{Oral|PosterCode}.pdf`

Your PosterCode is given in the programme (cf. www.pa.op.dlr.de/icam2009/programme/ICAM-agenda.pdf), starting with a capital letter (B, C, D, P, or S) followed by two digits.

4 CONCLUSIONS

This Volume shows to what extent the 125 co-authoring teams found the provided guidelines useful. The example got updated with overview figures of presentations in categories oral and poster and in topical groupings (Tab. 1). It is included in the Extended Abstract Volume to make a bit more explicit how an international scientific community – though diverse in many respects – is willing to cooperate on a voluntary basis. A short deadline before the meeting with some flexibility for late-comers and the avoidance of an extra charge appear to have contributed to the considerable number of contributions. It is hoped that the Volume of Extended Abstracts eases personal selections during the conference and preserves some of its contents.

Acknowledgements: *(9pt italics)*
We thank all contributors for their cooperation on a voluntary basis. The five sponsoring agencies DWD, DLR, KIT, NEC and WMO are acknowledged for their support and their trust in the organizers of ICAM-2009.

REFERENCES (e.g. article, book, proceedings; in 9 pt; second line indented for better distinction)

Bougeault, P., P. Binder, A. Buzzi, R. Dirks, R. Houze, J. Kuettner, R. B. Smith, R. Steinacker, and H. Volkert, 2001: The MAP Special Observing Period. *Bull. Amer. Meteorol. Soc.* **82** , 433–462.

Houze, R. A., Jr. 1993: *Cloud dynamics*. International Geophysics series, Volume **53,** Academic Press, 573 pp.

Schwitalla, T., G. Zängl, H.-S. Bauer, and V. Wulfmeyer, 2007: Convective initiation in the Black Forest region in high-resolution MM5 simulations. *Proc. 29th Intern. Conf. on Alpine Meteorology*, Chambery, France, 261–264.